



V5 Ground-Motion Model (GMM) for the Groningen Field

Re-issue with Assurance Letter

Julian J Bommer¹, Benjamin Edwards¹, Pauline P Kruiver², Adrian Rodriguez-Marek¹, Peter J Stafford¹, Bernard Dost³, Michail Ntinalexis¹, Elmer Ruigrok³ and Jesper Spetzler³

- 1. Independent consultant,**
- 2. Deltares,**
- 3. Royal Netherlands Meteorological Institute (KNMI)**

Datum March 2018

Editors Jan van Elk & Dirk Doornhof

General Introduction

The hazard in Groningen, due to earthquakes induced by the production of gas, is primarily presented by the ground motions to which buildings and people are subjected. The prediction of these ground motions is therefore critical for hazard and risk assessment.

This research was started in 2012 and is continuing with ever more ground motion data from Groningen earthquakes being collected. The Ground Motion Prediction Model (GMM) was therefore updated and progress documented regularly. In the Technical Addendum to Winningsplan 2013, a Ground Motion Prediction methodology based on a catalogue of tectonic earthquakes in southern Europe, was presented (Ref. 1). This methodology was inherently conservative, in the sense that it predicted ground motions which in future would more likely to be adjusted downwards than upwards.

In the report “Development of GMPEs for Response Spectral Accelerations and for Strong-Motion Durations (Version 1)” the status in May 2015 was documented (Ref. 2). An update of this document was issued in November 2015 which presented version 2 of the of the GMPE methodology (Ref. 3). This version of the Ground Motion Prediction Model was tailored to the Groningen situation (Ref. 4 to 7). In general, this update led to downward adjustment of assessed ground motions for larger earthquakes, resulting in a reduction of the assessed hazard. After incorporating some adjustments, this version of the GMM was used for the hazard and risk assessment supporting Winningsplan 2016, issued in April 2016.

Originally, an update of the GMM (version 3) was planned for July 2016, in support of the hazard and risk assessment for Winningsplan 2016. However, when early 2016 the deadline of submission for the Winningsplan was brought forward from July 2016 to April 2016, version 3 of the GMM could not be ready in time to be implemented in the hazard and risk assessment for this winningsplan.

Version 4 of the Ground Motion Model (GMM) was completed mid-2017 and shared with experts for an assurance review (Ref. 8). The current version of the GMM, version 5, has been updated based on the comments from the assurance review and was used in the Hazard, Building Damage and Risk Assessment of November 2017. The report describing GMM version 5 was issued in November 2017 (Ref. 9) together with this Hazard, Building Damage and Risk Assessment (Ref. 10). However, at that time the assurance process for the GMM version 5 was still in progress.

The current report is an update and re-issue of the GMM V5 report and additionally contains the Assurance Letter and short resumes of the Assurance Panel (Appendix I), and the full set of written comments on the first versions of the V4 and V5 GMM reports (Ref. 8 and 9), together with the detailed responses from the GMM development team (Appendices IX and X).

References:

- 1 Technical Addendum to the Winningsplan Groningen 2013; Subsidence, Induced Earthquakes and Seismic Hazard Analysis in the Groningen Field, Nederlandse Aardolie Maatschappij BV (Jan van Elk and Dirk Doornhof, eds), November 2013.
- 2 Development of Version 1 GMPEs for Response Spectral Accelerations and for Strong-Motion Durations, Julian J Bommer, Peter J Stafford, Benjamin Edwards, Michail Ntinalexis, Bernard Dost and Dirk Kraaijpoel, March 2015.
- 3 Development of Version 2 GMPEs for Response Spectral Accelerations and Significant Durations for Induced Earthquakes in the Groningen field, Julian J Bommer, Bernard Dost, Benjamin Edwards, Adrian Rodriguez-Marek, Pauline P Kruiver, Piet Meijers, Michail Ntinalexis & Peter J Stafford, October 2015
- 4 Geological schematisation of the shallow subsurface of Groningen (For site response to earthquakes for the Groningen gas field) – Part I, Deltares, Pauline Kruiver and Ger de Lange.
- 5 Geological schematisation of the shallow subsurface of Groningen (For site response to earthquakes for the Groningen gas field) – Part II, Deltares, Pauline Kruiver and Ger de Lange.
- 6 Geological schematisation of the shallow subsurface of Groningen (For site response to earthquakes for the Groningen gas field) – Part III, Deltares, Pauline Kruiver and Ger de Lange.
- 7 Modifications of the Geological model for Site response at the Groningen field, Deltares, Pauline Kruiver, Ger de Lange, Ane Wiersma, Piet Meijers, Mandy Korff, Jan Peeters, Jan Stafleu, Ronald Harting, Roula Dambrink, Freek Busschers, Jan Gunnink
- 8 V4 Ground-motion Model (GMM) for Response Spectral Accelerations, Peak Ground Velocity and Significant Duration in the Groningen field, Julian Bommer, Bernard Dost, Benjamin Edwards, Pauline Kruiver, Pier Meijers, Michail Ntinalexis, Adrian Rodriguez-Marek, Elmer Ruigrok, Jesper Spetzler and Peter Stafford, Independent Consultants, Deltares and KNMI, June 2017 with Parameter files - V4 Ground-Motion Model (GMM) for Response Spectral Accelerations, Peak Ground Velocity, and Significant Durations in the Groningen Field, Supplement to V4 GMM, Julian Bommer and Peter Stafford, Independent Consultants, June 2017
- 9 V5 Ground-Motion Model (GMM) for the Groningen Field, Julian J Bommer, Benjamin Edwards, Pauline P Kruiver, Adrian Rodriguez-Marek, Peter J Stafford, Bernard Dost, Michail Ntinalexis, Elmer Ruigrok and Jesper Spetzler, October 2017
- 10 Hazard, Building Damage and Risk Assessment, NAM (Jan van Elk and Dirk Doornhof), November 2017.

These reports are also available at the study reports page of the website www.namplatform.nl.



NAM

Title	V5 Ground-Motion Model (GMM) for the Groningen Field		Date	March 2018
			Initiator	NAM
Autor(s)	Julian J Bommer ¹ , Benjamin Edwards ¹ , Pauline P Kruiver ² , Adrian Rodriguez-Marek ¹ , Peter J Stafford ¹ , Bernard Dost ³ , Michail Ntinalexis ¹ , Elmer Ruigrok ³ and Jesper Spetzler ³	Editors	Jan van Elk & Dirk Doornhof	
Organisation	1. Independent consultant, 2. Deltares, 3. Royal Netherlands Meteorological Institute (KNMI)	Organisation	NAM	
Place in the Study and Data Acquisition Plan	<p><u>Study Theme:</u> Ground Motion Prediction</p> <p><u>Comment:</u> The prediction of Ground Motion is central to the hazard assessment. This report describes an update of the Ground Motion Prediction methodology (version 5) for the Groningen situation. It includes the Assurance Letter and comments from the Assurance Panel on the initial reports of GMM versions 4 and 5.</p>			
Directly linked research	(1) Hazard Assessment. (2) Fragility assessment of buildings in the Groningen region.			
Used data	Accelerograms from the accelerometers placed in the Groningen field. P- and S-wave velocity model sub-surface Groningen. Description of the shallow geology of Groningen.			
Associated organisation	KNMI			
Assurance	External assurance team has reviewed the report for GMM version 4 and 5. Comments from the assurance team on GMM version 4 and 5 are included in this report as appendices.			

V5 Ground-Motion Model for the Groningen Field

A report prepared for NAM

**Julian J Bommer¹, Benjamin Edwards¹, Pauline P Kruiver², Adrian Rodriguez-Marek¹,
Peter J Stafford¹, Bernard Dost³, Michail Ntinalexis¹, Elmer Ruigrok³, Jesper Spetzler³,**

1. Independent consultant, 2. Deltares, 3. Royal Netherlands Meteorological Institute (KNMI)

Revision 1

14 March 2018

TABLE of CONTENTS

Acknowledgements	ii
1. INTRODUCTION	1
2. EVOLUTION of GMM FRAMEWORK	3
2.1. Timeline of GMM development	3
2.2. Evolution of the ground-motion model	7
3. V5 GMM for AMPLITUDES at NS_B	16
3.1. Inversion of NS_B motions	16
3.2. Selection of forward simulation parameters	20
3.3. Parametric GMPEs for NS_B	27
3.4. Variability components	29
3.5. Comparison with V4 NS_B GMM	32
4. SITE AMPLIFICATION MODEL	39
4.1. Site response analyses	39
4.2. Zonation and amplification factors	45
4.3. Variability associated with AFs	50
4.4. Surface residuals of Groningen recordings	51
4.5. Comparison with V4 AFs and GMM	54
5. DURATION MODEL	56
5.1. Derivation of updated model	56
5.2. Comparison with V4 model	61
6. MODEL SUMMARY and IMPLEMENTATION	63
6.1. Complete GMM logic-tree	63
6.2. Sampling of variance components	74
7. CONCLUSIONS and FUTURE DEVELOPMENTS	80
8. REFERENCES	88
APPENDIX I Endorsement letter of review panel	93
APPENDIX II Slochteren earthquake recordings	99
APPENDIX III Component-to-component variability model	106
APPENDIX IV Median predictions of motion at NS_B	113
APPENDIX V Station vs zone linear AFs	126
APPENDIX VI Residuals of surface recordings	132
APPENDIX VII Median predictions of motion at surface	142
APPENDIX VIII Zeerijp earthquake recordings	165
APPENDIX IX V4 GMM review comments and responses	180
APPENDIX X V5 GMM review comments and responses	271

Acknowledgements

The report on the V4 ground-motion model includes almost three full pages of acknowledgements to the numerous individuals who have contributed in many important ways to the development of this work. Those expressions of gratitude and appreciation remain equally valid with regards to the V5 model.

In view of their critical role in providing detailed feedback on the draft V4 report and offering constructive suggestions that contributed to important refinements in this latest stage of model development, as well as the subsequent detailed review of the first issue of this report, we reiterate our debt of gratitude to the international GMM review panel, chaired by Jonathan Stewart and comprising Norm Abrahamson, Gail Atkinson, Hilmar Bungum, Fabrice Cotton, John Douglas, Ivan Wong and Bob Youngs. We cannot overstate the enormous value that has been added to the model development through the technical challenges and insightful observations that have been put forward by this illustrious panel of experts in the fields of ground-motion prediction and site response modelling.

We also add a note of thanks to the reviewers of the various journal papers that have been published from the work on the Groningen ground-motion model. Their comments and challenges have also been very valuable in assisting with the continued improvement of the GMM.

Renewed thanks are also due to Stephen Bourne, Steve Oates, Pourya Omidi and Tomas Storck for the invaluable feedback and testing of the model through implementation in the Groningen hazard and risk engine, and to Assaf Mar-Or for generating hazard and risk results that have provide very helpful insights into the performance of the model and changes from previous versions. We also thank Helen Crowley and Rui Pinho for keeping us informed of the ground-motion input needs for the derivation of building fragility functions for Groningen.

Finally, we must express our debt to Jan van Elk for continuing to provide the space and conditions to undertake this work and supporting for us in so many ways. The assistance of Dirk Doornhof and Jeroen Uilenreef in supporting Jan is also gratefully acknowledged.

1. Introduction

Following the magnitude M_L 3.6 Huizinge earthquake in August 2012, NAM has engaged in a major endeavour of data acquisition and model development to quantify the risk due to induced earthquakes in the Groningen field. A core component of the model for risk estimation is a ground-motion model (GMM) for the prediction of parameters characterising the shaking at the surface due to each earthquake scenario considered.

The Groningen GMM has been developed in successive stages, with the work beginning in the first half of 2013 when a very preliminary model was produced for the 2013 Winningsplan. Subsequently, over a period of four years, a much more sophisticated model has been developed in five successive and iterative stages, culminating in the V5 model presented in this report. The derivation of the previous four versions of the model were all documented in great detail in reports that collectively have a total length of 1,845 pages, supported by numerous other documents of even greater length presenting the underlying data collection activities to characterise the near-surface soil profiles across the Groningen field and the database of ground-motion recordings that have underpinned the model development. Additionally, several papers on different aspects of the model development process have been published in peer-reviewed journals. In view of the extensive documentation already available, this report presents a more succinct overview of the V5 model, presenting a summary of the model and brief narration of the modifications with respect to the V4 model, referencing earlier reports and published papers to guide the reader who seeks more detailed information.

Chapter 2 presents an overview of the evolution of the GMM for Groningen, including the incremental differences at each stage of development and most specifically the modifications of the V4 model included in the V5 model. The key features of the model are then explained in three sequential chapters: Chapter 3 presents the model for spectral accelerations and peak ground velocity (PGV) at the NS_B reference rock horizon; Chapter 4 presents the site amplification factors that transfer the rock motions to the ground surface; and Chapter 5 presents the model for durations. Chapter 6 summarises the complete guidance for implementing the GMM in terms of the logic-tree structure and the sampling of the variance components; for the user looking for a concise summary of the model without explanation of its derivation, this is fully self-contained in the sixth chapter. The report concludes with a brief discussion of the applicability of the current model and potential future developments.

In order to keep the main body of the report to an accessible length, additional information and plots are presented in 10 appendices. The first of these presents the credentials of the members of the international review panel and also includes the closing letter issued by this panel at the conclusion of their review of the V5 model as

presented in the first version of this report. Appendix II presents the recordings obtained during the Slochteren earthquake of May 2017, which were added to the database for the V5 model development.

Appendix III provides more detail of the final model for component-to-component variability. This is presented as an Appendix because while it represents a substantial advance with respect to how this component of variability was represented in earlier versions of the model, it is a fairly minor component of the model. Moreover, this appendix includes analyses conducted in response to the review panel comments on the V4 model regarding the potential influence of the instrument orientation on the component-to-component variability. In order to keep the main body of the V5 report as succinct as possible, this material is included in an appendix.

The following three appendices contain diagnostic plots to illustrate the performance of the V5 model: Appendix IV presents plots of median predictions in terms of response spectral accelerations at the NS_B horizon; Appendix V compares the NS_B to surface amplification factors calculated for the recording stations with the linear factors assigned to the zones in which they are located; and Appendix VI presents the residuals of the surface recordings with respect to the model predictions.

Appendix VIII presents the recordings from a significant earthquake—the third largest in the history of the Groningen field and the largest since the Huizinge earthquake of 2012—that occurred after the V5 model was completed and implemented. Simple comparisons are made between the V5 model predictions and the motions recorded during this earthquake.

Finally, Appendices IX and X present the full suite of review comments from the international expert panel on the V4 and V5 models, respectively, together with the complete set of responses from the GMM development team. In this way, there is full disclosure of the detailed review process that the model has undergone.

2. Evolution of GMM Framework

As noted in the Introduction, work on developing a ground-motion model for induced and triggered earthquakes in the Groningen field began more than four years ago and the model has evolved through various stages to reach the current formulation. The purpose of this chapter is to summarise the process both in terms of timelines and reviews of the various versions of the model, and also in terms of the evolution of the framework for the model.

2.1. Timeline of GMM development

In order to develop a probabilistic seismic hazard analysis for the 2013 Winningsplan, a seismological source model was developed that related the induced seismicity to reservoir compaction (Bourne *et al.*, 2014) and the hazard calculations realised through Monte Carlo simulations (Bourne *et al.*, 2015). A preliminary ground-motion model was developed within a short timeframe using the database available at that time, which included just 40 recordings from eight earthquakes with magnitudes in the range from M_L 2.7 to 3.6. The model was derived only for peak ground acceleration (PGA) and PGV, and was based on the European ground-motion prediction equation (GMPE) of Akkar *et al.* (2014) using hypocentral distance, R_{hyp} . The GMPE was deployed with an assumed V_{S30} of 200 m/s—which has since been found to be a very good estimate of the field average (Kruiver *et al.*, 2017)—with various coefficients adjusted with magnitude-dependent alternatives so that below about magnitude 4 the predictions would match the Groningen data. The model consisted of a single equation for each ground-motion parameter and was a deliberately conservative choice in terms of the expected motions from larger earthquakes. The model, described in Bourne *et al.* (2015), was also limited by not being specific to Groningen conditions for larger earthquakes that will generally drive hazard and risk estimates.

In order to develop a model that more closely reflects the specific source, path and site characteristics of Groningen earthquakes and also captures the range of epistemic uncertainty in extrapolations from the existing data to larger magnitudes, a process was initiated in late 2013 that has led to five successive versions of the GMM (Figure 2.1). The short timescales for each stage of model development are immediately apparent. The number of development and reporting stages was dictated by regulatory requirements to provide periodic updates and also the requirement to develop a model to underpin the hazard and risk calculations developed for the 2016 Winningsplan. The process has also included additional reviews by an international panel of ground-motion experts, which has been supplemented by the peer review of the various papers submitted for publication in seismological and earthquake engineering journals.

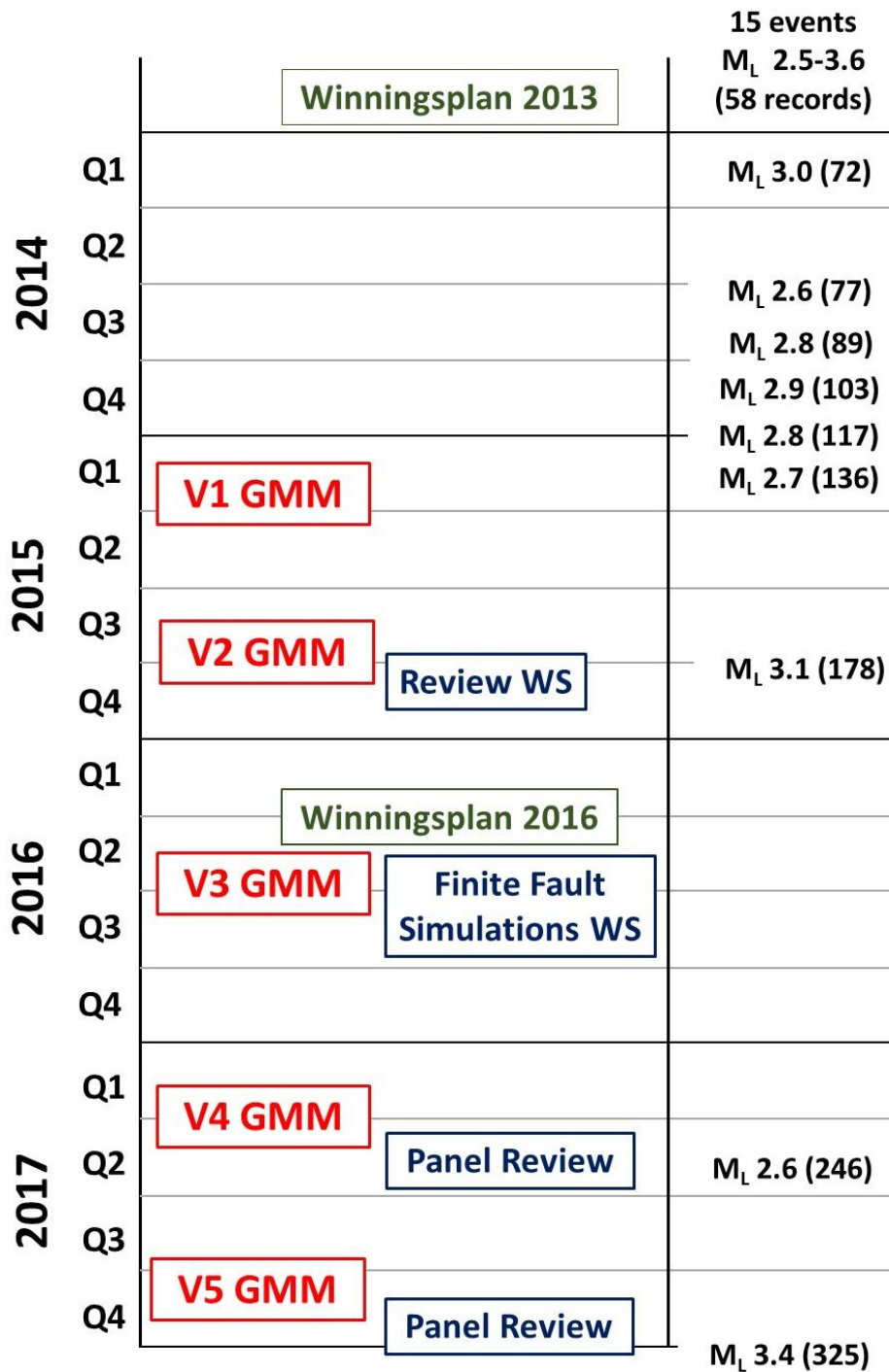


Figure 2.1. Timeline of GMM development for Groningen, with models indicated by date of issue of first report. The right-hand side indicates the growth of the ground-motion database in terms of recordings from events of M_L 2.5 and greater.

The technical advances in each stage of the model development, intended primarily to improve the representation of Groningen-specific conditions, are outlined below in Section 2.2. External factors that have influenced the process include the growth of the ground-motion database, aided by the expansion of seismic recording networks in the field (Dost *et al.*, 2017). At the end of 2013, the database contained just 58

records from 15 earthquakes; by the time of the V3 model development, the database had grown to 178 recordings from 22 earthquakes, thus more than doubling the average number of recordings per event. The database remained unchanged for the V4 model development, but for the V5 database 68 new recordings from the Slochteren earthquake of May 2017 were added; an overview of the recordings from this earthquake is given in Appendix II. Figure 2.2 shows the magnitude-distance distribution of the final V5 database.

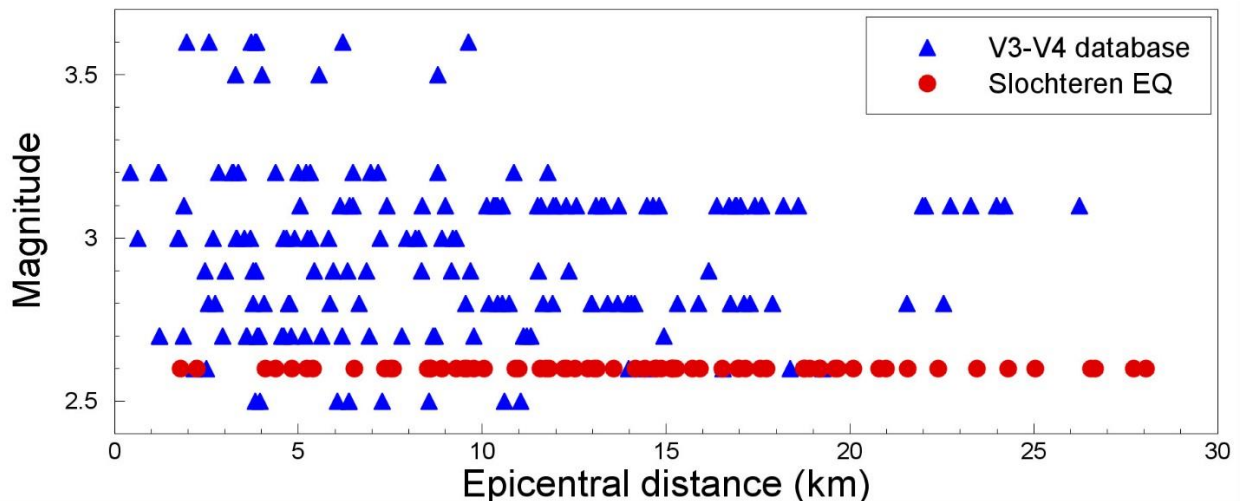


Figure 2.2. Distribution of the V5 Groningen ground-motion database in terms of local magnitude, M_L , and epicentral distance, R_{epi} .

Another important factor in the GMM development has been external review of the model, which has come from various sources including the Dutch State Supervision of Mines (SodM) and their expert advisors Dr William Ellsworth, Dr Art McGarr, and Professor Stefan Wiemer. Additionally, there were numerous review meetings with the Scientific Advisory Committee (SAC) chaired by Lucia van Geuns and some written comments from the SAC were also issued. Several questions and challenges on the GMM were posed to the development team, primarily by SAC members Dr Stefan Baisch and Professor Iunio Iervolino.

The GMM development also sought feedback and critical review from experts whose primary area of expertise is ground-motion modelling and site response analysis. An international panel was assembled consisting of Professor Gail Atkinson, Dr Hilmar Bungum, Professor Fabrice Cotton, Dr John Douglas, Professor Jonathan Stewart, Mr Ivan Wong, and Dr Bob Youngs. A two-day review workshop was conducted with the panel members on 27-28 October 2015, during which the V2 model was presented to the panel. The feedback included written comments from panel members both before and after the workshop in addition to the verbal comments

made during the workshop; all of these were taken into account in the development of the V3 model.

Critical review and suggestions for improvement of the model have also been provided at numerous stages by colleagues from URC (Upstream Research Company) at ExxonMobil, particularly with regard to the use of ground-motion simulations using finite rupture models. To discuss these approaches, a second workshop was held in London from 18-20 July 2016. The workshop was attended by several colleagues from URC and some invited external experts: Dr Luis Angel Dalguer, who has worked for many years on finite rupture simulations, and Drs Norm Abrahamson, Christine Goulet and Bob Youngs, who all have experience in the use of ground-motion simulations in GMPE development. The workshop began with a presentation of the V3 model, with comments and feedback from the participants, and then focused primarily on the best options for incorporating finite rupture simulations into the V4 model.

After the V4 model was developed and documented, the report was circulated to the members of the original review panel, plus Dr Abrahamson, and written review comments from all eight panel members were compiled by Professor Stewart who coordinated the review. These comments were taken into account in the issue of revised version of the V4 GMM report but most importantly were considered in the development of the V5 model. The comments on the V4 GMM and the GMM development team's responses are included in Appendix IX. The first issue of the V5 report was then submitted to the review panel, together with the responses to the V4 comments, in response to which the panel submitted new comments, together with editorial corrections. The full set of technical comments and the responses from the model development team are included in Appendix X. The closing letter from the review panel is in Appendix I, together with short biographies of each of the panel members.

The intervals of time allocated to each stage of model development have been very short, which has meant that the time available for exploratory analyses and iterations within each development stage has been extremely limited. While this schedule has created challenging conditions for the development of a stable and robust model, it has also brought some advantages in terms of the model being fully documented at each staging point and also implemented into the NAM seismic hazard engine, both of which have facilitated review and feedback. From this perspective, the V1, V3 and V4 models can all be viewed as internal checking points along the path of the model development toward each Winningsplan submission (Figure 2.1). The primary targets have been the risk calculations rather than simply generating hazard maps since only the former provide a rational basis for decision making (Bommer *et al.*, 2015a). The one exception to this, however, is the NEN-NPR seismic design code that the Dutch authorities have developed for the Groningen region, which adopted

hazard estimates based on the V4 GMM for the specification of seismic loading in its current revised issue.

2.2. Evolution of the ground-motion model

Before the Akkar *et al.* (2014) GMPE derived from recordings of tectonic earthquakes in Europe and the Middle East was adjusted to Groningen data in the small-magnitude range for the preliminary seismic hazard model, the original intention had been to adopt the GMPE of Dost *et al.* (2004), which had been derived from recordings of small-to-moderate magnitude induced earthquakes in gas fields in the northern Netherlands. The data were mainly from the Roswinkel gas field rather than Groningen but were also recorded on soft soil sites from shallow induced earthquakes and therefore seemed a logical choice for application to the Groningen field. However, the Dost *et al.* (2004) equations for PGA and PGV were found to grossly over-predict the recorded amplitudes of motion in the Groningen field. This was interpreted as being mainly due to the fact that in Groningen the high-velocity Zechstein salt layer lies above the gas reservoir—and is known to have a strong effect on the propagation of seismic waves ascending from ruptures initiating within the reservoir (Kraaijpoel & Dost, 2013)—whereas in the Roswinkel field the gas reservoir is above the Zechstein.

The observations prompted us to seek to develop a Groningen-specific model. The basic framework adopted for this was to invert the Fourier amplitude spectra (FAS) of surface motions in the field to estimate source, path and site parameters, and then to use simulations to estimate the motions from larger earthquakes. In order to capture the epistemic uncertainty associated with the extrapolations from small- to large-magnitude earthquakes, a logic-tree framework was adopted with the branches occupied by different versions of the simulation parameters, in effect following the ‘backbone’ GMPE approach (Atkinson *et al.*, 2014).

Figure 2.3 schematically illustrates the approach adopted for the V1 GMM (Bommer *et al.*, 2015b; Bommer *et al.*, 2016a).

The inversions identified optimal values of the parameters characterising the source, path and site, but in the forward simulations three different models for the stress parameter were adopted. While the V1 model was calibrated to Groningen conditions, it was considered deficient in terms of site response characteristics for two reasons. Firstly, the model included a field-wide site amplification function—inferred from the average amplification function for the recording network—without any lateral variation. Secondly, the amplification functions were linear and thus did not capture the potential effects of non-linear response of the soft soils under higher levels of acceleration.

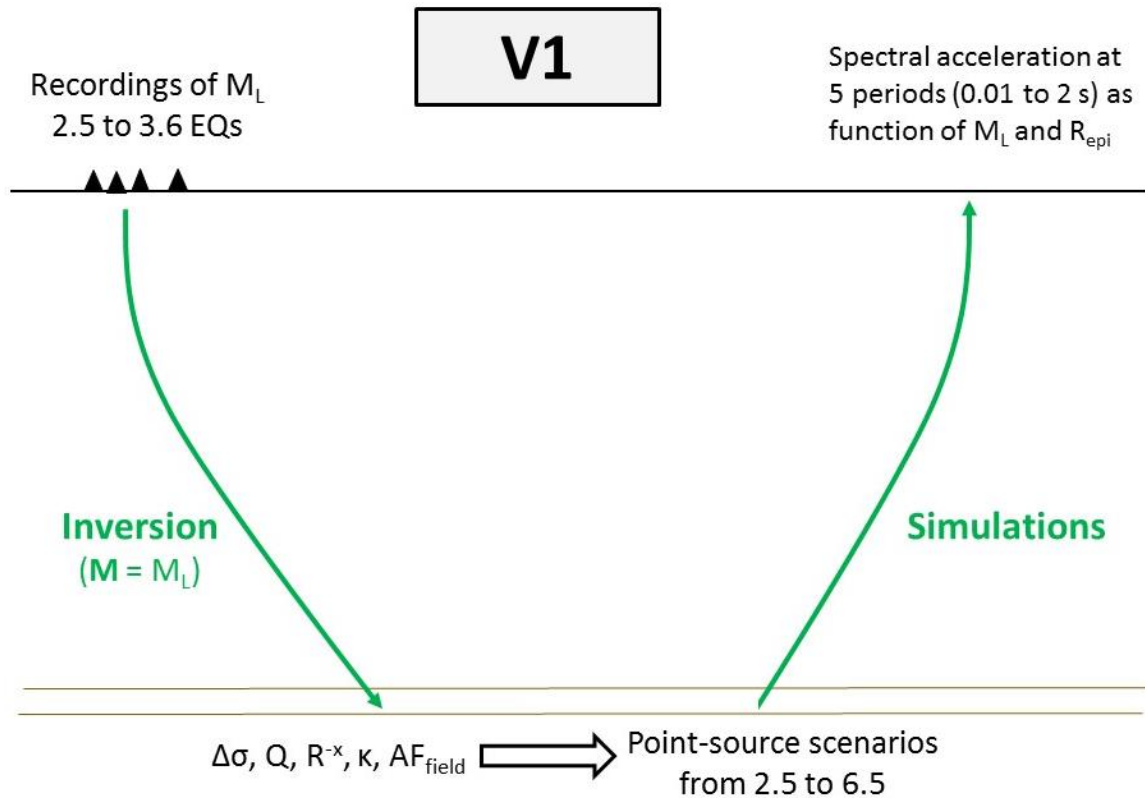


Figure 2.3. Schematic illustration of the development process adopted for the V1 GMM

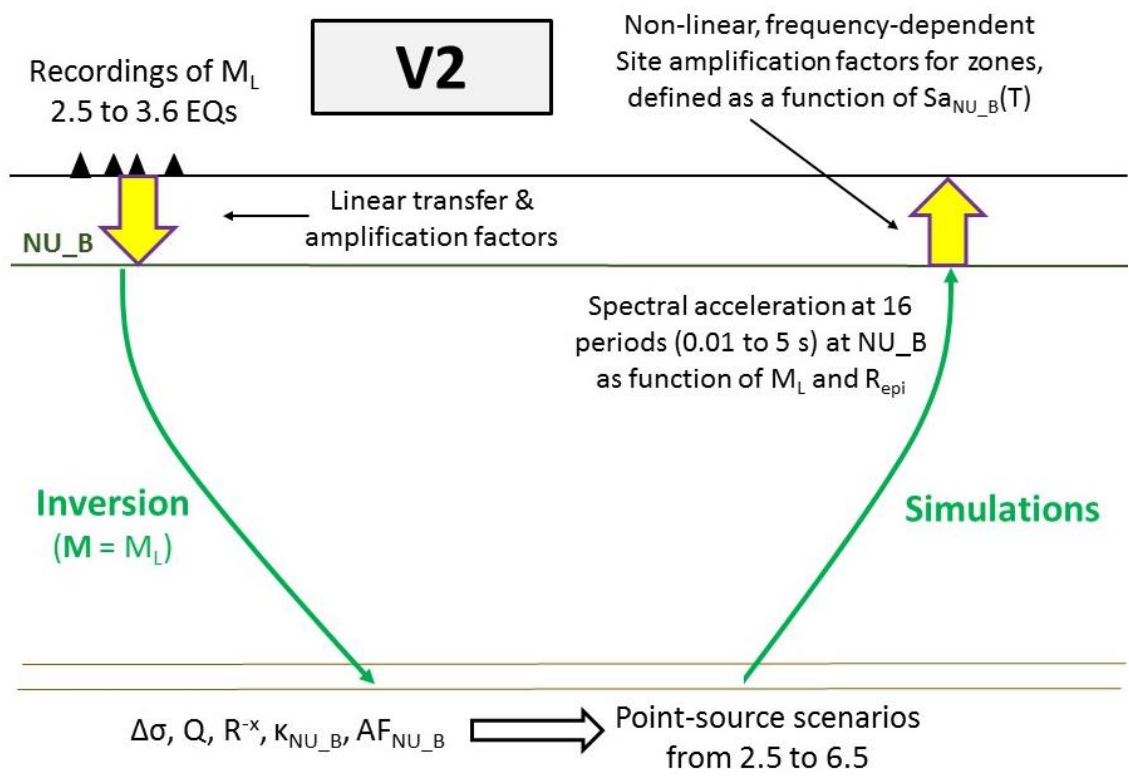


Figure 2.4. Schematic illustration of the development process adopted for the V2 GMM

The V2 model was the first model to capture local site effects (Bommer *et al.*, 2015c). This was done by developing predictive equations for a reference rock horizon and then combining these with non-linear site amplification functions for the overlying soil layers. The starting point was to deconvolve the FAS and the response spectra of the surface recordings using the shear-wave velocity (V_s) profiles developed for the field by Deltares (Kruiver *et al.*, 2017). A key assumption here was that since the recorded motions are weak, it could be assumed that the soil response was linear. For the V2 model, the reference rock horizon was the base of the Upper North Sea formation (NU_B) located at a depth of about 350 m (Figure 2.4). The forward simulations for the rock motions were performed for an increased range of response periods in order to match the definitions of the building fragility functions. The simulations were also used to generate FAS for a wide range of magnitude and distance combinations, and these were then used as input to RVT-based site response calculations to estimate amplification factors (AF) for the overlying soil layers. A zonation of the field, modified from a geological zonation, was defined such that within each zone an AF would apply at all locations for each response period.

The V3 model was a modification of the V2 GMM, with the most important change being to move the reference rock horizon to the more pronounced impedance contrast at the base of the North Sea supergroup (NS_B), located at a depth of 800 m (Figure 2.5).

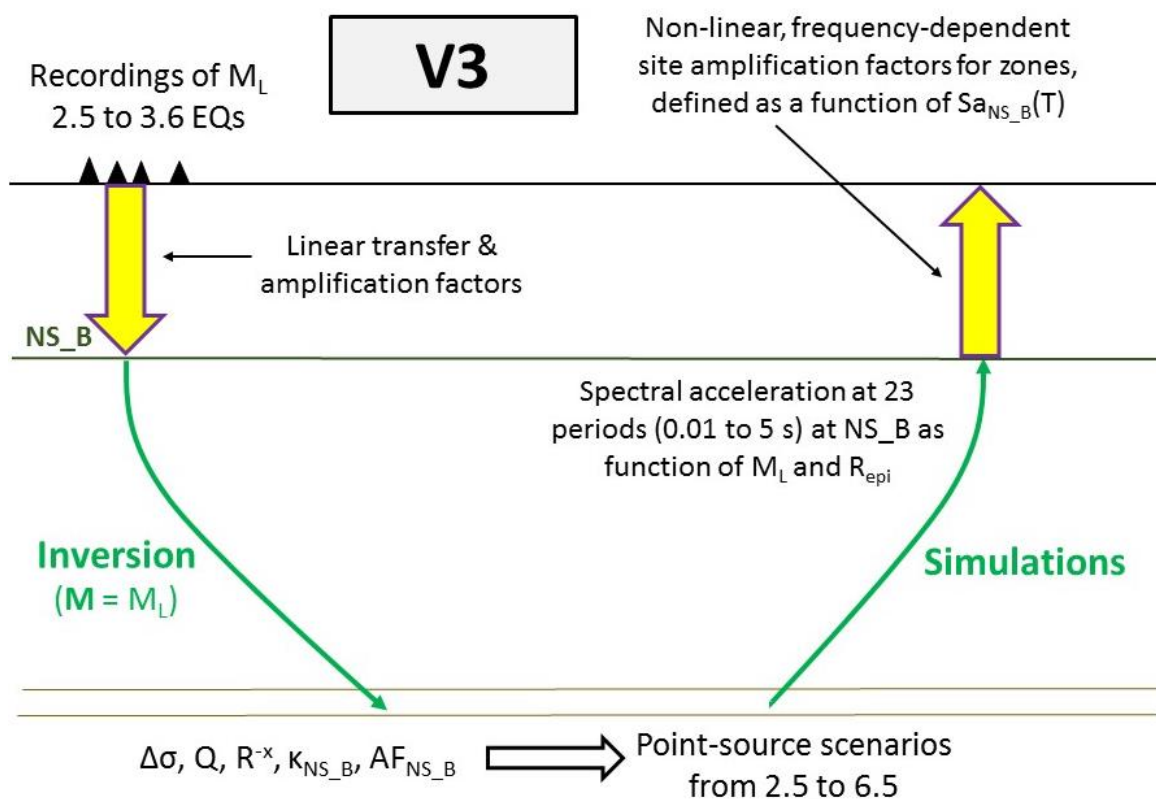


Figure 2.5. Schematic illustration of the development process adopted for the V3 GMM

In most other regards, the model derivation followed the same procedures, except that seven additional response periods were added in the short-period range to enable more realistic vertical spectra by application of V/H ratios. Both the NS_B reference horizon and the 23 target oscillator periods have remained fixed in subsequent versions of the model. The V3 GMM was documented in a report (Bommer *et al.*, 2016b) and also summarised in journal papers on the site response model (Rodriguez-Marek *et al.*, 2017) and the overall model (Bommer *et al.*, 2017a).

While the basic framework of the V3 GMM was largely retained for the V4 model, some important innovations were also made, as detailed in the report by Bommer *et al.* (2017b) and a paper by Bommer *et al.* (2017c). In Figure 2.6 the changes from the V3 to V4 model derivation are highlighted in red, and these include the following:

1. A move from point-source simulations using SMSIM (Boore, 2005a) to using simulations based on extended fault ruptures using EXSIM (Motezadian & Atkinson, 2005); this resulted in a change from epicentral distance (R_{epi}) to rupture distance (R_{rup}).
2. Scenario-dependence was introduced into the linear site amplification factors at short periods, an innovation not only for the Groningen project but in this field in general (Stafford *et al.*, 2017).
3. In the inversions, the previous assumption that moment and local magnitudes were equivalent was replaced by a relationship that indicated that for events of magnitude 2.5 and greater, moment magnitudes are on average 0.2 units smaller than M_L values.
4. The simulations included PGV in addition to spectral accelerations at 23 response periods since although not used in the risk model, this parameter is of interest because it is widely used to define tolerable levels of shaking.
5. Following an expert workshop on M_{max} for Groningen held in Amsterdam in March 2016, the largest magnitude for which the GMM needs to be applicable increased from **M** 6.5 to greater than **M** 7 (Bommer & van Elk, 2017).

The V5 GMM was intended to be a refinement of the V4 model, maintaining the same framework as illustrated in Figure 2.6, taking account of comments and suggestions from the review panel. Among the points raised by the reviewers was the calibration of the highest branch on the GMM logic-tree to match predictions from GMPEs derived from recordings of tectonic earthquakes. For the site response component of the model, particular focus was given to refining the magnitude- and distance-dependence of the linear AFs, and to accounting for uncertainty in the modulus reduction and damping (MRD) curves in the site-to-site variability. As has been noted in Section 2.1, an unforeseen modification was to add the recordings from the May 2017 Slochteren earthquake to the database.

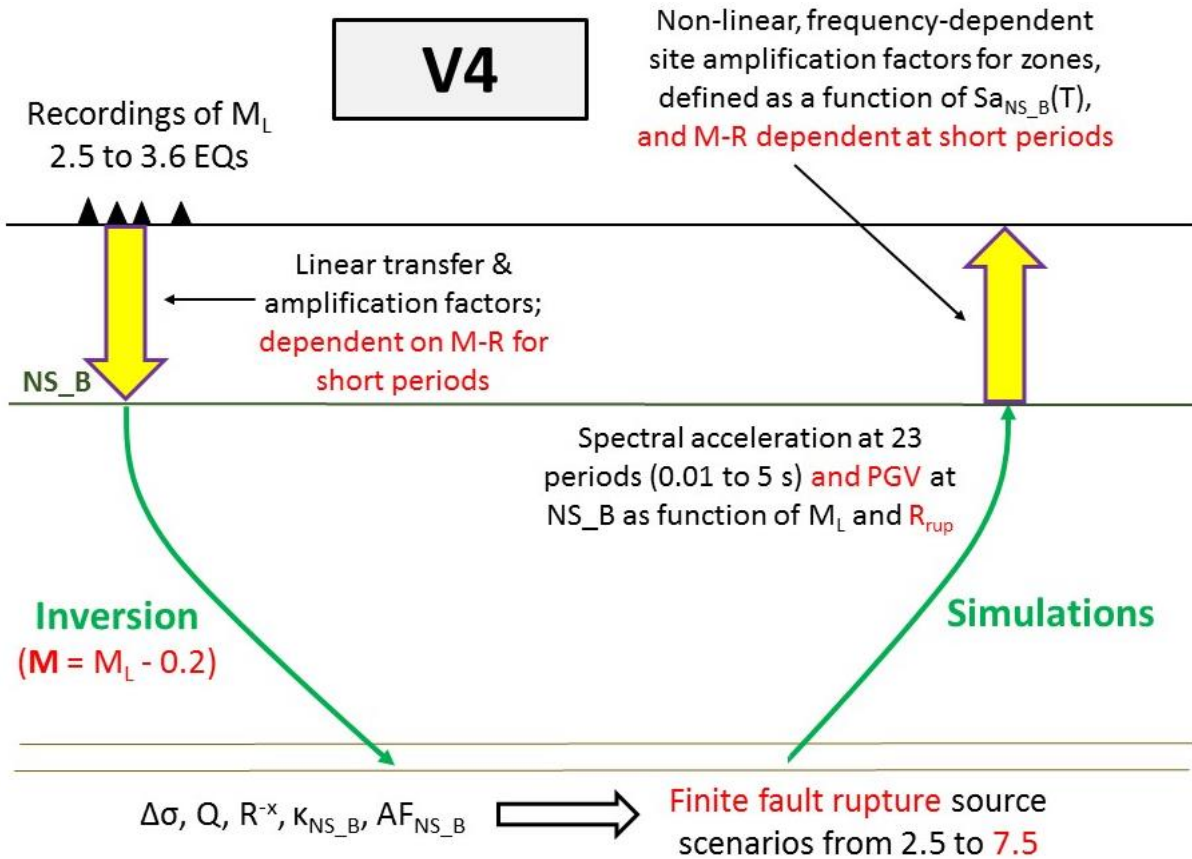


Figure 2.6. Schematic illustration of the development process adopted for the V4 GMM

However, there was another very important change from V4 to V5, which is the relationship between local and moment magnitudes in Groningen. Extension and refinement of the analyses that had previously suggested a systematic difference of 0.2 magnitude units between the two scales now concluded that for $M_L \geq 2.5$, the scales were in fact equivalent, on average (Dost *et al.*, 2018). Therefore, the V5 inversions were performed assuming $M = M_L$, as indicated in Figure 2.7. Although this is the only major change in the model derivation from V4 to V5, the M - M_L relationship exerts a major influence on inversions and consequently on the GMM; this is discussed in more detail in Section 3.5.

The M - M_L relationship used in the development of the V4 model is now considered to be inappropriate, and its correction now makes the V5 model a stable framework. As is discussed later in the report, the single application of an incorrect relationship between the magnitude scales for one of the five model development stages creates an exaggerated impression of the instability in the process.

The schematic illustrations in Figures 2.3 to 2.7 provide only very high-level illustrations of the processes involved. A more detailed overview is given in Figure 2.8, which highlights several of the additional inputs to the process, including the following:

- FAS and response spectra of recordings from the B-station accelerographs were transformed to the NS_B horizon using the V_S profiles from the field-wide model of Kruiver *et al.* (2017) modified over the uppermost ~30 m using *in situ* measurements (Noorlandt *et al.*, 2018). For the G-stations, where such *in situ* V_S measurements have not yet been made, rather than using surface accelerograms, recordings from geophones at 200 m depth were used to avoid the uncertainty in the highly influential uppermost part of the V_S profiles.
- In order to reduce the numbers of degrees of freedom in the inversion of the FAS at the NS_B horizon, some of the parameters were constrained independently. The kappa values were estimated directly using the method of Anderson & Hough (1984) and the geometrical spreading patterns were constrained with finite difference waveform simulations using a detailed 3D velocity model of the field.

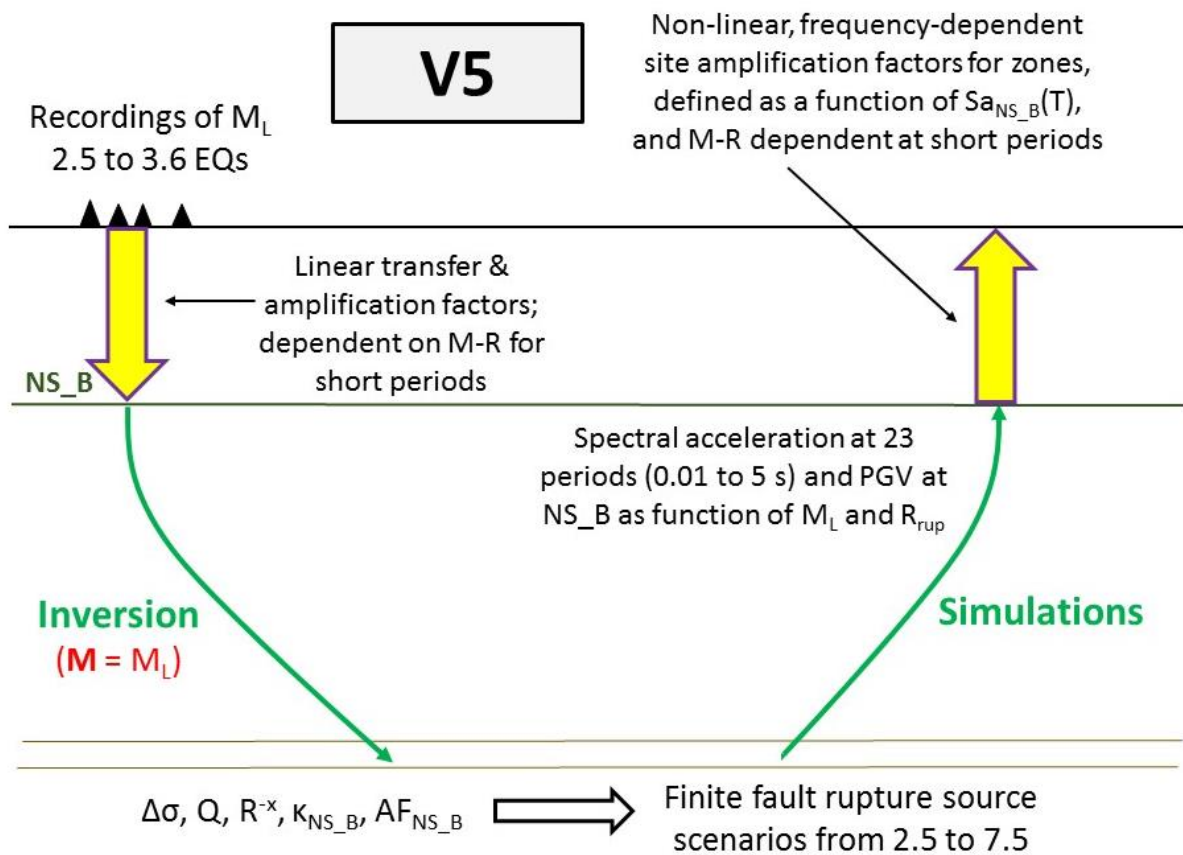


Figure 2.7. Schematic illustration of the development process adopted for the V5 GMM

Since the fragility functions for some building types in Groningen are defined in terms of both spectral accelerations and duration, a model has also been required for the prediction of the latter. In the V1 model, the duration was estimated simply using the Kempton & Stewart (2006) equation for durations with an assumed field-wide V_{S30} value of 200 m/s. In the V2 model, the duration GMPE of Afshari & Stewart (2016)

was modified to provide a better fit to the Groningen data, and a similar procedure was followed for the V3 GMM. For the V4 model, a new equation was derived from regression on the durations of simulated motions from EXSIM at the NS_B horizon, and the site amplification factors of Afshari & Stewart (2016) adapted to transfer the rock durations to the ground surface.

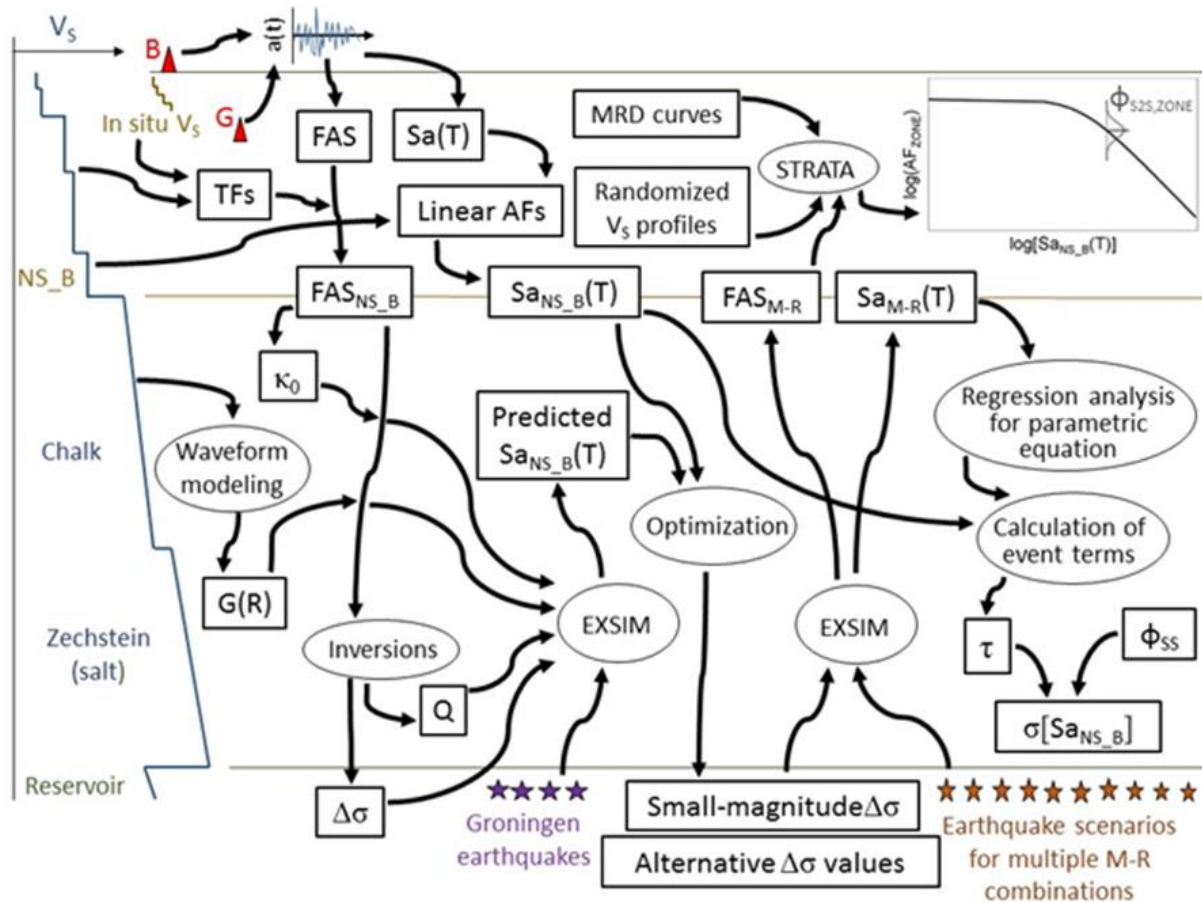


Figure 2.8. Illustration of the process for the derivation of the V4 and V5 GMM, adapted from Bommer *et al.* (2017a)

In closing this chapter, a brief comment is in order regarding the oscillator periods for which the model provides predictions of spectral accelerations. There are 23 target periods between 0.01 s and 5 s, the spectral acceleration at the former period being equivalent to PGA. This wide range of periods is covered so that the model may address all current and future requirements, but in assessing the model and its performance it is worth considering the response periods that are actually relevant to the risk calculations. Figure 2.9 displays information regarding the periods used to characterise the fragility functions for the 54 building types classified in the Groningen exposure database. For some building types, the spectral acceleration at the fundamental period, T1, is found to be sufficient to define the fragility function; for others, a second period, T2, and/or the duration is also required.

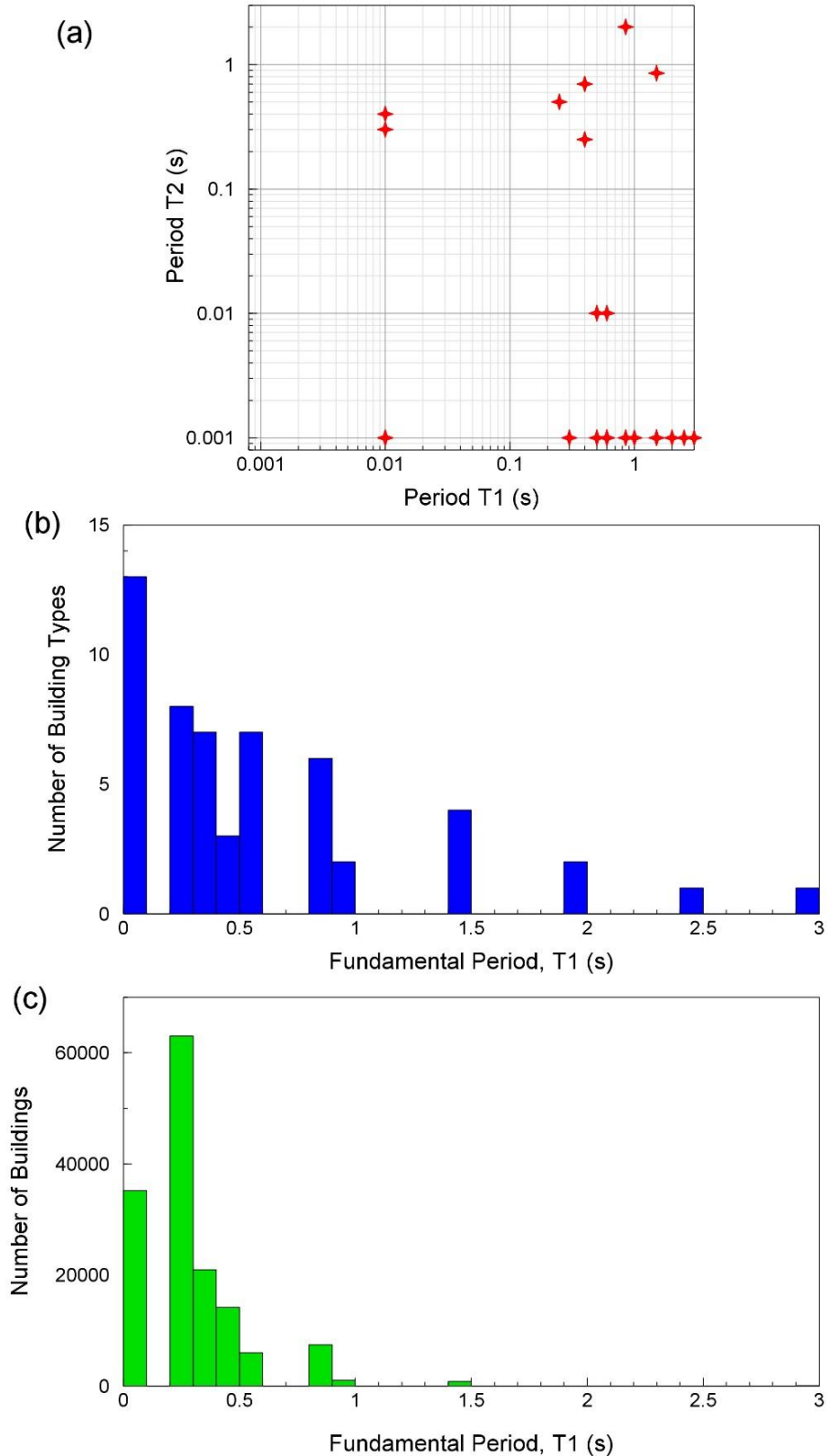


Figure 2.9. Characteristics of the V5 exposure database in terms of periods at which spectral accelerations define the fragility functions: (a) primary and secondary periods, in which a value of 0.001 s implies no secondary period; (b) numbers of building types in each period range; (c) numbers of buildings in each period range. Data provided by Helen Crowley.

The top plot shows the T1-T2 pairs, in which 0.001 s implies that the second period is not needed. There are fewer than 54 points on this plot because several building types have the same two controlling periods. The middle plot shows the distribution of building types with regards to the period T1; note that the first bar represents characterisation by $S_a(0.01s)$, or PGA. The lower plot shows the same information but in terms of the number of buildings in each period range, from which it is clear that apart from a large number of buildings characterised by PGA, the majority of the building stock has dominant periods in the range from 0.25 to 0.6 seconds. If one takes into account that these intermediate periods will often correspond to larger or taller structures, the distribution of exposed population would be even more concentrated in this period range. Periods beyond 1 second are of limited importance currently. The dense sampling of periods from 0.025 to 0.20 seconds has been primarily to allow the application of V/H ratios to lead to appropriate shapes for vertical response spectra; however, there has, to date, been little need for such spectra.

3. V5 GMM for Amplitudes at NS_B

The first part of the model for the prediction of $S_a(T)$ and PGV is a suite of ground-motion prediction equations (GMPEs) for the estimation of these parameters at the reference rock horizon (NS_B). The derivation of the V5 model for the motions at the rock horizon followed the same procedures as used in the V4 GMM development. However, three changes influenced the outcomes of this process. The first of these is minor updating of the soil properties tables (see Section 4.1) that led to minor modifications in the transfer functions used to translate the FAS of recordings at or near the surface to the NS_B horizon. The more significant changes were addition of a large number of recordings from the May 2017 Slochteren earthquake (Appendix II) and the update of the relationship between moment and local magnitudes in the Groningen region (Dost *et al.*, 2018). This chapter briefly summarises the modifications from the V4 rock model as a result of these changes to the input data and concludes with a comparison of the two models.

3.1. Inversion of NS_B motions

In view of the limited magnitude range of the earthquakes represented in the Groningen ground-motion database—with an upper limit of M_L 3.6—one of the key challenges in developing the GMM for the hazard and risk models has been the extrapolation to the largest magnitude currently considered, M 7.25. In order to accomplish this for the V5 Groningen GMM, motions are calculated using finite-fault, stochastic simulations. The method used is based on a discretised rupture model with dynamic corner-frequency (EXSIM: Motazedian & Atkinson, 2005; EXSIM_dmb: Boore, 2009). Each of the distributed sub-faults in this technique is assumed to be a point source (effectively a small magnitude earthquake), and can be characterised using the seismological parameters observed in events recorded in the Groningen gas field. More specifically, the seismological characteristics required for modelling ground motion using EXSIM are estimates of the source, path and site parameters that define the Fourier amplitude spectra (FAS) and duration of the motion. This section presents how the V5 GMM has been updated with respect to the V4 model. In all other aspects the inversion methodology and results remain as per the V4 GMM.

The ground-motion database, comprising recorded surface motions (B-stations) or 200 m borehole motions (G-stations), has been expanded by one event to 23 in the V5 model, and now includes 248 records, each of which has been deconvolved to the base of the North Sea supergroup (NS_B) horizon using the linear anelastic amplification functions corresponding to the velocity profile beneath each site (Figure 3.1). When deconvolving the borehole data within-column motions are used, such that the down-going waves are accounted for.

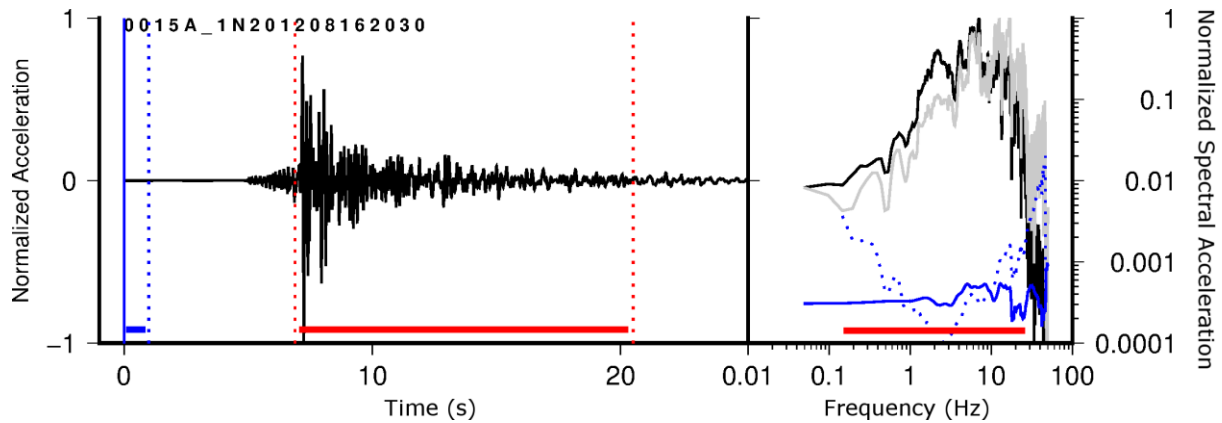


Figure 3.1. *Left:* example acceleration time series of the 2012 $M_L3.6$ Huizinge earthquake recorded at station 15 (GARST), 14 km from the epicentre. The period highlighted in red indicates the signal and in blue the noise. *Right:* Fourier amplitude spectrum of the acceleration time series. Black: as recorded at the surface; grey: deconvolved to the NS_B; solid blue: recorded noise; dotted blue: noise after deconvolution to the NS_B and low frequency adjustment; the frequency range highlighted in red shows the FAS used in inversions (SNR > 3)

The FAS of recordings, deconvolved to the NS_B horizon, were then used to determine the source, path and NS_B rock parameters for use in subsequent forward simulations. In a refinement to the inversion methodology used in the V4 GMM, a Bayesian-approach was implemented to reduce the strong trade-off between the event stress-parameter (and equivalently, f_{0i}) and κ . A prior distribution for the stress-parameter was produced using a median and log-normal standard-deviation. Standard deviations of 1.0, 1.25 and 1.5 (\log_{10} units) were tested (note that they do not directly relate to the posterior distribution of $\Delta\sigma$). 1.25 was selected as a compromise between the prior having limited influence (1.5, $\Delta\sigma$ outliers still present), and too-much (1.0, standard deviation of $\Delta\sigma < 0.2$): the aim being to reduce strong trade-offs, rather than controlling the median. Medians of the prior were 30, 50 and 70 bars (based on results using an initial uniform prior).

In the analyses (using three priors with median $\Delta\sigma = 30, 50, 70$ bar and 1.25 \log_{10} -unit standard deviation) Q values of 220-250 were obtained for an average shear-wave velocity of 2.6 km/s. In addition we determine site specific NS_B κ_0 of 0.01 to 0.045 s (5th, 95th percentiles). Figure 3.2 shows typical surface FAS fits using the resulting source (\mathbf{M} , $\Delta\sigma$) and path (Q) model along with site-specific amplification (including κ_0) computed using the NS_B corrected FAS, and applying the NS_B to surface transfer function. Using the 70, 50 and 30 bar priors resulted in median stress parameters of 40, 35 and 35 bars respectively (using a common Q, with site specific κ_0), indicating that the results are robust regardless of the choice of prior (Figure 3.3).

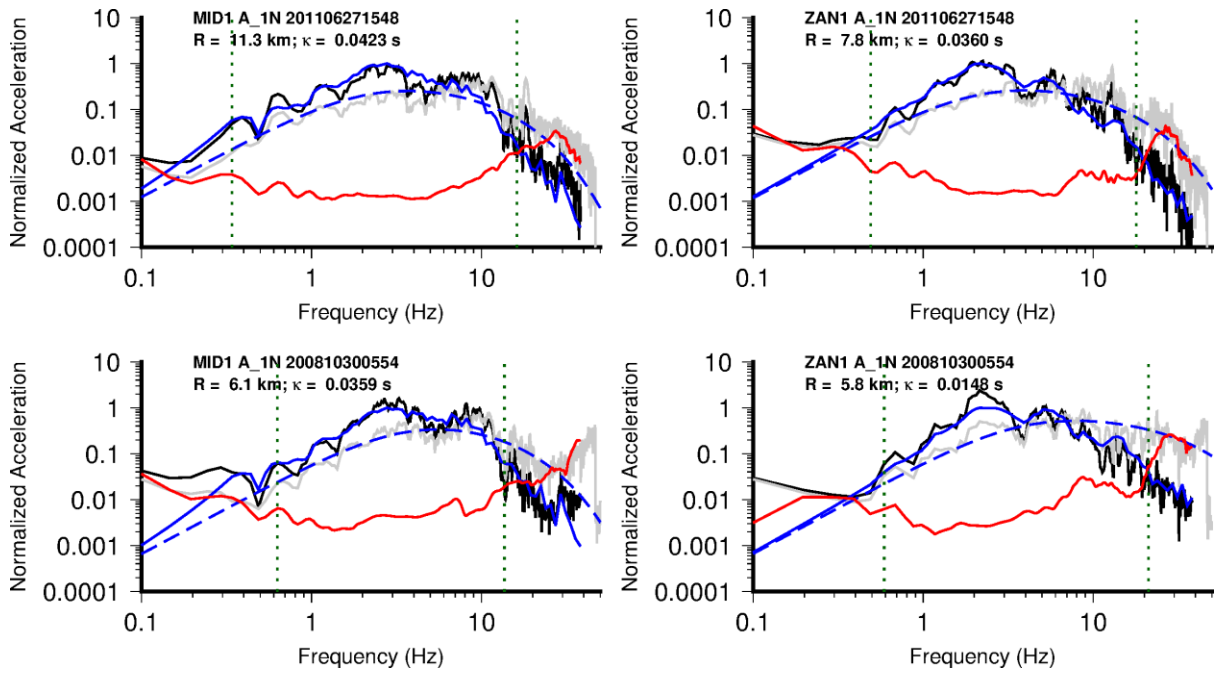


Figure 3.2. Comparison of observed (surface recordings at MID1 and ZAN1 accelerometers) and modelled FAS for two $M_L = 3.2$ events: top – 2011 Garrelsweer event ($f_0 = 2.1$ Hz); bottom – 2008 Westeremden event ($f_0 = 3.7$ Hz). Note absolute amplitudes are normalized such that only spectral shape is fit. Black line: surface acceleration FAS; red: surface noise FAS; grey: FAS deconvolved to NS_B using site transfer function; blue: modelled FAS (dashed: at NS_B; and solid: at surface).

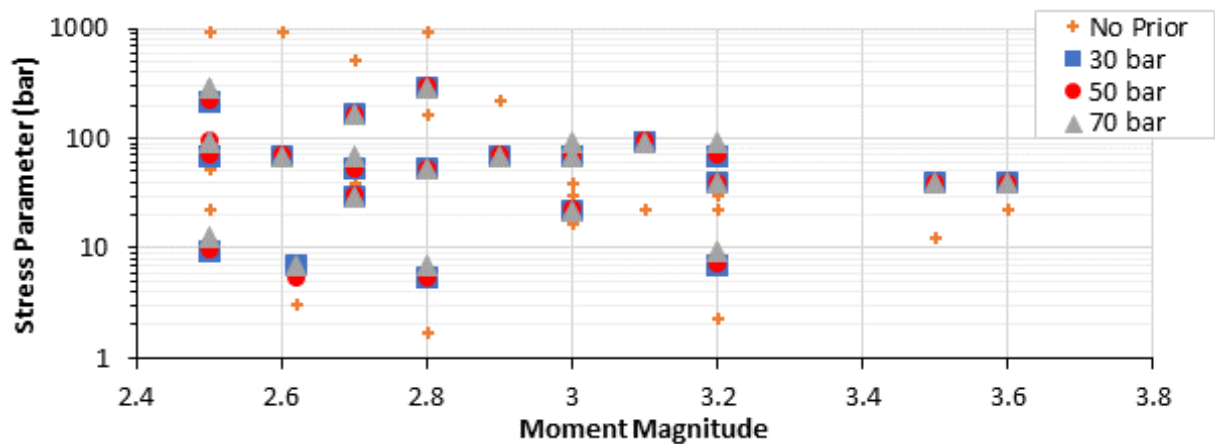


Figure 3.3. Best-fitting stress parameter for Groningen earthquakes using no prior, and 30, 50 and 70 bar priors in the stress-parameter distribution.

Using the long-period displacement plateau of the NS_B-corrected FAS, the geometrical decay function was inverted for along with average site amplification, fixing the moment magnitudes as determined by KNMI. The hinge points of the geometrical spreading function were selected to coincide with the distances observed during the full waveform simulations undertaken at Shell: 7 km and 12 km.

We assume that below 3 km (the minimum observed hypocentral distance), the decay is the same as between 3 to 7 km. The shape of the decay observed is similar (although less pronounced) to that seen during the simulations, indicating that the velocity structure has a strong impact on the recorded amplitudes as a function of distance. The decay rates observed were: $R^{-1.55}$ up to 7 km, $R^{-0.23 \pm 0.22}$ from 7 to 12 km, and $R^{-1.43 \pm 0.39}$ from 12 to 25 km. There is no error assigned to the first rate of decay, as it is conditioned on the selected M values (and segmentation distances). Although there are no data beyond around 25 km we assume R^{-1} , as indicated by the full waveform analyses. It is noted that the initial rate of decay is strongly dependant on the M values used in the inversion. In the previous V4 GMM, we used lower values of M (*i.e.*, assuming $M = M_L - 0.2$ rather than $M = M_L$), and therefore with seismic moments ~ 2 times weaker). This led to a stronger rate of decay in the first 7 km for the V5 model (and similar to the decay seen for the V3 model, which also used $M = M_L$). The reason for this is that the moment magnitude (and therefore seismic moment) sets the initial (source) amplitude, while the first observations occur at ~ 3 -7 km. The difference between source and observations then defines the initial rate of decay.

In order to define a field average amplification at the NS_B level, the (geometric) average amplification (source to NS_B) of all sites was computed. The amplification was found to be broadly frequency-independent between ~ 1 and 10 Hz and around 0.8-1.0 (albeit with a large standard deviation), suggesting that the effect of the velocity structure between the source (the reservoir) and the NS_B interface results, overall, in no significant resonance (Figure 3.4). The mild de-amplification between 1 and 10 Hz may be indicative of the velocity inversion present between the source and NS_B. At 0.6 Hz a pronounced peak exists which is also clear in the ground-motion residuals from previous GMMs. This feature is therefore retained. At high frequency the amplification increases, and plateaus at ~ 1.5 , consistent with expectations from quarter-wavelength modelling of the velocity profile.

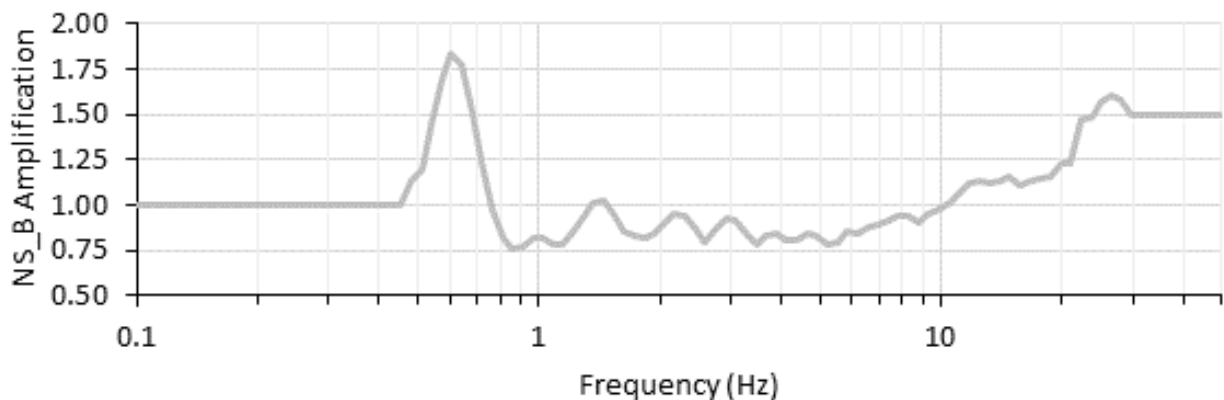


Figure 3.4. Network average source to NS_B amplification.

3.2. Selection of forward simulation parameters

Input ground motions are calculated using a finite-fault stochastic simulation methodology (EXSIM_dmb [version date: 17/10/2016]: Boore, 2009, based on EXSIM: Motazedian & Atkinson, 2005). This approach produces full time-histories and corresponding spectral ordinates by specifying a simplified seismological model (earthquake source, propagation and site effects).

The inversions discussed in Section 3.1 yield a range of possible combinations of source, path and site parameters that are consistent with the recorded data. While there is therefore an estimate of the mean value of each of the parameters obtained from the inversion, what is sought is the combination that when used in stochastic simulations yields predicted spectral ordinates that best reproduce the recordings. Based on the initial observations and spanning a broad range of the model space, we defined 72 parameter combinations based on: κ_0 values of 0.001, 0.005, 0.010, 0.015, 0.020 and 0.025 s; Brune stress parameter, $\Delta\sigma$, of 10, 30, 50, 60, 70, 80, 90, 100, 120, 150, 200 and 300 bar, and a Q value of 220. All simulations used the geometrical spreading model determined in Section 3.1, which was based on the segmentation distances from full waveform modelling. Source to NS_B amplification, based on the network-average, was relatively small, but non-negligible. The simulations were compared to the individual horizontal component response spectra at the NS_B horizon for all 20 spectral periods for which recorded data were available (0.01 to 2.5 s).

In order to assess the fit of each model the inter-event terms are calculated at each of the 20 periods. As for the V4 GMM, random-effect terms are calculated using:

$$\eta_i = \frac{\tau^2 \sum_{j=1}^{n_i} y_{ij} - \mu_{ij}}{n_i \tau^2 + \phi^2} \quad (3.1)$$

(Abrahamson & Youngs, 1992) with arbitrary starting values of the intra-event term $\phi=0.5$ and inter-event term $\tau=0.5$ (\log_{10}) and iterating until convergence. n_i is the number of records (y_{ij}) for the j^{th} event and μ_{ij} is the mean value of the j records for the i^{th} event. From the inter-event terms the average model bias is measured from the N events:

$$\text{bias}(T) = \frac{1}{N} \sum_{i=1}^N \eta_i(T) \quad (3.2)$$

As for the V4 GMM, the root-mean-square (RMS bias) and standard deviation [$\sigma(\text{RMS bias})$] over the period-specific values is taken after each simulation to provide a simulation specific (period independent) measure of model bias. Note that the RMS misfit will only be 0 in the case that the model is perfectly unbiased at all periods. Low $\sigma(\text{RMS bias})$ indicates that the residual misfit is consistent (either

consistently biased or unbiased), high values indicate period-to period differences in the bias are present. EXSIM performs time-domain simulation, and is significantly slower than SMSIM, which can use random-vibration theory to speed up the process when only peak-amplitude ordinates (e.g., SA) are required. For small magnitude events, EXSIM_dmb has been shown to produce the same results as SMSIM (Boore, 2009), as verified in the V4 GMM.

The results in terms of mean RMS bias is shown in Figure 3.5 versus stress parameter and κ_0 . The contour plot clearly shows the trade-off between the source and site terms, with increasing stress-parameter being accompanied by increased κ_0 to provide similar bias. The best fitting model for the motions at the NU_B horizon is found to have the following parameter combination based on the smallest RMS average misfit (bias) and sigma: $\Delta\sigma = 70$ bar; $\kappa_0 = 0.010$ s (RMS bias = 0.058 ± 0.087). The stress-parameter determined from the response spectra is higher than the average of ~35 bars determined from spectral analysis. It is noted, however, the approach here is to determine a full set of simplified parameters that reproduce the observed SA (and variability), rather than replicating the mean observed for the individual events.

Calibration to global GMPEs

The aim of the *upper* branch of the Groningen ground-motion model is to reflect ground motions observed for small **M** events in the gas field, while producing ground motions comparable with global tectonic seismicity when extrapolating to larger **M**. In order to calibrate the model at large magnitude we have performed a similar process to that described above for matching models with locally observed events. However, we now set the target as the PSA at 6 spectral periods (PGA, 0.1, 0.2, 0.3, 1 and 2 s) at magnitudes **M** = 5, 6 and 7, for logarithmically spaced distances of 0, 2.5, 5, 10 and 20 km and with $V_{S30} = 1500$ m/s (consistent with NS_B rock velocities). Normal faulting is assumed, with a dip of 75°. Six GMPEs were used as the target: three NGA-W2 models (BSSA14: Boore *et al.*, 2014; CY14: Chiou & Youngs, 2014; CB2014: and Campbell & Bozognia, 2014) in addition to the Eastern North America model YA15: Yenier & Atkinson (2015) and the European (RESORCE) models Aetal14: Akkar *et al.* (2014) and Betal14: Bindi *et al.* (2014). Due to the larger stress-drops expected for normal tectonic events, the grid-search was expanded to include 20 values between 50 and 1600 bars. Based on the work of Boore (2009), who compared SMSIM against EXSIM_dmb, and the comparisons undertaken here, SMSIM (with the R_{EFF} distance metric used for finite-fault approximation) was again used for the calibration.

Models with low bias (over the range of κ_0) and period-to-period variability in bias σ (RMS bias) use 200-400 bars (Figure 3.6). Assessing the fit was somewhat subjective due to the strong attenuation in the Groningen model, which was not exhibited in the GMPEs and leads to a greater spread of SA at moderate and short periods with distance (Figure 3.7).

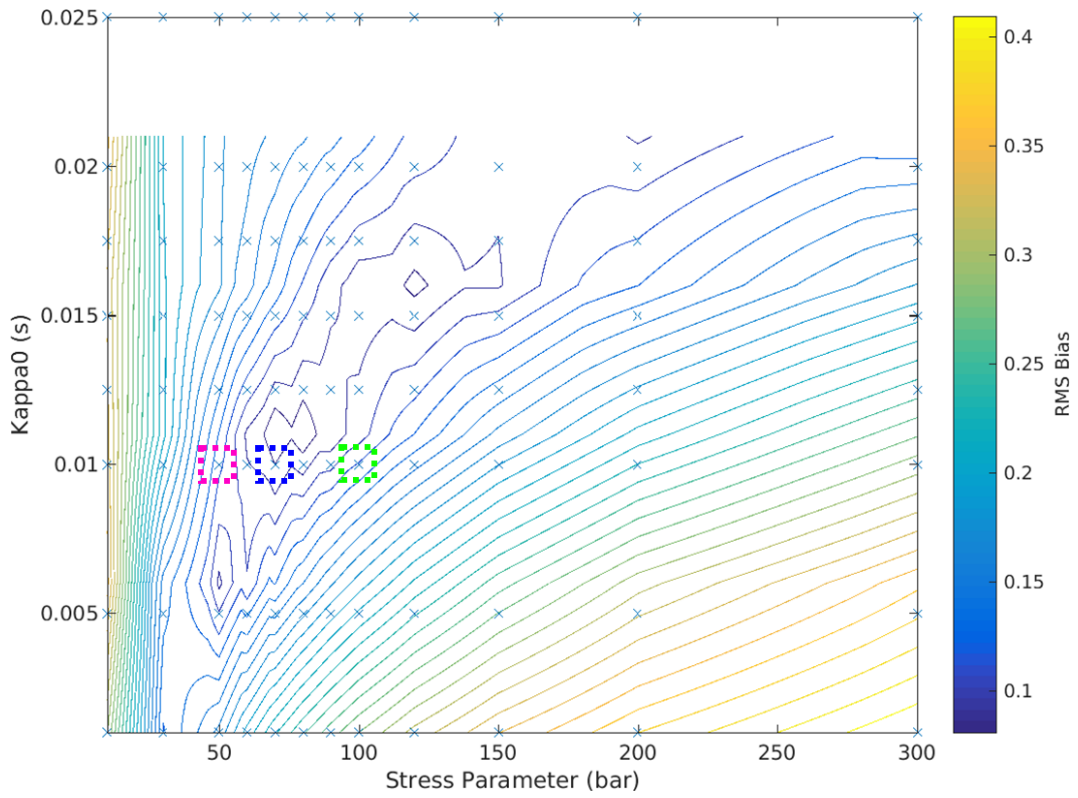


Figure 3.5. RMS bias contoured against stress parameter and κ_0 for $Q=220$. Dashed lines indicate the selected central (blue), lower (purple) and upper (green) model parameters for $M \leq 3.6$.

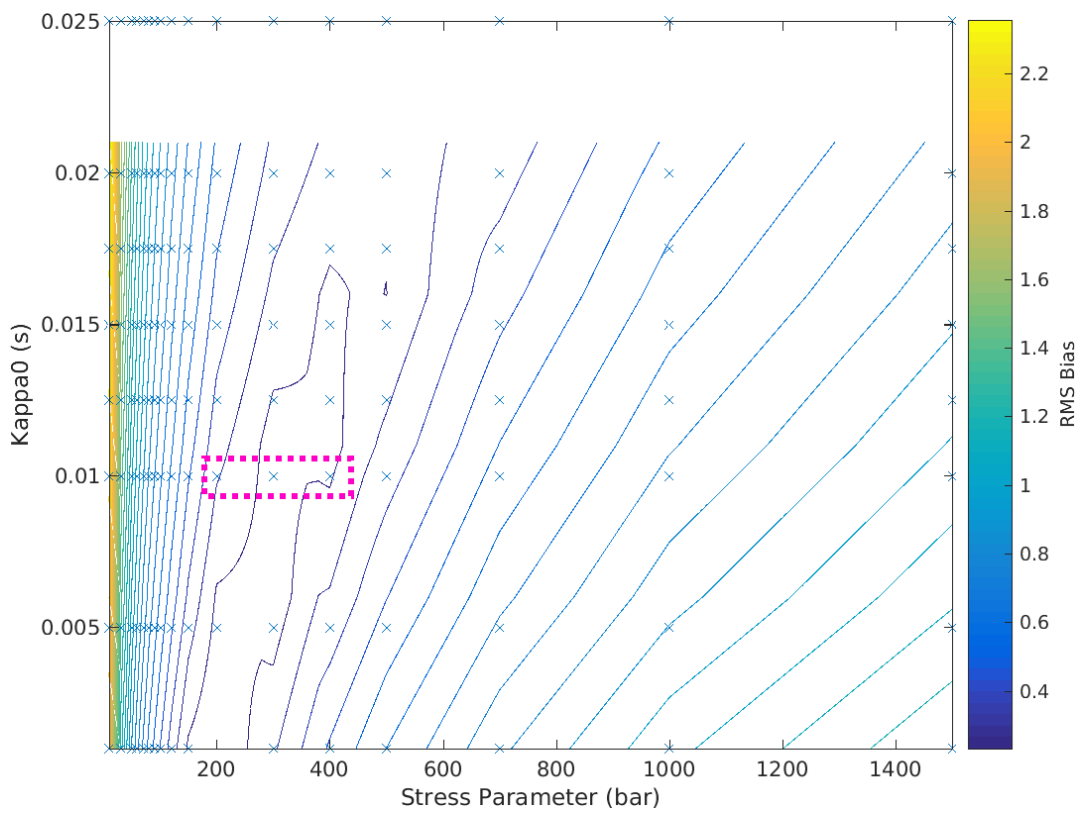


Figure 3.6. RMS bias against stress parameter and κ_0 for the NGA-W2 GMPE target PSA.

To be conservative, a model with ~ 300 bars was selected after inspection of the residual misfit plots to ensure that predicted motions for the upper model are consistent with (or, if necessary, exceed) tectonic seismicity across the range of periods. Effectively this means accepting a small positive model bias (*i.e.*, overestimation of long-period ground-motion) in order not to underestimate the short-period motions. A comparison of the simulated ground motions in terms of period, distance and magnitude is shown in Figure 3.7 for a 300 bar model. From these plots it can be appreciated that the upper branch of the V5 GMM does indeed mimic the GMPEs derived from tectonic earthquakes. The exception to this is most clearly visible in the middle frame of Figure 3.7, where it can be seen that the Groningen GMM predicts values lower than those obtained from the ENA model of Yenier & Atkinson (2015) as distance from the source increases, which is to be expected because Q values in the upper crust in Groningen are about an order of magnitude smaller than those typically found in ENA.

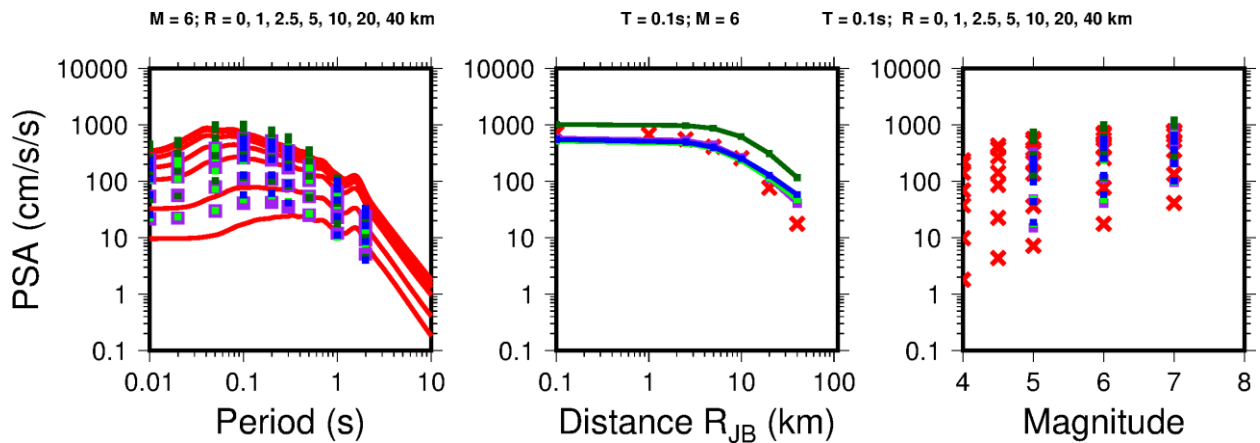


Figure 3.7. Comparison of simulations (upper model) using SMSIM RVT (R_{eff} version) (red) and the six GMPEs (blue: average NGA; purple/light green: RESORCE; dark green: ENA, $Z_{\text{hyp}}=10$ km). *Left*: SA vs. period. *Middle*: SA vs. distance. *Right*: SA vs. magnitude. All for scenarios indicated above panels.

Selection of lower, central and upper models

As for previous GMMs, for the forward simulations it was decided to use alternative values of the stress parameter to reflect the considerable epistemic uncertainty associated with extrapolation to much larger magnitudes. In the magnitude range covered by data ($M \leq 3.6$) the two central branches have a stress parameter of 70 bars (the best-fit model to local data, minimum bias), the lower branch 50 bars [with median bias to local data at moderate to short periods (0 to 0.2 s) $\sim -0.5\tau$ to $-\tau$] and—reflecting the possibility of the motions being similar to those from normal tectonic earthquakes—the upper branch has 100 bars [median bias to local data at short periods $\sim +0.5\tau$ to $+\tau$]. All models exhibit an increase of stress-parameter

with magnitude, reflecting the belief that for larger events, increasingly sampling greater depths of the crust, the low $\Delta\sigma$ values observed in the reservoir at low M are unrealistic. For the two central models (central *a* and central *b*), $\Delta\sigma$ rises to 140 bars and 220 bars at M 5, respectively, then remains constant. Similarly, the lower and upper models rise to 75 bars and 330 bars, respectively (Figure 3.8). The latter is designed to produce motions, given the Groningen-specific attenuation and site characteristics, which are similar to those observed globally, as shown previously. The lower model, with stress drops increasing to 75 bars for $M \geq 5$, is designed to reflect the fact that we do not believe that median stress drops at moderate and large magnitude could be lower than those observed for local seismicity in the reservoir. The overall spread of the models is designed to be consistent—increasing by a factor ~ 1.5 for each branch, apart from the lowermost branch, where 75 bars is chosen as the upper level for the lower model—with a ‘self-similar’ magnitude scaling (*i.e.*, consistent with the central models at low magnitude).

Table 3.1 summarises the full set of inputs to the simulations used to generate the motions at the NS_B reference for the derivation of the median GMPEs. For each of the model branches (lower, central *a/b*, and upper), response spectra were simulated using EXSIM_dmb for 2100 scenario events with $M = 2.0$ to 7.0 in steps of 0.25. For each scenario event a random epsilon was selected to define the length and width of the rupture. Recording locations were placed radially above the centre of the fault’s top edge at 0 km and then 25 distances logarithmically spaced between 1.0 and 79.5 km. For each distance, 8 sites were located, at 0 to 315° (in 45° steps). In total 1.75 million response spectra were calculated, or 436,800 for each of the model branches.

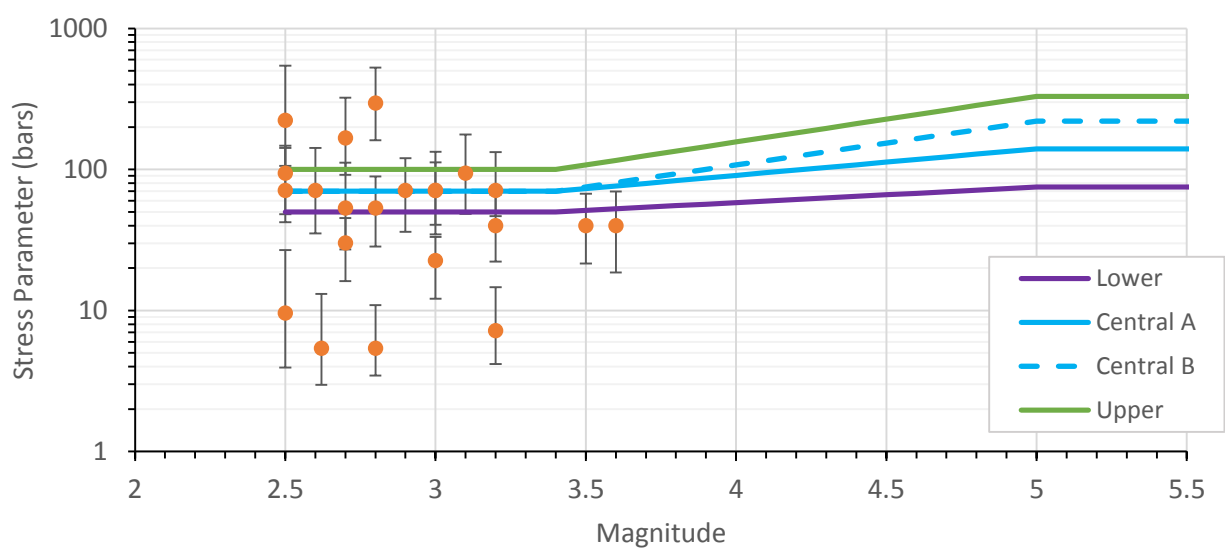


Figure 3.8. Estimates of stress drop together with confidence intervals as a function of magnitude, together with the four median models adopted for the simulations.

Table 3.1. EXSIM_dmb parameter values used in simulations for NS_B motions

Parameter	Symbol (units)	Value(s)	Notes
Density	ρ (g/cm ³)	2.6	
Shear-wave velocity	β (km/s)	2 3.5	M ≤ 4.5 (in reservoir) M ≥ 5.5 (Carboniferous) Linear interpolation between these magnitudes
Horizontal partition		0.707	
Radiation coefficient	θ	0.55	
Free surface	F	2	
Sub-fault source type		Brune (1970, 1971) ω^{-2}	
Top of rupture depth	Z_{top} (km)	3	
Seismogenic depth	Z_{seis} (km)	13	
Fault dip	Dip (degrees)	75	Average of observed 60 – 90 degrees.
Fault mechanism		Normal	
Fault width	W (km)	$\min(W(W\&C'94), [Z_{seis}-3]/\sin(\text{dip})]$	W(W&C'94): Width from Wells & Coppersmith (1994)
Fault length	L (km)	$L(W\&C'94)*(W/ W\&C'94)$	L(W&C'94): Length from Wells & Coppersmith (1994) Conserve area of fault A given by LxW in case limited by Z_{seis}
Hypocentre location	H($\Delta L, \Delta W$) (km, km)	Random, 0	Located randomly along strike, at 3 km depth (top of fault).
Slip velocity	V_{slip} (km/s)	0.8β	
Stress parameter (Lower, Central, Upper)	$\Delta\sigma$ [M ≤ 3.4] (bars)	50, 70, 70, 100	Linear interpolation of $\log(\Delta\sigma)$ with M
	$\Delta\sigma$ [M ≥ 5.0] (bars)	75, 140, 220, 330	
Geometrical spreading distances (R_{hyp})	R1, R2, R3 (km)	7, 12, 25	
Geometrical decay rates	$\lambda_1, \lambda_2, \lambda_3, \lambda_4$	-1.55, -0.23, -1.43, -1.00	
Path attenuation	Q	220	
Site attenuation	κ_0 (s)	0.010	
Source duration	T_s (s)	$1/0.4906\beta(\Delta\sigma/M_0)^{1/3}$	SI units
Path duration for sub-fault signals	T_p [R (km)]	$T_{5,75}/0.383$	V3 Groningen $T_{5,75}$ model for M = 3.0, $V_{s30}=1500$.
Rise time	T_s (s)	$1/f_0$	
Site amplification	A(f)	Network average NS_B	
Dynamic, pulsing percentage		50%	
Sub-fault averaging		RMS	
Scaling		(Acceleration FAS) ²	

Simulated NS_B motions

Figures 3.9 to 3.11 show simulated response spectral ordinates at the NS_B rock horizon for three different distances and, in each case, three different earthquake magnitudes. Each plot shows the simulations obtained with each of the four stress parameter branches that define the four branches of the median ground-motion logic-tree for the reference rock motions.

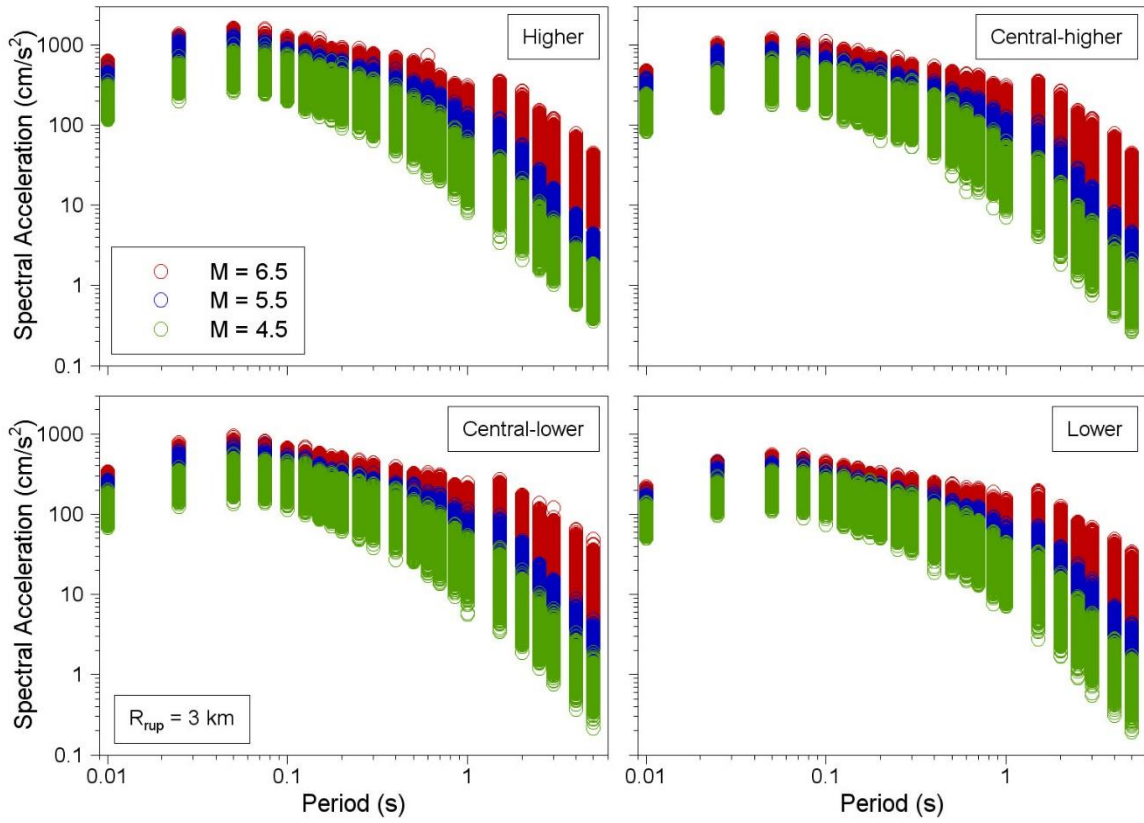


Figure 3.9. Simulated response spectra at NS_B at a rupture distance of 3 km

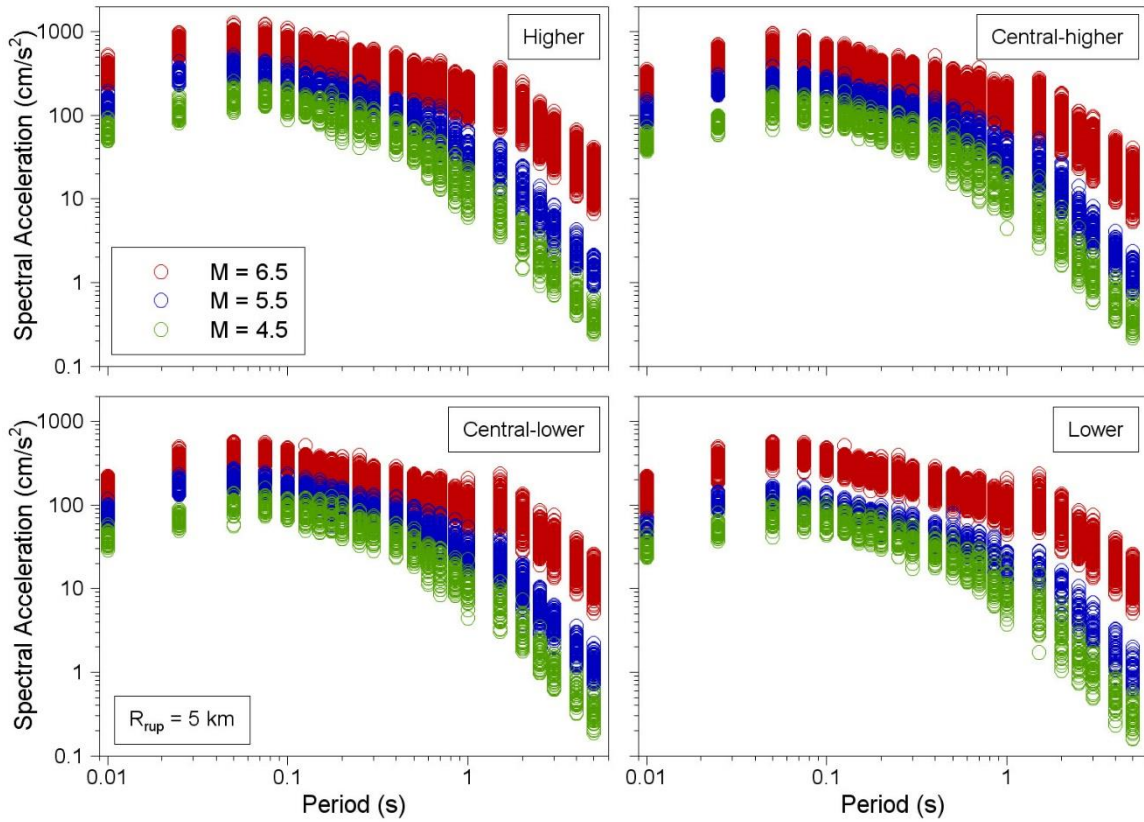


Figure 3.10. Simulated response spectra at NS_B at a rupture distance of 5 km

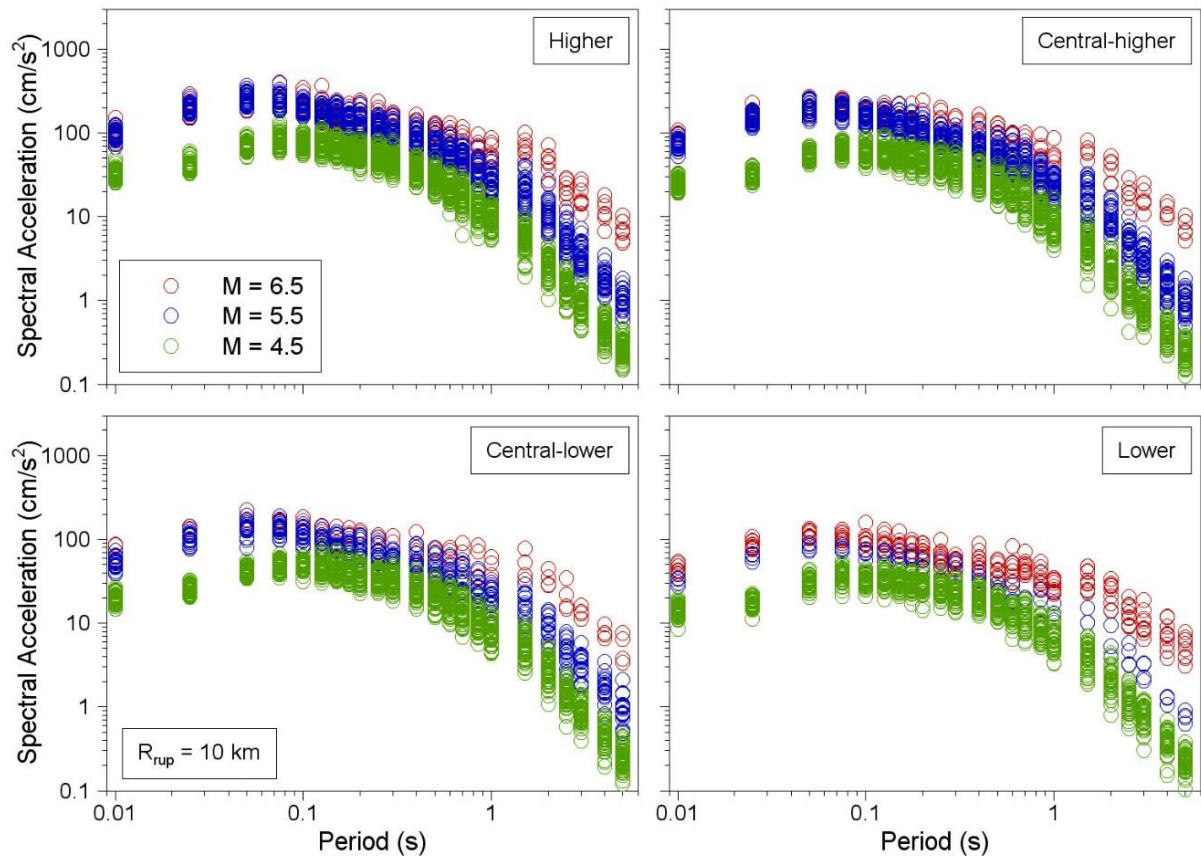


Figure 3.11. Simulated response spectra at NS_B at a rupture distance of 10 km

3.3. Parametric GMPEs for NS_B

The parametric GMPEs for Sa(T) and PGV at the NS_B were derived in exactly the same way as in the V4 model, performing simple regressions on the simulated motions. The functional form relating these ground-motion parameters to the local magnitude and the rupture distance is identical to that used for the V4 model, including the values of the hinging magnitudes for the changes in scaling and the hinging distances that control the changes in spreading functions.

The functional forms and their coefficients are all presented in Section 6.1 of this report. The equations are presented only in Chapter 6 to avoid unnecessary inflation of the length of the report and to thus provide a complete description of the GMM in a single section, for the convenience of potential users.

Figures 3.12 and 3.13 show plots of the outcomes from the regression against the simulations, for Sa(0.01s). The figures illustrate how well the regression fits the simulated motions at the NS_B horizon over the full range of magnitudes and distances for which the simulations were performed.

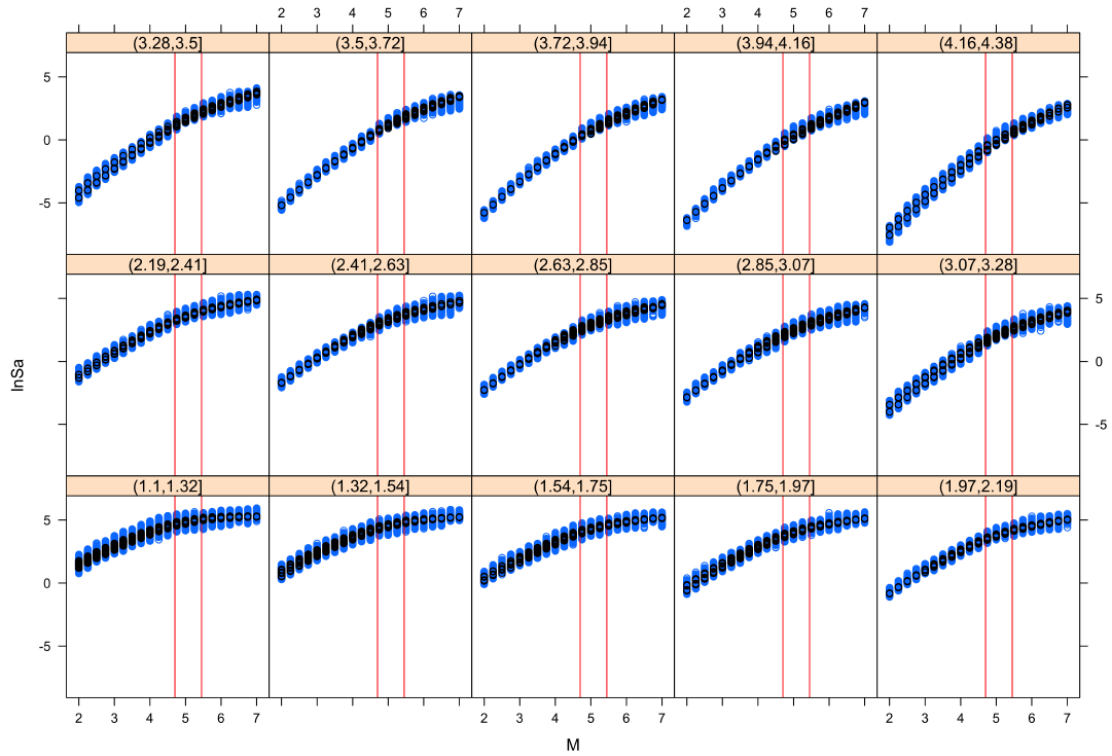


Figure 3.12. Comparison of regression results (*black*) with ESXIM simulations (*blue*) for PGA for different distances (ranges indicated by logarithmic values in header of each frame) against magnitude

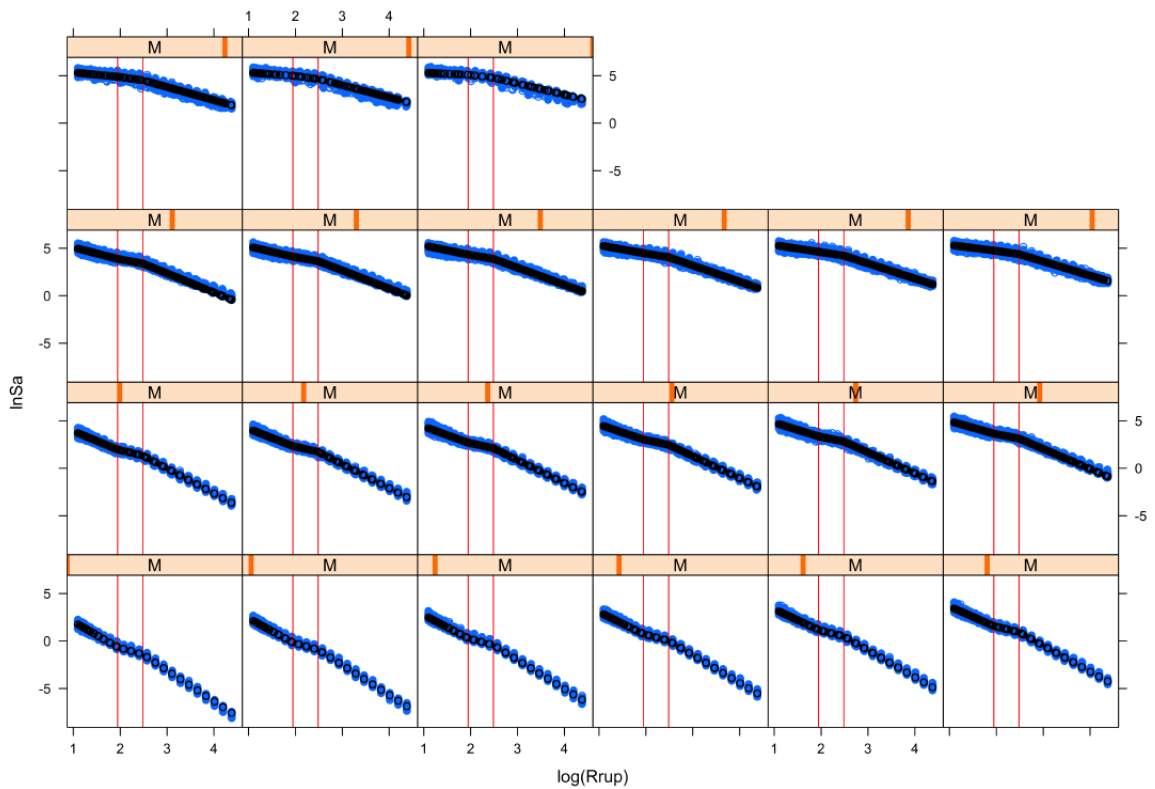


Figure 3.13. Comparison of regression results (*black*) with ESXIM simulations (*blue*) for PGA for different magnitudes (indicated by thick orange bars in header, with M increasing left to right) and distance; vertical red lines indicate control points for change of spreading function

3.4. Variability components

As for the V4 model, the variability components for the V5 model are primarily based upon an analysis of the small-magnitude data obtained in the Groningen field. The main exception to this statement is the use of comprehensive databases of tectonic earthquakes to place constraints upon the non-ergodic within-event variability.

The process followed to determine the between-event standard deviation is the same as that for the V4 model. Once the median model predictions were developed by running non-linear ordinary least squares regression analysis on the EXSIM simulation outputs, these model predictions were used to compute total residuals of the Groningen data. These field-specific data (either surface or borehole recordings) were transformed to the NS-B horizon. The total residuals are then partitioned into components using an advanced mixed effects regression approach that accounted for both magnitude uncertainties and spatial correlation, as well as crossed random effects for repeatable event and site effects. A more elaborate discussion of the approach taken, as well as the underlying mathematical framework, is provided in the V4 model report.

The mixed effects regression procedure was applied to each of the four model branches and the results obtained for $\ln(\tau)$ in each case are shown in Figure 3.14.

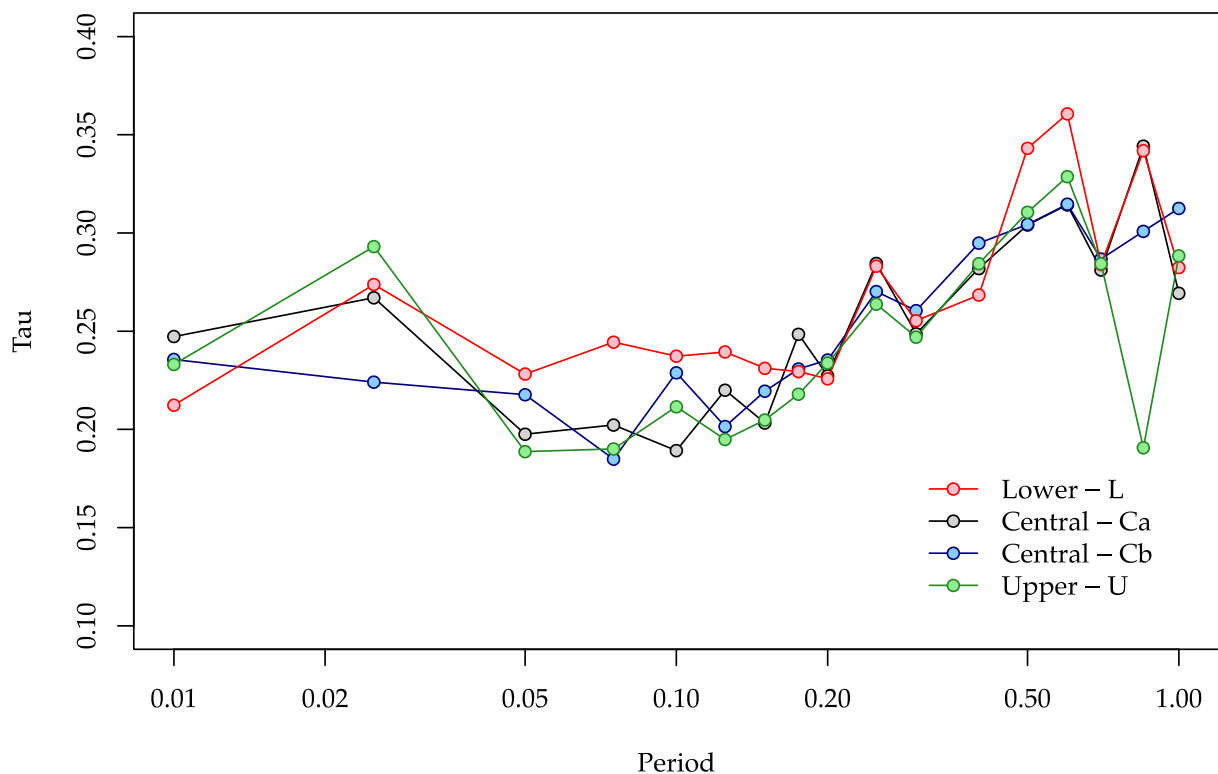


Figure 3.14. Estimates of the between-event standard deviation, in natural logarithms, for each of the four branches at the NS-B horizon.

The variation in the estimates of between-event variability arise from two primary sources. The first is associated with the fact that the stress parameter values are different for each of the four considered branches and so the median model predictions over the magnitude range for which data from the Groningen field exists differ from branch to branch. This difference in medians leads to differences in total residuals that then influence the way these residuals are decomposed in the regression analysis. The second reason is related to the stochastic nature of the advanced regression analysis that is performed. A Markov-chain Monte Carlo approach is adopted within a Bayesian framework to obtain estimates of the variance components. While multiple simulations are run for each branch, there will still be some degree of variability from simulation-to-simulation. Rather than being a negative point, for the present study this is viewed as an advantage as it allows some degree of epistemic uncertainty to be implicitly incorporated into the specification of the between-event standard deviations.

In order to develop a model for the between-event variability, the functional form adopted previously for the V4 model was again utilised. This function is a continuous function of response period as shown in Eq.(3.3):

$$\tau(T) = \sqrt{\tau_0^2 + [g(T)\tau_1]^2 + g(T)\tau_0\tau_1\tau_3} \quad (3.3)$$

where the function $g(T)$ is defined as in Eq.(3.4).

$$g(T) = \frac{2}{3} \left[\frac{1}{1 + \left(\frac{T}{\tau_2}\right)^2} \right]. \quad (3.4)$$

Independent fits of this model to the results shown in Figure 3.14 were made and this resulted in the set of parameters defined in Table 3.2.

Table 3.2. Parameters of the between-event standard deviation model

Branch	τ_0	τ_1	τ_2	τ_3
Lower, L	0.3335	0.4789	0.1982	-1.4434
Central, Ca	0.3068	0.6240	0.1028	-1.5605
Central, Cb	0.3132	0.5322	0.1299	-1.5269
Upper, U	0.3088	0.6348	0.1134	-1.5833

This model is able to capture the general variation of the between-event standard deviation well for all of the branches, as can be appreciated from the comparison between the regression outputs and the fitted models shown in Figure 3.15. The low

Tau estimates at 0.85 s for the upper branch is a result of sampling issues on one of the Markov chains and the result is discarded.

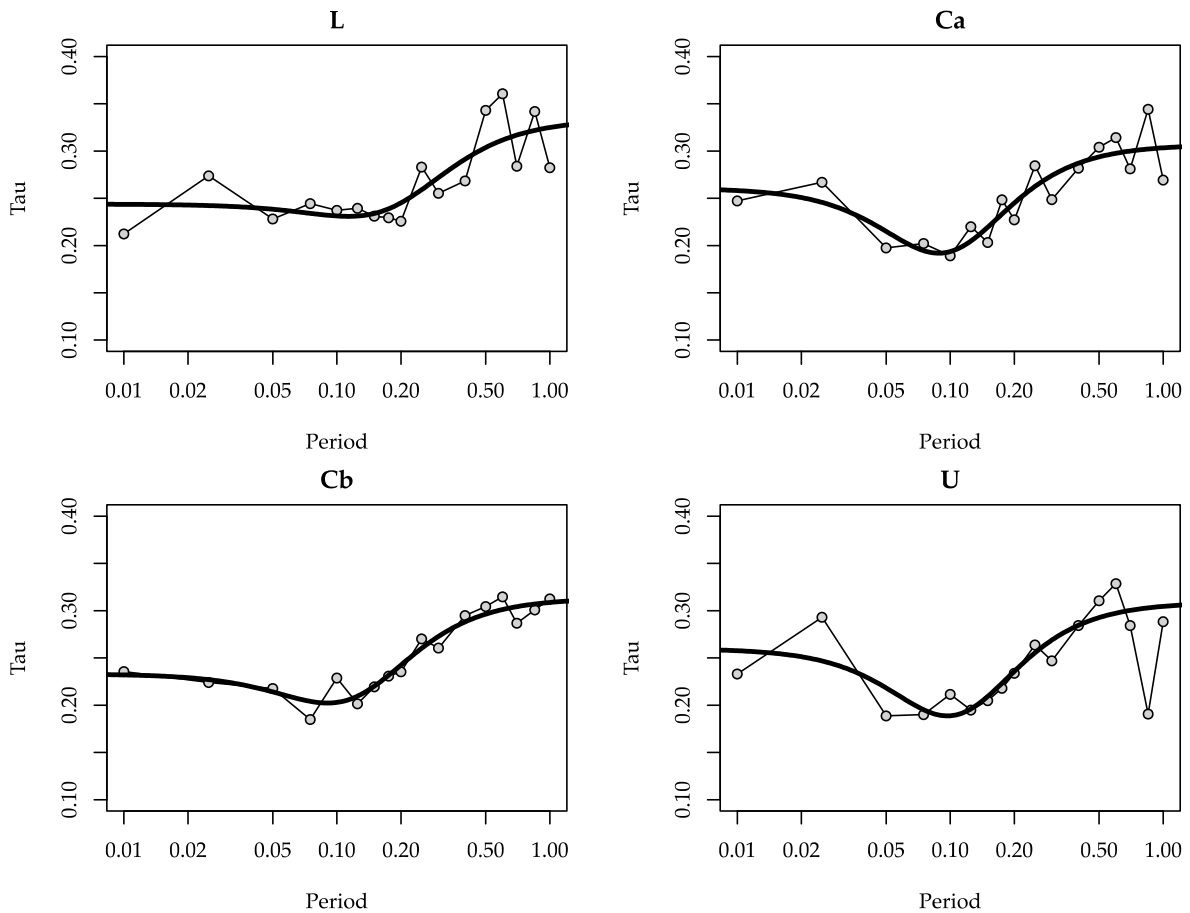


Figure 3.15. Model fits to the estimated between-event standard deviations. Note that for the upper branch, the anomalously low estimate at $T=0.85$ s is not used for the fitting.

The values of the between-event standard deviation for the V5 model have changed from those in the V4 model, as shown in Figure 3.16. For most periods of interest in the risk model for Groningen, the between-event standard deviations have increased, while at very short periods the model is now predicting lower values of between-event standard deviation. As the methodology remains consistent with that adopted for the V4 model, these differences are primarily attributed to the effect of the additional ground-motion records that have been added to the empirical database since the V4 model.

For the risk calculations, the geometric mean horizontal component of motion is transformed to the arbitrary horizontal component. This does not affect the median prediction but it requires the addition of the component-to-component variance to the variance associated with the geometric mean component. The strong polarisation of

several of the Groningen ground-motion recordings led to values of component-to-component variability in previous versions of the model that are appreciably higher than those generally found from datasets of recordings from tectonic earthquakes. The model for the component-to-component variability has been updated in the derivation of the V5 model to capture the distance dependence of the polarisation and also to diminish with increasing magnitude to become similar to tectonic models at the magnitude level beyond which triggered Groningen earthquakes would be assumed to have the characteristics of tectonic events. The derivation of this new model is presented in Appendix III.

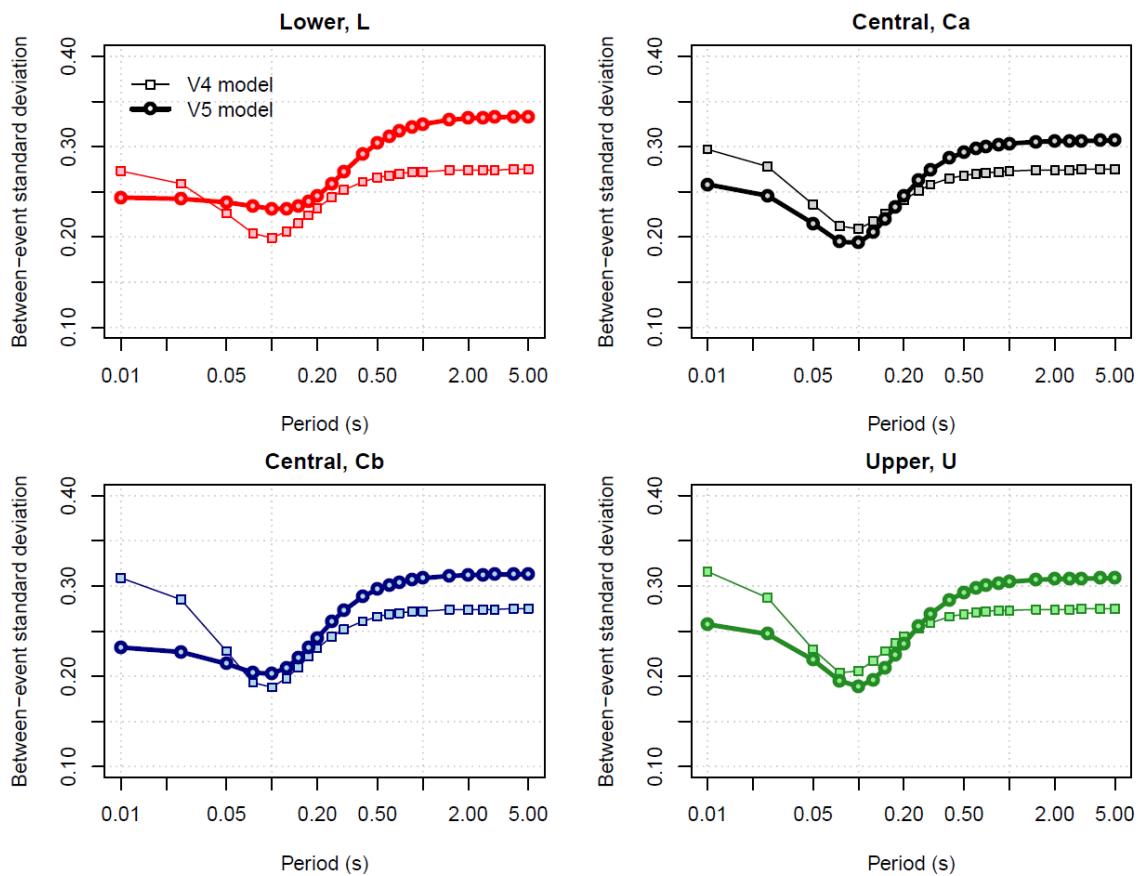


Figure 3.16. Comparison of the between-event standard deviations for the V4 and V5 models.

3.5. Comparison with V4 NS_B GMM

The derivation of the V5 model for NS_B motions followed exactly the same steps as used for the V4 model, but differences have arisen due to changes in the data. The variability model has altered slightly; while the within-event non-ergodic standard deviation remains unchanged the addition of the Slochteren data resulted in a modest increase in the between-event standard deviation except at the shortest oscillator periods, as shown in Figure 3.16.

The weights on the logic-tree branches carrying these four GMPEs were also unchanged from the V4 model since the rationale underlying the choice of those weights has not changed. The median predictions, however, have changed much more dramatically. The predictions from both models are compared in several plots presented in Appendix IV, from which it can be appreciated that except for short response periods and large earthquake magnitudes, the amplitudes predicted by the V5 model are appreciably lower than those from the V4 model. This is shown more clearly in Figures 3.17 and 3.18, which plot ratios of the predicted accelerations from the central-higher (Cb) and upper (U) models. The reduction in amplitudes is up to 20-30% in some cases. This is partly the result of the addition of the large number of recordings from the 2017 Slochteren earthquake to the database since the recorded amplitudes from that event were exceptionally low, leading to a reduction of about 10% with respect to the V4 GMM in the intermediate period range (see Appendix II for a detailed discussion of these data and their impact on the model derivation).

The primary cause for the change in NS_B amplitudes from V4 to V5, however, is the change in the relationship between local and moment magnitudes. Preliminary work on the relationship between M and M_L in the Groningen field indicated that for events larger than M_L 2.5 (in other words, those of relevance to the derivation of the GMM), values of M were, on average, consistently 0.2 units smaller than M_L . This relationship was implemented in the V4 inversions and caused a marked change in the estimates of the stress parameters and the near-source geometric spreading rate; in previous versions of the model, it has been assumed that the two magnitude scales were equivalent in the range of interest. Subsequent work, using a larger database of Groningen earthquakes and more detailed analyses, demonstrated conclusively that in fact the previous assumption that $M = M_L$ was in fact valid (see Dost *et al.*, 2018). Therefore, for the V5 model derivation, the assumption of equivalence of the two magnitude scales was once again invoked, now supported by empirical data from the region. Figure 3.19 shows the ratio of simulated motions obtained from the V5 model to those that would have been obtained from the V4 model; for the magnitude-distance combinations generally found to dominate the hazard and risk estimates in Groningen, the change in the magnitude relationship clearly caused a significant reduction. Figure 3.19 actually reflects the influence of both the change in the magnitude definition and the addition of the Slochteren data, but the former is the dominant influence since the fitting is by event rather than by record and the Slochteren earthquake is only one of 23 events in the V5 database.

Although the change of the magnitude definition from the V4 to V5 models has had a marked effect, it is important to emphasise that the current model is well supported and it is the V4 model that was subject to a change that is not supported by local data (an occurrence that can be attributed to the very aggressive schedule on which the different versions of the model have been generated; see Section 2.1).

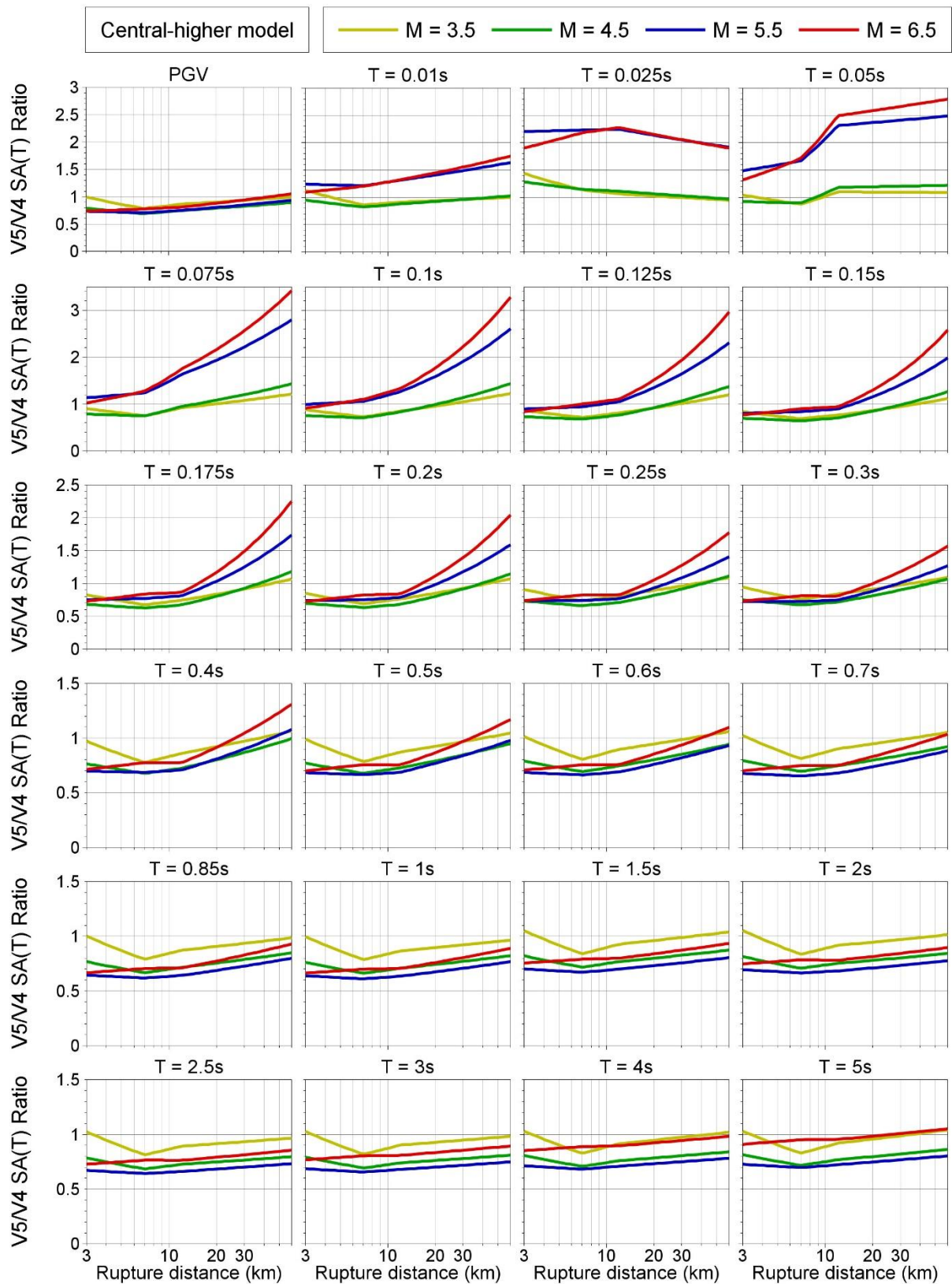


Figure 3.17. Ratios of predicted medians at NS_B from the central-higher (Cb) branch of the V5 to V4 models, plotted against distance for four magnitudes

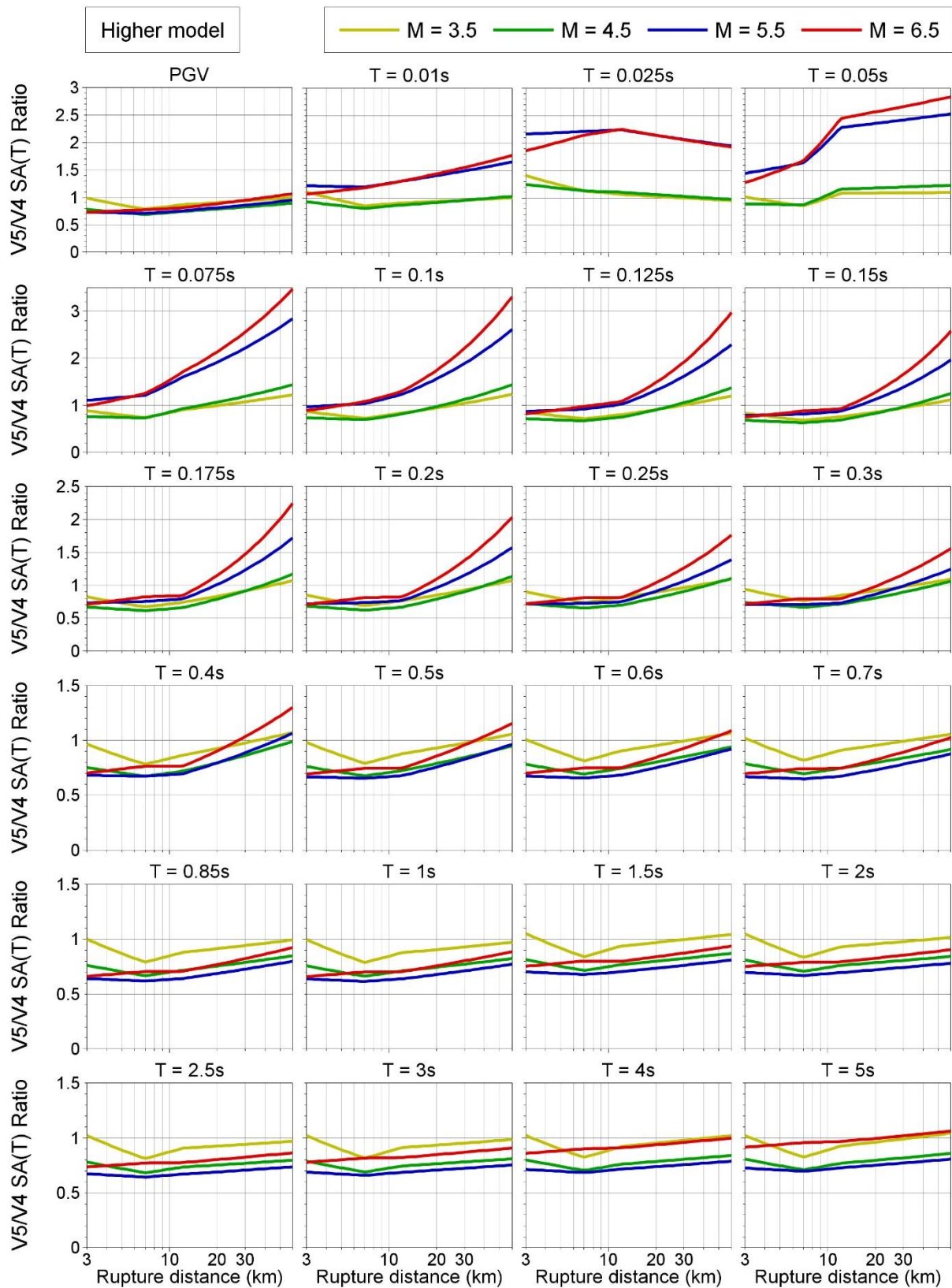


Figure 3.18. Ratios of predicted medians at NS_B from the upper (U) branch of the V5 to V4 models, plotted against distance for four magnitudes

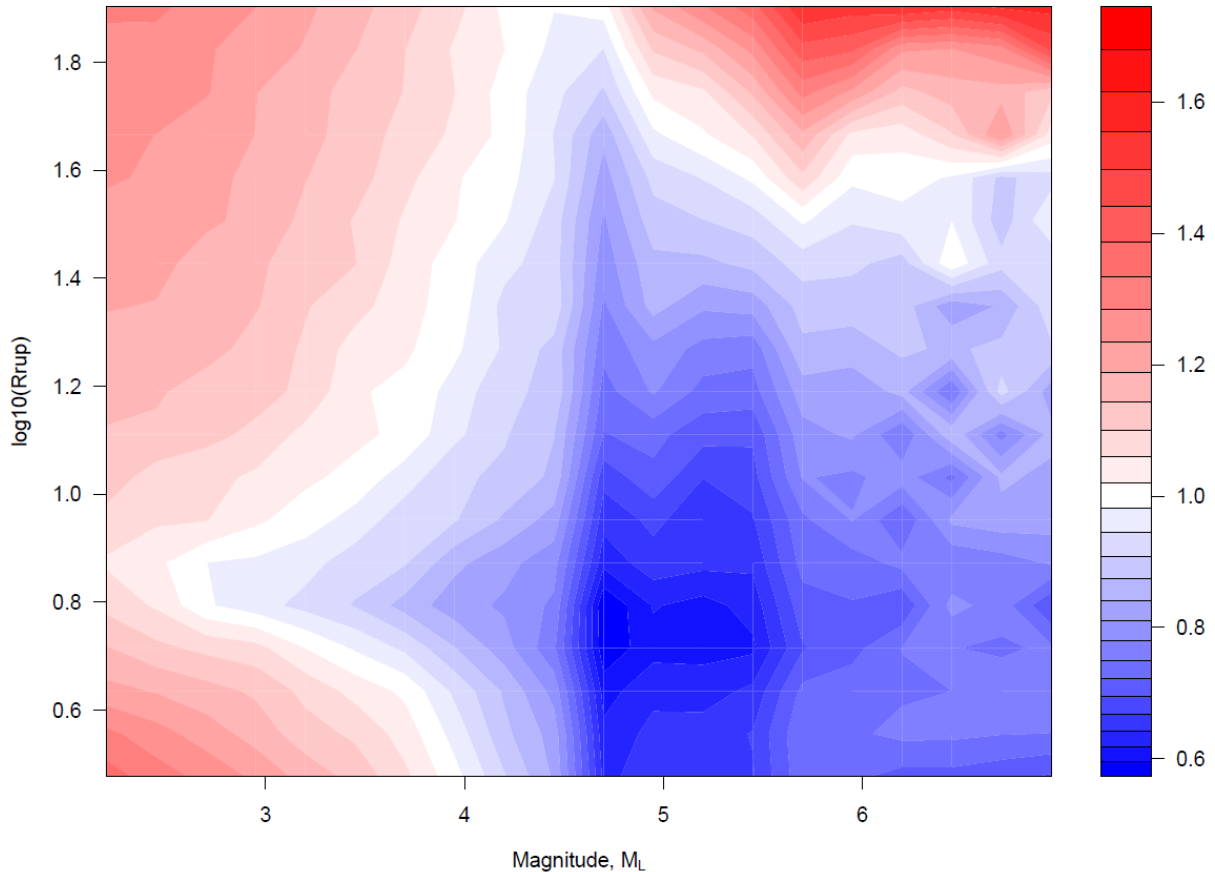


Figure 3.19. Ratios of V5 Sa(0.5s) at NS_B to those obtained invoking the $\mathbf{M} = M_L - 0.2$ relationship in the inversions, as a function of magnitude and distance

Although the models are not directly comparable because of the change of distance metric associated with moving from point-source earthquake representations to finite rupture modelling, the GMM has actually been quite stable from V3 to V5, as illustrated in Figures 3.20 to 3.22. These plots also compare the models with predictions from two NGA-West2 models, confirming that for larger events the models predict motions similar to those from tectonic GMPEs (except at longer distances because of the lower Q values). We note in passing that the generation of predicted response spectra for earthquakes of magnitude $\mathbf{M} \geq 2$ does represent a significant extrapolation of the NGA-West2 models.

The reader is also referred to Appendices IX and X for additional discussions of the selection of the source, path and site parameters used in the simulations to generate the GMM. In those Appendices, numerous questions raised by the international review panel have been answered with additional analyses, plots and explanations that should enable a better understating of the technical bases for the current model.

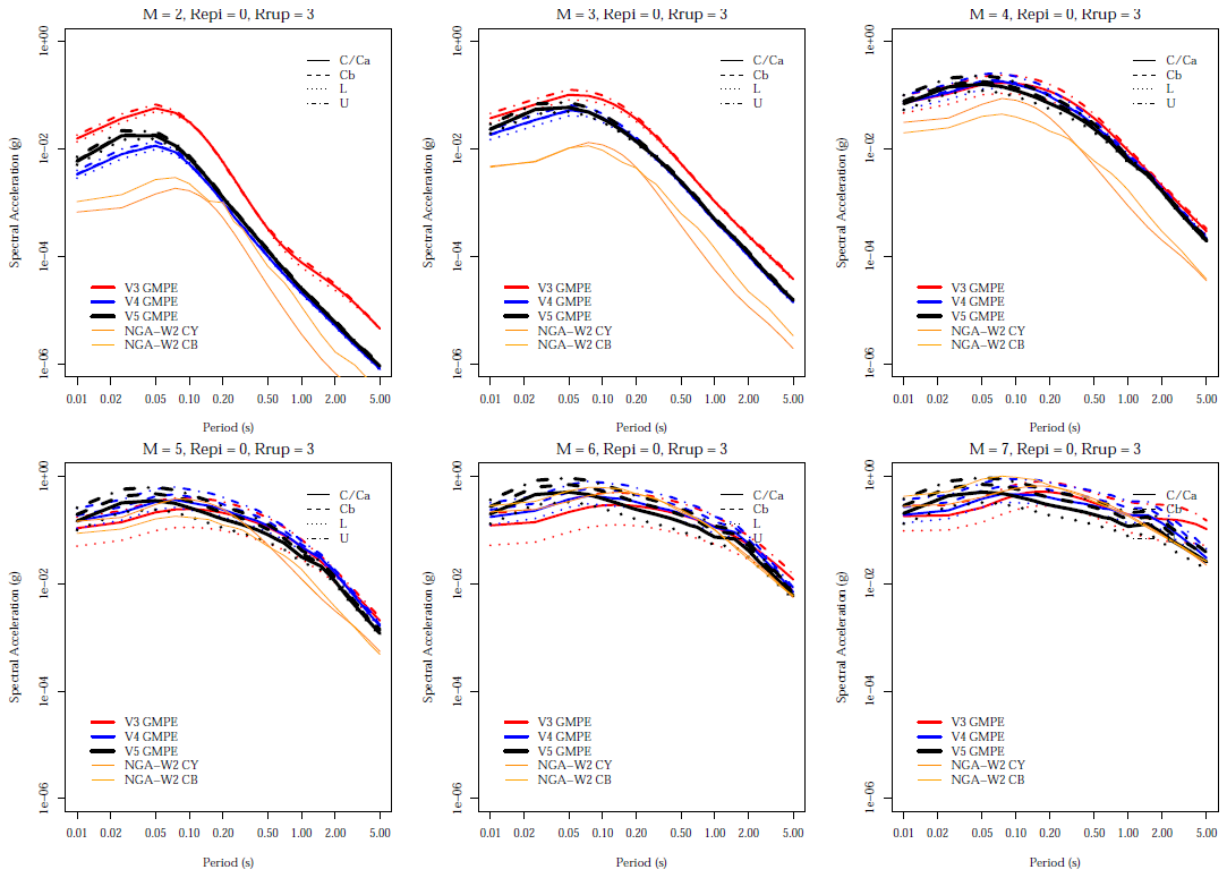


Figure 3.20. Comparison of predicted median spectral ordinates from the V3, V4 and V5 for an epicentral distance of 0 km, together with predictions from two NGA-West2 models.

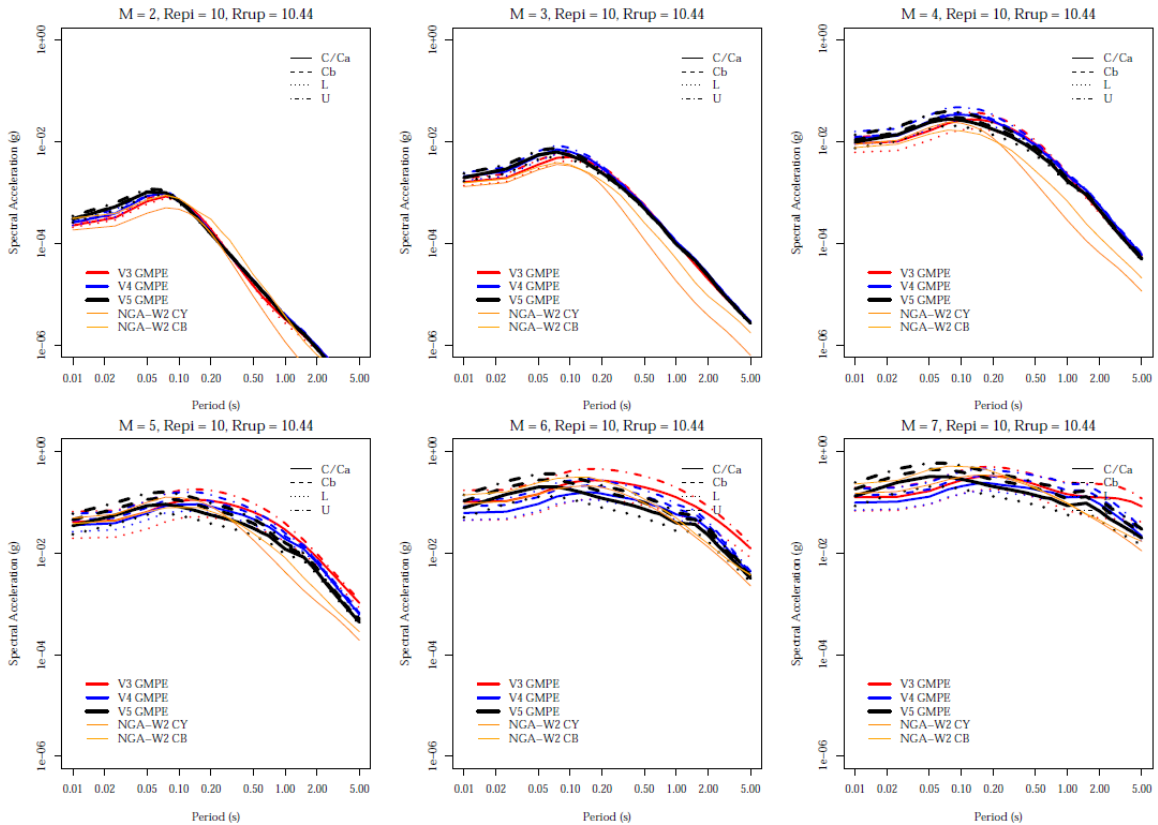


Figure 3.21. Comparison of predicted median spectral ordinates from the V3, V4 and V5 for an epicentral distance of 10 km, together with predictions from two NGA-West2 models.

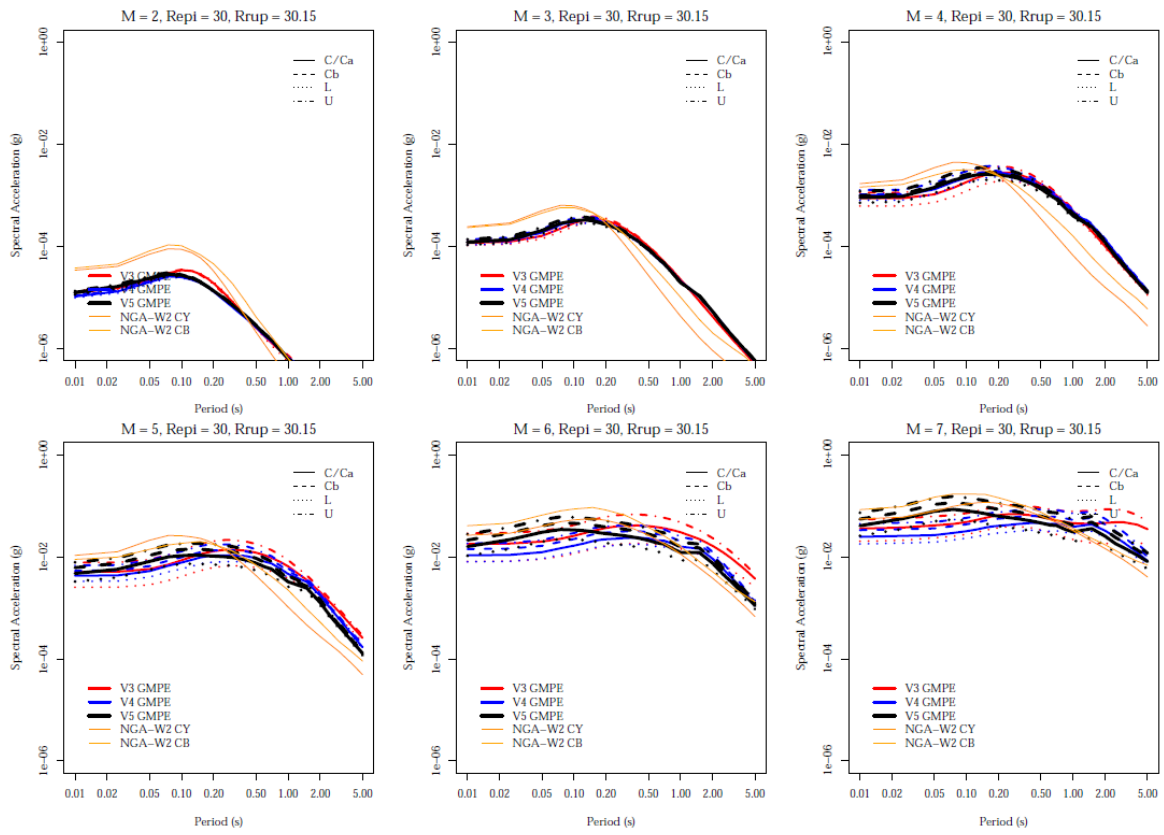


Figure 3.22. Comparison of predicted median spectral ordinates from the V3, V4 and V5 for an epicentral distance of 30 km, together with predictions from two NGA-West2 models.

4. Site Amplification Model

The site amplification model transforms the ground-motion predictions at the NS_B horizon to the ground surface. The framework of the V5 site response model—including the field zonation—is very similar to that of the V4 model, but some subtle differences are discussed in the first three sections of this Chapter. Thereafter, the residuals of the recorded surface motions with respect to the new model are discussed and the chapter closes with a brief comparison between the site response characteristics of the V4 and V5 models.

4.1. Site response analyses

The site response analyses were performed according to the same set-up as for GMM V4 (Bommer *et al.*, 2017b). Several adjustments were made with respect to the input FAS motions at NU_B and their sampling, and to the geomechanic look-up table.

Input motions

A new set of 3,600 input FAS motions at NU_B was used as input for the STRATA site response calculations. These motions span a magnitude **M** range from 1.5 to 7.5 with steps of 0.1 (**M**=1.5-5.0) and 5.25, 5.5, 5.75, 6.0, 6.25, 6.5, 7.0, 7.25, 7.5. The rupture distance ranges from 3.0 to 60 km in 20 log-spaced steps. These ranges enable the derivation of the M-R dependence of AF (section 4.2). The derivation of the new FAS motions is described in Chapter 3.

The set of 3,600 FAS motions was ranked according to their PGA and subsequently divided into 10 groups instead of the 5 groups in GMM V4, because of the much larger number of motions. The FAS motions per group are shown in Figure 4.1 and 4.2.

The required inputs to the STRATA analyses are both an FAS and an estimate of the duration, for which the significant duration corresponding to 5-75% of the total Arias intensity is used. The durations are modelled using the equation of Boore & Thompson (2014) and the averages reported for 50 time-histories randomly generated for each FAS. The significant durations for the corresponding magnitudes in V4 and V5 are similar, ranging from 1.1 to 14 s (median 4.8 s) for V4 and 0.6 to 12 s (median 3.9 s) for V5. The significant durations of the higher magnitudes (**M** 6.25 – 7.5) which were added in V5 are longer, ranging from 5 to 37 s (median 11 s).

The duration was adjusted such that the PGV of the input FAS motion in the RVT-FAS analysis using STRATA corresponded to the PGV of the simulated time signals

(D_{75-5}) using EXSIM that were input for the FAS. The corrected duration D_{corr} is given by:

$$D_{corr} = \frac{D_{75-5}}{0.64} \quad (\text{Eq. 4.1})$$

This correction produces PGVs in STRATA that are a few percent too low for low ranks and a few percent too high for high ranks, apart from the strongest motions (maximum 19%). The median relative difference between PGVs from EXSIM and PGVs from corrected durations in STRATA for all ranks is -0.5%.

One motion per group of ranked motions was randomly selected as input motion for each voxel stack, corresponding to 10 STRATA calculations per voxel stack as compared to 5 in GMM V4. The sampling of all signals for all calculations is shown in Figure 4.3. On average, each motion is sampled 391 ± 20 times. The sampling of FAS motions of two small and two large zones is shown in Figure 4.4. Because of the much larger number of motions divided into 10 groups, not all motions are sampled in the smaller zones (top panels of Figure 4.4). All motions are sampled in the larger zones (bottom panel of Figure 4.4). Overall, the selection of the NS_B motions for input to the site response analyses was judged to be sufficiently random.

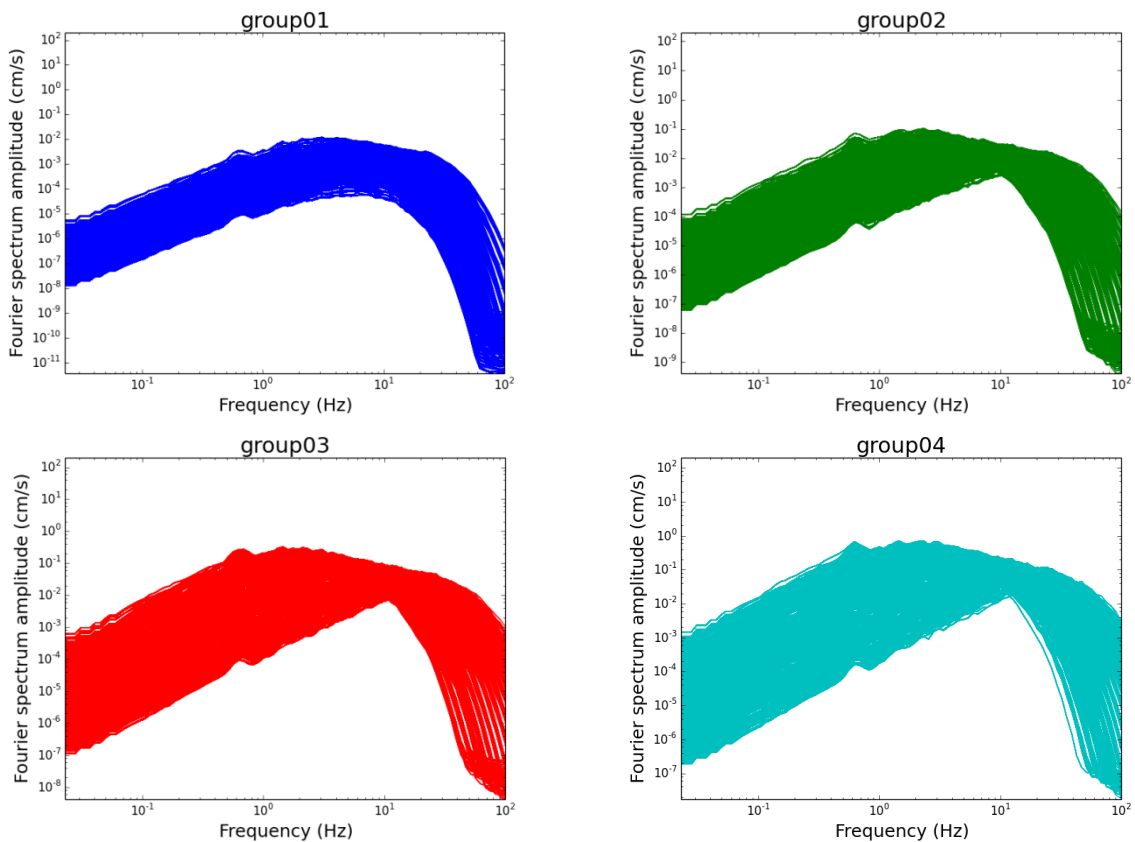


Figure 4.1. FAS generated at the NS_B horizon for use in RVT-based site response analyses for groups 1 to 4

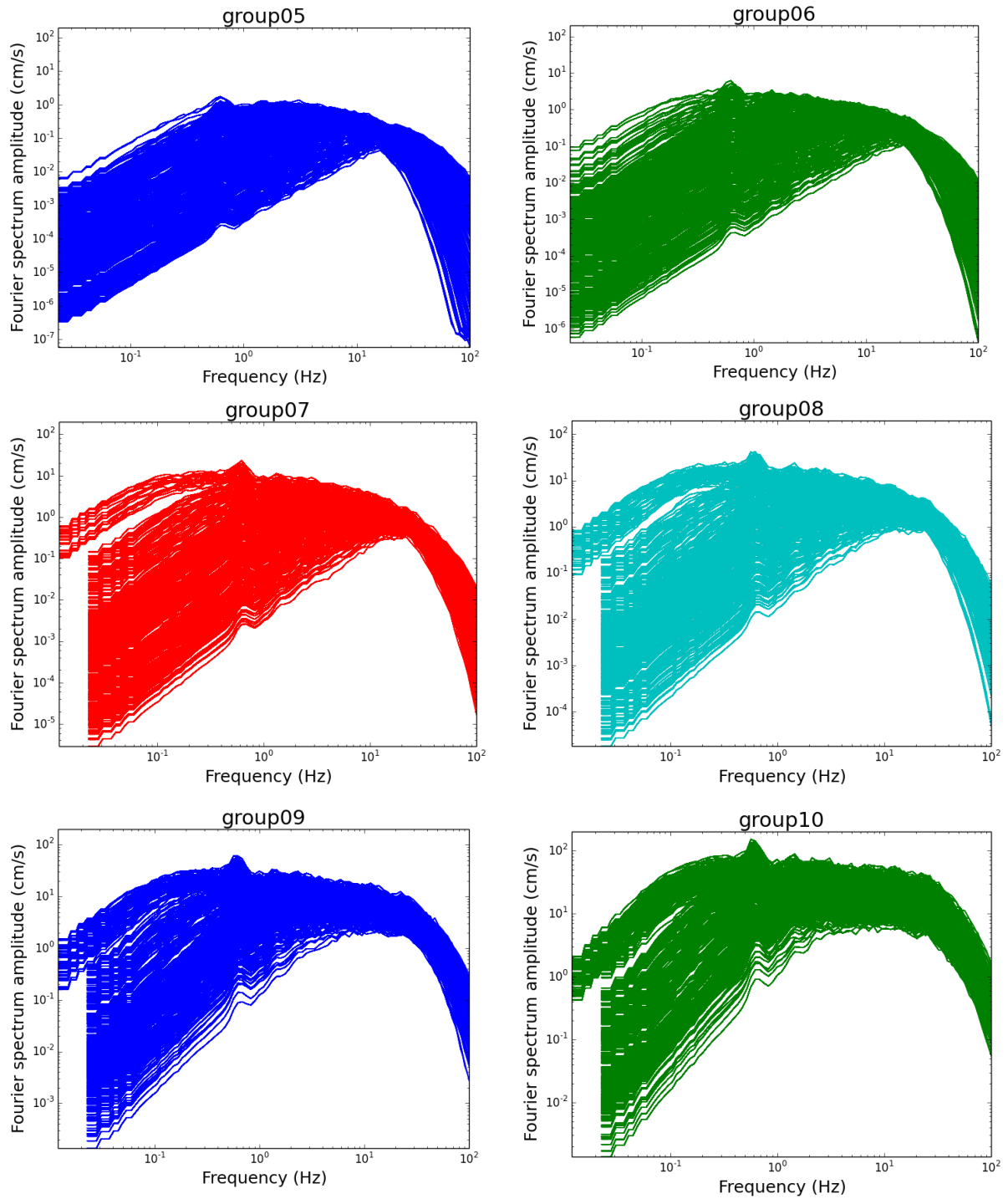


Figure 4.2. FAS generated at the NS_B horizon for use in RVT-based site response analyses for groups 5 to 10.

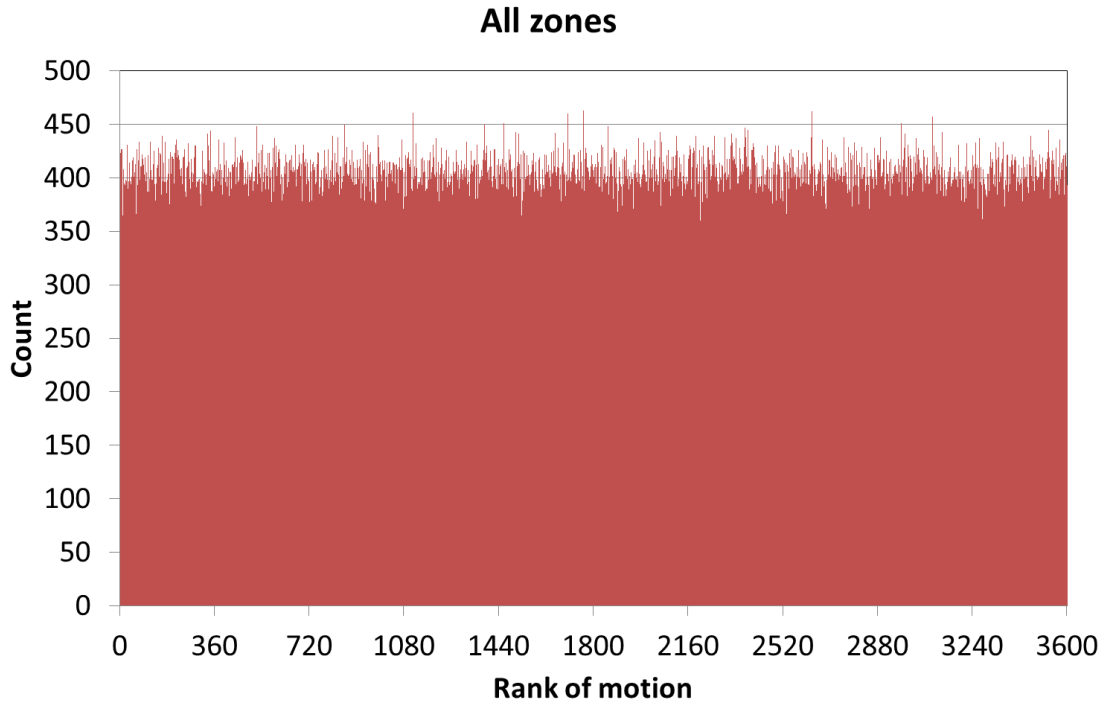


Figure 4.3. Sampling of the 3,600 NS_B FAS in the site response analyses over the whole field

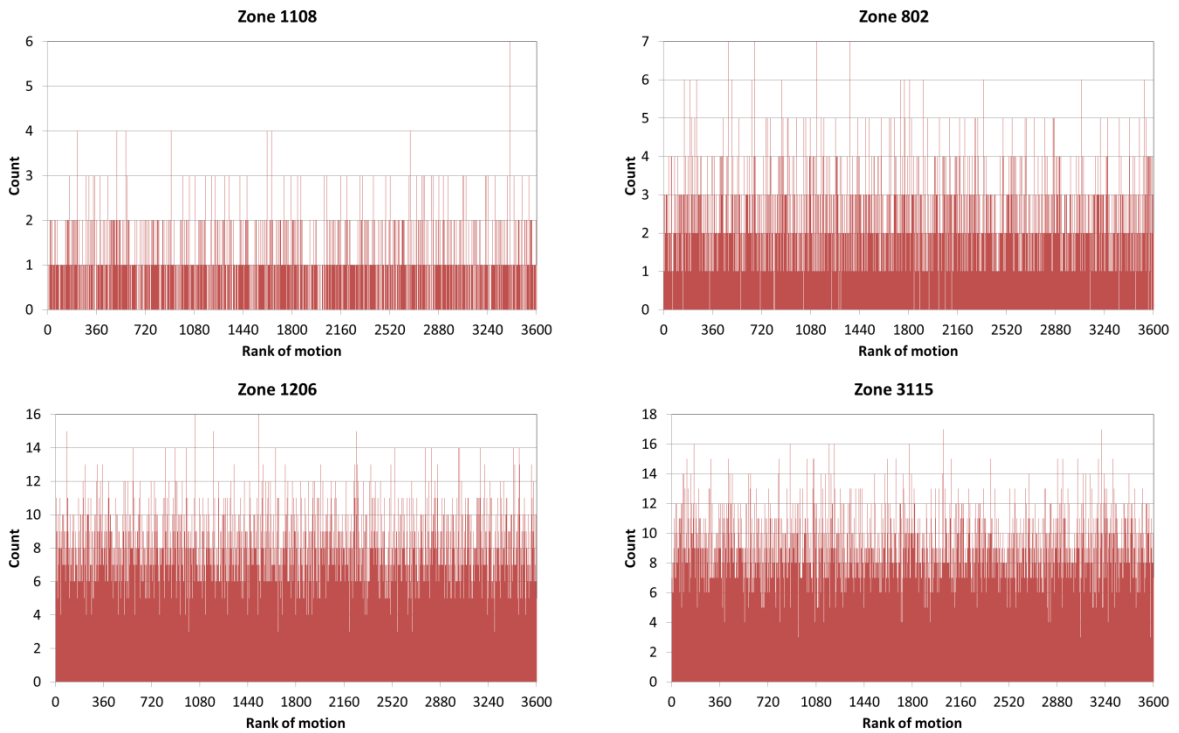


Figure 4.4. Sampling of the 3,600 NU_B FAS in the site response analyses for four of the geological zones. Top panels show the sampling for two small zones, bottom panels the sampling for two large zones.

Update of geomechanic look-up table

Results from laboratory test from Groningen samples became recently available (van Essen, 2017). The samples were taken at the Eemskanaal levee in the province of Groningen, in the toe and the crest of the levee. Cone penetration tests were also performed at these locations. The combination of laboratory data and CPT soundings enables the calibration of empirical relations between CPT parameters and undrained shear strength S_u for Groningen for the sampled stratigraphy-lithology combinations. The empirical relations were updated for three soil types: Naaldwijk clay, Holland peat and Basal peat.

For Naaldwijk clay, the relation $S_u = q_{net}/17$ follows the laboratory derived S_u much better than the earlier assumed $S_u = q_{net}/14$ (Figure 4.5). The empirical relation between S_u and vertical effective stress σ'_{v0} for V5 has been based on the CPT data set using $S_u = q_{net}/17$. The CPT based data were used rather than the laboratory data, because the CPT data represent a much larger data set and cover a larger vertical effective stress range.

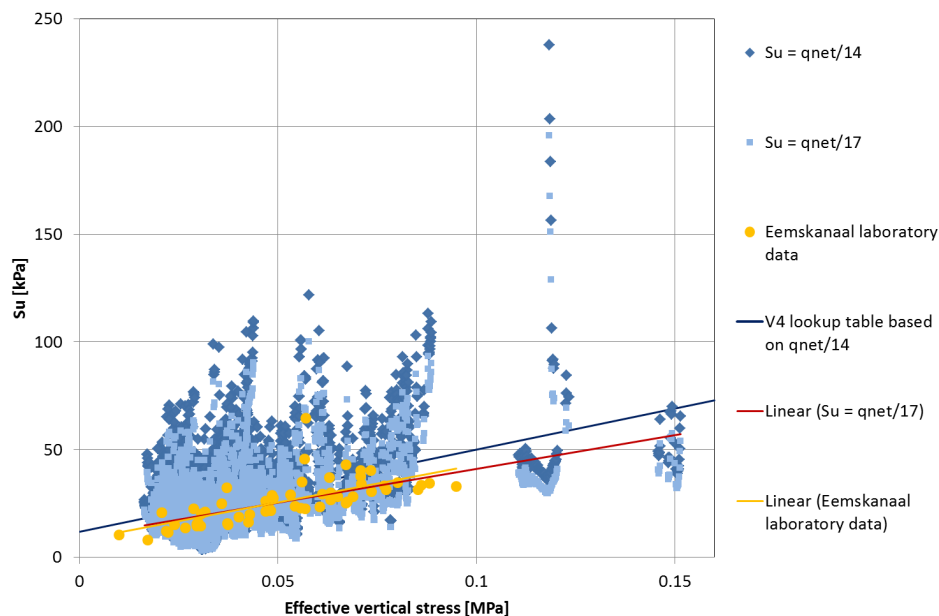


Figure 4.5. CPT derived and laboratory data for S_u for Naaldwijk clay (NA), including linear regression lines.

For other types of clay, the laboratory data were insufficient to justify a deviation from earlier assumed $S_u = q_{net}/14$. Therefore, no changes relative to GMM V4 were made for clays, other than Naaldwijk clay.

The Holland peat and Basal peat are well represented in the laboratory data and less abundant in the CPT data set. The data are shown in Figures 4.6 and 4.7 for Holland peat and Basal peat respectively. In both cases, the laboratory data are regarded as

better representatives of S_u values than the CPT-derived S_u . Therefore, the updated empirical relation between S_u and vertical effective stress σ'_{v0} for V5 has been based on the linear regression through the laboratory data.

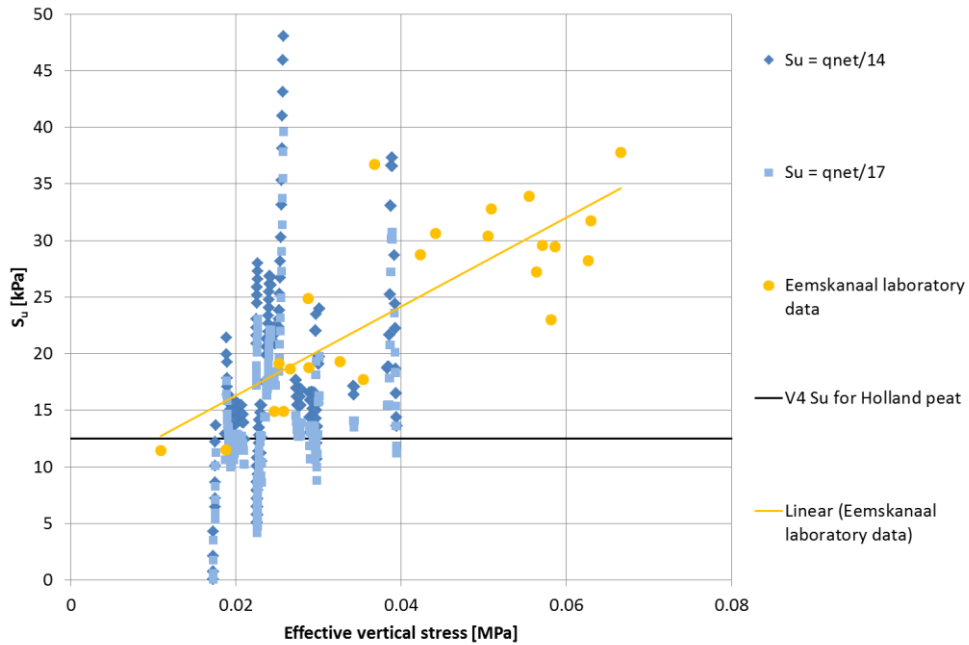


Figure 4.6. CPT derived and laboratory data for S_u for Holland peat (NIHO), including V4 relation and linear regression line through laboratory data for V5.

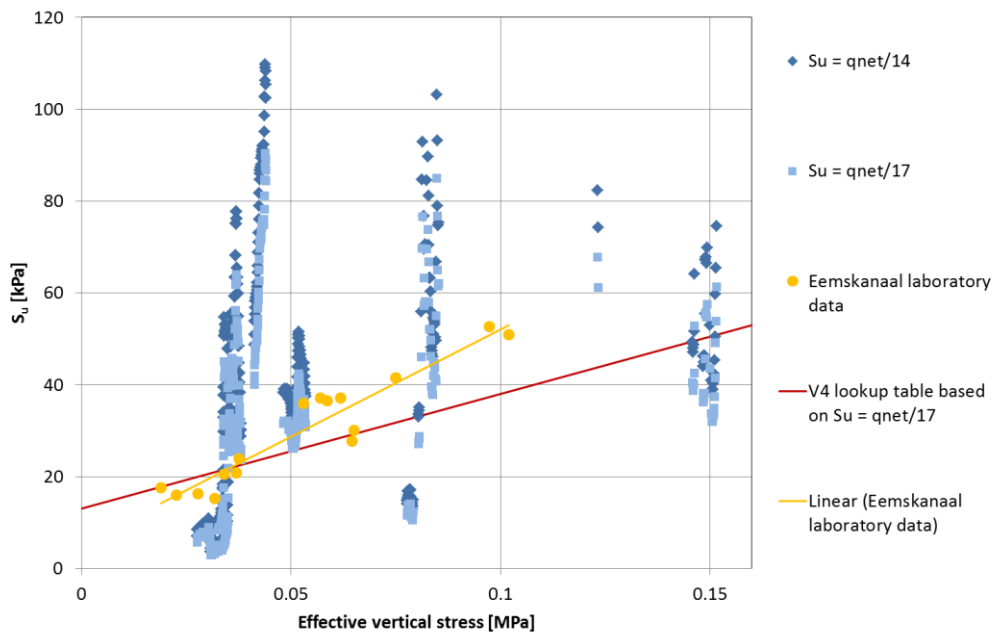


Figure 4.7. CPT derived and laboratory data for S_u for Basal peat (NIBA), including V4 relation and linear regression line through laboratory data for V5.

The updated empirical relations are summarised below and replace the equations in Tables V.3 and V.4 in Appendix V of the GMM V4 report (Bommer *et al.*, 2017b):

- Naaldwijk clay (NA): $S_u = 0.31 \sigma'_{v0} + 10$ [in kPa]
- Holland peat (NIHO): $S_u = 0.39 \sigma'_{v0} + 8$ [in kPa]
- Basal peat (NIBA): $S_u = 0.47 \sigma'_{v0} + 5$ [in kPa]

Update of MRD curves for Groningen peat

Additional tests were being conducted on Holland peats that were sampled in the field at three locations in Groningen (Zwanenburg & Konstantinou, 2016; Zwanenburg *et al.*, 2017). The MRD curves were determined in lab experiments. Several tests were performed to cover the full strain range in order to construct the Groningen specific MRD curves for Holland peat. In total 20 k_0 -CRS tests, 20 static Direct Simple Shear tests, 26 Resonant column tests and 10 cyclic Direct Simple Shear tests have been conducted at Ruhr Universität Bochum, Norwegian Geotechnical Institute and Deltares. The lab program also provided additional information about the undrained shear strength of Holland peat. The test results were used to improve the geomechanic input parameters and to adjust the parameters for the Darendeli type formulae for Holland peat in V5 as follows:

- For the modulus reduction curve:
 - $\gamma_{ref} = 2\%$, independent of the consolidation stress.
 - $a = 0.8$
- For the damping curve, retain the previous V4 values:
 - $D_{min} = 2.512 \cdot (\sigma'_{v0}/p_a)^{-0.2889}$.
 - $b = 0.712$.

The MRD parameter values for the older Basal peat were not adjusted, because these were not tested in the lab and they behave different from Holland peat due to the recent sediment load.

4.2. Zonation and amplification factors

The V4 zonation was preserved for the V5 GMM. Moreover, the approach used to compute the amplification functions for the zones was similar to that for the V4 GMM, with the only change being the functional form of the linear part of the amplification factors (AF). These changes were introduced because the analyses performed in the V4 GMM led to persistent biases between the AFs computed for the stations and the AFs computed for the zones. This bias was determined to arise from a poor characterisation of the magnitude and distance dependence of the AFs.

The magnitude and distance dependence in the AFs is discussed at length in Stafford *et al.* (2017), who suggest that for magnitudes between about 2.5 and 4.5, the elastic AFs have a nearly linear dependence on magnitude and distance. These

conclusions are based on numerical and theoretical analyses and are backed by empirical data from the KiK-net array. In the V4 GMM, the magnitude and distance dependence for the zones could not be fully captured because the sampling of magnitude and distance of the input motions was not sufficiently broad. In the V5 GMM model, the sampling of magnitude and distance covers the entire range of interest for the hazard model (see Section 4.1).

The model for the AF of the zones is given below. These equations replace Eqs.(8.4) to (8.7) of the V4 GMM report. For each zone and each response period (including PGV), the median amplification factor is given by:

$$\ln(AF) = f_1^* + f_2 \ln\left(\frac{Sa_{NS_B,g} + f_3}{f_3}\right) \quad (4.2)$$

where f_2 and f_3 are model parameters, and $Sa_{NS_B,g}$ is the spectral acceleration at the NS_B horizon and is given in units of g (the acceleration of gravity). When the equation is applied to PGV, $Sa_{NS_B,g}$ is replaced by PGV_{NS_B} in units of cm/s. The parameter f_1^* is magnitude-and distance-dependent. For spectral acceleration, it is given by:

$$f_1^* = [a_o + a_1 \ln(R)] + [b_0 + b_1 \ln(R)][\min(M, M_{ref}) - M_{ref}] \quad (4.3)$$

where M is moment magnitude (**M**), R is closest distance in km, a_o , a_1 , b_0 , and b_1 are model parameters, and M_{ref} is given by:

$$M_{ref} = M_1 - \frac{\ln(R) - \ln(3)}{\ln(60) - \ln(3)}(M_1 - M_2) \quad (4.4)$$

where M_1 and M_2 are model parameters.

For PGV, the parameter f_1^* is given by:

$$f_1^* = \begin{cases} [a_o + a_1 \ln(R)] + [b_0 + b_1 \ln(R)](M - M_{ref}) & \text{for } M \leq M_{ref} \\ [a_o + a_1 \ln(R)] + d(M - M_{ref}) & \text{for } M > M_{ref} \end{cases} \quad (4.5)$$

where $M_{ref} = M_1$ and a_o , a_1 , b_0 , b_1 , d , and M_1 are model parameters. Each of the model parameters in Eqs.(4.3) to (4.5) are oscillator-period dependent. The model is only applicable for $M \geq 2$. In addition, the amplification factor $\ln(AF)$ in Eq.(4.2) is subject to both upper and lower limits, AF_{max} and AF_{min} . These limits are the same as those applied to the AFs in the V4 GMM model. The linear portion of the model (Eqs. 4.3 and 4.5) was also used to compute the linear AFs for the stations (see Figure 2.7).

The parameters of Eqs.(4.2) to (4.5) were obtained in a similar manner as in the derivation of the V4 GMM. The parameters were obtained from maximum likelihood

regressions of the AFs computed from the site response analyses described in Section 4.1. Since some of the parameters have interdependences, some constraints were placed on these parameters. Namely, parameter f_3 is chosen from a preliminary analysis and is assumed to be the same for all zones. Parameters M_1 , M_2 , a_1 , b_1 , and f_2 were smoothed sequentially (one at a time) after initial regressions. Parameters M_1 , M_2 , a_1 , and b_1 were also constrained to be within the 5th and 95th percentiles of their respective values computed for all the stations. After each smoothing, the regression analyses were repeated.

Figure 4.8 shows the amplification factors for all the zones for a magnitude of **M** 4.5 and a distance of 5 km. These AFs can be compared with the V4 AFs shown in Figure 9.5 from the V4 GMM report (Bommer *et al.*, 2017b). Figure 4.9 plots the ratios of AFs of the V5 divided by the V4 model for four magnitude-distance combinations. The lower AFs at short periods were expected because of the positive bias with respect to recorded motions that was seen in the residuals of the V4 GMM model and which has been addressed in the V5 model development. For periods longer than about 0.2 seconds, the AFs in the V5 GMM are only slightly (less than 5%) lower than in the V4 GMM model.

Figure 4.10 plots the AFs for all the zones in the Groningen field for a fixed scenario (**M** = 4.5 and **R** = 5 km) and selected periods. The spatial distribution of AFs is similar to that observed in the V4 GMM (Figure 9.18 in Bommer *et al.*, 2017b).

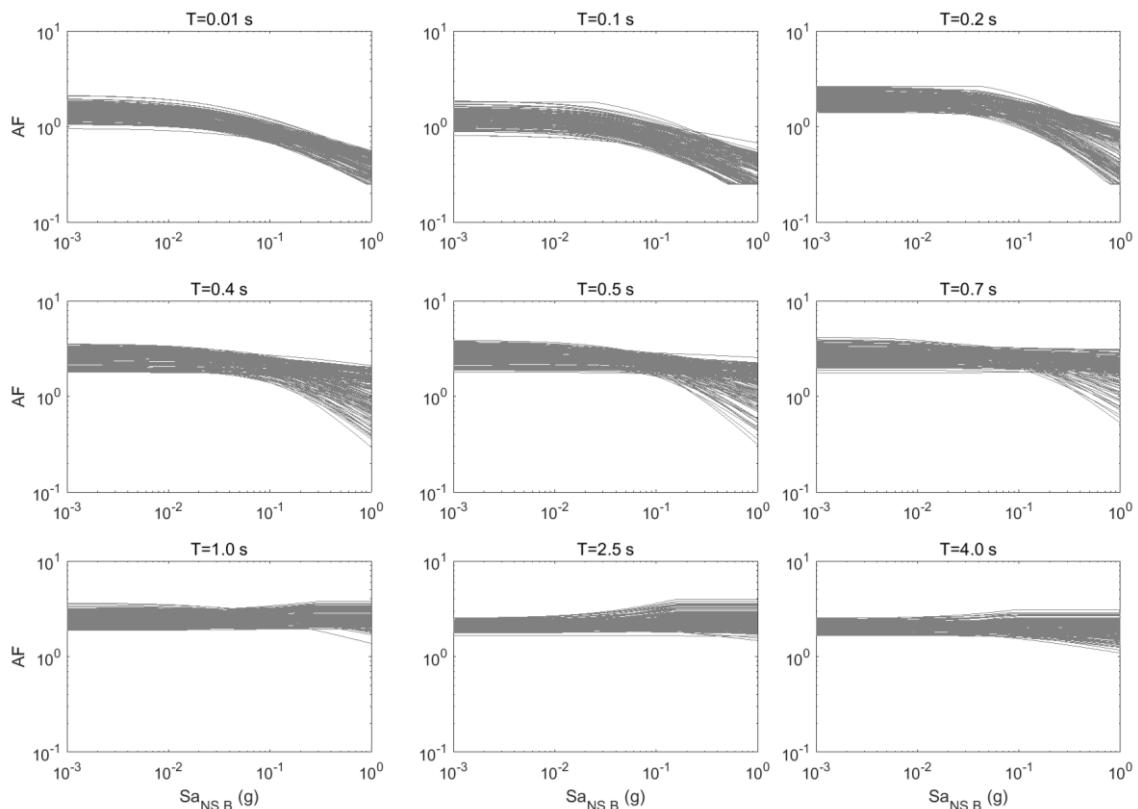


Figure 4.8. Fitted AF functions for all zones for selected periods (for $M=4.5$ and $R=5$ km)

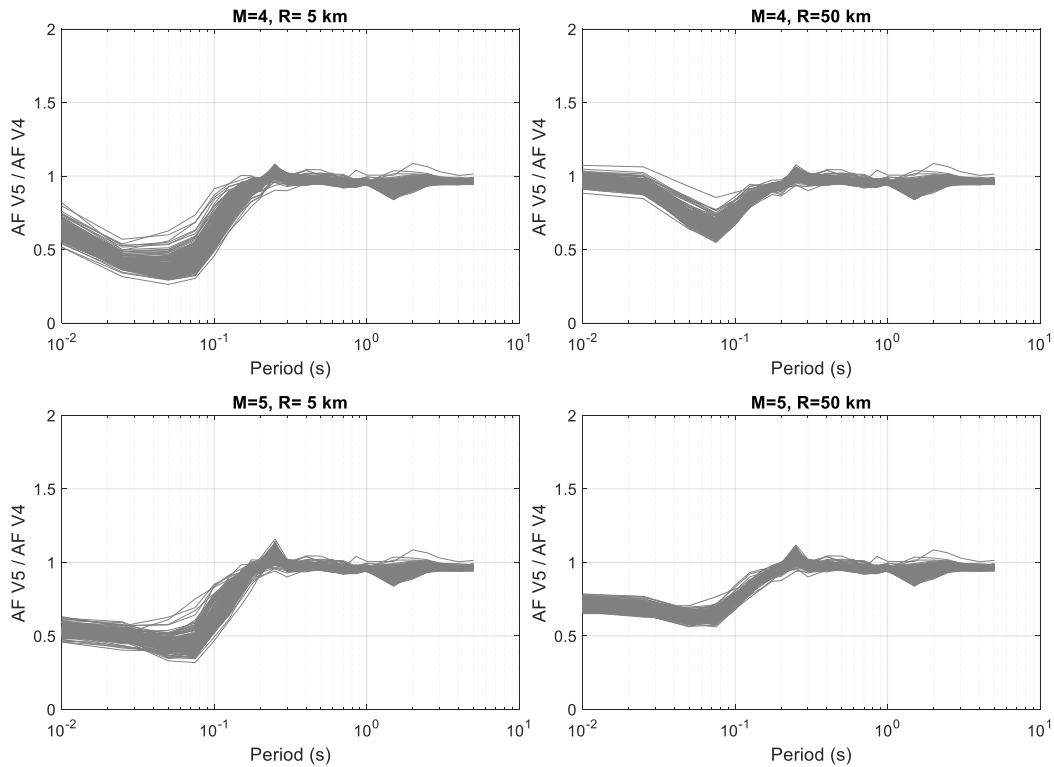


Figure 4.9. Ratios of AFs of V5 GMM over V4 GMM for all the zones. Each plot corresponds to a selected magnitude/distance combination. Spectral accelerations at rock were selected using the V5 GMM rock model.

An important check for the model validity is that the AFs computed for a station for the magnitude-distance combinations of recorded motions should fall within the range of site-to-site variability of the corresponding zone AFs. Figure 4.11 shows this comparison for two selected stations. Additional figures for other station/zone combinations are given in Appendix V. In general, the station AFs are within a range of two standard deviation of the zone AFs, however, there are some biases that are seen at very low periods (zone AFs are lower than station AFs), and at a period of about 0.1 seconds (zone AFs are higher than station AFs). These differences occur because of deviations from the assumed linearity of AFs with respect to magnitude and distance.

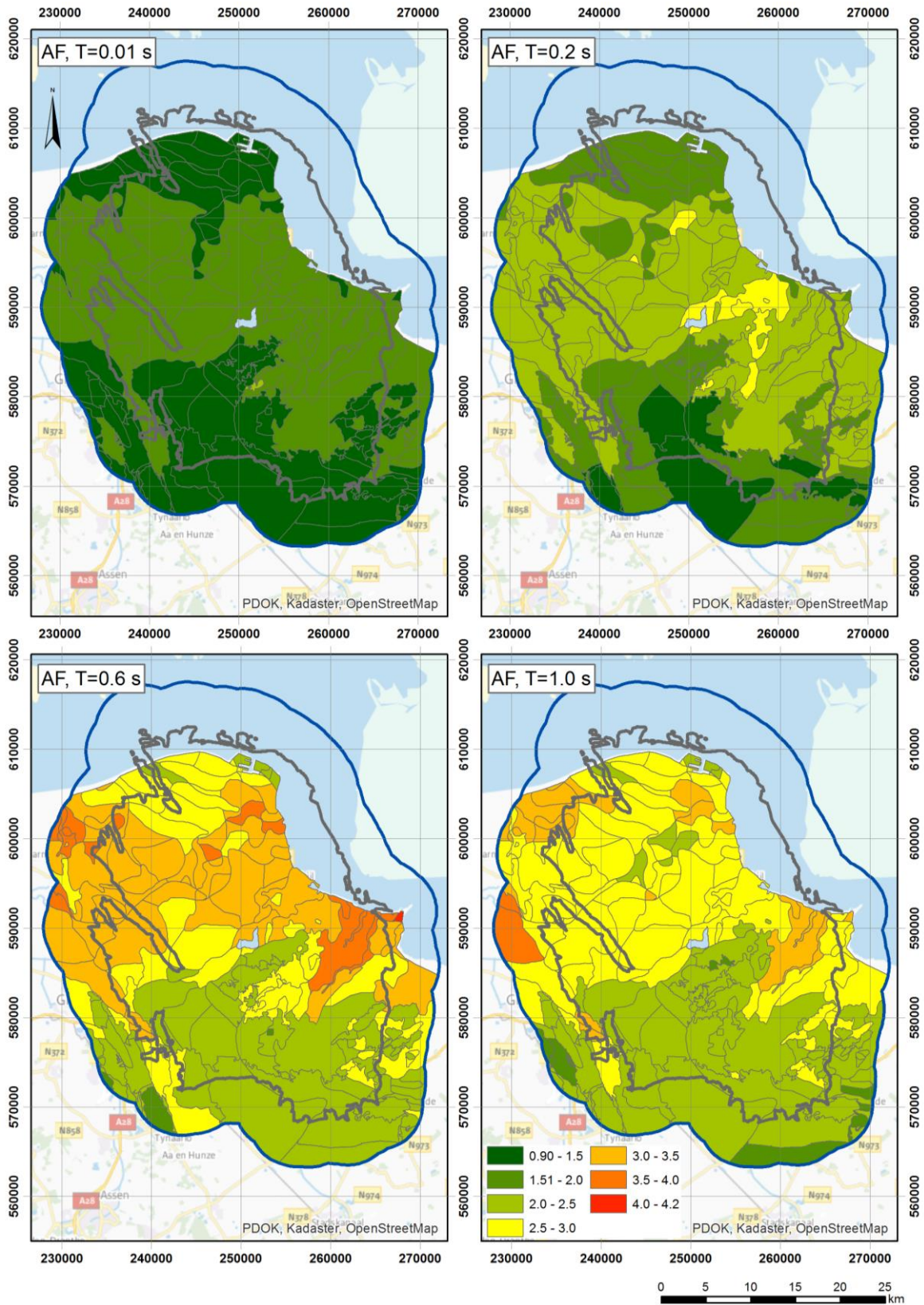


Figure 4.10. Weak motion AFs (e^{f1^*}) for the zones in the Groningen region. The AFs are shown for a $M=4.5$, $R=5$ km scenario and selected periods

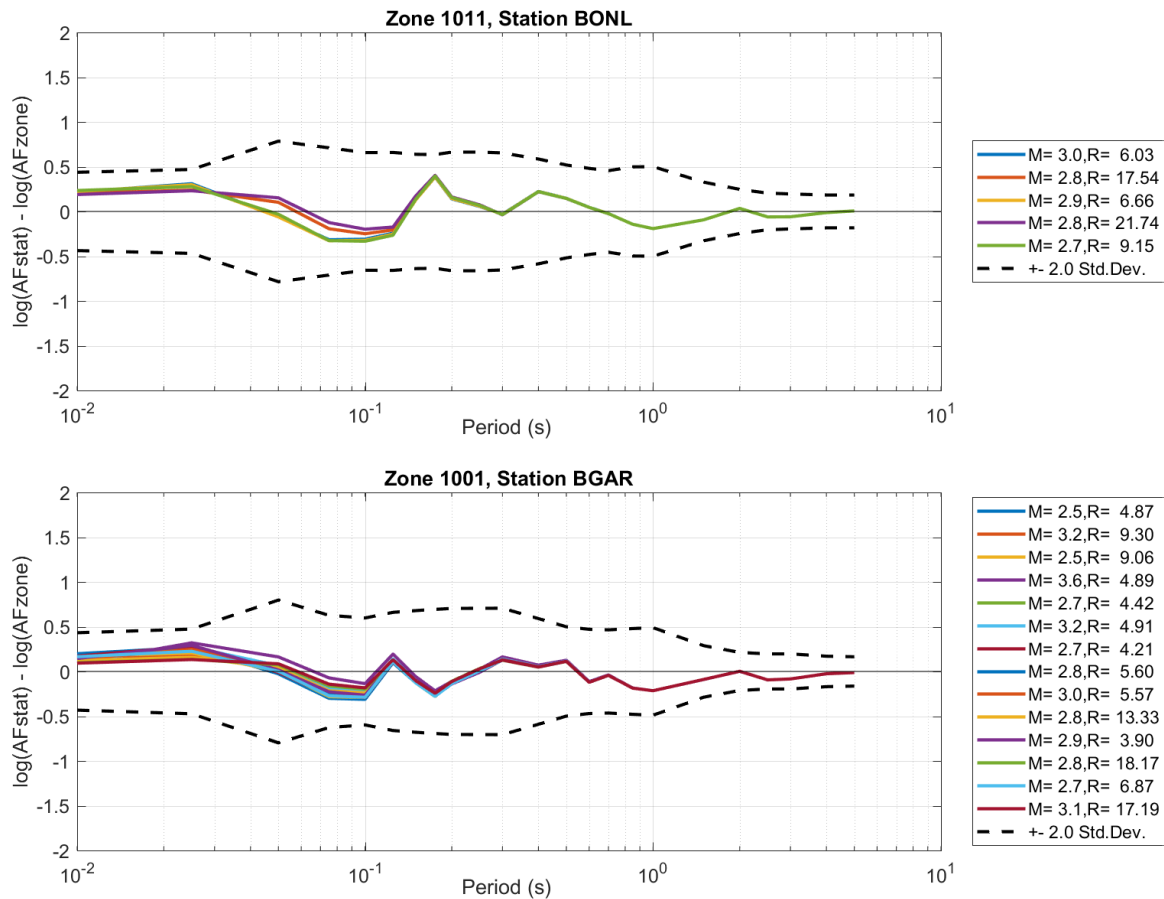


Figure 4.11. Comparison of linear AF for selected stations and the corresponding zone where the station is located. AFs are shown for the magnitude and distance pairs that correspond to recorded motions at each station. Similar plots for all other B-station recordings are given in Appendix V.

4.3. Variability associated with AFs

The model for site-to-site variability (ϕ_{S2S}) was developed in a similar way as for the V4 GMM, with the only difference being that in the V4 GMM model, the ϕ_{S2S} for large values of Sa_{NS_B} ($\phi_{S2S,2}$) was constrained to always be higher than or equal to the value for low values of Sa_{NS_B} ($\phi_{S2S,1}$). This constraint was not applied in V5 GMM because often the uncertainty at low intensities was larger than at high intensities because of the complexity resulting from magnitude and distance dependence. Figure 4.12 plots the difference in ϕ_{S2S} values between V5 GMM and V4 GMM. Overall, the values of $\phi_{S2S,1}$ for periods lower than about 0.2 seconds increased with respect to the V4 GMM. On the other hand, values of $\phi_{S2S,2}$ are generally the same for both models at longer periods.

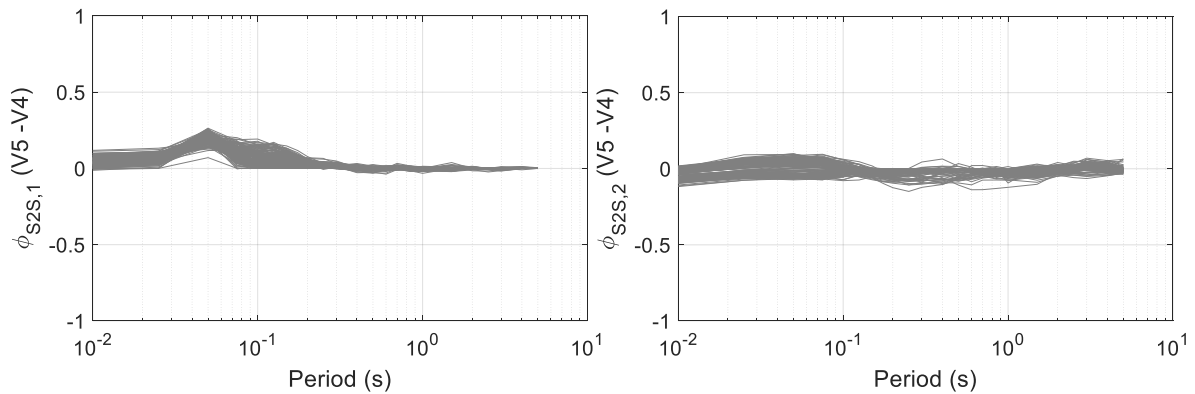


Figure 4.12. Difference in ϕ_{S2S} values between the V5 GMM and the V4 GMM. The plot on the left is for low intensity values ($\phi_{S2S,1}$), and the plot on the right is for high intensity values ($\phi_{S2S,2}$).

The values of $\phi_{S2S,1}$ for all the zones in the Groningen region are shown in Figure 4.13. The spatial distribution of these values is similar to the distribution in the V4 GMM (see Figure 9.19 in Bommer *et al.*, 2017b).

4.4. Surface residuals of Groningen recordings

Residuals have been calculated at the surface by first calculating the residuals at the NS_B horizon (see Section 3.4) and then subtracting these from the total residuals. Plots showing the residuals de-composed into between-event and within-event components at the NS_B, and the site response residual at the surface, are shown for all 24 amplitude-based parameters in Appendix VI. Overall, the residuals are well behaved, showing no trends and, at longer periods, rather small scatter. Bearing in mind the process of building the model and the use of zone-wide AFs in forward modelling, the fit to the surface recordings is remarkably good.

In the V4 model, it was noted that at short periods, there was overestimation due to M-R dependence of the AFs not being well captured; Figure 4.14 shows that in the V5 model, this issue has been resolved. This was a key objective of V5 GMM development stage.

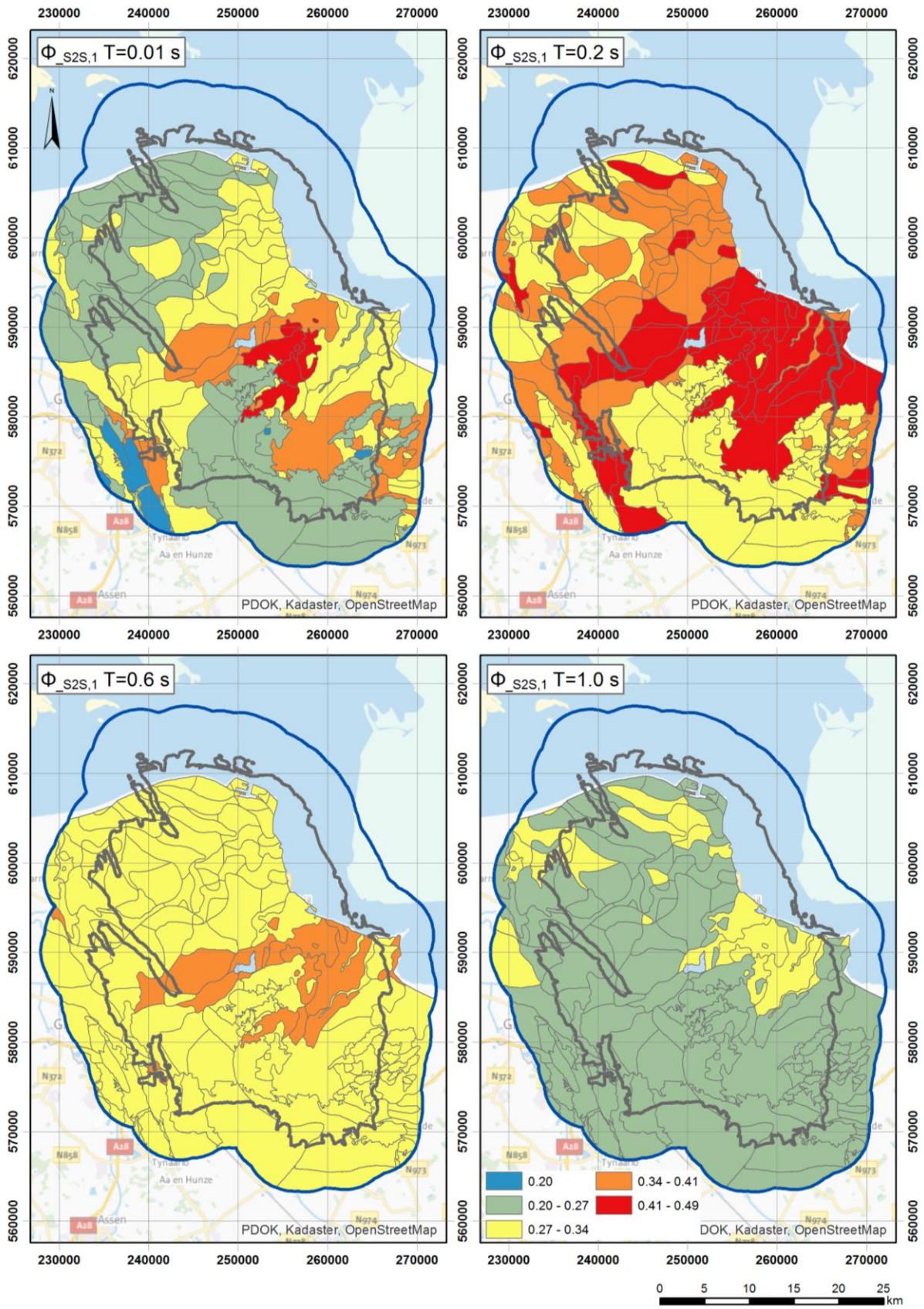


Figure 4.13. $\phi_{s2s,1}$ values for selected period and for all zones in the Groningen region

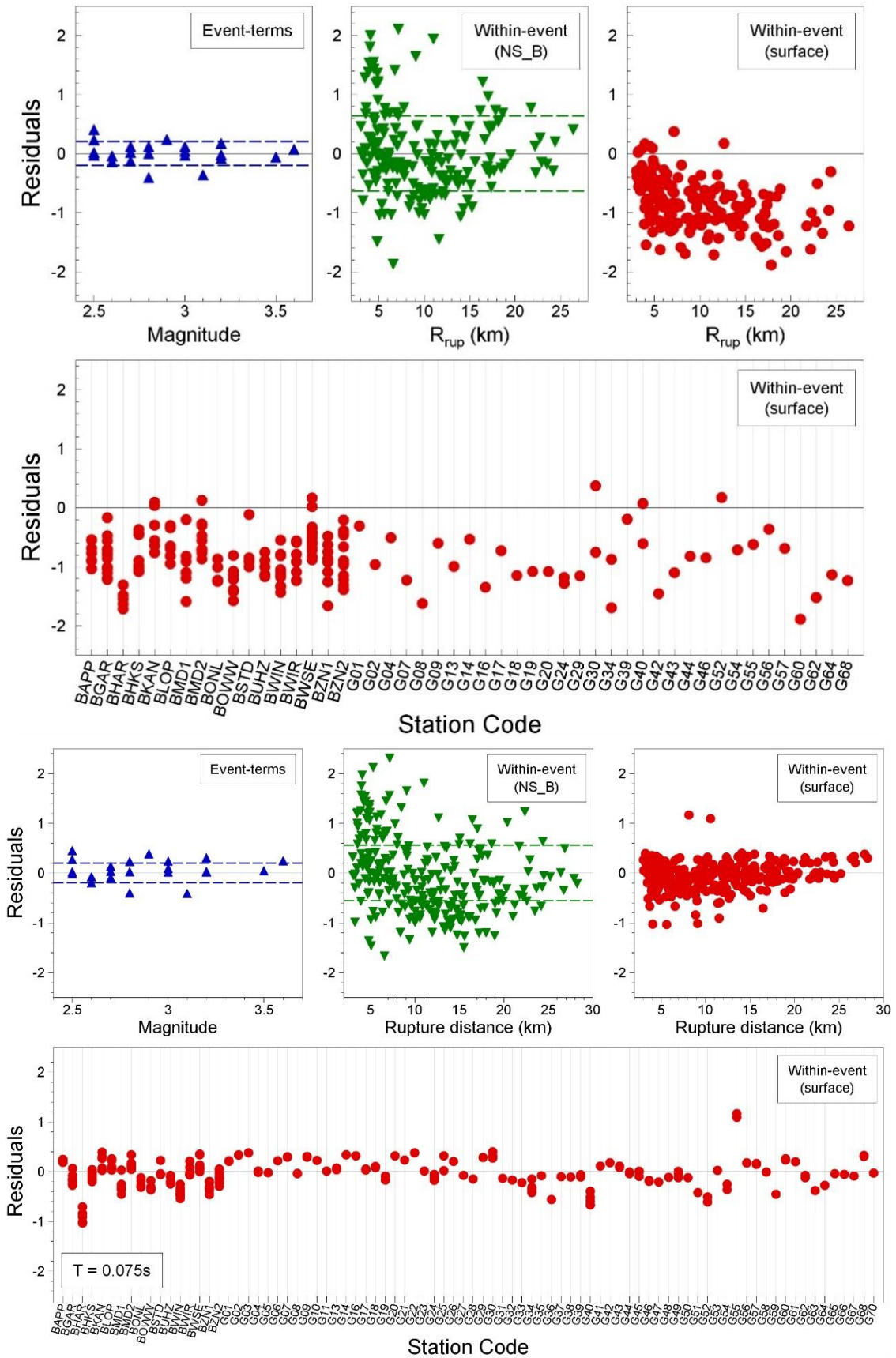


Figure 4.14. Decomposed residuals of surface motions for Sa(0.075s) from the V4 (*upper*) and V5 (*lower*) models

4.5. Comparison with V4 AFs and GMM

Appendix VII shows plots of the predicted median response spectra from the V5 model at the ground surface together with the motions at the NS_B horizon, the latter to illustrate the effects of the amplification factors. In each of these plots, the surface motions from the V4 GMM are also shown for comparison. For the smaller magnitudes, predictions from the V3 are also included; however, because that model was based on point source representation of earthquakes, larger magnitudes require assumptions regarding the conversion from R_{epi} to R_{rup} that make meaningful comparisons very difficult.

The general pattern observed between the predictions from the V4 and V5 models is that the latter predicts lower amplitudes at the surface. This reduction is not primarily due to changes in the site amplification model since median AFs have mostly reduced slightly (see Figure 4.9 and specific examples in Figure 4.15) and the site-to-site variability has increased a little (see Figure 4.10 and specific examples in Figure 4.16); these two changes will, to some extent, cancel each other out. The main reason for the lower predicted surface motions is the changes to the NS_B model (Section 3.5), in which amplitudes dropped mainly because of the updated magnitude scale correlation and, to a lesser extent, because of the inclusion of the data from the 2017 Slochteren earthquake.

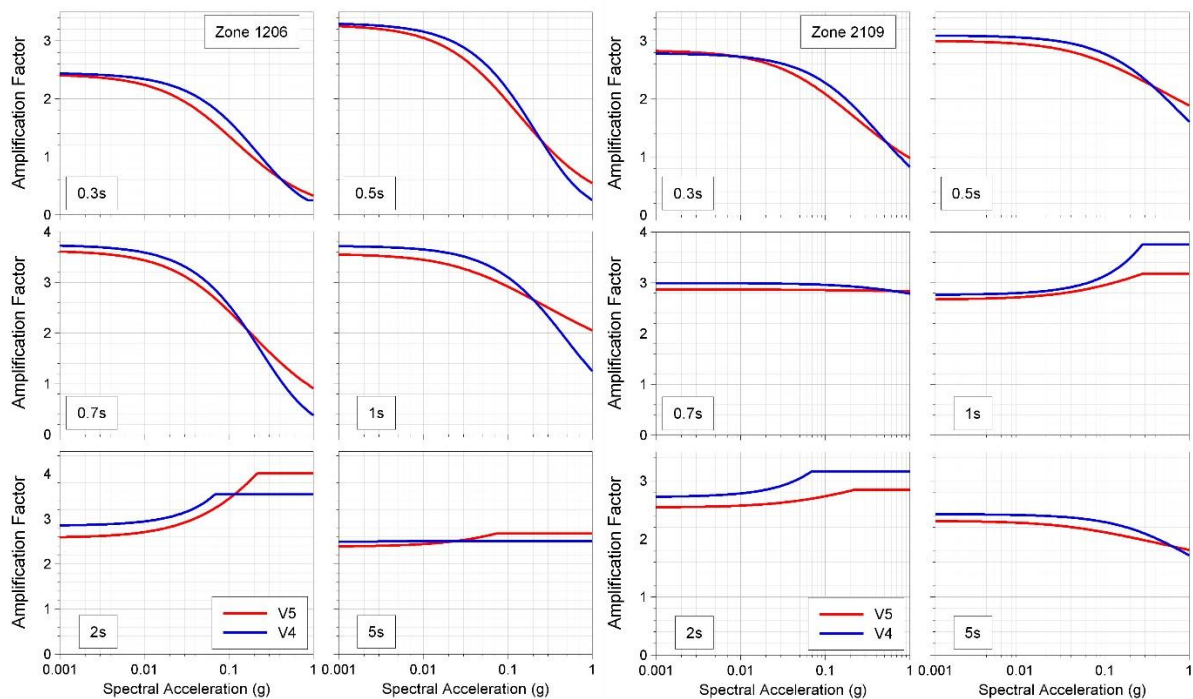


Figure 4.15. Comparison of median AFs from the V4 (blue) and V5 (red) models at six response periods. *Left:* Zone 1206, *Right:* Zone 2109.

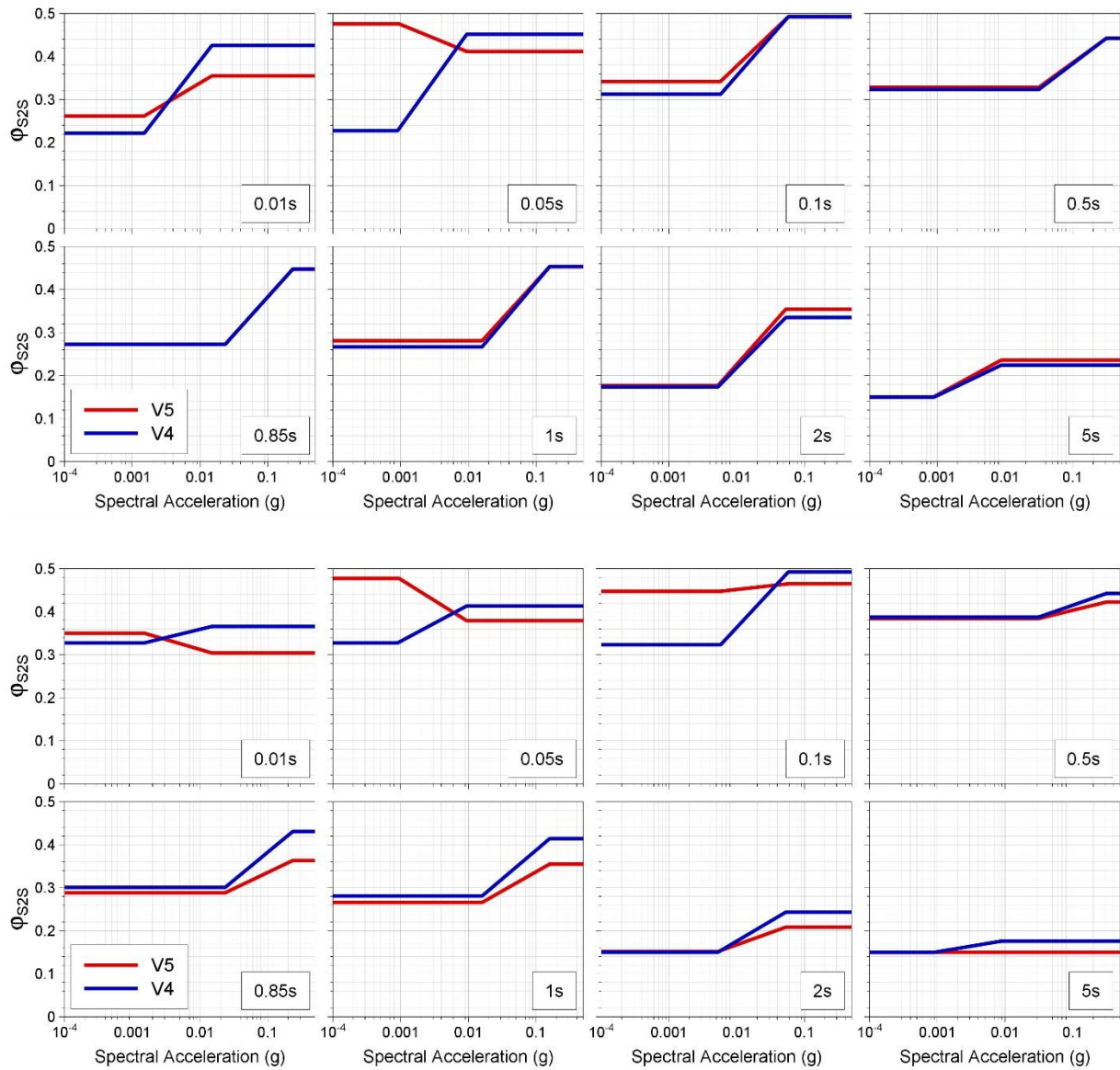


Figure 4.16. Comparison of site-to-site variability from the V4 (blue) and V5 (red) models at six response periods. *Upper*: Zone 1206, *Lower*: Zone 2109.

5. Duration Model

As has been noted earlier in Chapter 2, for some building types in the Groningen exposure database the fragility functions are defined in terms of both spectral accelerations and the duration of the ground shaking, for which the significant duration defined between 5% and 75% of the total Arias intensity is adopted as the preferred definition.

The general approach used to derive the V5 duration model was essentially the same as that used in the V4 model development; this chapter briefly explains the subtle differences and then compares the results from the two models.

5.1. Derivation of updated model

The duration model was developed by performing regression analyses directly upon the outputs of the EXSIM simulations. This is the same process as was followed during the development of the V4 duration model. The EXSIM simulations use the prediction equation originally developed for use in the V3 model to describe the durations of time-series originating from each sub-source of the finite fault ruptures represented by EXSIM. This V3 model has previously been shown to work well for small events and is able to capture some important field-specific attributes of the path scaling. However, the V3 duration model performed poorly when extrapolated to the prediction of large-magnitude, long-distance scenarios. The approach of using EXSIM to generate synthetic accelerograms and fitting the duration model to these outputs performed well for the V4 duration model and so the approach was retained for the V5 model.

Figure 5.1 presents an example of the duration values derived from the EXSIM simulations plotted against distance for three magnitude values. A noteworthy feature of the durations obtained from the EXSIM simulations is that the rate of duration increase with distance reduces as the magnitudes increase. This magnitude-dependence of the distance scaling of duration is consistent with what is commonly observed from tectonic earthquakes.

The simulated duration values shown in Figure 5.1 represent part of a much larger database of simulated duration values. In total, 436,800 simulated durations were generated for each of the four model branches and these simulated data and thereafter regarded as 'empirical data' for the purposes of developing the V5 duration model. That is, the duration model arises from a regression analysis conducted treating the EXSIM duration outputs as observed duration values. However, the variance components for the duration model are obtained by making use of the real observed duration values from the Groningen field.

As the overall process adopted for the development of the V5 duration model is the same as that for the V4 model, the main differences arising between the V4 and V5 duration models therefore relate to the fact that source durations are sensitive to level of stress drop. As the V5 model adopts a new set of stress drop branches the duration model is updated to reflect these new branches. Furthermore, the additional ground-motion recordings used in the V5 database dictates that the estimates of the variance components differ between the V4 and V5 models.

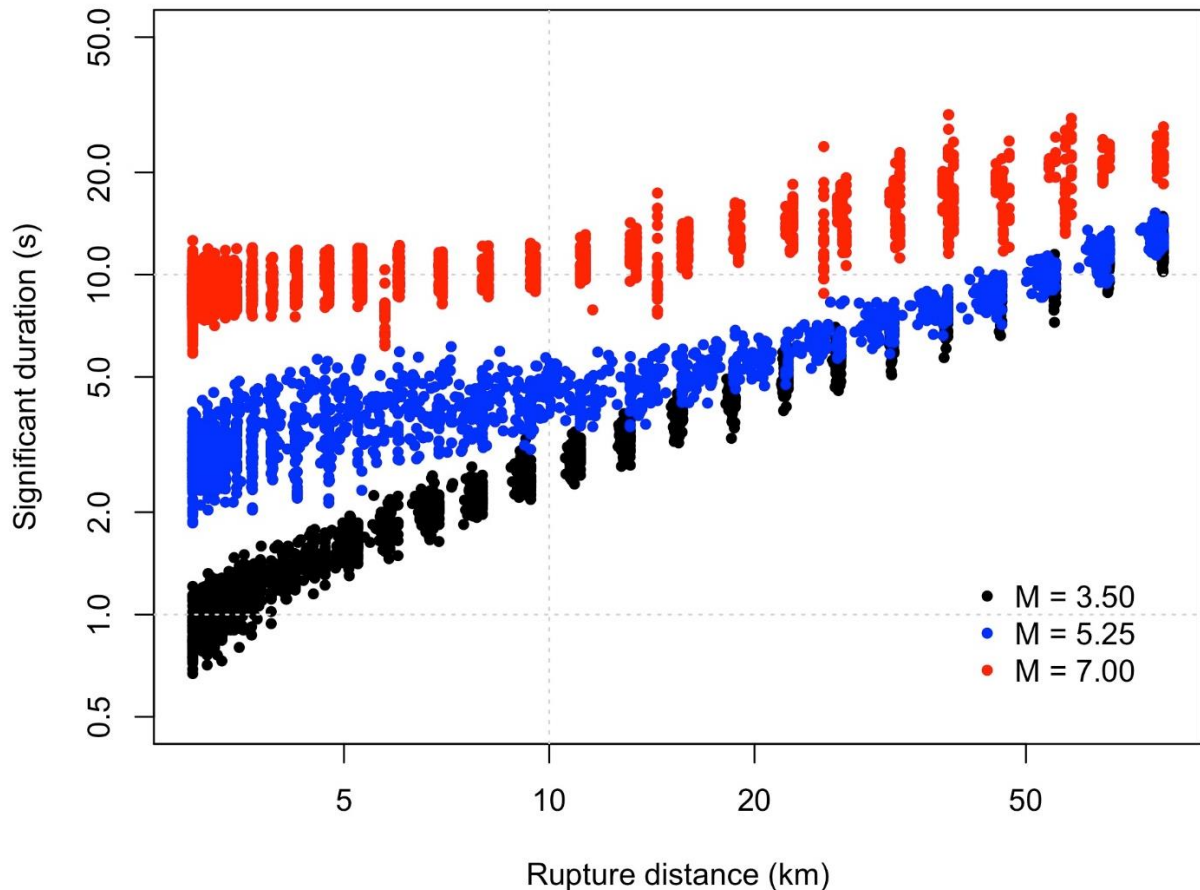


Figure 5.1. Example significant duration values derived from EXSIM simulations for three magnitude values.

The functional form used for the duration model remains the same as that in the V4 model, but the magnitudes at which fundamental changes in scaling take place have been modified slightly. This modification reflects the adjustment to the relationship between local and moment magnitudes used in the V5 model. For both the V4 and V5 models the EXSIM simulations were performed in terms of moment magnitude (which is the natural magnitude scale to use for that software). Therefore, when changes in the duration predictions arose as a result of changes to the expected scaling of rupture dimensions, changes in stress parameter with magnitude, or changes in the rupture velocity with magnitude, the points at which these changes

occurred were defined as a function of moment magnitude. For the V4 duration model, the functional form was defined in a piecewise manner to reflect differences in scaling associated with these points, but the particular locations where scaling changed were converted to be defined in terms of local magnitude. For the V5 model, the adopted equivalence between local and moment magnitudes means that the points at which scaling changes are now slightly adjusted to be more directly aligned with the breaks in scaling incorporated into the EXSIM simulations.

The overall functional form for the V5 duration model is defined in terms of contributions from the source, path and site:

$$\ln D_{5-75\%} = g_{src}(M) + g_{path}(R_{rup}, M) + g_{site}(V_{S,30}) \quad (5.1)$$

The inclusion of the site response term reflects the fact that durations are directly predicted to the surface horizon rather than being predicted to NS_B first and then mapped to the surface.

The source scaling is a function of magnitude only and is defined in Eq.(5.2):

$$g_{src}(M) = \begin{cases} m_6 + m_7(M - 5.25) & \text{for } M \leq 5.25 \\ m_6 + m_8(M - 5.25) + m_9(M - 5.25)^2 & \text{for } M > 5.25 \end{cases} \quad (5.2)$$

where the magnitude used for the source term is constrained to not be less than 3.25, *i.e.*, $M \equiv \max(M, 3.25)$.

The path scaling is linear in log-rupture distance for distances beyond 12km (informed by the numerical waveform modelling), while at closer distances there is a degree of nonlinear scaling. The overall path function is defined as:

$$g_{path}(R_{rup}, M) = \begin{cases} (r_6 + r_7M) \left[\ln \left(\frac{R_{rup}}{3} \right) \right]^{r_8} & \text{for } R_{rup} \leq 12\text{km} \\ (r_6 + r_7M) \left[\ln \left(\frac{12}{3} \right) \right]^{r_8} + (r_9 + r_{10}M) \ln \left(\frac{R_{rup}}{12} \right) & \text{for } R_{rup} > 12\text{km} \end{cases} \quad (5.3)$$

In a similar manner to the source scaling, the magnitude value that is passed into the path scaling function is constrained to equal a value within the range 3.25 to 6.0. Hence, the magnitude in Eq.(5.3) can be expressed as $M \equiv \min[\max(M, 3.25), 6.0]$.

The site scaling is adopted from the model of Afshari & Stewart (2016), but is adjusted to simply reflect the difference in shear-wave velocity that exists between the NS_B horizon, to which the EXSIM durations correspond, and the surface. The

parameterisation of the surface velocity is made using the average shear-wave velocity over the uppermost 30 m. The site scaling is therefore:

$$g_{site}(V_{S,30}) = \phi_1 \ln \left[\frac{\min(V_{S,30}, V_1)}{V_1} \right] \quad (5.4)$$

with $\phi_1 = -0.2246$ and $V_1 = 600$ m/s. These site response parameters are kept constant for all of the four model branches.

The model coefficients for the magnitude and distance scaling for each of the four branches is presented in Table 5.1. The computation of the variance components is made using the same procedure outlined in Section 3.4, but as the total residuals are computed directly from the surface motions, the regression estimates τ and ϕ , rather than τ and ϕ_{SS} . These parameters are also included in Table 5.1.

Table 5.1. Coefficients of the median V5 duration model

Coefficient	Lower, L	Central, Ca	Central, Cb	Upper, U
m_6	1.0138	1.0077	0.9829	0.9444
m_7	0.6912	0.6864	0.6763	0.6627
m_8	0.9453	0.9247	0.9143	0.9513
m_9	-0.1202	-0.1314	-0.1335	-0.1567
r_6	2.4617	2.4515	2.4537	2.4752
r_7	-0.3998	-0.3982	-0.3970	-0.4004
r_8	0.7099	0.7105	0.7078	0.7106
r_9	1.1584	1.1545	1.1370	1.1200
r_{10}	-0.1207	-0.1192	-0.1143	-0.1090
τ	0.3937	0.3961	0.3922	0.3935
ϕ	0.5400	0.5401	0.5398	0.5399

In applications to the risk model, the arbitrary rather than geometric mean component of the duration is required, which necessitates the addition of the component-to-component variance. The derivation of this quantity is presented in Appendix III.

The general scaling of the V5 duration model is shown with respect to distance for a number of magnitude values in Figure 5.2 and with respect to magnitude for a number of distances in Figure 5.3. It is clear from both figures that the impact of the stress parameter branches is typically modest at small to intermediate magnitude values, but that there is some non-negligible dependence for larger magnitudes.

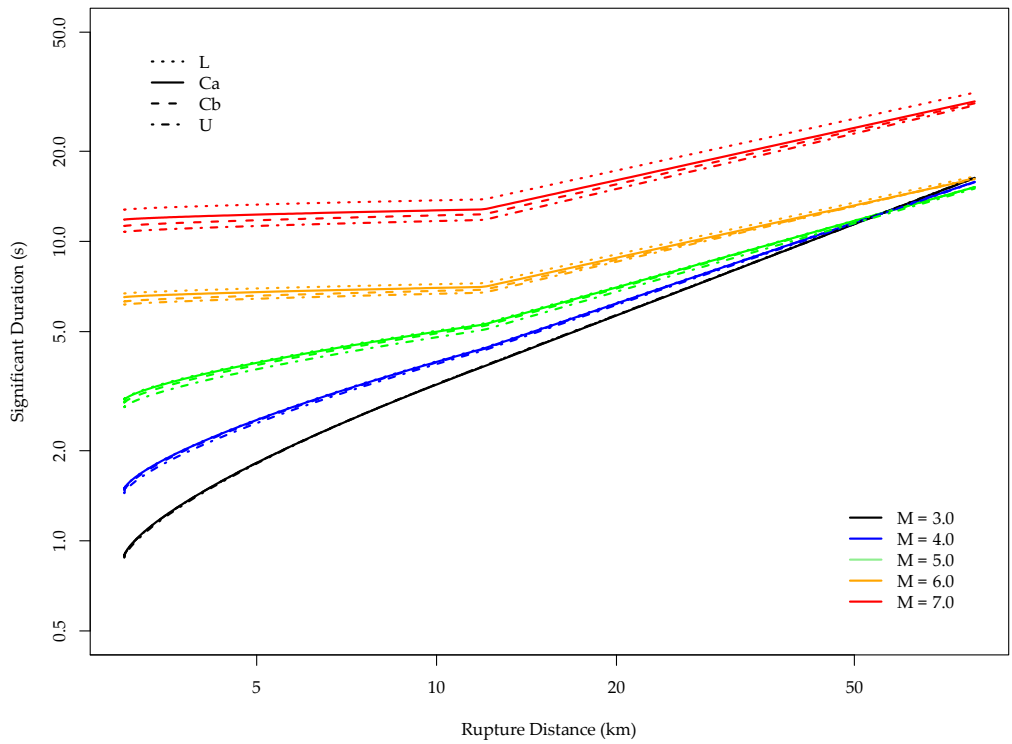


Figure 5.2. Predicted scaling of significant duration with distance for a number of magnitude values. V_{S30} is taken at 200m/s in all cases.

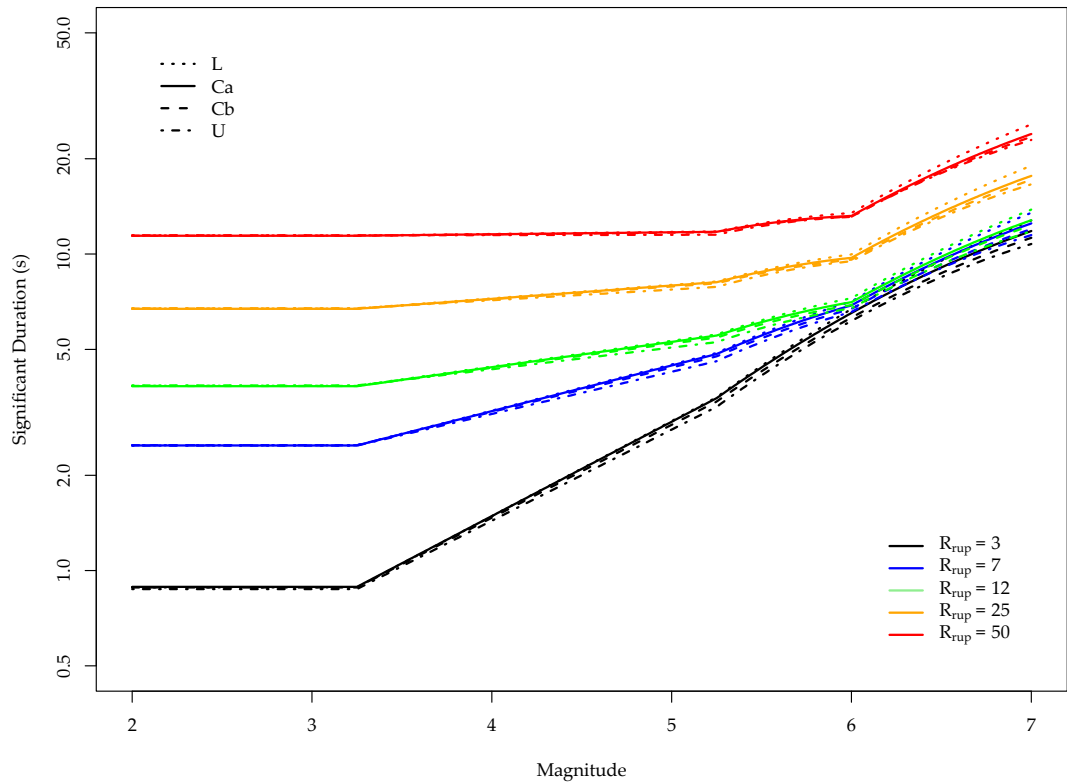


Figure 5.3. Predicted scaling of significant duration with magnitude for a number of distance values. V_{S30} is taken at 200m/s in all cases.

5.2. Comparison with V4 model

The predictions of the V5 duration model are broadly consistent with those of the V4 model for many scenarios of relevance to the Groningen risk model. Given that both models make use of the V3 prediction model to define the sub-source duration values and the scaling of these sub-source contributions with distance, it is not surprising to see very consistent predictions of both magnitude and distance scaling in both the V4 and V5 models. This consistency can be appreciated for each of the four branches in Figure 5.4.

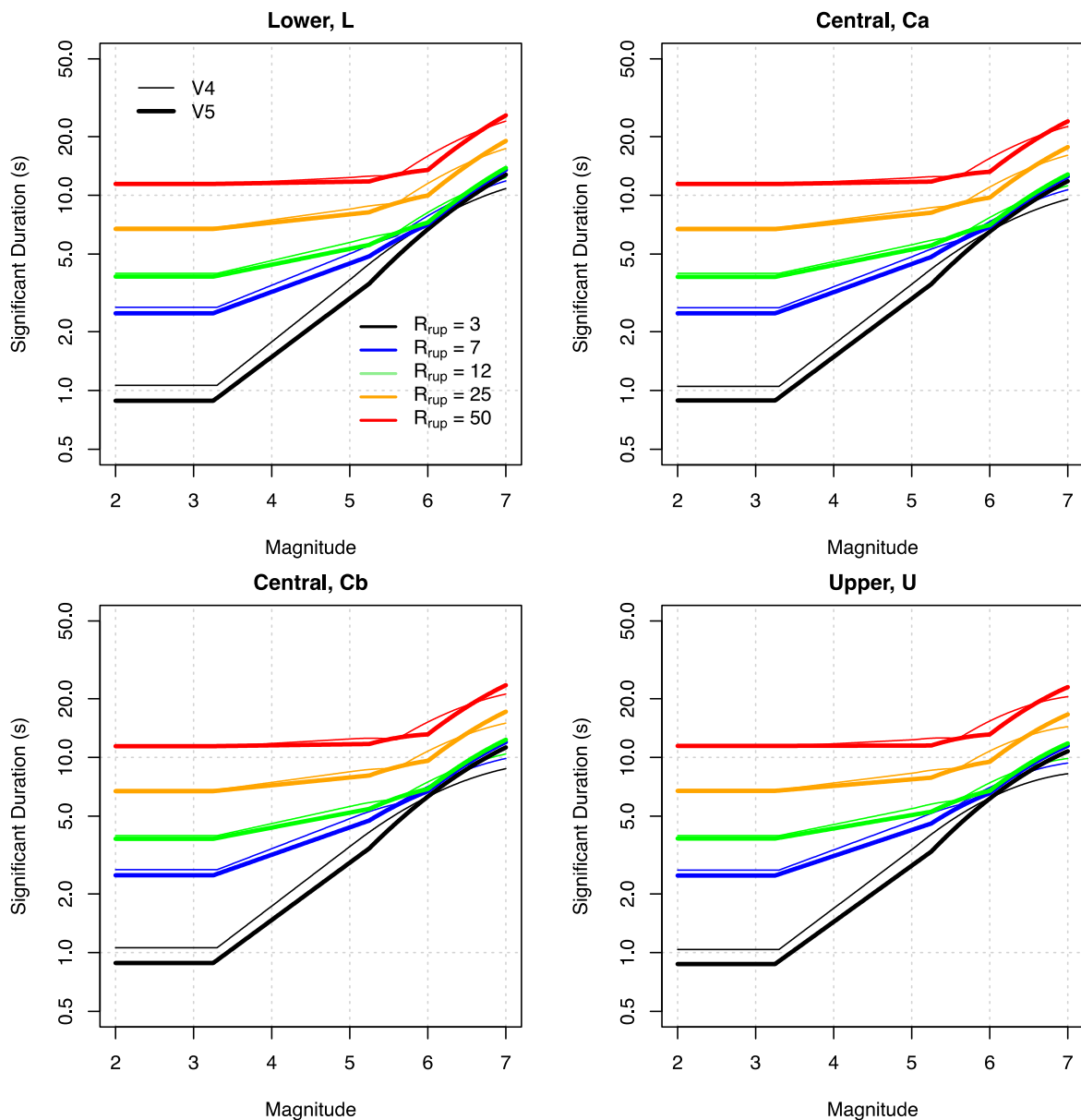


Figure 5.4. Comparison of duration predictions from the V4 and V5 models with respect to magnitude for a number of different distances. Note that predictions are shown here for a consistent value of moment magnitude, *i.e.*, the V4 model predictions are converted from local magnitude to moment magnitude.

However, there are non-trivial differences between the V4 and V5 model predictions for the shortest distances where the effects of the changes in stress parameter between these models is most significant. Figure 5.4 shows that the V5 duration model consistently predicts shorter durations at short distances than its V4 counterpart. These shorter durations reflect the higher values of stress parameter that have been adopted in the V5 model. At larger distances the influence of the source duration is not as strong and so the predictions for both V4 and V5 become more aligned. Similarly, the distance scaling shown in Figure 5.5 reinforces this point showing that differences tend to reduce as one moves farther away.

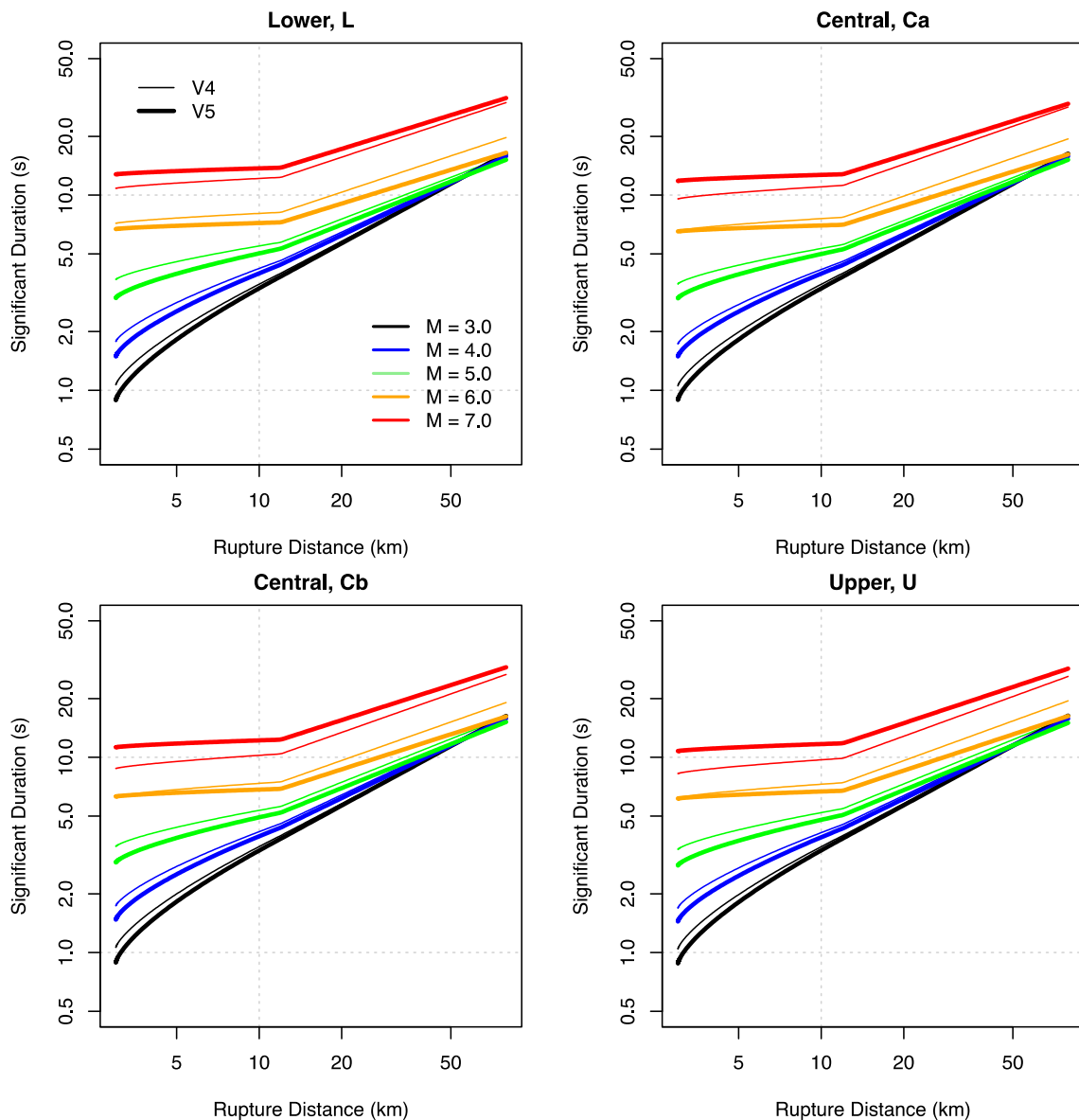


Figure 5.5. Comparison of duration predictions from the V4 and V5 models with respect to rupture distance for a number of different magnitude values. Note that predictions are shown here for a consistent value of moment magnitude, *i.e.*, the V4 model predictions are converted from local magnitude to moment magnitude.

The variance components for the duration model are treated differently between the V4 and V5 models. As discussed in Section 6.2, the V5 risk model computes ground-motion fields (of both spectral amplitude and duration) at the NS_B horizon, and then propagates these through to the surface. In the V4 model the correlations that exist between the spectral amplitudes and duration was handled in an approximate manner that allowed only the total standard deviation of durations at the surface to be modelled. In the more correct approach adopted in V5, it becomes necessary to decompose the total standard deviation into between-event and within-event components.

Since there is almost no magnitude scaling in the duration predictions over the magnitude range spanning the Groningen data, the total residuals for duration computed in each branch are very similar. The variance components are also similar as a result. As can be seen from Table 5.1, the average between-event standard deviation over the four model branches in V5 is 0.3939, while the average within-event standard deviation is 0.5400. The corresponding total standard deviation is 0.6683 for the V5 model and this is slightly larger than the value of 0.6354 obtained from the V4 model.

6. MODEL SUMMARY and IMPLEMENTATION

As noted in Chapter 1, this chapter provides a concise summary of the complete model for those interested in its implementation. This means that some information is repeated from previous chapters but for the convenience of the user the complete model is presented here in its entirety. Section 6.1 presents the basic model elements, including the equations and their coefficients, as well as identifying all of the electronic supplements where the model parameters are listed; in previous GMM reports, similar information was included as an Executive Summary. Section 6.2 provides instructions for the sampling of the variance components.

6.1. Complete GMM logic-tree

The V5 Groningen ground-motion model (GGMM) has the same basic structure as the V4 model: equations for the prediction of accelerations at the NS_B rock horizon combined with frequency-dependent non-linear site amplification factors (AF) assigned to zones defined throughout the study area (onshore gas field plus 5 km buffer). As for the V4 model, the model provides predictions of 5%-damped spectral accelerations [Sa(T)], at 23 periods and peak ground velocity (PGV); in all cases, the geometric mean of the horizontal components is predicted. As in V4, the predictions at the NS_B horizon are a function of local magnitude (M_L) and rupture distance (R_{rup}). Additionally, the model predicts the duration of shaking (D_{S5-75}) directly at the ground surface, as a function of M_L , R_{rup} and V_{S30} .

The functional form of the predictive equations is essentially the same as in V4 (apart from the model for AF) and the logic-tree structure is also the same, with four branches for the median predictions and two branches for the within-event variability. The field zonation is identical with exactly the same 160 zones defined by the X-Y coordinates of the voxels included within each zone. The median V_{S30} values for each zone are also unchanged from the V4 model.

This section summarises the basic elements of the V5 model as required for its implementation in hazard and risk calculations. The coefficients and additional values (such as the site amplification zonation) are included in supplementary CSV files identified in the text.

Equations for Median Motions at NS_B Rock Horizon

The equations for predicting the median ground-motion parameters at the NS_B rock horizon are a function of only magnitude (M_L) and distance (R_{rup}); hereafter, these are specified simply as M and R, the latter measured in km. The model has exactly the same functional form as the V4 model for motions at the NS_B horizon and can

be represented as comprising a source component and a path component, the latter being a function of magnitude and distance:

$$\ln(Y) = g_{source}(M) + g_{path}(R, M) \quad (6.1)$$

where Y is either Sa(T) in cm/s² or PGV in cm/s. The source-related terms are segmented into three ranges of magnitude:

$$g_{source}(M) = m_0 + m_1(M - 4.7) + m_2(M - 4.7)^2 \quad M \leq 4.7 \quad (6.2a)$$

$$g_{source}(M) = m_0 + m_3(M - 4.7) \quad 4.7 < M \leq 5.45 \quad (6.2b)$$

$$g_{source}(M) = m_0 + m_3(5.45 - 4.7) + m_4(M - 5.45) + m_5(M - 5.45)^2 \quad M > 5.45 \quad (6.2c)$$

Similarly, the path terms are also segmented into ranges of rupture distance:

$$g_{path}(R, M) = (r_0 + r_1M) \ln\left(\frac{R}{3}\right) \quad R < 7 \quad (6.3a)$$

$$g_{path}(R, M) = (r_0 + r_1M) \ln\left(\frac{7}{3}\right) + (r_2 + r_3M) \ln\left(\frac{R}{7}\right) \quad 7 \leq R < 12 \quad (6.3b)$$

$$g_{path}(R, M) = (r_0 + r_1M) \ln\left(\frac{7}{3}\right) + (r_2 + r_3M) \ln\left(\frac{12}{7}\right) + (r_4 + r_5M) \ln\left(\frac{R}{12}\right) \quad R \geq 12 \quad (6.3c)$$

There are four versions of the median equations for Y at the NS_B horizon, as summarised in Table 6.1; these models correspond to different values of the stress parameter, $\Delta\sigma$. There are two central models, both having the same value of the stress parameter in the magnitude range of the existing Groningen data; at larger magnitudes, the stress parameters rise to lower (Ca) and higher (Cb) values.

Table 6.1. Weights on the four branches for median predictions at NS_B.

Branch	Model	Code	Weight
1	Lower	L	0.1
2	Central – lower	Ca	0.3
3	Central – upper	Cb	0.3
4	Upper	U	0.3

The coefficients of equations (6.2) and (6.3) for the four individual models are presented in the file [gmpe_medians_NS_B_20170724_v5.csv](#).

Sigma Model for NS_B Rock Horizon GMPEs

The sigma model representing the aleatory variability in the values of $\ln(Y)$ from Eq.(6.1) includes a between-earthquake component, τ , and a within-earthquake component, ϕ_{SS} . If Y_μ is the median value obtained from Eqs.(6.1)-(6.3), then two different quantities may be predicted by sampling from the components of variability: Y_{GM} , the geometric mean component (to be used for hazard mapping), and Y_{arb} , the arbitrary component (to be used in risk calculations):

$$\ln(Y_{GM}) = \ln(Y_\mu) + \varepsilon_E \tau + \varepsilon_S \phi_{SS} \quad (6.4a)$$

$$\ln(Y_{arb}) = \ln(Y_\mu) + \varepsilon_E \tau + \varepsilon_S \phi_{SS} + \varepsilon_C \sigma_{C2C} \quad (6.4b)$$

The ε values are standard normal variates that represent the numbers of standard deviations from the each of the normal distributions; σ_{C2C} is the component-to-component variability. The component-to-component variability model has changed appreciably from the V4 model and now includes dependence on both magnitude and distance. The component-to-component variance is defined by the following equations for the value at different periods, T:

$$\sigma_{c2c}^2(M, R) = 0.026 + 1.03[5.6 - \min(5.6, \max[M, 3.6])]R^{-2.22} \quad T \leq 0.1s \quad (6.5a)$$

$$\sigma_{c2c}^2(M, R) = 0.045 + 5.315[5.6 - \min(5.6, \max[M, 3.6])]R^{-2.92} \quad T \geq 0.85s \quad (6.5b)$$

For periods in between 0.1 and 0.85 seconds, the following interpolation is used:

$$\sigma_{c2c}^2(T, M, R) = \sigma_{c2c}^2(0.1, R) + \left[\frac{\log(T) - \log(0.1)}{\log(0.85) - \log(0.1)} \right] [\sigma_{c2c}^2(0.85, R) - \sigma_{c2c}^2(0.1, R)] \quad (6.6)$$

The component-to-component variability of duration is also defined and presented later in this section.

A unique value of between-earthquake variability is associated with each period (and PGV) and there are two equally-weighted branches for the within-event variability. The between-earthquake variability values are modified from V4 but the values of the within-event variability are identical to those used in the previous model. The complete logic-tree for motions at the NS_B horizon is illustrated in Figure 6.1. The values of the sigma components are presented in the file [gmpe_sigmas_NS_B_20170831_v5.csv](#).

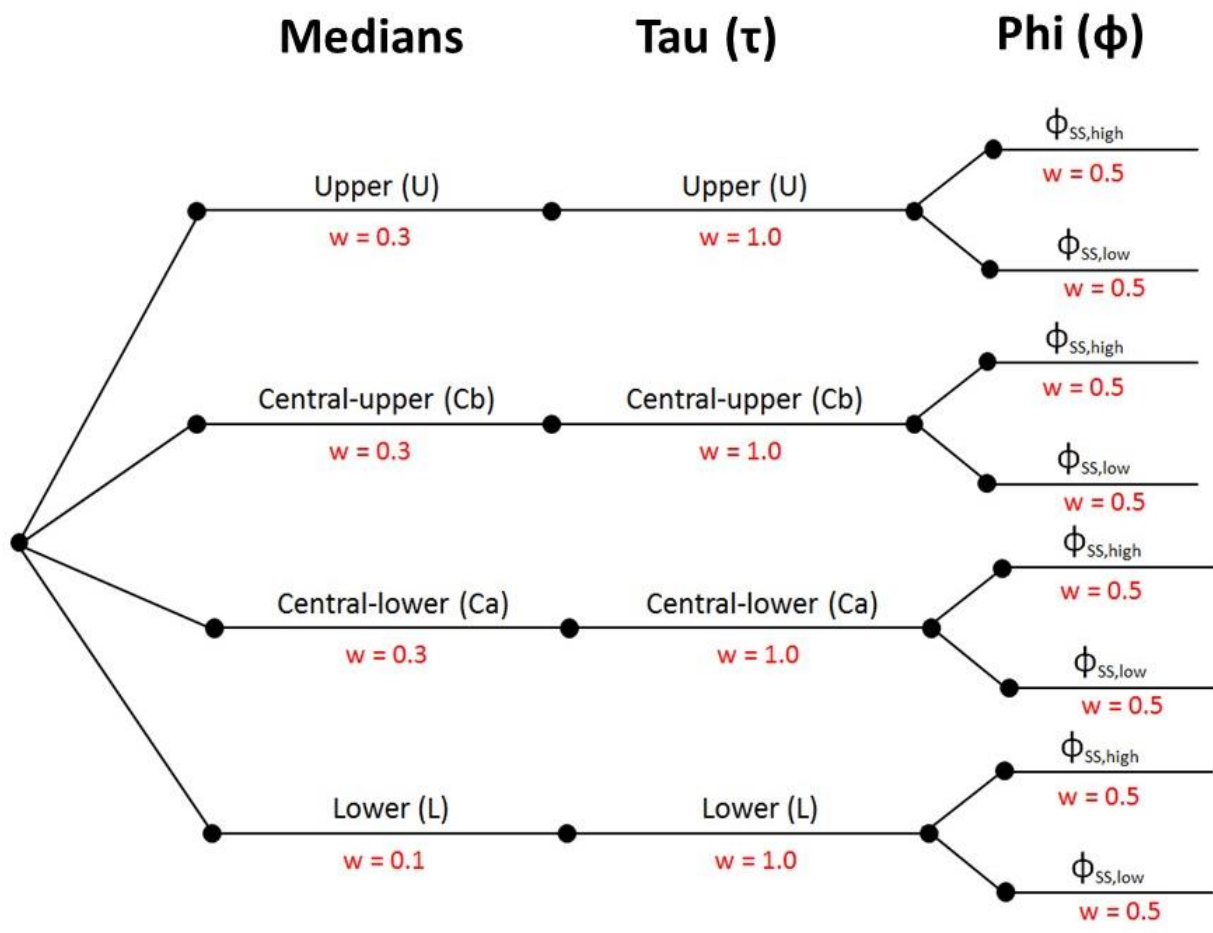


Figure 6.1. Logic-tree structure for model for motions at the NS_B horizon

Field Zonation

The study area is divided into **160** zones having a common set of AFs for both Sa(T) and PGV (Figure 6.2). The zones are defined by a numerical code; the zones and their geographical limits are identical to those defined for the V4 model. A list of 140,862 voxel squares of 100 x 100 m—each identified by the RD coordinates of their centre—and the zone to which each voxel is identified is provided in the following file: [gmpeSurfaceZonation_20170824_v5.csv](#). The content of the file is identical to that in [gmpeSurfaceZonation_20170131_v4.csv](#), but a new file has been created in order to have a consistent set of CSV files defining the parameters of the V5 model.

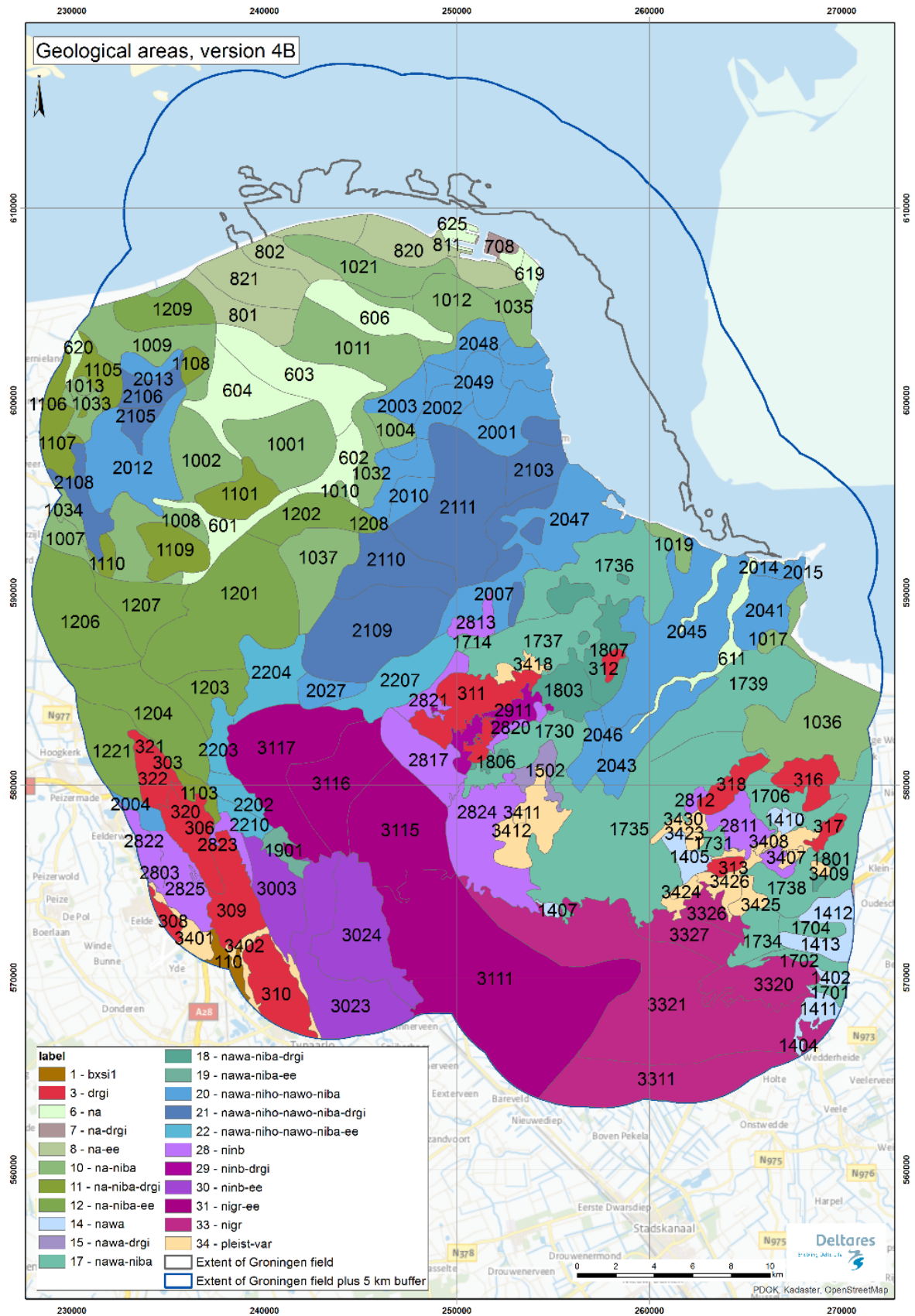


Figure 6.2. V5 zonation of the Groningen field for site amplification factors

Median Non-Linear Soil Amplification Factors

For each of the 160 zones and each ground-motion parameter (spectral acceleration at 23 periods and PGV), the amplification factors, AF, are defined as follows:

$$\ln[AF(Sa)] = f_1^* + f_2 \ln\left(\frac{Sa_{NS_B,g} + f_3}{f_3}\right) \quad (6.7a)$$

$$\ln[AF(PGV)] = f_1^* + f_2 \ln\left(\frac{PGV_{NS_B} + f_3}{f_3}\right) \quad (6.7b)$$

In Eq.(6.7a), $Sa_{NS_B,g}$ is the spectral acceleration at the NS_B horizon, expressed in units of g (981 cm/s²); in Eq.(6.7b), PGV_{NS_B} is the PGV value at the same reference rock horizon, in units of cm/s. This general formulation is unchanged from the V4 model, but the functional form for the first term on the right-hand side has been modified, as explained below.

The first term on the right-hand side of Eq.(6.7), f_1^* , is the exponent of the linear part of the amplification factors. The term is magnitude- and distance-dependent and for Sa(T) this dependence is defined by the following equation:

$$f_1^* = [a_0 + a_1 \ln(R)] + [b_0 + b_1 \ln(R)] [\min(M, M_{ref}) - M_{ref}] \quad (6.8)$$

where M_{ref} is given by:

$$M_{ref} = M_1 - \left[\frac{\ln(R) - \ln(3)}{\ln(60) - \ln(3)} \right] (M_1 - M_2) \quad (6.9)$$

where M_1 and M_2 are model parameters.

For PGV, f_1^* , is given by:

$$f_1^* = [a_0 + a_1 \ln(R)] + [b_0 + b_1 \ln(R)] (M - M_1) \quad M \leq M_1 \quad (6.10a)$$

$$f_1^* = [a_0 + a_1 \ln(R)] + d(M - M_1) \quad M > M_1 \quad (6.10b)$$

The model parameters a_0 , a_1 , b_0 , b_1 , M_1 and M_2 are all given for all periods and all zones in the file **gmpeSurfaceAmplificationModel_20170826_v5.csv**. For PGV, the same parameters are given but M_2 is given as -99 since this coefficient is not used for this ground-motion parameter. The coefficient d used in Eq.(6.10b) is also included in the file, and is entered as 0 for Sa(T). The values of $\ln(AF)$ in Eqs.(6.7a) and (6.7b) are subject to upper and lower limits of AF_{max} and AF_{min} , which are also

included in the same file. It should be noted that the model for AF is only applicable for magnitudes greater than or equal to $M_L 2$.

Site-to-Site Variability Model

The variability in the site amplification factors is given by the standard deviation ϕ_{S2S} , which is defined as a tri-linear function as defined in the following equations (and illustrated in Figure 6.3):

$$\phi_{S2S} = \phi_{S2S,1} \quad Sa_{NS_B,g} < Sa_{Low} \quad (6.11a)$$

$$\phi_{S2S} = \phi_{S2S,1} + (\phi_{S2S,2} - \phi_{S2S,1}) \left[\frac{\ln(Sa_{NS_B,g}) - \ln(Sa_{low})}{\ln(Sa_{high}) - \ln(Sa_{low})} \right] \quad Sa_{Low} \leq Sa_{NS_B,g} \leq Sa_{High} \quad (6.11b)$$

$$\phi_{S2S} = \phi_{S2S,2} \quad Sa_{NS_B,g} > Sa_{High} \quad (6.11c)$$

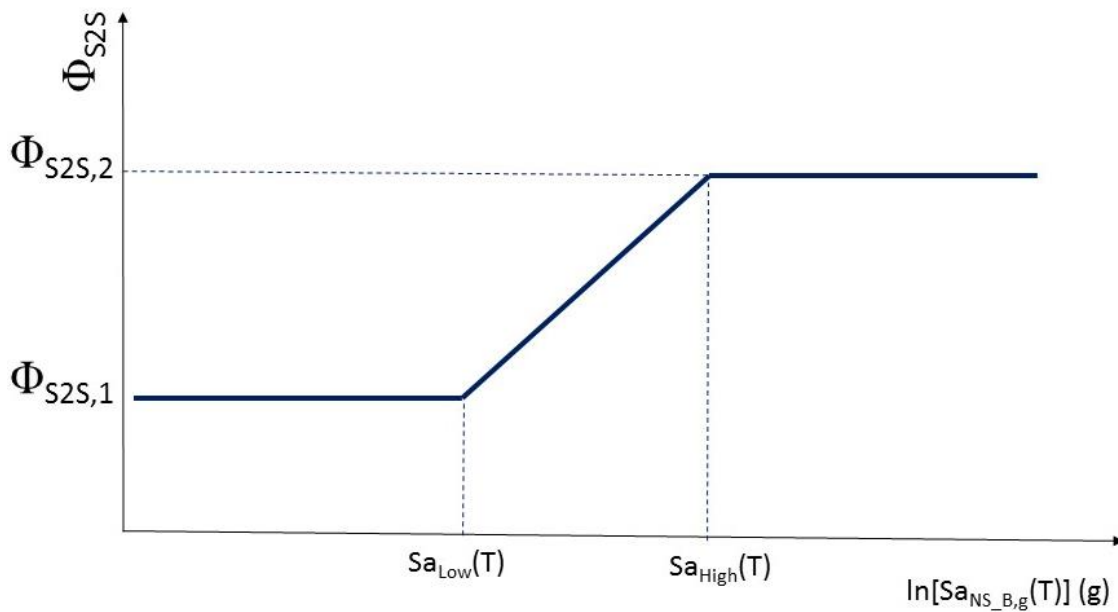


Figure 6.3. Schematic illustration of the site-to-site variability model. The values on the x-axis is the spectral acceleration at the NS_B, expressed in units of g, or the PGV value in cm/s. In either case, the value is obtained by application of Eqs.(6.1) to (6.4)

The four parameters defining the site-to-site variability model for $Sa(T)$ at all 23 periods and also for PGV in each of the 160 site amplification zones are listed in the file [gmpeSurfaceAmplificationModel_20170826_v5.csv](#).

Period-to-Period Correlation of Residuals of Sa(T)

For the risk calculations, values of Sa(T) calculated at a given location for different periods, T, must account for the period-to-period correlations of the residuals. The correlation coefficients, to be applied to all components of variability, for Sa(T) at all 23 periods are exactly the same as those used in the V4 model and these are provided in the CSV file: [gmpe_period2period_correlations_20170824_v5.csv](#). The content of this file is identical to the file provided with the V4 model ([gmpe_period2period_correlations_20170131_v4.csv](#)) but a new file has been created to create a consistent suite of input files for the V5 model.

For convenience, an additional file ([gmpe_im2im_correlations_20170901_v5.csv](#)) has been provided that includes the full correlation matrix for both spectral ordinates and durations (as discussed in Section 6.2).

Duration Model

The model for the prediction of durations has the same functional form as the V4 model, only the magnitudes at which the breaks in scaling occur and the actual coefficients having been changed. As before, the model has four branches that should each be used in conjunction with the corresponding median branch on the predictions for Sa(T) and PGV. The median predictions of the duration, D_{S5-75} (significant duration based on the accumulation from 5% to 75% of the total Arias intensity), is comprised of a source component and a path component to obtain the NS_B motions, plus a site component that transforms the rock motions to the ground surface:

$$\ln(D_{S5-75}) = f_{source}(M) + f_{path}(R, M) + f_{site}(V_{S30}) \quad (6.12)$$

The source function is defined as:

$$f_{source} = m_6 + m_7(\max[M, 3.25] - 5.25) \quad M \leq 5.25 \quad (6.13a)$$

$$f_{source} = m_6 + m_8(M - 5.25) + m_9(M - 5.25)^2 \quad M > 5.25 \quad (6.13b)$$

The path function is dependent on both distance and magnitude:

$$f_{path} = (r_6 + r_7 M') \left[\ln\left(\frac{R}{3}\right) \right]^{r_8} \quad R \leq 12 \quad (6.14a)$$

$$f_{path} = (r_6 + r_7 M') \left[\ln\left(\frac{12}{3}\right) \right]^{r_8} + (r_9 + r_{10} M') \ln\left(\frac{R}{12}\right) \quad R > 12 \quad (6.14b)$$

where, $M' = \min[\max(M, 3.25), 6.0]$ (6.14c)

The site term is very simple:

$$f_{site}(V_{S30}) = -0.2246 \ln\left(\frac{\min(V_{S30}, 600)}{600}\right) \quad (6.15)$$

The duration model requires V_{S30} as an input parameter. The median V_{S30} value for each of the 160 site amplification zones is listed in the supplementary electronic file **gmpeSurfaceZonationVs30_20170826_v5.csv** (which contains exactly the same information as **gmpeSurfaceZonationVs30_20170131_v4.csv**). A map showing these median V_{S30} values is presented in Figure 6.4. Since the largest value of V_{S30} for any zone is 270 m/s, the logarithmic term in Eq.(6.15) will always be the ratio $V_{S30}/600$.

The coefficients of Eqs.(6.13) and (6.14) are all listed, for all four branches, in the file **gmpeDuration_20170903_v5.csv**. The total variability in the duration predictions is given by the sigma values in Table 6.2; the component-to-component variability for the duration is given by:

$$\sigma_{c2c}^2 = 0.0299 + 2.434[5.6 - \min(5.6, \max[M, 3.6])]R^{-1.95} \quad (6.16)$$

this variability is sampled conditioned on the residual of the amplitude-based parameter, using the correlation coefficients in Table 6.3. The sigma values are also provided in the file **gmpeDuration_20170903_v5.csv** and the correlation coefficients are provided in the additional supplementary electronic file **gmpeDuration_Sa_Correlations_20170826_v5.csv** (which contains the same values as **gmpeDuration_Sa_Correlations_20170131_v4.csv**). The four duration branches are to be implemented in combination individually with the corresponding median branch for spectral accelerations and PGV.

Table 6.2. Sigma components for $\ln(D_{S5-75})$

Branch	1	2	3	4
Model	Lower	Central-lower	Central-upper	Upper
$\tau[\ln(D_{S5-75})]$	0.3937	0.3961	0.3922	0.3935
$\phi[\ln(D_{S5-75})]$	0.5400	0.5401	0.5398	0.5399

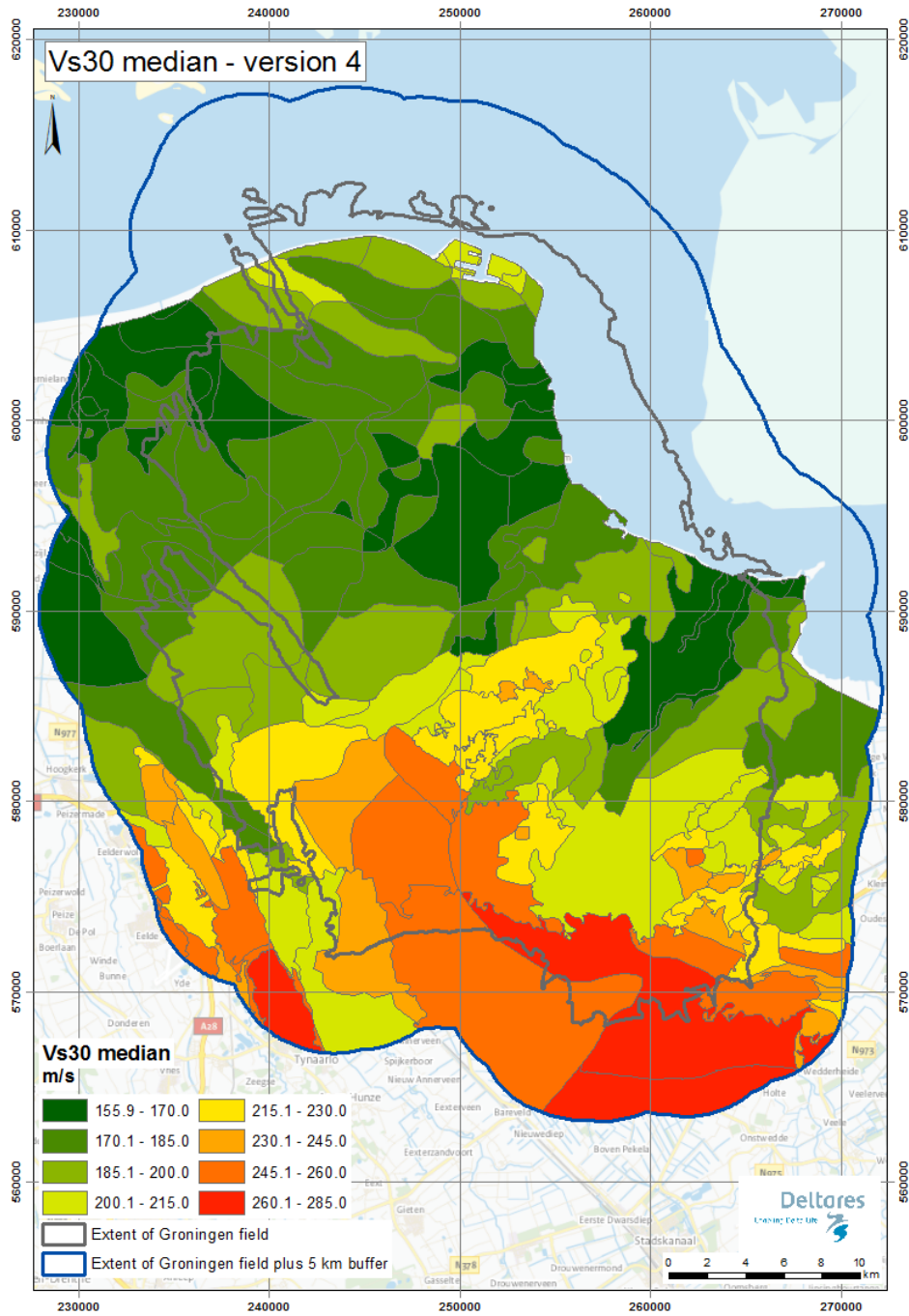


Figure 6.4. Median V_{S30} values of each zone

Table 6.3. Correlation coefficients for the residuals of duration and $S_a(T)$ or PGV (applicable for both between event and within event correlations)

T [s]	0.01	0.025	0.05	0.075	0.1	0.125	0.15	0.175	0.2	0.25	0.3	0.4
ρ	-0.45	-0.45	-0.45	-0.45	-0.39	-0.39	-0.39	-0.39	-0.39	-0.39	-0.39	-0.33
T [s]	0.5	0.6	0.7	0.85	1	1.5	2	2.5	3	4	5	PGV
ρ	-0.28	-0.24	-0.21	-0.17	-0.13	-0.05	-0.01	0.02	0.05	0.09	0.12	-0.26

Summary List of Electronic Supplements

1. gmpe_medians_NS_B_20170724_v5.csv
2. gmpe_sigmas_NS_B_20170831_v5.csv
3. gmpeSurfaceZonation_20170824_v5.csv
4. gmpeSurfaceAmplificationModel_20170826_v5.csv
5. gmpe_period2period_correlations_20170824_v5.csv
6. gmpeDuration_20170903_v5.csv
7. gmpeSurfaceZonationVs30_20170826_v5.csv
8. gmpeDuration_Sa_Correlations_20170826_v5.csv
9. gmpe_im2im_correlations_20170901_v5.csv

These files are all contained in the folder “V5 GMM electronic supplements”, which is made available as a zipped file of the same name.

6.2. Sampling of variance components

The GMM developed for induced seismicity in the Groningen gas field predicts spectral accelerations (SA) at 23 response periods (T), peak ground velocity (PGV) and significant duration (D) at the ground surface as a function of local magnitude (M), rupture distance (R) and site classification. For all intensity measures the motion is first predicted at a bedrock horizon (NS_B) and then amplification factors (AF) are applied to these rock amplitudes to obtain the surface motions. While field-specific probabilistic AFs (functions defining the distribution of amplification) are developed for SA and PGV, in the case of significant duration a global deterministic V_{S30} -dependent AF is adopted and applied throughout the field. The AFs are defined for PGV and for SA at each period and for each of the 160 zones defined over the field. Values of duration are predicted using a unique value of V_{S30} for each of the zones. Note that SA for an oscillator period of 0.01 s is assumed equivalent to peak ground acceleration (PGA).

The prediction of the median values of SA, PGV and D is relatively straightforward, simply applying the relevant values of M_L and R for each earthquake-site combination, and then applying the relevant AF or V_{S30} depending on the zone within which the site is located. However, the models predict distributions of values rather than unique estimates of SA, PGV and D. In all cases, the intensity measures (SA, PGV and D) are log-normally distributed and their joint distribution is assumed to be multivariate log-normal. For both model development and sampling it is convenient to work with the log-transformed intensity measures such that variation about the median motion for a given scenario is defined by a symmetric normal distribution (or multivariate normal). The scale of the variation in this transformed space is defined by a standard deviation. The total standard deviation in ground-motion prediction models is usually represented by the symbol sigma (σ) and the total residuals are

then defined by the product of σ and epsilon (ϵ) the number of standard deviations sampled (and a standard normal variate).

The purpose of this document is to define the procedures for sampling the aleatory variability in the prediction of the ground-motion parameters. The hazard and risk model for the Groningen field uses Monte Carlo simulations and therefore the focus is on the random sampling of ϵ values in each ground-motion realisation. The process is schematically illustrated in Figure 6.5, which depicts the estimation of SA for a single value of T at three locations (over two zones) as a result of a single earthquake. In practice, however, the implementation is somewhat more complicated because the sampling of variance components must also respect correlations between parameters and spatial correlation as well. In the following, the first subsection defines the different components of variability and then the issue of spatial correlation is discussed. After that, the sampling is discussed for different applications of increasing complexity with regards to the variability.

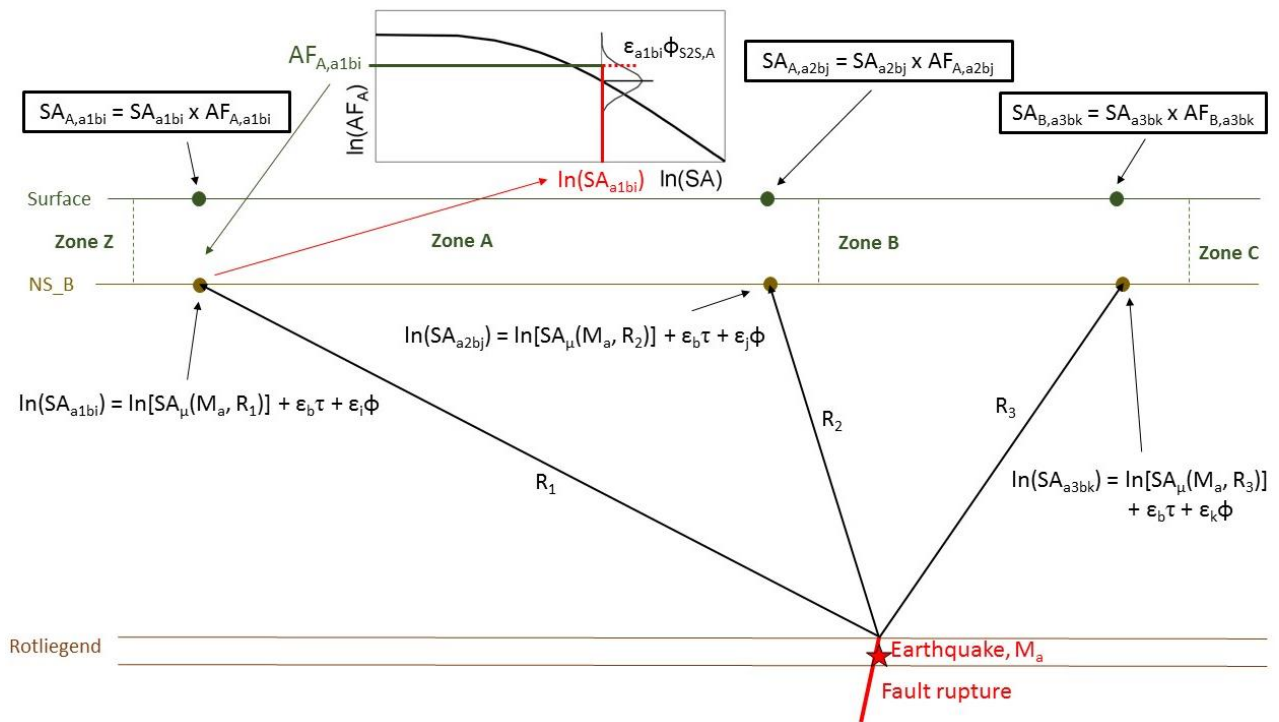


Figure 6.5. Schematic illustration of the calculation of SA at three surface points, in two zones, for an earthquake of magnitude M_a and an event-term of $\epsilon_b\tau$; in this simple example, the within-event variability is sampled without considering spatial correlation (Bommer *et al.*, 2017c).

Components of Variability in the Groningen GMM

The components of variability defined in the Groningen GMM are listed in Table 6.4, indicating also which ground-motion parameters they are related to and where they

are applied both in terms of a reference horizon and in the calculation of hazard or risk.

Table 6.4. Elements of ground-motion variability in the Groningen GMM

Symbol	Description	GM Parameter ¹	Horizon ²	H or R ³	Epsilon ⁴
σ_{GM}	Standard deviation of geometric mean of ground-motion parameters	SA(T), PGV	NS_B	Hazard	ε_{GM}
σ_{arb}	Standard deviation of arbitrary component of ground-motion parameters	SA(T), PGV, D	NS_B	Risk ⁵	ε_{arb}
τ	Between-event variability of ground-motion parameters	SA(T), PGV, D	NS_B	H & R ⁵	ε_E
ϕ_{SS}	Within-event non-ergodic variability of amplitude-based parameters	SA(T), PGV, D	NS_B	H & R ⁵	ε_S
σ_{c2c}	Component-to-component variability of spectral accelerations	SA(T), D	NS_B	Risk	ε_c
ϕ_{S2S}	Site-to-site variability associated with AFs	SA(T)	Surface	H & R	ε_Z

Notes: 1 – The ground-motion parameters to which it applies; 2 – Reference elevation at which applied; 3 – Whether used in hazard or risk calculations; 4 – Symbol for normalised residual used to sample distribution; 5 – PGV is not currently employed in probabilistic risk calculations, while D is not employed in hazard calculations.

The total variability on the geometric mean ground-motion amplitudes is given by:

$$\sigma_{GM} = \sqrt{\tau^2 + \phi_{SS}^2 + \phi_{S2S}^2} \quad (6.17)$$

whereas the total variability of the arbitrary component of motion is given by:

$$\sigma_{arb} = \sqrt{\tau^2 + \phi_{SS}^2 + \phi_{S2S}^2 + \sigma_{c2c}^2} \quad (6.18)$$

The total variability on the duration is conceptually also decomposed into these different elements, but because the amplification effects are treated as being known and deterministic $\phi_{S2S} \equiv 0$ and $\phi = \phi_{SS}$, noting that normally $\phi^2 \equiv \phi_{SS}^2 + \phi_{S2S}^2$.

There are two correlation functions defined for ground-motion residuals as well, and their characteristics are summarised in Table 6.5. Both of these correlation models are used to construct the full correlation matrix that is required for the sampling process within the risk calculations.

Table 6.5. Correlations of residuals in the Groningen GMM

Symbol	Description	GM Parameter ¹	Horizon ²
ρ_{T2T}	Period-to-period correlation of spectral accelerations	SA at multiple T	NS_B
ρ_{SA-D}	Correlations of spectral acceleration and duration	SA(T) and D	NS_B

Notes: 1 – The ground-motion parameters to which it applies; 2 – Reference elevation at which employed.

Spatial Correlation of Ground Motions

Another correlation of ground-motion residuals is that which occurs spatially since observations from dense recording networks have revealed that epsilon values at closely-spaced locations tend to be correlated rather than being entirely random.

For the calculation of Group Risk or any other aggregate measure of the seismic risk, the spatial correlation of ground motions is important since it leads to pockets of higher-than-average and lower-than-average ground motions rather than simply random spatial variation of the amplitudes. The coincidence of a pocket of higher-than-average ground motions with a group of seismically vulnerable structures will result in higher estimates of Group Risk than when spatial correlation of the ground motions is ignored. Although the primary focus of the risk modelling is Individual Local Personal Risk (ILPR, which is a location-specific measure), Group Risk estimates may be needed and for this reason, spatial correlation does need to be considered.

A Groningen-specific model for spatial correlation of ground motions, defined as a function that varies continuously with the distance separating two points, has not yet been derived (see Chapter 7). For the current (V5) risk modelling purposes, it is proposed to approximate the spatial correlation with a simpler model that assumes perfect correlation within each of the 160 site amplification zones and no within-event correlation between one zone and another. In practice, this correlation of ground-amplitude amplitudes is not perfect because the NS_B motions, the AFs and σ_{c2c} all depend on M and R, and the value of R will vary for different grid points within a zone. Consequently, the while the correlation of the within-event residuals is perfect, the actual ground-motion amplitudes over the zone will vary spatially. Once the field-specific model is ready, the degree to which this approximation mimics the real spatial correlation will be explored, but for the current phase of risk modelling it is proposed to constrain the sampling of variability elements such as to approximate spatial correlation in the simplified manner indicated above. However, there is no requirement to invoke spatial correlation in the hazard calculations.

Sampling Variability in Hazard Calculations for PGV and SA(T)

When hazard maps are generated in terms of these 24 parameters (*i.e.*, spectral accelerations at 23 response periods plus PGV), they are treated completely independently. The uniform hazard response spectra (UHRS) at specified location are obtained from individual hazard curves for SA at the 23 response periods. The hazard is calculated at grid points defined across the field, usually with several grid points located within each site response zone.

The sequence of sampling of variability to be followed in generating the hazard estimates is therefore as follows:

1. For each earthquake and GM parameter, a value of ε_E is randomly sampled.
2. For each grid point, the NS_B motion is calculated randomly sampling ε_S ; this means that spatial correlation is ignored at the reference rock horizon.
3. For each grid point, the median surface motion is estimated by applying the AF value conditioned on the realisation of the NS_B motion (including the two components of variability sampled in steps #1 and #2).
4. The final surface motion at each location is then calculated by randomly sampling ε_Z ; here again, spatial correlation is ignored and the site-to-site variability is therefore interpreted as being due to spatial variability of the soil profiles and dynamic soil properties within the zone.

Sampling Variability in Ground-motion Values for Risk Calculations

When ground-motions at the surface are predicted for the purpose of providing inputs to risk calculations, a number of differences arise when compared to the same predictions within the hazard calculations. One of these is that the component-to-component variability needs to be added in order to obtain estimates of the arbitrary component of motion rather than the geometric mean. Secondly, spatial correlation needs to be approximated as was described earlier. And finally, since the risk calculations are made for several building types at a given location—which have different vibration periods and some of which have different vibration periods along their two axes—the period-to-period correlations of the spectral accelerations also need to be sampled. Similarly, as fragility curves for some typologies utilise both spectral amplitude and duration, the correlation between these intensity measures must also be taken in to account. The sampling sequence now becomes as follows:

1. For each earthquake, the covariance matrix for between-event residuals is sampled in order to obtain a vector ε_E that contains between-event residuals for all 23 spectral ordinates as well as duration. This can be expressed mathematically as $\varepsilon_E = [\varepsilon_E(T_1) \ \cdots \ \varepsilon_E(T_{23}) \ \varepsilon_E(D)]^T$. The correlation matrix can be defined as:

$$\boldsymbol{\rho} = \begin{bmatrix} \boldsymbol{\rho}_{Sa(T),Sa(T)} & \boldsymbol{\rho}_{Sa(T),D} \\ \boldsymbol{\rho}_{D,Sa(T)} & \rho_{D,D} \end{bmatrix} = \begin{bmatrix} \rho_{Sa(T_1),Sa(T_1)} & \rho_{Sa(T_1),Sa(T_2)} & \cdots & \rho_{Sa(T_1),D} \\ \rho_{Sa(T_2),Sa(T_1)} & \rho_{Sa(T_2),Sa(T_2)} & \cdots & \rho_{Sa(T_2),D} \\ \vdots & \vdots & \ddots & \vdots \\ \rho_{D,Sa(T_1)} & \rho_{D,Sa(T_2)} & \cdots & \rho_{D,D} \end{bmatrix} \quad (6.19)$$

2. For each zone, the NS_B motion for the arbitrary component needs to reflect both the variability suggested by ϕ_{SS} as well as the component-to-component variability associated with σ_{c2c} . Rather than sample separate sets of epsilon values for each of these components individually, a vector of epsilon values $\boldsymbol{\varepsilon}_A = [\varepsilon_A(T_1) \cdots \varepsilon_A(T_{23}) \varepsilon_A(D)]^T$ is generated. For each ground-motion measure, the residual of the arbitrary component is given by $\varepsilon_A \sqrt{\phi_{SS}^2 + \sigma_{c2c}^2} \equiv \varepsilon_S \phi_{SS} + \varepsilon_c \sigma_{c2c}$. That is, the covariance matrix from which $\boldsymbol{\varepsilon}_A$ is sampled has diagonal elements that are defined by $\phi_{SS}^2 + \sigma_{c2c}^2$ (for all spectral ordinates and for duration). The off-diagonal elements of the covariance matrix make use of the same correlation matrix elements as used for the sampling of the between-event residuals. The sampled values of $\boldsymbol{\varepsilon}_A$ are used at all grid points within a zone to approximate spatial correlation.
3. For each grid point, the median surface motion is estimated by applying the AF value conditioned on the realisation of the NS_B motion (including the two components of variability $\boldsymbol{\varepsilon}_E$ and $\boldsymbol{\varepsilon}_A$ sampled in steps #1 and #2). Note that for the duration there is no conditioning and the AF for each zone depends purely upon the V_{S30} value for the zone.
4. The final surface motion at each location is then calculated by randomly sampling ε_Z ; for a given period, the same value of ε_Z should be invoked at every grid point within a zone in order to represent spatial correlation.

7. CONCLUSIONS and FUTURE DEVELOPMENTS

The V5 model is the product of work conducted over many months and the outcome of several cycles of iteration and critical review. The model meets all of the objectives defined for ground-motion prediction in the Groningen field in terms of reflecting local source, path and site conditions, and also capturing the epistemic uncertainty associated with extrapolation from recordings of small-magnitude induced earthquakes to the estimation of ground motions generated by larger triggered earthquakes. The model also meets all of the requirements for hazard and risk modelling in terms of the predicted ground-motion parameters.

In this closing chapter, some features of the GMM—including the assumption of linear site response for the existing records—are briefly discussed and potential future developments are outlined.

Non-Linear Site Response in Current Database?

The basic framework for developing the Groningen GMMs, from V2 to V5, has involved removing linear site amplification from the recorded motions to transform the motions to the NS_B rock horizon, and then transferring predicted NS_B motions from larger earthquakes to ground surface using non-linear AFs (Figure 2.8). The assumption that the records in the Groningen database have only been affected by linear site amplification is reasonable considering that most of the earthquakes recorded in the field are smaller than M_L 3.2, and the largest earthquake is only M_L 3.6 (Figure 2.2). There are no direct means to verify that this assumption holds. However, this assumption seems to be corroborated by the comparison of site amplification functions obtained from the inversion of the seismological model with the linear surface-to-NS_B transfer functions (see Figures 5.16 and 5.17 in the V4 GMM report, Bommer *et al.*, 2017b).

In this section we explore this assumption using the V5 GMM zone amplification factors (AFs). Figure 7.1 plots the ratio of the zone AFs using the full model (see Section 4.2) and the AFs using only the linear portion of this model [e.g., only f_1^* , see Eq.(4.2) in Section 4.2]. For each station, the AFs are computed for the magnitude-distance combinations that correspond to the recorded motions at these stations. Observe that the assumption of linearity holds for periods greater than about 0.2 seconds. For a period of 0.01 seconds, the largest deviation from linearity is for Station BMD1 for the M_L 3.6 Huizinge earthquake. The station is at a distance of only 3.59 km. In this case, the non-linear AF are 11% smaller than the linear factors. The largest deviations from the linear assumption occur at a period of 0.05 seconds. The largest deviation occurs also for the BMD1 Huizinge recording (the non-linear AF is 30% lower than the linear AF).

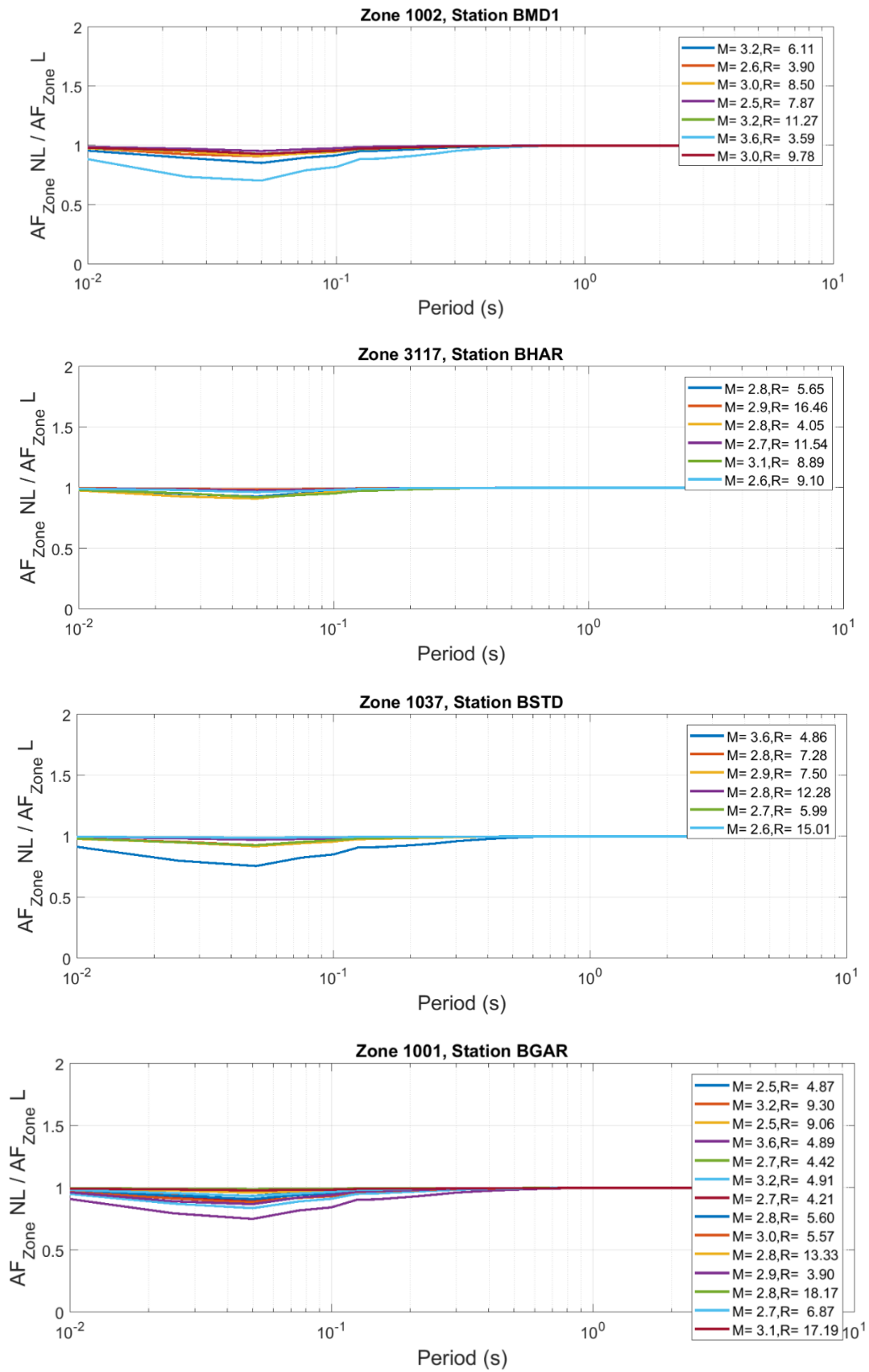


Figure 7.1. Ratios of nonlinear AFs ($AF_{Zone\ NL}$) to linear AFs ($AF_{Zone\ L}$) for selected stations. The AFs are computed using the Zone AF model. Spectral accelerations at the NS_B boundary are computed from the V5 GMM using the Central-upper branch.

The zone AFs are largely consistent with the assumption of linearity. The inversions that are conducted to develop the NS_B model use the full bandwidth of the recordings, hence the possible deviations from linearity at high frequencies ($0.02 \text{ s} \leq T \leq 0.075 \text{ s}$) should not affect the model greatly, other than possibly a slight over-estimation of kappa at the NS_B interface. However, only the recordings for the strongest earthquakes could lead to deviations from non-linearity. Since all the records are used in the inversion (Figure 2.2), it is unlikely that the value of kappa is affected very strongly. Equally, the stress parameter estimates may also have been affected by underestimation of the NS_B motions at a few short periods for a few of the records. However, since the stress parameters are estimated from inversion of all of the records using the full range of frequencies, the effect would not be very large. The logic-tree structure, as discussed below, already allows for greater stress parameter values in the magnitude range of the field database.

Another effect of the deviation from linearity is that there may be an under-estimation of motions for the short periods where these deviations are observed. However, at these periods the site-to-site variability values have increased significantly from previous versions of the model (see Figures 4.12 and 4.15 in Section 4.3). Moreover, these periods are not of high relevance to the current risk model (see Figure 2.9).

The alternative approach of accounting for potential non-linear behaviour in the site response for the small-magnitude earthquakes recorded at the stations would necessitate an iterative approach for the development of the model. This approach would require multiple repetitions of the full suite of site response analyses and consequently would be computationally very costly. Considering that the small deviations from non-linearity are unlikely to have a large effect on the risk model and since uncertainty in the GMM logic-tree extends to the small-magnitude range of the data, the decision was made to maintain the framework assuming linear AFs for the existing database and to accept the potential minor bias in the model derivation.

Stability of the GMM and the NEN-NPR

The V5 GMM is the outcome of an iterative development process that has involved incremental evolution at each stage. In many regards the model has been stable since V2 or V3, when the basic framework of predicting motions at a buried rock horizon to be combined with non-linear AFs was established. Although it is difficult to compare the V3 and V5 models because of their use of different distance metrics, the model has been stable in several respects apart from the apparent fluctuations related to the use of an $M-M_L$ relationship in the V4 model derivation that is now understood to be inappropriate to the Groningen region. The current model is considered to be stable and has sufficient uncertainty bounds to be used with confidence for the foreseeable future. As has been noted previously, the uncertainty range increases with earthquake magnitude but is non-trivial even in the small magnitude range (Figure 7.2). The lower and higher branches in the magnitude range of the existing data cover such features as the reduction due to addition a

new, low-stress parameter event, on the one hand, and the potential minor underestimation of the stress parameters due to the assumption of fully linear site response for all records in the existing database, on the other.

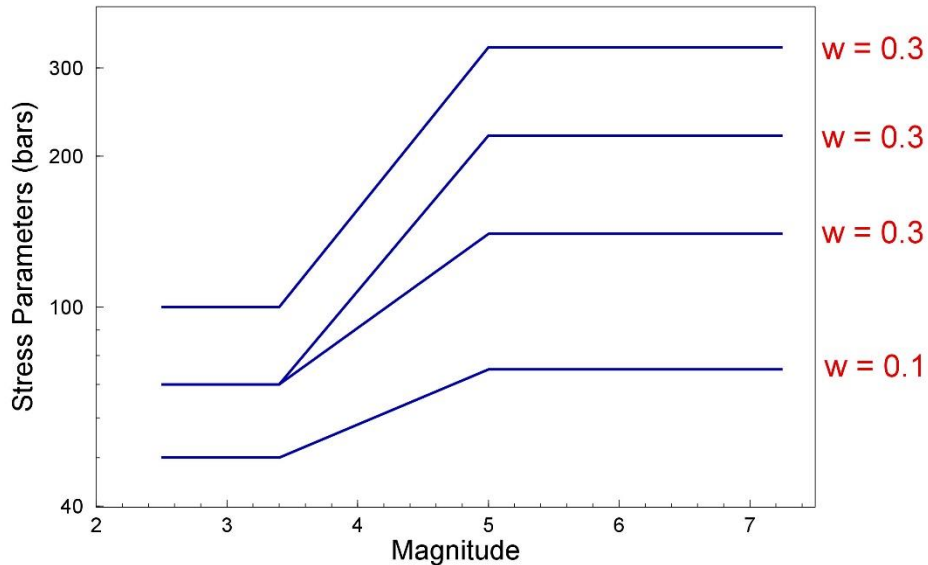


Figure 7.2. Stress parameters and associated weights underlying the V5 GMM logic-tree; note the range of uncertainty even in the magnitude interval covered by the data

Since the 2016 Winningsplan was based on the V2 model (see Figure 2.1), the V3 and V4 models would have no real significance other than staging posts in the model development, which while time-consuming in terms of documentation did facilitate review and feedback. However, the V4 GMM has acquired additional relevance because it was used in the recent update of the NEN-NPR building code for the Groningen region. This is one more consequence of the imposed schedule for responses to the Groningen earthquakes. However, it is now clear that the current version of the NEN-NPR code is based on a conservative ground-motion model, which is consistent with the purpose and objective of codes for earthquake-resistant design of buildings.

Spatial Correlation of Groningen Ground-Motions

The primary metric used to quantify seismic risk in the Groningen field is local personal risk (LPR), which is specific to individual buildings or locations. However, other metrics are also considered, including Group Risk (GR) that is an aggregate measure over the complete exposure database. The calculation of GR is sensitive to spatial correlation of the ground motions, for which reason the instructions for implementation of the GMM presented in Section 6.2 are aimed at ensuring an approximation to a realistic spatial correlation model. Work planned in the coming weeks will derive a Groningen-specific spatial correlation model, which will then be compared to the implied distribution of spatial correlation lengths from the

implementation of the variability sampling instructions within the framework of site amplification factors on non-uniform size. The expectation is that the comparison will confirm the current approximation as an acceptable and conservative approximation.

The data that will be used to derive the spatial correlation model will be partly obtained from the flexible network that is gathering closely-spaced recordings from dense arrays of geophones (Figure 7.3). These data will be added to the recordings from the three permanent accelerograph networks now operating in the region: the KNMI permanent surface accelerographs (B-stations), the KNMI operated borehole arrays of geophone plus surface accelerographs (G-stations), and the TNO-operated network of accelerographs in houses and public buildings (Figure 7.4). The Groningen-specific spatial correlation model, and its comparison with the effective spatial correlation model in the current risk implementation, will be presented in the forthcoming paper by Stafford *et al.* (2018).

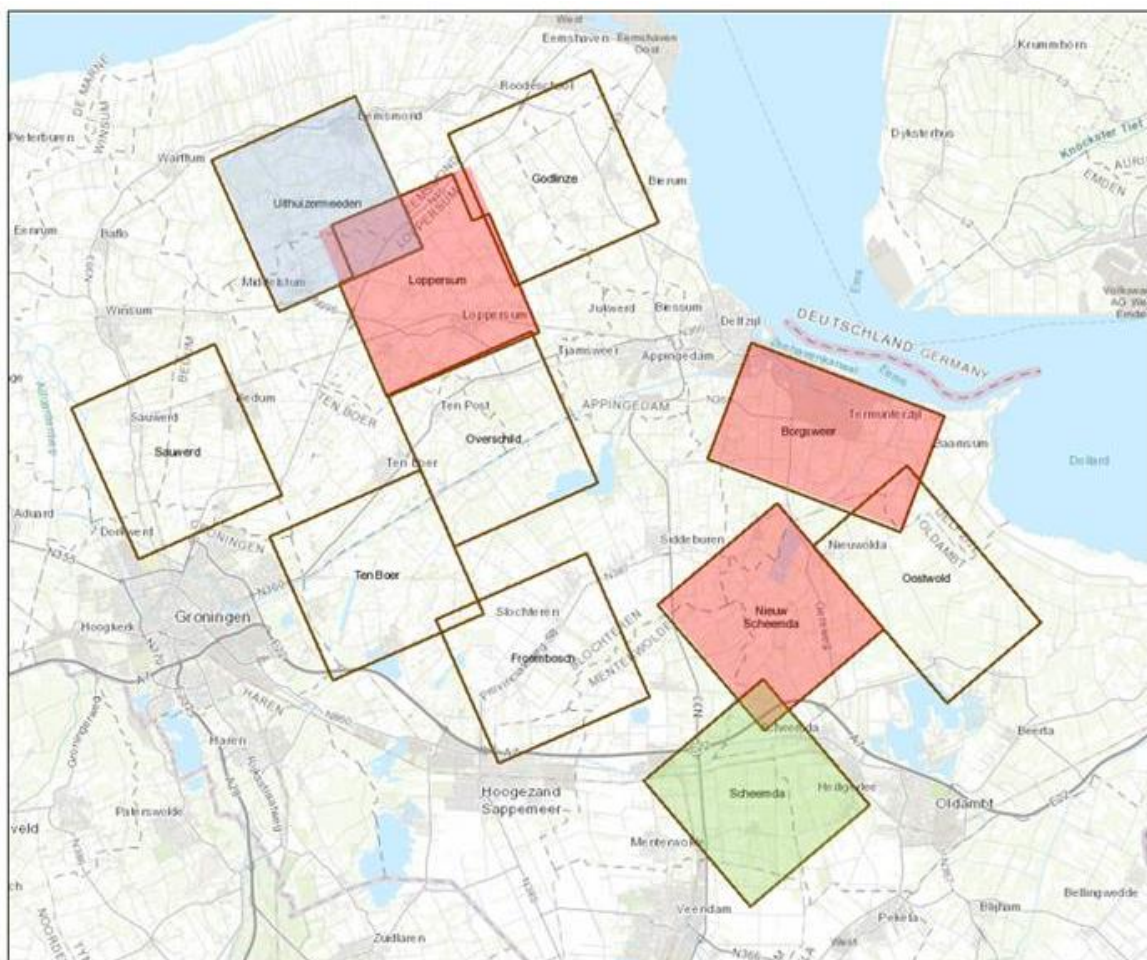


Figure 7.3. Deployment areas (“patches”) for the NAM flexible network of 400 geophones, where the instruments are installed for periods of about 6 weeks. The red areas have already been covered, the green was the most recent area of installation and the blue the next location to be targeted. The blank areas are planned deployment areas; the deployment has since progressed. (Courtesy of Remco Romijn, NAM).

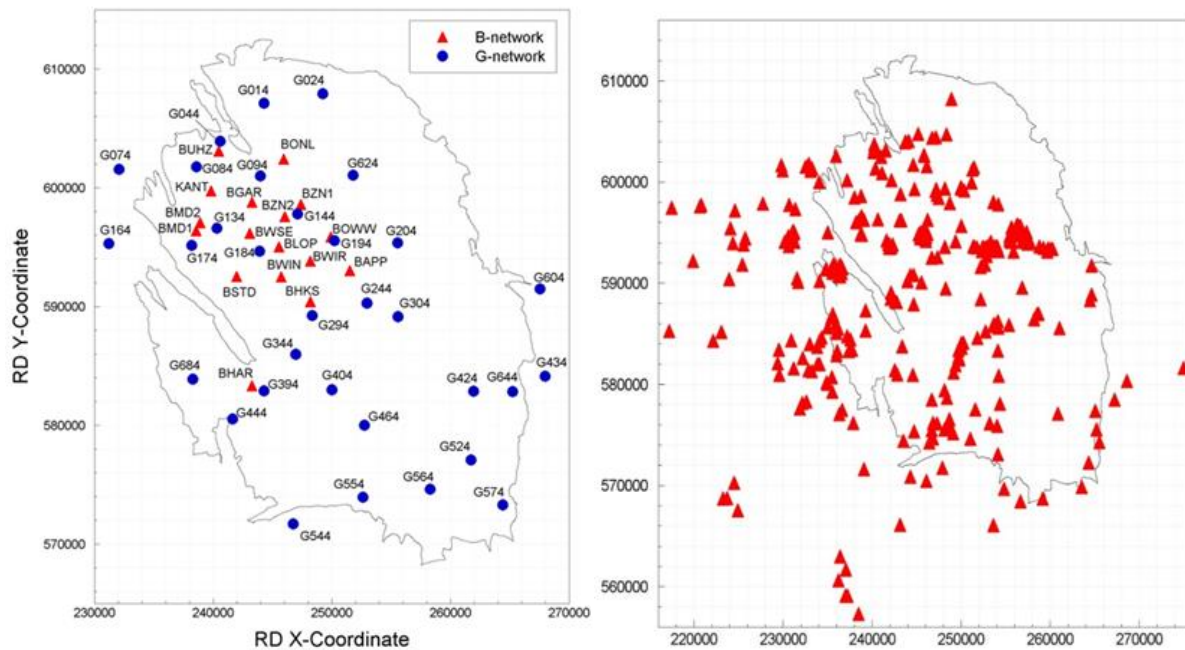


Figure 7.4. Accelerograph networks in Groningen: *Left*: B-station and G-station operated by KNMI; *Right*: TNO-operated instruments in houses and public buildings

Regarding the TNO network, to date these recordings have not been used in the model derivation because of concerns regarding the installation of many of the accelerographs above floor level (Figure 7.5). In order to investigate the degree to which the structural response of these buildings may have influenced the recordings—and therefore the degree to which they can be used as representations of the actual ground motion—experiments have been conducted. In full-scale shaking table tests on a model of a Groningen house conducted at LNEC in Lisbon, the installation of TNO instruments on wall brackets was reproduced together with a second instrument correctly installed at the base of the building (Figure 7.6). Recordings obtained from these instruments are now being processed and are being analysed to ascertain whether recordings from instruments such as those depicted in Figure 7.5 can be used for the derivation of the spatial correlation model.

In conjunction with the assessment of the usability of recordings from those TNO-operated accelerographs installed at some height on a wall (which have been excluded from the database compiled for the study of spatial correlation), work is also underway to assess the usability of recordings from the instruments installed within NAM's production facilities. Analyses are also being undertaken to assess the level of consistency of the surface recordings from the G-stations and the B-stations, and also of the NS_B motions that would result from deconvolution of the surface recordings and the 200-m deep geophone recordings of the G-network. All of these analyses will be documented to establish the database to be used in future refinements of the Groningen GMM.



Figure 7.5. Examples of TNO instruments installed above ground level



Figure 7.6. Reproduction of the TNO installation of accelerographs at ground level and at a higher level on a full-scale model subjected to shake table testing at LNEC

Future Updates of the Groningen GMM

While it has been necessary to develop the GMM for Groningen through a series of short and intense iterations, with each development stage lasting about 7 months on average, there is no intention to produce a V6 model on a similar schedule. Having now reached a mature stage of model development, it is expected that the V5 model will be used for the coming period and any revision will be undertaken on a less rushed timetable.

Notwithstanding the commitment to henceforth implement modifications to the GMM in a more measured manner than that which has marked the development to date, if new hazard and risk estimates are to be presented towards the end of 2018, it is possible that some minor modifications may be made. The first of these would be if the analysis of spatial correlation were to indicate that the approximation achieved through the current rule for sampling variability (Section 6.2) is not an acceptable representation of the field-specific model. The options that could be considered in such a case are modification of the variance sampling rules or the introduction into the risk engine of the Groningen-specific spatial correlation model. The latter option is potentially much more demanding and could only be contemplated if there were sufficient time for implementation and checking through cross-validation.

The second, and more modest, modification would be to include logic-tree branches for between-event variability, as issue that has been raised by the international review panel (see Appendices IX and X). In the current model, no epistemic uncertainty has been included on this parameter and it would be a logical extension of the general modelling approach to introduce branches for alternative Tau values. Since most modern GMPEs with heteroskedastic sigma indicate that Tau values at larger magnitudes are lower than those at small magnitudes such branches can be expected to be skewed towards lower values compared to the V5 model. The basis for alternative Tau branches is now being explored.

As new data becomes available—in the form of recordings from new earthquakes or improved characterisation of the shallow or deep sub-surface—sensitivity analyses will first be performed to gauge the likely impact on the model. New data are being collected and it is also expected that each new earthquake will significantly expand the database by virtue of the number of ground-motion recording instruments now operating in the Groningen field. This point was illustrated by the magnitude ML 3.4 Zeerijp earthquake of 8 January 2018, the third largest event to have occurred in the field. A preliminary analysis of the recordings from this earthquakes is presented in Appendix VIII of this report.

In terms of major changes to the current model, the medium-term objective will be to move towards a more fully non-ergodic ground-motion model. This is discussed in Appendices IX and X as part of the dialogue with the international review panel.

8. References

- Abercrombie, R.E. (1995). Earthquake source scaling relationships from -1 to 5 M_L using seismograms recorded at 2.5 km depth. *Journal of Geophysical Research* **100**, 24015-24036.
- Abrahamson, N.A. & R.R. Youngs (1992). A stable algorithm for regression-analyses using the random effects model. *Bulletin of the Seismological Society of America* **82**, 505-510.
- Afshari, K. & J.P. Stewart (2016). Physically parameterized prediction equations for significant duration in active crustal regions. *Earthquake Spectra* **32**(4), 2057-2081.
- Akkar, S., M.A. Sandikkaya & J.J. Bommer (2014). Empirical ground-motion models for point- and extended-source crustal earthquake scenarios in Europe and the Middle East. *Bulletin of Earthquake Engineering* **12**(1), 359-387. *Erratum: 12*(1), 389-390.
- Anderson, J.G. & S.E. Hough (1984). A model for the shape of the Fourier amplitude spectrum of acceleration at high frequencies. *Bulletin of the Seismological Society of America* **74**, 1969-1993.
- Atkinson, G.M., J.J. Bommer & N.A. Abrahamson (2014). Alternative approaches to modeling epistemic uncertainty in ground motion in probabilistic seismic-hazard analysis. *Seismological Research Letters* **85**(6), 1141-1144.
- Bindi, D., M. Massa, L. Luzi, G. Ameri, E. Pacor, R. Puglia & P. Augliera (2014). Pan-European ground-motion prediction equations for the average horizontal component of PGA, PGV, and 5%-damped PSA at spectral periods up to 3.0 s using the RESORCE dataset. *Bulletin of Earthquake Engineering* **12**(1), 391-430.
- Bommer, J.J., H. Crowley & R. Pinho (2015a). A risk-mitigation approach to the management of induced seismicity. *Journal of Seismology* **19**(2), 623-664.
- Bommer, J.J., B. Dost, B. Edwards, P.P. Kruiver, P. Meijers, M. Ntinalexis, B. Polidoro, A. Rodriguez-Marek & P.J. Stafford (2015c). *Development of Version 2 GMPEs for response spectral accelerations and significant durations from induced earthquakes in the Groningen field*. Version 2, 29 October 2016, 515 pp.
- Bommer, J.J., B. Dost, B. Edwards, P.J. Stafford, J. van Elk, D. Doornhof & M. Ntinalexis (2016a). Developing an application-specific ground-motion model for induced seismicity. *Bulletin of the Seismological Society of America* **106**(1), 158-173.
- Bommer, J.J., B. Dost, B. Edwards, P.P. Kruiver, P. Meijer, M. Ntinalexis, A. Rodriguez-Marek & P.J. Stafford (2016b). *Development of V3 GMPEs for response spectral accelerations and significant durations from induced earthquakes in the Groningen field*. Version 0, 8 July 2016, 476 pp.
- Bommer, J.J., B. Dost, B. Edwards, P.P. Kruiver, P. Meijer, M. Ntinalexis, A. Rodriguez-Marek, E. Ruigrok, J. Spetzler & P.J. Stafford (2017b). *V4 Ground-Motion Model (GMM) for Response Spectral Accelerations, Peak Ground Velocity, and Significant Durations in the Groningen Field*. Version 2.1, 23 June 2017, 541 pp.

Bommer, J.J., B. Dost, B. Edwards, P.P. Kruiver, M. Ntinalexis, A. Rodriguez-Marek, P.J. Stafford & J. van Elk (2017c). Developing a model for the prediction of ground motions due to earthquakes in the Groningen gas field. *Netherlands Journal of Geoscience* **96**(5), s203-s213.

Bommer, J.J., B. Edwards, P.P. Kruiver, A. Rodriguez-Marek, P.J. Stafford, B. Dost, M. Ntinalexis, E. Ruigrok & J. Spetzler (2017d). *V5 Ground-Motion Model for the Groningen Field*. 30 October, 161 pp.

Bommer, J.J., P.J. Stafford & J.E. Alarcón (2009). Empirical equations for the prediction of the significant, bracketed and uniform duration of earthquake ground motion. *Bulletin of the Seismological Society of America* **99**(6), 3217-3233.

Bommer, J.J., P.J. Stafford, B. Edwards, B. Dost & M. Ntinalexis (2015b). *Development of version 1 GMPEs for response spectral accelerations and for strong-motion durations*. Version 2, 21 June 2015, 304 pp.

Bommer, J.J., P.J. Stafford, B. Edwards, B. Dost, E. van Dedem, A. Rodriguez-Marek, P. Kruiver, J. van Elk, D. Doornhof & M. Ntinalexis (2017a). Framework for a ground-motion model for induced seismic hazard and risk analysis in the Groningen gas field, The Netherlands. *Earthquake Spectra* **33**(2), 481-498.

Bommer, J.J. & J. van Elk (2017). Comment on “The maximum possible and maximum expected earthquake magnitude for production-induced earthquakes at the gas field in Groningen, The Netherlands” by Gert Zöller and Matthias Holschneider. *Bulletin of the Seismological Society of America* **107**(3), 1564-1567.

Boore, D.M. (2005a). *SMSIM – Fortran programs for simulating ground motions from earthquakes: Version 2.3—A revision of OFR 96-80*. US Geological Survey Open-File Report 00-509, 55 pp.

Boore, D.M. (2005b). Erratum: Equations for estimating horizontal response spectra and peak acceleration from western north American earthquakes: A summary of recent work, by D.M. Boore, W.B. Joyner and T.E. Fumal. *Seismological Research Letters* **76**(3), 368-369.

Boore, D.M. (2009). Comparing stochastic point-source and finite-source ground-motion simulations: SMSIM and EXSIM. *Bulletin of the Seismological Society of America* **99**, 3202-3216.

Boore, D.M., J.P. Stewart, E. Seyhan & G.M. Atkinson (2014). NGA-West2 equations for predicting PGA, PGV, and 5% damped PSA for shallow crustal earthquakes. *Earthquake Spectra* **30**(3).

Boore, D.M. & E.M. Thompson (2014). Path durations for use in the stochastic-method simulations of ground motions. *Bulletin of the Seismological Society of America* **104**(5), 2541-2552.

Bourne, S.J., S.J. Oates, J. van Elk & D. Doornhof (2014). A seismological model for earthquakes induced by fluid extraction from a subsurface reservoir. *Journal of Geophysical Research Solid Earth* **119**, doi: 10.1002/201JB011663.

Bourne, S.J., S.J. Oates, J.J. Bommer, B. Dost, J. van Elk & D. Doornhof (2015). A Monte Carlo method for probabilistic hazard assessment of induced seismicity due to conventional natural gas production. *Bulletin of the Seismological Society of America* **105**(3), 1721-1738.

Brune, J.N. (1970). Tectonic stress and spectra of seismic shear waves from earthquakes. *Journal of Geophysical Research* **75**, 4997-5009.

Brune, J.N. (1971). Correction. *Journal of Geophysical Research* **76**, 5002.

Butcher, A., R. Luckett, J.P. Verdon, J.-M. Kendall, B. Baptie & J. Wookey (2017). Local magnitude discrepancies for near-event receivers: Implications for the U.K. traffic-light scheme. *Bulletin of the Seismological Society of America* **107** 532-541.

Campbell, K.W. & Y. Bozorgnia (2007). *Campbell-Bozorgnia NGA Ground Motion Relations for the Geometric Mean Horizontal Component of Peak and Spectral Ground Motion Parameters*. PEER Report 2007/02, Pacific Earthquake Engineering Research Center, University of California at Berkeley, 240 pp.

Campbell, K.W. & Y. Bozorgnia (2014). NGA-West2 ground motion model for the average horizontal components of PGA, PGV, and 5%-damped elastic pseudo-acceleration response spectra. *Earthquake Spectra* **30**(3), 1087-1115.

Chiou, B.S.J. & R.R. Youngs (2014). Update of the Chiou and Youngs NGA model for the average horizontal component of peak ground motion and response spectra. *Earthquake Spectra* **30**(3), 1117-1153.

Deichmann, N. (2006). Local magnitude, a moment revisited. *Bulletin of the Seismological Society of America* **96**, 1267-1277.

Deichmann, N. (2017). Theoretical basis for the observed break in M_L/M_W scaling between small and large earthquakes. *Bulletin of the Seismological Society of America* **107**, 505-520.

Dost, B., B. Edwards & J.J. Bommer (2018). The relationship between M_w and M_L – a review and application to induced seismicity in Groningen, the Netherlands. *Seismological Research Letters*, DOI: 10.1785/0220170247.

Dost, B. & D. Kraaijpoel (2013). *The August 16, 2012 earthquake near Huizinge (Groningen)*. KNMI. <http://www.knmi.nl/knmi/library/miscellaneousreport.html>

Dost, B., E. Ruigrok & J. Spetzler (2017). Development of probabilistic seismic hazard assessment for the Groningen gas field. *Netherlands Journal of Geoscience* **96**(5), s235-s245.

Dost, B., T. van Eck & H. Haak (2004). Scaling of peak ground acceleration and peak ground velocity recorded in the Netherlands. *Bolletino di Geofisica Teorica ed Applicata* **45**(3), 153-168.

Edwards, B., B. Allmann, D. Fäh & J. Clinton (2010). Automatic computation of moment magnitudes for small earthquakes and the scaling of local to moment magnitude. *Geophysical Journal International* **183**, 407-420.

Edwards, B. & J. Douglas (2014). Magnitude scaling of induced earthquakes. *Geothermics* **52**, 132-139.

Edwards, B., T. Kraft, C. Cauzzi, P. Kästli & S. Wiemer (2015). Seismic monitoring and analysis of deep geothermal projects in St Gallen and Basel, Switzerland. *Geophysical Journal International* **201**, 1020-1037.

- Grünthal, G., R. Wahlstrom & D. Stromeyer (2009). The unified catalogue of earthquakes in central, northern, and northwestern Europe (CENEC)-updated and expanded to the last millennium. *Journal of Seismology* **13**, 517-541.
- Hanks, T. C. & D. M. Boore (1984). Moment-magnitude relations in theory and practice. *Journal of Geophysical Research* **89**, 6229-6235.
- Kempton, J.J. & J.P. Stewart (2006). Prediction equations for significant duration of earthquake ground motions considering site and near-source effects. *Earthquake Spectra* **22**(4), 985-1013.
- Kraaijpoel, D. & B. Dost (2013). Implications of salt-related propagation and mode conversion effects on the analysis of induced seismicity. *Journal of Seismology* **17**(1), 95-107.
- Kruiver, P. P., E. van Dedem, E. Romijn, G. de Lange, M. Korff, J. Stafleu, J.L. Gunnink., A. Rodriguez-Marek, J.J. Bommer, J. van Elk & D. Doornhof (2017). An integrated shear-wave velocity model for the Groningen gas field, The Netherlands. *Bulletin of Earthquake Engineering* **15**(9), 3555-3580.
- Motazedian, D. & G.M. Atkinson (2005). Stochastic finite-fault modelling based on a dynamic corner frequency. *Bulletin of the Seismological Society of America* **95**, 995-1010.
- Munafò, I., L. Malagnini & L. Chiaraluce (2016). On the relationship between M_w and M_L for small earthquakes. *Bulletin of the Seismological Society of America* **106**, 2402-2408.
- Noorlandt, R.P., P.P. Kruiver, M.P.E. de Kleine, M. Karaoulis, G. de Lange, A. Di Matteo, J. von Ketelhodt, E. Ruigrok, B. Edwards, A. Rodriguez-Marek, J.J. Bommer, J. van Elk & D. Doornhof (2018). Characterisation of ground-motion recording stations in the Groningen gas field. *Journal of Seismology*, DOI: 10.1007/s10950-017-9725-6.
- Rodriguez-Marek, A., P.P. Kruiver, P. Meijers, J.J. Bommer, B. Dost, J. van Elk & D. Doornhof (2017). A regional site-response model for the Groningen gas field. *Bulletin of the Seismological Society of America* **107**(5), 2067-2077.
- Stafford, P.J., Rodriguez-Marek, A., B. Edwards, P.P. Kruiver & J.J. Bommer (2017). Scenario dependence of linear site effect factors for short-period response spectral ordinates. *Bulletin of the Seismological Society of America* **107**(6), 2859-2872.
- Stafford, P.J., B.D. Zurek, M. Ntinalexis & J.J. Bommer (2018). Extensions to the Groningen ground-motion model for seismic risk calculations: component-to-component variability and spatial correlation. *In preparation for special issue of Bulletin of Earthquake Engineering on 'Induced Seismicity and its Effect on the Built Environment'*.
- van Essen, H. (2017). *Proevenverzameling Noorderzijvest - Deelverzameling ten behoeve van dijkversterking Eemskanaal*. Deltares report 1220173-024-GEO-0071, 30 May 2017 (in Dutch).
- Wells, D.L. & K.J. Coppersmith (1994). New empirical relationships among magnitude, rupture length, rupture width, rupture area, and surface displacement. *Bulletin of the Seismological Society of America* **84**, 974-1002.
- Yenier, E. & G.M. Atkinson (2015). Regionally adjustable generic ground-motion prediction equation based on equivalent point-source simulations: Application to central and eastern North America. *Bulletin of the Seismological Society of America* **105**, 1989-2009.

Zwanenburg, C. & M. Konstantinou (2016). *Assessment of dynamic properties for peat - Factual Report*. Deltares report 1209862-011-GEO-0003, 4 November 2016.

Zwanenburg, C., M. Konstantinou & P. Meijers (2017). *Dynamic behaviour of Groningen peat - Analysis and parameter assessment*. Deltares report 1209862-011-GEO-0005, 24 March 2017

APPENDIX I

International Review Panel

As explained in Chapters 1 and 2 of this report, the development of the Groningen GMM has undergone extensive peer review by an international panel of experts in the fields of ground-motion prediction and site response characterisation. The full set of written comments on the first versions of the V4 and V5 GMM reports, together with the detailed responses from the GMM development team, are presented in Appendices IX and X, respectively. This appendix presents the closure letter from the review panel issued following their review of the V5 mode, and also includes brief biographies of the panel members.

January 15 2018

Mr Jan van Elk
Nederlandse Aardolie Maatschappij B.V. (NAM)
Schepersmaat 2,
9405 TA Assen, The Netherlands

Dear Mr. van Elk:

The undersigned are members of an international panel of experts in earthquake ground motion modelling, which was engaged at various intervals since July 2015 to review the development of ground motion models for the Groningen field. Panel reports presenting our assessments have been submitted for the Version 4 model (May 2017) and the Version 5 model (January 2018).

Our overall assessment of the modeling effort to date is that it has produced a state-of-the-art model that is well suited for its purpose of regional ground motion prediction to support hazard and risk studies in the Groningen field. While our most recent review of the draft Version 5 report resulted in some technical and editorial comments, these issues do not impact the fundamental viability of the model that has been developed.

Respectfully submitted,



Jonathan P. Stewart (Chair)



Norman A. Abrahamson



Gail M. Atkinson



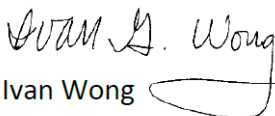
Hilmar Bungum



Fabrice Cotton



John Douglas



Ivan Wong



Robert R Youngs

Professor Jonathan P Stewart (chairman)

Jon Stewart is a civil engineer with Masters and PhD degrees in geotechnical engineering. He is currently full Professor and head (chair) of the Department of Civil & Environmental Engineering at the University of California Los Angeles (UCLA) and Fellow of the American Society of Civil Engineers (ASCE). Professor Stewart is widely regarded as one of the foremost global experts in the characterisation of dynamic site response and its influence on earthquake ground motions. He has received numerous awards and accolades for his research, the most recent being the prestigious William B. Joyner Lecture (2016) and the Bruce Bolt Medal (2018) both awarded jointly by Seismological Society of America and the Earthquake Engineering Research Institute. Professor Stewart served as editor-in-chief of the ASCE *Journal of Geotechnical and Geoenvironmental Engineering* from 2007 to 2010, and has served as editor of *Earthquake Spectra* since 2013. He has published over 100 papers related to geotechnical earthquake engineering and seismic ground-motion characterisation in peer-reviewed journals, including being co-author of one of the NGA-West2 GMPEs published in 2014. Professor Stewart has served in many US and international technical committees and projects, including leadership roles in the Global Ground Motion Prediction Equations Project of GEM (Global Earthquake Model) and as member of the international advisory panel for New Zealand ground motion national hazard model.

Dr Norman A Abrahamson

Norm Abrahamson obtained a PhD in Seismology from the University of California at Berkeley and is currently adjunct professor in Civil and Environmental Engineering at both UC Berkeley and UC Davis. Dr Abrahamson has been engaged in practice as well as research throughout his 30-year career, working both as a consultant for seismic projects around the world and as an employee at PG&E in California where he was the technical lead for seismic hazard assessments for the Diablo Canyon nuclear power plant and 170 dams throughout northern California. He also led the PG&E seismic research program for 20 years. He is widely regarded as the world leader in the field of earthquake ground-motion prediction and probabilistic seismic hazard assessment. In 2012, he was the recipient of the Bruce Bolt Medal in recognition of work in the field of ground-motion prediction. Dr Abrahamson has produced ground-motion models for active crustal, stable continental and subduction regions, and has played pivotal roles in major projects for GMPE development such as NGA-West, NGA-West2 and NGA-East. He has extensive experience in consultancy projects related to ground-motion characterisation and seismic hazard analyses, including leadership roles in the US Department of Energy Extreme Ground-Motion Project, the PEGASOS project for Swiss nuclear power plant sites, the SWUS project for nuclear power plants in the southwest United States, and for hydroelectric dams in British Columbia, Canada.

Professor Gail M Atkinson

Gail Atkinson is a seismologist and currently holds the positions of Professor and NSERC/TransAlta/Nanometrics Industrial Research Chair in Hazards from Induced Seismicity in the Department of Earth Sciences at Western University, Ontario, Canada. Professor Atkinson's research covers a wide range of topics related to earthquake hazards and particularly the development of ground-motion prediction equations (GMPEs). She has produced GMPEs for Eastern North America, active crustal regions (NGA-West and NGA-West2 models), and more recently for induced earthquakes. Professor Atkinson has published more than 200 papers on earthquake ground motions, seismic source characterisation and site response; her work is widely cited, as demonstrated by her *h*-index that is above 50. She has served as President of the Seismological Society of America, and also as President of the Canadian Geophysical Union. She was the 2007 Bill Joyner Memorial Lecturer.

Dr Hilmar Bungum

Hilmar Bungum is a seismologist who obtained his PhD from the University of Bergen in 1974. Between 1987 and 2007, Dr Bungum was Deputy Director of NORSAR in Oslo, and he has also held adjunct professor appointments in geophysics and seismology at the Universities of Bergen and Oslo. He has published extensively on tectonics, observational seismology, seismic source modelling, ground-motion prediction and probabilistic seismic hazard analysis (PSHA). Dr Bungum has also served for many years as an editorial board member for both *Journal of Seismology* and *Journal of Earthquake Engineering*. He has extensive experience in both research and consultancy projects related to seismic hazard analysis around the world. His experience as a reviewer in such projects includes assessment of the seismic hazard studies performed for nuclear power plant sites in Finland, on behalf of the regulator, and as chairman of the Participatory Peer Review Panel (PPRP) in SSHAC Level 3 PSHA studies for nuclear power plant sites in South Africa and Spain.

Professor Fabrice Cotton

Fabrice Cotton current holds the chair of Engineering Seismology and Seismic Hazard at the University of Potsdam, Germany. He is the head of the "seismic hazard and risk dynamics" section of the German Research Centre for Geosciences (GFZ) and he is also chairing the GEM (Global Earthquake Model) Science Board. He obtained his PhD in seismology in 1996 and then worked for five years as a researcher in the seismic hazard team of the French Nuclear Safety Institute (IRSN Fontenay aux Roses, France) before taking up an academic position at the Joseph

Fourier University in Grenoble. His research interests are mainly focused on the analysis of earthquake source properties (kinematic source inversion, stress-drop variability), ground-motion prediction in stable continental regions and seismic hazard assessment. He has published over 100 journal papers on these topics and his work has been highly cited (*h*-index > 35). Professor Cotton has participated in many international projects related to earthquake hazard assessment including the PEGASOS project for PSHA at Swiss nuclear power plants and the SIGMA project in France. He is also an associate editor of the *Bulletin of the Seismological Society of America*.

Dr John Douglas

John Douglas obtained his PhD in Engineering Seismology in 2001 from Imperial College London after which he worked as post-doctoral researcher on the European Strong-Motion Database. He subsequently worked as a senior engineering seismologist at the French Geological Survey (BRGM) for over a decade during which time he was engaged on both research and commercial projects related to natural hazards. Dr Douglas is current Chancellor's Fellow (Lecturer) in the Centre for Intelligent Infrastructure within the Department of Civil and Environmental Engineering of the University of Strathclyde, UK. He has published extensively on the characterisation and prediction of earthquake ground-motions, including those due to induced earthquakes. He also maintains the global compendium of GMPEs at www.gmpe.org.uk. Dr Douglas is associate editor of the *Bulletin of the Seismological Society of America*, *Earthquake Spectra* and the *Bulletin of Earthquake Engineering*. In 2011 he won the quadrennial Young Researcher Prize (*Prix du Jeune Chercheur*) of the French Association of Earthquake Engineering (AFPS).

Ivan Wong

Ivan Wong is a seismologist and geologist specialising in seismic hazard analysis and currently works as senior principal seismologist at Lettis Consultants International in California. He has several decades of experience in the assessment of earthquake hazards for critical projects worldwide, including work on more than 200 dams in the U.S., Canada, Thailand, Eritrea, and Egypt; bridges, tunnels and pipelines; mining facilities and tailings dams in the western US, Peru, Brazil, Colombia, Ecuador, and Chile; nuclear power plants and waste repositories; cogeneration plants; and LNG facilities and offshore petroleum platforms. Ivan served as project manager for the probabilistic seismic hazard analysis (PSHA) and probabilistic fault displacement hazard analysis (PFDHA) conducted for the Yucca Mountain radioactive waste repository in Nevada, USA. In 2017, he was appointed by California Governor Jerry Brown to serve on the Alfred E. Alquist Seismic Safety Commission for a term of four years. In recent years, a major focus of Ivan's work

has been related to induced seismicity. He has analysed numerous cases of induced seismicity throughout the U.S. and western Canada including the Rocky Mountain Arsenal in Colorado, Permian Basin in west Texas, eastern Ohio, and The Geysers, California. He co-authored guidelines such as the US Department of Energy's Protocol and Best Practices for Geothermal Energy-Induced Earthquakes and the US Interstate Oil and Gas Compact Commission's technical and regulatory criteria on injection-induced seismicity. He is a long-serving associate editor of the *Bulletin of the Seismological Society of America* and past member of the editorial board of *Earthquake Spectra*.

Dr Robert R Youngs

Bob Youngs is a civil engineer who earned Masters and PhD degrees in geotechnical engineering from the University of California at Berkeley. A founding member and vice-president of the specialist consultancy firm Geomatrix, he is now a Principal Engineer at Wood plc (formerly AMEC Foster Wheeler Environment & Infrastructure, Inc.) in Oakland California. Dr Youngs has more than 40 years of consulting experience, with primary emphasis in hazard and decision analysis. He has pioneered approaches for incorporating Earth sciences data and their associated uncertainties into probabilistic hazard analyses. The focus of this work has been on developing quantitative evaluations of hazard by combining statistical data and expert judgment. Dr Youngs has considerable experience in developing ground motion models and assessing earthquake hazards in a variety of tectonic environments utilising SSHAC processes. He was a member of the research teams that developed EPRI's seismic hazard assessment for nuclear power plants in the CEUS in 1988, as well as EPRI-sponsored research projects to assess ground motions (1993) and maximum magnitudes (1994) for the CEUS. He was also a member of the project team for the NRC project to develop response spectral shapes for analysis of nuclear facilities (NUREG/CR-6728) in 2001, and for the EPRI SSHAC Level 3 project to characterise ground motions in the CEUS for analysis of nuclear facilities in 2004 as well as the update of these models executed in 2013. He was a member of ground motion development teams for SSHAC Level 3 projects in British Columbia, Washington State, California, and the current NGA East project for the CEUS. Dr Youngs has completed seismic hazard analyses of existing and proposed nuclear power plants throughout the United States (including in Alabama, Florida, Illinois, Louisiana, Massachusetts, Michigan, New York, North Carolina, and Washington) and internationally, including in Bulgaria, Canada, Slovakia, Switzerland (PEGASOS project) and Spain. Dr Youngs was awarded the 2012 Jesuit Seismological Award by the Eastern Section of the Seismological Society of America for contributions to observational seismology

APPENDIX II

Slochteren Earthquake Recordings

A magnitude M_L 2.6 earthquake occurred towards the south of the Groningen field on 27 May 2017 near the town of Slochteren (Figure A2.1). This was the first event of $M_L \geq 2.5$ to contribute records to the ground-motion database used for the derivation of the GMM since the V3 database was established with 178 accelerograph recordings obtained from 22 earthquakes with local magnitude in the range from M_L 2.5 to M_L 3.6; the database remained unchanged for the V4 GMM.

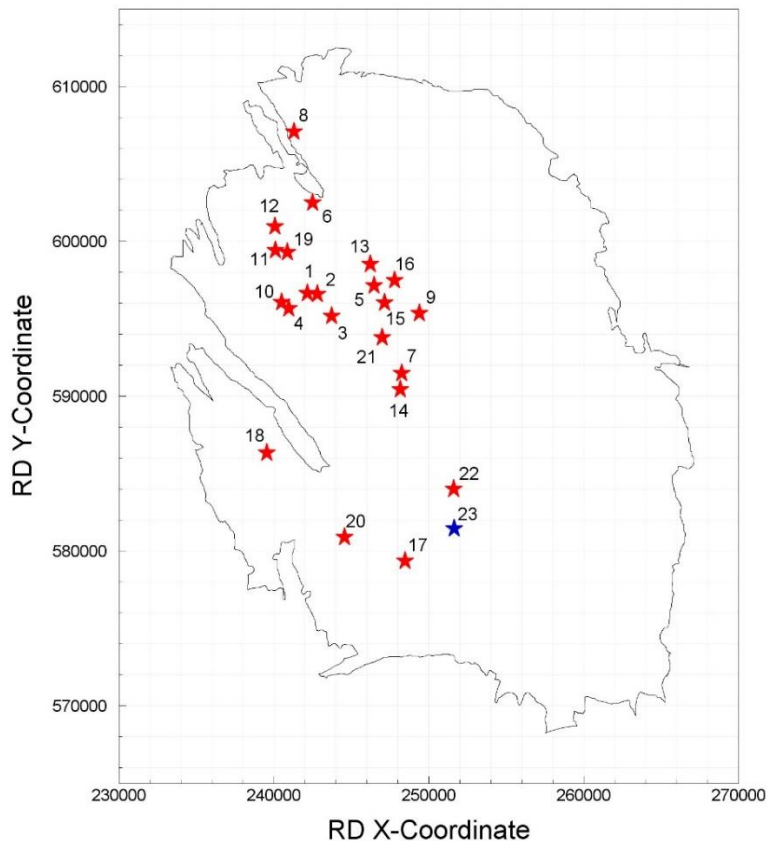


Figure A2.1. Epicentres of the 22 earthquakes in the V3-V4 Groningen ground-motion database and the May 2017 Slochteren event (*blue star*)

The recordings from the Slochteren event were processed rapidly in order to be incorporated to the database used for the derivation of the V5 GMM. The earthquake added 68 new recordings to the database—and increase of almost 40% compared to the V3 and V4 versions—predominantly from the G-stations, including several stations that had not contributed to the database previously. Before this event, the largest number of recordings from a single event were the 44 accelerograms of the

M_L 3.1 Hellum earthquake, which was the last event added to the V3 database. With the expansion of the recording networks in the region, it can now be expected that future earthquakes will routinely generate similar numbers of recordings.

The PGA values recorded in the Slochteren earthquake are compared with those from previous earthquakes in Figure A2.2. The largest horizontal PGA value was 0.035g. While this is much smaller than the maximum value of 0.082g recorded in the 2012 Huizinge earthquake—in itself a very low level of motion compared to those observed in destructive earthquakes in tectonically active regions—it did appear large in comparison to previous earthquakes of comparable magnitude. The value of 0.035g has been exceeded in five previous earthquakes, the smallest of which was of magnitude M_L 2.9. This highest PGA was recorded at less than 2 km from the earthquake epicentre. As can be appreciated from Figure A2.2, the majority of the recorded amplitudes were rather low, even compared to the existing database.

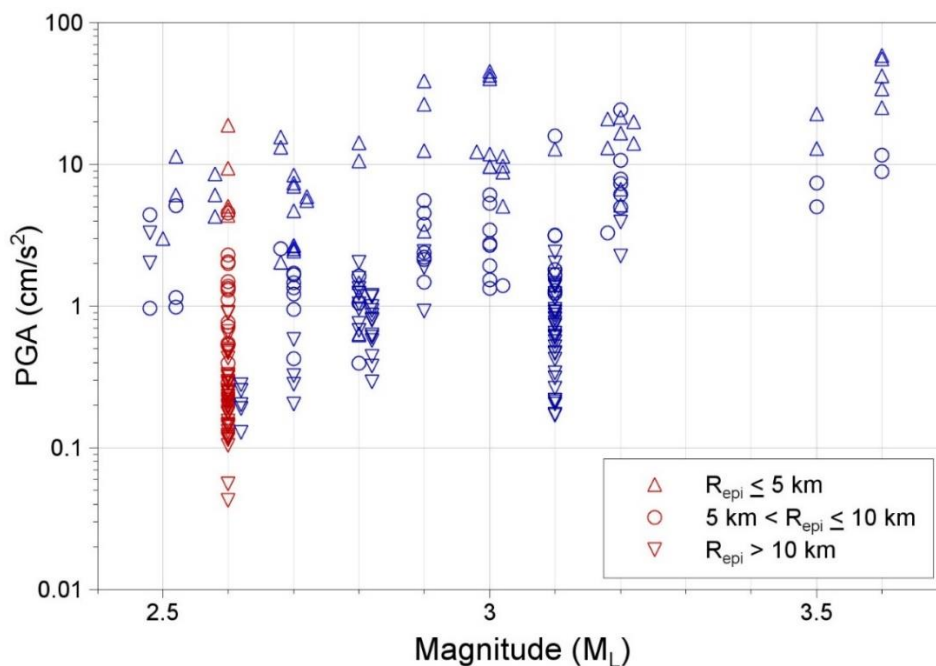


Figure A2.2. Geometric mean horizontal PGA values against magnitude in the Groningen database, with symbols indicating ranges of epicentral distance. The red symbols correspond to the May 2017 Slochteren event. Where two or more events have the same magnitude, the symbols are displaced slightly left and/or right for clarity.

The recording exhibiting the largest peak acceleration of 0.035g displays features typical of the Groningen data, namely highly-polarised horizontal components with the high PGA value associated with a pronounced and isolated peak in the motion (Figure A2.3). As already observed in the database, for individual components of motion the values of PGA and duration exhibit a strong inverse correlation (Figure A2.4).

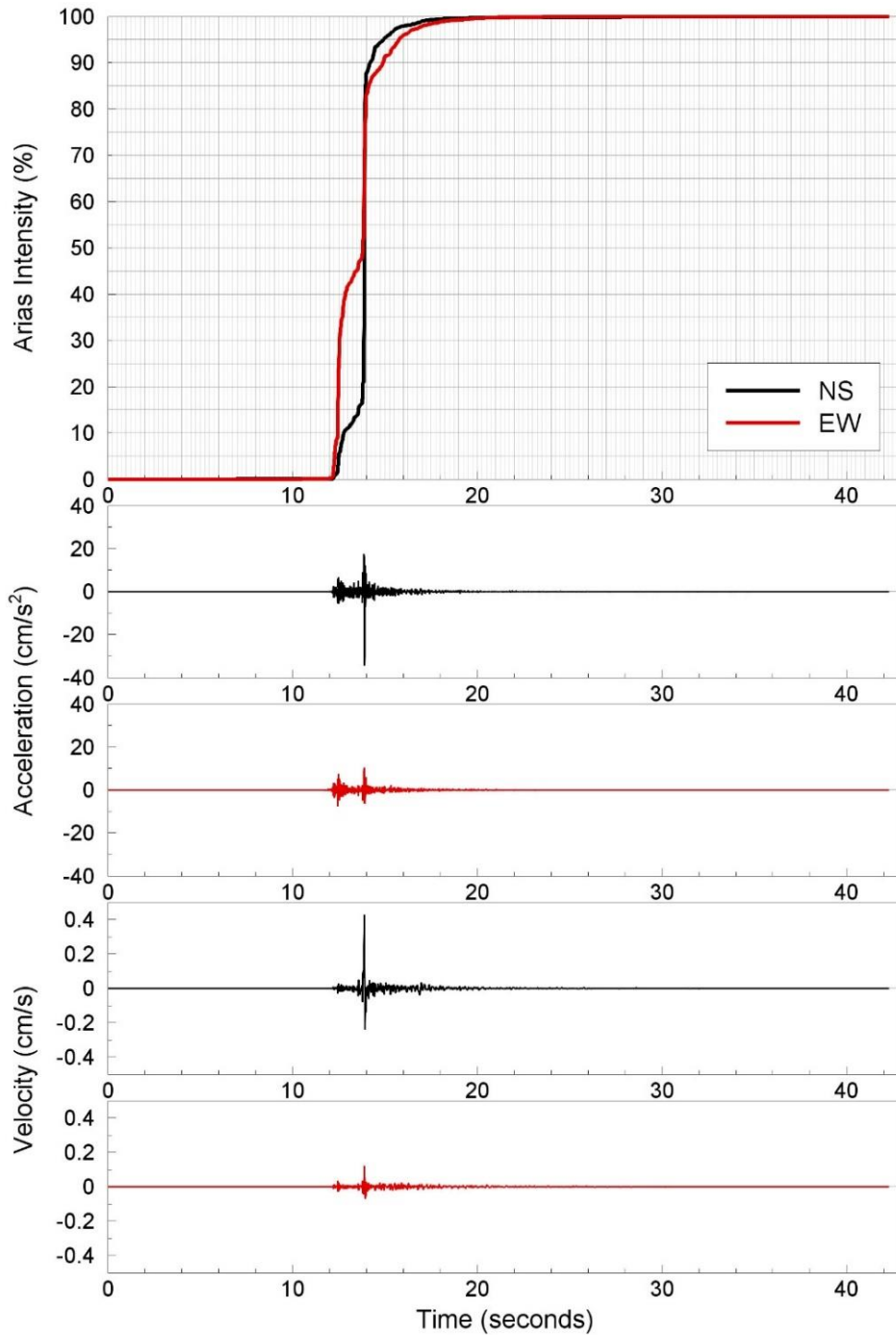


Figure A1.3. Horizontal acceleration and velocity components from the G46 station recordings of the Slochteren earthquakes and the Husid plots showing the distribution of the energy in the motion over time

The degree of polarization of the horizontal motions at short epicentral distances is illustrated in Figure A2.5, in which it can be seen that for two recording stations (G46 and G50), the ratios of the two horizontal peaks—of both acceleration and velocity—is about 3.

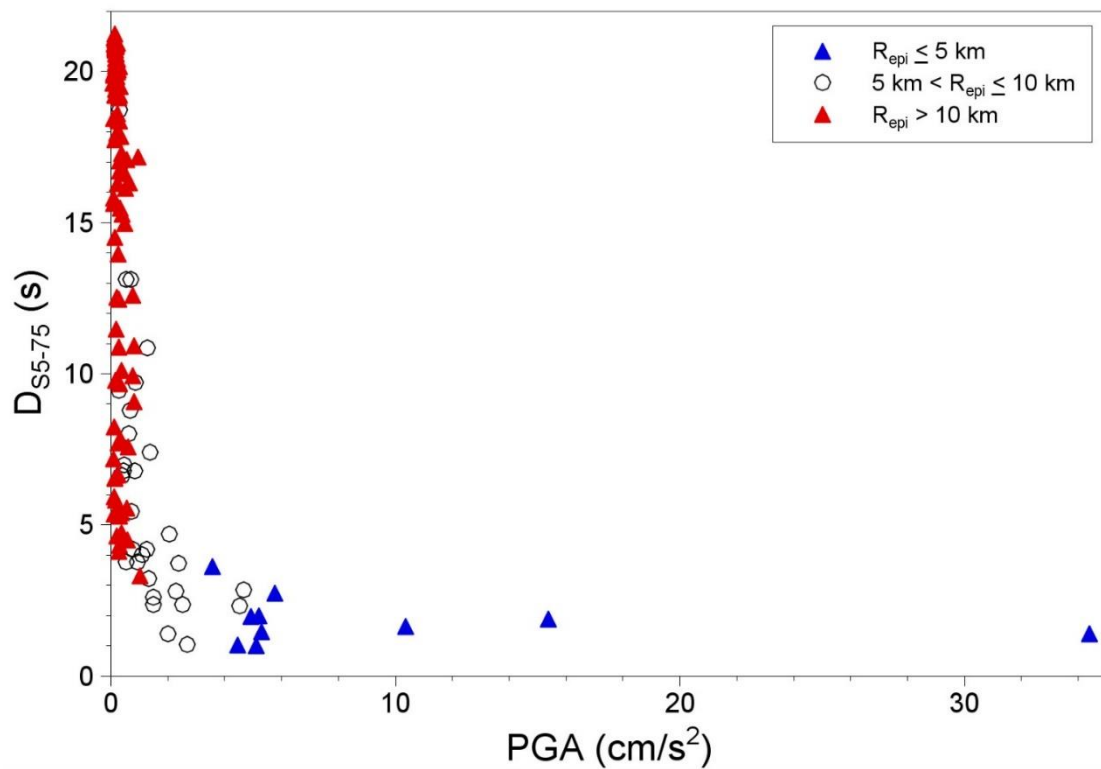
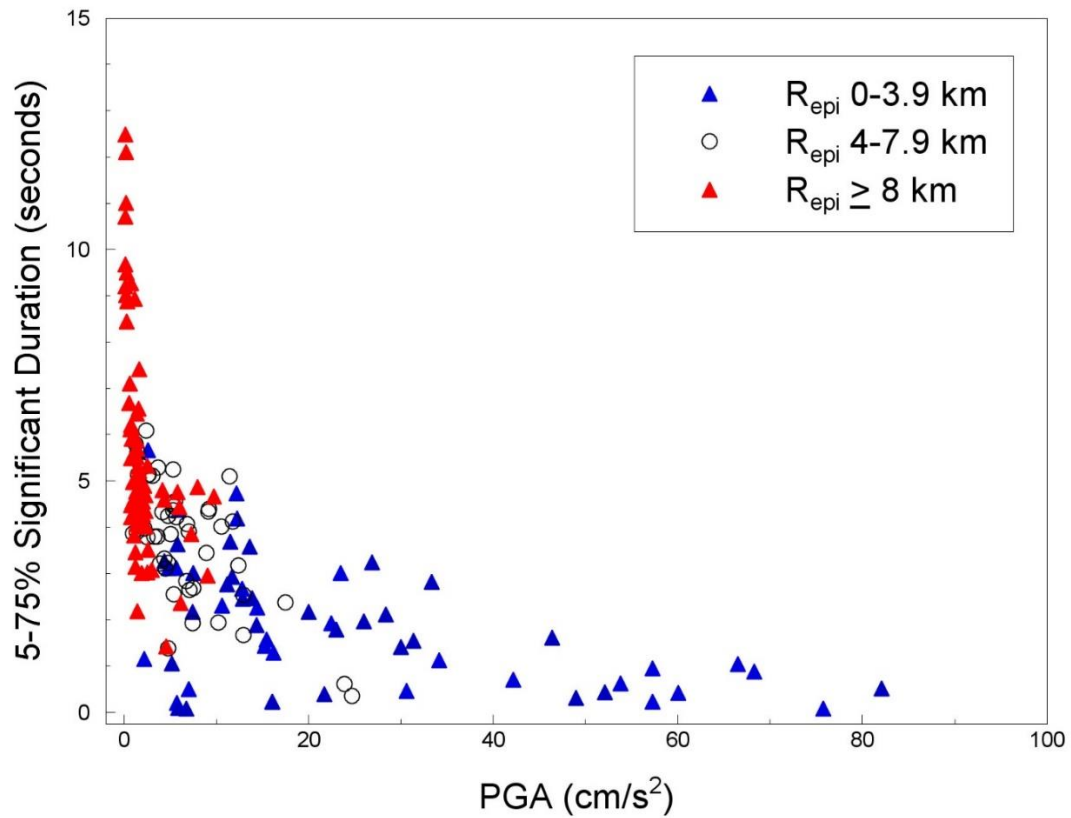


Figure A2.4. *Upper*: Individual component values of PGA and significant duration in the Groningen ground-motion database, showing the strong inverse relationship between these two parameters; *Lower*: Similar plot using only the Slochteren data.

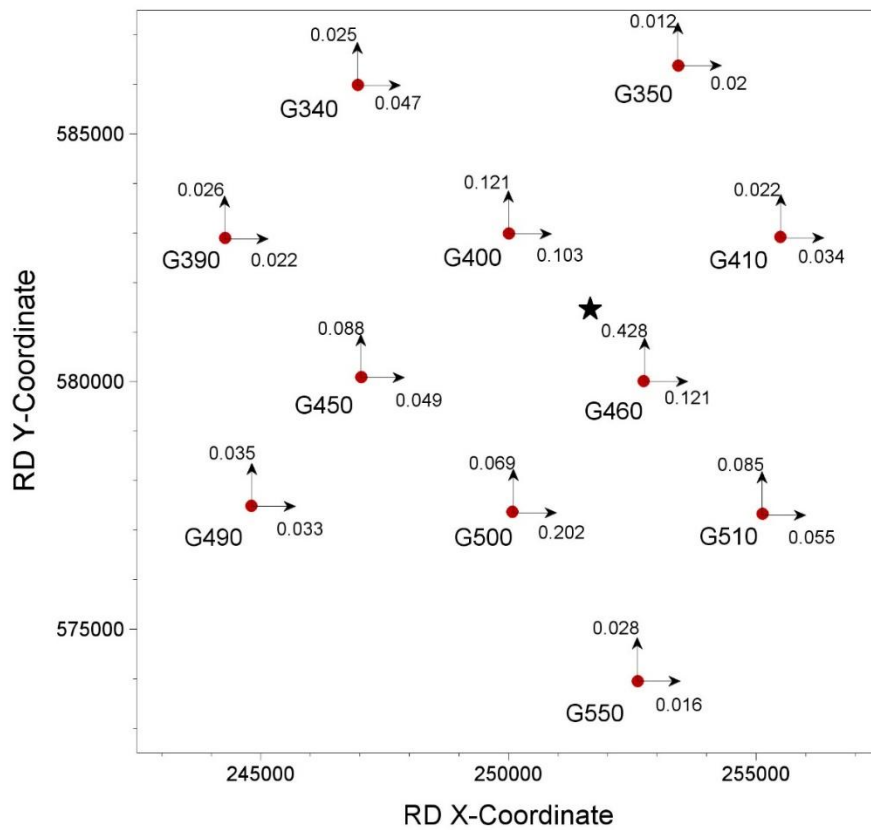
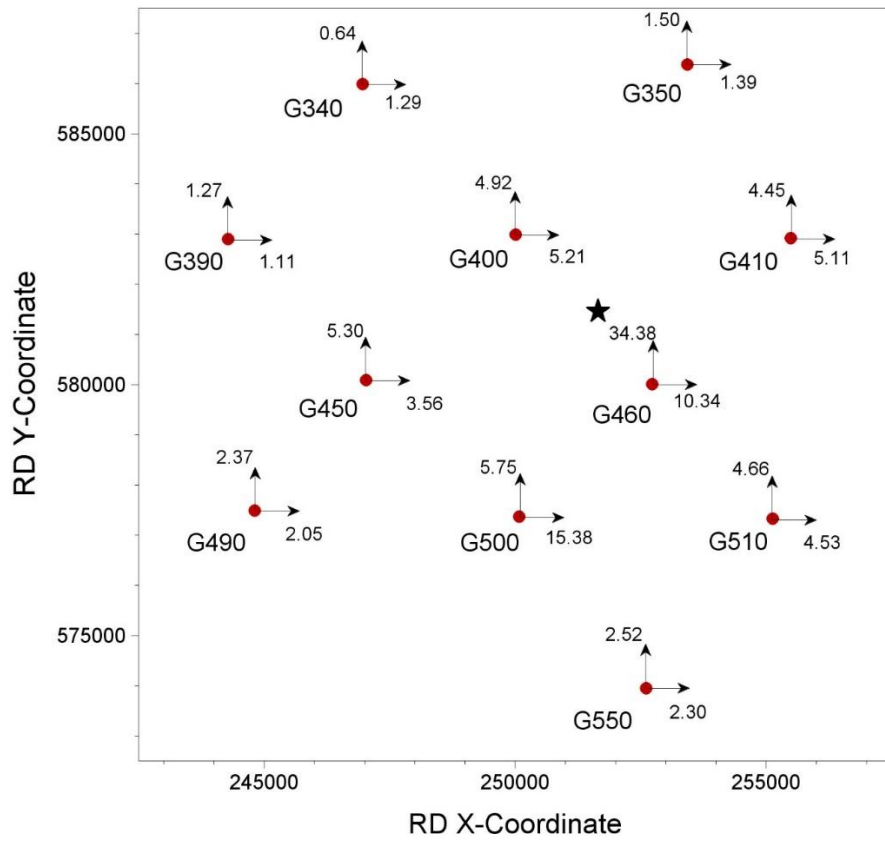


Figure A2.5. *Upper:* Accelerograph stations within ~8 km of the epicentre (*black star*) of the Slochteren earthquake, showing the PGA values (cm/s²) on the NS and EW components; *Lower:* Similar plot for PGV (cm/s).

Despite the relatively high peaks of the strongly-polarised near-source recordings, as noted earlier the overall pattern observed is that on average the amplitudes of motion from this earthquake are rather low. Calculating the residuals of geometric mean PGV with respect to the V4 GMM, the event-term is found to be one inter-event standard deviation below the median level for that model. The relatively weak nature of this earthquake is also confirmed by the event terms found from the simulations for the V5 model (Figure A2.6).

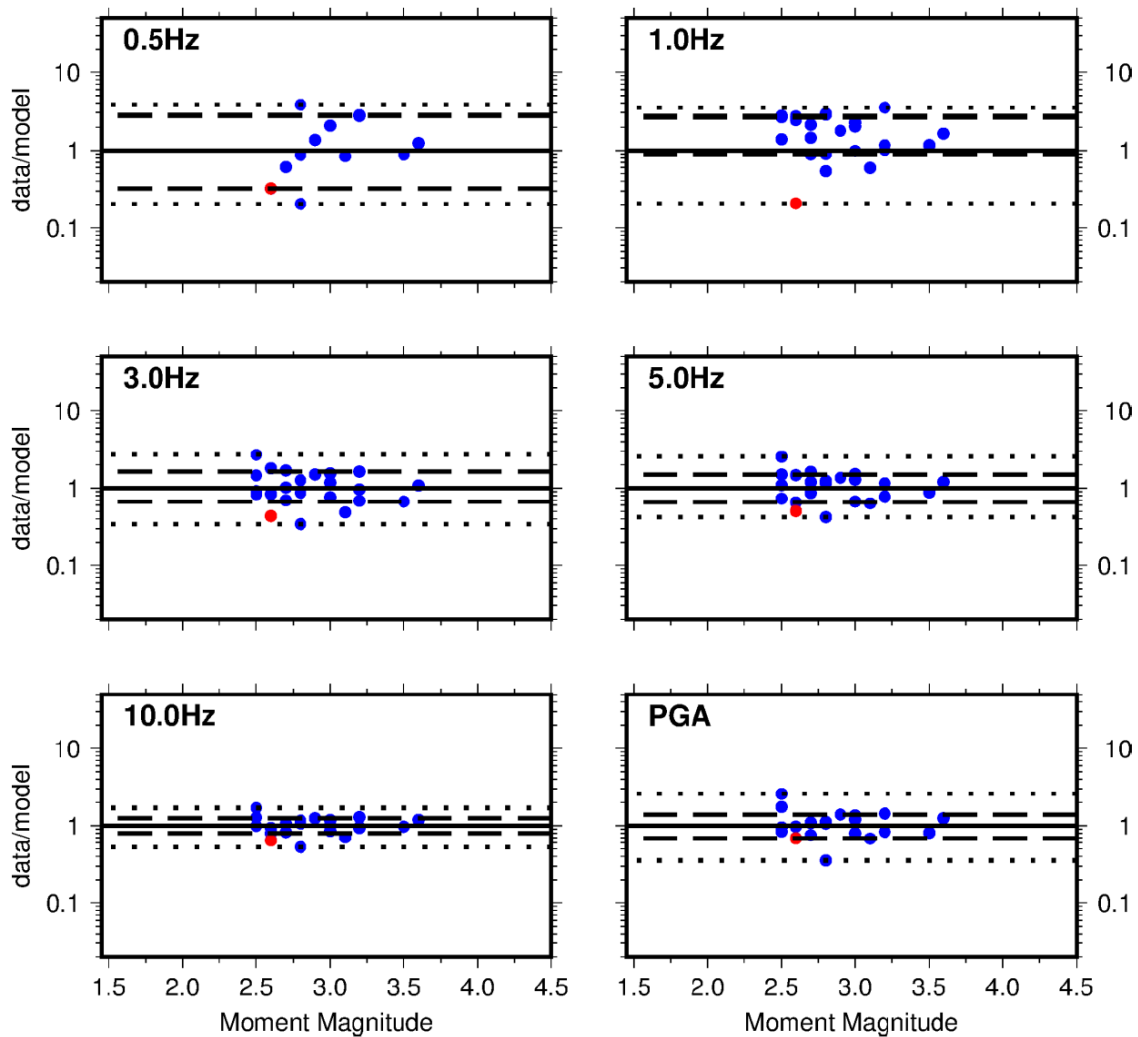


Figure A2.6. Between-event terms for the Central-lower (Ca) simulations with the V5 model; the red dots correspond to the Slochteren earthquake. The solid line indicates equivalence, the dashed and dotted lines indicate the one and two standard deviation levels.

Figure A2.7 shows the effect of repeating the V5 inversions without the Slochteren recordings, which leads to an optimal solution with a higher kappa value at the NS_B horizon and a higher value of the stress parameter, if it assumed that this applies to both of the central branches. The combined effect of these two changes is shown in Figure A2.8, which shows that in the range of intermediate periods (0.1-0.5 s) the

reduced stress parameter leads to a ~10% reduction in amplitudes, while at shorter periods the kappa increase appears to cancel out the effect.

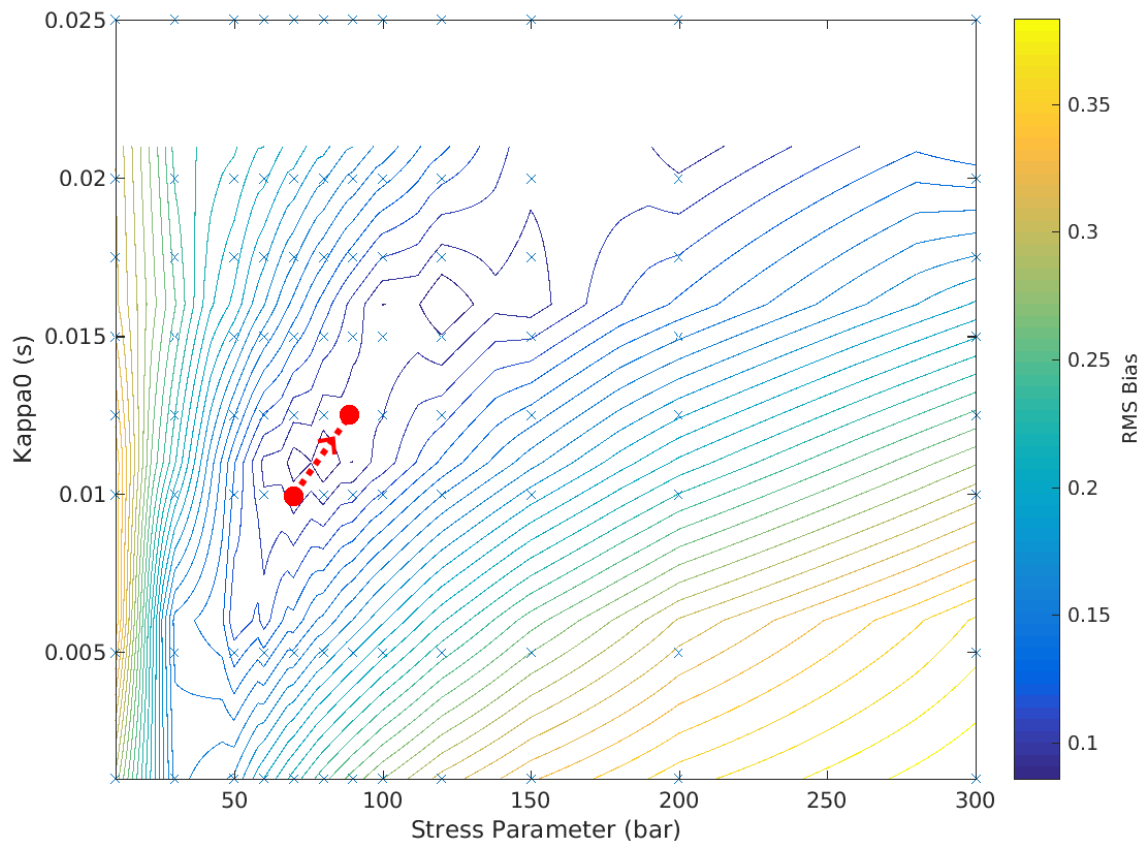


Figure A2.7. Change in optimal model parameters caused by removal of Slochteren data

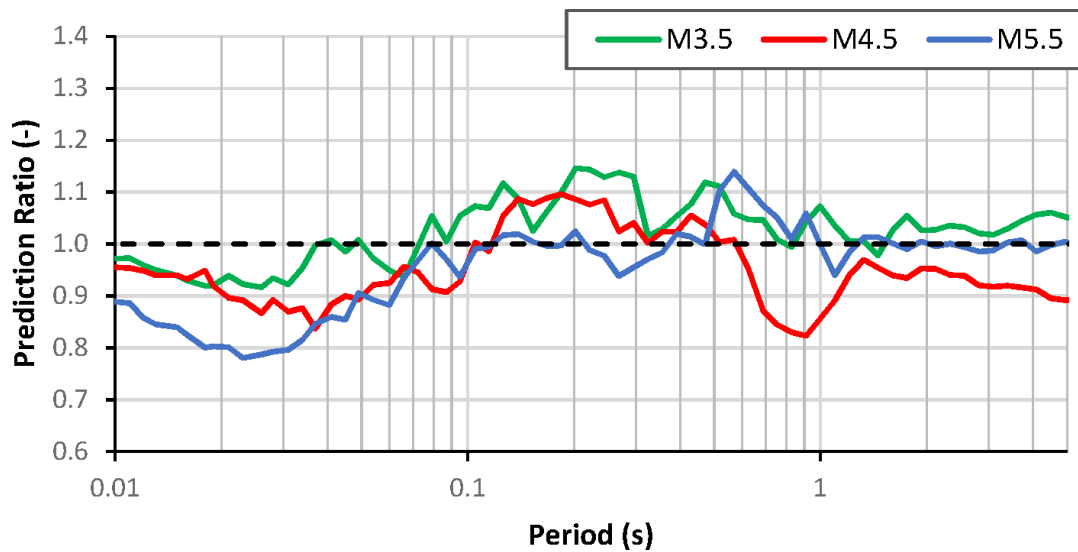


Figure A2.8. Ratios of simulated motions from V5 inversions excluding and including the recordings of the Slochteren event

APPENDIX III

Component-to-Component Variability Model

A3.1 Introduction

The risk calculations for the Groningen field require the use of the arbitrary instead of the geometric mean component of spectral acceleration and duration. This is predicted by sampling a normal distribution considering the geometric mean predictions of the Groningen GMMs as the mean and the component-to-component variability as the standard deviation. Previous estimates of the component-to-component variability of the Groningen ground-motion database yielded significantly larger values than those observed in published ground-motion models and calculated for other strong-motion databases. Research into the cause of this difference during the development of the V3 model (Bommer *et al.*, 2016b) showed that the variability values obtained are related to the distances of the records considered. The derivation of a new distance-dependent model is therefore important to take this effect into account. Additionally, a component-to-component variability model for duration was also derived to estimate the arbitrary component of duration. The following work is summarised in this Appendix: (a) the derivation of a new field-averaged model similar to the V3/V4 model, (b) the derivation of a distance- and magnitude- dependent model, and (c) the derivation of the model for duration.

A3.2 Field-averaged model for c2c variability of spectral acceleration

The component-to-component variability with respect to the geometric mean at each period is given by the following equation (Boore, 2005b):

$$\sigma_{c2c}^2 = \frac{1}{N} \sum_{j=1}^N \left(\frac{\ln Y_{1j} - \ln Y_{2j}}{2} \right)^2 \quad (\text{A3.1})$$

where Y1 and Y2 are the spectral accelerations at that period from the two horizontal components of the j^{th} record, and N is the total number of records.

Because of the scarcity of data beyond the period of 1 s, it was decided by Bommer *et al.* (2015c) for the V2 and V3/V4 models to use the values of Campbell & Bozorgnia (2007), scaled to match the Groningen values up to a period of 1 second. A simple tri-linear fit was then applied to the values to produce the final model, in order to eliminate erratic period-to-period variations.

Figure A3.1 shows the component-to-component variance calculated for the V3/V4 Groningen ground-motion database, the values reported by Boore (2005b) and by

Campbell & Bozorgnia (2007) as well as the final model used in the V3 and V4 GMMs. An equivalent V5 model (referred to as “V3 updated”) derived by repeating the process identically – but with the inclusion of the data recorded during the 26 May 2017 M_L 2.6 Slochteren earthquake – is also shown.

The variances calculated with the updated model are between 10% and 15% lower than those corresponding to the V3/V4 database. As a result, the best fit to the data is provided by scaling the Campbell & Bozorgnia (2007) values by 2.05 instead of 2.25. The value calculated for PGV is 0.283 and coincides with the value obtained by scaling the Campbell & Bozorgnia (2007) value for PGV by 2.05.

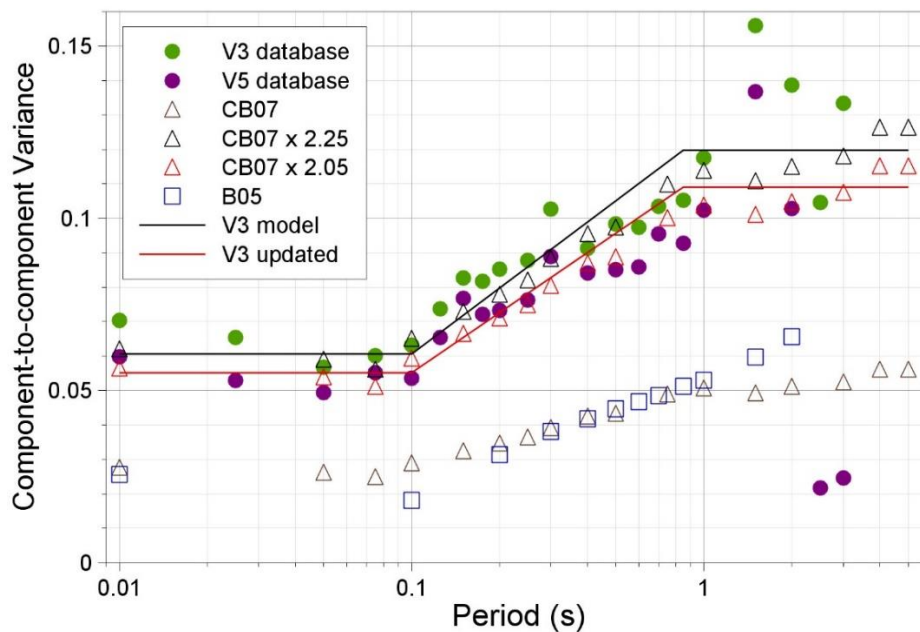


Figure A3.1. The component-to-component variances of the Groningen data (*solid circles*) and their approximation by the scaled values from Campbell & Bozorgnia (2007), simplified by a trilinear trend

A3.3 Distance-dependent model for c2c variability of spectral acceleration

The decrease of variability observed from V3/V4 to V5 in Figure A3.1 is most likely due to the change in the distance distribution of the database due to the inclusion of the Slochteren data, which generally consist of more distant recordings than the existing database. Using a field-averaged model when distance has significant influence has the disadvantage that the component-to-component variability is underestimated in the short distances and overestimated in longer distances.

Figure A3.2 shows the individual component-to-component variances of the arbitrary components of each record with respect to the geometric-mean acceleration, against distance, the values of the model presented in Section A3.2 (in red), the values of Campbell & Bozorgnia (2007) and the values of several functional forms of which the

fit to the data was tested. The functional form in orange is finally selected for the V5 distance-dependent model because it matches the observations of high polarisation at short distances and quickly converges to the tectonic values in longer distances. This functional form is:

$$\sigma_{c2c}^2 = s_1 + s_2 e^{s_3 + s_4 \ln(R)} \quad (\text{A3.2})$$

This expression can be re-written more simply as:

$$\sigma_{c2c}^2(R) = c_1 + c_2 R^{c_3} \quad (\text{A3.3})$$

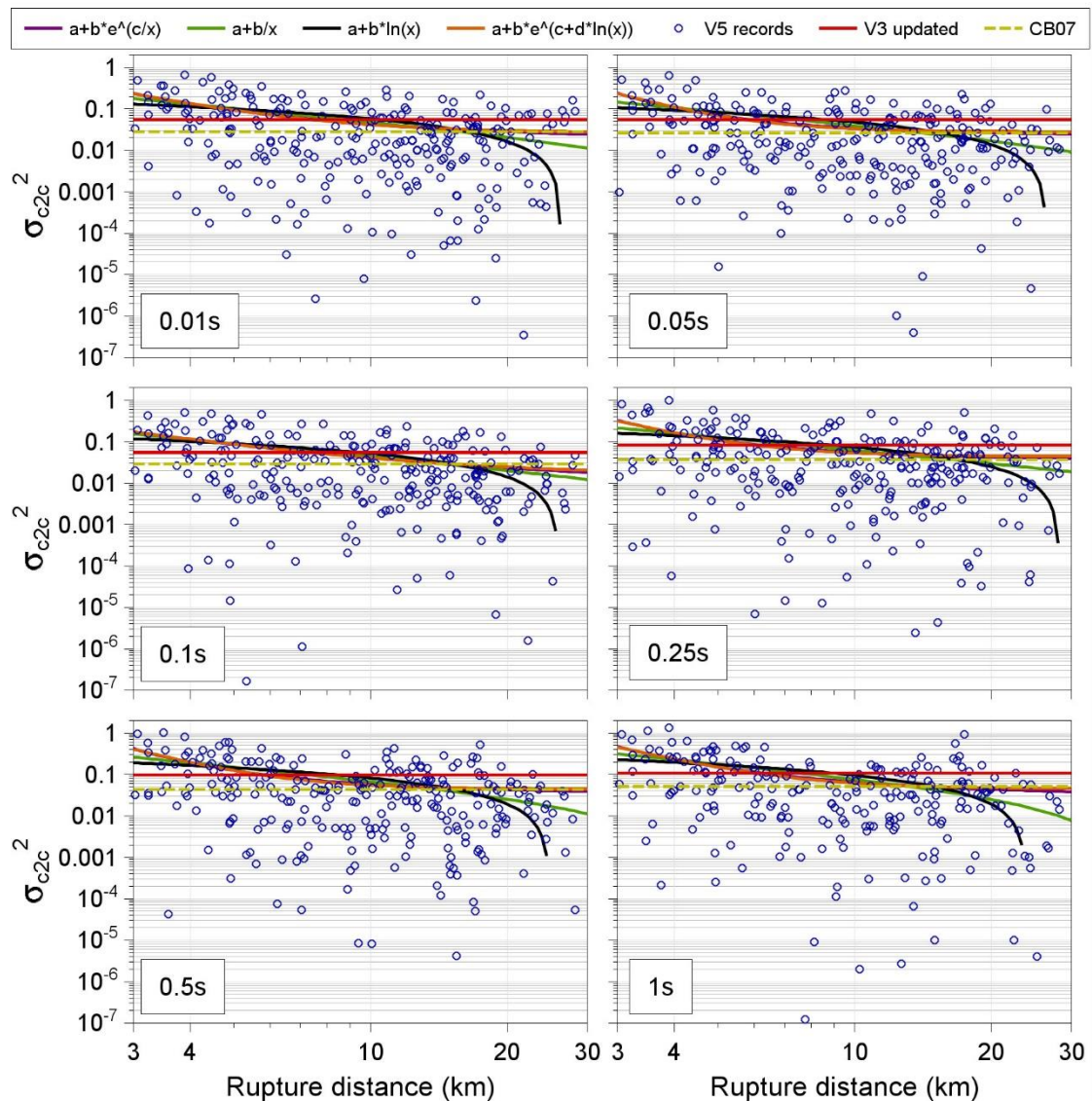


Figure A3.2. The component-to-component variances of the Groningen records at six periods compared to possible functional forms of a distance-dependent model

Figure A3.3 presents the component-to-component variance calculated by Eq.(A3.3)

for different distances and using coefficients obtained from regressions performed for each period individually. In order to eliminate erratic period-to-period fluctuations, we fix the model to a tri-linear form similar to the V3/V4 model, whereby a constant value will be used for periods below 0.1s and another for periods greater than 0.85s, and the values for intermediate periods will be a result of linear interpolation of the two in the $\log(T)$ space. Figure A3.4 shows the new model that results from this simplification.

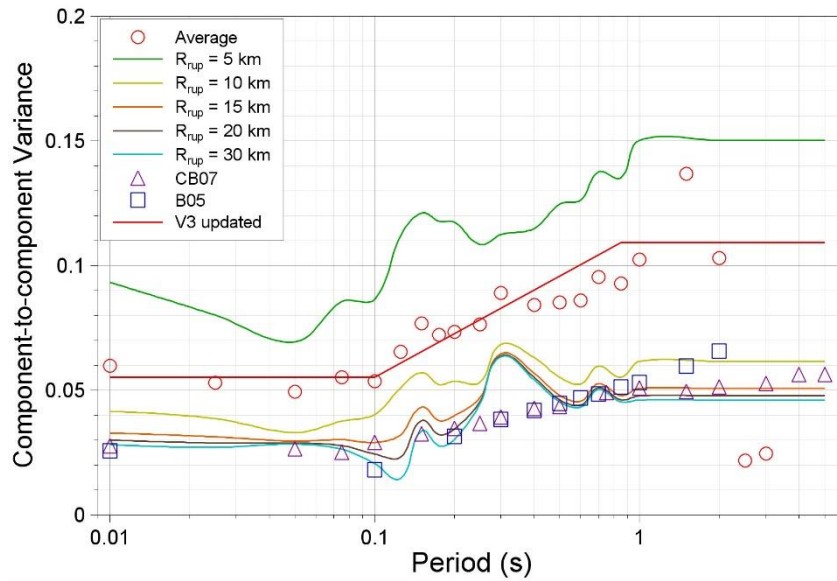


Figure A3.3. The component-to-component variability model for Groningen as obtained by individual regressions at each period, at different distances, compared to the data average, the updated V3 model and the tectonic models.

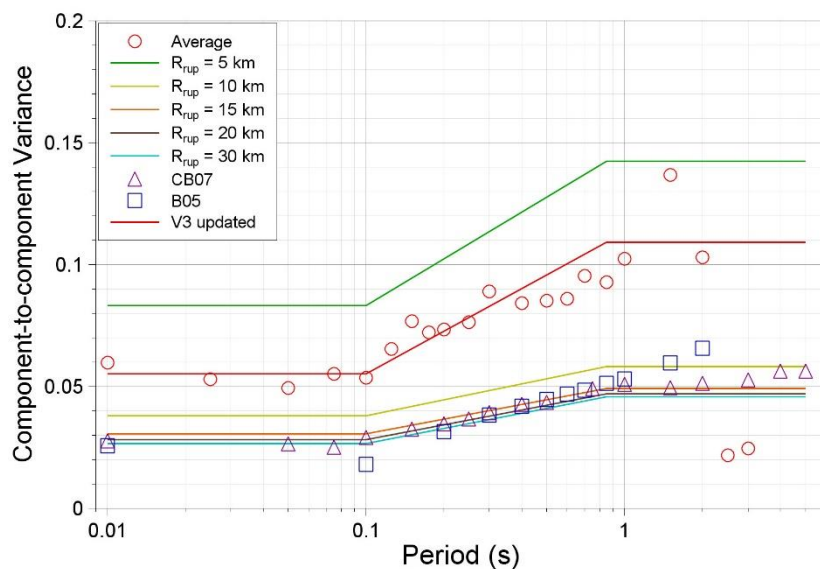


Figure A3.4. The component-to-component variability model for Groningen at different distances, compared to the data average, the updated V3 model and the tectonic models.

The high values exhibited for short distances will have a significant impact on the risk calculations, which begs the question of whether this polarisation will also persist at larger magnitudes. The polarisation observed is very likely an effect of the clear radiation pattern emitted by the nearly-point sources of small magnitude events. As ruptures elongate and events acquire the characteristics of tectonic earthquakes with larger magnitudes, it is most likely that polarisation will diminish as multiple points with opposite and different radiation patterns contribute to the waveforms recorded. Hence, we do not expect the component-to-component variability at large magnitudes to be different from that presented by published tectonic models. Therefore, we apply a magnitude-dependence to the model, whereby it will be fully applicable as presented in Figure A3.4 for the magnitude range of the data (until M 3.6) and converge linearly to tectonic values over two units of magnitude (until M 5.6). The final form of the V5 component-to-component variability model is presented in Eqs.(A3.4-6) and is shown in Figures A3.5 and A3.6.

$$\sigma_{c2c}^2(M, R) = 0.026 + 1.03[5.6 - \min(5.6, \max[M, 3.6])]R^{-2.22} \quad \text{for } T \leq 0.1\text{s} \quad (\text{A3.4})$$

$$\sigma_{c2c}^2(M, R) = 0.045 + 5.315[5.6 - \min(5.6, \max[M, 3.6])]R^{-2.92} \quad \text{for } T \geq 0.85\text{s} \quad (\text{A3.5})$$

$$\sigma_{c2c}^2(T, M, R) = \sigma_{c2c}^2(0.1, M, R) + \left[\frac{\log(T) - \log(0.1)}{\log(0.85) - \log(0.1)} \right] [\sigma_{c2c}^2(0.85, M, R) - \sigma_{c2c}^2(0.1, M, R)]$$

for $0.1\text{s} < T < 0.85\text{s}$ (A3.6)

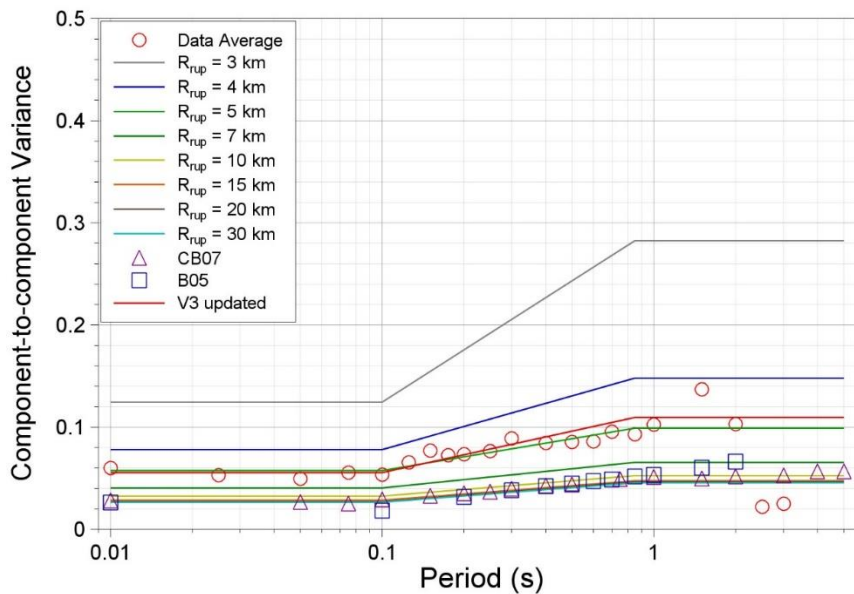


Figure A3.5. The component-to-component variance model for Groningen at different distances for $M \geq 4.5$ compared to the data average, the updated V3 model and the tectonic models.

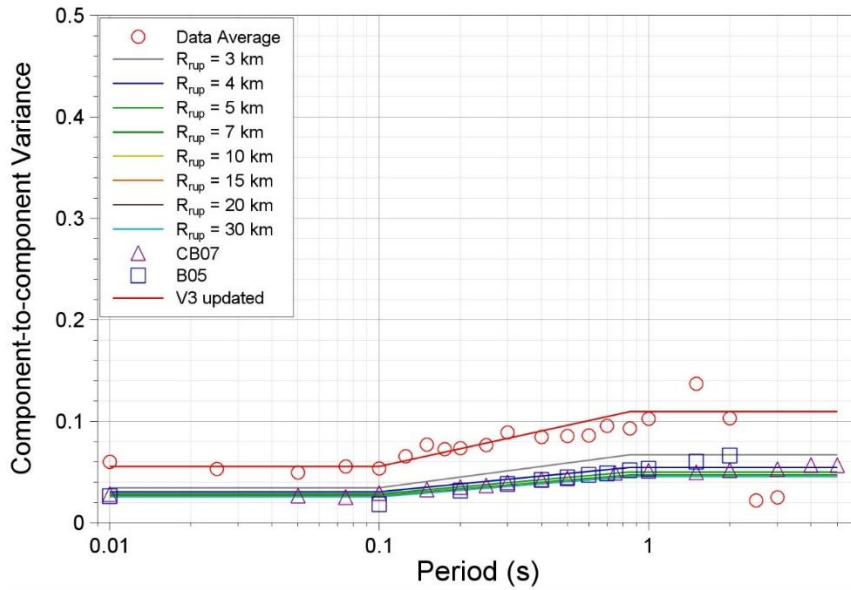


Figure A3.6. The component-to-component variance model for Groningen at different distances for $M_{L5.5}$ compared to the data average, the updated V3 model and the tectonic models.

A3.3 Distance-dependent model for c2c variability of duration

An equivalent model is derived for duration and presented in Eq. (A3.7). Figure A3.7 compares the model to the individual component-to-component variances of duration of the arbitrary components of the records.

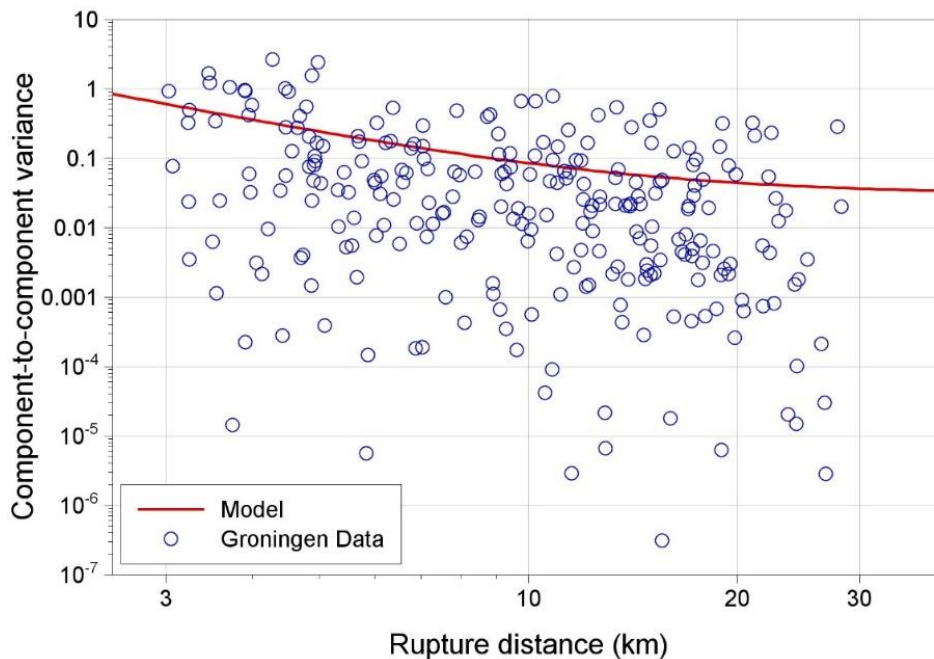


Figure A3.7. Comparison of the V5 durations c2c variability model and the component-to-component variances of the durations of the Groningen records

The model has the same functional form as the model for spectral acceleration, and has been fixed to converge to the values of the tectonic model of Bommer *et al.* (2009) at large magnitudes and longer distances:

$$\sigma_{c2c}^2(R) = 0.0299 + 2.434[5.6 - \min[5.6, \max(M, 3.6)]]R^{-1.95} \quad (\text{A3.7})$$

Figure A3.8 displays the magnitude scaling of the model at different distances.

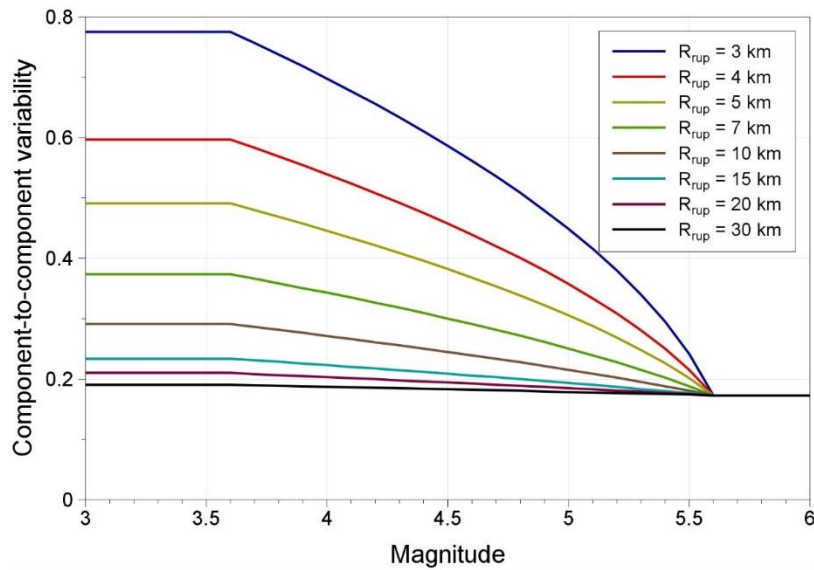
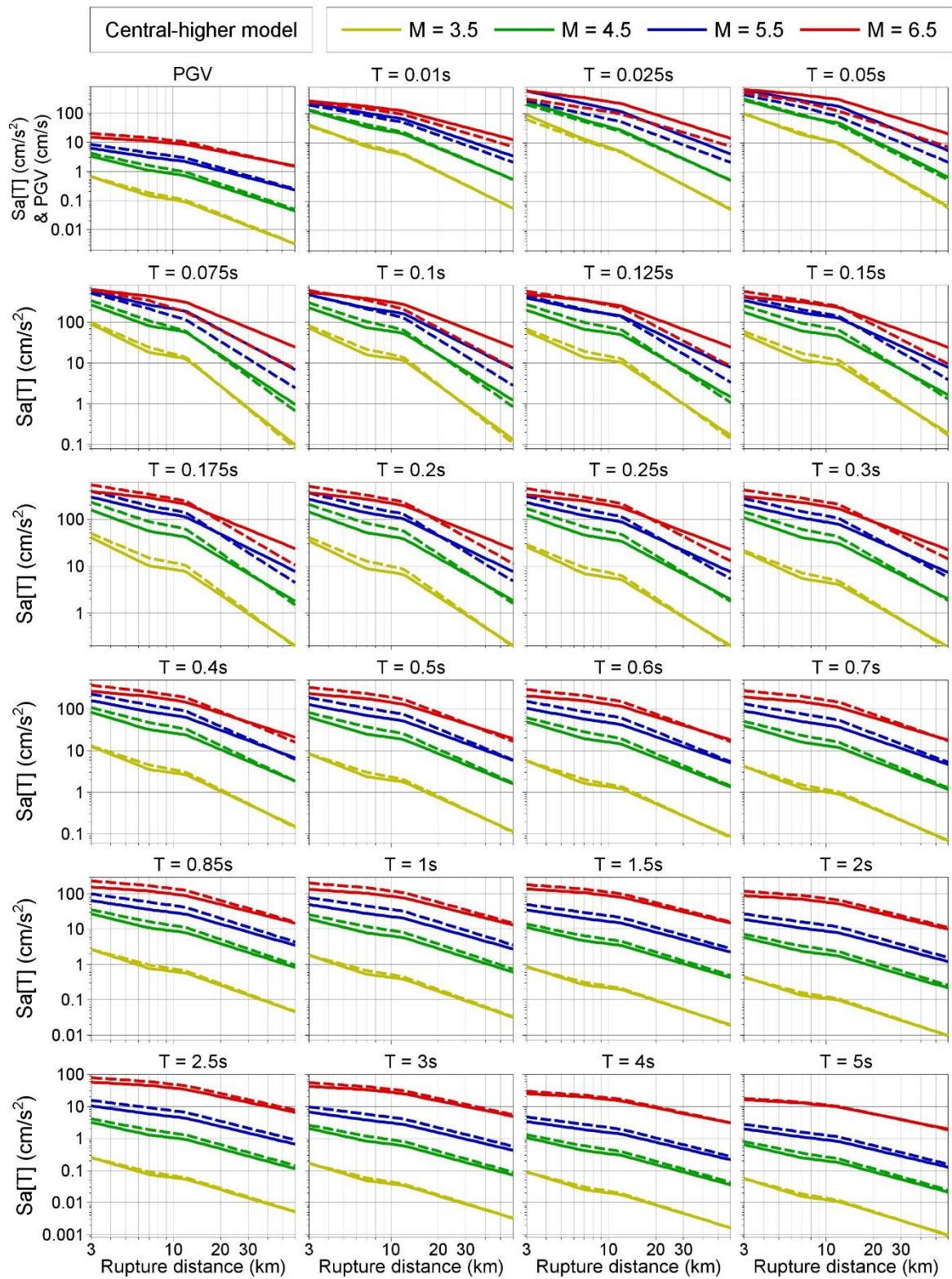
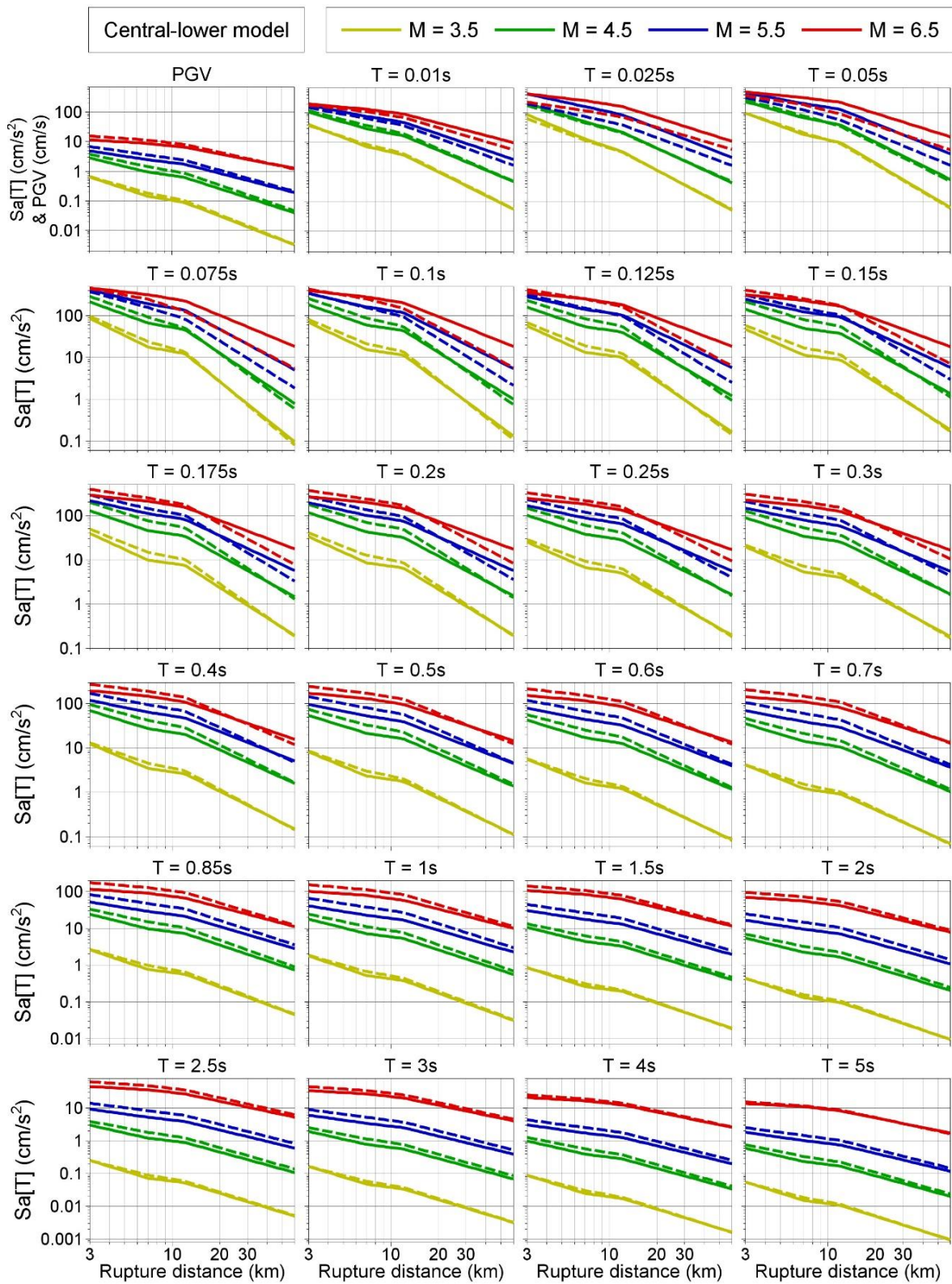
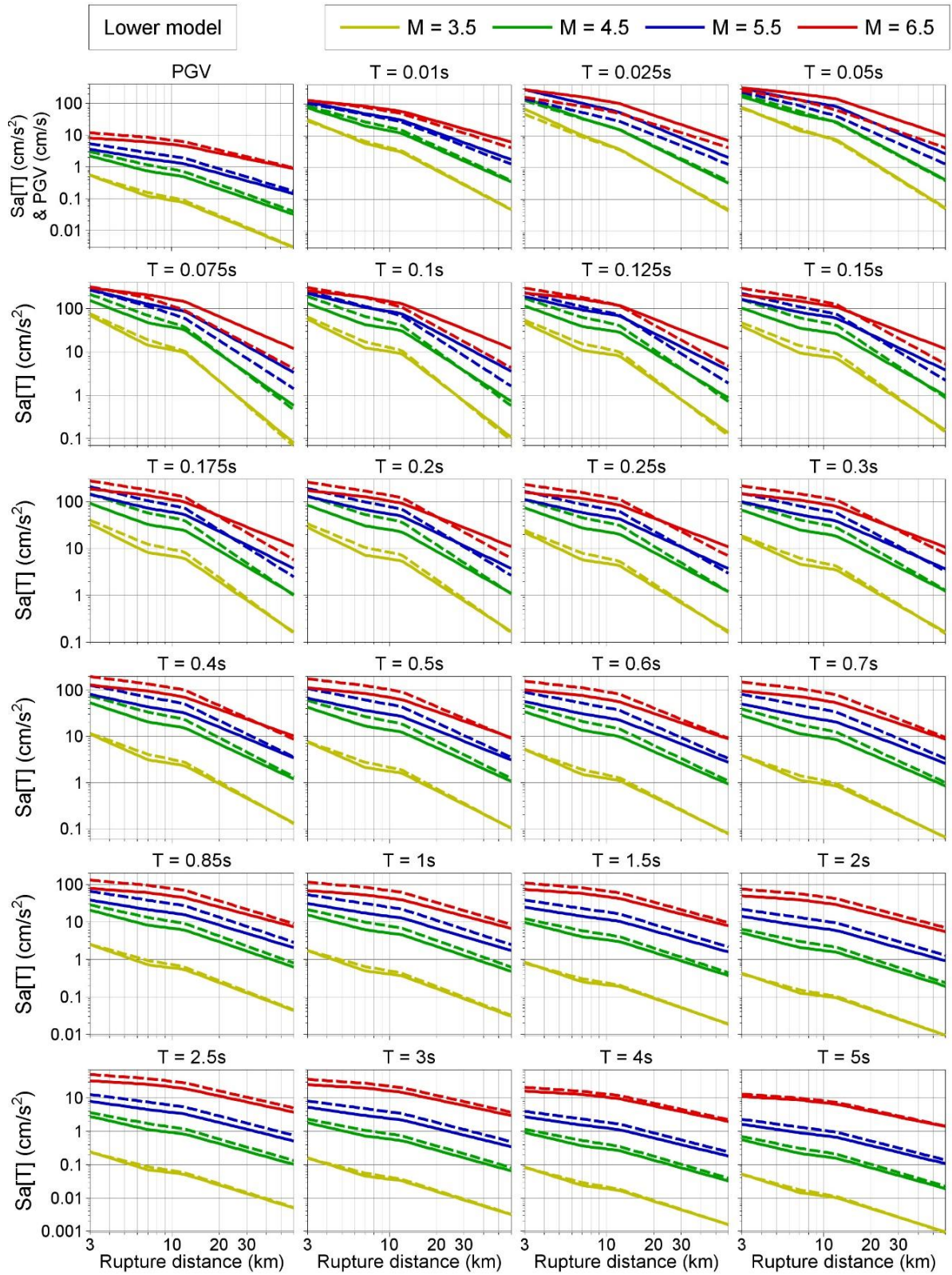


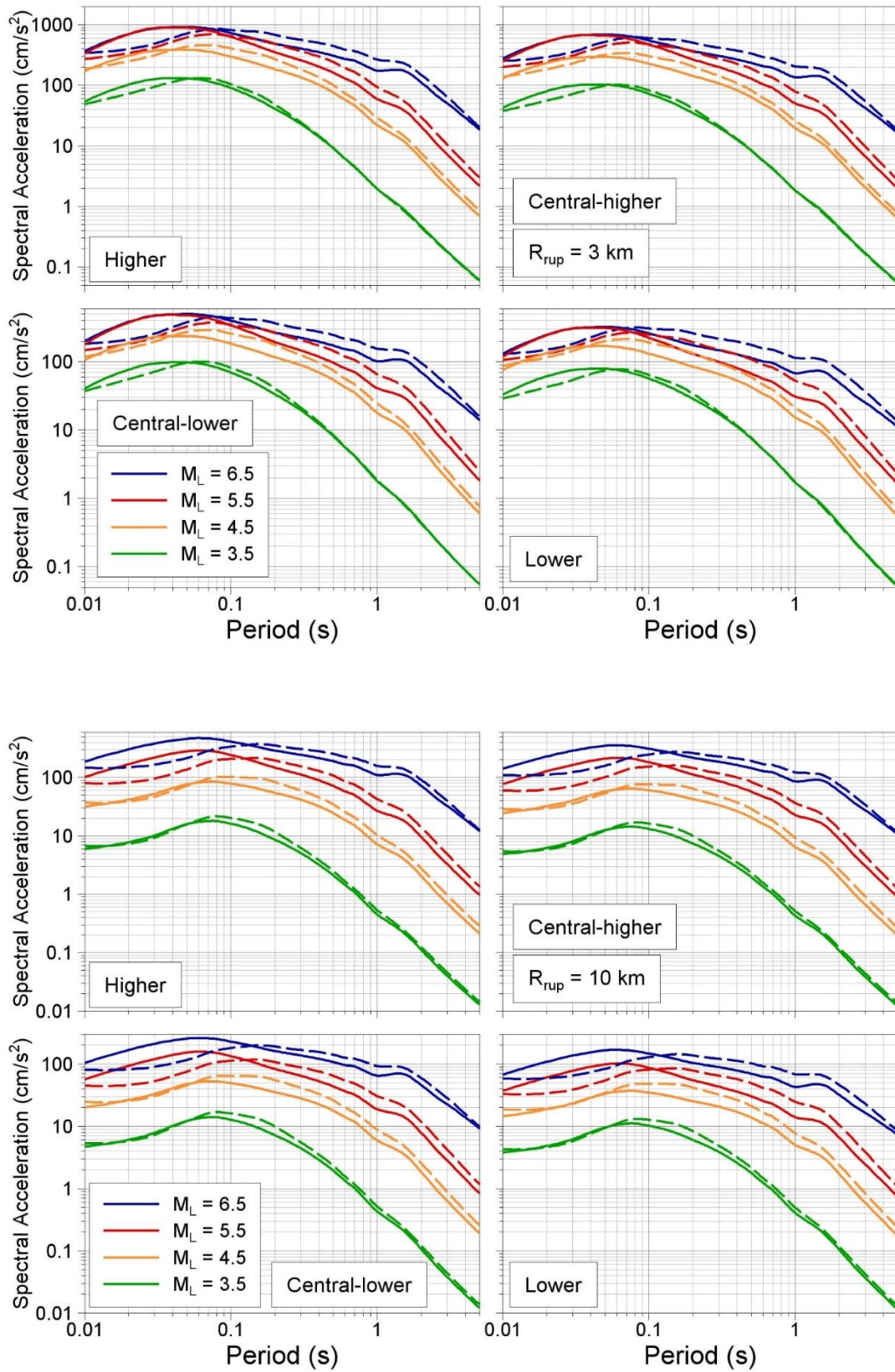
Figure A3.8. Comparison of the V5 durations c2c variability model and the component-to-component variances of the durations of the Groningen records

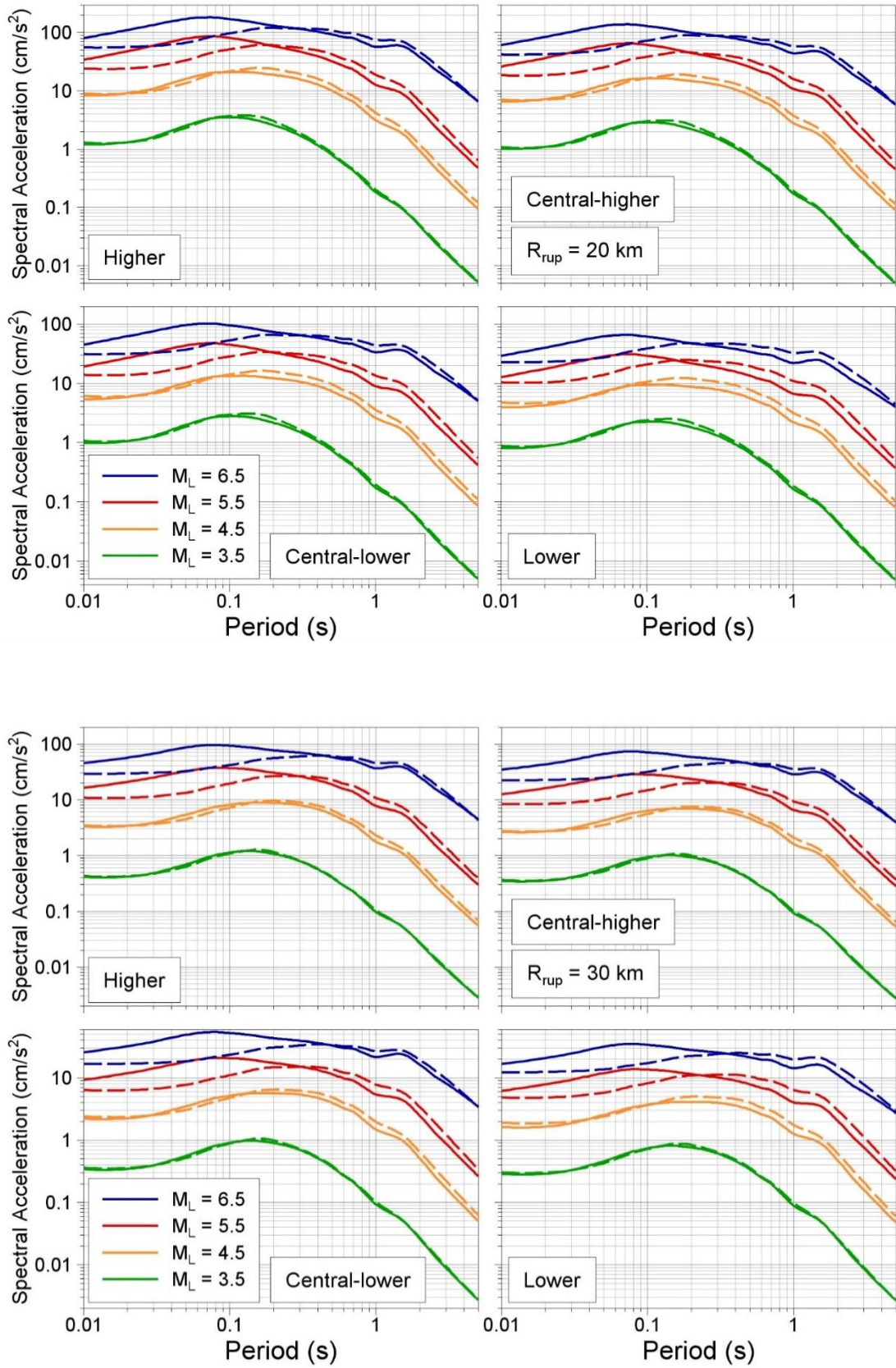


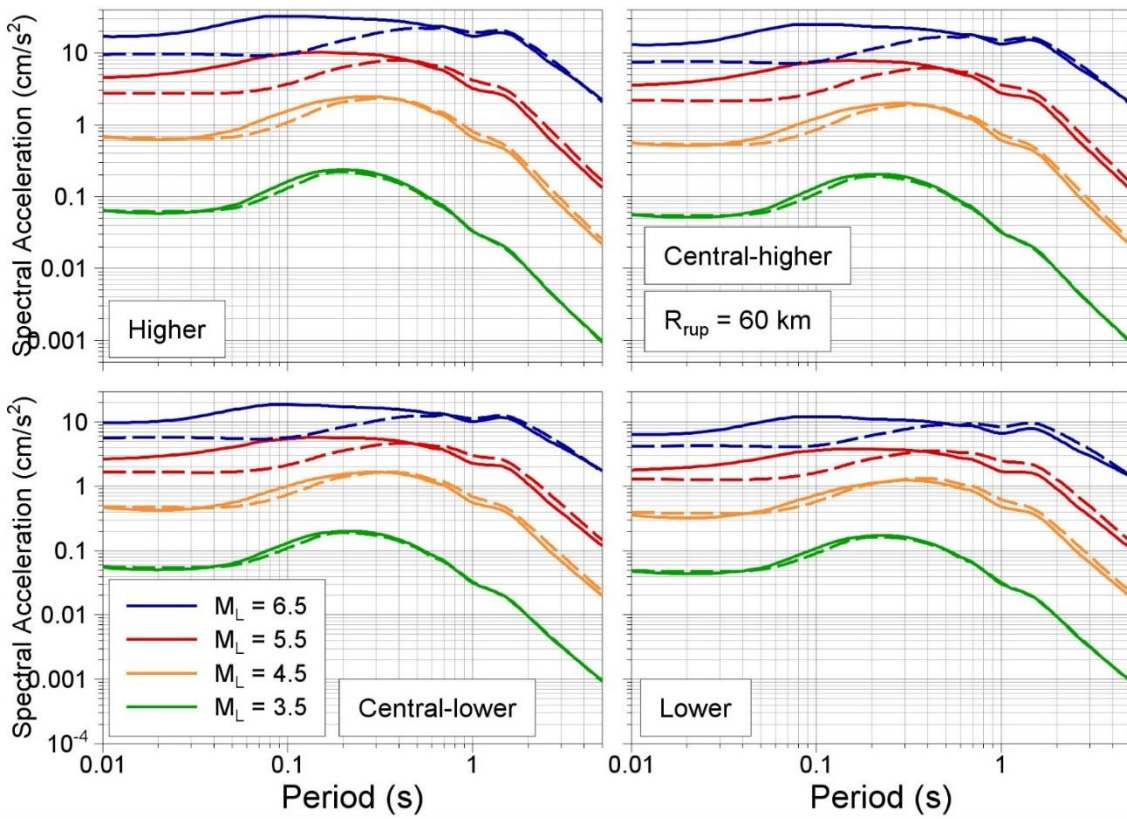
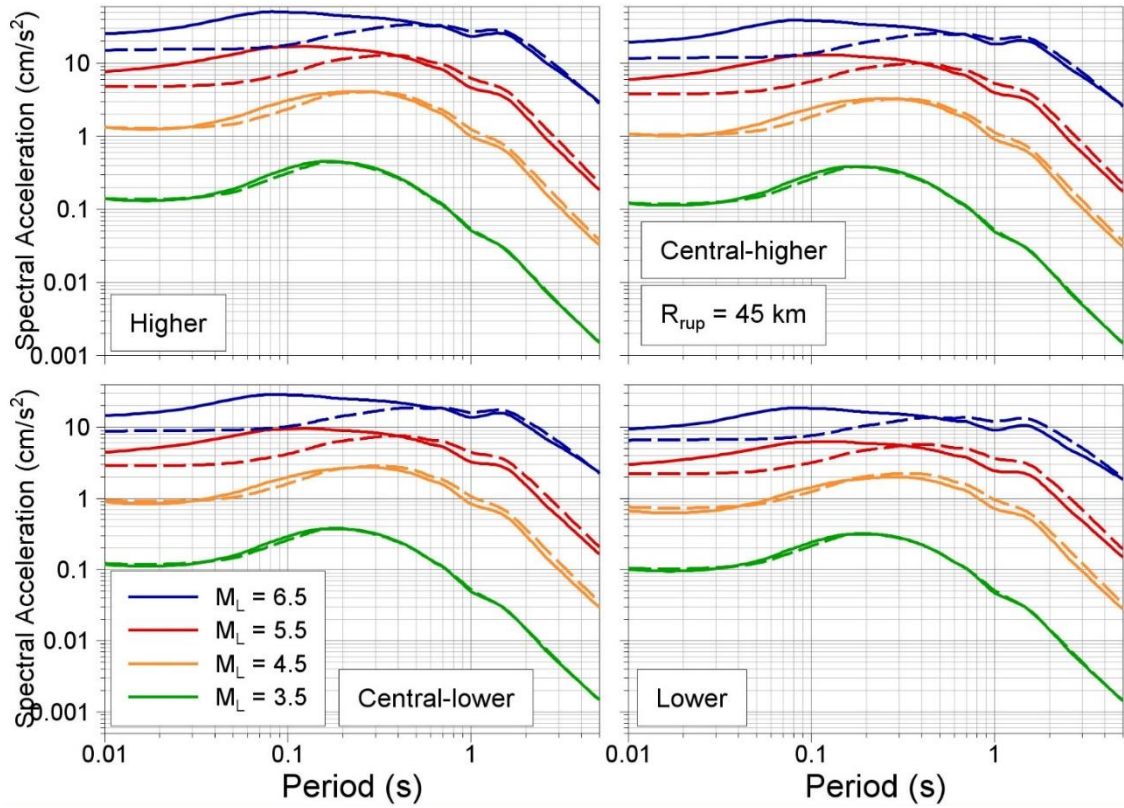




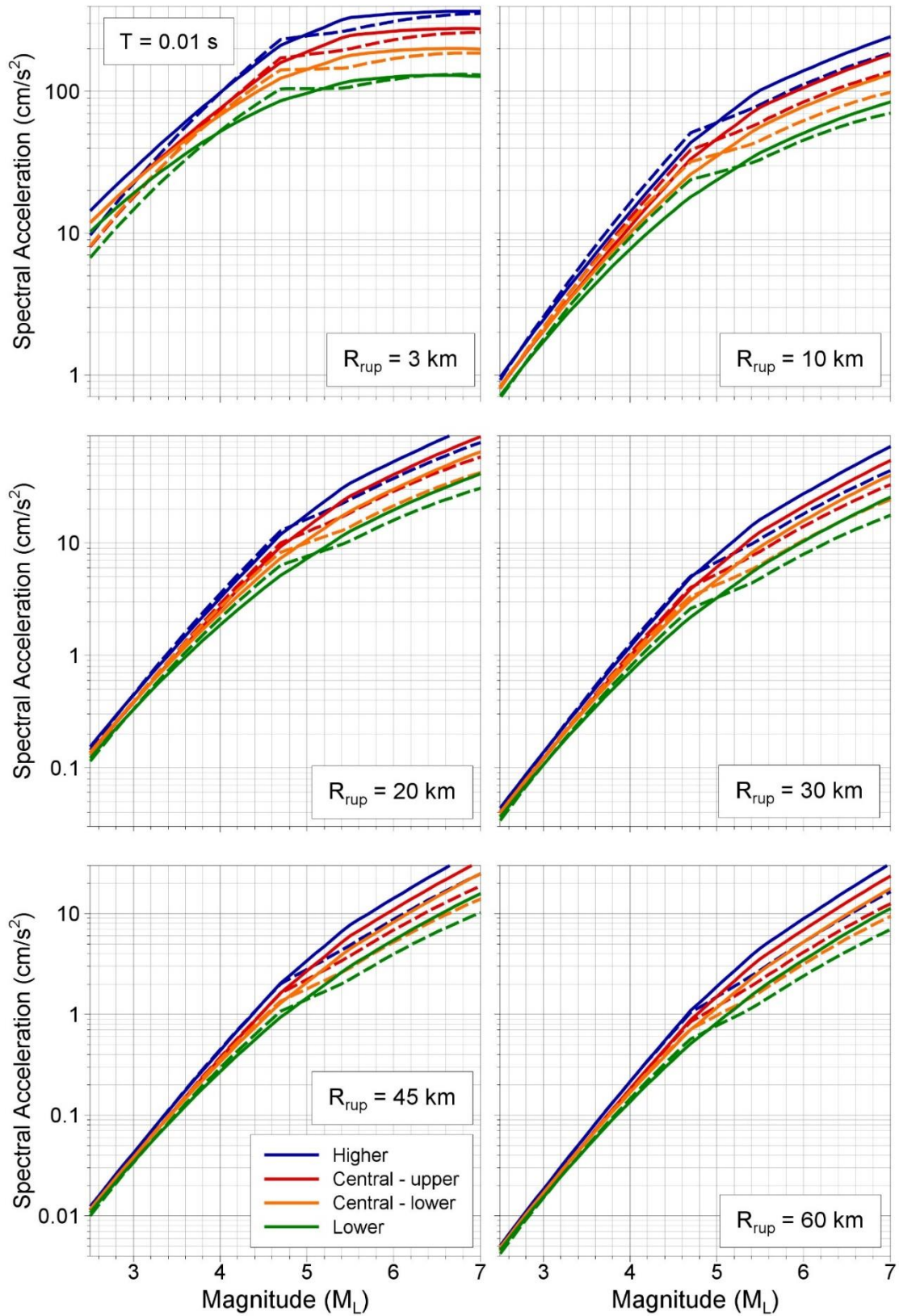
A4.2 Response Spectra

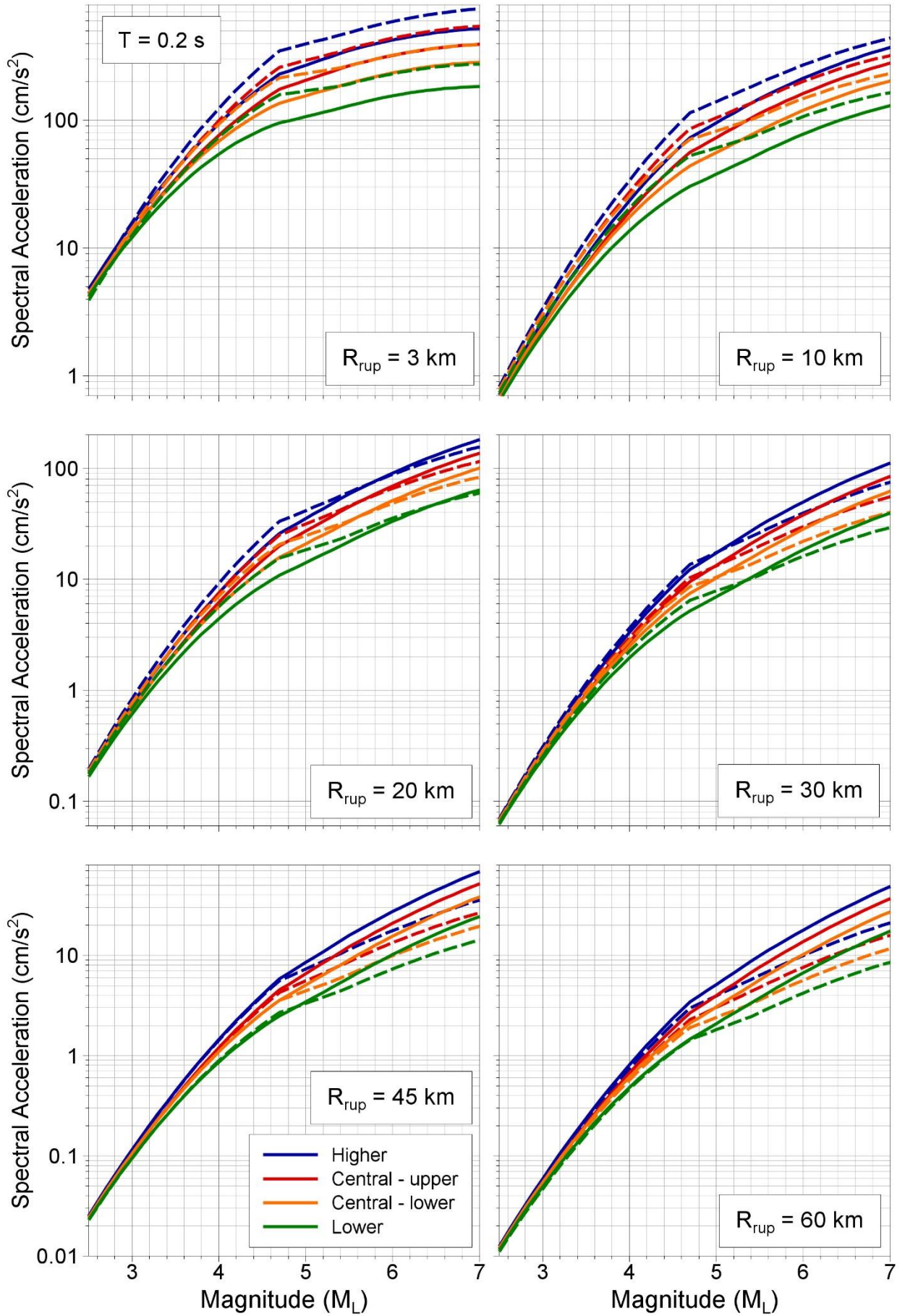


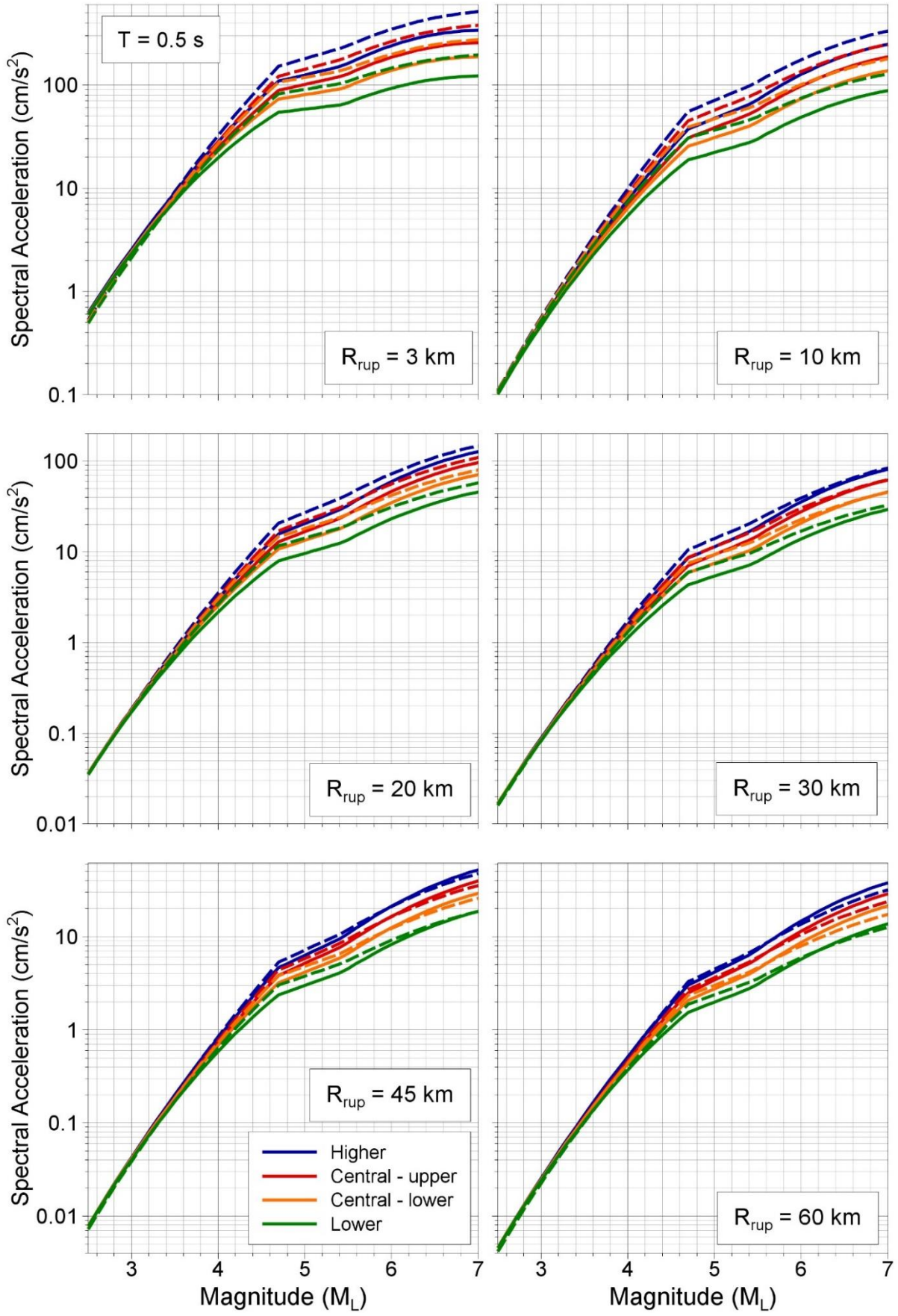


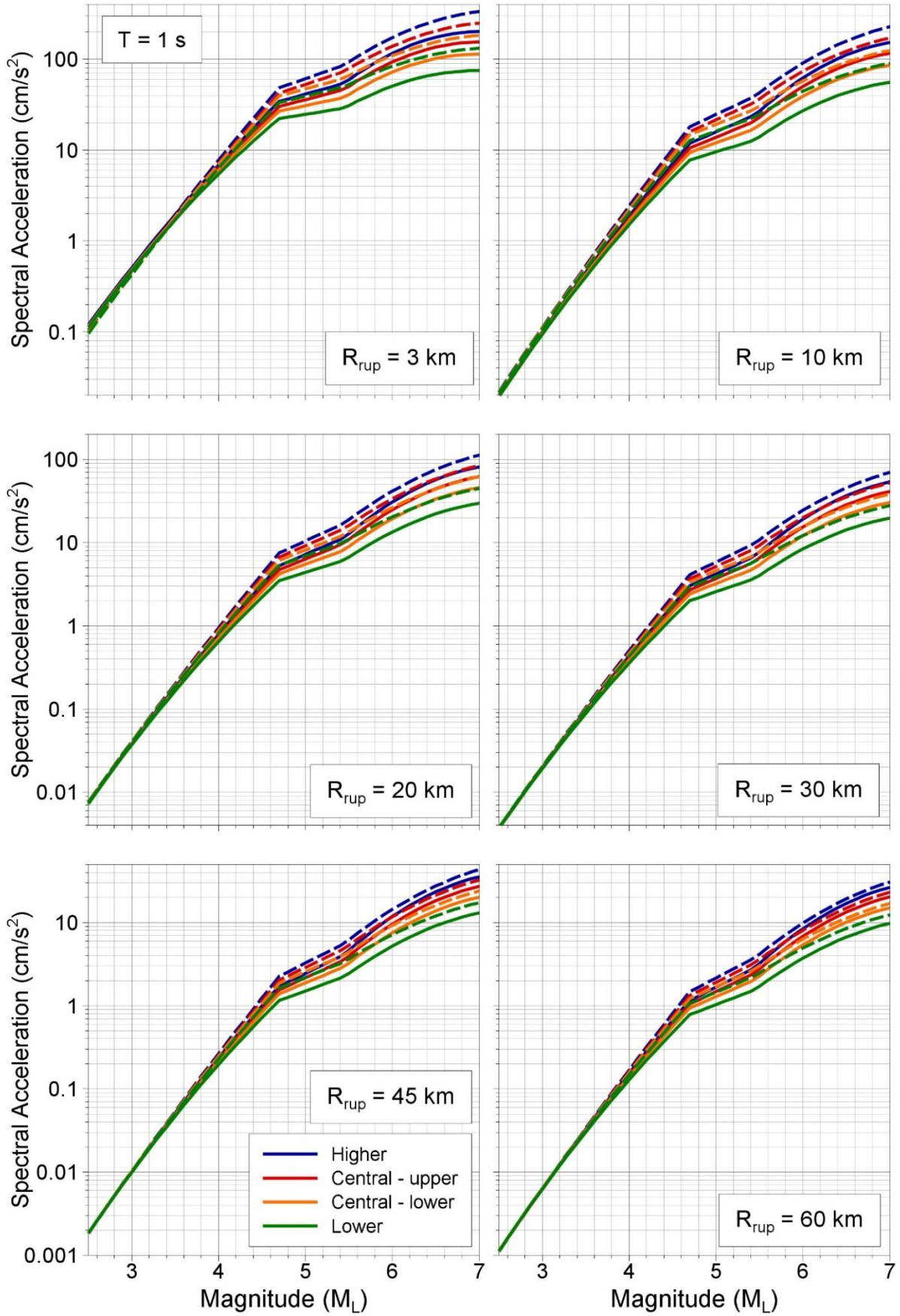


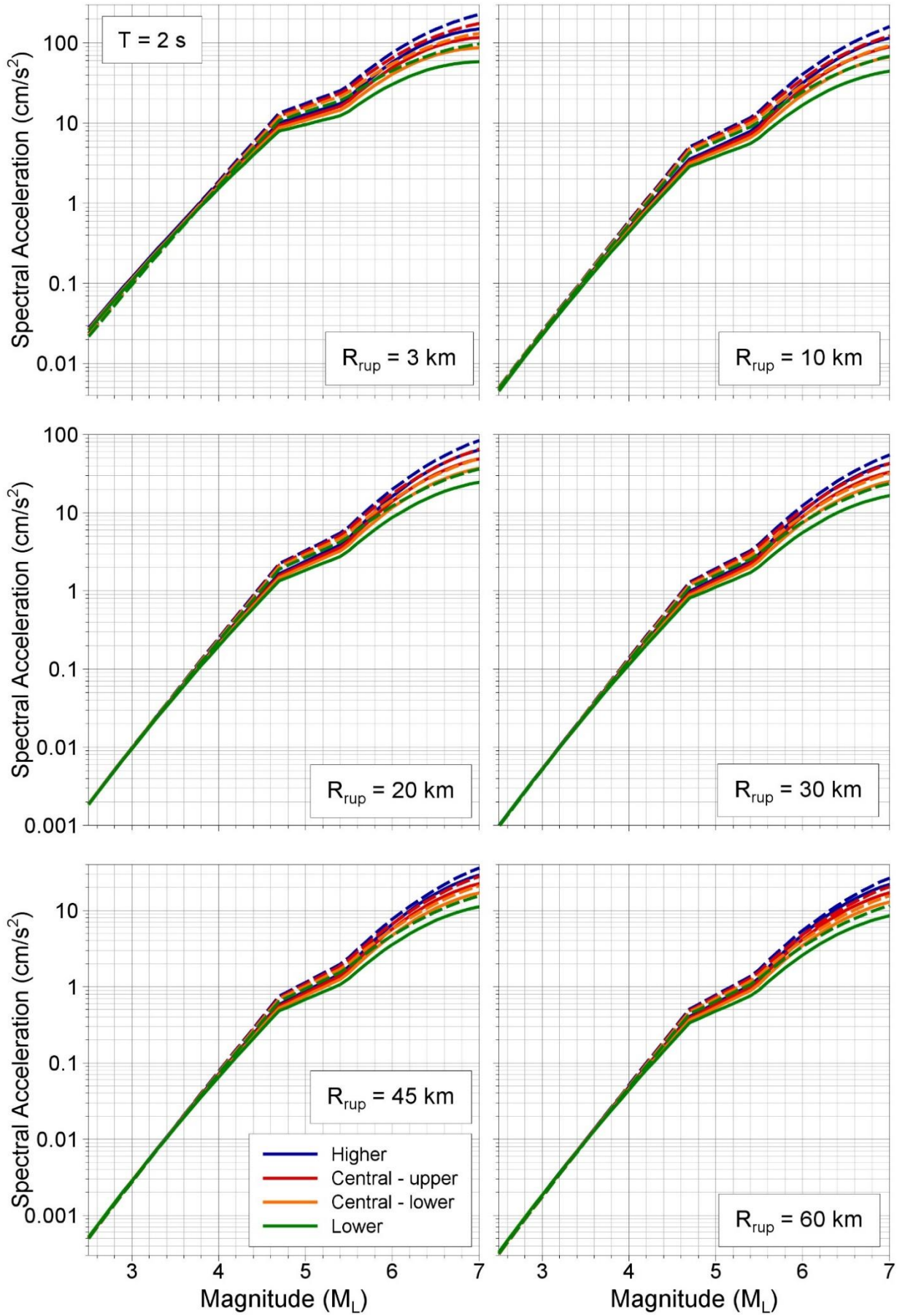
A4.3 Plots of median predictions at NS_B shown with respect to magnitude

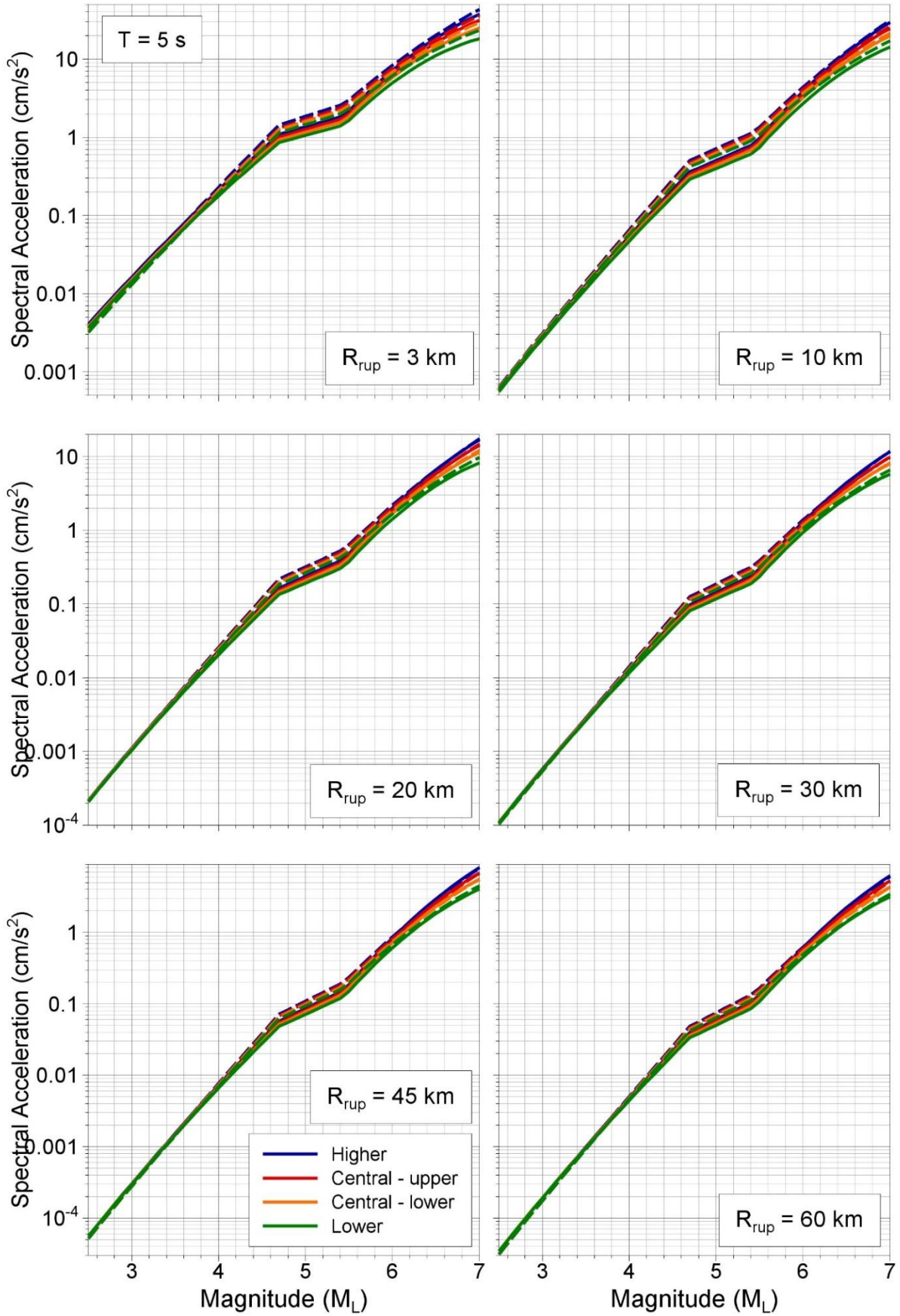






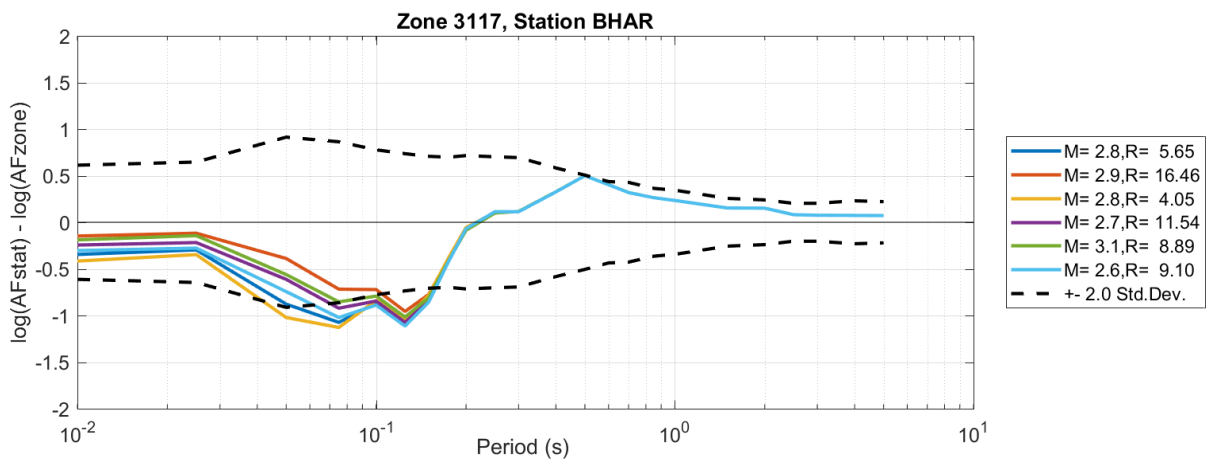
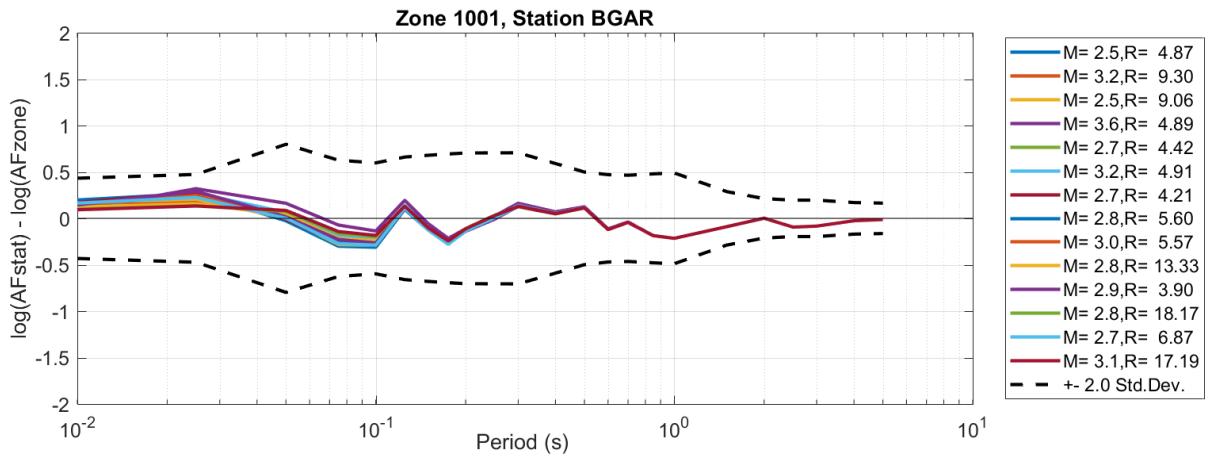
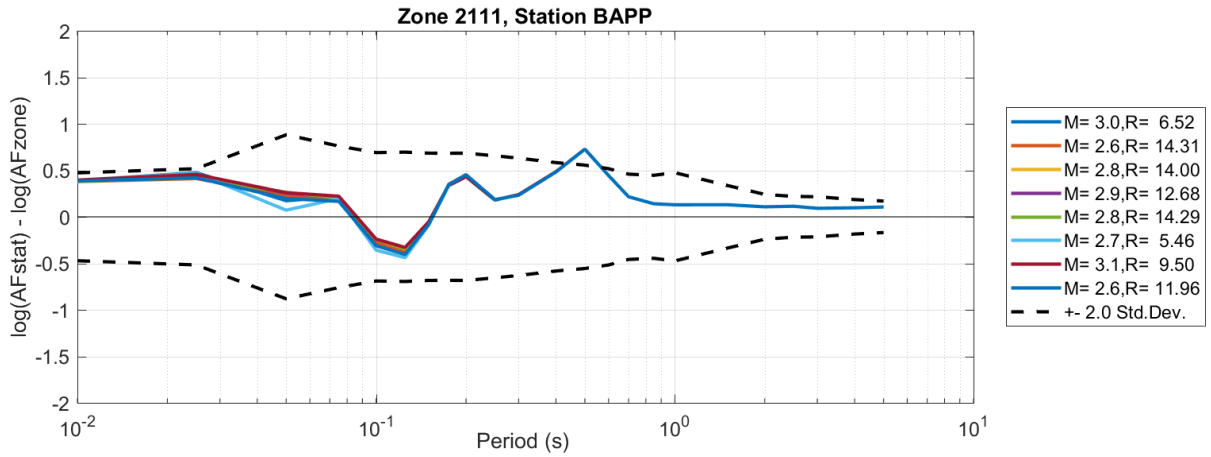


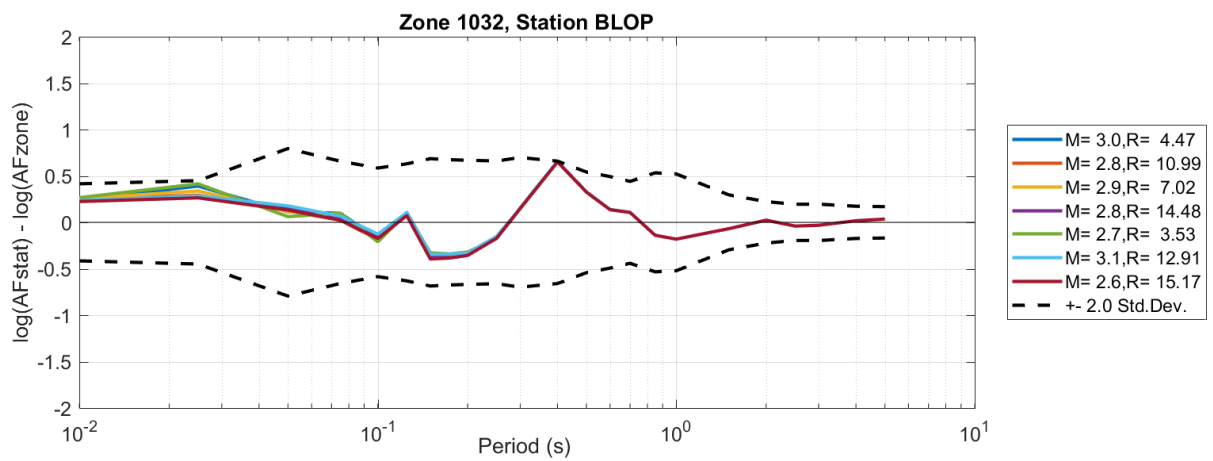
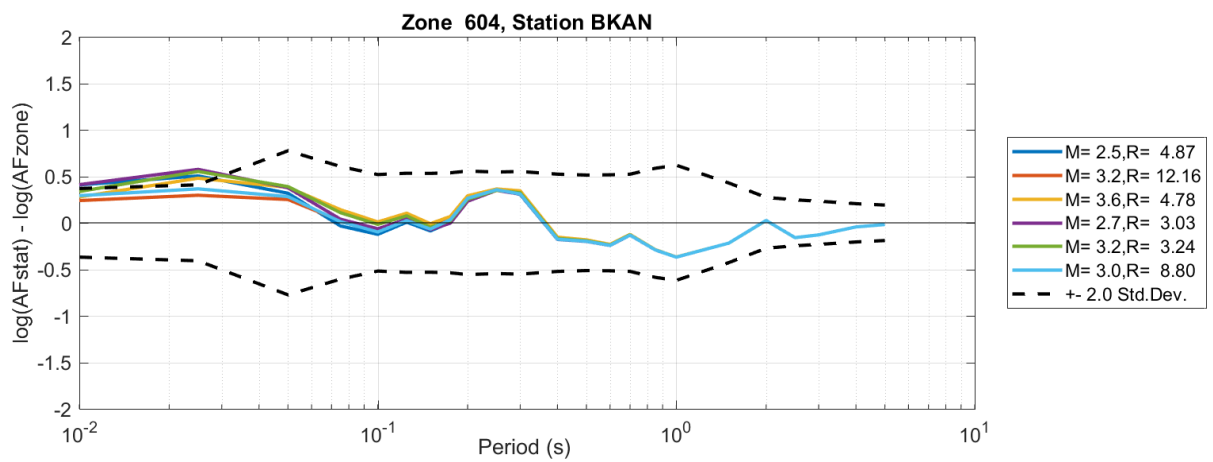
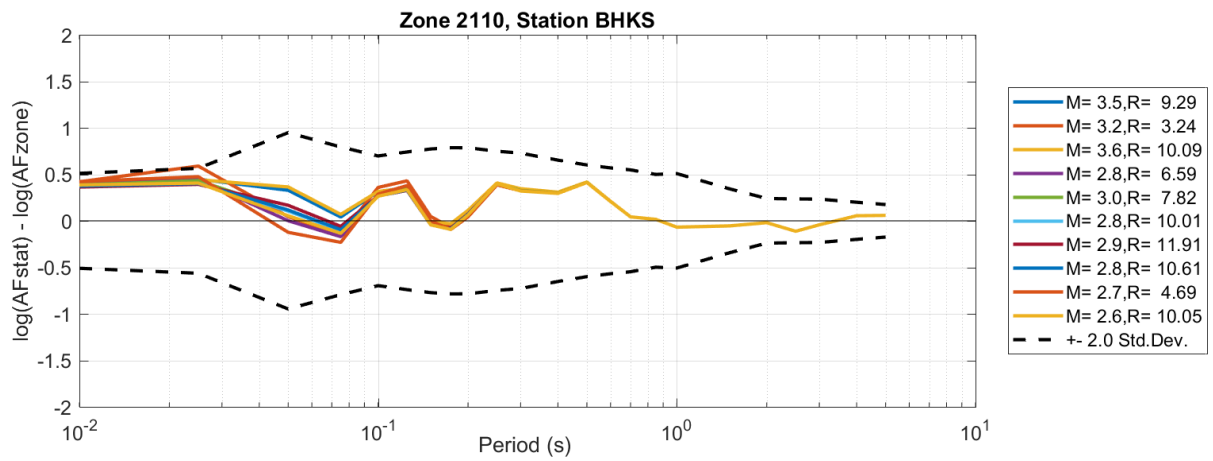


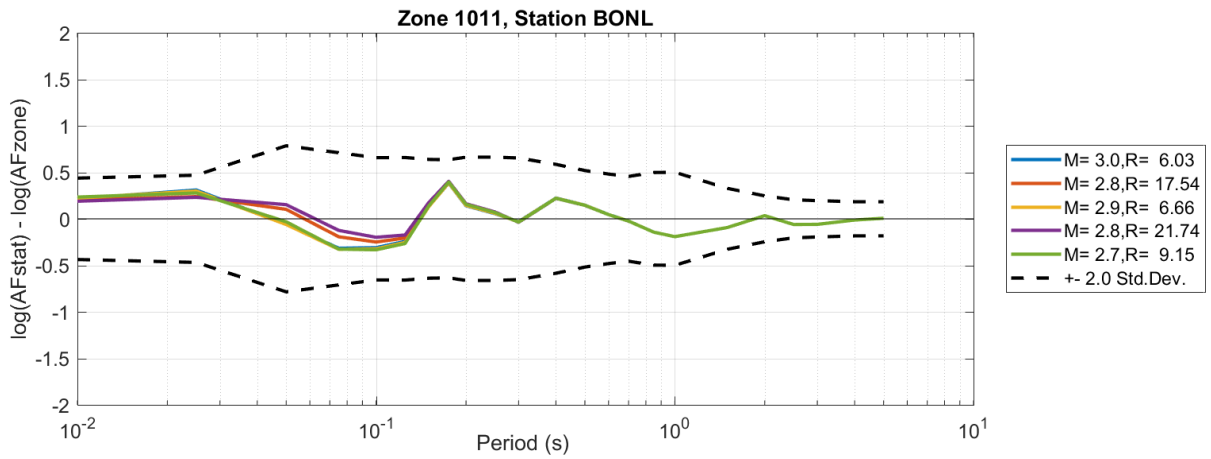
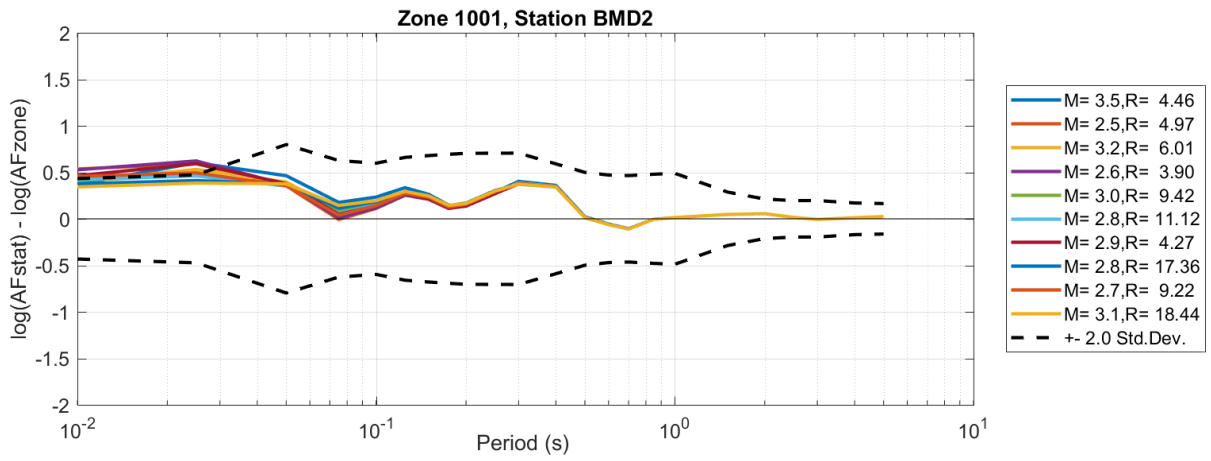
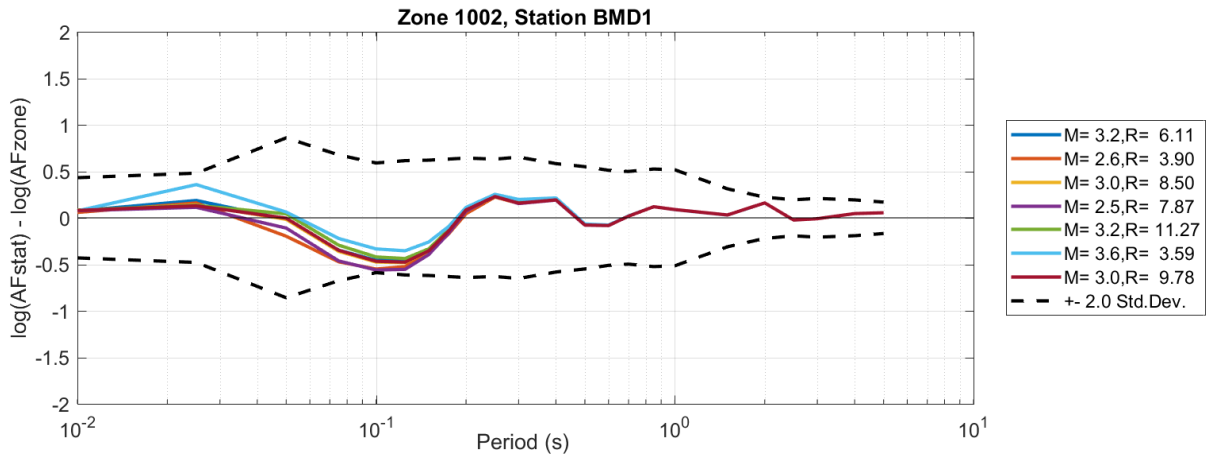


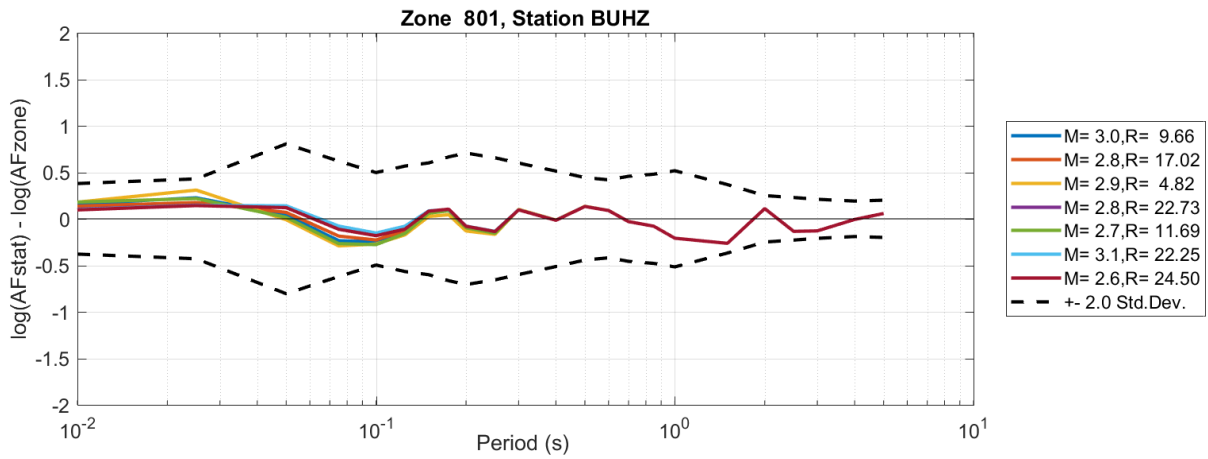
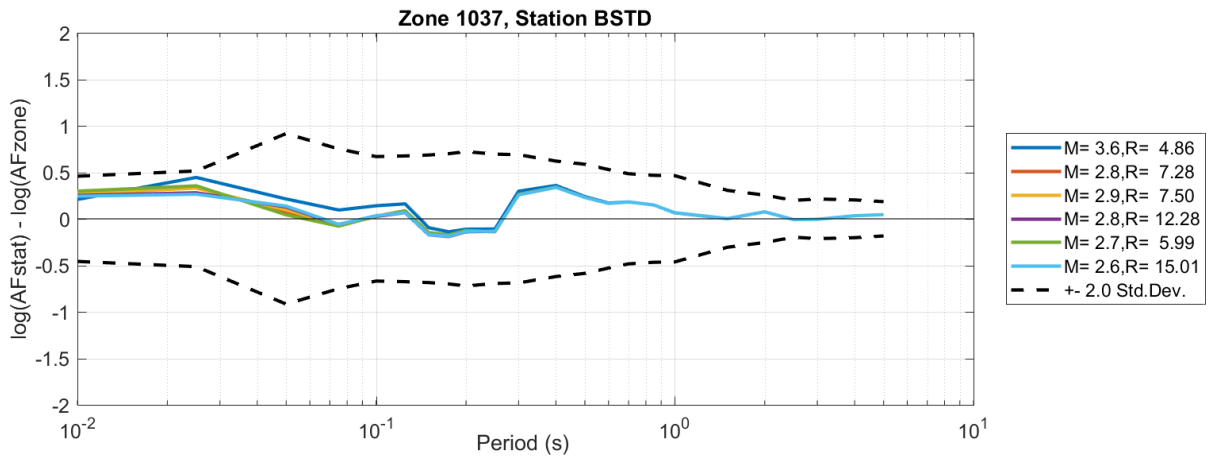
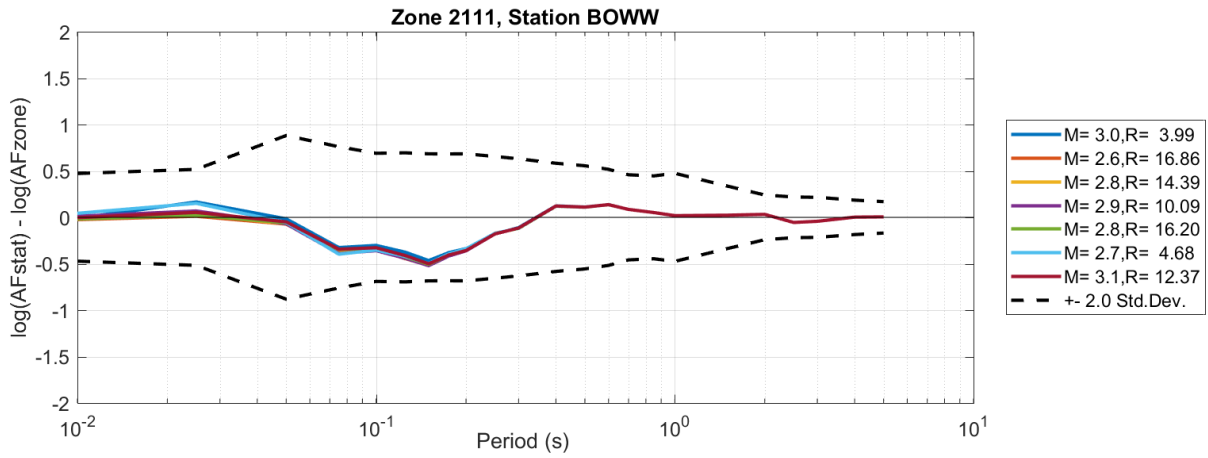
APPENDIX V

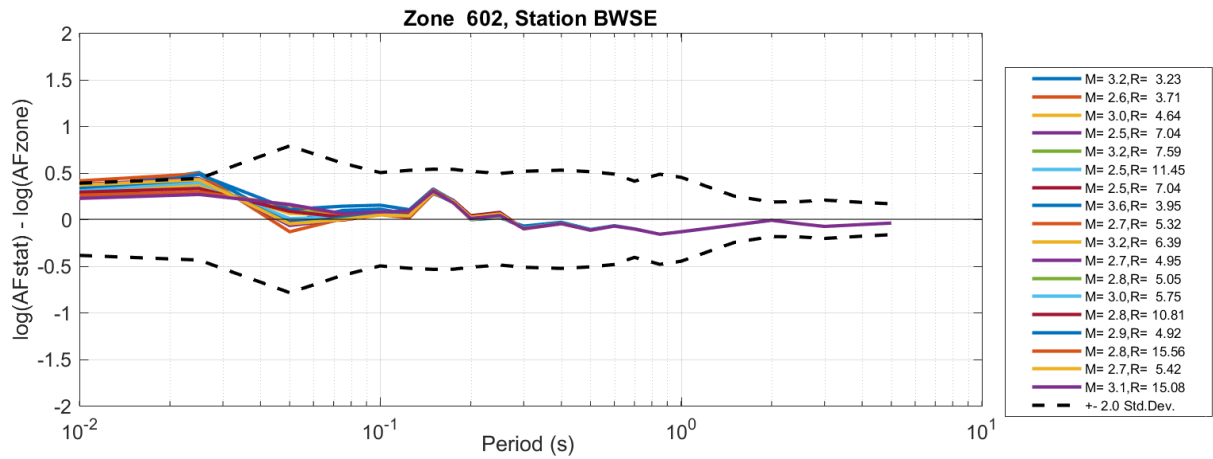
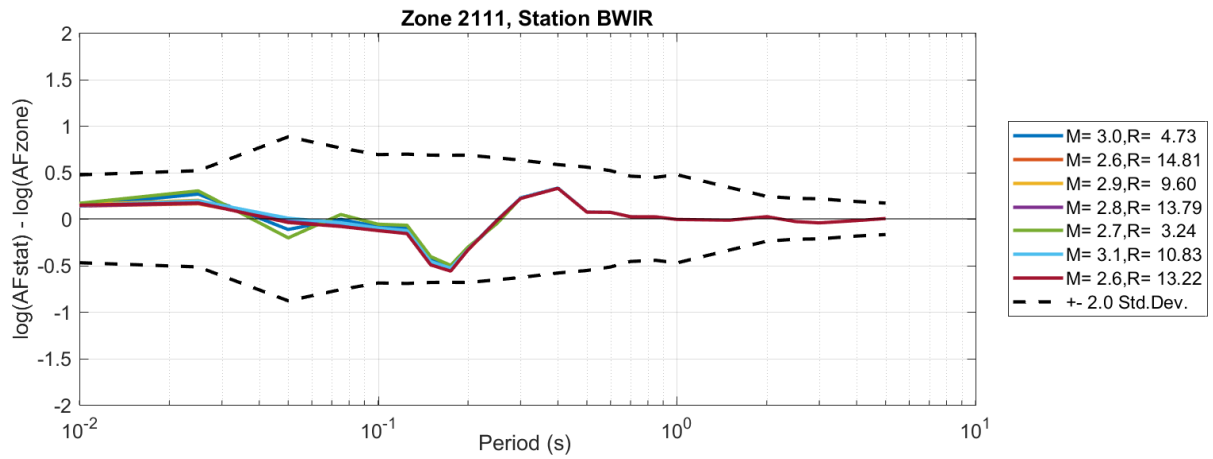
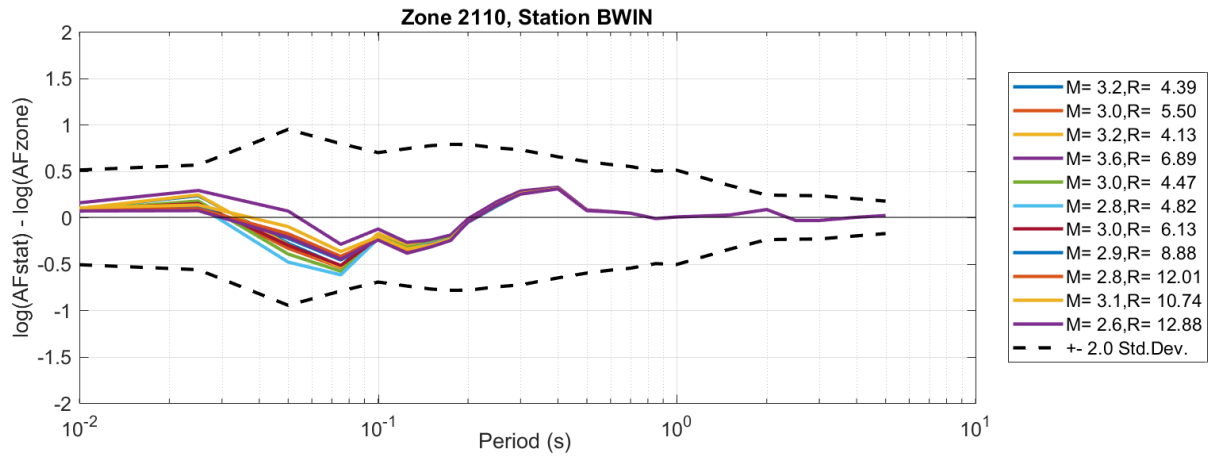
Stations vs Zone Linear AFs

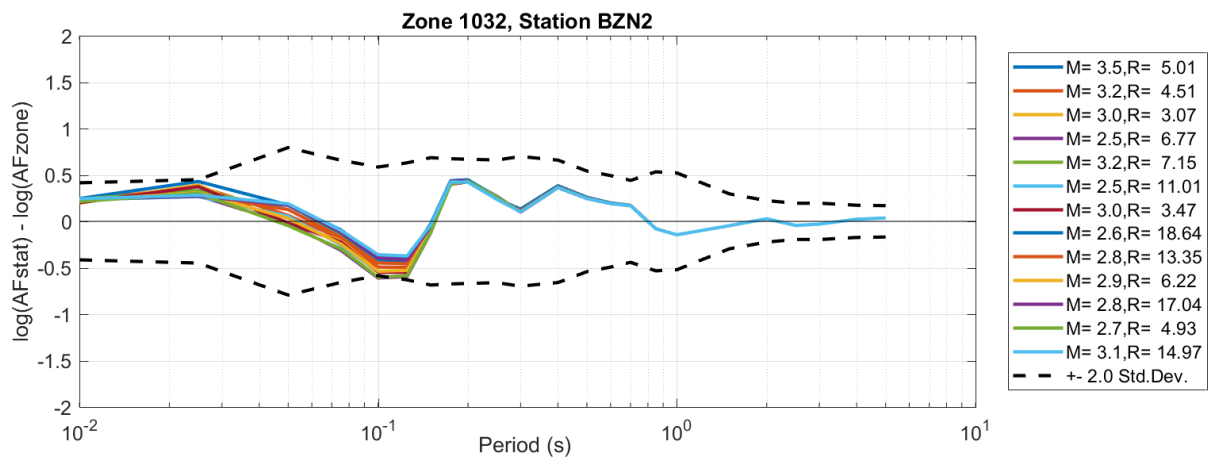
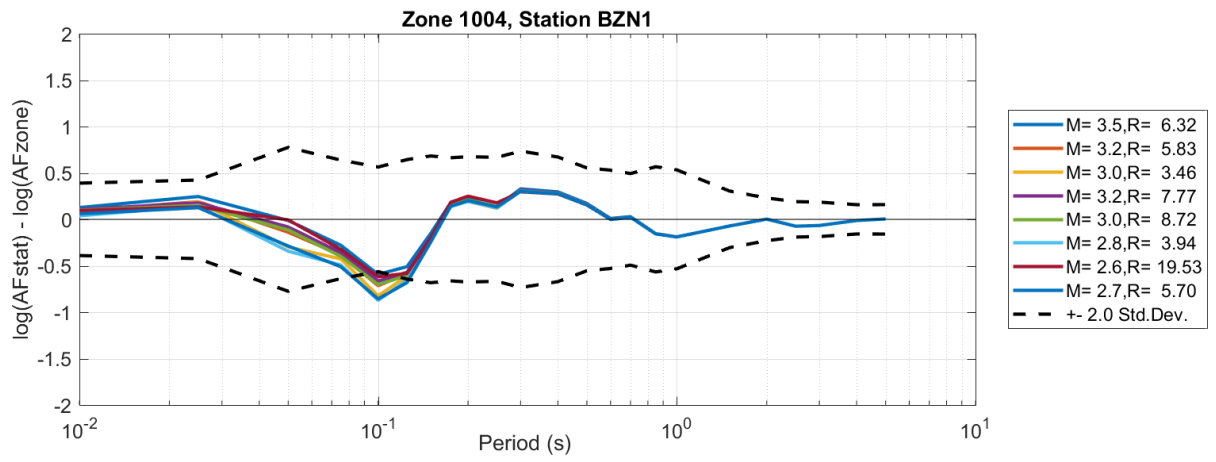








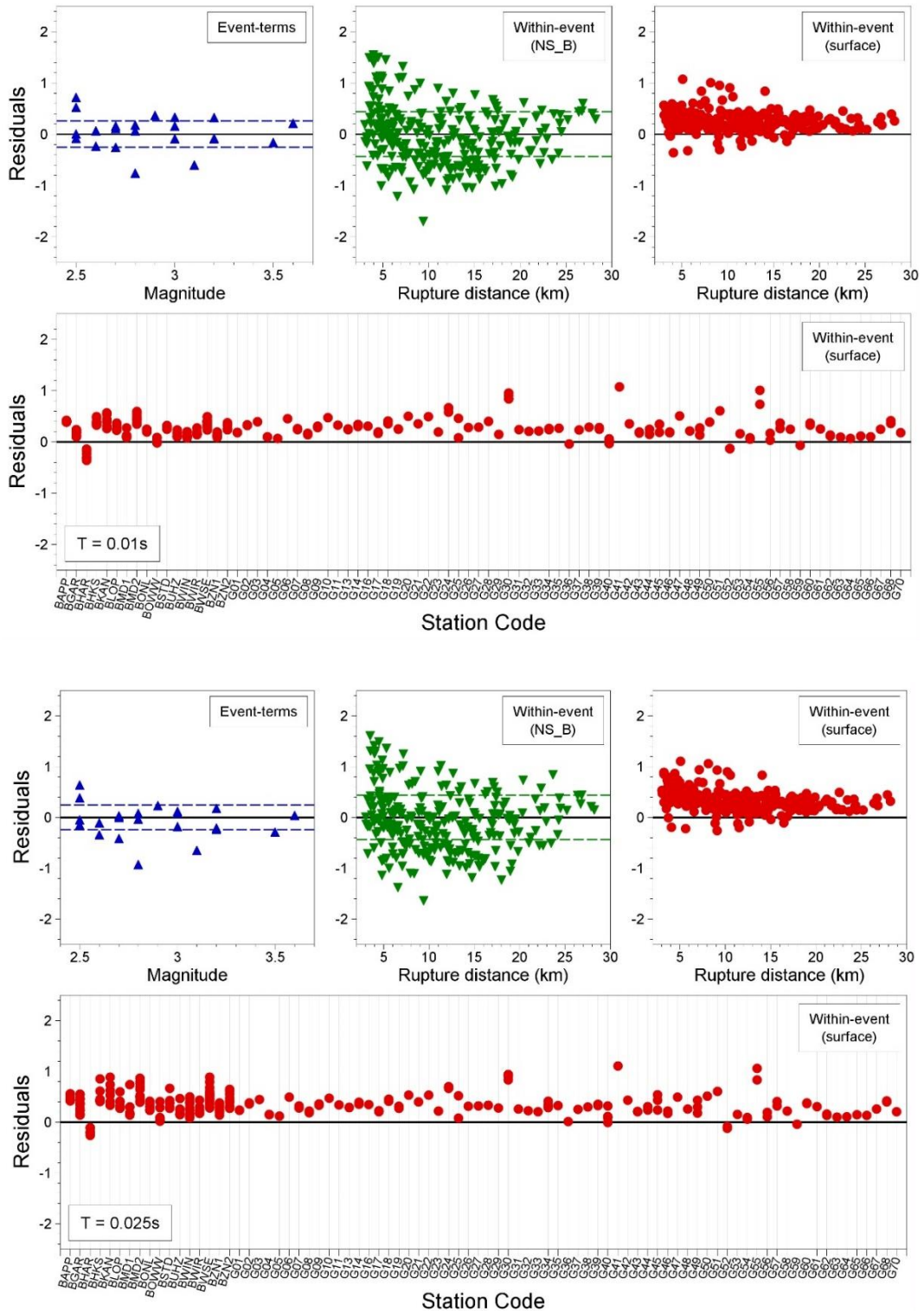


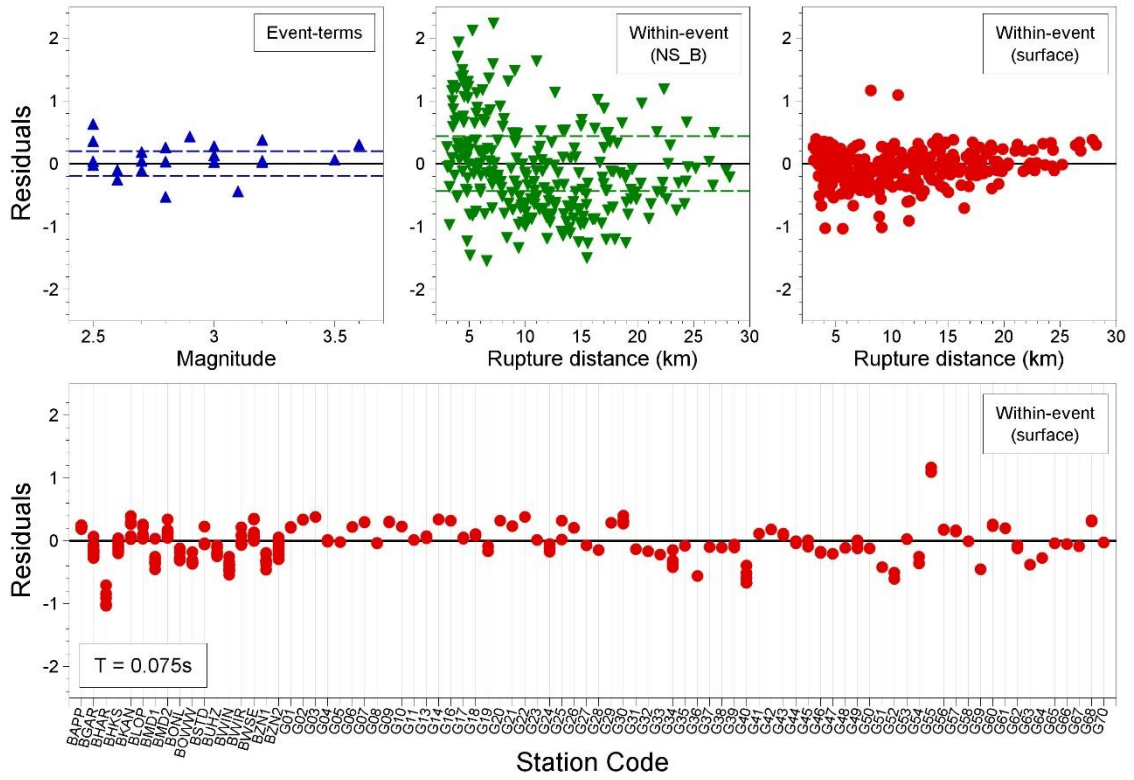
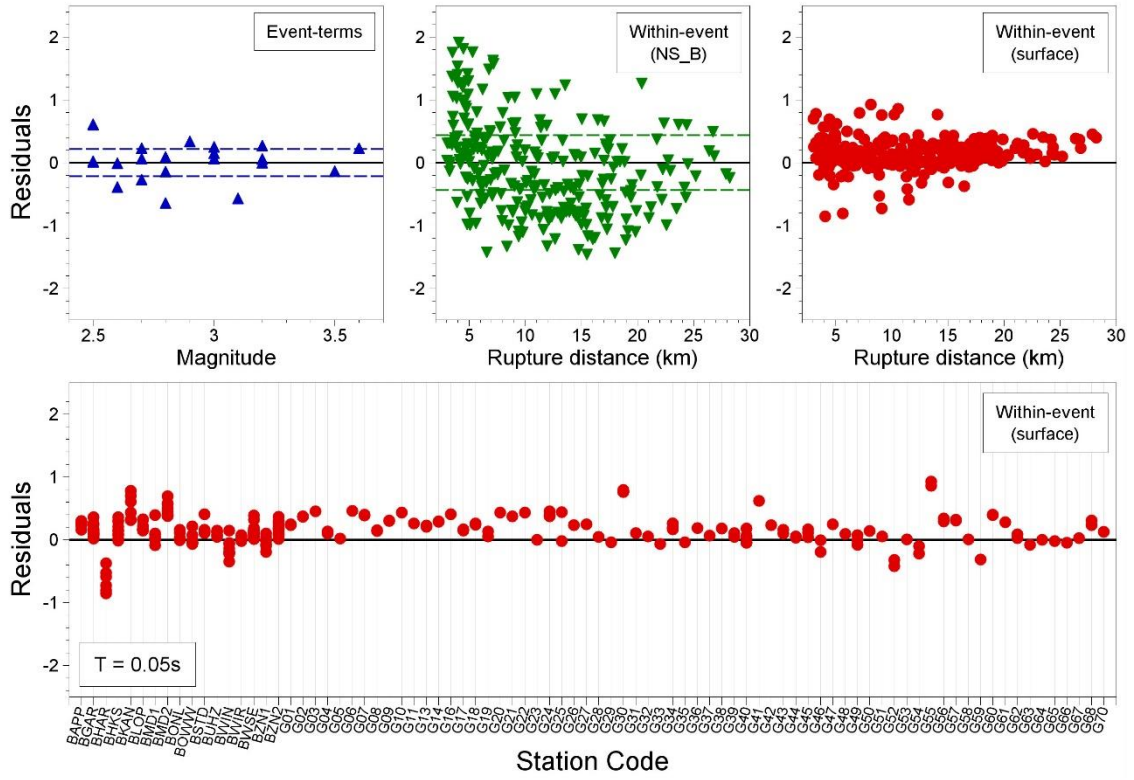


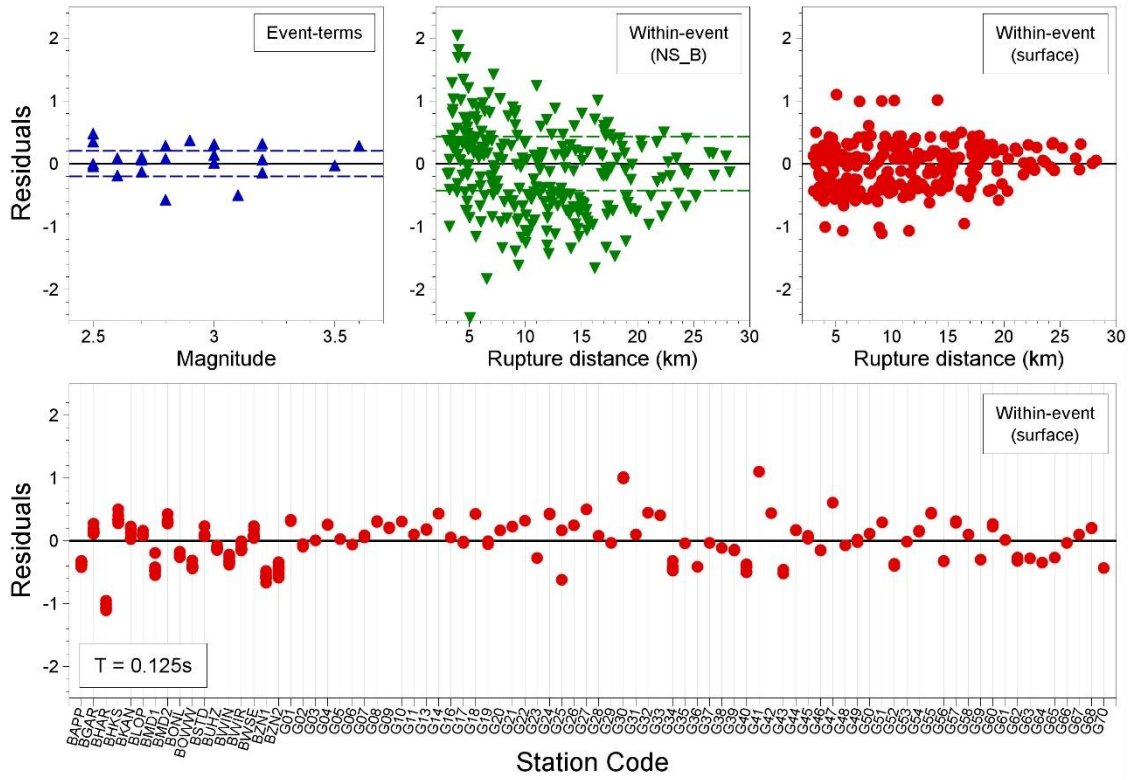
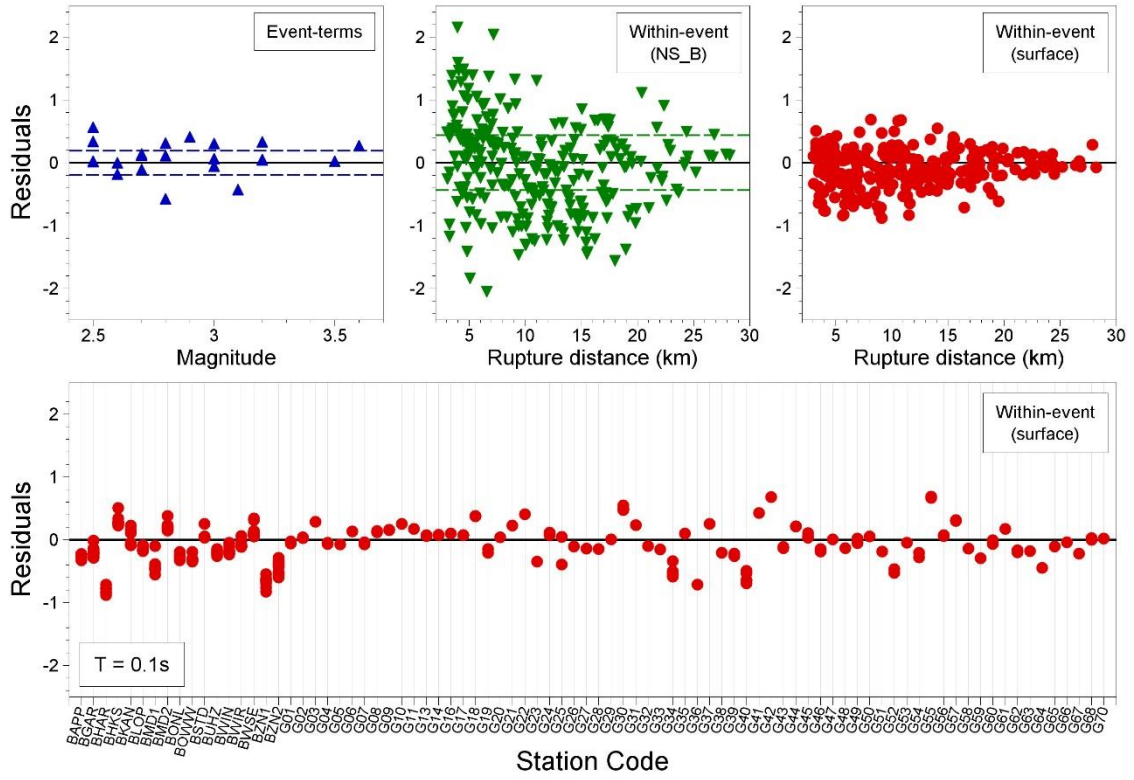
APPENDIX VI

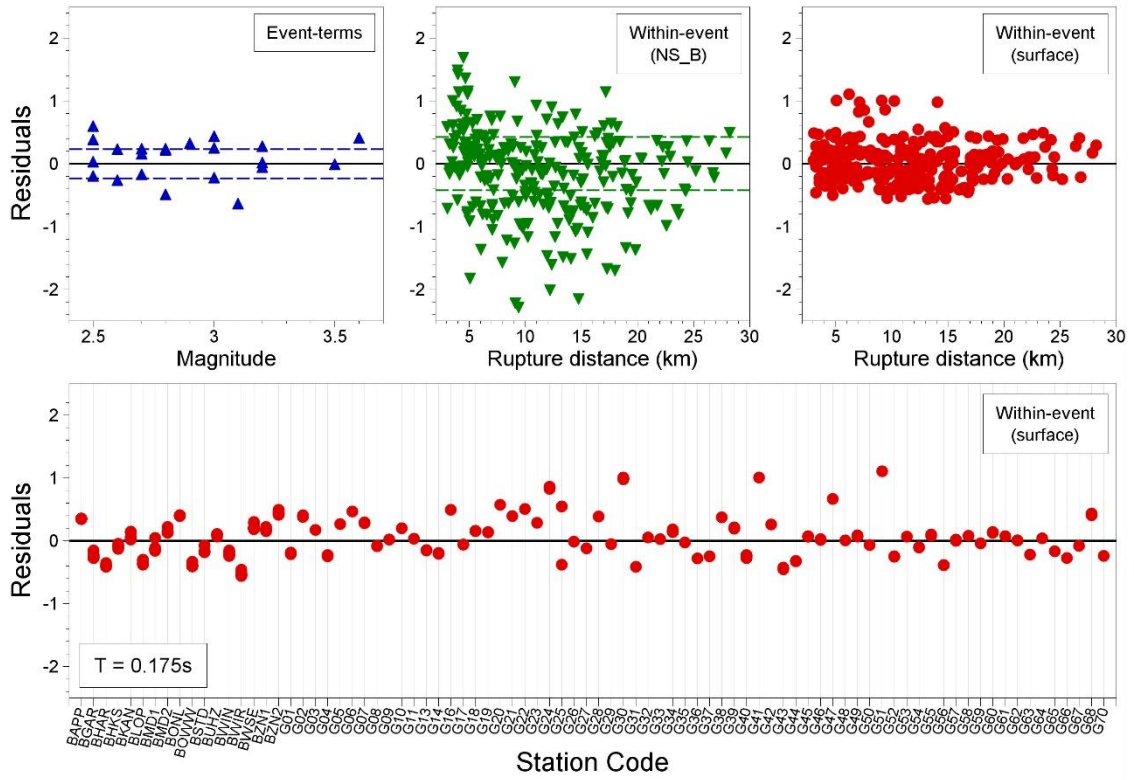
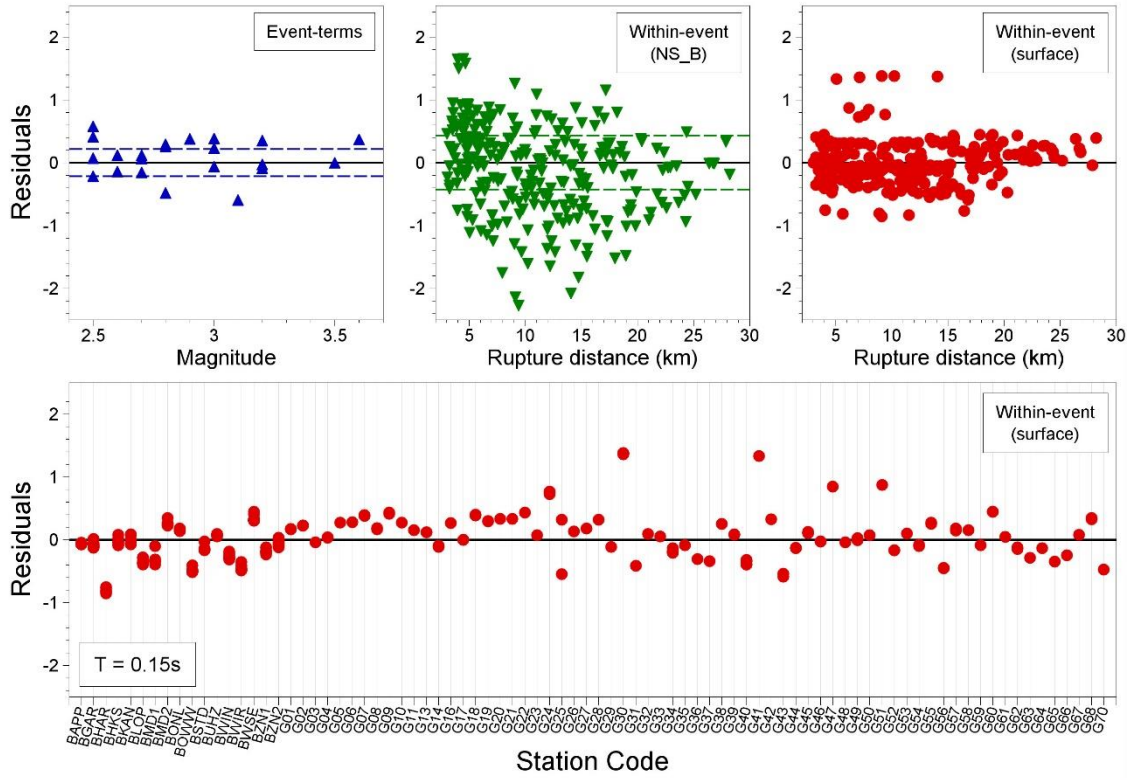
Surface Residuals of Groningen Recordings

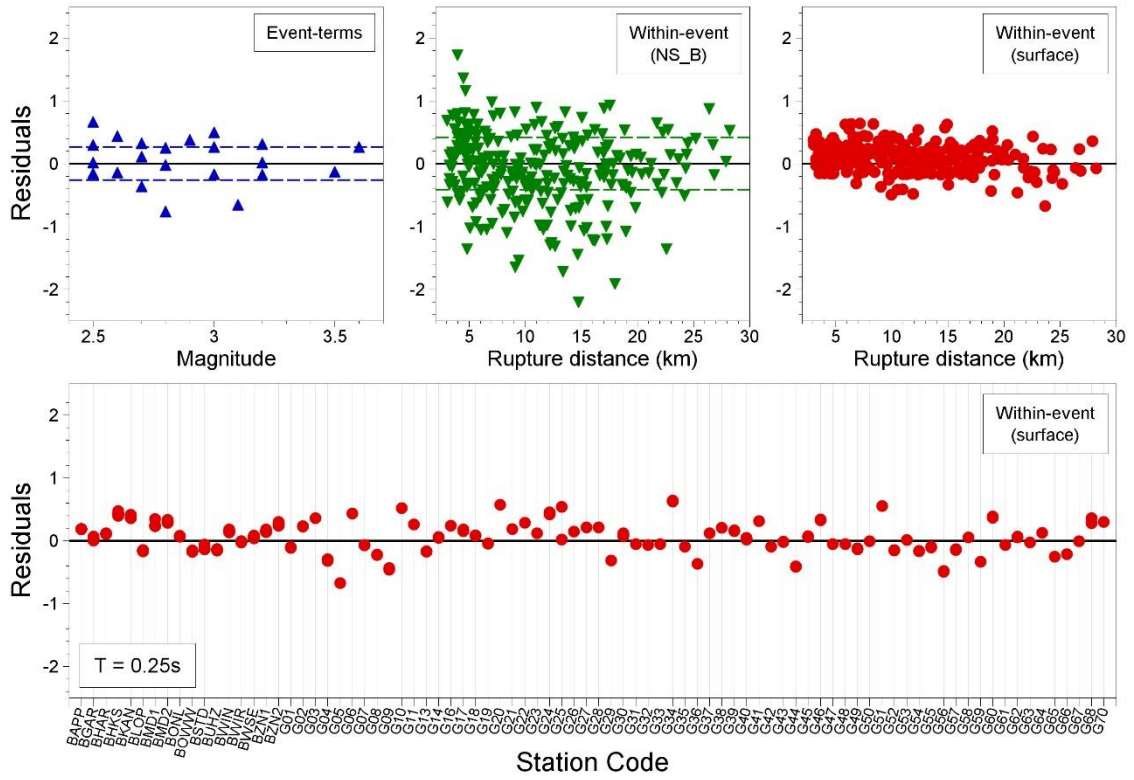
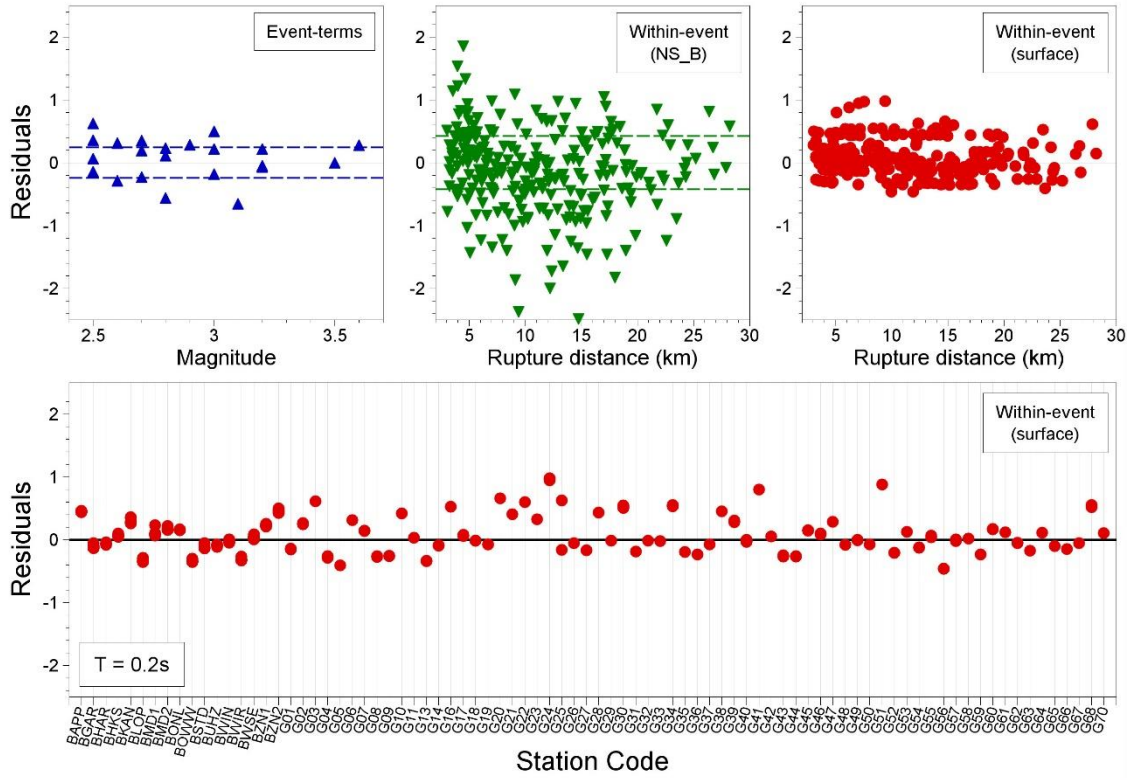
Presented in the plots are residuals of the Central-lower model obtained using $\phi_{SS,low}$.

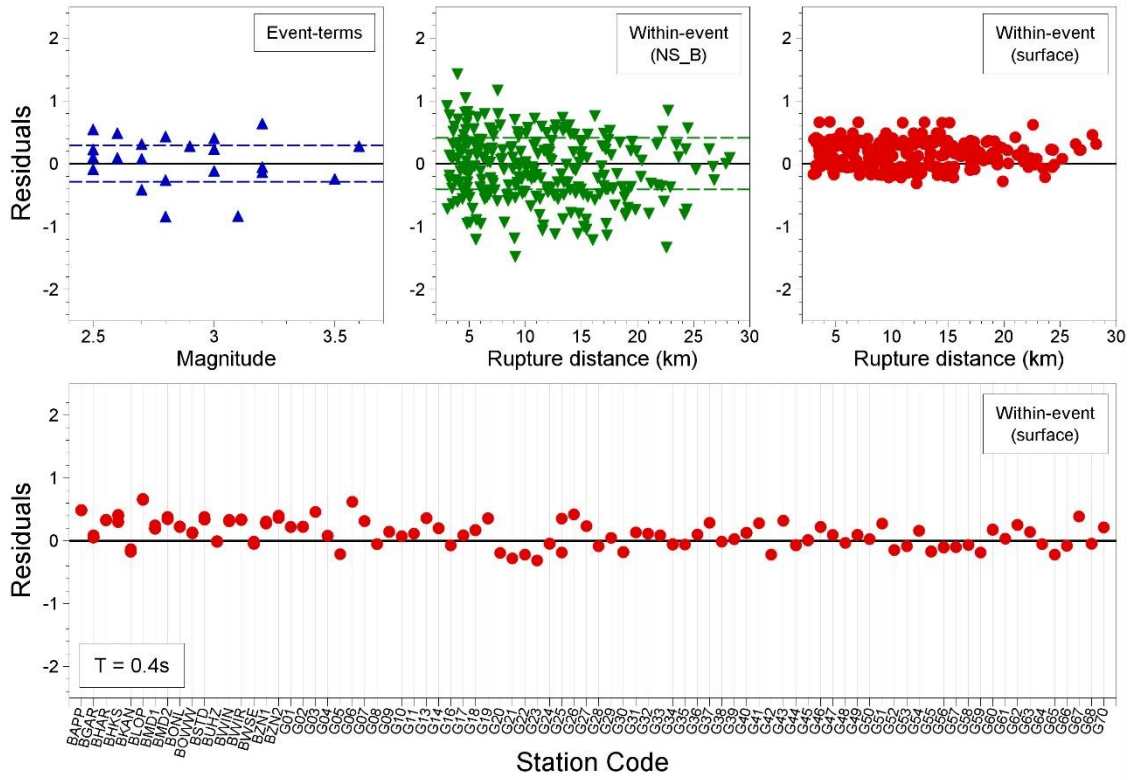
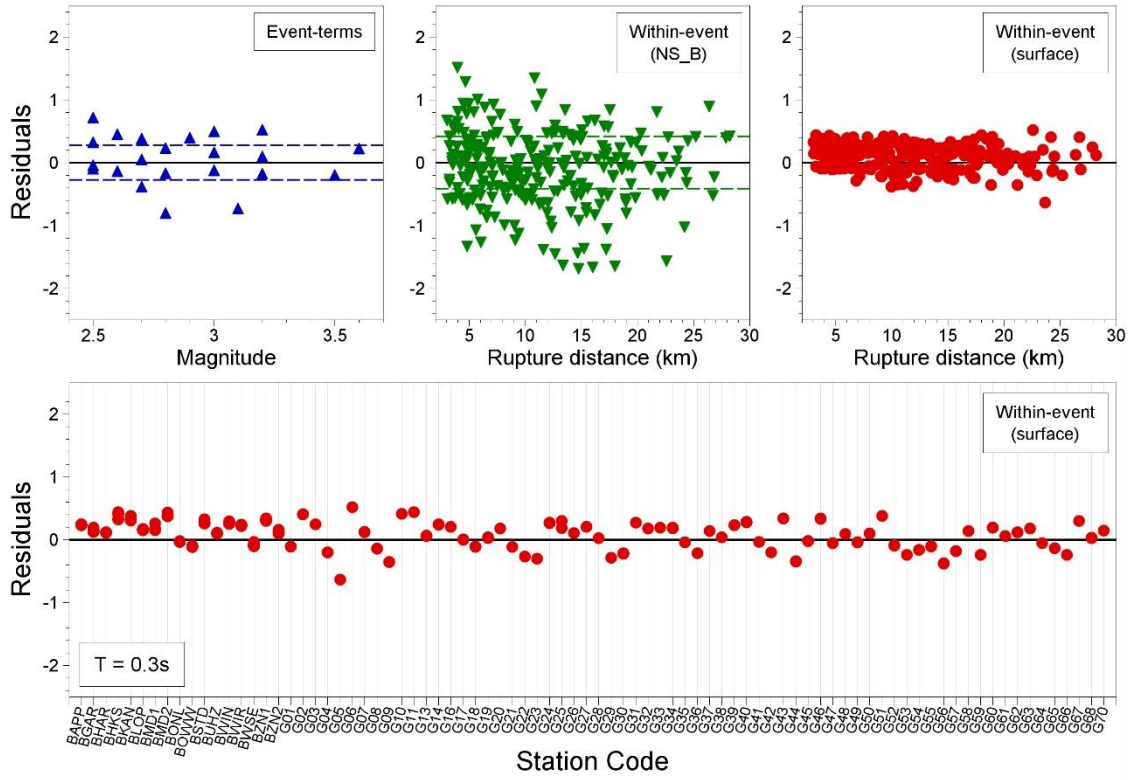


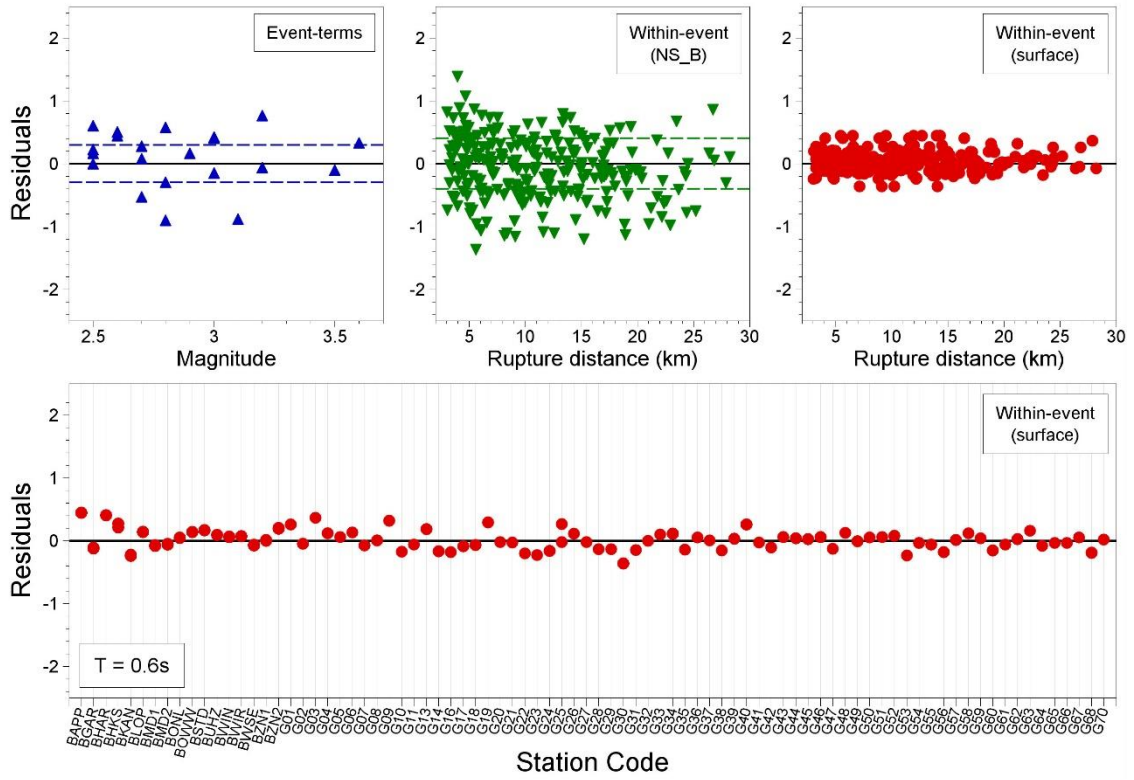
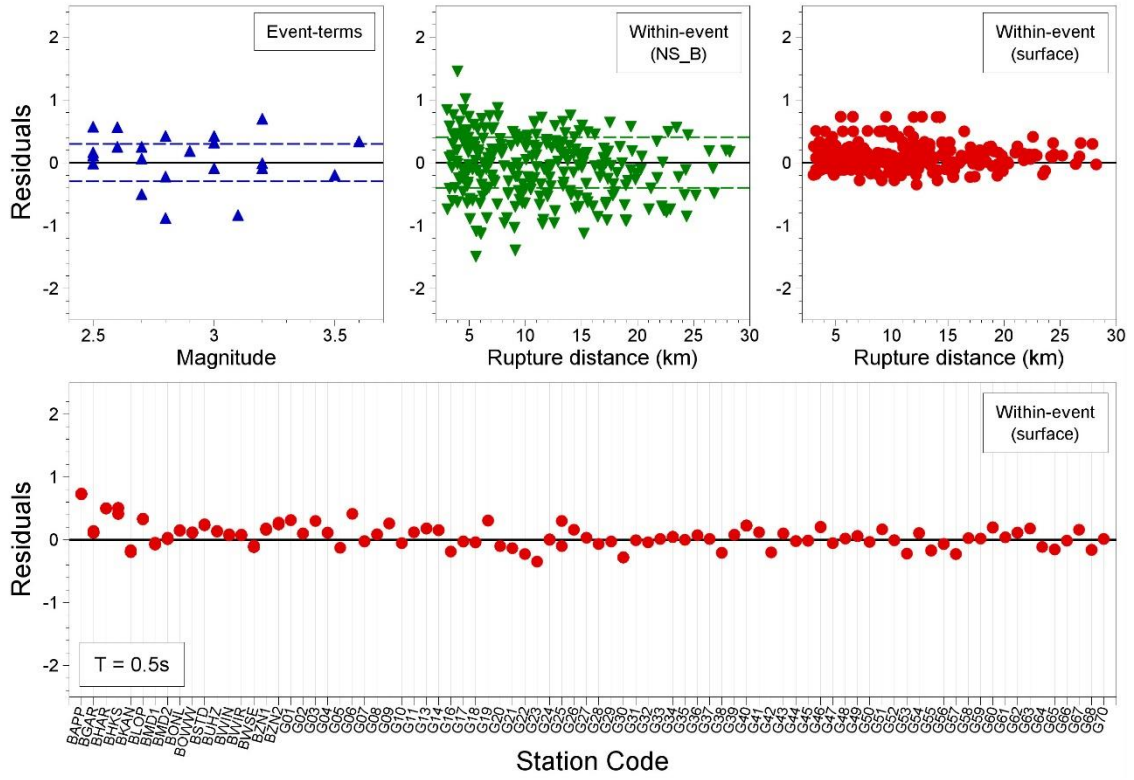


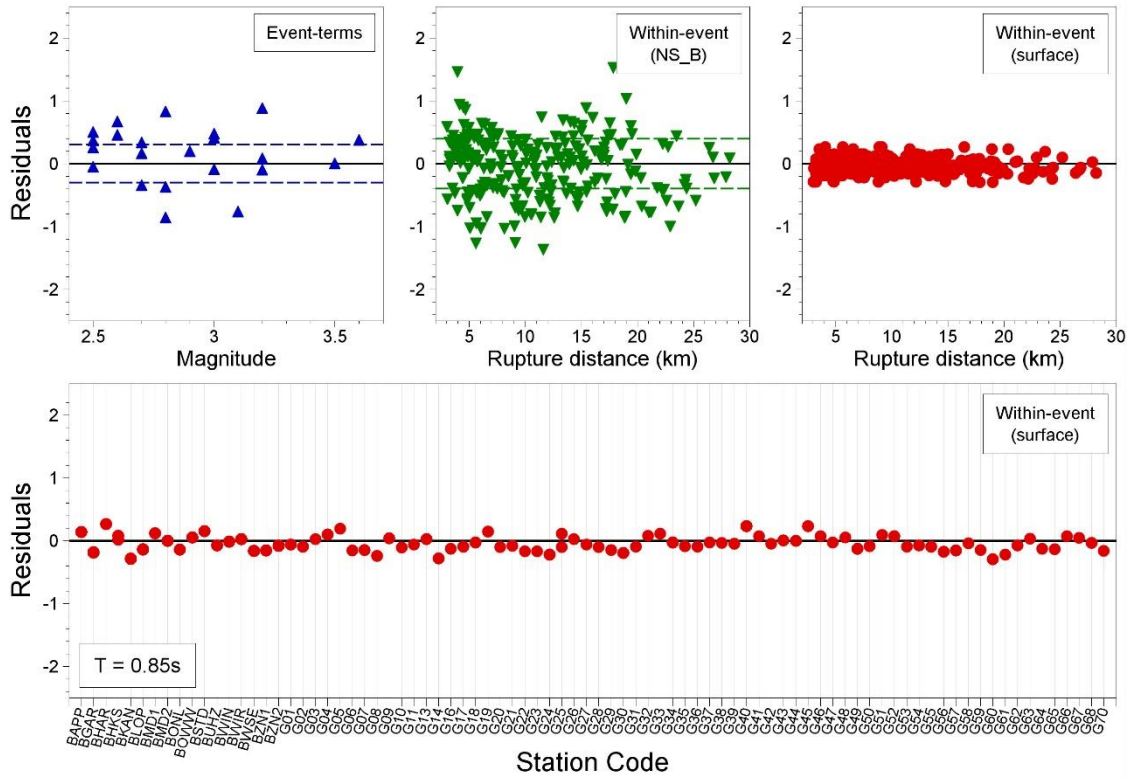
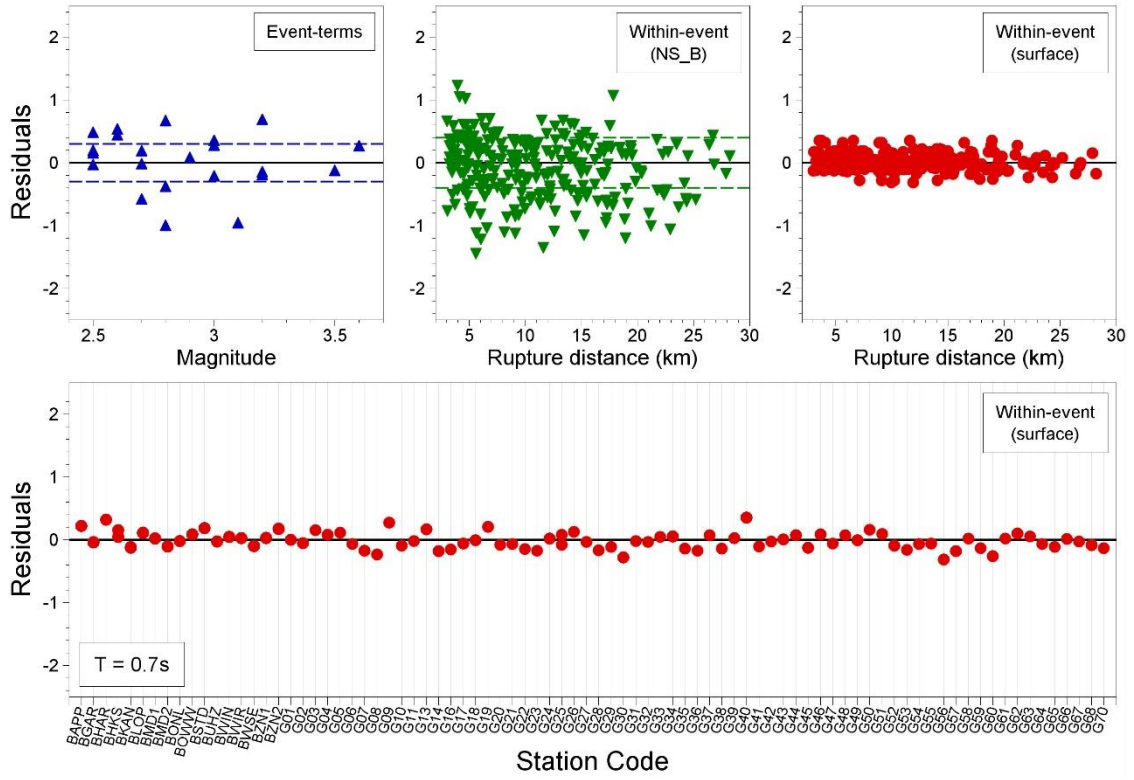


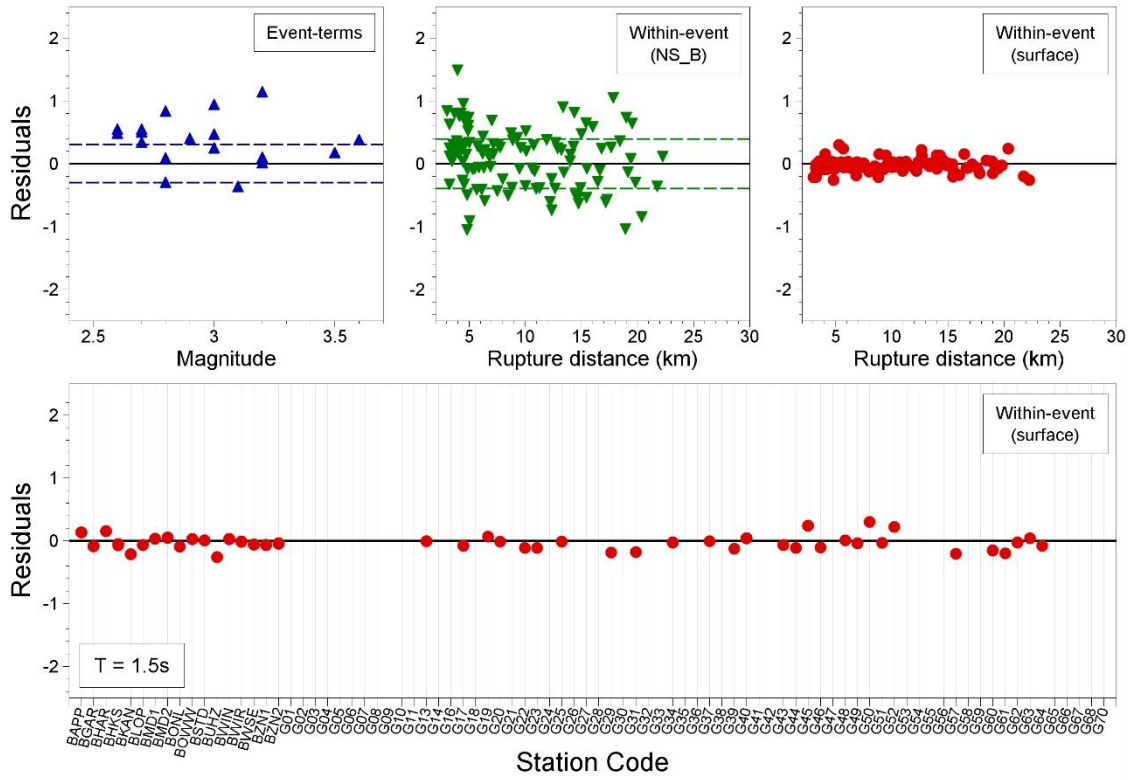
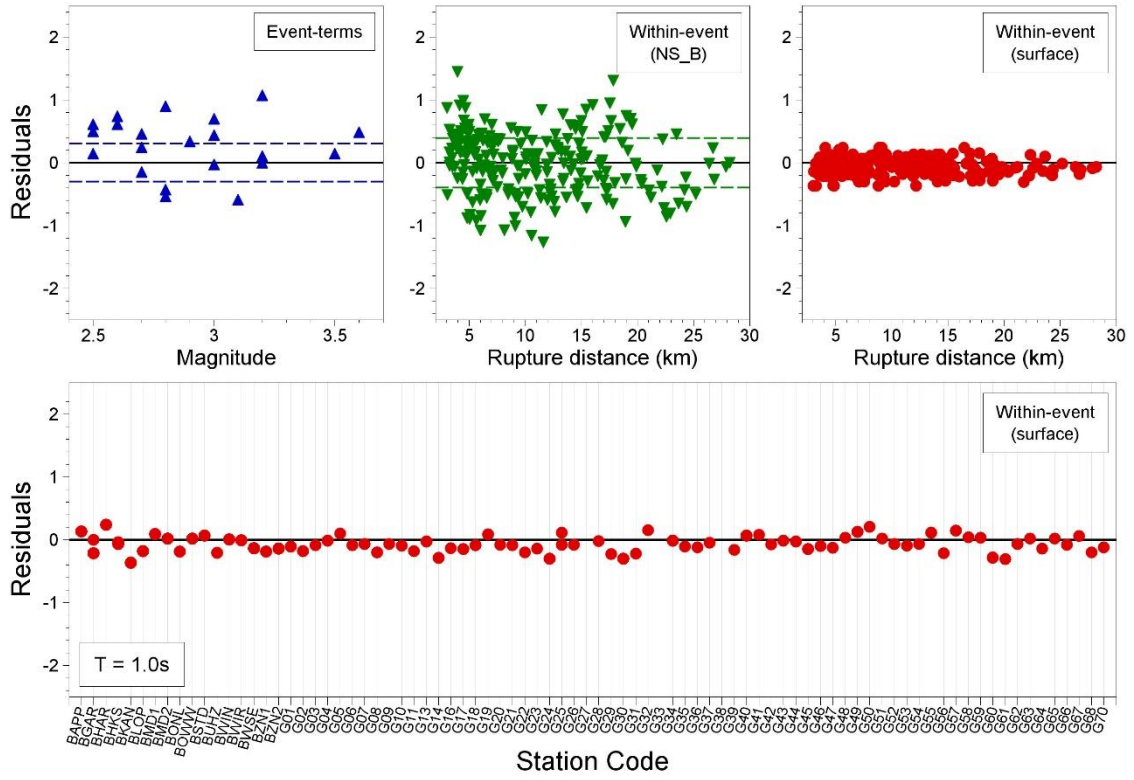


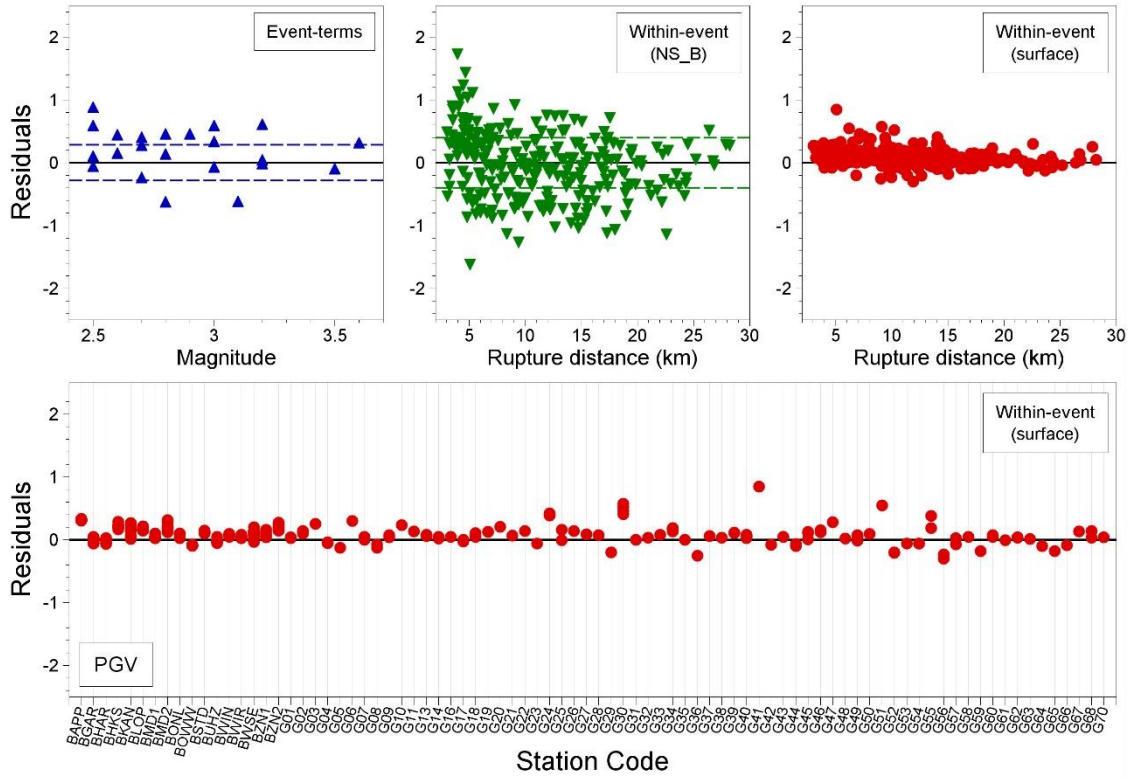






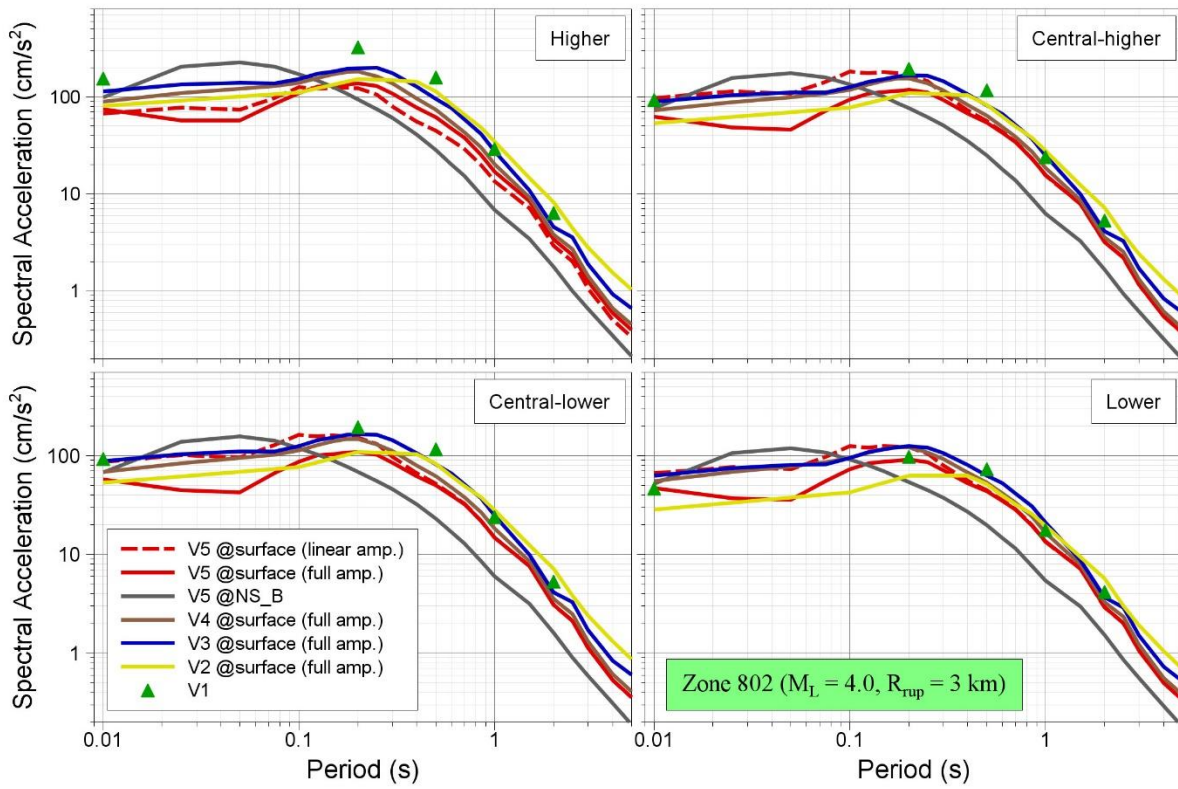


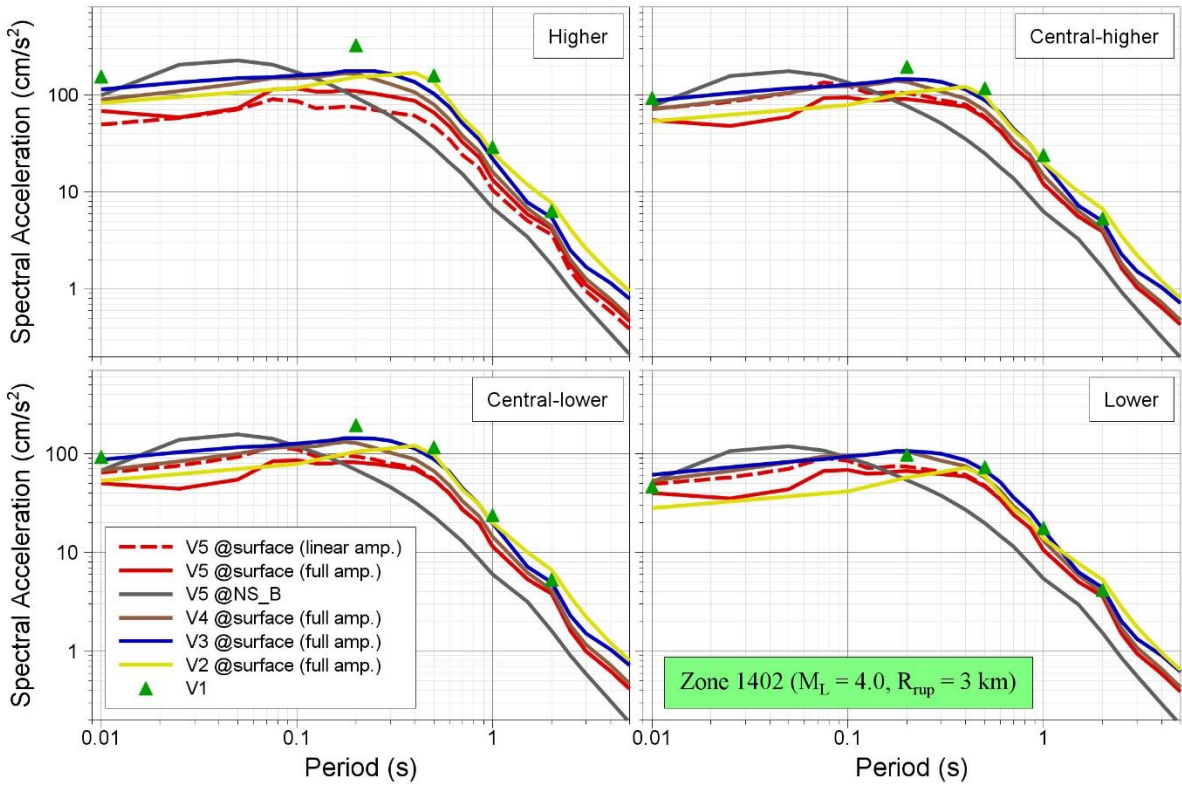
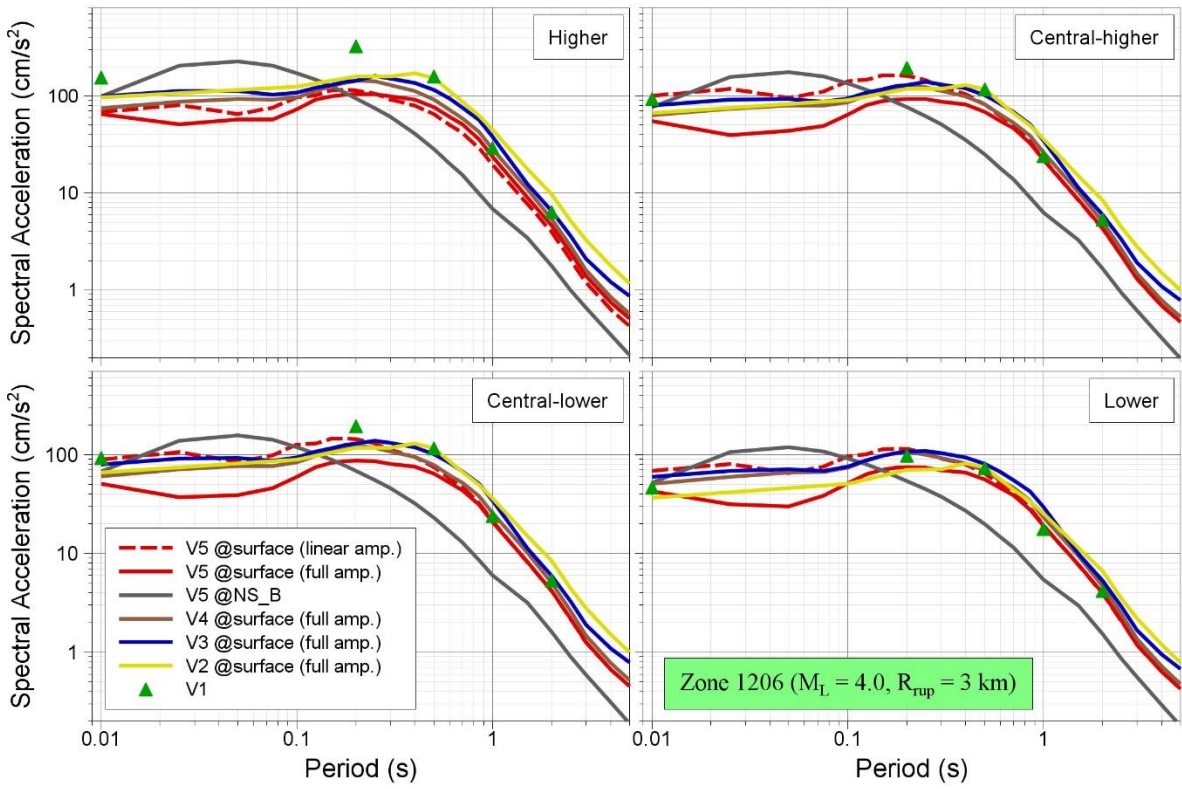


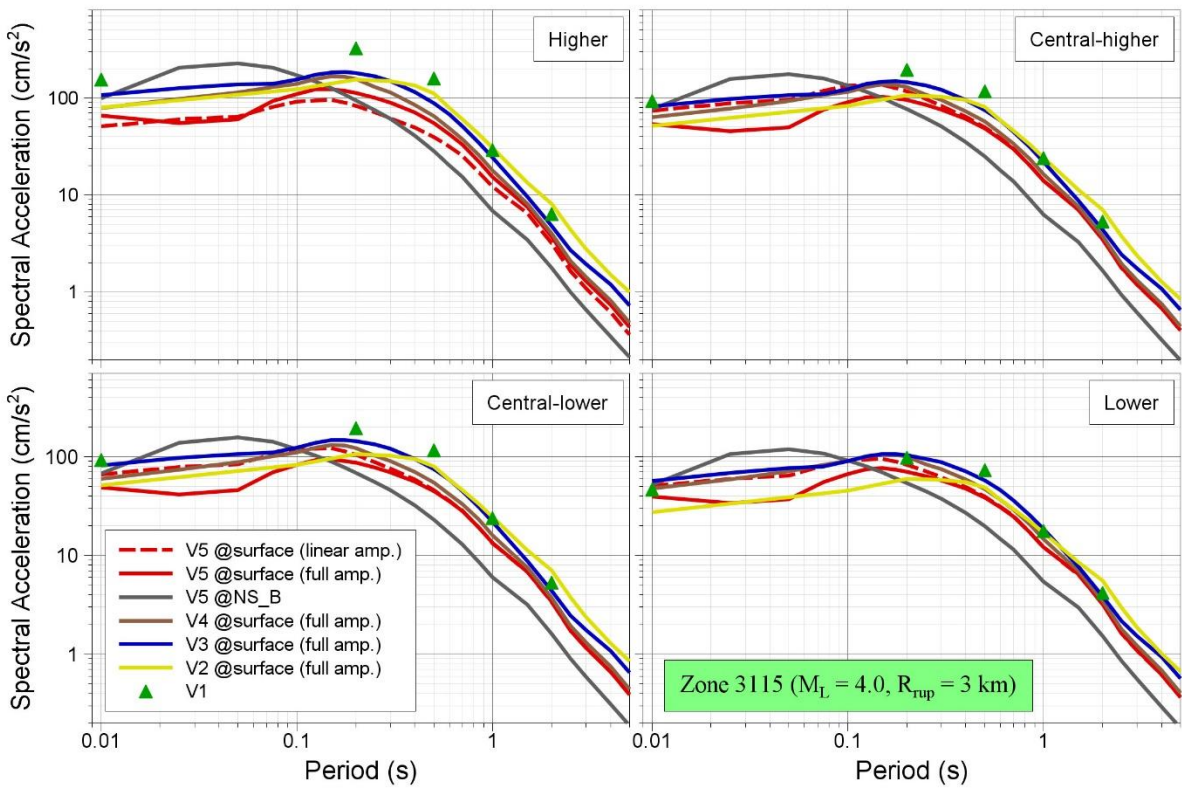
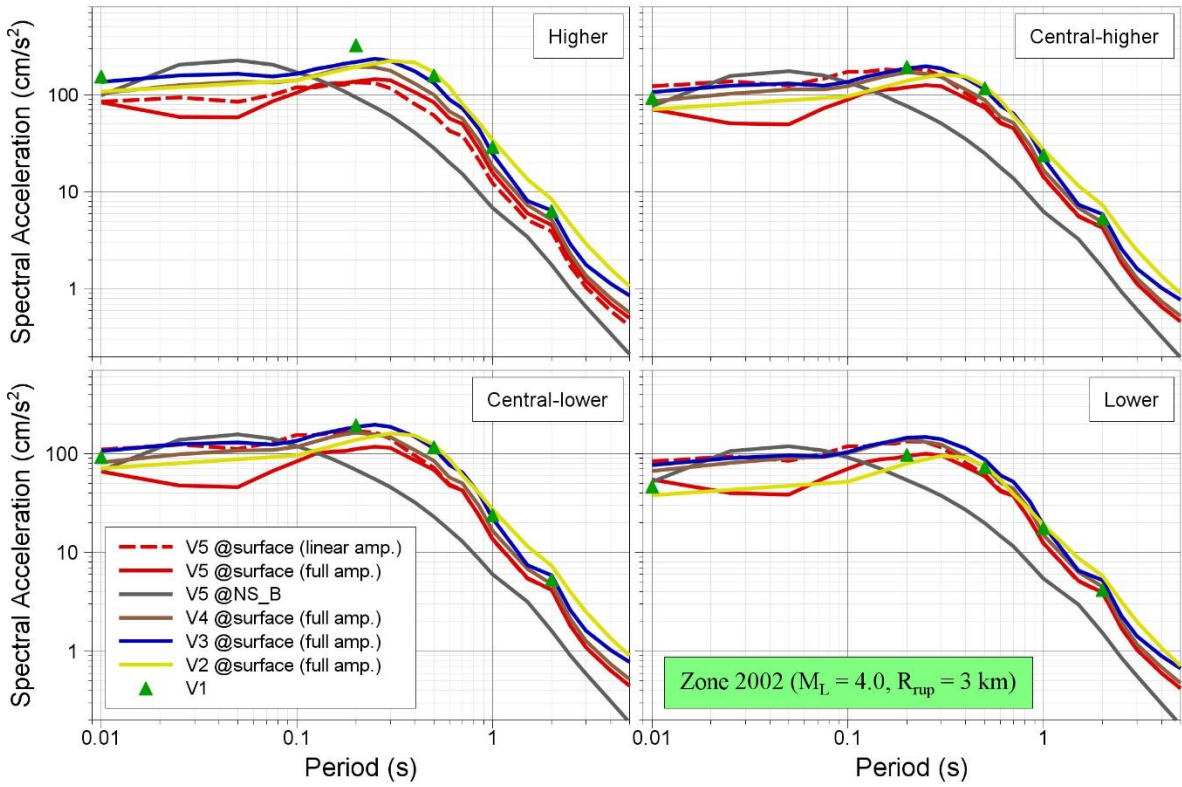


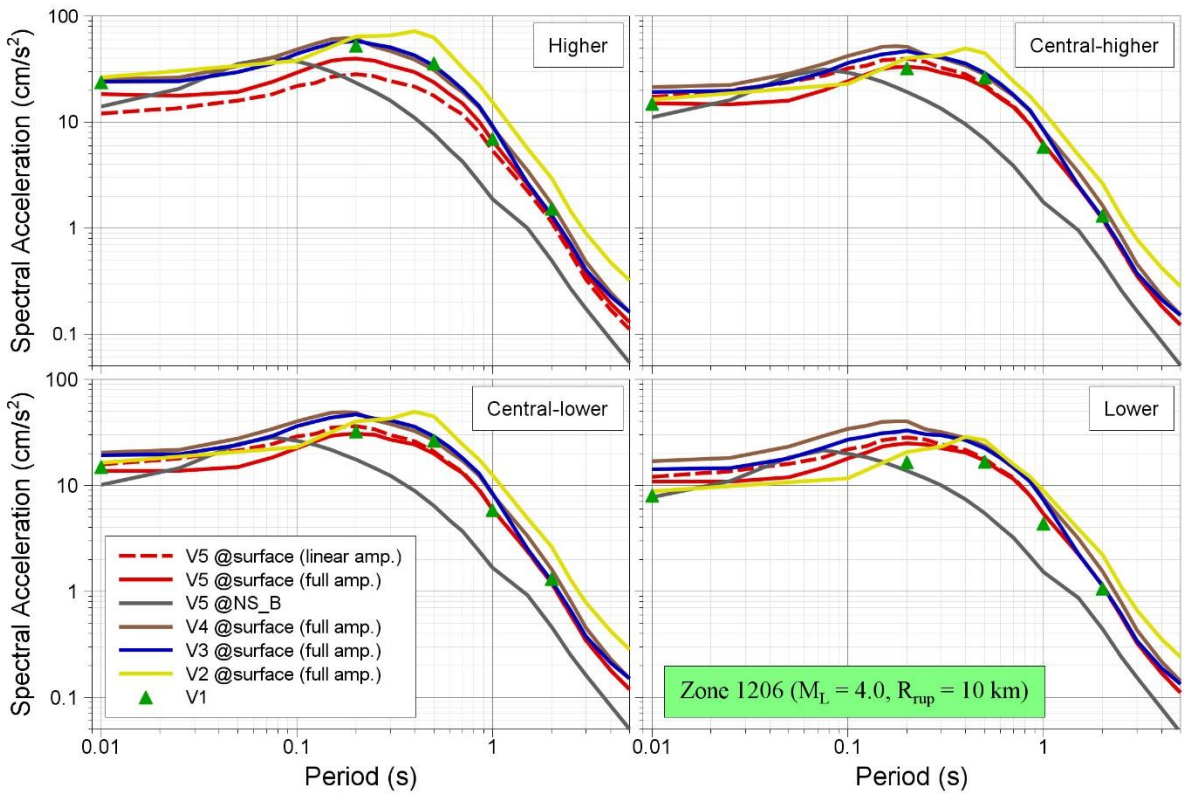
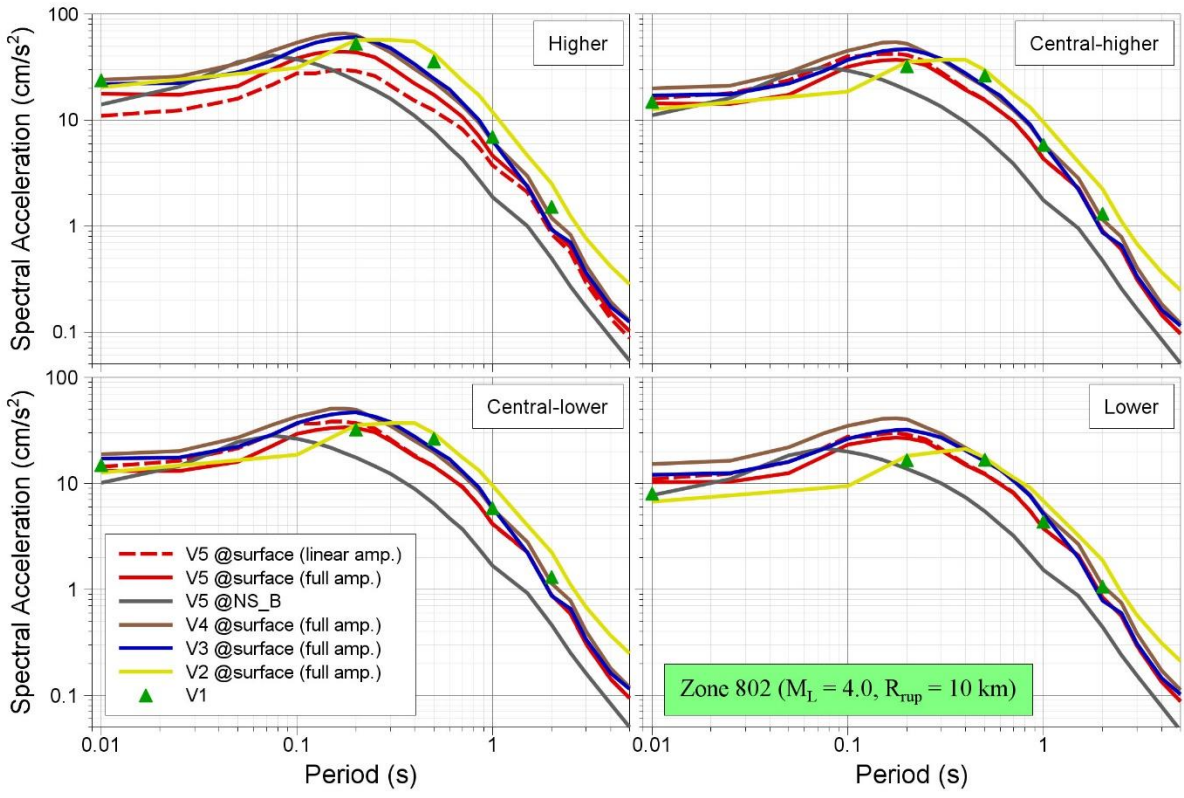
APPENDIX VII

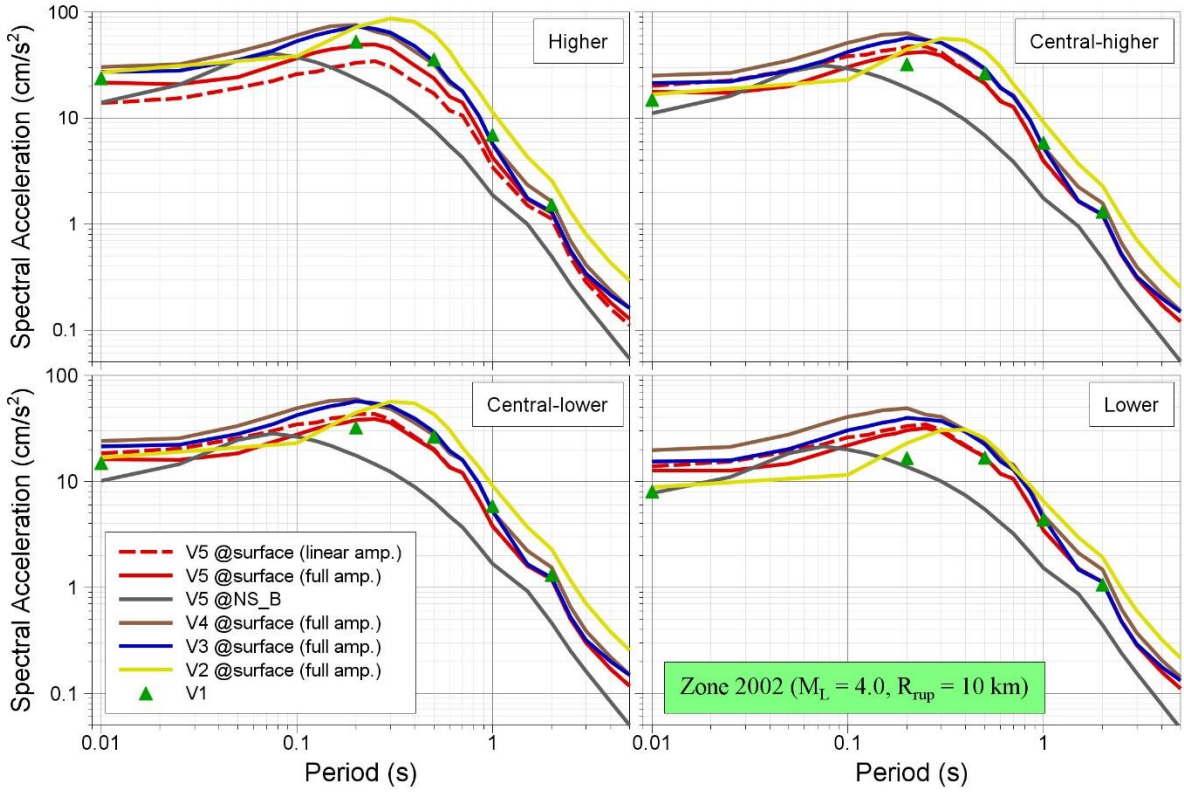
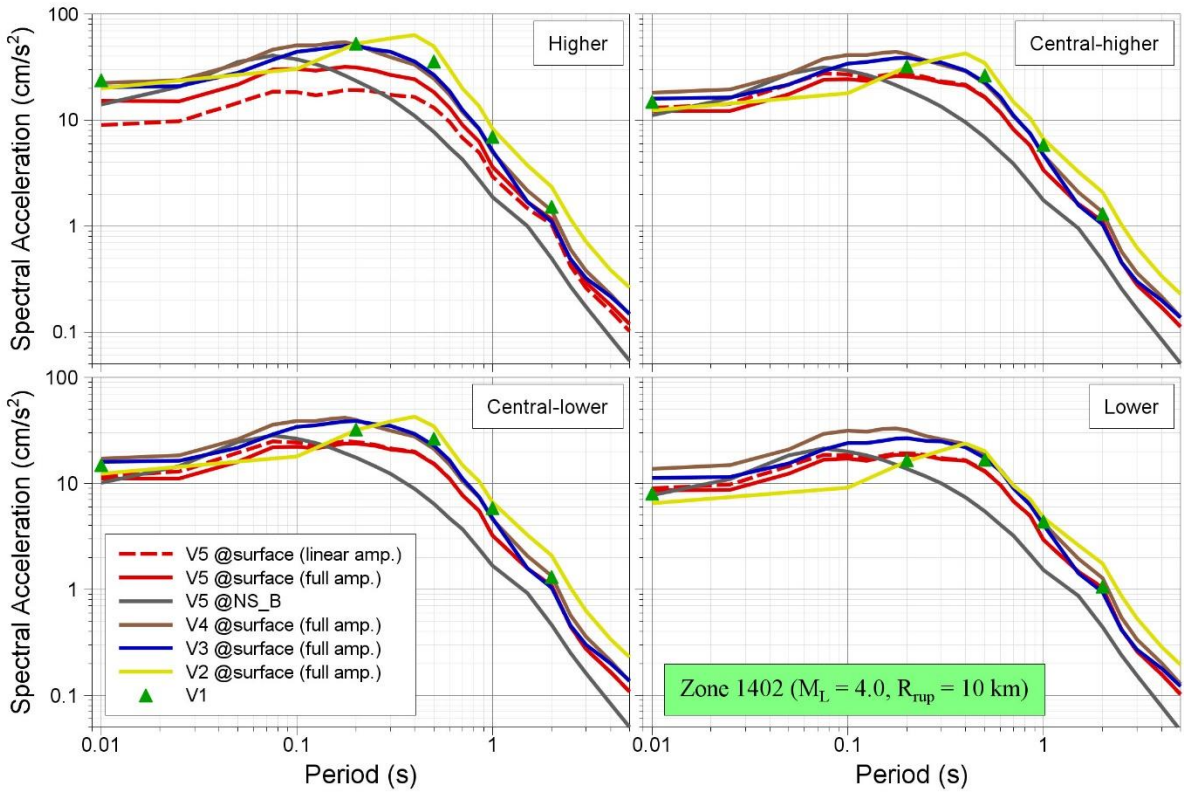
Median Predictions of Motions at Surface

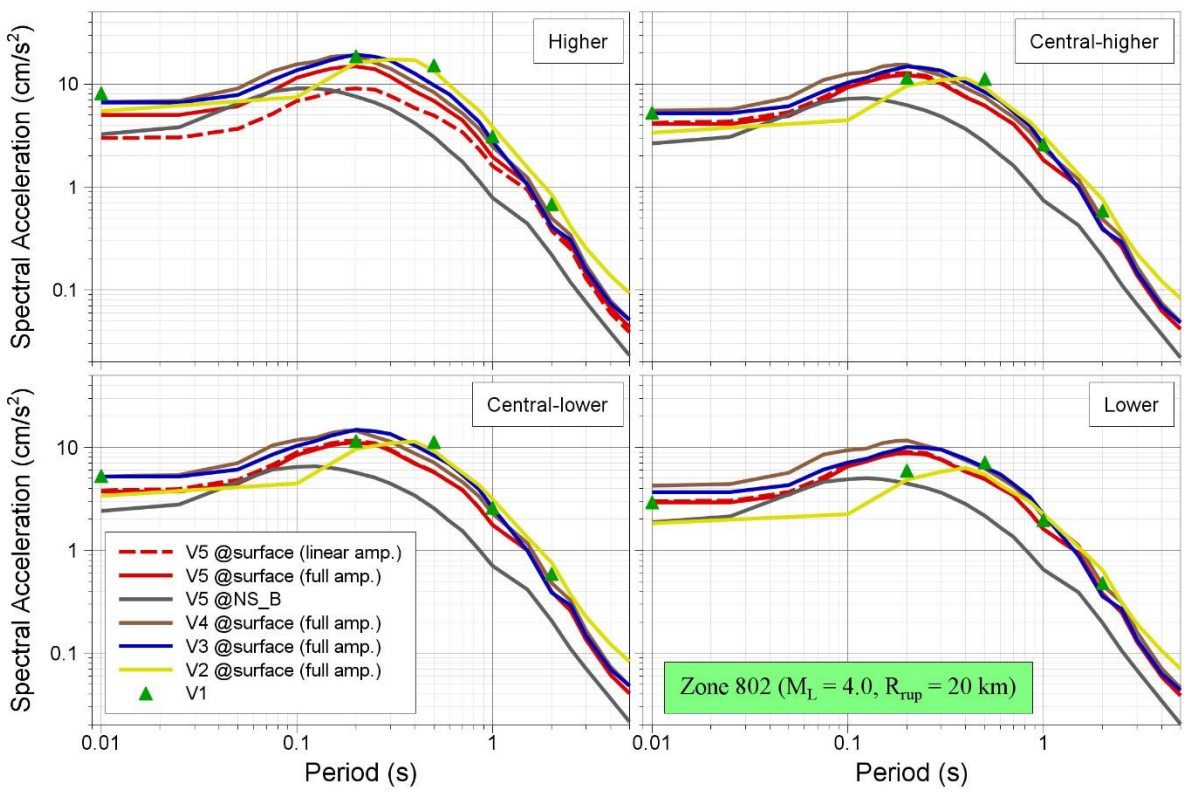
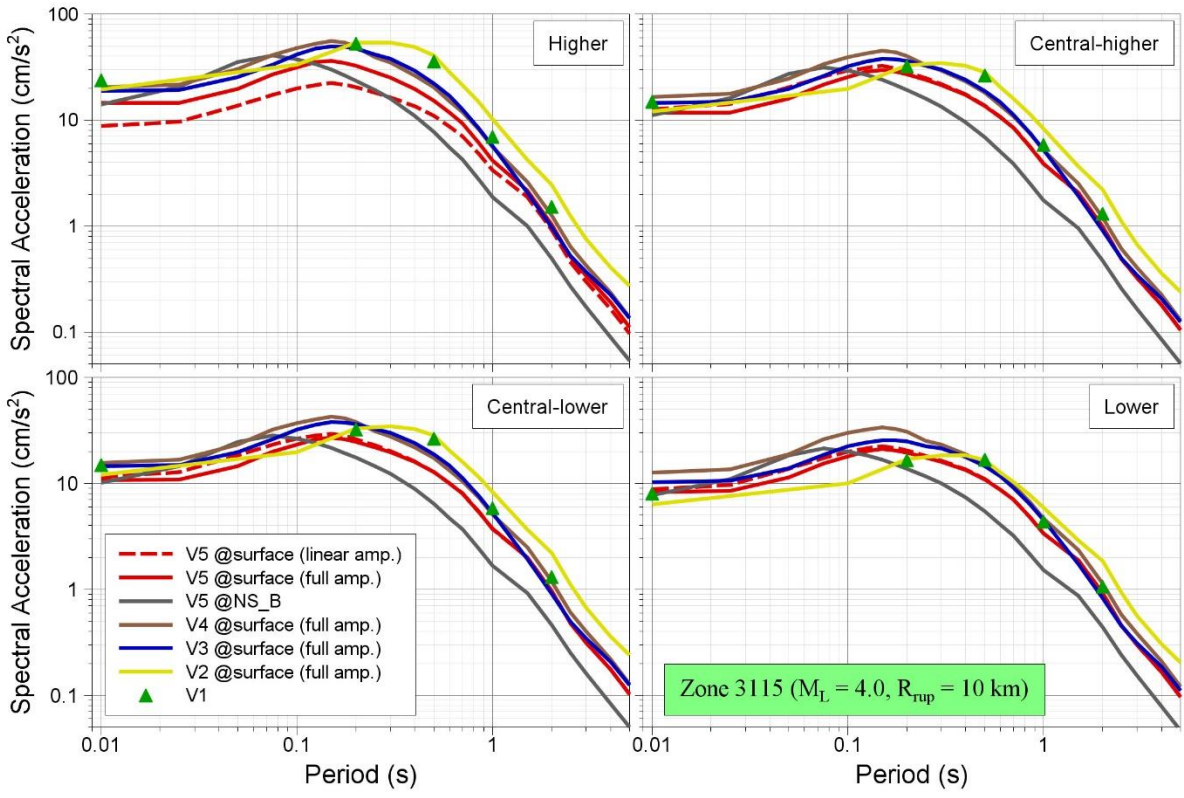


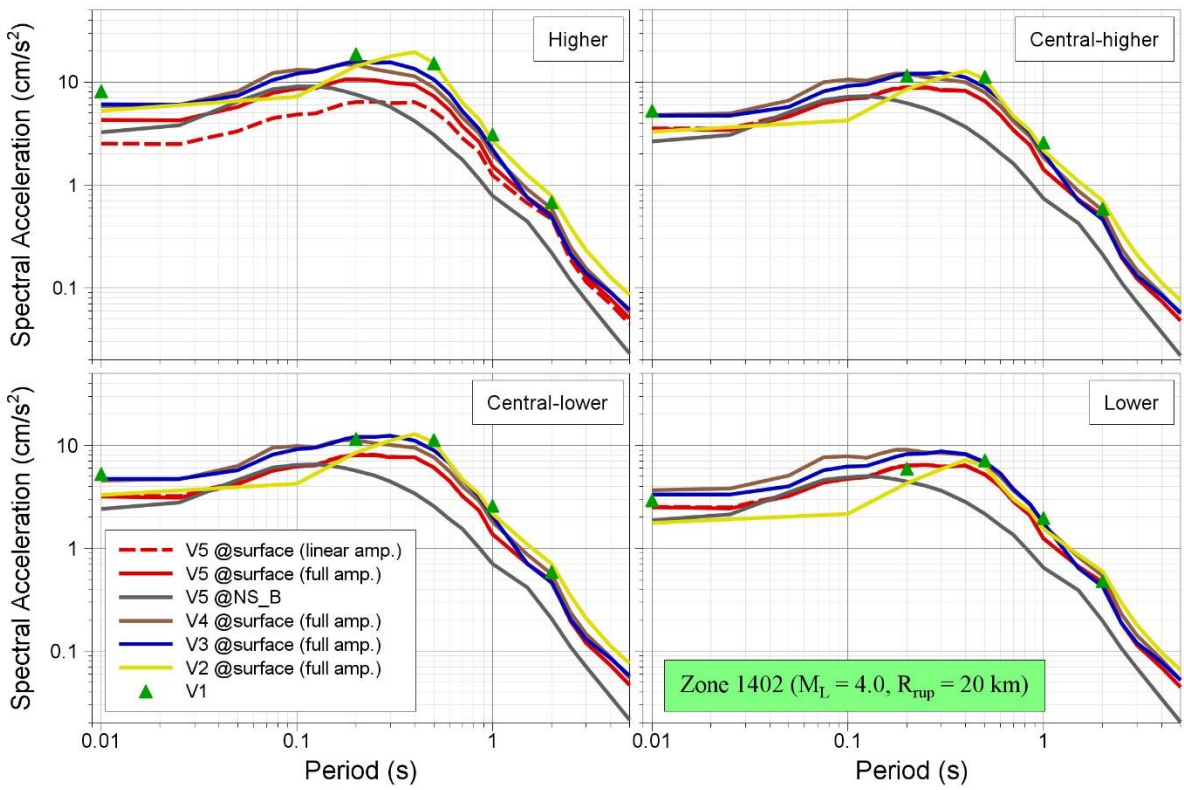
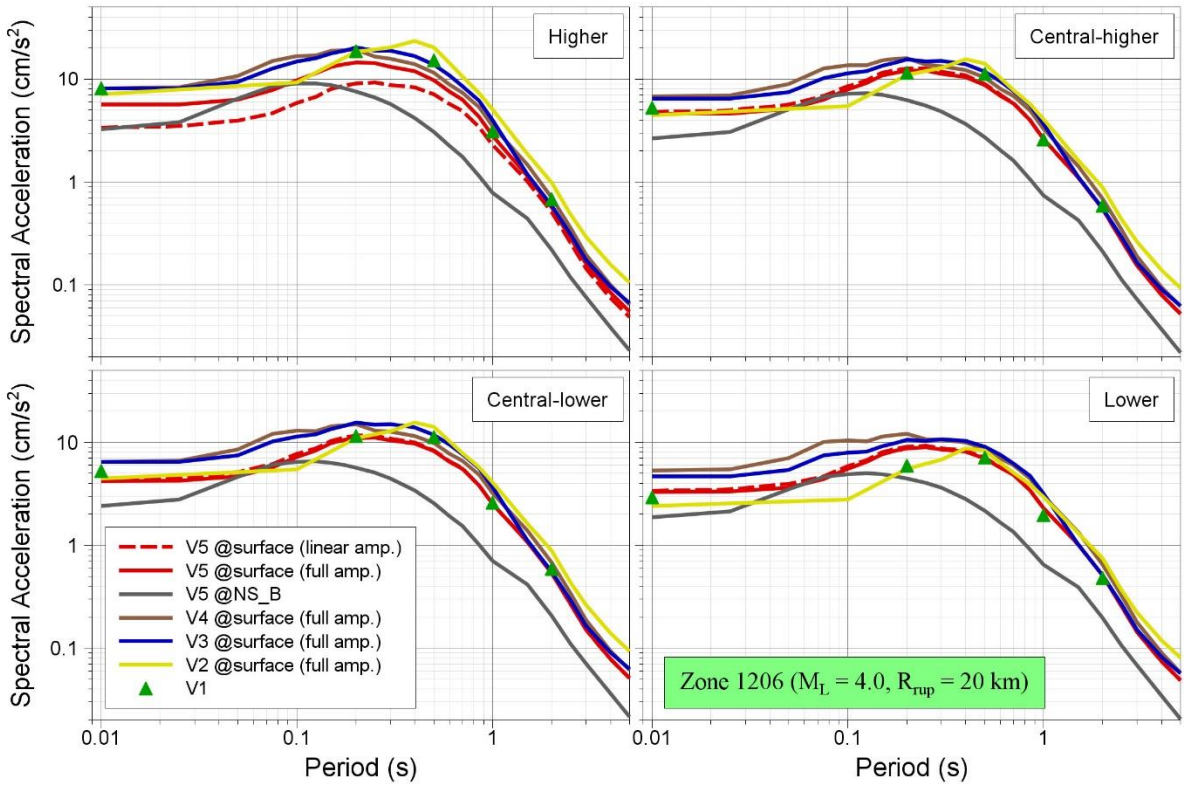


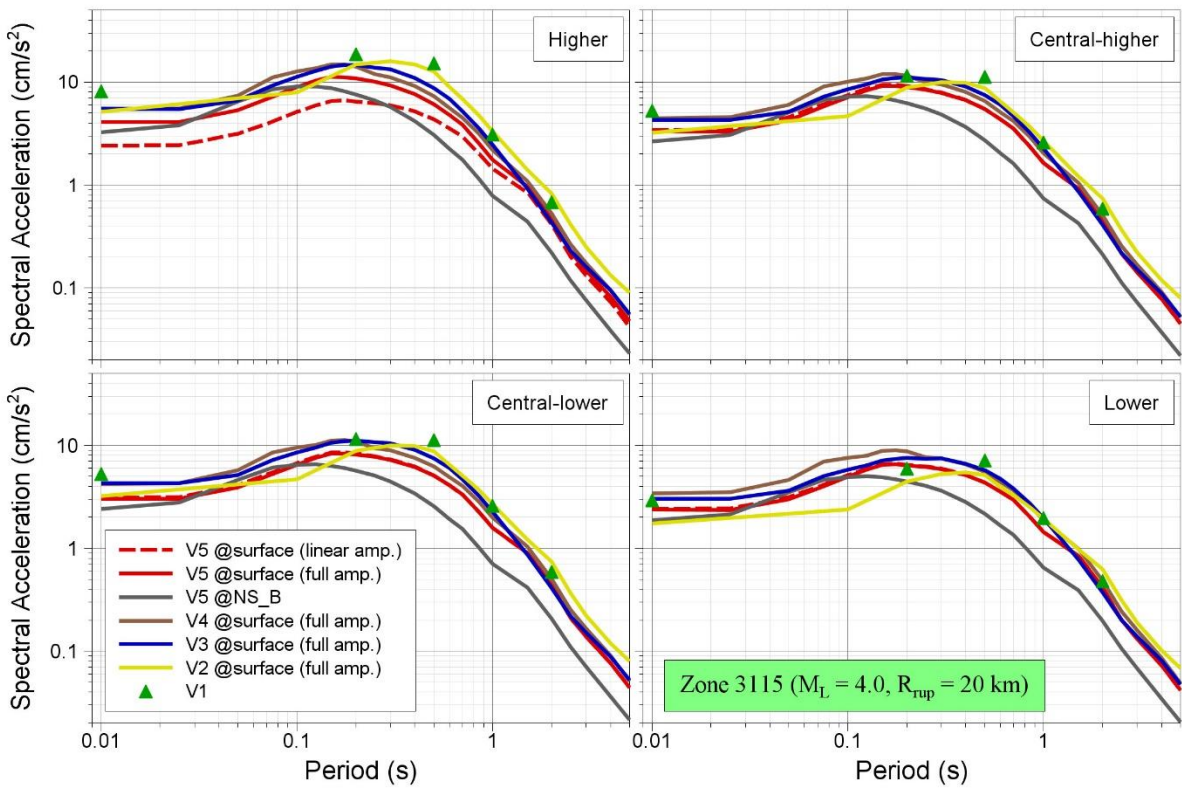
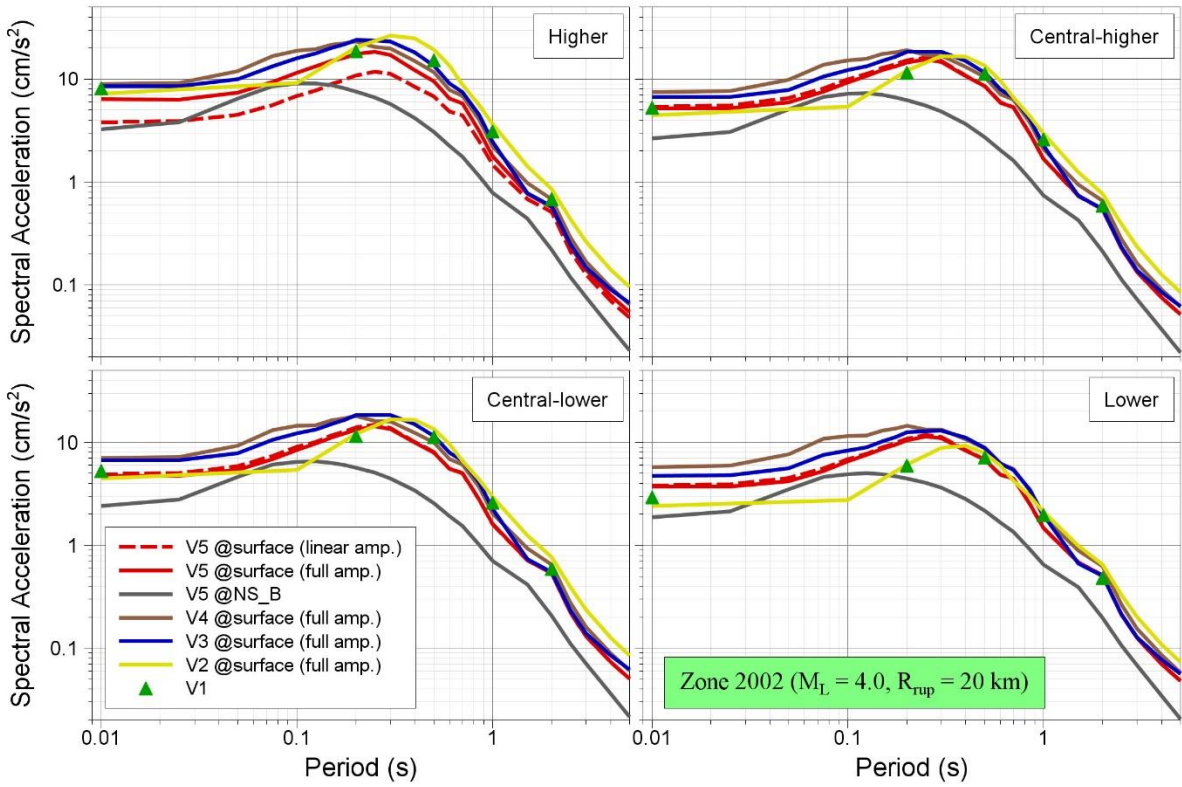


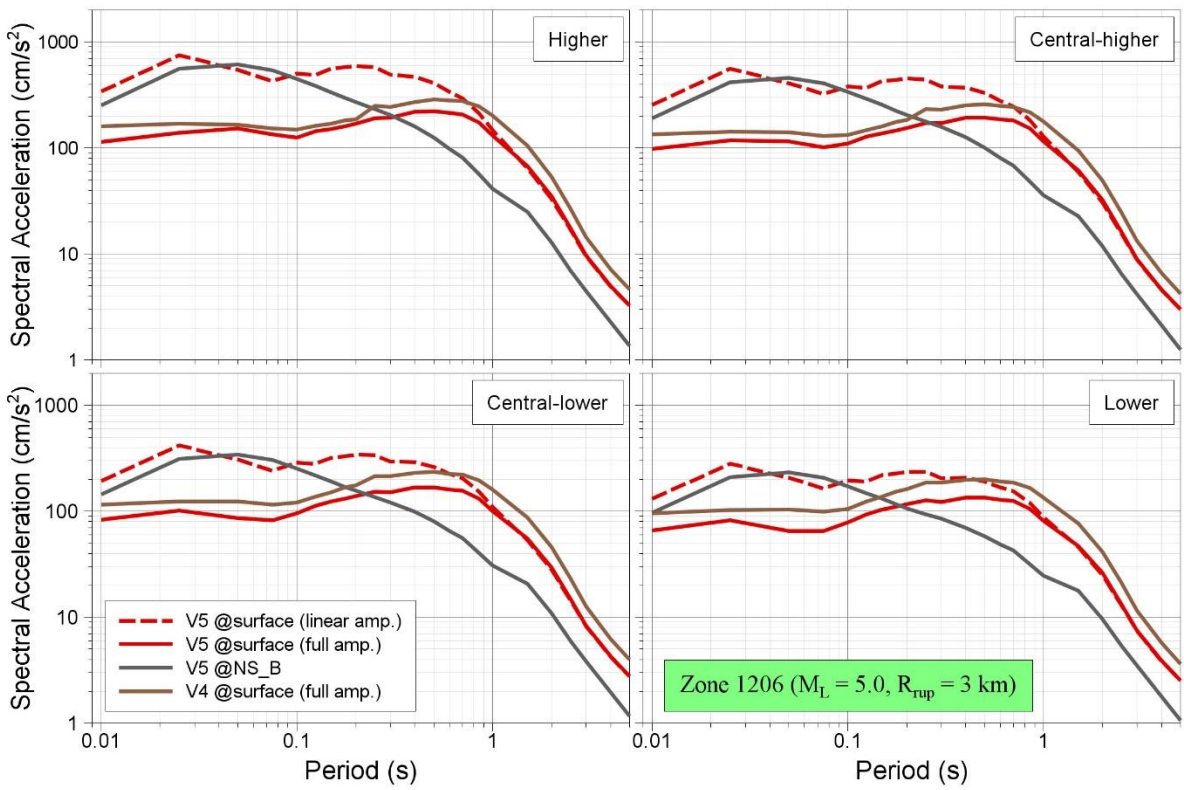
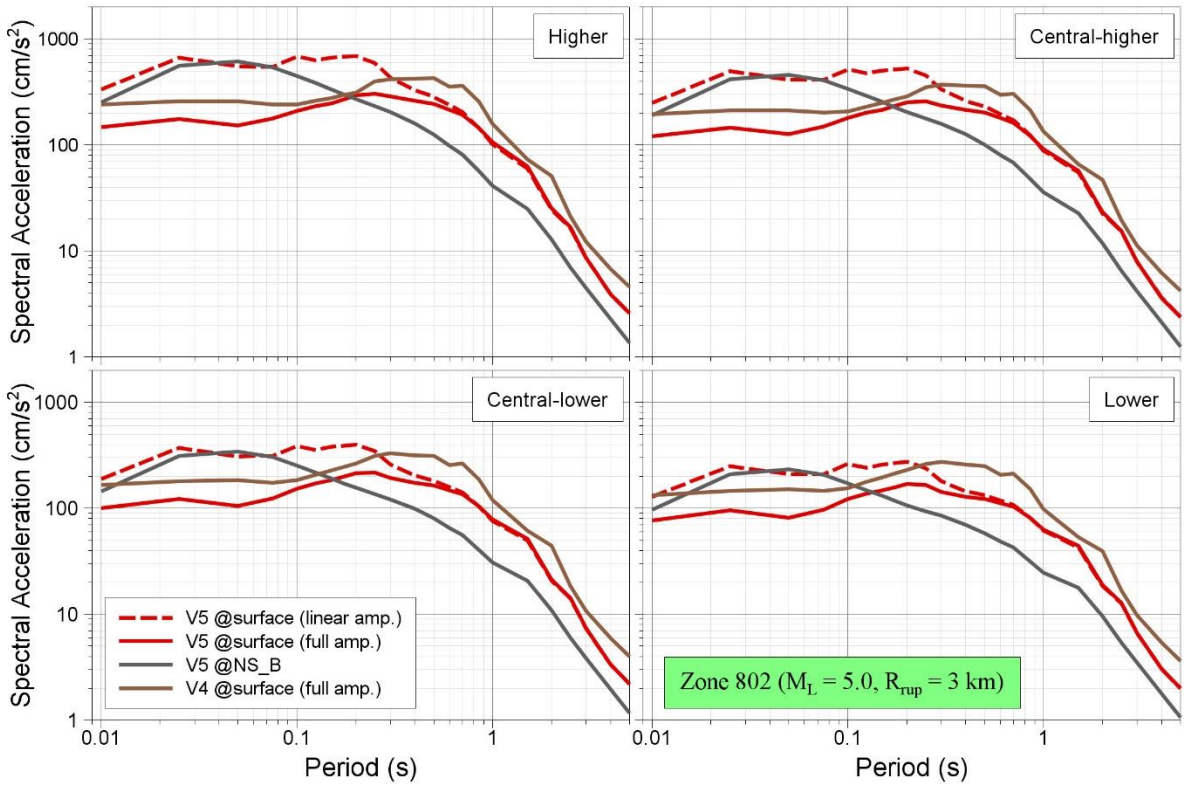


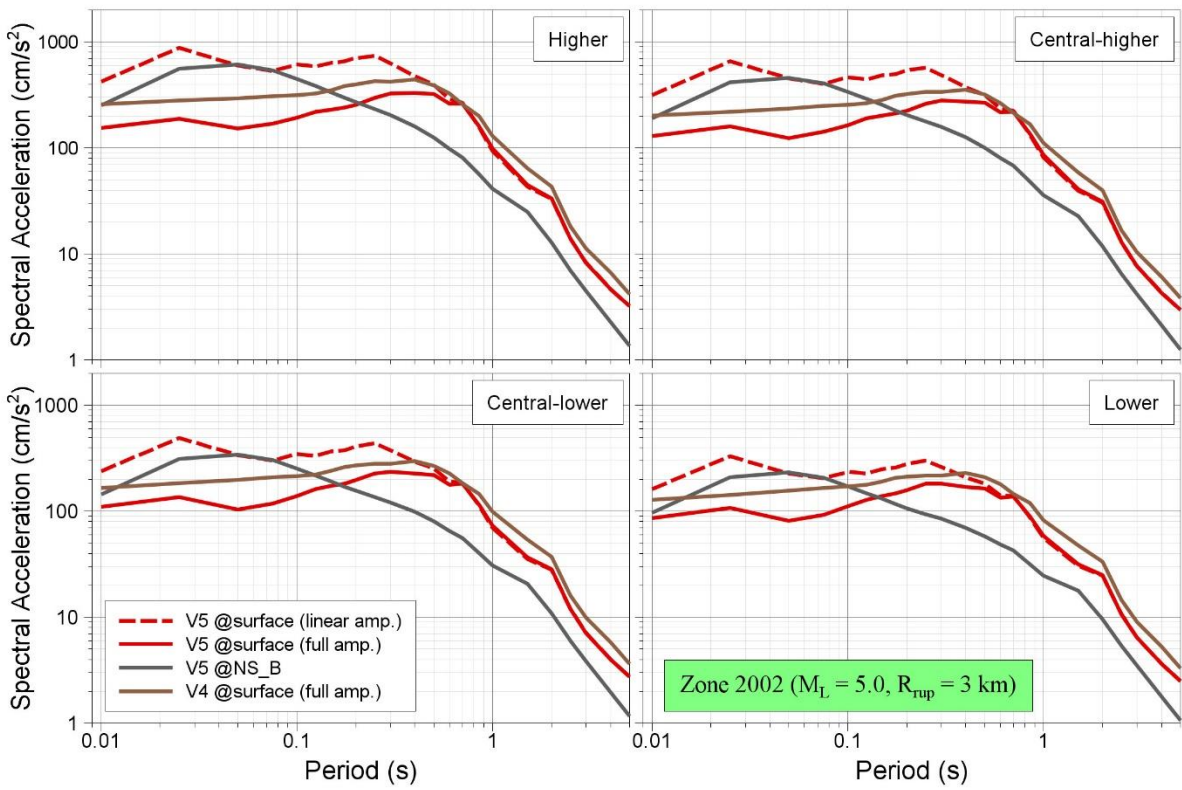
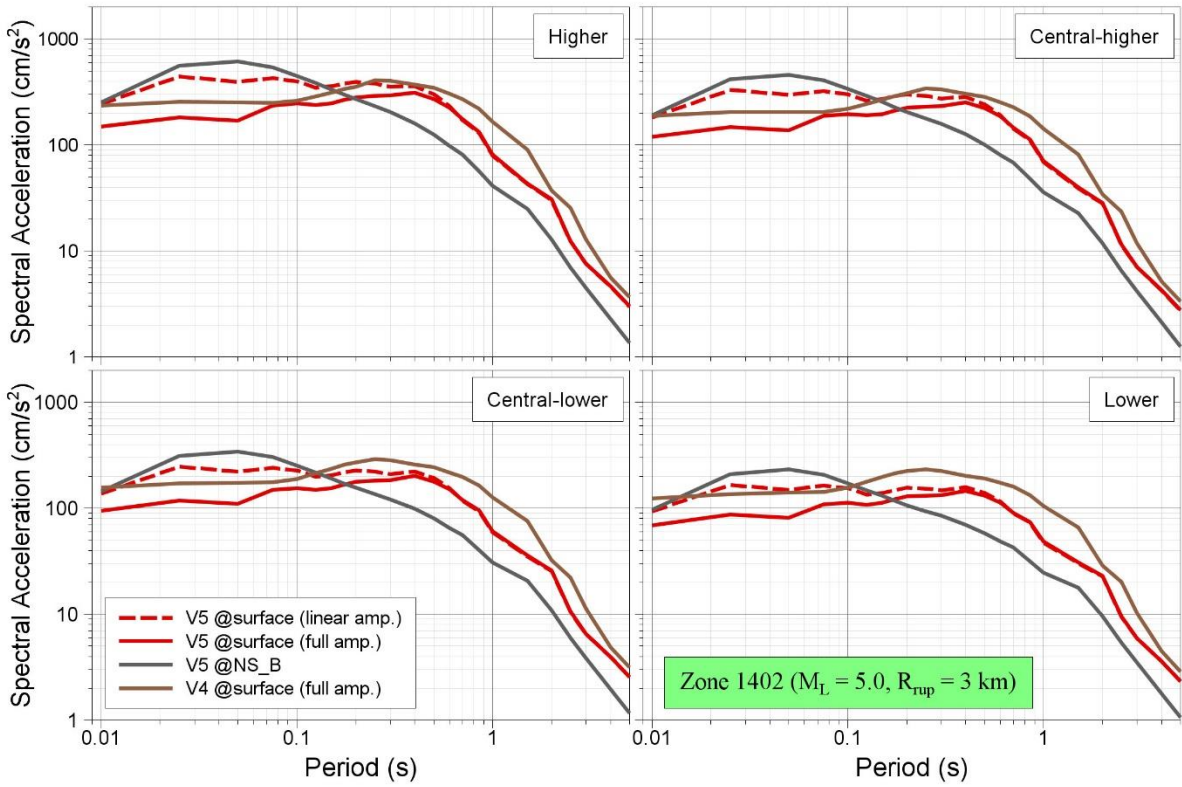


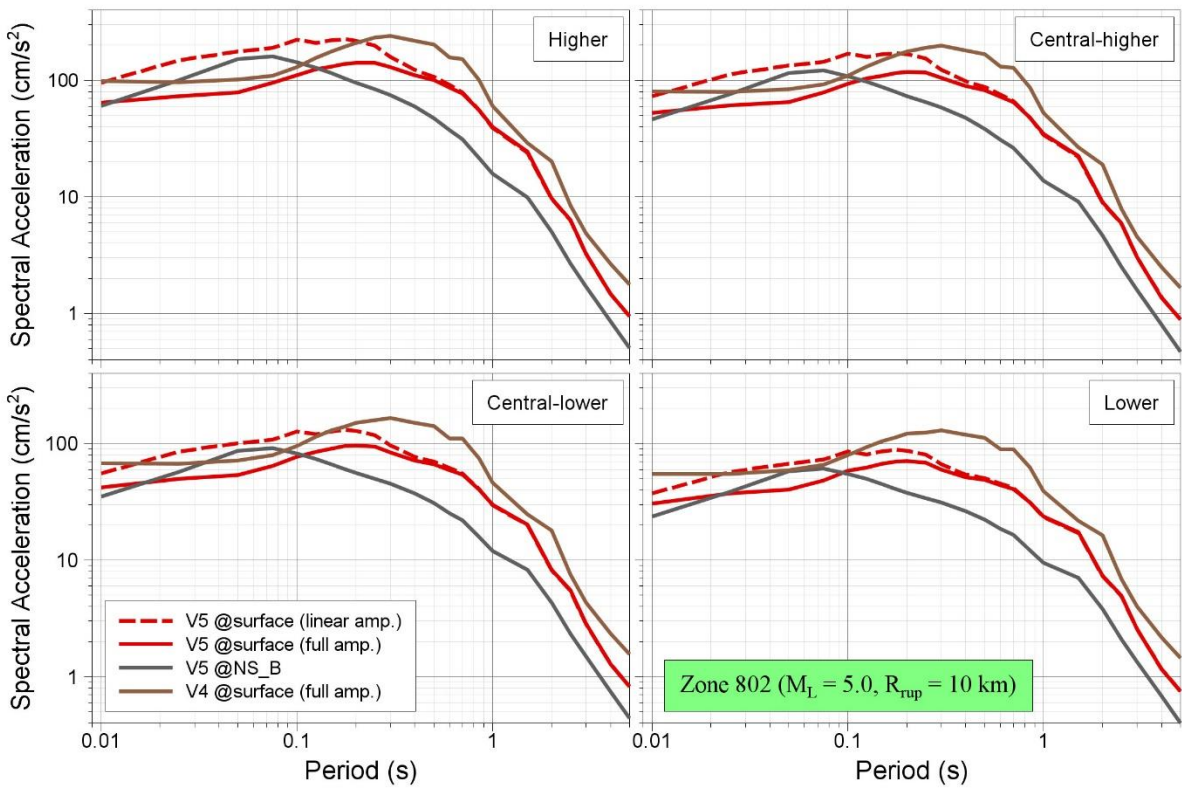
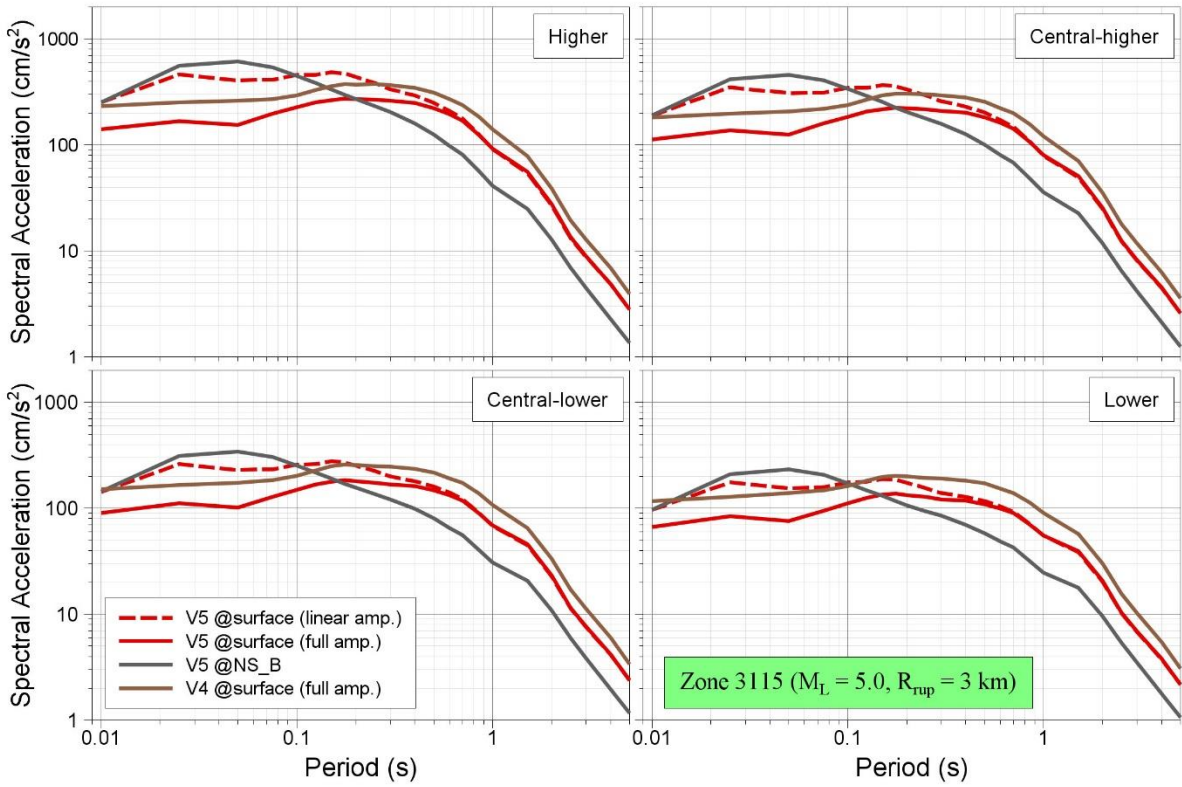


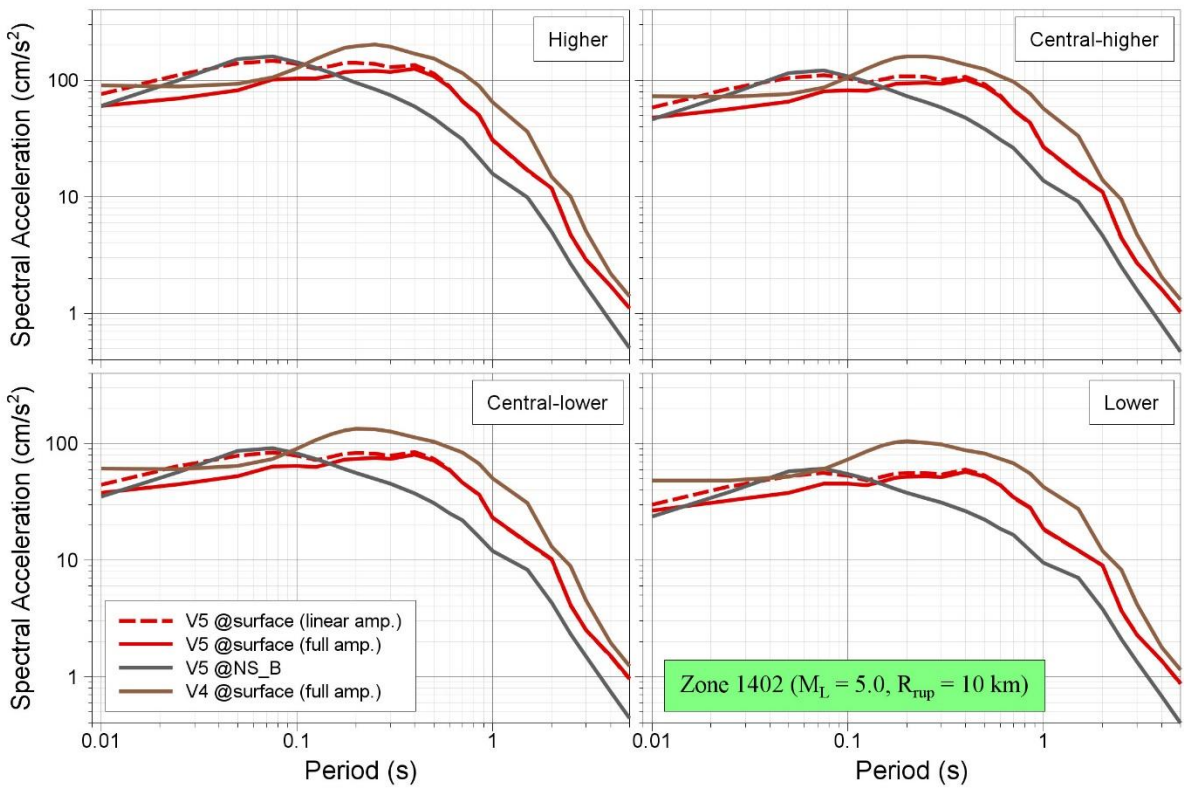
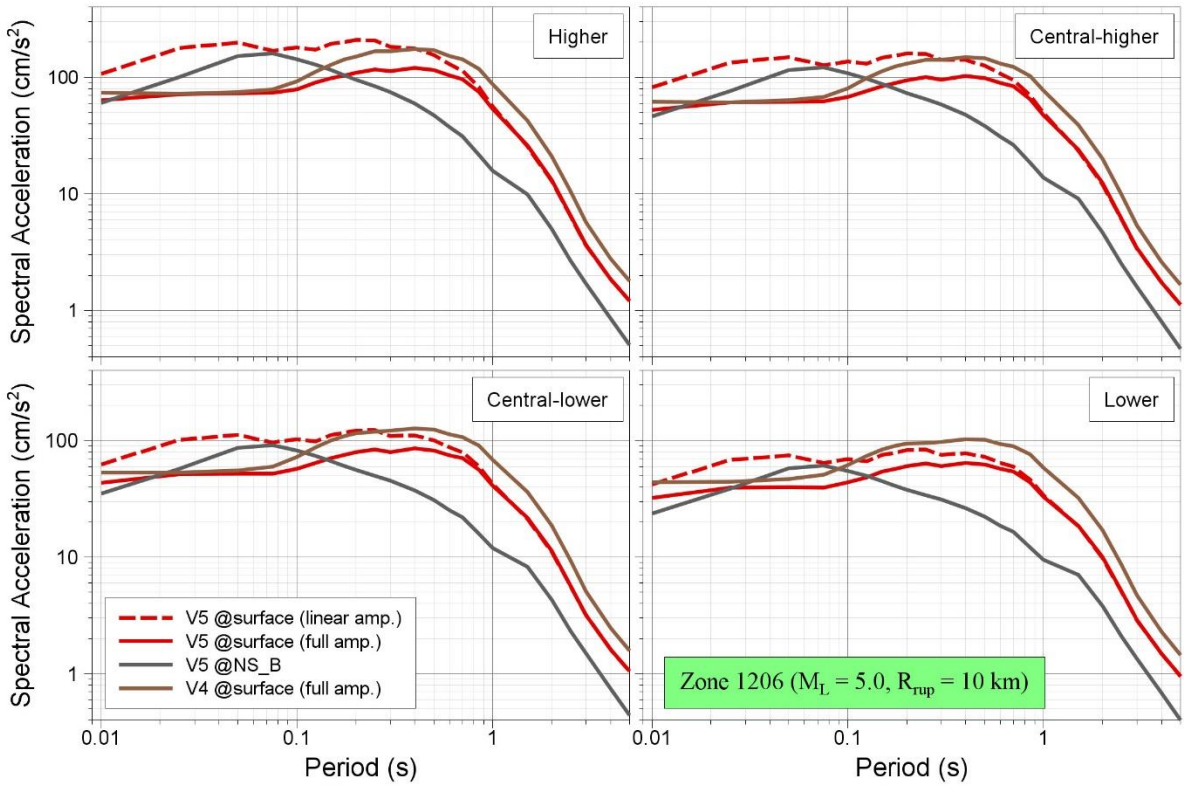


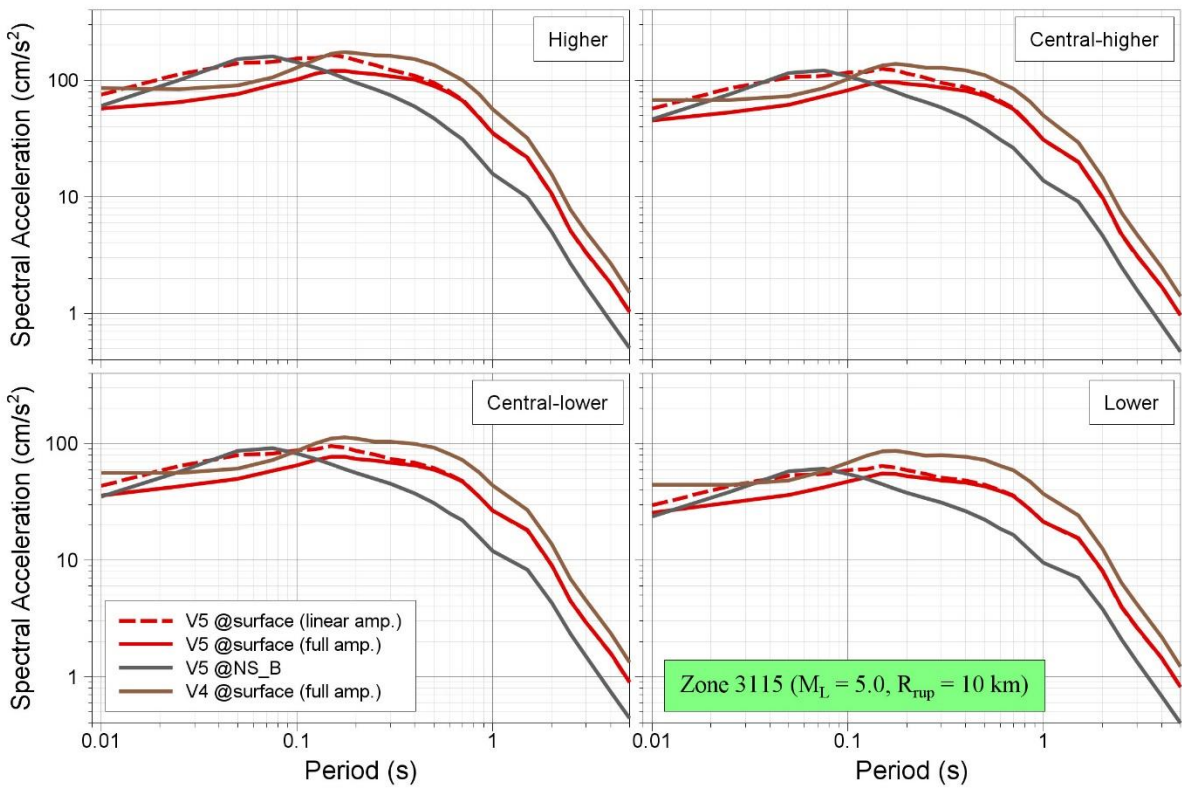
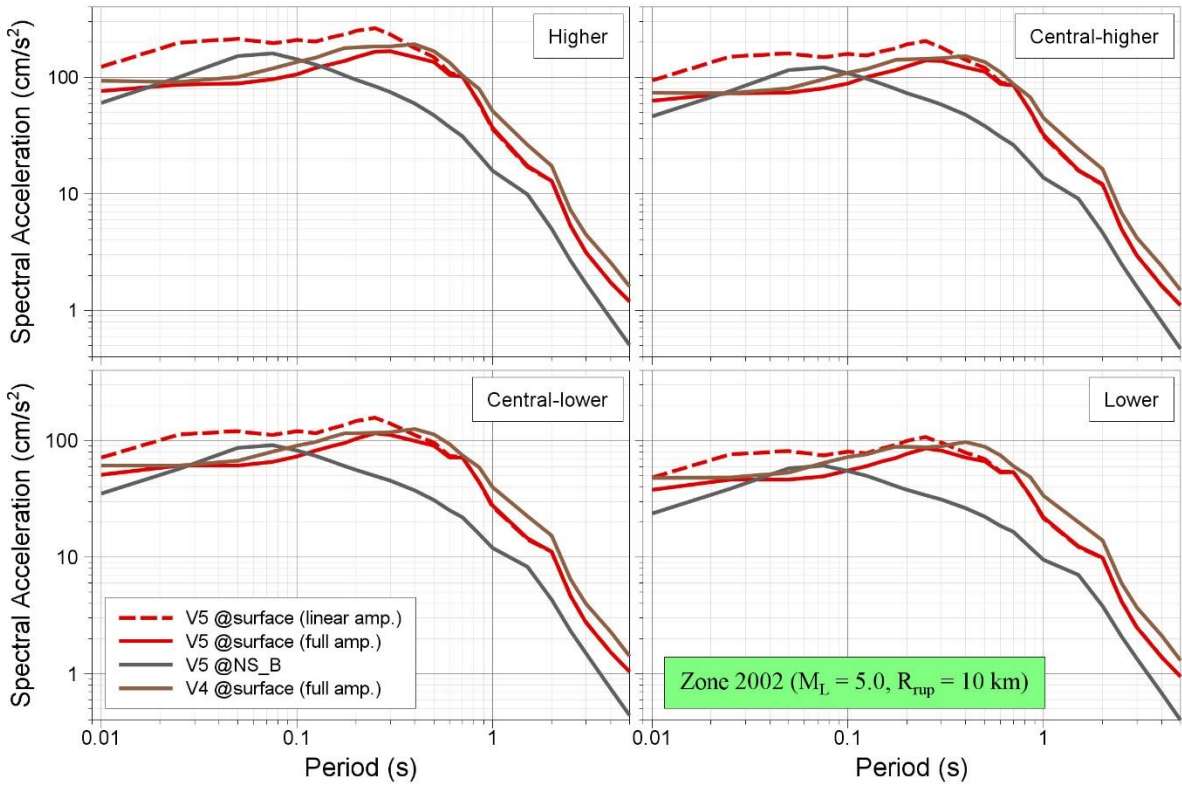


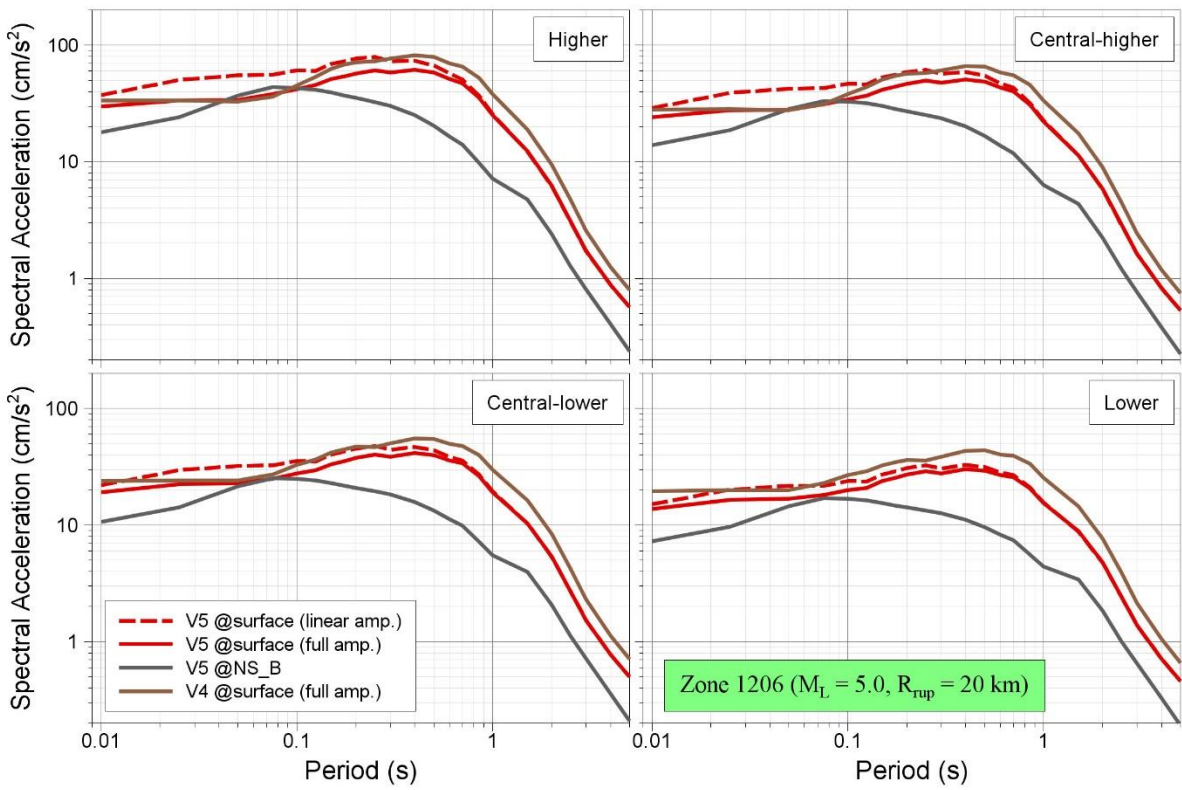
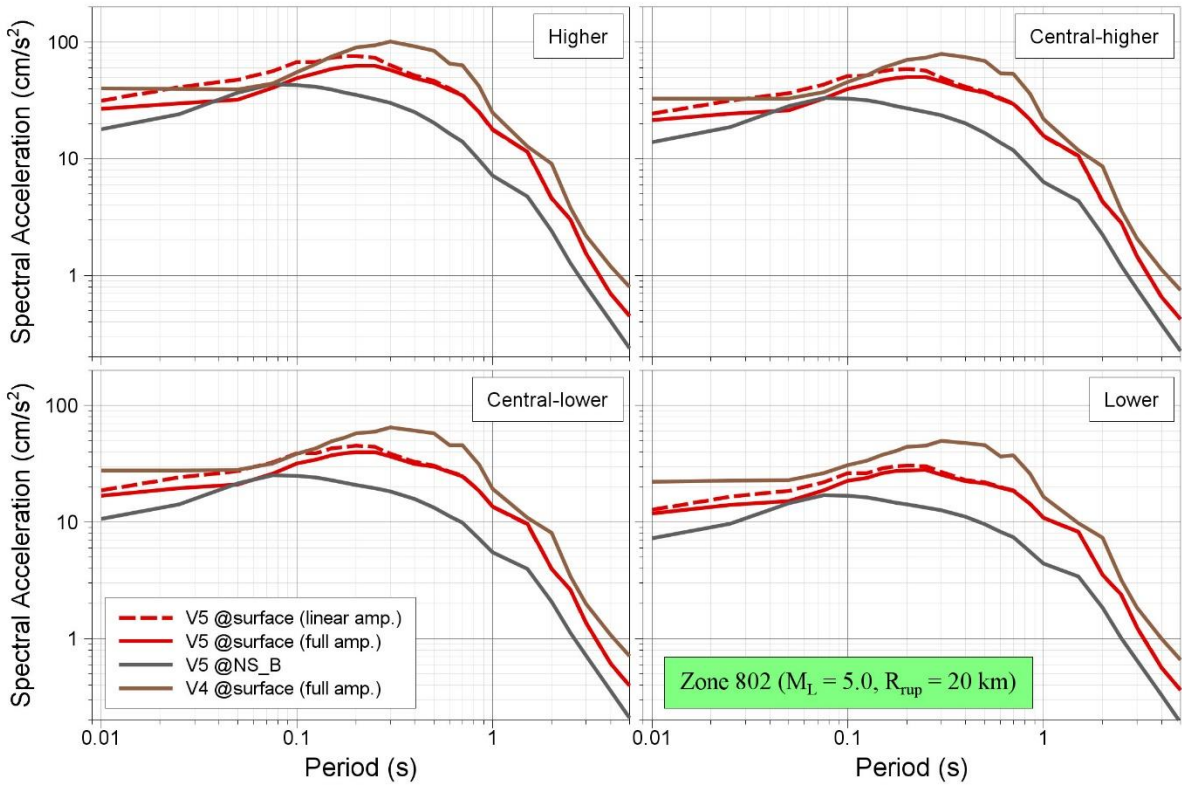


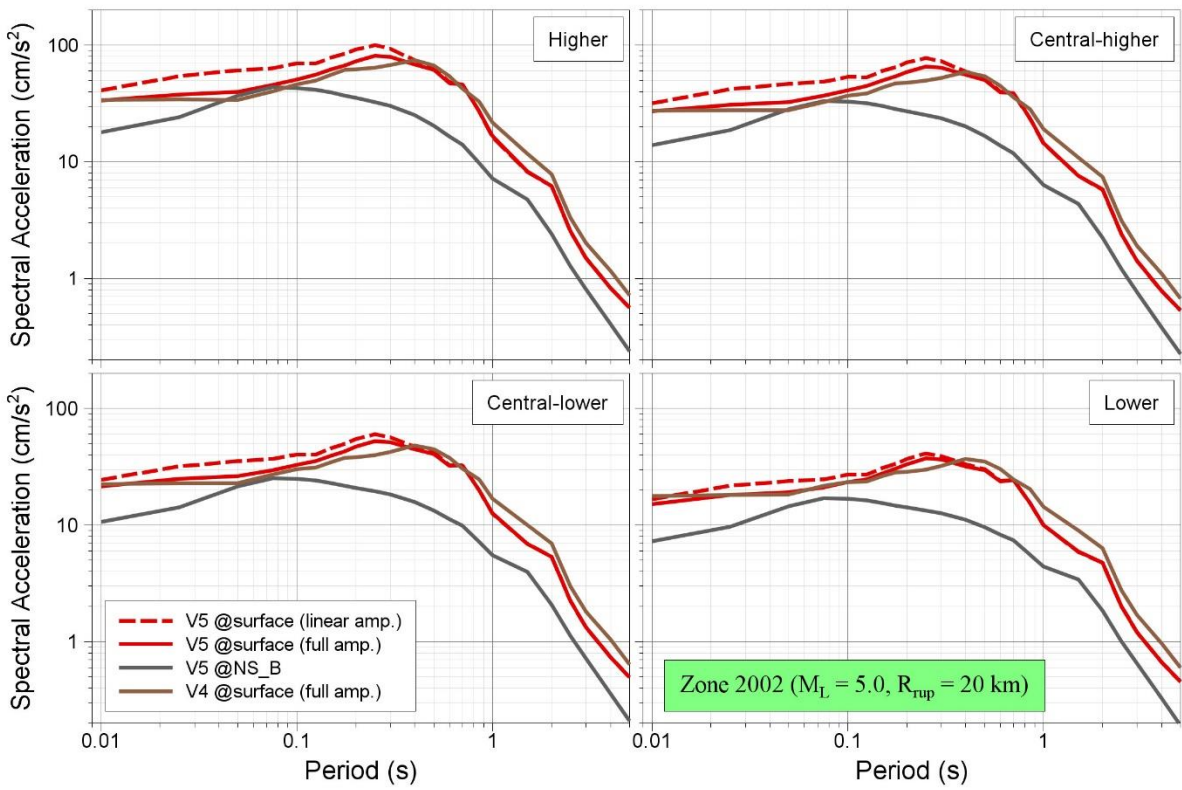
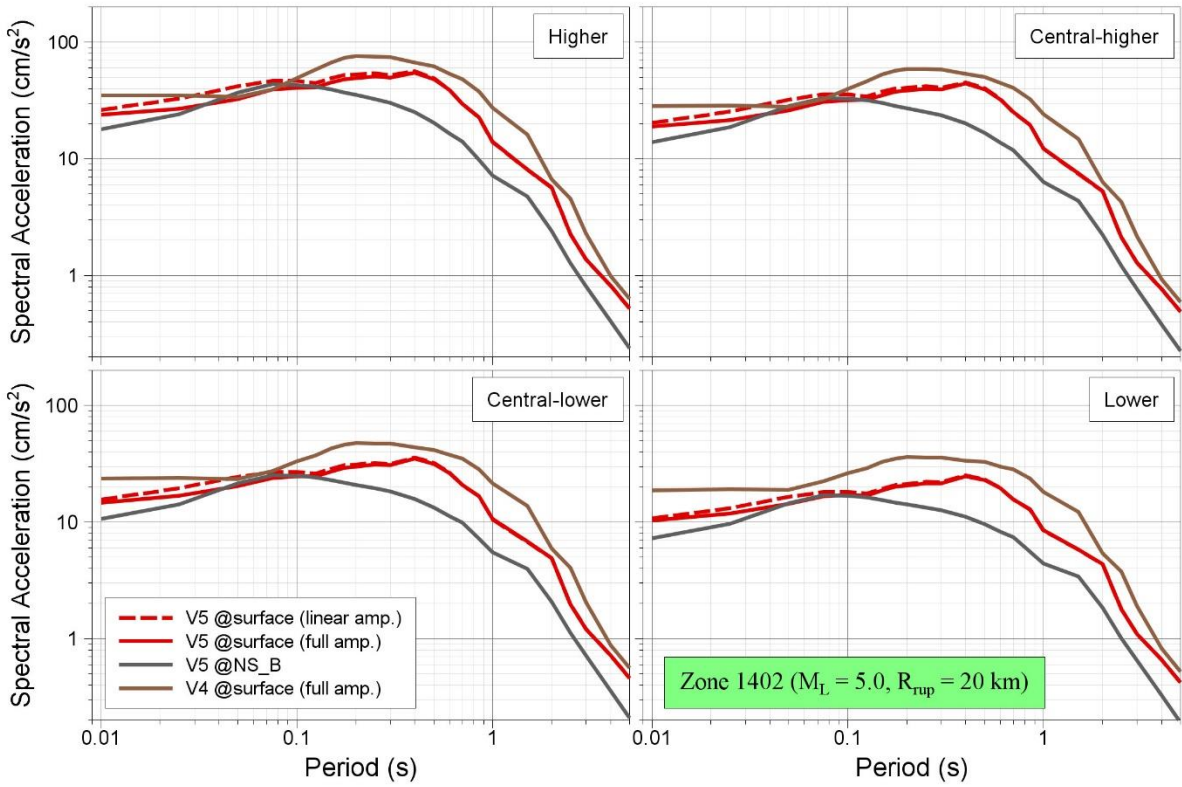


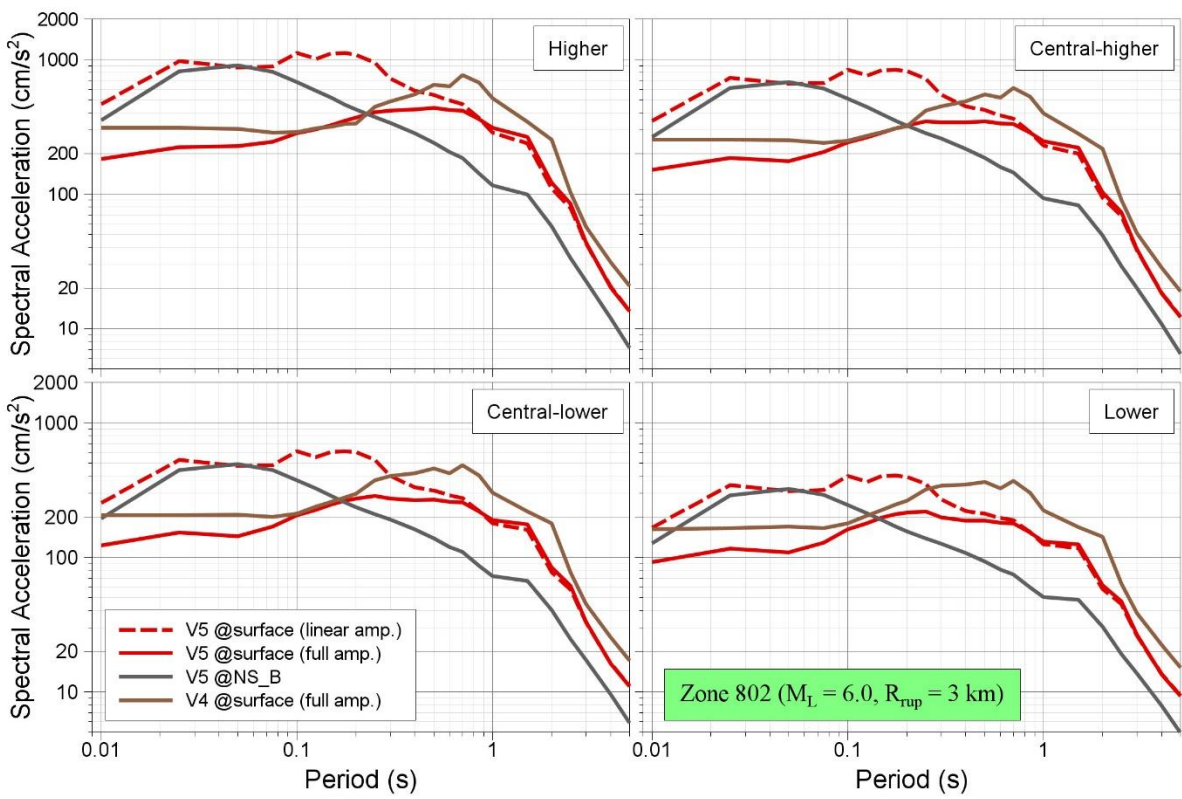
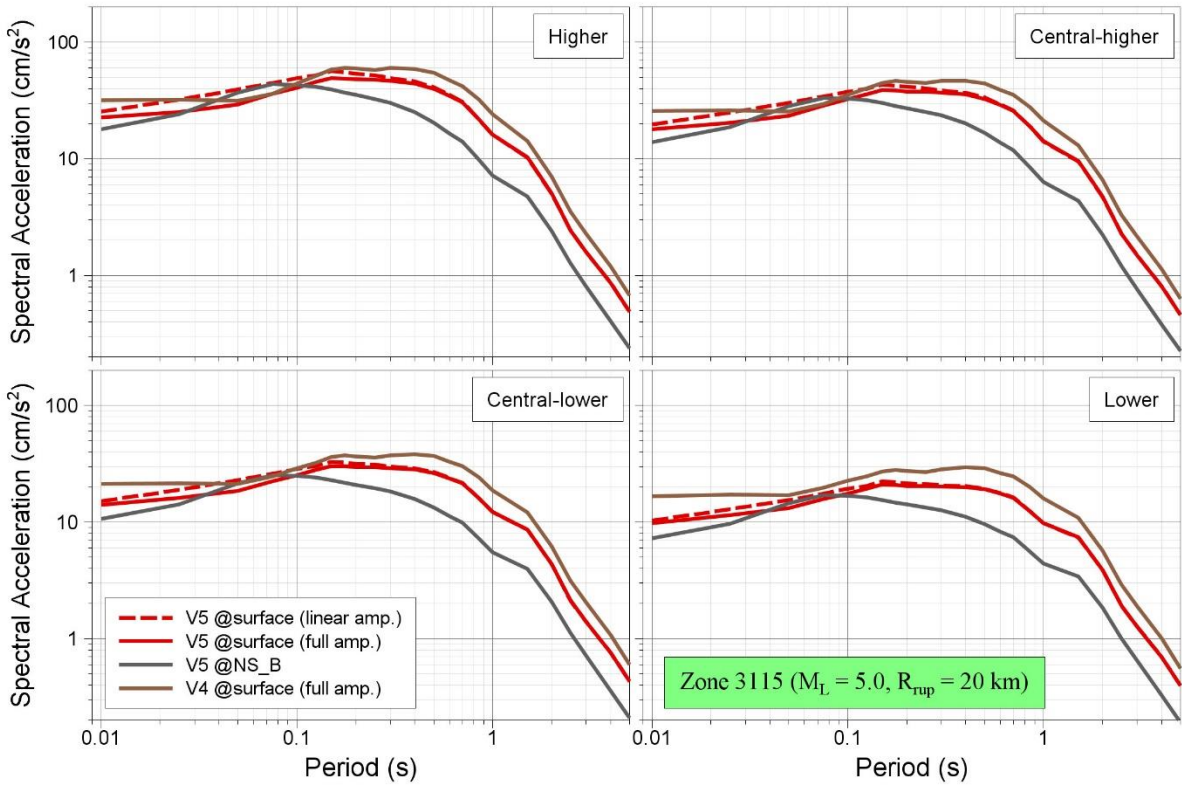


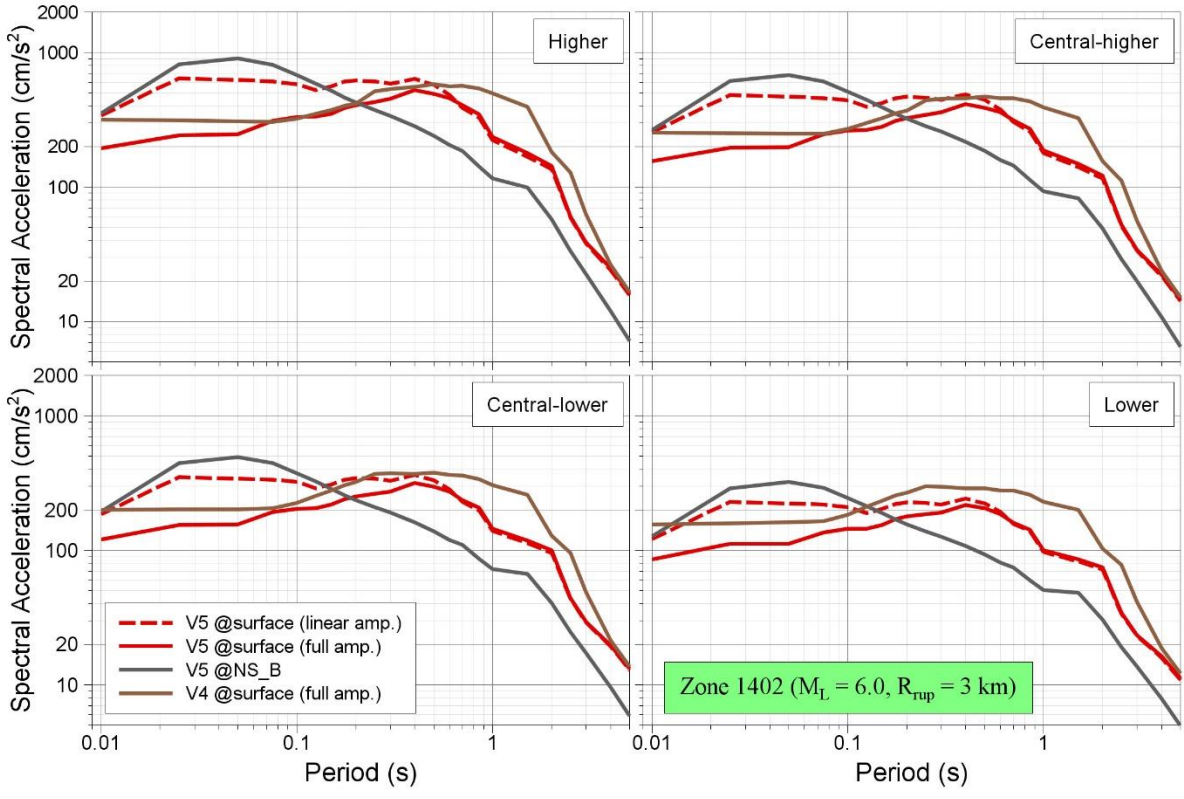
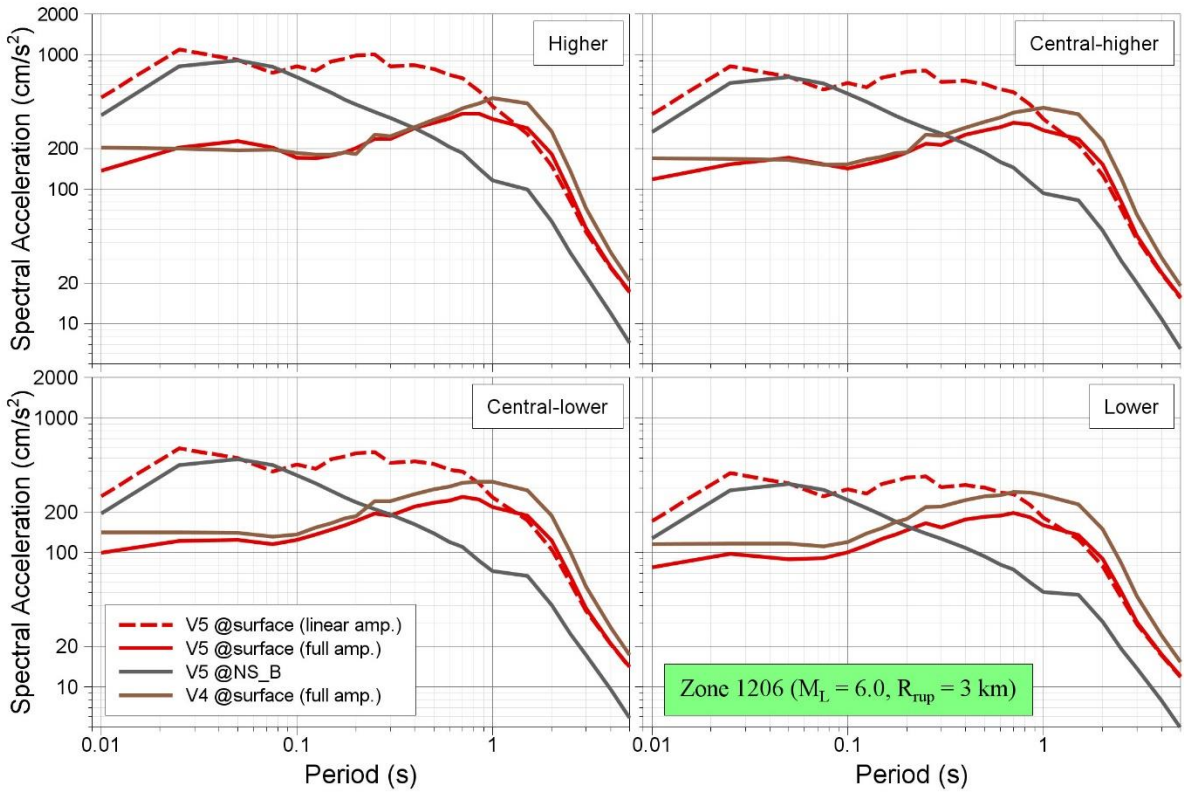


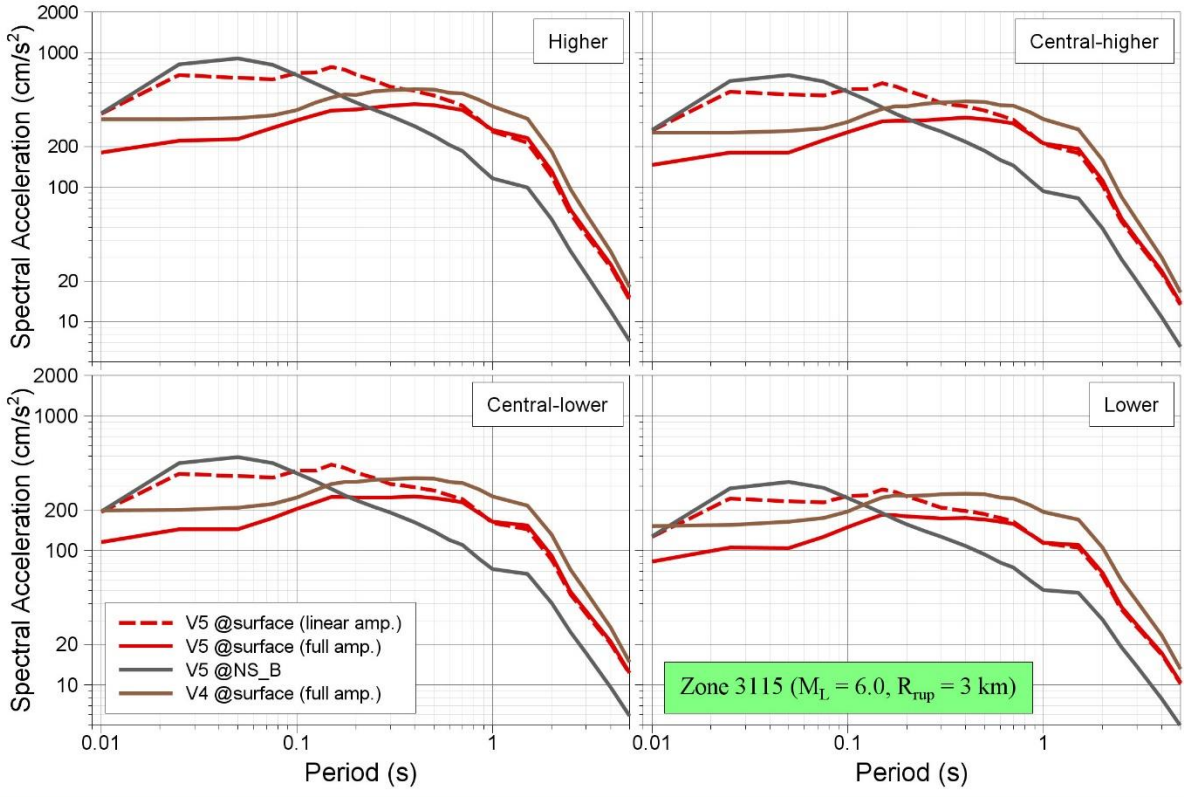
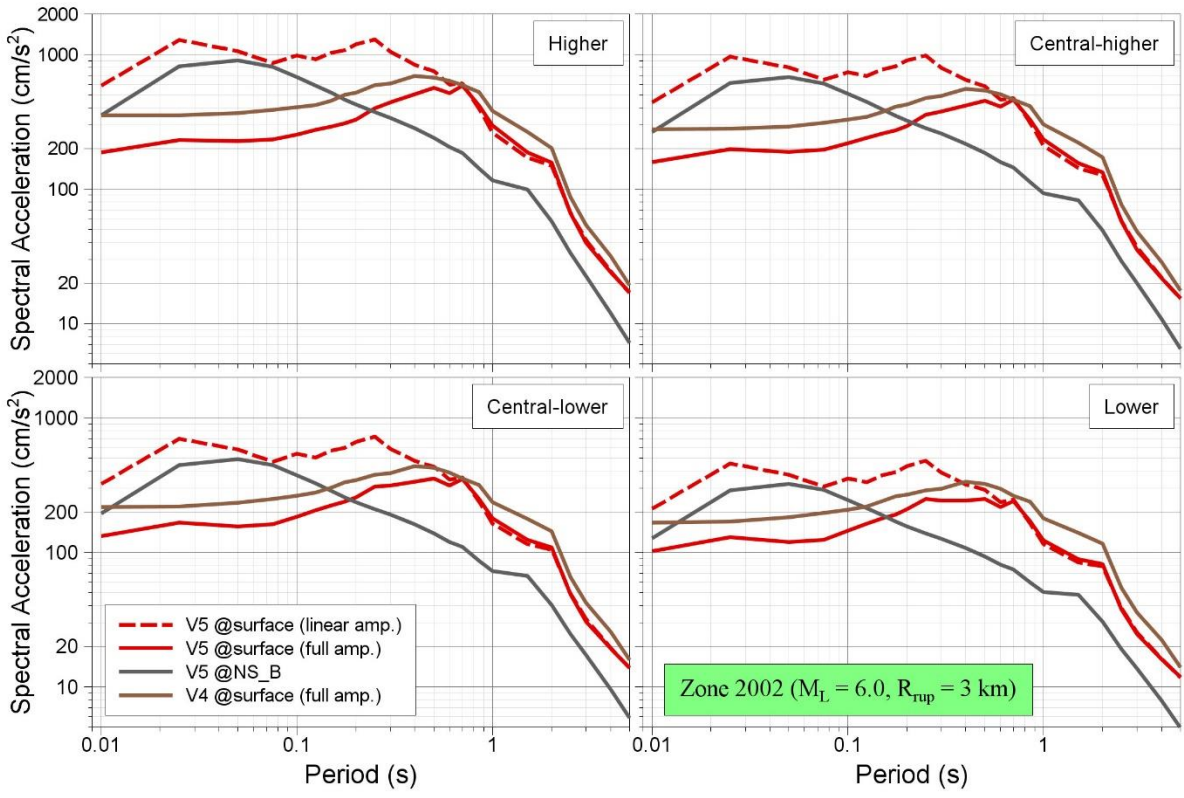


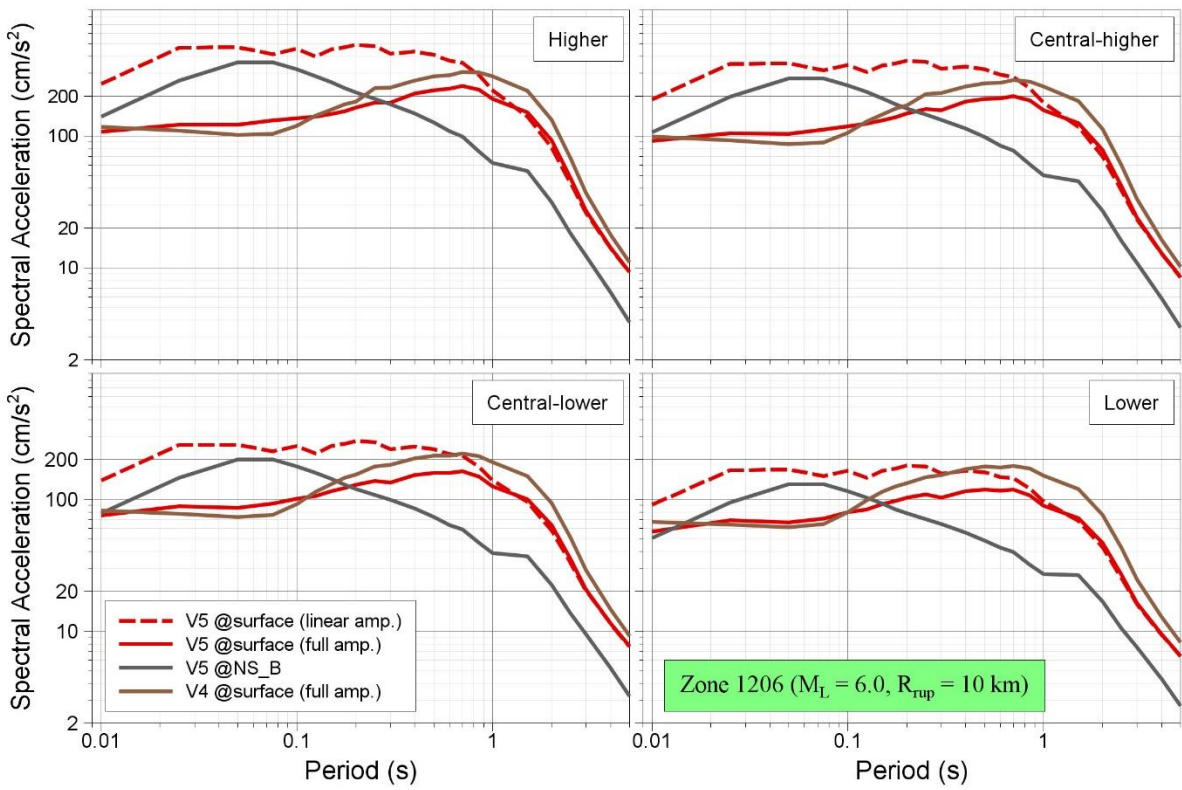
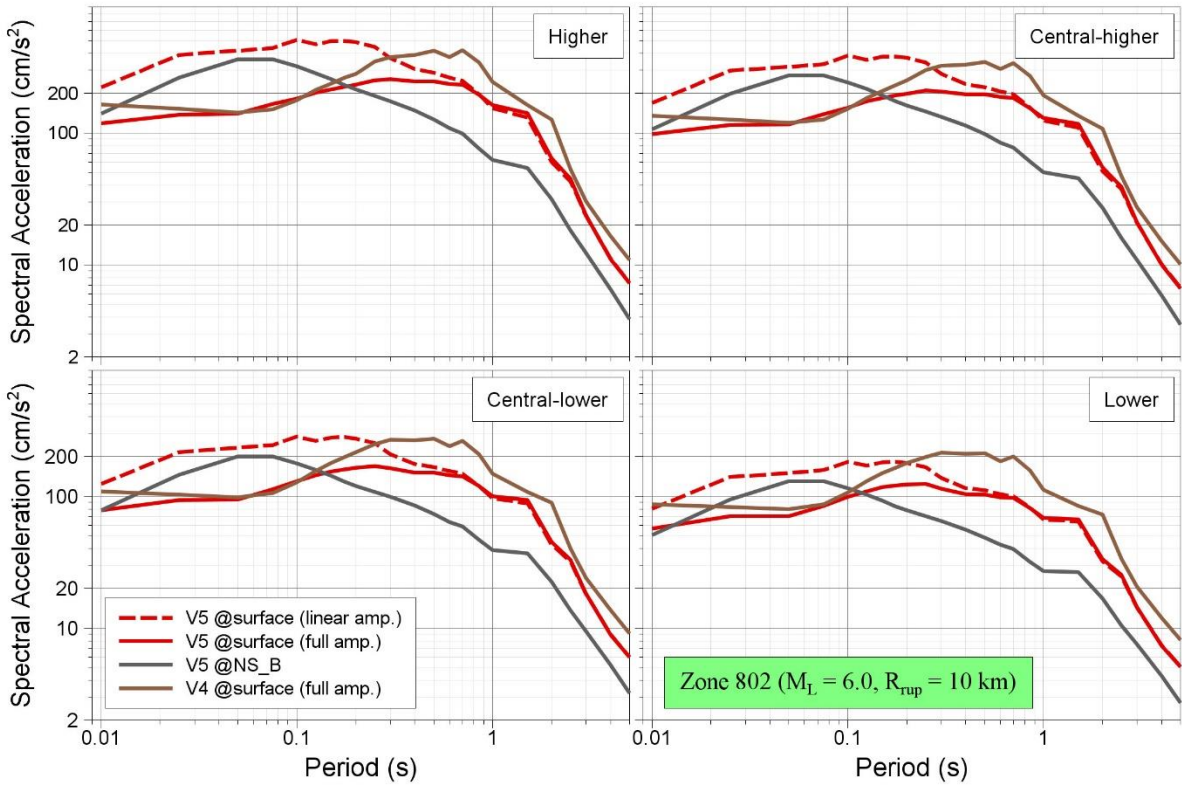


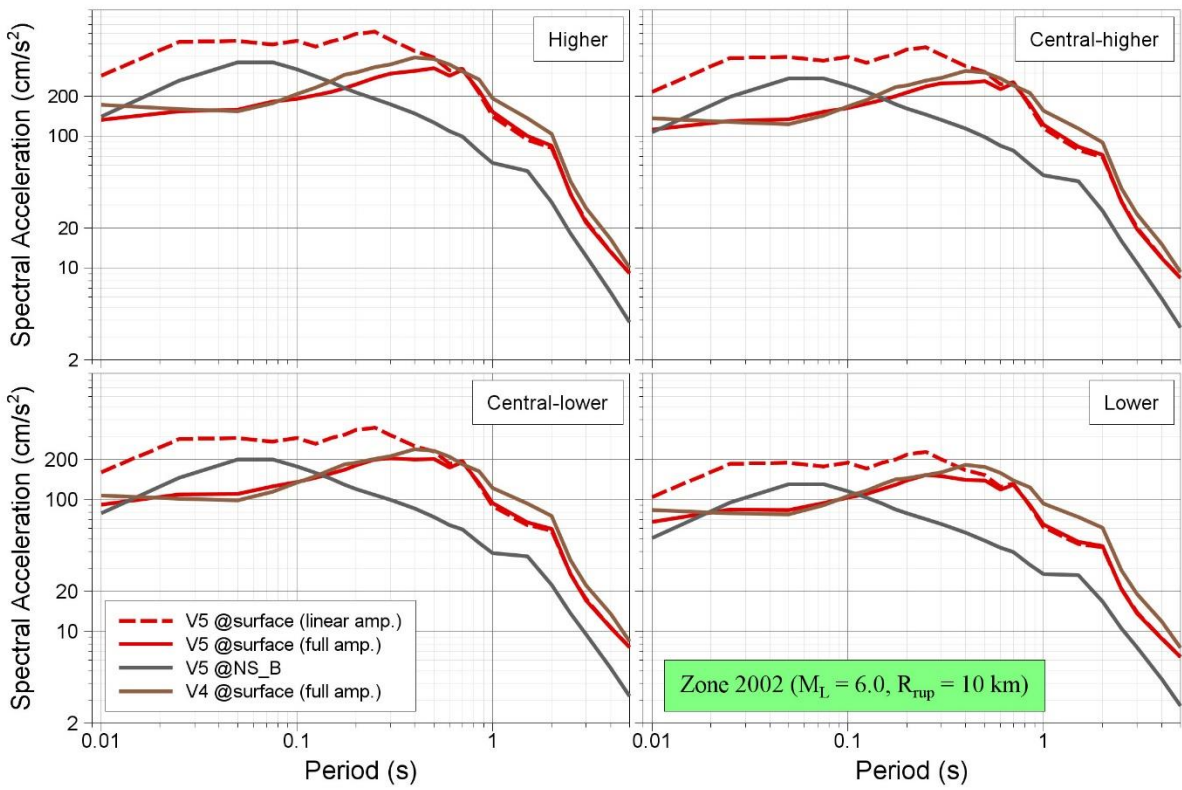
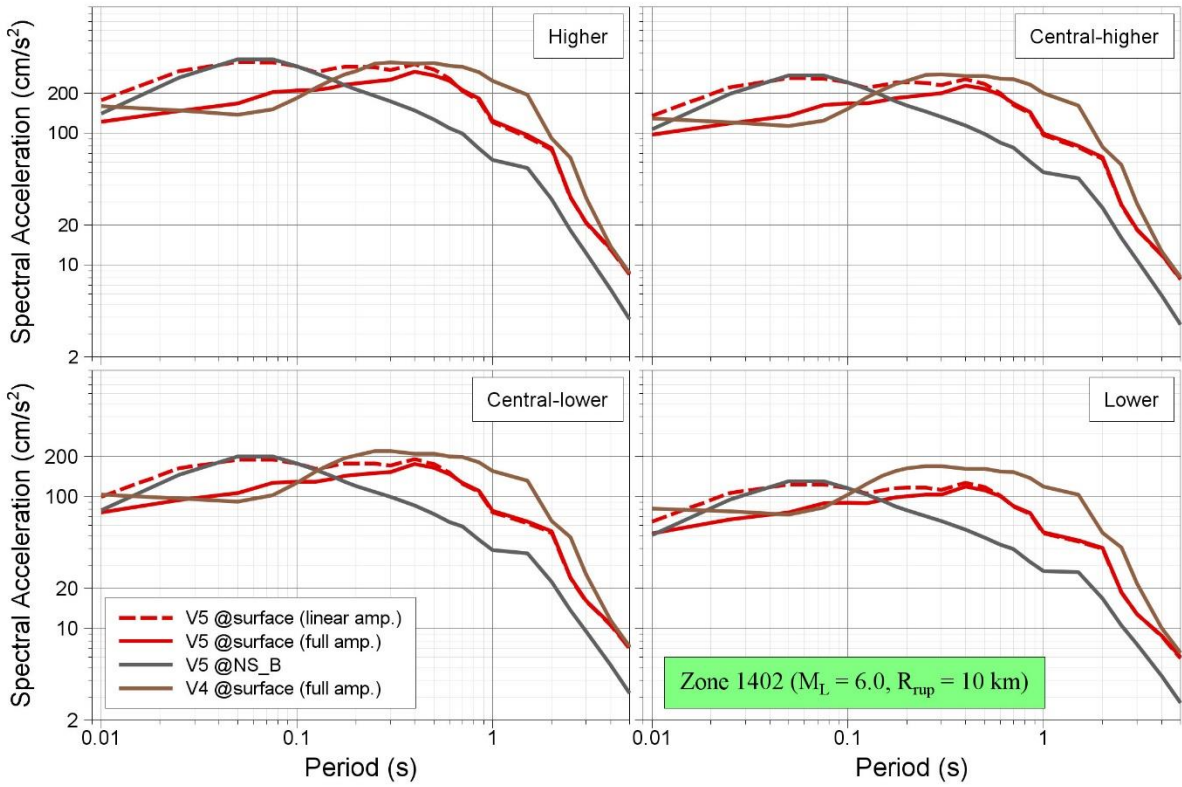


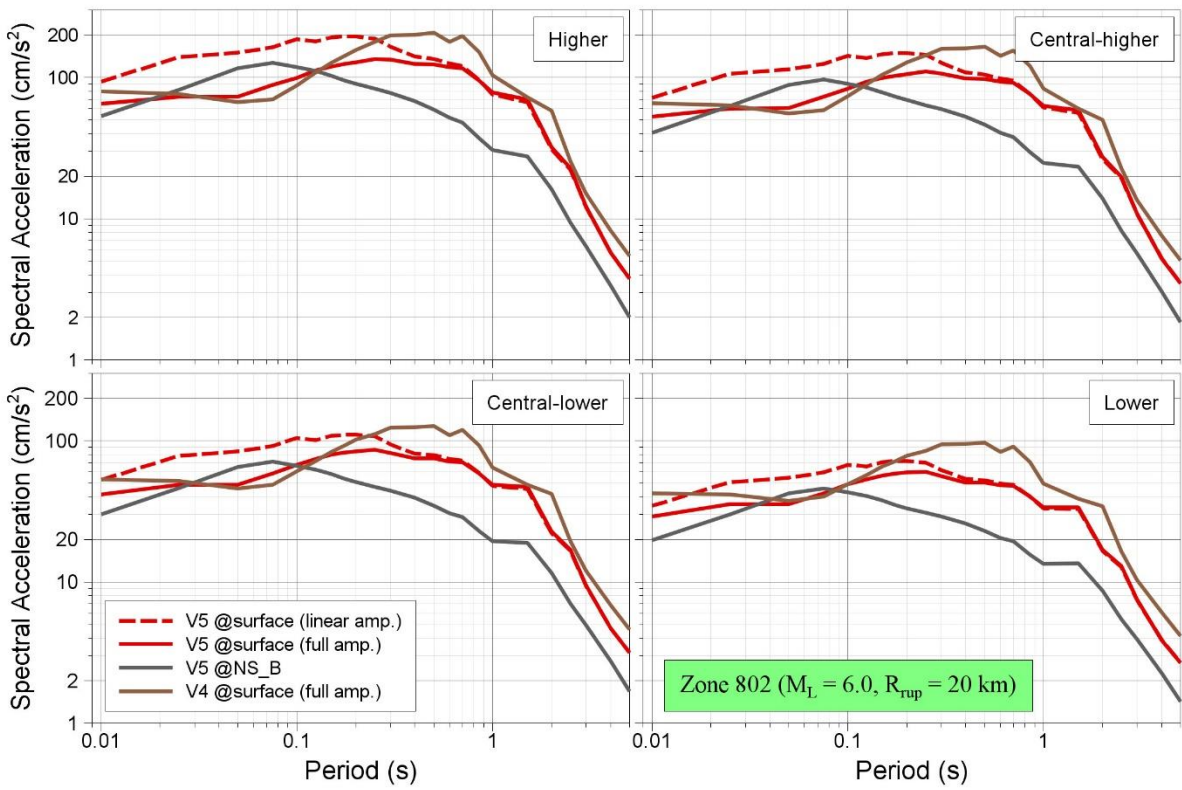
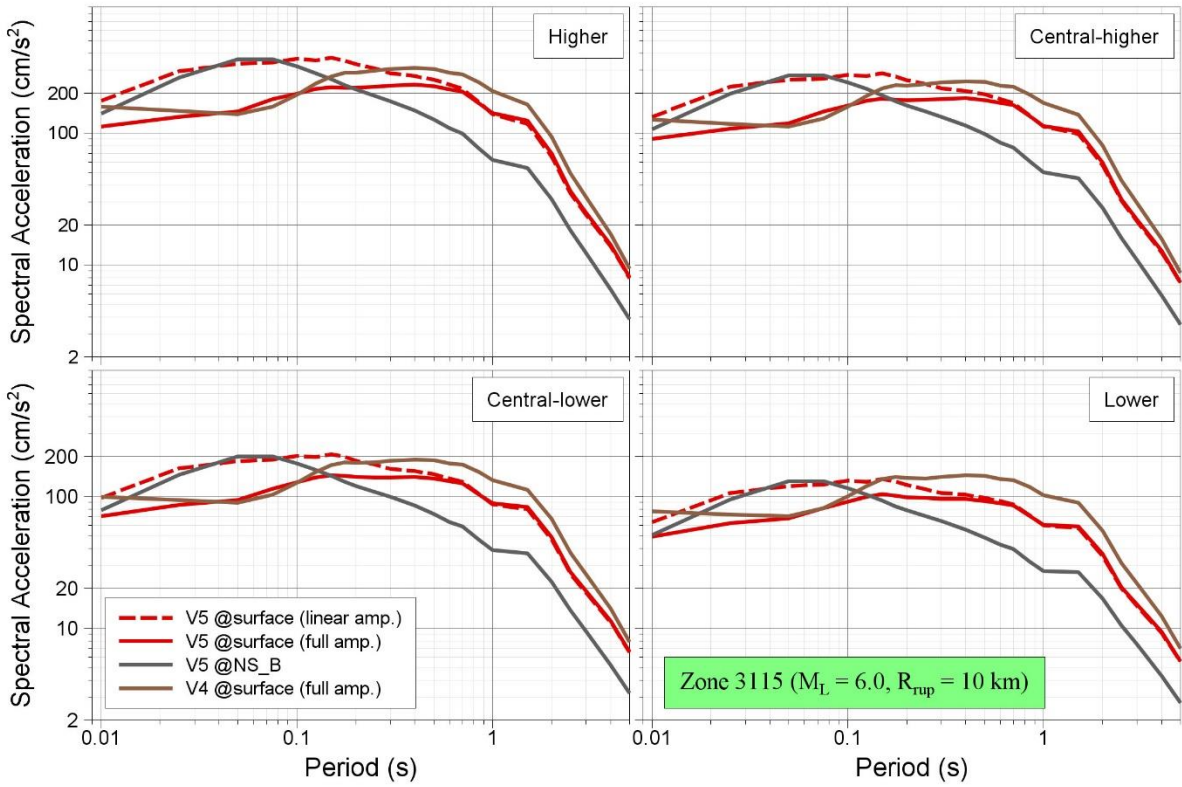


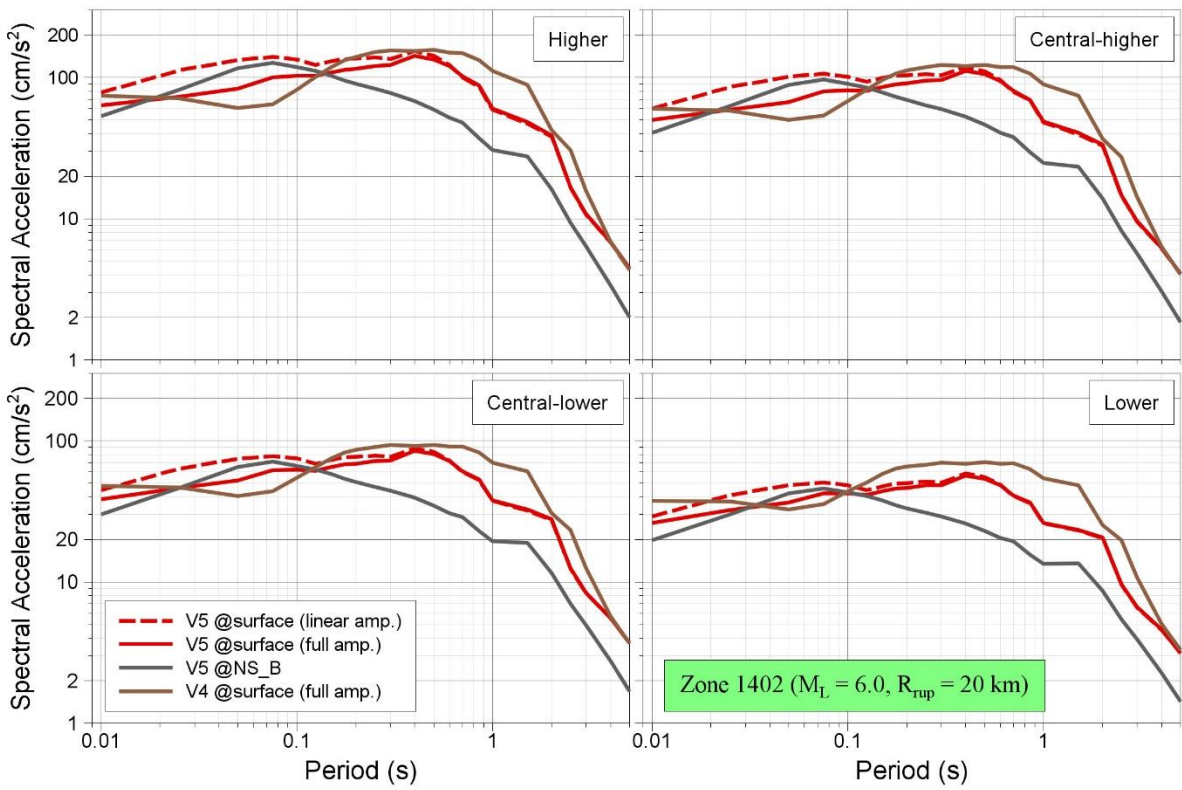
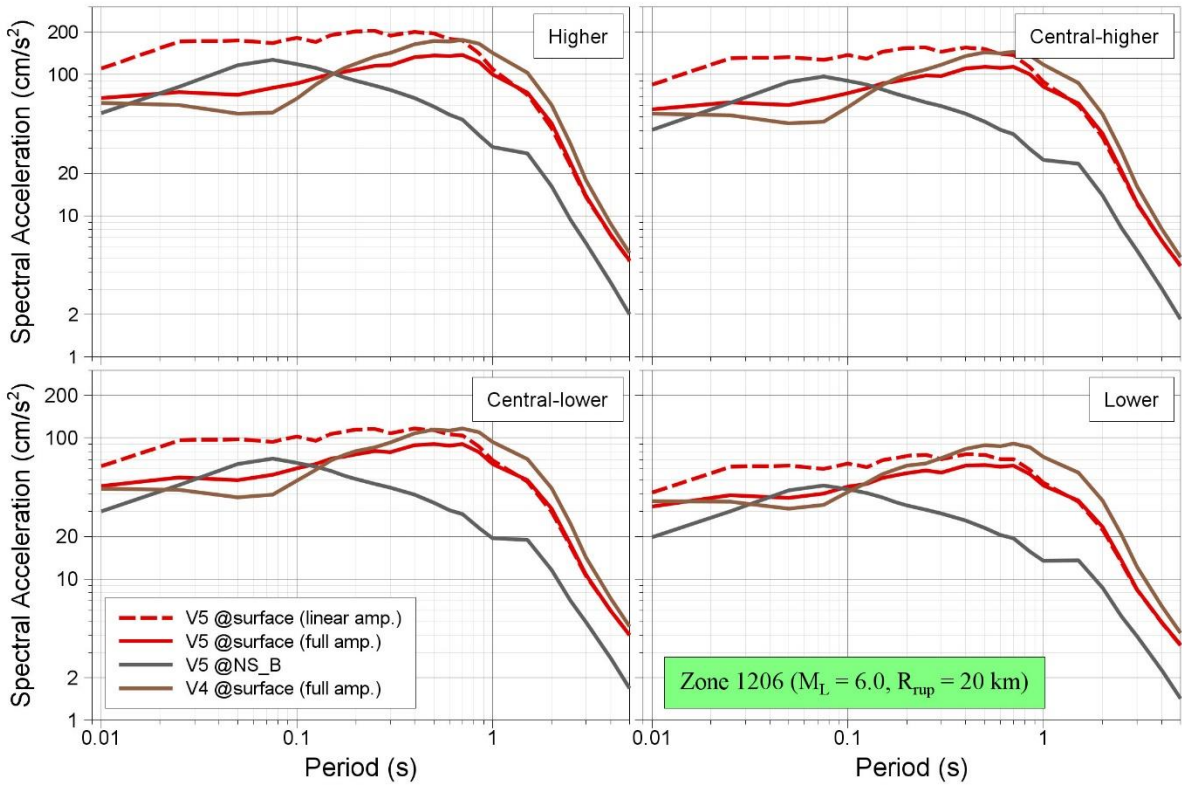


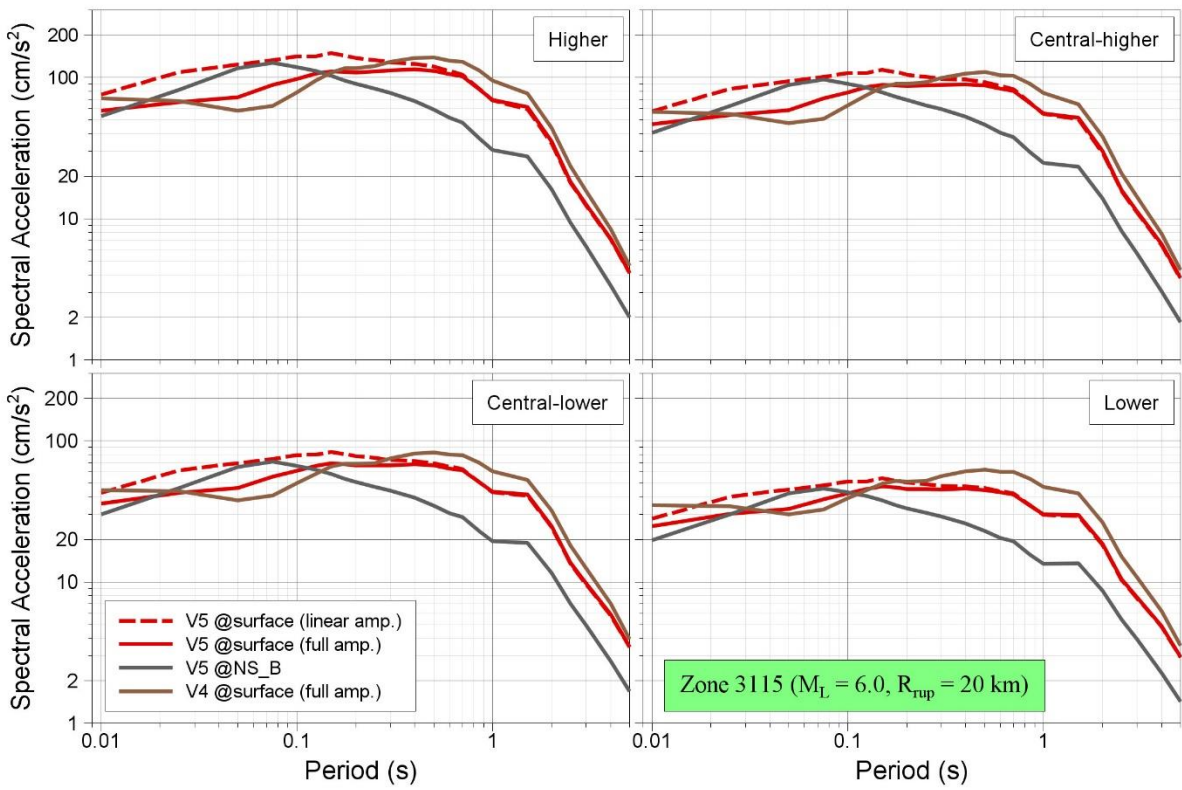
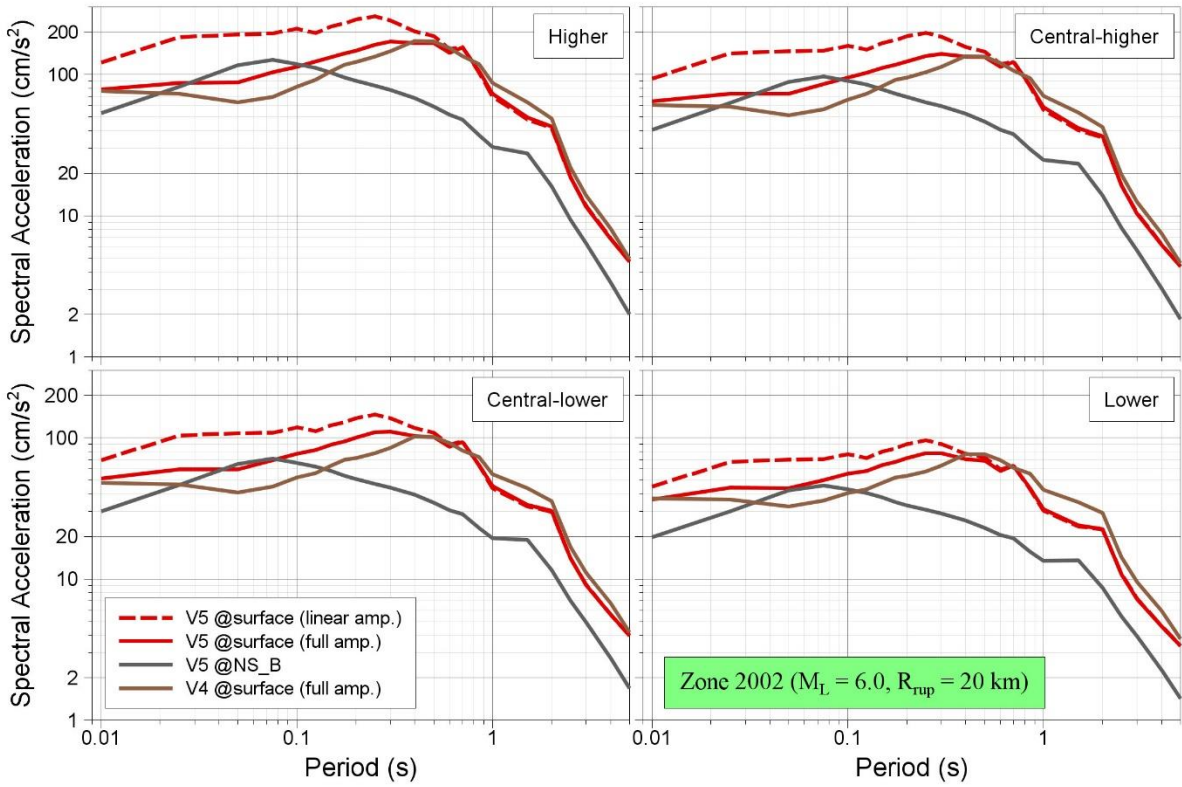












APPENDIX VIII

Preliminary Analysis of the Ground-Motion Recordings from the Zeerijp Earthquake of 8 January 2018

This appendix presents a brief overview and preliminary analysis of the ground-motion recordings obtained during this recent earthquake. This report was issued four days after the earthquake as part of NAM's response to the event.

Introduction

On Monday 8 January 2018 at 14:00:52 UTC (3 pm local time), an earthquake occurred near the village of Zeerijp in the municipality of Loppersum (Figure A8.1).

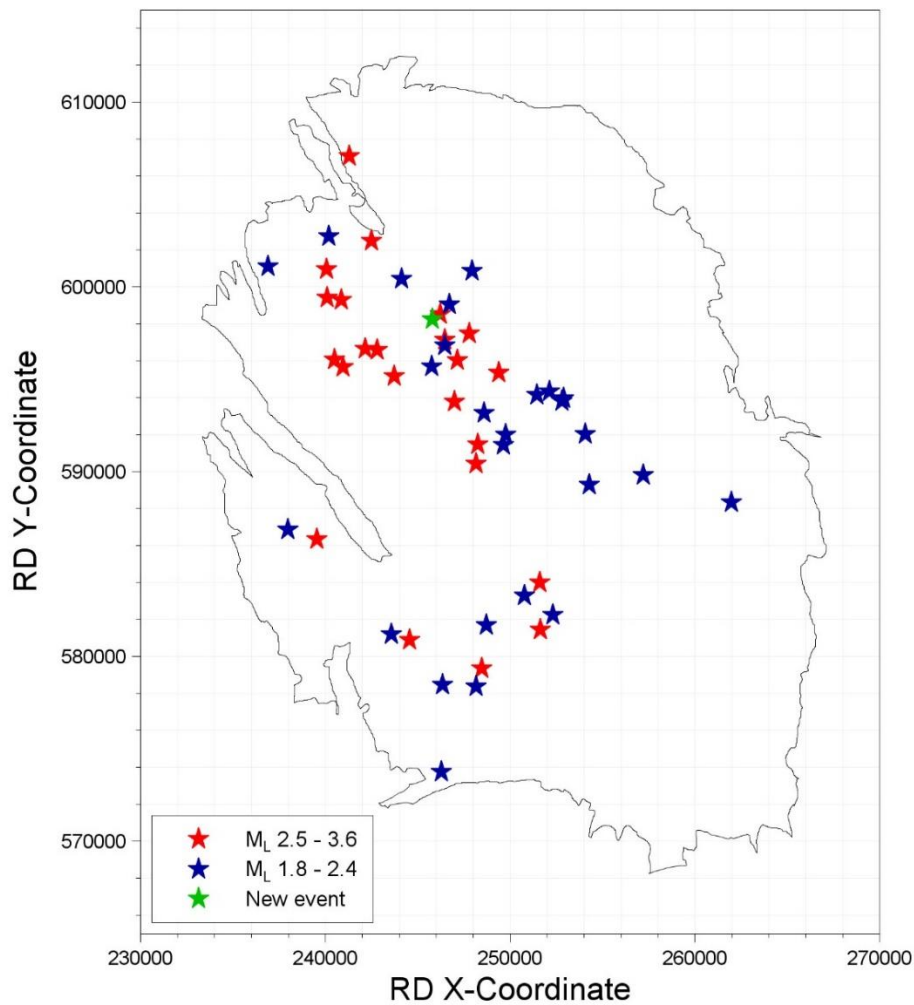


Figure A8.1. Epicentre of Zeerijp earthquake (*green star*) together with epicentres of previous earthquakes of $M_L \geq 2.5$ (*red stars*) and of $M_L 1.8-2.4$ (*blue stars*)

In common with all induced earthquakes in the Groningen field, a focal depth of 3 km was assigned by KNMI, who reported a local magnitude of M_L 3.4. This is the third largest earthquake to have occurred in the Groningen field, the largest being the M_L 3.6 Huizinge earthquake of August 2012 and the second largest the M_L 3.5 Westerendem earthquake of August 2006.

In keeping with trend during more recent earthquakes such as the M_L 3.1 Hellingwold earthquake of September 2015 and the M_L 2.6 Slochteren earthquake of May 2017 (Figure A8.2), the latest earthquake has triggered a large number of accelerograms, as a direct result of the expansion of the strong-motion recording networks in the Groningen field (Dost *et al.*, 2017). The Slochteren earthquake, despite its modest magnitude, contributed almost 70 new recordings to the Groningen ground-motion database.

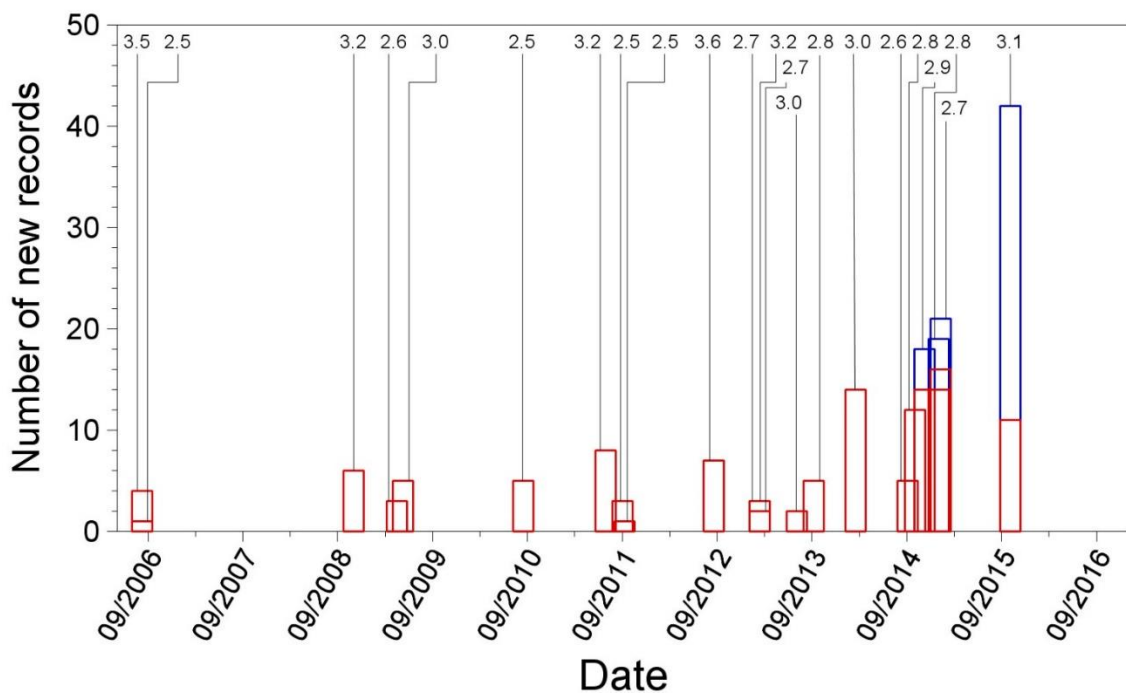


Figure A8.2. Diagram illustrating the timing of earthquakes of $M_L \geq 2.5$ in the Groningen field and the number of records yielded by the permanent KNMI network (B-stations, red) and by the expanded borehole geophone network (G-stations, blue). The 2017 Slochteren earthquake added an additional 68 records to the database. Figure from Bommer *et al.* (2017c).

The KNMI portal (<http://rdsa.knmi.nl/opencms/nl-rssm>) made accelerograms from the earthquake available within an hour of the event and 79 three-component recordings were downloaded and processed for this preliminary assessment of the motions. Figure A8.3 shows these recordings in the magnitude-distance occupied by the database used to derive the current ground-motion model used for seismic hazard and risk analyses in the Groningen field. This report presents an overview of the

recorded motions in terms of their amplitudes and durations, and discusses how the recorded amplitudes of motion compare with predictions from the ground-motion models. The discussions focus primarily on peak ground acceleration (PGA), which is assumed equal to the spectral acceleration at a period of 0.01 seconds, and peak ground velocity (PGV), which has been shown to correlate very well with the spectral acceleration at a period of 0.3 seconds for the Groningen data (Figure A8.4).

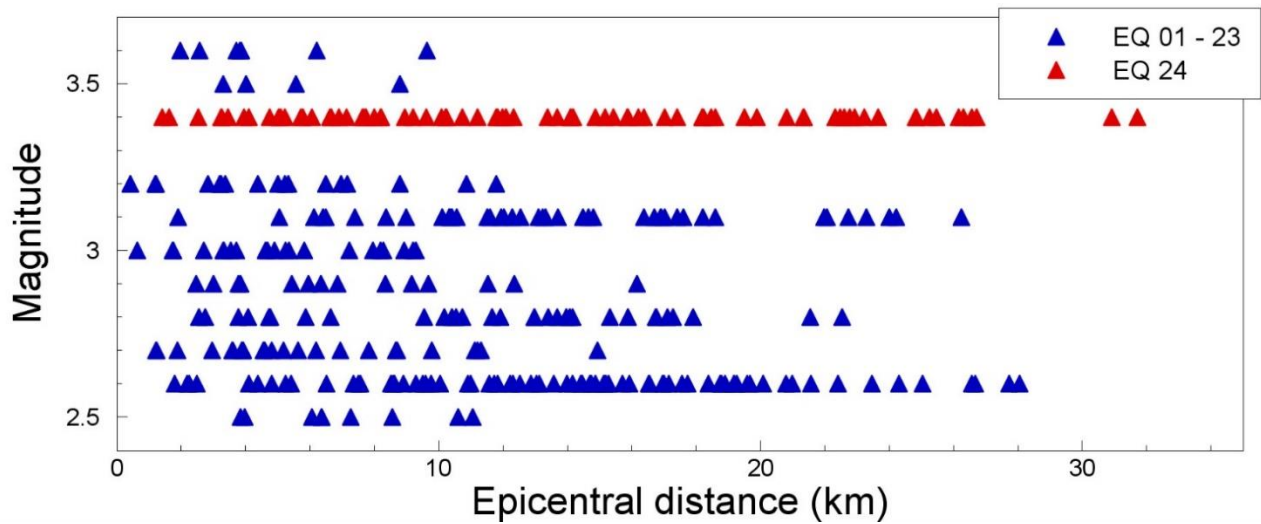


Figure A8.3. Magnitude-distance distribution of the Groningen strong-motion database including the recordings of the 2018 Zeerjip earthquake

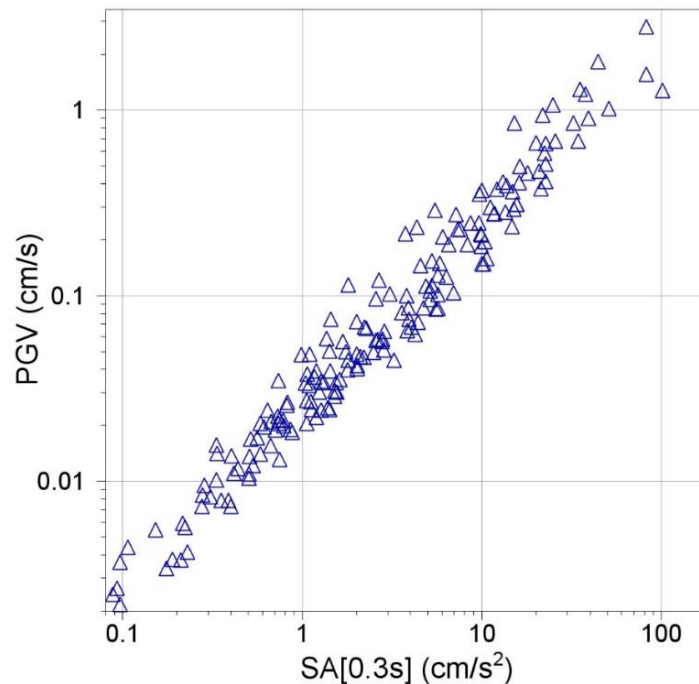


Figure A8.4. Correlation between values of PGV and spectral accelerations at 0.3 seconds for the Groningen strong-motion database (Bommer *et al.*, 2017c)

Peak Ground Accelerations and Velocities

Figure A8.5 shows the larger horizontal values of PGA and PGV from each recording obtained during the Zeerjip earthquake plotted against the distance of the recording site from the epicentre. The largest amplitudes were obtained at the BGAR station located 2.5 km from the epicentre: the PGAs recorded at this station are 108.4 cm/s^2 on the EW component and 71.0 cm/s^2 on the NS component. The largest PGV values are at the same station are 3.19 cm/s (EW) and 1.98 cm/s (NS). The EW component of the BGAR station is the only record to exceed to previous maximum PGA value recorded during the Huizinge earthquake.

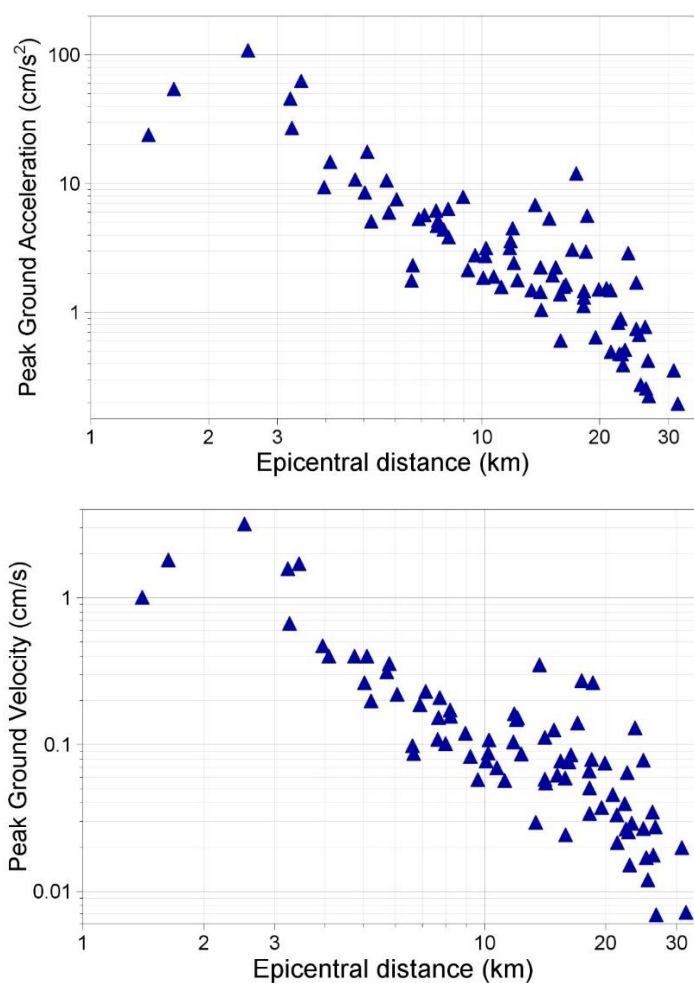


Figure A8.5. Larger as-recorded horizontal components of PGA (*upper*) and PGV (*lower*) recorded during the Zeerjip earthquake plotted against epicentral distance

A striking feature of Figure A8.5 are the lower amplitudes recorded closer to the epicentre at the BZN1 and G140 stations. The differences are unlikely to be explained by differences in site profiles since all three stations have almost identical values of the time-averaged shear-wave velocity over the upper 30 metres (Kruiver

et al., 2017; Noorlandt *et al.*, 2018), which are all equal to 192 or 193 m/s. Figure A8.6 shows the horizontal components of PGA and PGV obtained within 5 km of the epicentre, from which it can be appreciated that the very strong polarisation often observed in Groningen recordings (*e.g.*, Bommer *et al.*, 2017a) is not particularly marked for this event.

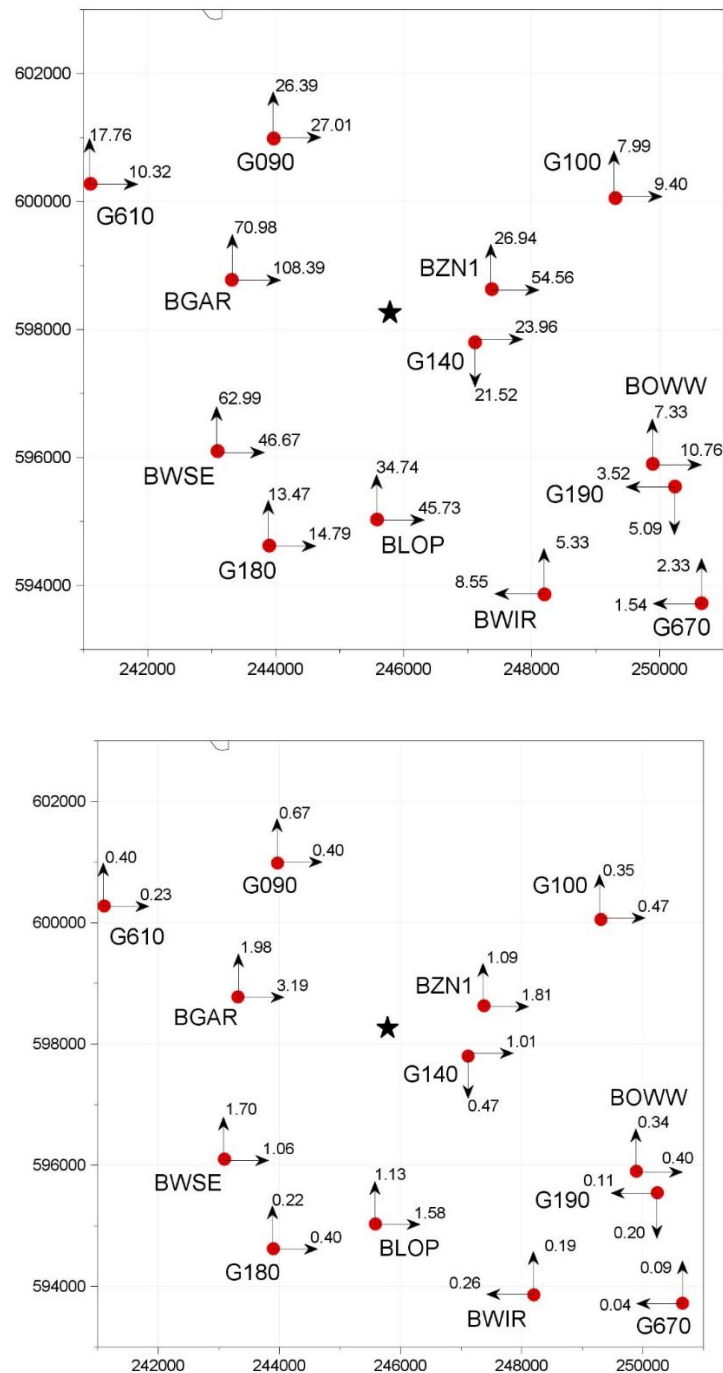


Figure A8.6. Horizontal components of PGA (*upper*) and PGV (*lower*) recorded during the Zeerijp earthquake at epicentral distances of less than 5 km; units are cm/s² and cm/s, respectively.

As already shown in Figure A8.3, the amplitudes decay rapidly with distance although the effect of simultaneous arrivals of direct and critically refracted/reflected waves leads to an increase in amplitudes at some locations between 12 and 20 km from the epicentre. However, these effects do not lead to significant absolute amplitudes at those distances and it is clear from Figures A8.7 and A8.8 that outside of the epicentral area the motions are generally of very low amplitude: $< 0.02g$ for PGA and < 0.3 cm/s for PGV.

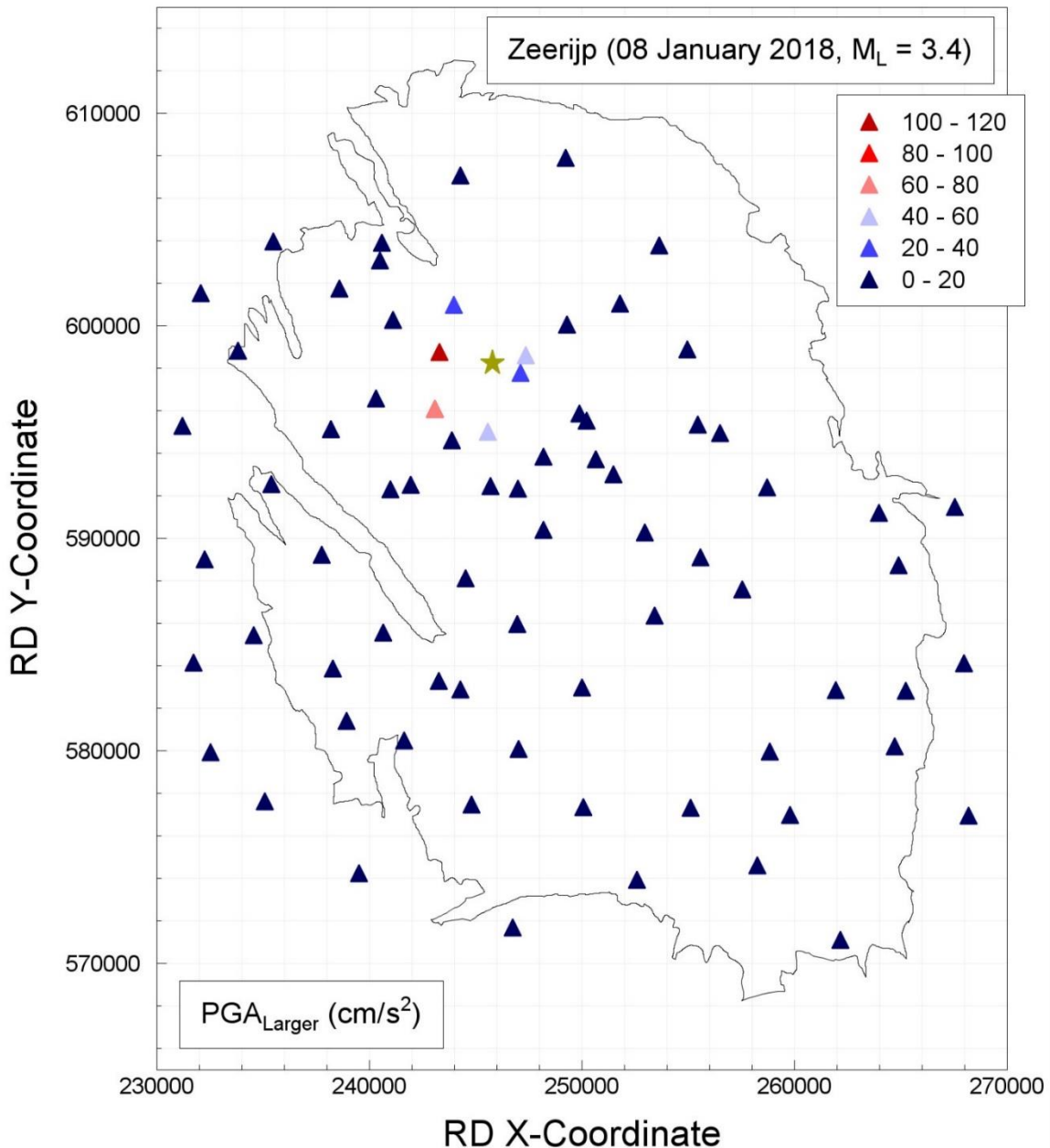


Figure A8.7. Map showing ranges of the larger component of PGA (cm/s^2) recorded at each station

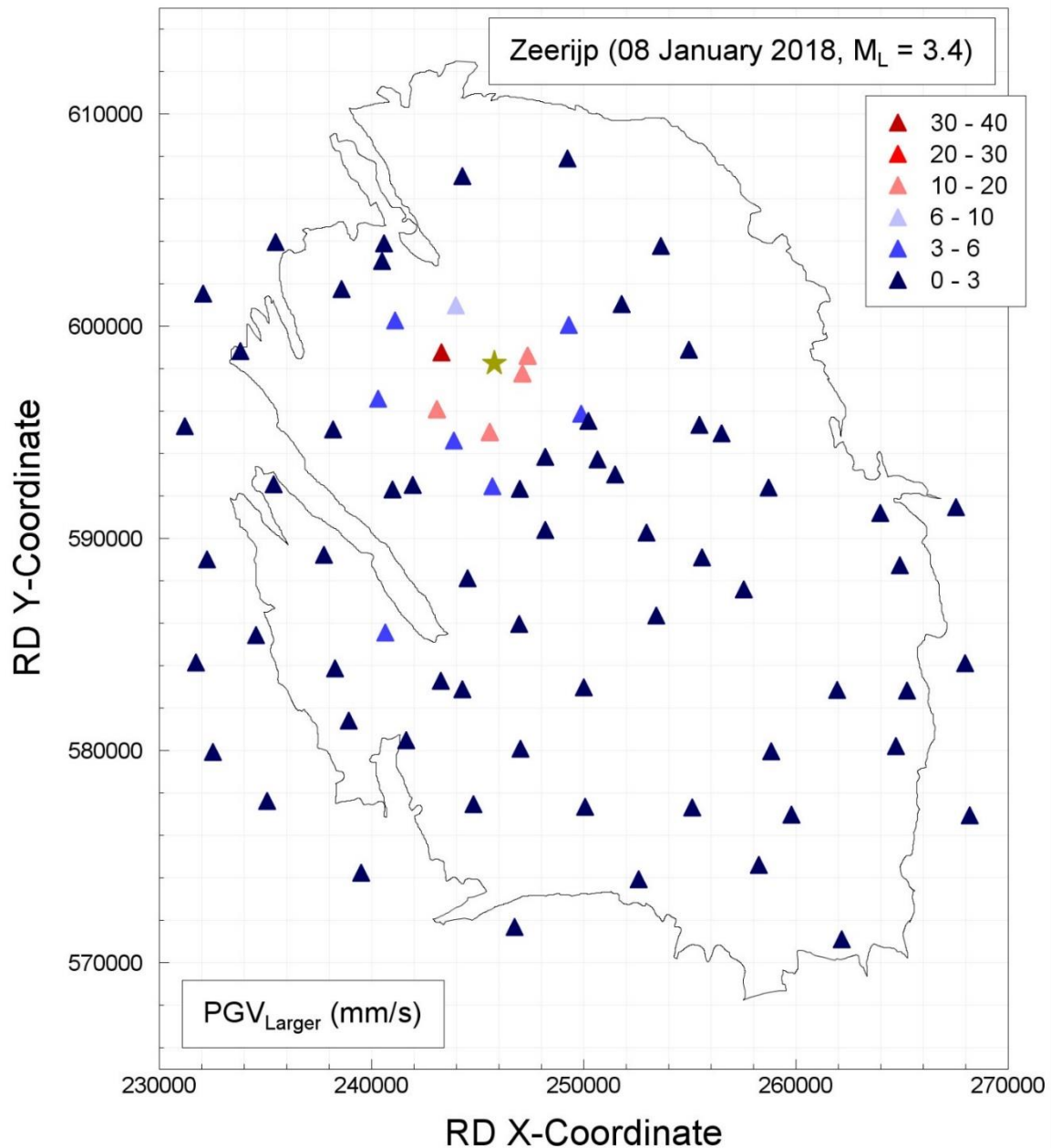


Figure A8.8. Map showing ranges of the larger component of PGV (note units: mm/s) recorded at each station

Overall, with the single exception of the EW component of the BGAR record, the motions are generally consistent with those observed in previous earthquakes. Figure A8.9 shows the geometric mean horizontal components of PGA and PGV plotted against magnitude together with the corresponding values from the complete database. The most striking feature is how this earthquake has contributed a large number of low-amplitude recordings, a feature also clearly visible for the M_L 2.6 Slochteren and M_L 3.1 Hellum earthquakes, reflecting the expansion of the recording networks in the Groningen field.

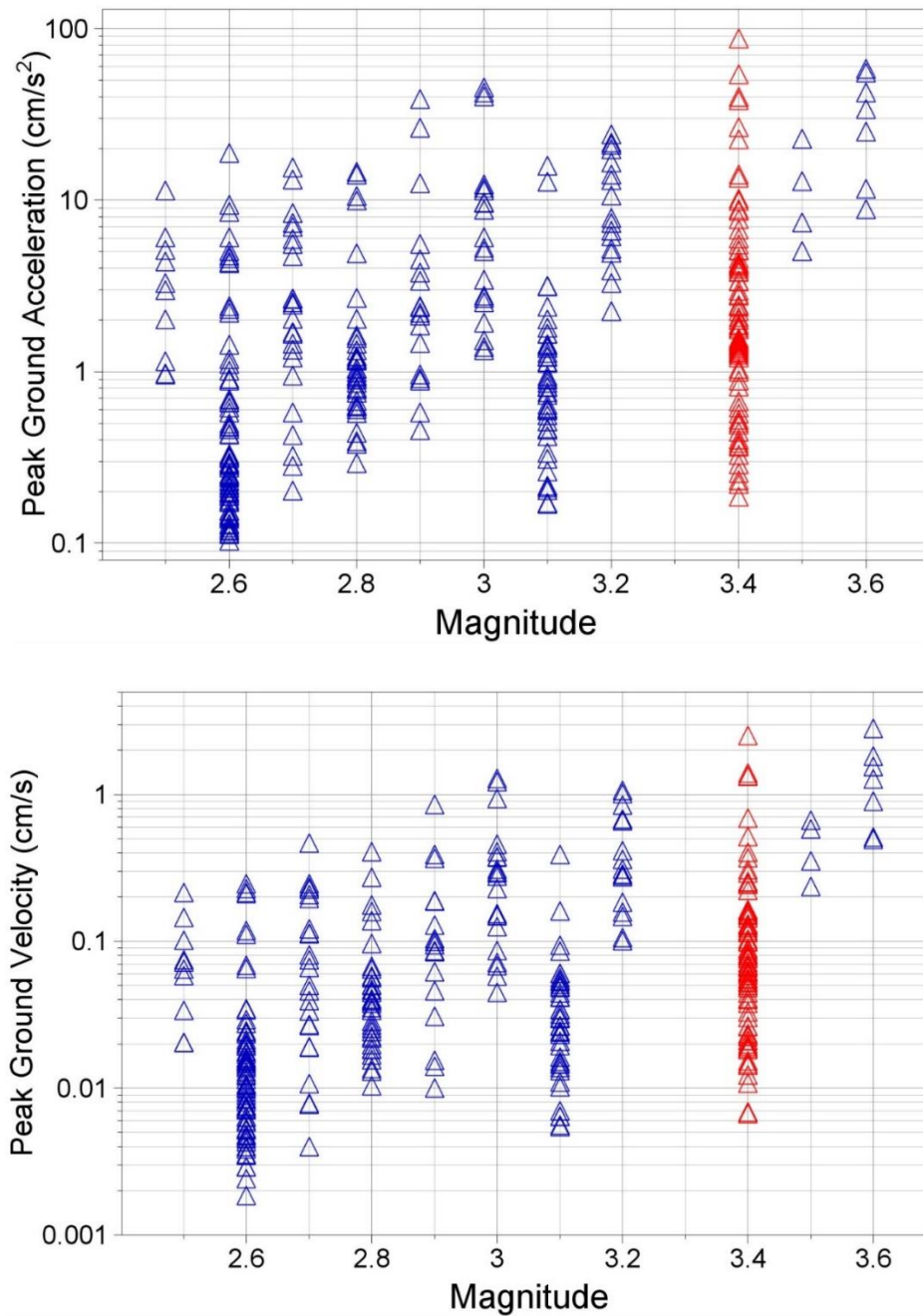


Figure A8.9. Geometric mean horizontal components of PGA (*upper*) and PGV (*lower*) recorded during the Zeerijp earthquake (*red*) and in previous earthquakes (*blue*) plotted against local magnitude

Ground-Motion Durations

The maximum amplitude of ground shaking, whether represented by PGA or PGV, provides a simple indication of the strength of the motion but the potential for adverse effects—such as damage to masonry buildings or triggering liquefaction—also depends on the duration or number of cycles of the motion.

A feature that has been consistently observed in the Groningen ground motions is a very pronounced negative correlation between PGA and duration, with high amplitude motions consistently associated with shaking of very short duration (Bommer *et al.*, 2016a). The same pattern is observed in the recordings of the Zeerijp earthquake, as shown in Figure A8.10. The largest value of PGA, recorded on the EW component at the BGAR station, is associated with a duration of less than half-a-second (0.43 s). The second highest PGA value is also from the BGAR station and is associated with a duration of just 0.54 s.

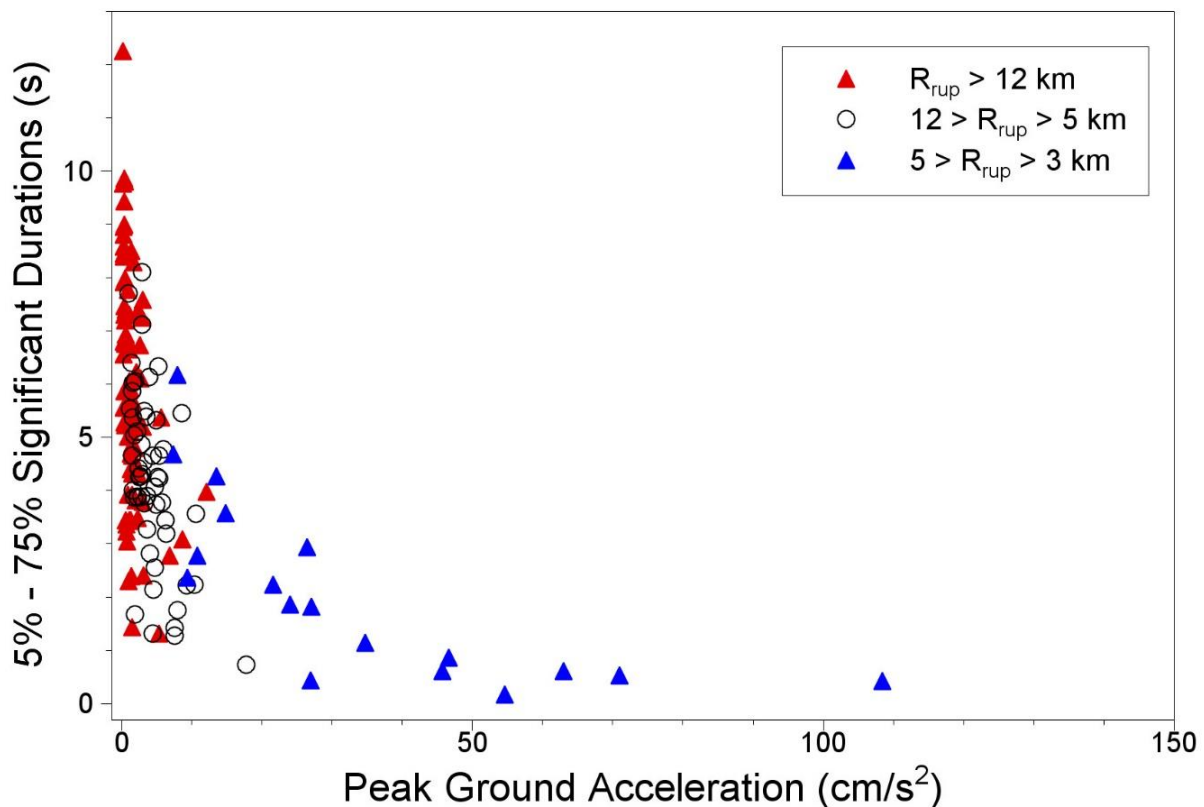


Figure A8.10. Pairs of PGA and significant duration for individual components of the Zeerijp records, with symbols indicating the rupture distance of the recording.

The horizontal components of both acceleration and velocity from this station are shown in Figure A8.11, which also shows the build-up of Arias intensity (which is a measure of the energy in the motion) over time. The strong concentration of the energy in a single pulse of motion is immediately apparent. An equally pronounced case is seen for the BZN1 recording—the second closest instrument to the epicentre and source of the fourth largest value of PGA—where the larger amplitude component is associated with a significant duration of just 0.17 s (Figure A8.12).

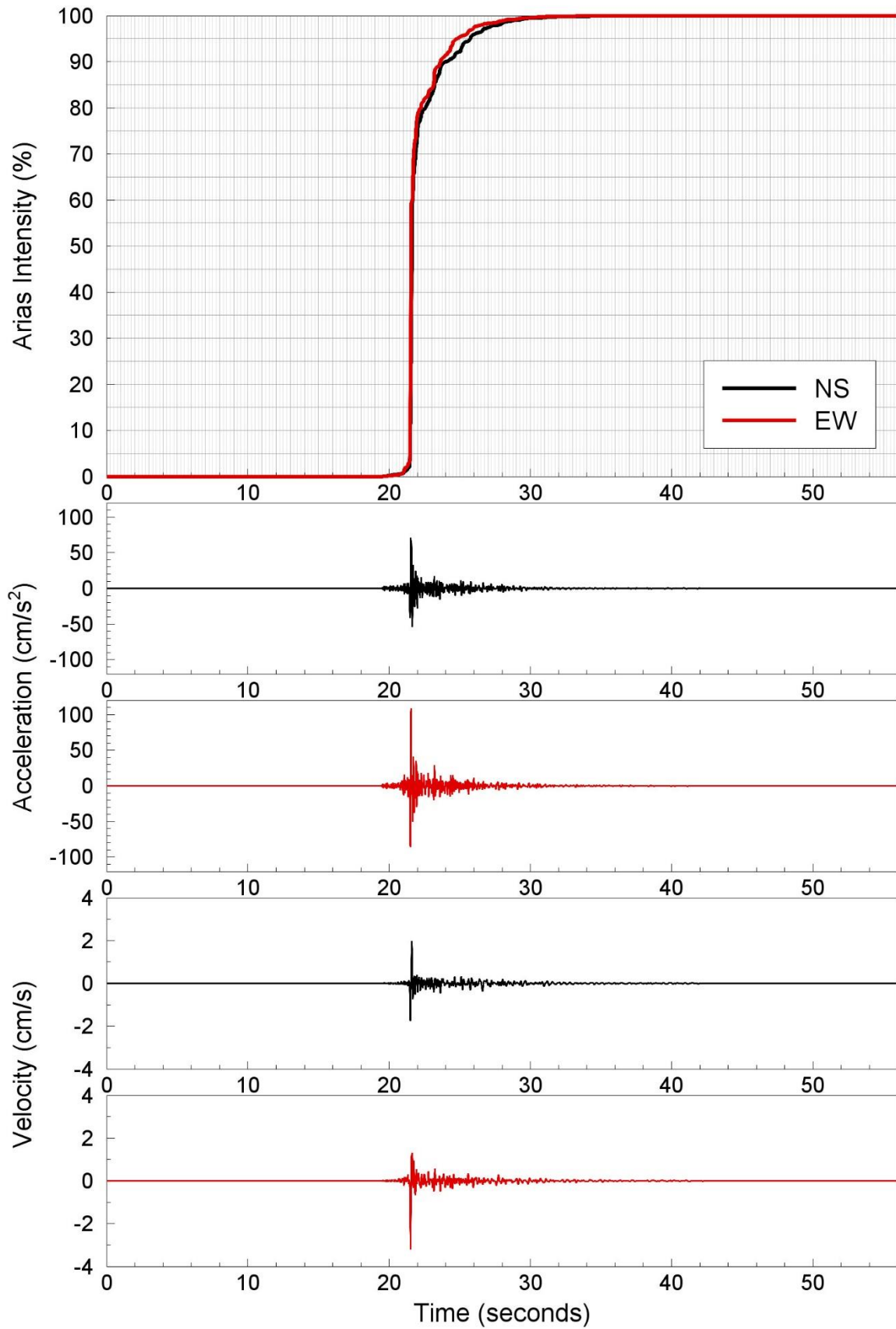


Figure A8.11. Horizontal components of acceleration and velocity from the BGAR station; the upper frame shows the accumulation of Arias intensity (energy) over time.

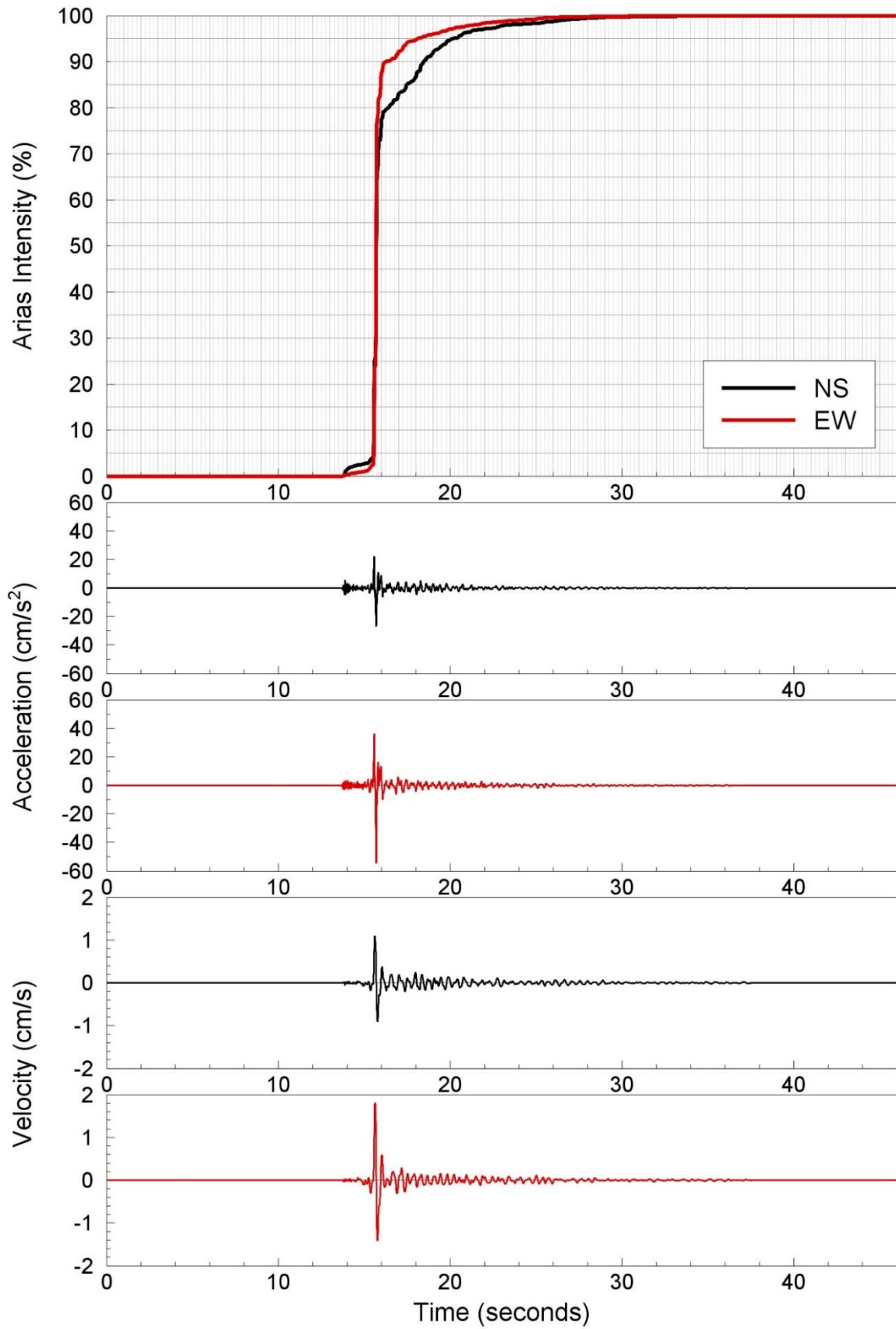


Figure A8.12. Horizontal components of acceleration and velocity from the BZN1 station; the upper frame shows the accumulation of Arias intensity (energy) over time.

Spectral Accelerations and Comparison with Ground-Motion Models

The fragility functions used in the estimation of seismic risk in the Groningen field are defined in terms of response spectral accelerations at various oscillator periods (Crowley *et al.*, 2017). The horizontal acceleration response spectra from the BGAR recordings of the Zeerjip earthquake are shown in Figure A8.13. The peaks at about 0.07 and 0.15 seconds are consistent with the calculated linear amplification factors for this station, although it must be recognised that some non-linear could have been caused by this earthquake at such close distance to the station (Bommer *et al.*, 2017d). The very different shapes of the spectra around 0.1 second, however, is likely to reflect source effects and the radiation pattern of seismic energy.

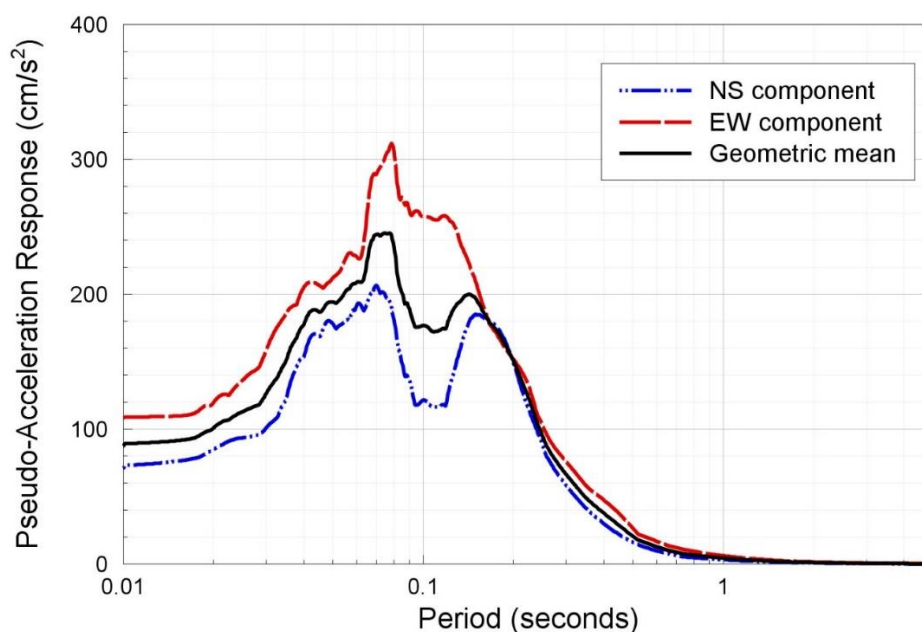


Figure A8.13. Horizontal response spectra from the BZN1 (upper) and BGAR (lower) stations

For this preliminary analysis, the key question of interest is whether the motions recorded in this earthquake are consistent with the current ground-motion model (GMM) being used in the Groningen field. The current model is the V5 GMM developed last year (Bommer *et al.*, 2017d) and we have simply calculated the total residuals at the surface for different ground-motion parameters. In each case, the residual is the natural logarithm of the ratio of the observed (recorded) to the median predicted value, so a residual of 0.7 indicates that the recorded value was underestimated by a factor of 2 by the model and a residual of -0.7 would indicate over-prediction by a factor of 2. Figure A8.14 shows the residuals of PGA and PGV with respect to the V5 GMM plotted against rupture distance. In both cases, the scatter is very considerable but it can also be observed that the PGA residuals are

well centred about the zero line, which suggests that the model provides a reasonable overall fit to the data. For the PGV values, the residuals are slightly shifted towards negative values, which indicates that on average the model is over-predicting the level of peak ground velocity. The same patterns in the residuals are observed for spectral accelerations, S_a , at other periods, with the residuals at short periods being generally centred (Figure A8.15) while at longer periods there is a consistent pattern of over-prediction by the V5 GMM (Figure A8.16).

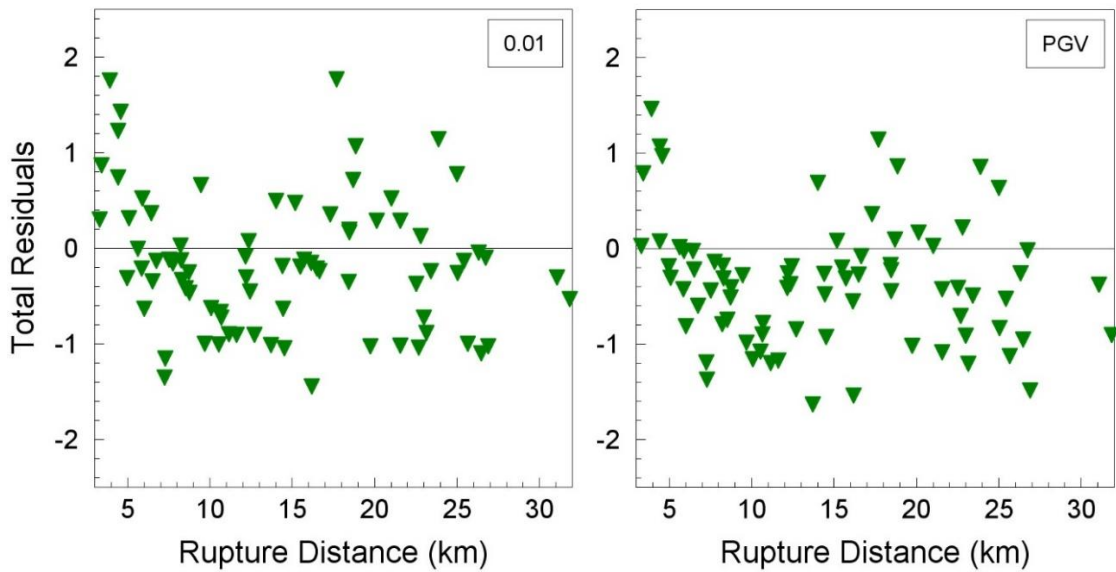


Figure A8.14. Residuals of PGA (*left*) and PGV (*right*) with respect to the central branch of the V5 GMM plotted against rupture distance.

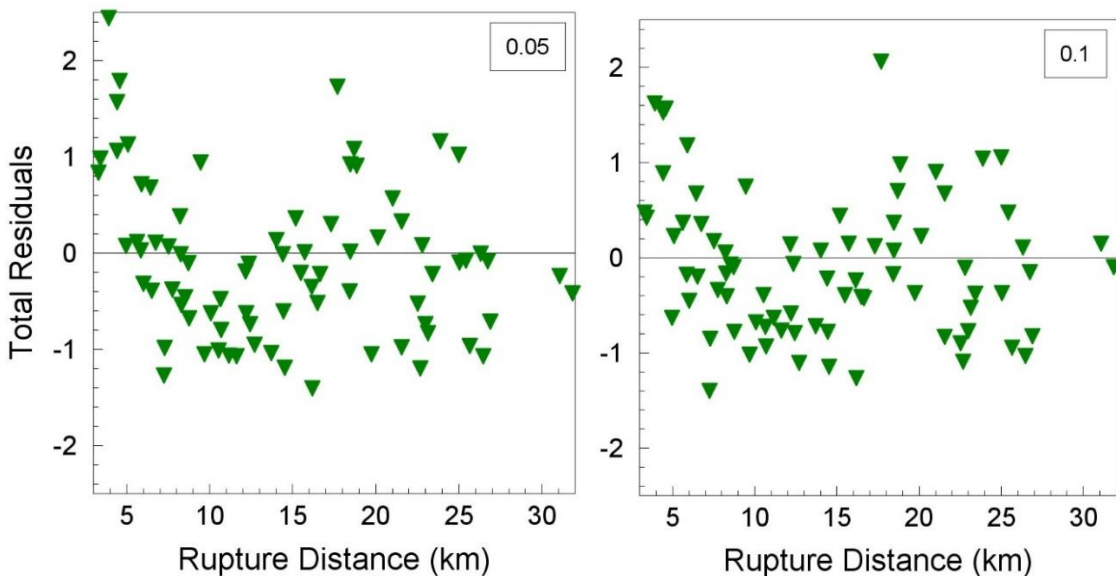


Figure A8.15. Residuals of $S_a(0.05s)$ (*left*) and $S_a(0.1s)$ (*right*) with respect to the central branch of the V5 GMM plotted against rupture distance.

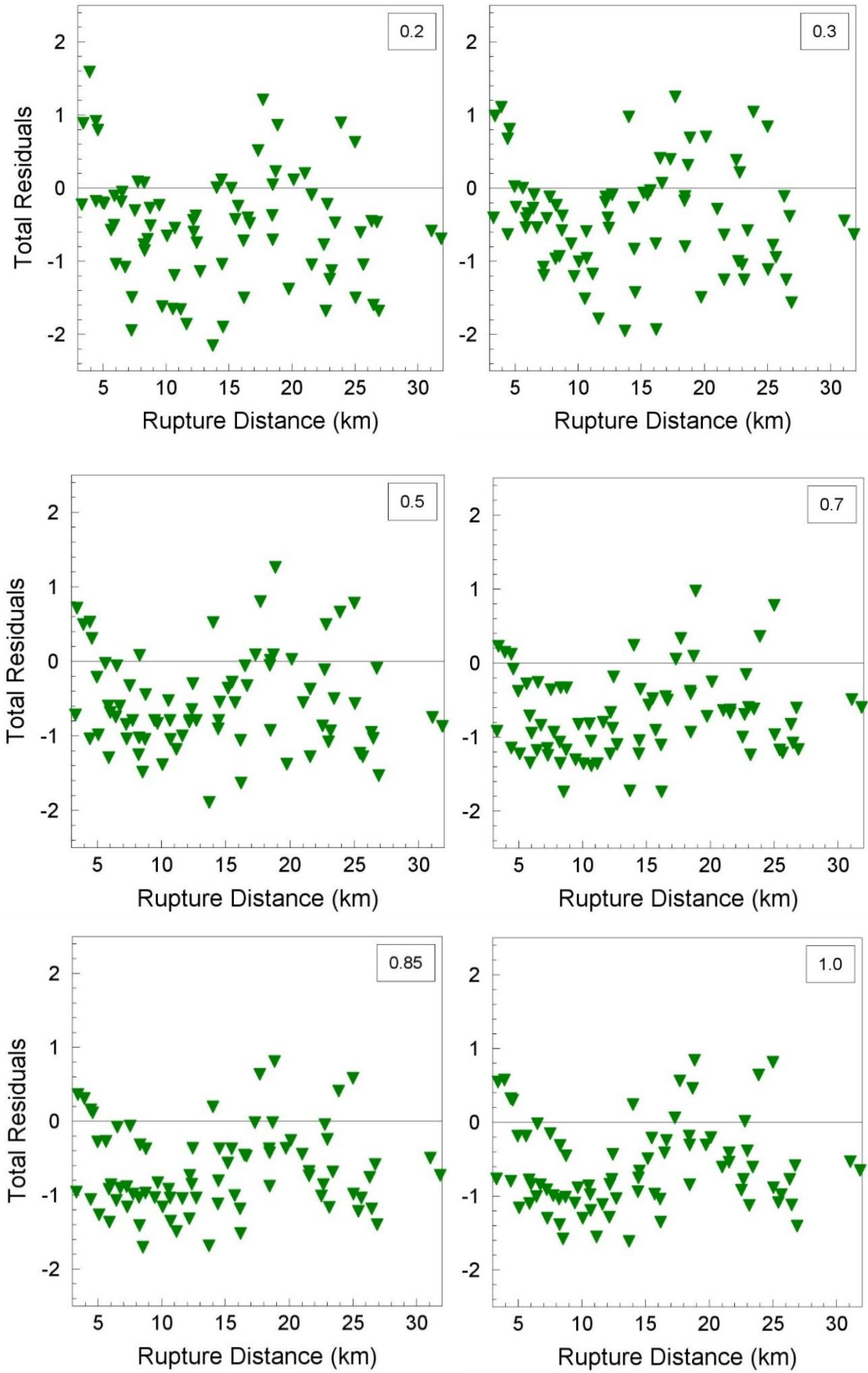


Figure A8.16. Residuals of $S_a(T)$ at six response periods, T , against distance

Concluding Remarks

The M_L 3.4 Zeerjip earthquake of 8 January 2018 has contributed a large body of ground-motion recordings that will inform and enrich the ongoing work of developing hazard and risk estimation models. The largest component of PGA recorded in this earthquake is $0.11g$, which exceeds the previous maximum of $0.08g$ recorded in the 2012 M_L 3.6 Huizinge earthquake. However, the largest value of PGV—which is generally considered a better indicator of the damage potential of the motion—recorded in this latest event is 3.19 cm/s , which is smaller than the value of 3.46 cm/s recorded in the Huizinge earthquake. Moreover, the duration of the new maximum PGA is just 0.43 seconds; the duration of the $0.08g$ component from Huizinge was 0.52 seconds, also very short but fractionally longer.

An important observation is that the motions recorded in the Zeerjip earthquake are broadly consistent with the predictions from the ground-motion model currently deployed in the seismic hazard and risk modelling for Groningen at short ($< 0.1\text{ s}$) response periods. At longer response periods, the model tends to over-predict these recorded motions.

APPENDIX IX

Review Comments and Responses on the V4 GMM Report

The first version of the V4 GMM report was issued on 29 March 2017 and was submitted to the international review panel (see Appendix I). Editorial and technical comments were received from the panel a few weeks later and a revised version of the V4 report, taking account of all the editorial comments and also some of the technical comments, was issued on 23 June 2017. The revised V4 GMM report was submitted to the panel together with the responses to the editorial comments.

The technical comments were mostly addressed in the development of the V5 model and the responses to these comments were submitted to the review panel together with the first version of the V5 GMM in mid-December 2017. The complete report containing the comments and responses is reproduced here as issued, including self-contained references; the only modification has been the page numbers, which are continuous with the rest of this report.

TABLE of CONTENTS

1. INTRODUCTION	182
2. MAIN REVIEW COMMENTS	184
2.1. Stress parameter and model performance at large magnitudes	184
2.2. Inversion and parameter uncertainties	188
2.3. Local-to-moment magnitude conversion and its effects	193
2.4. EXSIM documentation	196
2.5. Fully non-ergodic model	199
2.6. Tau model	199
2.7. Event depths	204
2.8. Use of H/V spectral ratios	205
2.9. Soil shear strength as restraint on stress-strain backbone curves	212
2.10. Ground response analysis input motions	213
2.11. Site amplification bias and implications for suitability of EQL analyses	213
2.12. Component-to-component variability	220
2.13. Function for duration model	227
3. ADDITIONAL REVIEW COMMENTS	230
3.1. Chapter 1: Introduction	230
3.2. Chapter 2: Overview of V4 GMM	231
3.3. Chapter 3: Groningen ground-motion database	231
3.4. Chapter 4: Characterisation of recording stations	233
3.5. Chapter 5: Inversions for Source, Path and Site Parameters	239
3.6. Chapter 6: GMPEs for reference rock horizon	242
3.7. Chapter 7: Site response model	247
3.8. Chapter 8: Site response analyses	248
3.9. Chapter 9: Zonation for site amplification functions	250
3.10. Chapter 10: Sigma model	251
3.11. Chapter 11: Application and extension of GMM for $S_a(T)$	255
3.12. Chapter 12: GMPE for duration	262
3.13. Chapter 13: Concluding remarks	263
4. CONCLUDING REMARKS	264
5. REFERENCES	266

1. Introduction

The development of models for the prediction of ground motions due to induced earthquakes in the Groningen gas field in the Netherlands has been an evolutionary process, passing through several distinct stages (Bommer *et al.*, 2017d). Fully functional and documented versions of the model have been issued at different times. At three critical stages, the ground motion model (GMM) has undergone peer review by international experts. The key model development and review stages can be summarised as follows:

- V1 GMM issued in March 2015. This was the first model calibrated to the specific condition of the Groningen field and included a logic-tree formulation to capture epistemic uncertainty. Peer-reviewed for publication in the *Bulletin of the Seismological Society of America* (Bommer *et al.*, 2016a).
- V2 GMM issued in October 2015. This model included a zonation of the field with non-linear, frequency-dependent amplification factors. The model was reviewed by an expert panel (Gail Atkinson, Hilmar Bungum, Fabrice Cotton, John Douglas, Jonathan Stewart, Bob Youngs and Ivan Wong) during a workshop held in London on 27-28 October 2015, followed by written comments submitted by individual panel members.
- V3 GMM issued in July 2016, using a new and deeper reference rock horizon. This model was discussed at a workshop held in London on 18-20 July 2016 with the participation of geophysicists from Shell and ExxonMobil and a small group of international experts (Norm Abrahamson, Luis Angel Dalguer and Bob Youngs). The participants provided feedback on the model in general but the key focus of the workshop was the transition from point-source to extended-rupture based simulations. The V3 model was also peer-reviewed for publication in *Earthquake Spectra* (Bommer *et al.*, 2017a).
- V4 GMM issued in March 2017, similar in many regards to the V3 model but with several important refinements and additions, the most important of which was the adoption of rupture distance instead of epicentral distance.

The V4 GMM report (Bommer *et al.*, 2017b) was reviewed in detail by a panel comprising the experts who had participated in the review workshops. The panel was chaired by Jonathan Stewart and included Norm Abrahamson, Gail Atkinson, Hilmar Bungum, Fabrice Cotton, John Douglas, Bob Youngs and Ivan Wong. The panel sent their review comments 15 May 2017 in the form of a formal review report and an Excel file with 249 editorial comments. On 23 June 2017, a revised version of the V4 GMM report was issued (Bommer *et al.*, 2017c) and shared with the review panel, together with responses to each of the editorial comments.

This document now addresses the response of the Groningen GMM to the formal review comments on the V4 model. In each case, we explain how the comments was accommodated in the revision of the V4 GMM report or in the development in the V5

GMM (Bommer *et al.*, 2017e), where appropriate. For a few comments, we provide rebuttals to explain why we do not believe that a modification is needed or else explain how the issue is to be addressed in longer-term developments beyond the V5 GMM, which was produced to a tight schedule in order to be available for the V5 hazard and risk results that NAM was required to deliver on 1st November 2017.

In Chapters 2 and 3 of this report, we reproduce *ad verbatim* the review panel comments (highlighted in blue Times New Roman font in order to be more easily distinguished) and provide immediately below our responses. The report concludes with a brief discussion of the current status of the model development and future perspectives.

2. Main Review Comments

The review report issued by the expert panel highlighted 13 main substantive issues. These are addressed in the following sections.

2.1. Stress parameter and model performance at large magnitudes

A fundamental limitation of the developed GMMs is the lack of calibration of the ground motions for magnitudes beyond the data range. The approach taken is to use branches for alternative values of stress parameter that are applied in the GMM development (through EXSIM simulations). Because it is typical for stress parameter values to increase with magnitude below some magnitude range, above which they become constant, it is not possible to convincingly bound the range for stress parameter based on the Groningen small-M data. Thus, of necessity, a large uncertainty needs to be assumed for this aspect of the GMM development, and experience from other regions needs to be invoked. A fuller discussion of what regions were considered, and why, would be helpful in this regard. Reference is made to NGA-W2 models, but reference to European models, especially those representing normal faulting environments, should be added – as well as reference to models for shallow events in central and eastern North America. Consideration of these additional models may influence the center and range of stress parameters considered in model development, particularly at large magnitudes; this would likely require additional work as part of V5 model development.

We agree with the reviewers that a fundamental, and general, limitation of ground-motion prediction lies in scenarios beyond the coverage of local data. However, we argue that the GMM presents a solution to this data limitation, accounting for the increased epistemic uncertainty through multiple logic-tree branches, whilst maintaining a high degree of predictive power for smaller ($M < 3.6$) events where local data exists. Nevertheless, we agree that, while our approach accounts for a broad range of uncertainty in extrapolating to large M , the specific approach of calibration of EXSIM simulations to GMPEs developed using data from seismically active regions can be improved from that presented in the V4 GMM by using multiple GMPEs.

Taking in light the reviewers' suggestions, the V5 model is now calibrated against:

- a) A suite of NGA-W2 GMPEs (BSSA14: Boore *et al.*, 2014; CY14: Chiou & Youngs, 2014; CB2014: and Campbell & Bozognia, 2014), primarily comprising Californian data and large global events;
- b) Two GMPEs [Aetal14: Akkar *et al.* (2014a) and Betal14: Bindi *et al.* (2014)] based on European and Middle-East data.
- c) The Eastern North America model YA15: Yenier & Atkinson (2015).

All GMPEs are used with normal faulting and $V_{s30} = 1500$ m/s. The V5 report summarises the process undertaken, which remains unchanged from V4 apart from

using the additional comparison GMPEs. Additional plots are presented in Figures 2.1 to 2.3 in this response.

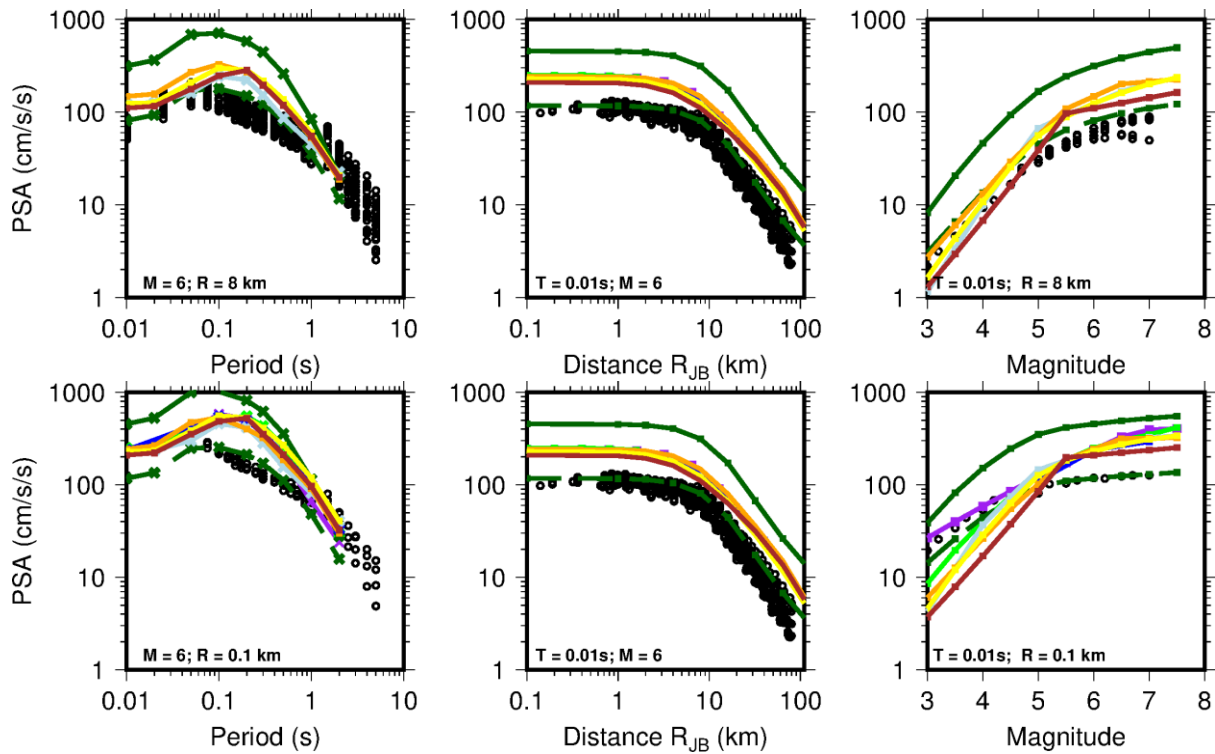


Figure 2.1. EXSIM simulations (circles) for the *lower GMM* compared against several GMPEs. Scenarios are indicated in the labels. Dark green: YA15 (dashed = 3 km source, solid = 10 km source); yellow: CB14; orange: CY14; purple: Aetal14; light green: Beta14; brown: Boore *et al.* (2014); light-blue: Abrahamson *et al.* (2014)

The comparisons with NGA-W2 and RESORCE models indicate broad similarity, with differences that are accountable to the selection of lower, central or upper models. The strategy for selection of the upper model, defined as the ‘most tectonic-like’, was to ensure overall similarity in the predictions (using bias estimators), but allowing predictions at larger distances and shorter periods to deviate in mind of the attenuation differences. In Figure 2.3 (the upper GMM) the predictions are shown to envelope the range of GMMs (NGA, RESORCE and ENA). The ENA model (for tectonic like predictions – with hypocentre depth at 10 km), as typical of stable continental models, presents an upper-bound to the predictions.

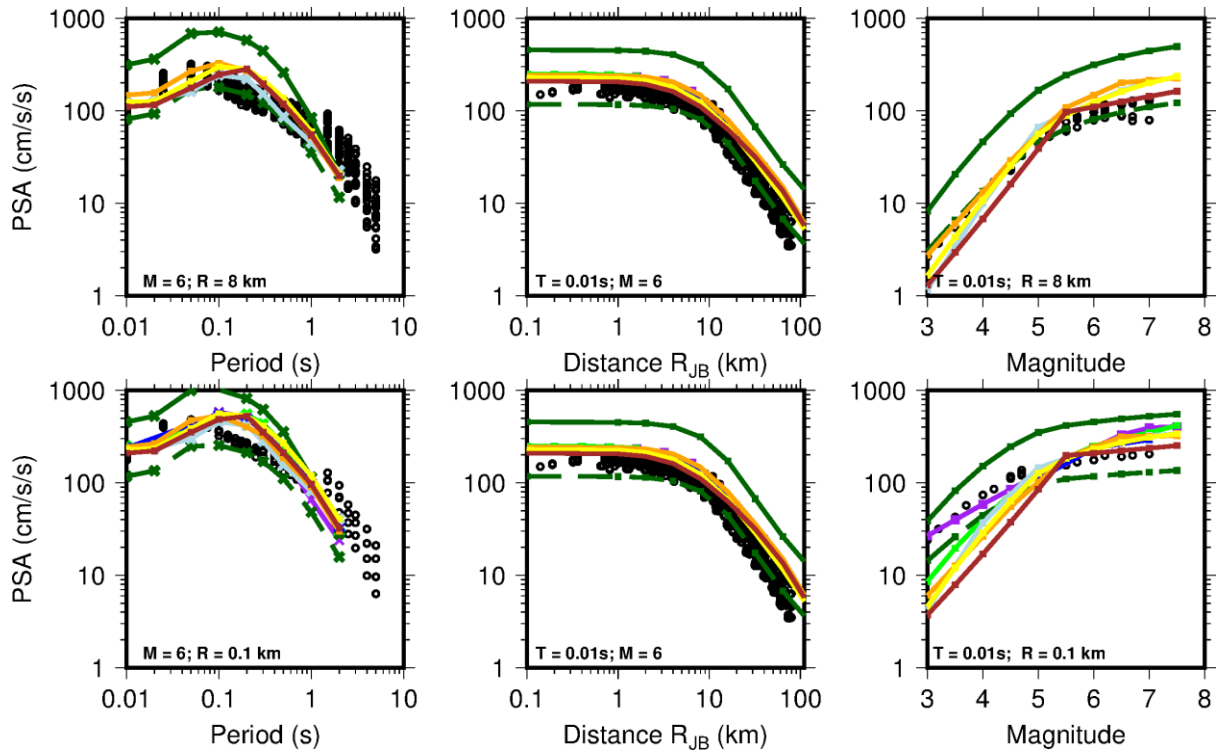


Figure 2.2. EXSIM simulations for the *central-a GMM* compared against several GMPEs. See Figure 2.1 for details

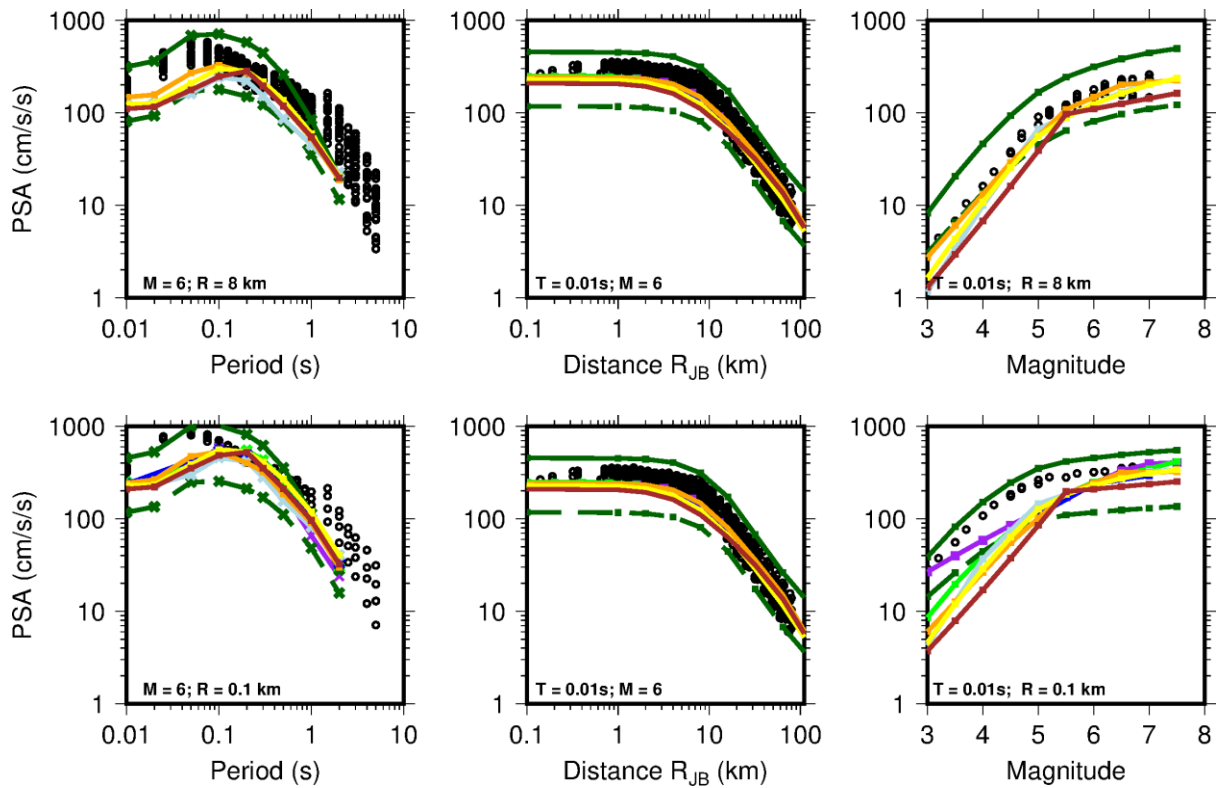


Figure 2.3. EXSIM simulations for the *upper GMM* compared against several GMPEs. See Figure 2.1 for details

Another issue that affects confidence in the scaling of the GMMs to larger magnitudes concerns the use of EXSIM as the simulation platform for GMM development. We agree that EXSIM has advantages in handling the geometric issues of finite-fault scaling; however a significant limitation is that EXSIM is not nearly as well calibrated (i.e. using large databases over a broad range of magnitudes and distances) as is the equivalent point source approach. Calibrations of EXSIM have been generally limited to specific events with known geometries, as in the exercises carried out for its original development and in subsequent validation exercises for its implementation on the SCEC broadband platform. For the Groningen GMM, for which an application-specific calibration is not feasible, it is not clear that there are advantages to using EXSIM over an equivalent point source.

We were very surprised to read this comment in the report and wonder if it is really a consensus view of the full panel? We appreciate that point-source simulations have been well calibrated and that valuable work has been done on effective distances to approximate the near-source distance saturation effects, but we are modelling earthquakes up to M 7.25 (the upper limit of the Mmax distribution) and are not really content with representing the ground-motion fields from larger events as emanating from a single point. Indeed, the Workshop held in London in July 2016 was specifically intended to address this issue and to choose the most appropriate approach to finite rupture simulations. At that Workshop, we were challenged very strongly—and with good justification—by Norm Abrahamson for using point-source representations even for the larger triggered earthquake scenarios and strongly encouraged to move to finite ruptures and the use of rupture distance. The presentations at that Workshop on the SCEC calibration exercises and the use of simulations in NGA-East and other projects convinced us that the best option was, without any doubt, to use EXSIM. The simulations at smaller magnitudes from EXSIM and SMSIM at smaller magnitudes were checked against one another as a check (see responses in Section 2.4). We need to bear in mind that the ultimate goal of this GMM is for application not in hazard calculations but in risk estimation, and being able to more accurately represent the ground-motion field and the numbers of buildings affected by different ground-motion levels for larger-magnitude earthquake scenarios is very important.

One more advantage of moving to EXSIM is that we now have a duration prediction model that extrapolates to larger distances and larger magnitudes in physically meaningful way; for obvious reasons, we could never have made progress with the duration model using point-source simulations.

In any case, regardless of whether simulations are based on finite fault or equivalent point source simulations, the final GMM needs a more comprehensive justification in its application to larger magnitudes. This can be achieved through comparisons of its magnitude scaling behaviour against GMMs that have been validated over a wide magnitude range. Some comparisons are made to the Atkinson (2015) GMM, but other GMMs that are believed to have suitable scaling characteristics for comparison should also be included. The Abrahamson et al (2014) GMM should be considered because it has appropriate near-distance

scaling over the full magnitude range. For central and eastern North America, the Yenier and Atkinson (2015) GMM includes a term that allows the stress parameter to be scaled with respect to magnitude and focal depth, making it applicable to induced events. In addition, a range of European GMM models are available and should be considered, selecting those with appropriate attributes.

We feel that these points were at least partly addressed in our responses to an earlier comment in this section. The suggested GMPEs have been incorporated into the comparison. Since three NGA-West2 GMPEs were already used in the calibration, we did not include the Abrahamson *et al.* (2014) model to avoid biasing the result toward this dataset – furthermore it is not significantly different to the three selected NGA-W2 models in the parameter space of interest. However, this GMPE is shown in Figures 2.1 to 2.3, for completeness.

The lower GMM displays similarity to the Yenier & Atkinson (2015) ENA model for shallow (3 km) hypocentres at all but the shortest periods ($T < 0.05$ s). The magnitude scaling is also consistent with various GMPEs – but most similar to the shape (but not necessarily amplitude) of the YA15 model – which was earlier found to be appropriate in an analysis of magnitude scaling in the Groningen data. Many of the GMPEs have a decay at low magnitudes that is too steep (at short distances, but not at greater distances) – resulting in an under-prediction of amplitudes available in the Groningen database. The central model is most similar to the range of GMPEs, across all distances and magnitudes, although shows (as for all GMMs) a shorter-period peak owing to the low κ_0 reference horizon, and also displays similar magnitude scaling to the lower GMM: similar to most GMPEs at 8 km, but displaying higher amplitudes for small events at very short distance. The upper GMM is designed to ensure that predicted amplitudes are consistent with—or exceed—GMPE predictions for moderate to large events at all but the longest distances (accounting for the low Q environment). Comparing with the GMPEs in Figure 2.3, only the YA15 model for deep (10 km) hypocentres exceeds the GMM. Since this is an ENA based model – with very weak attenuation – we treat this model as an upper bound in the comparisons.

2.2. Inversion and parameter uncertainties

Using deconvolved data, fits are performed to set the Brune source corner frequency, the spectral displacement plateau, and κ_0 . There are many uncertainties in this process, including magnitude conversion (local to moment – see comment M3) and source velocity β . We recognize that some of these parameters need to be fixed in the inversion, and the uncertainty in the process can be represented by the resulting spread of the inverted parameters, reflecting data variability.

We agree with the reviewers, and have provided, where possible, estimates of parameter uncertainty in the V4 and V5 reports to reflect this. We would note that

while uncertainty still remains, in linking full waveform modelling, site response modelling and estimates of Q from previous studies we have been able to greatly decouple the significant trade off of parameters. The model has remained robust throughout several iterations of the GMM, with significant changes in parameters (stress, geometrical attenuation) due mainly to a change in how \mathbf{M} was determined. The latter point has been explored in detail, with a paper submitted to *Seismological Research Letters* on the topic (see also Appendix II of the V5 report).

It is unclear from the current text how reference site amplification $T(f)$ is determined. Is that part of the inversion or it is set separately using quarter-wavelength theory or similar? The amplification is stated as being close to one in Chapter 5, but how can this be distinguished from stress parameter? Wouldn't more amplification imply lower stress parameters?

The site transfer function, $T(f)$, is determined by post-processing the residual misfit of the FAS after fitting the Brune far-field model (for example, see Edwards *et al.*, 2013). This element has remained the most stable throughout the GMM development and is shown in Kruiver *et al.* (2017) to provide remarkably consistent amplification estimates at individual stations to those from shear wave 1D velocity modelling.

While some trade-off is possible, the fact that the NS_B component is calibrated over all stations (assuming a homogeneous NS_B response) will decouple this to a great extent. Note that the amplification is frequency dependent (and magnitude, distance independent for the FAS), while the effect of the stress parameter is magnitude dependent. In the response domain a trade-off would be stronger (due to the sensitivity of the oscillator to lower frequencies), but the NS_B $T(f)$ is determined based on FAS and applied in the subsequent optimisation of PSA.

Another related issue is trade-offs between correlated parameters. The inversion should consider what parameters can be constrained by the available data. The correlation matrix of the parameter estimates from the inversion should be provided to demonstrate which parameters are reliable and which just trade off with other parameters. Some specific concerns in this regard:

- Given the narrow range of distances in the data set (epicentral distances <25 km), it may not be possible to estimate both Q and κ ;
- κ and stress may be highly correlated; and
- Near-fault distance attenuation slope and stress parameter may be highly correlated.

This issue is well documented, and we acknowledge that significant trade-offs and uncertainties do lie in the deconvolution of source, path and site specific terms. As noted in previous comment responses, the inversion has benefited greatly from a variety of independent analysis and modelling that has resulted in significantly reduced degree of non-uniqueness – conditioned on the results of (a) **M** (provided by KNMI), the shape of the geometrical decay (Shell/NAM), **Q** (KNMI), and site response (Deltares/NAM). In order to highlight the benefit of this information—and in response to the request for covariance matrices—Figure 2.4 shows the unconstrained covariance of the NS_B inversion problem (the only information used is the site response, which deconvolves the motions to the NS_B). Covariance is calculated using the normalised percentage (%/100) deviation in spectral parameters that would lead to similar (5% worse) misfit: essentially describing how the spectral parameters change to provide a similarly well-fitting model. These changes are split into two main categories: those involving a positive and those a negative change in $\Delta\sigma$.

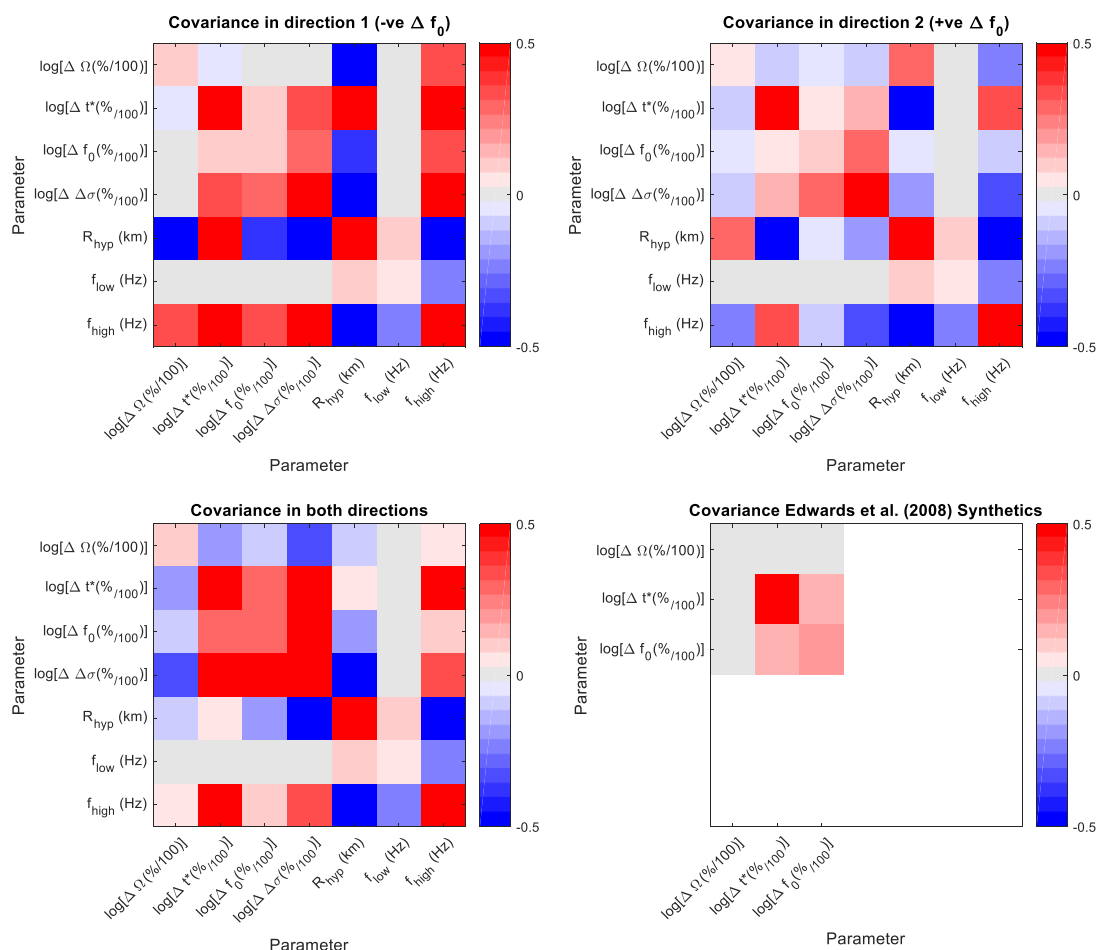
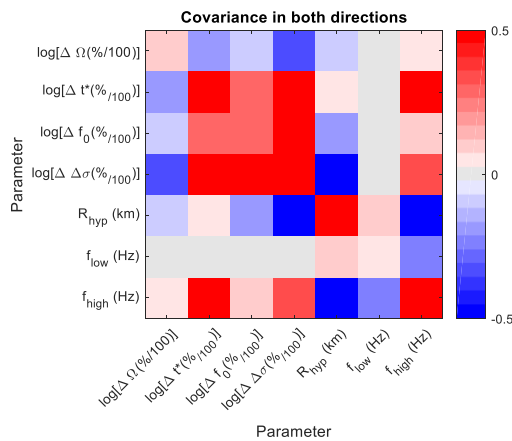


Figure 2.4. Covariance matrices for the spectral inversion problem with site response constraint (i.e. NS_B deconvolved motions). Covariance is calculated using the percentage (%/100) deviation in spectral parameters leading to similar (5% worse) misfit for (top left) reductions in f_0 (and $\Delta\sigma$), (top right) increases in f_0 ; (bottom left) both increases and decreases in f_0 and (bottom right) the synthetics of Edwards *et al.* (2008)

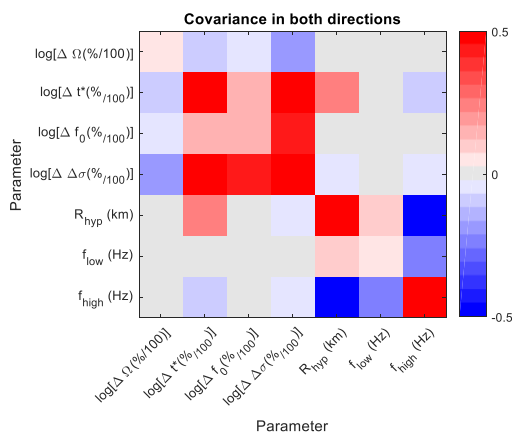
The covariance shows similar behaviour to those seen in previous synthetic and bootstrapping approaches: higher f_0 (or $\Delta\sigma$) are compensated by higher whole path attenuation (t^* - also denoted κ_r or $\kappa(r)$ in this context). Uncertainties in individual parameters are dominated by uncertainty in t^* and f_0 . It is noted that the parameter adjustment required depends on the upper fitting frequency (f_{high} and the distance (which is also correlated to f_{high}). The covariances are also dependent for many parameters, on the style of change (increase or decrease in f_0).

Figure 2.5 shows the effect on the covariance of the additional constraints, from using a common event corner and prior $\Delta\sigma$, to the final inversion that uses the average Q and κ from the previous stage. The sequence shows how the uncertainties and covariances are successively decreased. Note that f_0 and $\Delta\sigma$ are correlated by definition.

Site response constraint only:



Add bayesian $\Delta\sigma$ and event common f_0 :



Final inversion (site, event f_0 , Q, bayesian $\Delta\sigma$):

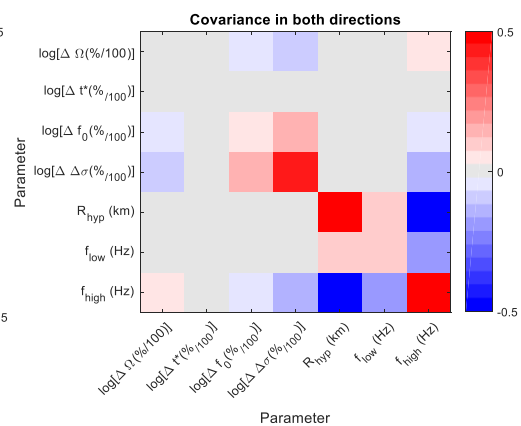


Figure 2.5. Covariance matrices for the spectral inversion problem. Covariance is calculated using the percentage (%/100) deviation in spectral parameters leading to similar (5% worse) misfit for both increases and decreases in f_0 at (top left) inversion constrained only by site response information; (bottom left) constrained by site response and Bayesian prior $\Delta\sigma$; (bottom right) final inversion including site response, prior $\Delta\sigma$ and Q model

The patterns in Figure 2.5 show, therefore, how our strategy—given additional constraint—removes the strong trade-offs present in the original problem. What may remain, nevertheless is bias – which results from incorrect constraint being applied. We believe that the constraints are justified based on the independent agreements: for instance, site response and Q have been measured using various methods. The stress parameter strongly converged to similar medians independent to the median of the prior, indicating that this is a robust solution.

Given these issues, it is not clear that the stress parameters shown in Figures 5.18 and 5.19 are reliable or if they are biased due to trade-offs with κ_0 and near-distance slope.

As argued in response to the previous comment, we believe the trade-offs are minimised using the approach adopted. Nevertheless this does involve introducing possible sources of bias: the most obvious being the Q and κ_0 values determined in the initial inversion stage. Stress parameters are conditioned on these values – and therefore, while the trade-off is controlled, choosing the wrong Q model (and corresponding κ_0) may lead to bias – potentially evident in systematic shifts. Due to the fact that the recordings are unusually close ($R < 25$ km), we believe this is not the case. To test this, two alternative models have been developed: one with $Q = 100$ and one with $Q = 400$ (*c.f.* $Q = 220$ as used in the V5 model). These limits represent a conservative range over which Q may be found (based on results from inversion of surface and NS_B corrected data, *e.g.*, bootstrap analysis, changing datasets from V1 to V4). Using these Q models, corresponding κ_0 values are determined for the sites, then the second inversion stage is run, applying those Q and κ_0 values (*i.e.*, inversion corresponding to the covariance matrix in the bottom right of Figure 2.5). The slope of the geometrical spreading function remains almost identical (changing by 0.02-0.03). The average stress parameters change minimally for both the increased and decreased Q (and corresponding κ_0) from an average of 4.5 MPa to 4.1 MPa and 4.4 MPa respectively. We note that these changes are also inconsistent with those expected given a trade-off existing (*i.e.* decrease Q – stronger attenuation = increase stress parameter, and vice versa). We are therefore confident that the inversion of Fourier amplitudes is – given the \mathbf{M} and site response information – robust. We note that the subsequent refinement of the stress parameter during the optimisation for PSA prediction changes the value of ~ 4 -5 MPa slightly (the central model used 7 MPa), however – the PSA optimisation is again conditioned on the use of Q and geometrical spreading determined in the Fourier analysis – hence a similarly low level of trade off would be expected. We attribute the shift in stress parameter to a change in the focus of frequency (Fourier analysis tends to put more weight on high frequencies whereas response domain analyses put more weight on lower frequencies).

2.3. Local-to-moment magnitude conversion and its effects

The relationship between M_L and M is important. This has been assumed as $M = M_L - 0.2$, but this is not well justified, especially as the gradient on Fig. 2.2 is not unity. It is generally held that a change in the slope of this relationship is to be expected at small magnitudes. For example, Deichmann (2017) shows that M_L vs M should scale as 1.5: 1 for small earthquakes ($< \sim 4$), as a consequence of the effects of Q and the Wood-Anderson response (see also Goertz-Allman et al., 2011). The slope of $M-M_L$ on Fig. 2.2, considering all data points, appears to be ~ -0.25 . Given the preponderance of evidence that M_L-M is likely not a simple 1:1 scaling, this relationship should be improved.

A significant effort was focussed on resolving this issue – as detailed in Appendix II of the V5 report, which is itself a summary of a paper submitted to SRL. We indeed found that the 1:1 slope was valid only at $M_L > 2$, and below this we observe similar trends to those found in the literature (Figure 2.6) over the entire magnitude range of interest this leads to:

$$M = 0.056262 * M_L^2 + 0.65553 * M_L + 0.4968 \quad (2.1)$$

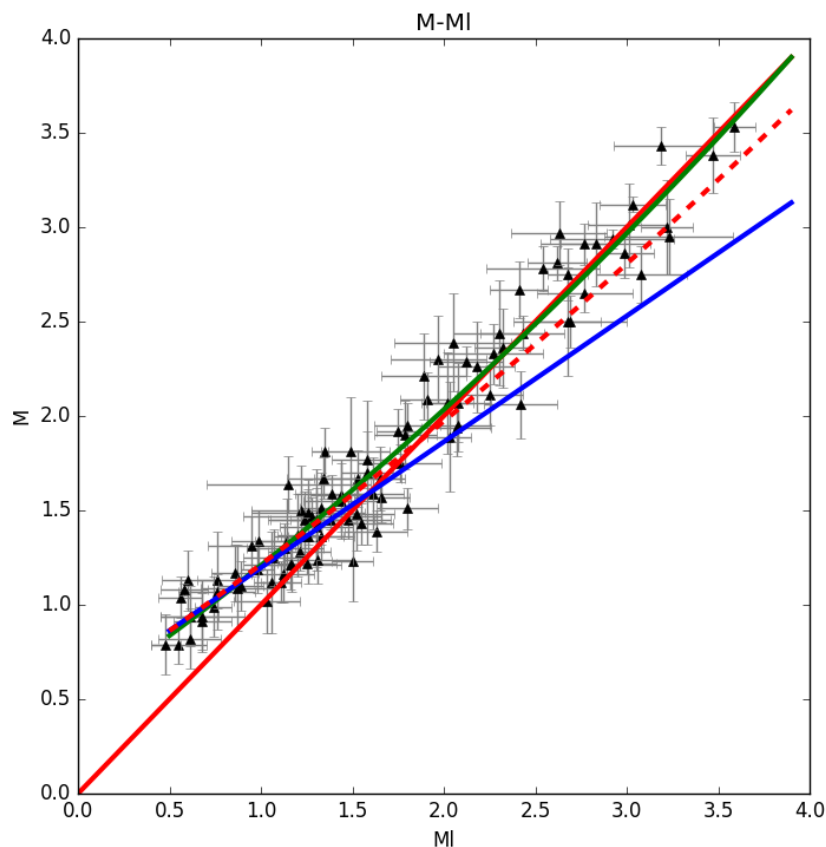


Figure 2.6. Moment magnitude M as a function of local magnitude M_L . In green the proposed quadratic relation is shown. In red-dashed, the Grünthal *et al.* (2009) relation and in blue the Munafò *et al.* (2016) relation.

The ultimate use of the conversion is to link the M_L values that characterize seismicity with the GMMs. Since the GMMs are based on simulated motions, it is straightforward to develop the appropriate conversion relationship by running the simulated time series through a Wood-Anderson response and calculating M_L for the simulated records. In this way, you could develop an M_L - M relation that is internally-consistent with the simulations used in the GMM development. We recognize that this would likely be a V5 model task.

This is a good suggestion and has been investigated by implementing the V5 GMM using Random Vibration Theory. We found that the results of the empirical model presented in V5 Appendix II are consistent with those using the V5 GMM (Figure 2.7). The RVT simulations predict a stronger bend at low magnitudes, but this analysis seems to support the use of $M = M_L$ for $M > 2.5$ and below this $M > M_L$. Note that simulations are carried out at the NS_B. Differences in M_L may be expected due to amplification and attenuation effects between the NS_B and the -200 m borehole level where M_L is typically measured.

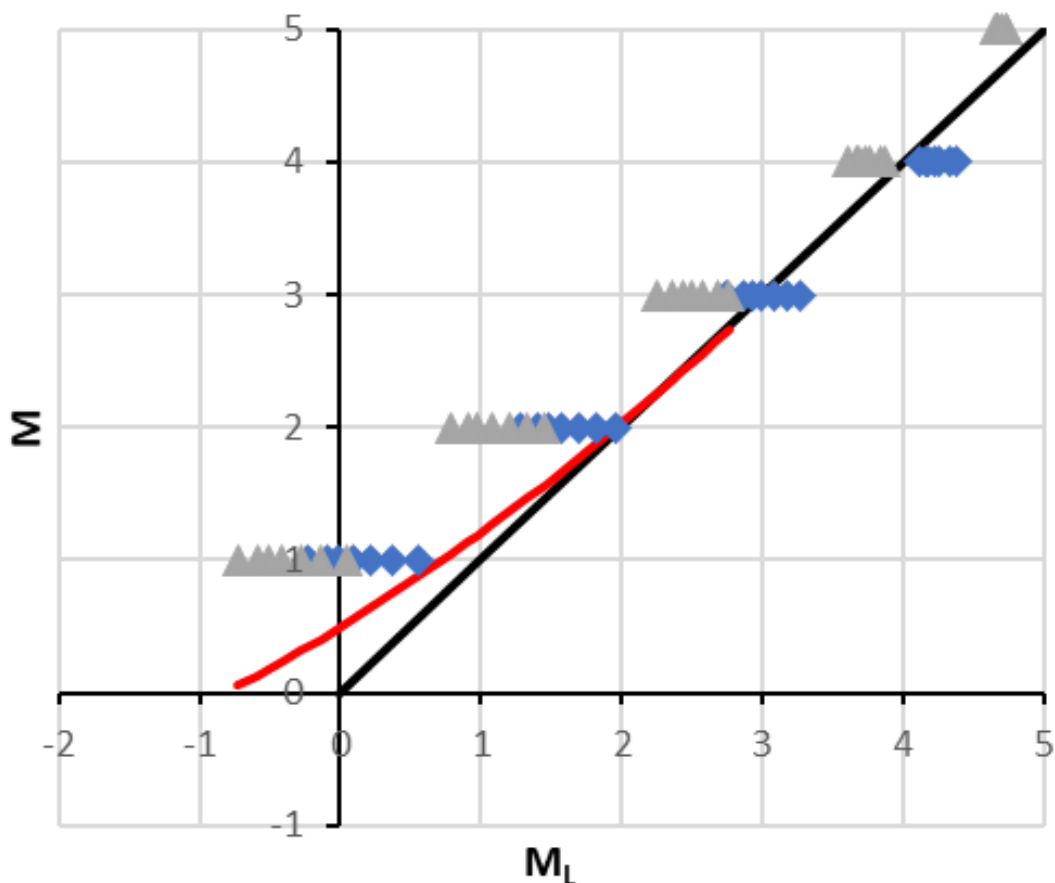


Figure 2.7. M_L calculated using the standard KNMI equations for events of magnitude M simulated with the V5 GMM at the NS_B. Grey: 7MPa, blue 14 MPa. Red line: $M:M_L$ equation in Appendix II of the V5 GMM

Comment M2 noted the trade-offs between parameters that inevitably result from the inversion procedure. There is a connection between that general issue and the magnitude conversion. The initial decay rate of amplitudes is strongly dependent on the \mathbf{M} values used in the inversion, as noted by the authors. For example, the V3 model assumed $\mathbf{M}=\mathbf{M}_L$ and got a steep decay in the first 7 km, $R^{-1.7}$; by contrast, V4 assumes $\mathbf{M}=\mathbf{M}_L-0.2$ and gets $R^{-1.2}$. This is an unfortunate coupling between the $\mathbf{M}-\mathbf{M}_L$ conversion and geometric spreading that has a large impact on amplitudes in the first 7 km, which are important. This coupling is not necessary. A calibration constant could be used to level the source amplitudes to the moment constraint. Or, equivalently, another hinge could be added at 2.5 or 3 km, with a decay from the epicentre to the source that would be fixed in such a way as to force the source amplitudes to agree with the moment (i.e. a leveling hinge). This would uncouple the near-distance attenuation of amplitudes on the surface from the values of \mathbf{M} , and thereby allow a more accurate representation of the amplitude decay at close distances that is predicted by the theoretical modeling.

The reality is that there is little reliable evidence for the slope of the geometrical decay in the first 3 km hypocentral distance (i.e., within the subsurface). We agree that, ideally the full waveform simulations could be used to determine this – however, all evidence so far points to the fact that such simulations, whilst informative, are highly variable and depend on issues such as: source mechanism, source location, azimuth, degree of heterogeneity of the velocity model. The source features are not possible to forecast in the context – we attempted to determine an ‘average’ to overcome this. However, the overriding issue is the fact that the slope of the decay is strongly dependent on the heterogeneity of the velocity model. While the 3D model is amongst the best available, it still assumes sharp and regular impedance contrasts at lithological boundaries that may lead to over-estimation of wave-propagation effects (including the slopes of ‘decay’). The slope of the simulations was therefore – in this application – deemed unreliable. We nevertheless used the hinge points, which were generally constant across all modelling strategies.

The idea that we can impose an arbitrary hinge point at a distance below which we have data (i.e., $R_{hyp} < 3$ km) would indeed partly decouple the \mathbf{M} and 0-7 km decay (Figure 2.8). The reviewers should note, however that the coupling then simply shifts from \mathbf{M} and the 0-7 km decay to \mathbf{M} and the 0-3 km decay (where there is no data). Since we are not confident this would improve the model – and simply shifts the issue nearer the source, the strategy has not been implemented for V5.

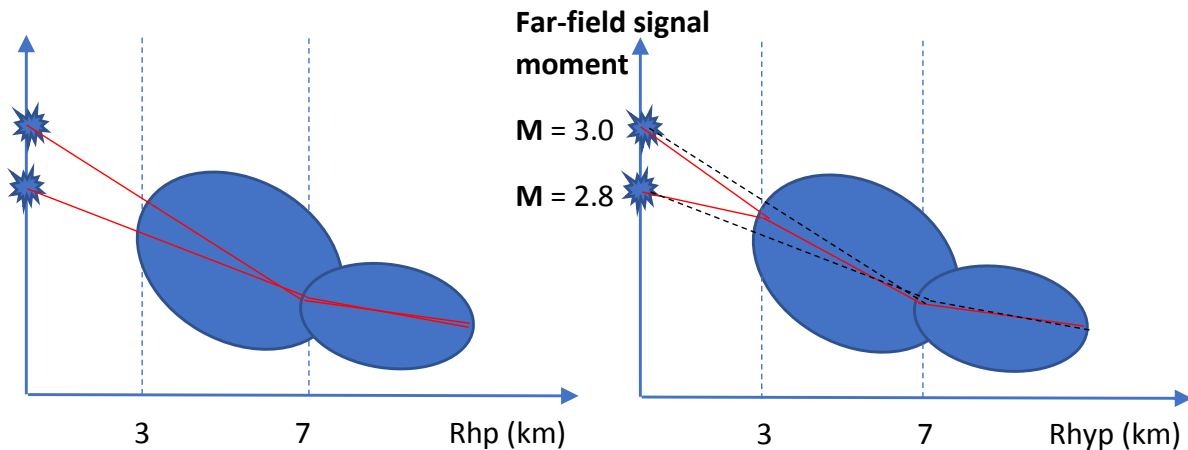


Figure 2.8. Schematic example of imposing an arbitrary hinge point at distance $R_{hyp} = 3$ km. *Left:* strategy using both data and M to determine decay 0-7 km. *Right:* strategy with 3 km hinge, decay 3-7 km defined by data alone, dashed lines show the decay from the left panel.

Based on comments in Chapter 13, we understand that M_L - M relationship will be addressed in the V5 model development. We hope the comments provided here are useful in planning that future work.

We are very grateful for the review comments, which have helped to direct this area of the model development. We believe that we now have a stable relationship between the two magnitude scales and indeed the only reason that this has seemed to be an unstable element of the modelling was the use of a preliminary estimate of the relation between M_L and M —since proven to be incorrect—in the derivation of the V4 GMM.

2.4. EXSIM documentation

There is a lack of information concerning the EXSIM simulations performed to develop the GMMs. Over what magnitude, distance ranges were they run? EXSIM has not generally been used for magnitudes <4 . Please provide specific values of magnitude, distance, number of subsources, etc. for the EXSIM simulations.

For each of the model branches (lower, central a/b, and upper), response spectra were simulated using EXSIM_dmb for 2100 scenario events with $M = 2.0$ to 7.0 in steps of 0.25 . For each scenario event a median and random epsilon was selected to define the length and width of the rupture (within the 3-13 km seismogenic depth). Recording locations were placed radially above the centre of the fault's top edge at 0 km and then 25 distances logarithmically spaced between 1.0 and 79.5 km. For each distance 8 sites were located, at 0 to 315 degrees (in 45 degree steps). In total 1.75 million response spectra were calculated, or 436,800 for each of the model branches. Further parameter settings are detailed in the V5 GMM (Table 3.1), and reproduced here in Table 2.1 for convenience.

Table 2.1. EXSIM_dmb parameter values used in simulations for NS_B motions

Parameter	Symbol (units)	Value(s)	Notes
Density	ρ (g/cm ³)	2.6	
Shear-wave velocity	β (km/s)	2 3.5	M \leq 4.5 (in reservoir) M \geq 5.5 (Carboniferous)
Horizontal partition		0.707	
Radiation coefficient	θ	0.55	
Free surface	F	2	
Sub-fault source type		Brune (1970, 1971) ω^{-2}	
Top of rupture depth	Z_{top} (km)	3	
Seismogenic depth	Z_{seis} (km)	13	
Fault dip	Dip (degrees)	75	Average of observed 60 – 90 degrees.
Fault mechanism		Normal	
Fault width	W (km)	$\min(W(W\&C'94), [Z_{seis}-3]/\sin(\text{dip})]$	W(W&C'94): Width from Wells & Coppersmith (1994)
Fault length	L (km)	$L(W\&C'94)*(W/ W\&C'94)$	L(W&C'94): Length from Wells & Coppersmith (1994) Conserve area of fault A given by LxW in case limited by Z_{seis}
Hypocentre location	H($\Delta L, \Delta W$) (km, km)	Random, 0	Located randomly along strike, at 3 km depth (top of fault).
Slip velocity	V_{slip} (km/s)	0.8β	
Stress parameter (Lower, Central, Upper)	$\Delta\sigma$ [M \leq 3.4] (bars)	50, 70, 70, 100	Linear interpolation of $\log(\Delta\sigma)$ with M
	$\Delta\sigma$ [M \geq 5.0] (bars)	75, 140, 220, 330	
Geometrical spreading distances (R_{hyp})	R1, R2, R3 (km)	7, 12, 25	
Geometrical decay rates	$\lambda_1, \lambda_2, \lambda_3, \lambda_4$	-1.55, -0.23, -1.43, -1.00	
Path attenuation	Q	220 600	M \leq 4.5 (in reservoir) M \geq 5.5 (Carboniferous)
Site attenuation	κ_0 (s)	0.010	
Source duration	T_s (s)	$1/0.4906\beta(\Delta\sigma/M_0)^{1/3}$	SI units
Path duration for sub-fault signals	T_p [R (km)]	$T_{5,75}/0.383$	V3 Groningen $T_{5,75}$ model for M = 3.0, V_{s30} =1500.
Rise time	T_s (s)	$1/f_0$	
Site amplification	A(f)	Network average NS_B	
Dynamic, pulsing percentage		50%	
Sub-fault averaging		RMS	
Scaling		(Acceleration FAS) ²	

The reviewers note that EXSIM is generally not used for events below **M** = 4. This is correct, probably because it is slower than SMSIM being limited to time-domain runs. It is also worth noting that in the past EXSIM did not produce output that was consistent with SMSIM for point source (small) events. This issue was resolved by Boore (2009), who modified EXSIM—hence our use of this modified version:

EXSIM_dmb. We believe both EXSIM and EXSIM_dmb now both use the same correction. A comparison of EXSIM_dmb runs and SMSIM is included here (Figure 2.9) showing the conformity of the methods at $M < 4$.

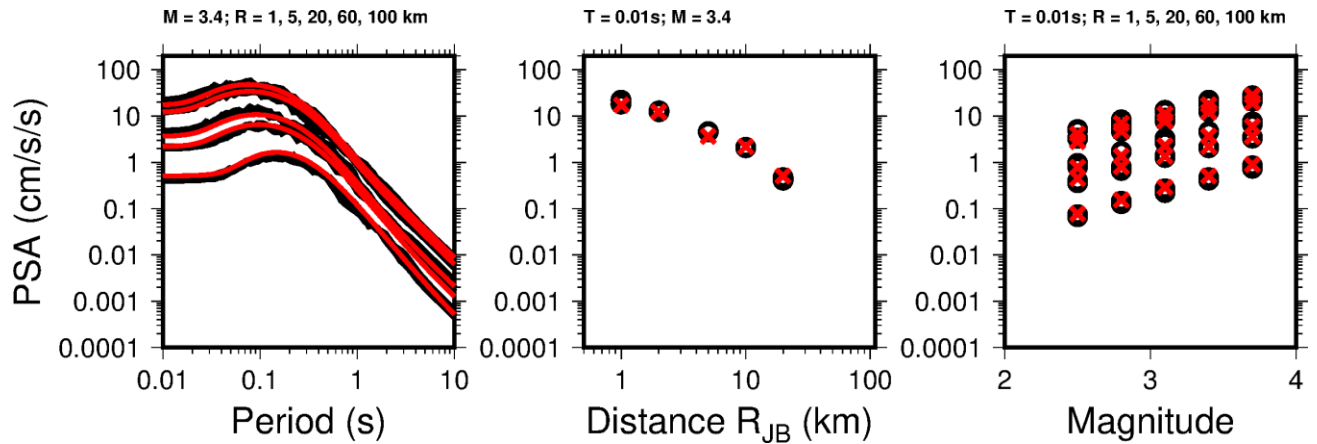


Figure 2.9. Comparison between EXSIM_dmb and SMSIM (RVT implementation) for an identical seismological model. Black: EXSIM_dmb; red: SMSIM (RVT). *Left*: PSA vs. period. *Middle*: PSA vs. distance. *Right*: PSA vs. magnitude. All for scenarios indicated above panels

A further question arises as to the level of sub-faulting required. A test of using 0.1×0.1 km sub-faults at $M = 4$ showed almost no difference to using a single sub-fault (Figure 2.4.2). The sub-fault size was therefore set to 1.5×1.5 km.

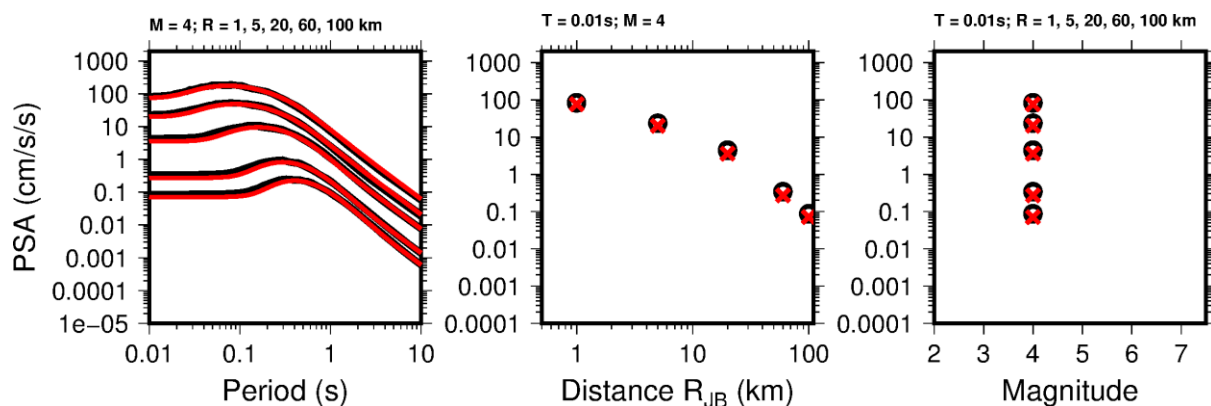


Figure 2.10. Comparison between EXSIM_dmb and SMSIM (RVT implementation) for an identical seismological model. Black: EXSIM_dmb; red: SMSIM (RVT). *Left*: PSA vs. period. *Middle*: PSA vs. distance. *Right*: PSA vs. magnitude. All for scenarios indicated above panels. 0.1×0.1 km sub-faults are used.

2.5. Fully non-ergodic model

The authors have developed a partially non-ergodic model by considering the effects of site-specific site response. This is commendable. However, the data compiled in this study might allow a fully non-ergodic model to be considered (including non-ergodic path effects). In the V5 model development, the authors could consider the spatially variability of their GMM following the approach of Landwehr et al. (2016, BSSA). An anisotropic path effects model could be set up to allow new data to update the model over time.

While we agree that this is most likely the direction that the Groningen model should evolve towards, we do not believe that we currently have sufficient data to constrain such a model. The development of the V4 model made use of a maximum of 178 records from 22 events, while the updated V5 model database had a maximum of 246 records from 23 events (with many of the additional records being made in boreholes).

Work is currently underway on two fronts that will potentially take us toward a fully non-ergodic model (at least a non-ergodic path and site model). On one front an extended database of recordings from both mobile temporary arrays and instruments housed in buildings is being compiled for the purposes of enabling a spatial correlation model to be developed. At the same time, detailed numerical simulations of ground-motion fields are being made from which spatial correlations are being computed. Naturally, if good agreement can be found between the correlations in the empirical and seismologically-simulated ground-motion fields then we can make use of the numerical simulations to separate out apparent spatial correlation from systematic path effects.

This is all work in progress and it was not possible to consider the Landwehr *et al.* (2016) approach for the V4 or V5 models.

Note that in order to get to a fully non-ergodic model we also need to obtain more information about the region-specific source effects. This is already proving challenging for the various small events that have been recorded, but is clearly far more challenging when forecasting region-specific behaviour of the as-yet unseen larger events that are entertained in the hazard and risk calculations.

2.6. Tau model

As shown in Figure ES.2, the tau model is directly linked to the median models through the stress parameter model used in the simulations. We have two concerns in this regard:

1. It is not clear that the model adequately represent epistemic uncertainty on τ . The statistical uncertainty on the estimates of τ from mixed-effects analysis could inform the epistemic uncertainty on τ independent of the median models. This would apply at small magnitudes where τ is constrained by data.

2. The use of the τ from small magnitude events to estimate this dispersion at large magnitudes is questionable. While the results shown in Figure 10.17 appear reasonable, but there should be a comparison to global and European models. Consideration should be given to applying alternate global models for τ at large magnitudes.

These issues would likely need to be addressed in a V5 model.

The use of statistical uncertainty to constrain epistemic uncertainty in the between-event variability is made problematic due to the relatively small numbers of events. For the well-constrained short period ordinates the coefficient of variation in between-event variability is around 35% while it increases to around 60% for the largest ordinates (the specific numbers depend upon the stress drop branch and the response period considered). An additional issue that we face for this particular statistical dataset is that the magnitude values are concentrated in a region where site effects actually have a strong impact upon the apparent magnitude scaling of the models. It is therefore not entirely clear to what extent the epistemic uncertainty should be placed directly upon source parameters or upon site components in order to represent the apparent between-event variability.

Most studies of tectonic motions suggest that between-event variability decreases with increasing magnitude. Our model takes the estimates constrained by the small magnitude events and holds the level of this between-event variability constant in projecting to larger magnitude events. If the previous tectonic studies are correct, then this should suggest that our estimates of between-event variability are conservative for the larger events.

Making a direct comparison with global and European models reveals that our V4 and V5 between-event variabilities are quite significantly lower than those of the European models and slightly lower than those of the NGA models (as represented by the Boore & Atkinson, 2008, model) – see Figure 2.11. For periods of greatest interest to the risk model, the V5 model has between-event variability that is typically higher than the V4 model, and so is closer to the tectonic levels suggested by the Boore & Atkinson (2008) model. We entirely expect to have lower between-event variability than these generic regional/global models because of the field-specific nature of our dataset. However, it is very difficult to know, or to estimate, how far below these tectonic models we should be.

That said, if we make use of statistical uncertainty from the mixed effects formulation to inform possible levels of epistemic uncertainty in the between-event variability then we would need to entertain the possibility of levels of between-event variance that are significantly greater than fully ergodic regional models. We believe that this is excessive given the very regional nature of our study and the fact that elsewhere we are assuming that all events originate from the same depth.

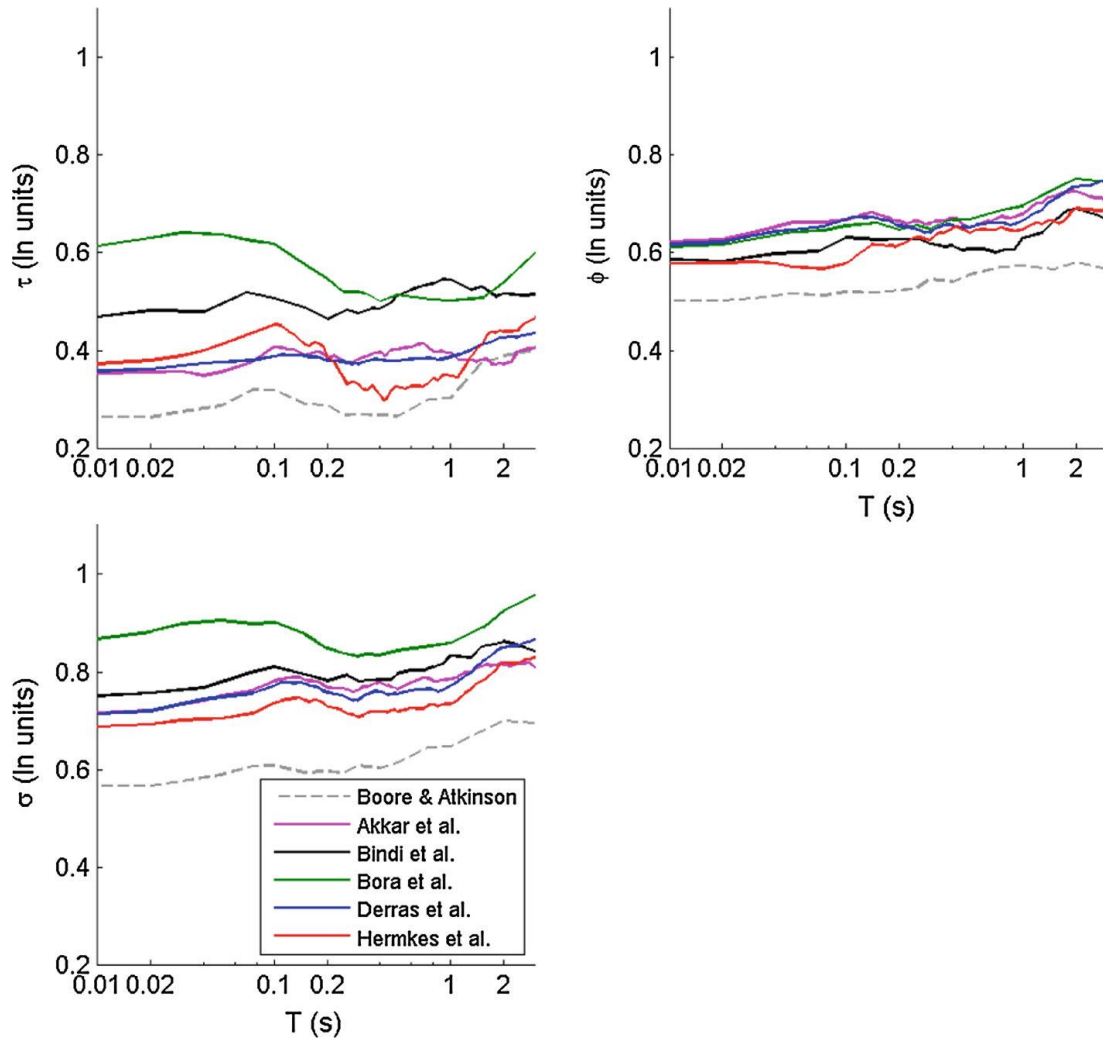


Figure 2.11. Comparison of variance components in recent European ground-motion models, including the Boore & Atkinson (2008) levels for reference. From Douglas *et al.* (2014).

It should also be noted that our estimates of the between-event variability take into account factors such as magnitude uncertainty, spatial correlations and random effects for individual stations. The levels of variability that people are used to seeing usually do not consider any of these effects and the between event variabilities that are typically published are excessively high as a result (even without accounting for the ergodic effects).

In summary, we feel that our dataset is still not rich enough to enable estimates of statistical uncertainty to inform levels of epistemic uncertainty in the between event variability – especially at long response periods. Additionally, it is difficult to make direct comparisons between our estimates and published values from regional and global studies because of the fact that these studies use a quite different (and much simpler) approach to estimating variance components (and their estimates are usually over-estimated).

Sec 6.5, statistical analysis to reduce τ (p 109-118). This section describes regression methodologies used during residuals analyses. A random effect was added to address the uncertainty in earthquake magnitude. This approach allows magnitude errors to be removed from the event term (and τ); however, the true magnitude for the earthquake must be the same be the same for all spectral periods. There are several methods that can be used to do this. For example: (1) expand the covariance matrix to include all spectral periods at once, or (2) run the periods separately, then find the best (average) true magnitude for all periods, then re-run each period using a fixed best magnitude. Approach (1) leads to a much larger covariance matrix that can be difficult to converge. Approach (2) has been applied for the California subset of the NGA-W2 data base by Kuehn and Abrahamson (2017).

The text does not discuss this issue. Based on the formulation in the report (Eq. 6.15), it looks like the regression is run with magnitude uncertainty that is independent for each period. In this case, the corrected magnitude will be different for each period. This leads to too large of a reduction in τ . That is, if a single best magnitude was used for all periods, then the period-to-period differences in the magnitude uncertainty would go back into the event terms and increase τ .

Both of the above comments are very closely related and so are responded to collectively. The approaches suggested by the reviewers were explored during the process of developing the V5 ground-motion model. The primary issue associated with the simultaneous consideration of all periods is the need to impose the between-period correlation structure for each level of the hierarchical model. That is, we need to define inter-period correlations for the within-event residuals, the between-event residuals and the between-site residuals – all at the buried NS-B horizon. The analyses conducted needed to make assumptions about these correlations that cannot be verified, but are clearly questionable. Essentially the same inter-period correlation model was used for all levels of the model so that the total inter-period correlation is consistent with that used in the risk calculations.

Following the approach of Kuehn & Abrahamson (2017) is computationally more straight-forward, but neglects these inter-period correlations and so is not directly comparable. Figure 2.12 shows the estimates of the magnitude random effects that are obtained following the Kuehn & Abrahamson (2017) approach. The idea that is that after computing the mean random effects across all periods that these can then be fixed (effectively changing the magnitudes of the events) and the variance partitioning can be repeated. However, upon doing this, the current data set (maximum of 246 records from 23 events per period with the longest period having just 30 records from 11 events) gives results that simply cannot be supported – almost all of the between-event variability is mapped over to the magnitude random effects. For comparison, the Kuehn & Abrahamson (2017) approach was applied to 5719 records from 184 events and with minimum numbers of records per event being imposed.

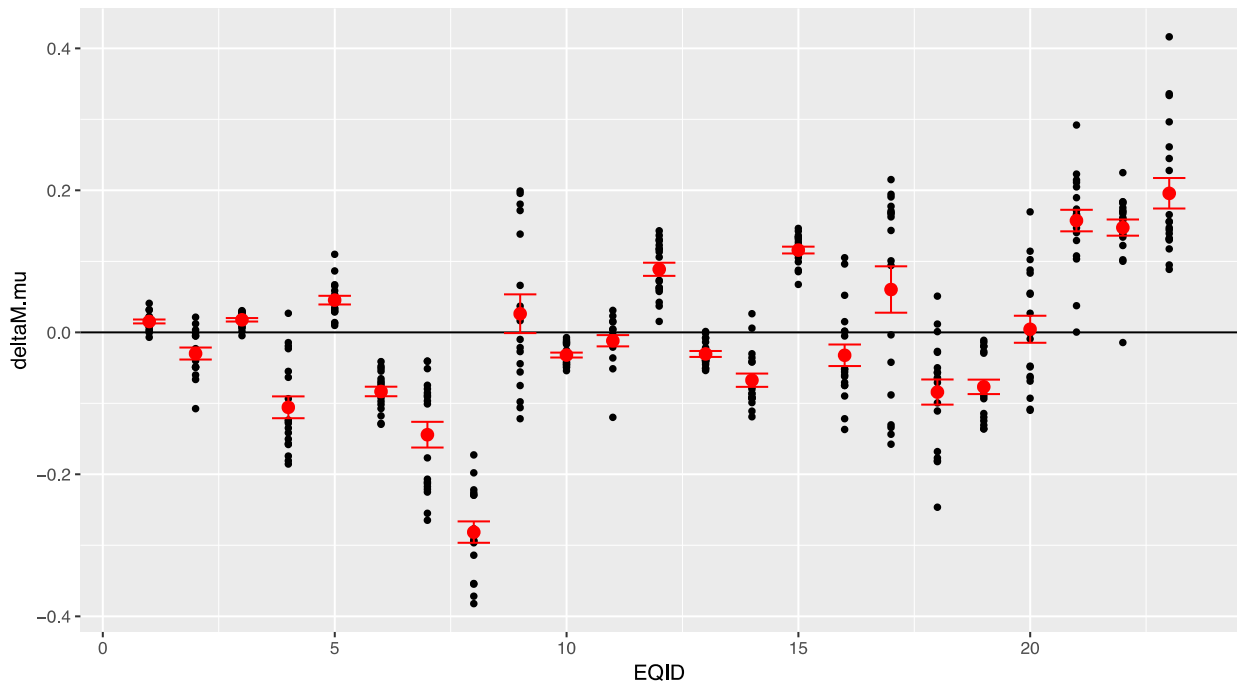


Figure 2.12. Estimates of the magnitude random effect for each event computed on a period-by-period basis (black dots) along with the mean estimate across these periods (red markers and error bars).

The primary issue is associated with the way in which the regression analysis is performed. The concern of the reviewers is that but not enforcing the same value of the random effect for magnitude (and site) for each event (and station) that we will be allowing too much freedom for the magnitude random effects to ‘steal’ variability from what should be allocated to the between-event variability. However, in our approach this does not happen. Although the random effect for each magnitude can vary from period to period (as seen in Figure Y), the actual variability in the magnitude random effects is still fixed at a known amount. Therefore, while the actual random effects can assume unrealistic values by varying across periods, the variance estimates themselves are constrained. Therefore, if the magnitude uncertainty is set to be 0.2 for a given event, then the variance decomposition will force this to be equal to this value regardless of what the actual random effect ends up being. For the Markov-chain Monte Carlo based approach adopted for the V5 model (which is the same as the approach adopted for the V4 model) this has been verified using synthetic data with known variance contributions.

At any given response period we have the total variability defined by our total residuals. Unlike the Kuehn & Abrahamson (2017) approach, we are not solving for the parameters of our median model, our model is effectively fixed by the EXSIM simulations. We then partition this total variability among the between-event, between-site and within-event components while reserving a fixed known amount that is associated with the effects of the known magnitude uncertainty.

The original review comments above were made in response to the approach adopted in the V4 model. After a significant amount of testing, including following the approach advocated by the reviewers, we reached the conclusion that our original approach was not underestimating the between-event variability.

We recommend that the report explain how the magnitude uncertainty was treated for different spectral periods.

In light of the above investigations, the variance partitioning was therefore maintained on a period-by-period basis and again considered the effects of individual magnitude uncertainty, random effects for both event and station and spatial correlation effects. The full individual magnitude uncertainty is forced to be sampled from each event.

The addition of new records to the V4 dataset actually meant that the between-event standard deviation increased from the V4-V5 models. The reason for this can, at least partly, be explained by looking at the systematic bias in the random effects from the most recent events in Figure 2.12. This effect may be related to differences between surface and borehole recordings, but is an issue that needs more time and recordings to be resolved. However, the change in the between-event variability has not arisen as a result of us having changed the regression methodology.

2.7. Event depths

All events are assumed to originate at 3 km. Please reference a source document with a summary of seismicity to justify the depth. What is the thickness of the reservoir? Is there a related range about the 3 km? One of the panel members on the source working group (Wong) thought events were relocated, which led to some events occurring below the reservoir.

The gas reservoir ranges in thickness from about 150 to 300 m, but in some locations is offset by faults by up to one reservoir thickness. The depth to the top of the reservoir also varies slightly across the field, but 3 km is assumed as an average depth of the gas-bearing Rotliegend sandstone layer that holds the gas reservoir. Considerable effort has been invested in re-locating the hypocentres of Groningen earthquakes and these studies have all converged to placing the hypocentres within the reservoir. The Dutch seismological service, KNMI, has performed its own re-locations and published the results in *Geophysical Journal International* (Spetzler & Dost, 2017). They conclude that at least three-quarters of the earthquakes re-located in their study are located within the Rotliegend, with a fifth of the events possibly in the underlying Carboniferous just below the base of the reservoir. However, the

reported depths for those events are such that within the range of variation of the reservoir depth and thickness, location of the hypocentres within the reservoir cannot be precluded. A small number of events were also located at shallower depths, presumably within thin and brittle anhydrite layers within the overlying Zechstein salt; however, these events are of very small magnitudes (well below the lower limit considered in the GMM development). There is high confidence and general agreement that the events of relevance to the hazard and risk modelling ($M_L \geq 2.5$) are located within the reservoir, but no attempt has been made to refine these depths or to randomize the depths in the forward modelling.

Has the significance of the assumption that rupture proceeds downward from 3 km been considered? We understand this detail of the source modeling was discussed in source characterization workshops – please reference suitable documents to justify this assumption.

Absolutely. The Mmax workshop concluded that earthquakes of up to magnitude 5 would occur primarily as ruptures within the reservoir (*i.e.*, induced events) whereas larger magnitude earthquakes (*i.e.*, triggered events) would be associated with ruptures propagating downwards into the Carboniferous. This is reflected in the source modelling for the simulations by setting reservoir parameters ($\beta = 2$ km/s, $Q = 220$) for smaller events ($M \leq 4.5$) and parameters appropriate to the Carboniferous rock ($\beta = 3.5$ km/s, $Q = 600$) for large event ($M \geq 5.5$), with linear transitions between these values over the intervening magnitudes; this is indicated in Table 2.1.

2.8. Use of H/V spectral ratios

Chapter 4 describes the characterization of ground motion recording sites, which is based on site-specific measurements in the upper 50 m and regional models at larger depths. Since some of the measurements were based on MASW methods, there is a good chance that H/V spectral ratios could be computed, from which the fundamental period of the recordings site could be obtained. These periods could be compared to those implied by the V_s models, thus providing valuable calibration.

We concur with that exploring the relationship between the fundamental periods of the recording sites inferred from the H/V ratios of ground-motion recordings and from the calculated transfer functions is a useful calibration exercise. Kawase *et al.* (2011), for example, have shown that the horizontal-to-vertical ratios of the Fourier amplitude spectra (FAS) of recorded ground motions are related to the transfer functions for the site, and in the PEGASOS Refinement Project this approach to identifying the site period was found to work very well in many circumstance (Renault *et al.*, 2014). Instead of the MASW recordings, we used the time-histories from the ground-motion recording stations. Figure 2.13 shows two examples of the comparison of H/V ratios, averaged over several recordings, with the transfer

functions, from which it can be appreciated that there is very good agreement in terms of frequency associated with the peak.

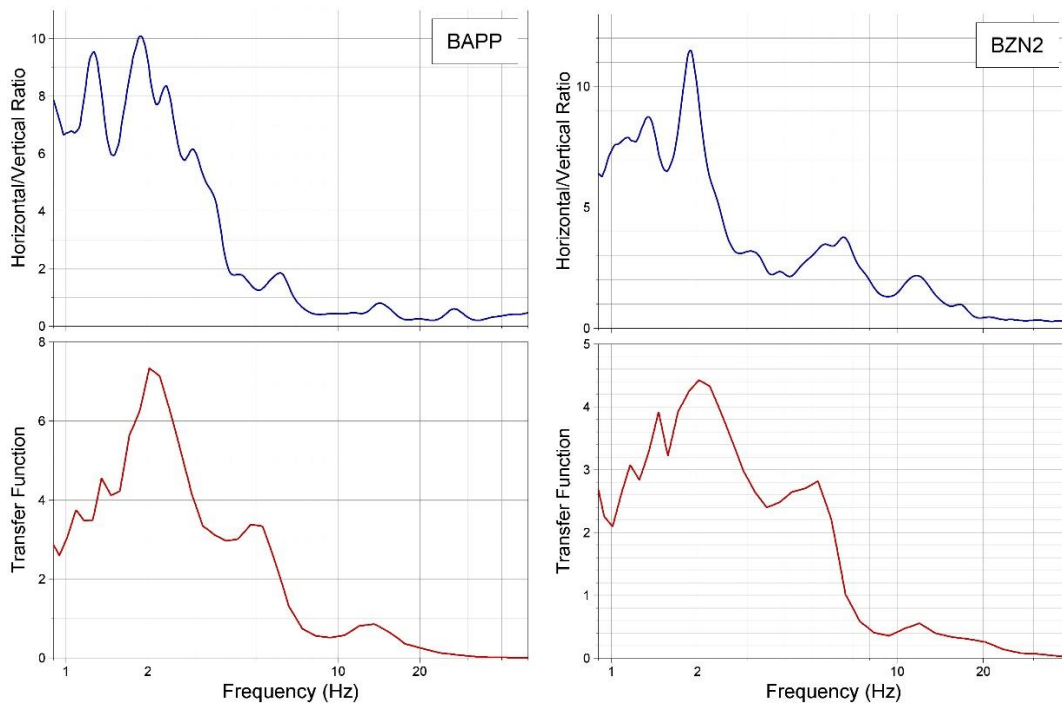


Figure 2.13. Comparison of average H/V ratios of the FAS from several recordings (*top*) with the transfer functions (*bottom*) calculated for two of the surface accelerograph stations

Figure 2.14 summarises the results for all of the B-stations, comparing the frequency of the H/V peak with the frequency associated with the peak of the transfer function. The agreement between the two estimates of the dominant frequency is generally good: for about a third of the stations, the difference is not more than 10%, and for half of them it is within 15%. There are only four stations for which the dominant frequency of the transfer function differs by more than 30% from the frequency of the H/V peak. Two of these are shown in Figure 2.15, from which it can be appreciated that there is a strong peak on the calculated transfer function (TF) for BMD2 that does match the H/V ratio, but there is a second peak of very slightly higher amplitude. At BGAR, again there are peaks that match in frequency, but there is a second—and much stronger—peak on the H/V ratio.

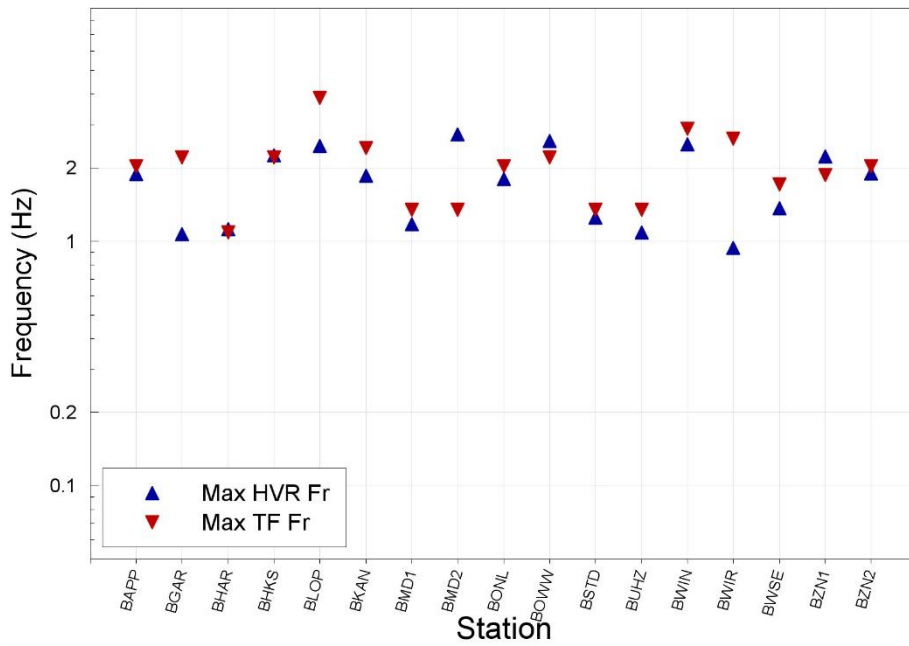


Figure 2.14. Frequencies associated with peaks of H/V ratios (*blue*) and TFs (*red*)

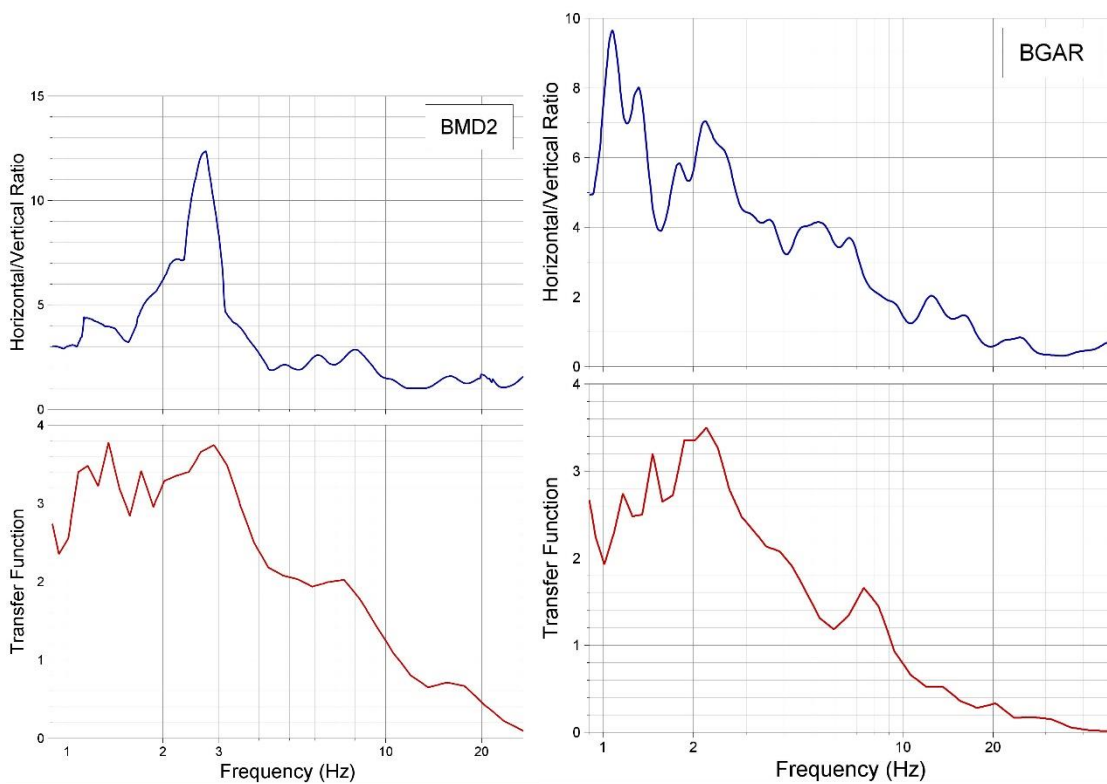


Figure 2.15. Comparison of average H/V ratios of the FAS from several recordings (*top*) with the transfer functions (*bottom*) calculated for two of the surface accelerograph stations

For the G-stations, we are fortunate to be able to refer to independent work conducted at Stanford University under funding from Shell (rather than NAM). The

work presented by Spica *et al.* (2018) uses passive noise recordings from the G-station accelerographs and from the geophones at 50, 100, 150 and 200 m depth. The work is based on interpreting the H/V spectral ratios from these recordings in terms of the Diffuse Field Assumption, which links the ratios to retrieval of Green's functions through autocorrelation of the ambient seismic field. Combining H/V inversion and borehole interferometry, they obtain V_s profiles at the G-stations down to 200 m depth Figure 2.16).

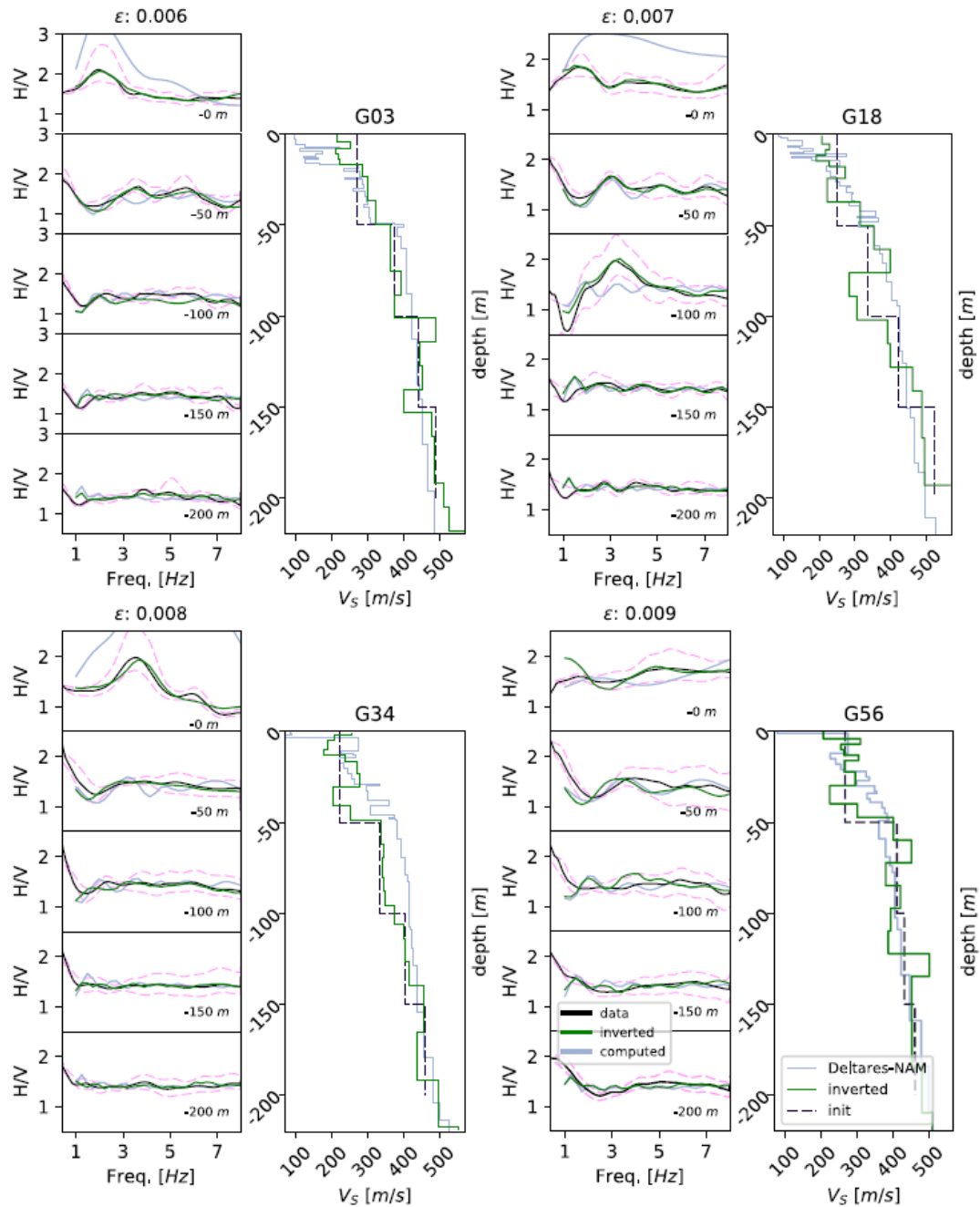


Figure 2.16. Results from Spica *et al.* (2018) for four G-stations. In each case, the left-hand plot shows the recorded (*black*) and inverted (*green*); the right-hand plots show the V_s profiles obtained from their analysis (*green*), their starting model (*black, dashed*) and the model from the NAM model (*cyan*) of Krüver *et al.* (2017).

Spica *et al.* (2018) note the generally good agreement with the velocity model developed from the GeoTop model for the construction of the GMM: “We successfully obtained complex V_S velocity profiles of the shallow sub-surface at different borehole sites in the Groningen area. Velocity models are globally in good agreement with previous site characterization for the region (Kruiver *et al.* 2017).” They also note that the agreement is excellent at depths of 100 m and greater, but that at shallower depths the two studies find similar trends—“that is, some high contrast with a higher local velocity at approximately the same depth”—it is also noted that V_S values from the two models differ by up to a factor of two. For us, this observation vindicates the choice to use the 200 metre-geophone recordings from the G-stations rather than the surface accelerograms in order not to rely on deconvolutions obtained using transfer functions calculated from shallow velocity profiles that were not confirmed by measurement.

It could be that a site amplification model that uses V_{S30} and site period would be of equal value to, or better than, the zonification models.

The choice to use 1D site response analyses throughout the entire Groningen field was dictated by the desire to capture subtleties of the site response that could not be captured by the use of simple proxies, such as V_{S30} and site period. While proxy-based models can replicate site response trends, a full 1D site response analysis is able to capture details of the site response that are not amenable to a simple parameterization. This is particularly the case for the Groningen site where amplification at some frequencies can be controlled by resonances of shallower portions of the profile, while at other frequencies site response is controlled by resonances of deeper portions of the profile. This would necessitate the use of different pairs of proxies for different frequencies, which would negate the simplicity of a proxy-based model.

However, the suggestion of the reviewers is valuable. We explore the reviewers’ suggestion by plotting the predictions of the parameters of the zonal amplification function model as a function of V_{S30} . Figure 2.17 shows the predicted linear amplification factors (AF) for $M=5$ and $R=10$ km. Observe that at most periods there is a strong correlation between the AF and V_{S30} . For longer periods, this correlation follows a linear trend in log-log space, as predicted by empirical models built into modern GMPEs. In fact, at some period (e.g., $T=0.6$ s), the fit is remarkable and it is clear that V_{S30} could have been used as a proxy for the zones’ AF values. However, at other periods (e.g., $T=0.1$ s) the scatter is large indicating that the use of V_{S30} would not have predicted the AFs as accurately as 1D site response analyses. As suggested by the reviewers, the scatter would have been somehow reduced by the use of site period, but even if site period is considered, the scatter remains high.

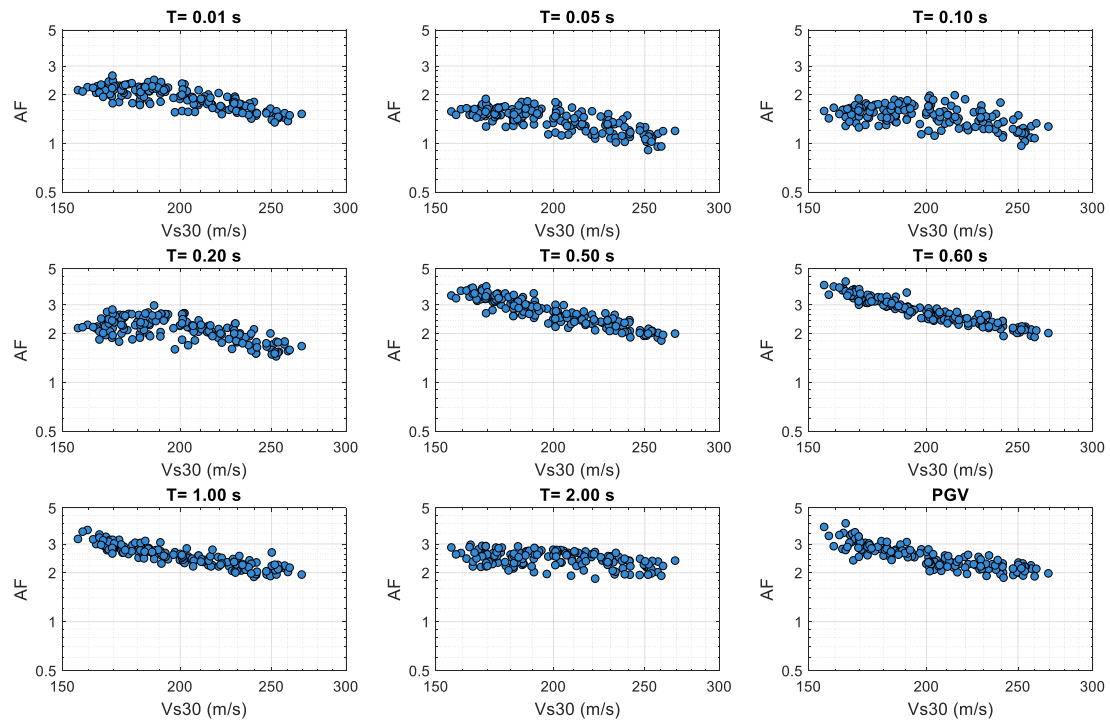


Figure 2.17. Zone amplification factors (AF) for selected periods plotted versus the V_{S30} of each zone. The AF are computed for $M=5$, $R=10$ km.

It is also important to note that the linear trend with V_{S30} is not valid for very soft zones at short periods. In these cases, the relationship between AF and V_{S30} could only have been determined from multiple site response analyses, hence negating the advantage of a simpler, proxy-based model.

Figure 2.18 plots the parameter f_2 as a function of V_{S30} . This parameter indicates the strength of nonlinearity: the more negative the value, the stronger the reduction of AFs as ground motion intensity increases. Observe that in some cases the trend with V_{S30} is clear, while in other cases there is large scatter, with large variations in the value of f_2 for a single value of V_{S30} . This scatter remains even after considering the site period as an additional parameter. The data in Figure 2.18 suggests that a V_{S30} model would have resulted in larger scatter for scenarios that induce strong nonlinearity. This is largely due to the fact that there is a range of soil types in the Groningen field which have distinct nonlinear behaviour (e.g., peats, clays, and sands). For this reason, the use of proxies alone could not accurately predict nonlinear behaviour since V_{S30} alone cannot serve as a predictor of soil type. The adoption of geologically-based zones allows for the grouping of areas that have commonalities in the soil composition, and hence reduces the predicted scatter in the prediction of AFs.

The limitations of a proxy-based model can also be shown by selecting zones that have common proxies, and comparing the predicted AFs for these zones. Figure 2.19 plots the predicted linear AF for $M=5$ and $R=10$ km for zones that have V_{S30}

values within 20 m/s, and site periods within 0.2 s. Note that even for this tight range of values, there is significant scatter in the AF, reinforcing the conclusions listed above. In fact, at $T=0.3$ s the AF varies from 2.2 to 3.1, despite the narrow range of values of the selected proxies.

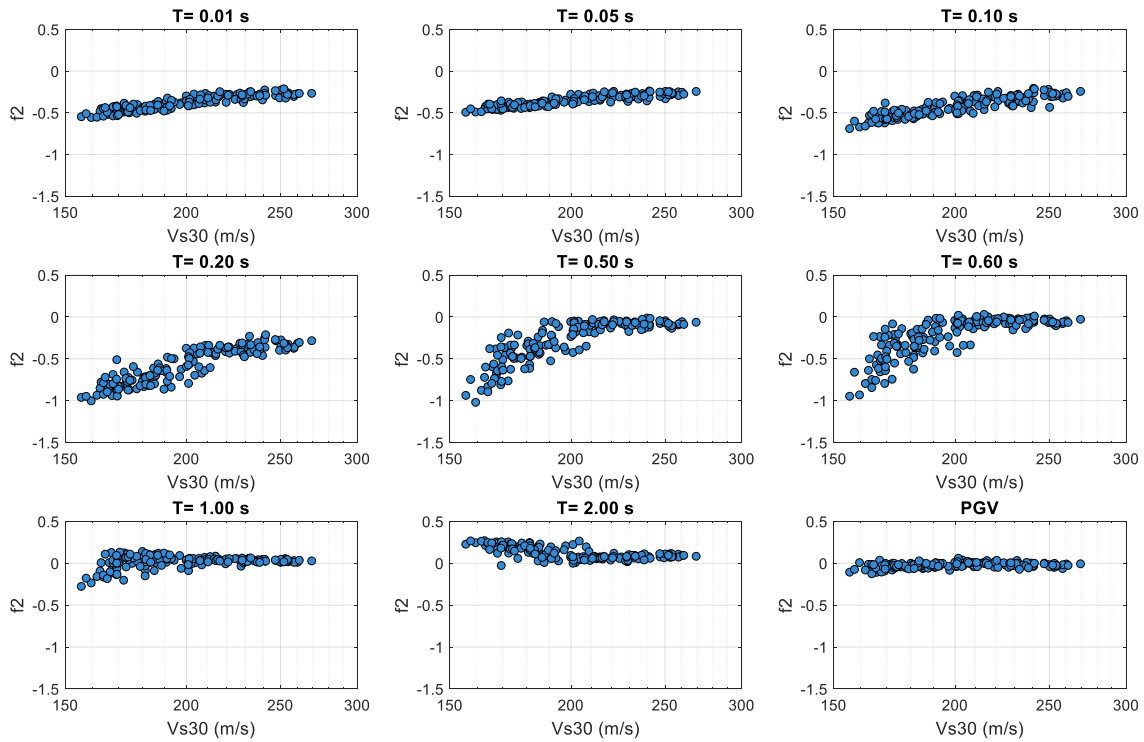


Figure 2.18. Parameter f_2 for each zone plotted versus V_{S30} of each zone.

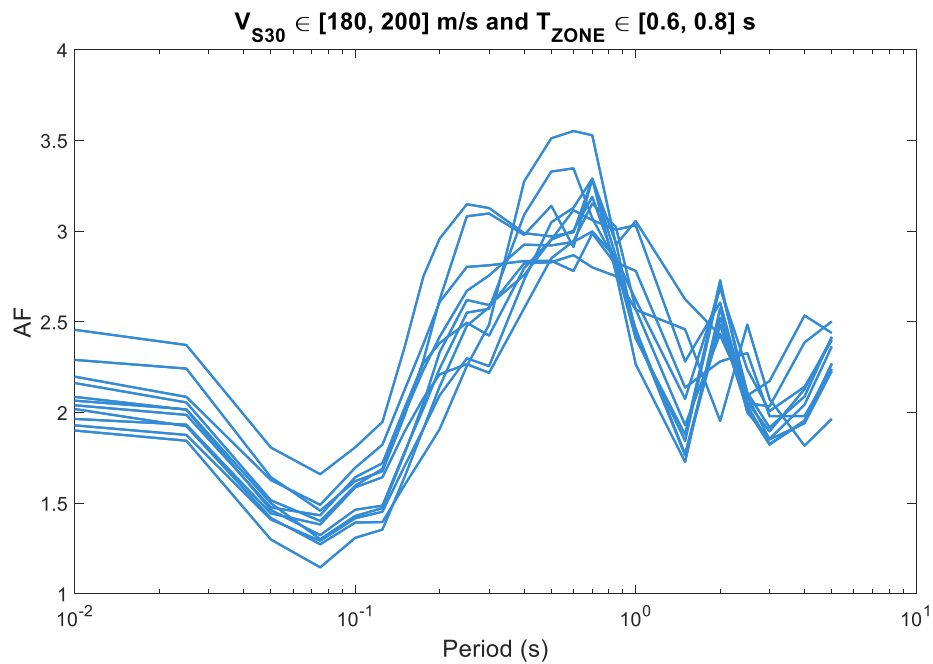


Figure 2.19. Linear AF versus period for zones that belong to the indicated range of V_{S30} and site periods (T_{ZONE}).

Taken collectively, Figures 2.17 to 2.19 could also be interpreted as indicating that a proxy-based model would do a decent job in predicting AFs for the Groningen field. Nonetheless, the selected approach captures details of the site response that are not captured by proxy-based models, and hence is considered more appropriate for capturing site effects across the Groningen field.

2.9. Soil shear strength as restraint on stress-strain backbone curves

In Chapter 7, a constant value of $N_k = 14$ is used to relate shear strength to CPT tip resistance. This parameter carries large uncertainty (approximate range of 10-50). Given that additional soil testing seems to be planned as future work, we recommend that shear strength testing (in situ vane shear or lab) be undertaken near sites of CPT soundings to set a material-specific value of N_k for the simulations. This could significantly impact ground response analysis results at large strains.

During the course of the project, laboratory data became available from the Eemshaven levee. Both OCR and S_u were determined for shallow sediments. These data were analysed and compared to the S_u and OCR data based on the CPT data set. The results are described in Section 4.1 of the GMM V5 report. In summary, the factor N_k was adjusted to 17 for Naaldwijk clay (see Figure 4.5 of the GMM V5 report, reproduced below for convenience as Figure 2.20).

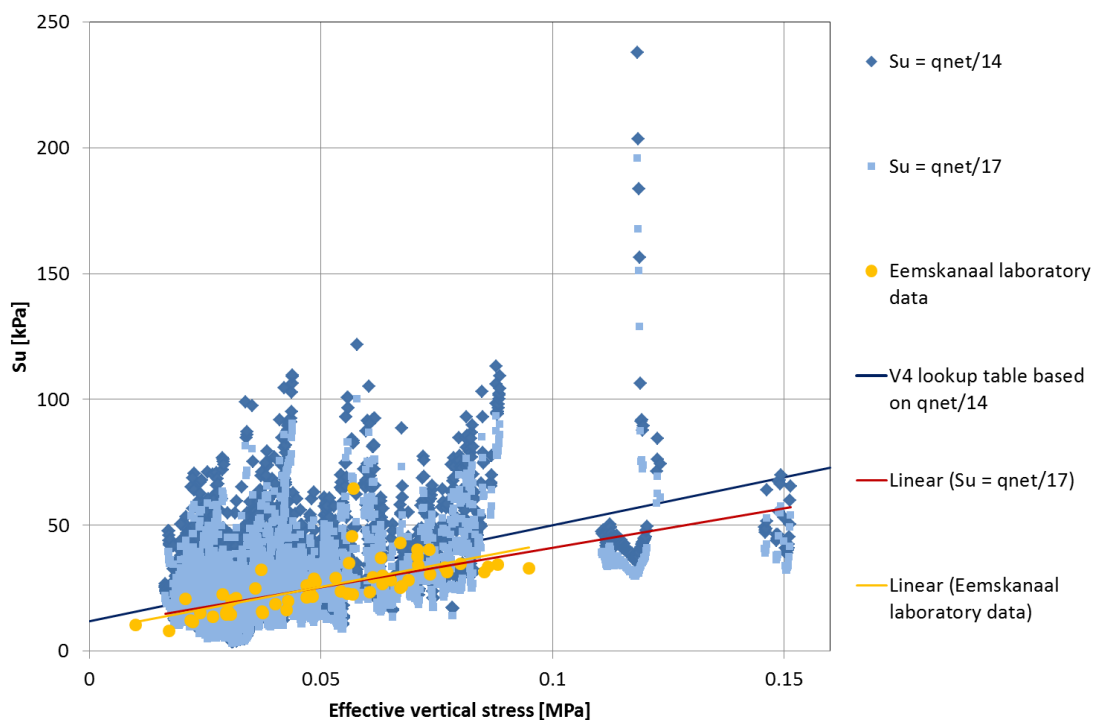


Figure 2.20. CPT derived and laboratory data for S_u for Naaldwijk clay (NA), including linear regression lines

For Holland peat and Basal peat, the laboratory data were used to convert effective vertical stress to S_u . The need to use N_k for these two soil types is no longer there. For other types of clay, the laboratory data were insufficient to justify a deviation from earlier assumed $N_k = 14$. Therefore, no changes relative to GMM V4 were made for clays, other than Naaldwijk clay. Additionally, the laboratory data for OCR were regarded as not reliable. Therefore, we did not use the laboratory data to adjust the geomechanic look-up table with respect to OCR.

We will monitor future developments in laboratory measurements in Groningen and include results in the geomechanical look-up table when new data become available.

2.10. Ground response analysis input motions

In Section 8.2, the use of SMSIM to evaluate input motions for ground response analyses is described. Why not use motions already computed for GMM development from EXSIM? Were the stress parameters used in the SMSIM simulations consistent with those used for EXSIM?

This was an error in the original V4 GMM report: the input motions are simulated using the same method (EXSIM) and parameters as used to calculate response spectra for the GMPE derivation.

2.11. Site amplification bias and implications for suitability of EQL analyses

In Sections 9.4 and 11.2, the authors document apparent bias in the site amplification model. This is attributed to differences between site-specific profiles used in inversion and zone-based profiles used for forward analysis. While we can understand that biases of this sort could be present for a given site, if the zonation is appropriate, these differences should average to zero across all of the sites. Accordingly, the presence of a persistent difference is concerning.

The biases discussed in Section 9.4 and shown in Figures 9.25 to 9.29 of the V4 GMM report (Bommer *et al.*, 2017c) were the result of a model that did not properly account for the magnitude scaling of short period amplification factors (Stafford *et al.*, 2017). The biases shown on these figures are strongly magnitude dependent. In fact, a close examination of these figures shows that the ratio is close to one for earthquakes with magnitude greater than 3.5. The bias for low magnitudes resulted from a mismatch between the magnitude-dependency of the amplification factors computed for the stations and those computed for the zones. The V5 GMM corrected for these biases (see Figure 4.11 and Appendix V in the V5 GMM report; this figure is reproduced below as Figure 2.21 for the convenience of the reviewers).

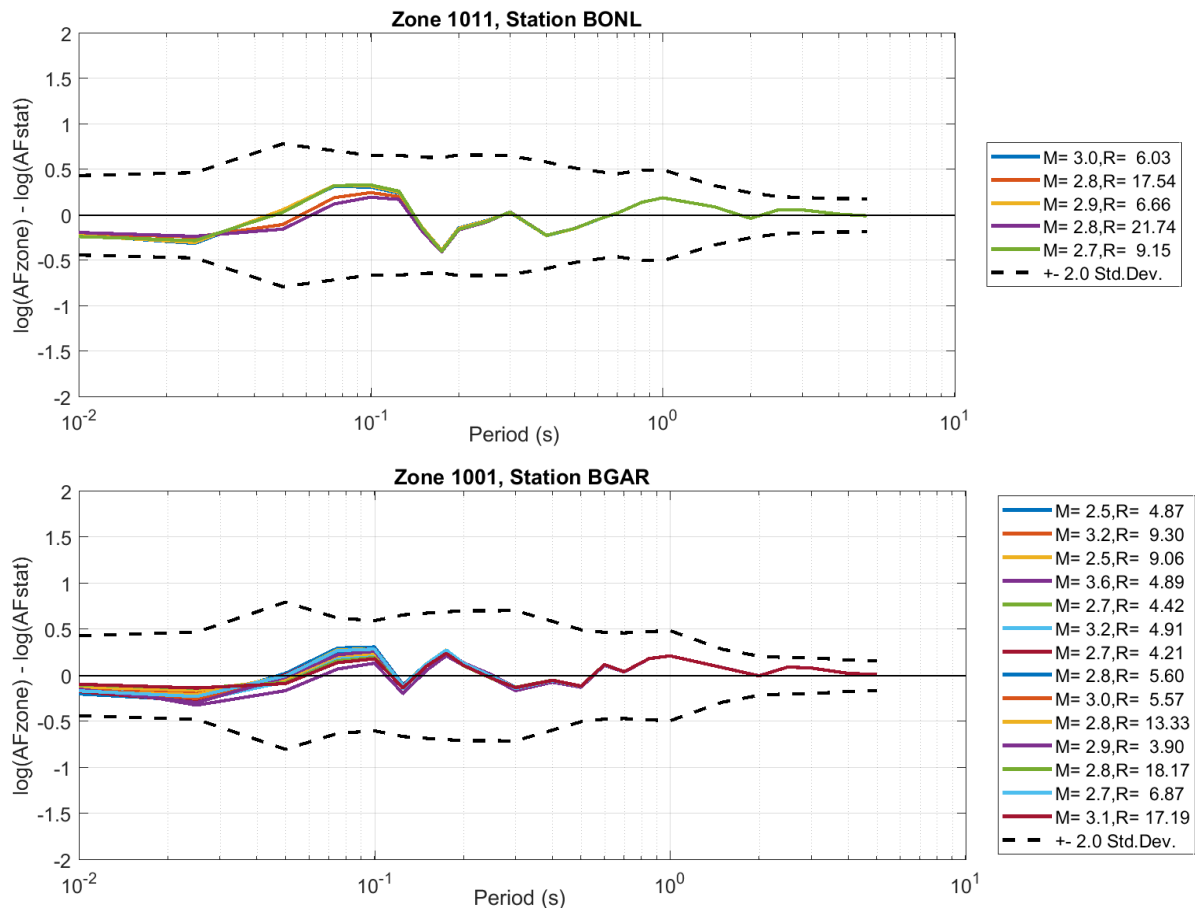


Figure 2.21. Comparison of linear AF for selected stations and the corresponding zone where the station is located. AFs are shown for the magnitude and distance pairs that correspond to recorded motions at each station.

The bias in the amplification functions had propagated to the residuals of the model, as pointed out by the reviewers and as discussed in Section 11.2 in the V4 GMM report. The corrections introduced in the magnitude (and distance) dependence of the amplification factors also removed these biases (see Figure 4.14 of the V5 GMM report).

It is interesting that the bias is only present for spectral accelerations at short periods. This is the same period range where equivalent-linear methods tend to be problematic relative to nonlinear methods. This leads us to wonder if zonation is really the cause of the problems, or perhaps this is an artifact of the equivalent-linear analyses being used for the forward analyses, which may be returning unrealistic spectral shapes. A visual assessment of the spectral shapes returned by equivalent-linear analyses can be made to judge whether the results may be unreliable (see Section 2.4.1 of Stewart et al. 2014).

The bias observed in the V4 model was largely due to issues with scenario dependence and it has been removed from the V5 model through refined modelling of that scenario dependence.

The comment of the reviewers regarding the potential limitations of equivalent linear analysis (EQL) is valid. Despite this, we have confidence in the results of the EQL analyses. We have done an extensive literature review (Section 8.1 in the V4 GMM report) to justify our choice of method. The shape of the amplification functions versus period also is compatible with the nature of the profiles. The nonlinear trends also match expected behaviour for very soft soils, with stronger nonlinearity at higher frequencies. However, we also acknowledge the potential limitations of EQL analyses and we adopt a relatively high model error as a lower bound to the site-to-site variability (Figure 9.11 in the V4 GMM report).

It is also important to mention that the primary reason to use random-vibration based EQL analyses is that the approach adopted by the ground motion characterization team requires a large number of site response analyses. To conduct these number of analyses would not be possible if more complex (*e.g.*, nonlinear analyses) were adopted. A secondary, but important, reason to use EQL analyses is that the correlation between damping and the high-frequency attenuation parameter κ_0 is straight forward in frequency-domain analyses, but not so in time-domain analyses. This is important because the approach adopted requires that the selected low-strain damping be compatible with a target value of $\Delta\kappa$ (*i.e.*, the additional high-frequency attenuation resulting from site response alone). This value can be computed using Eq.(7.20) of the V4 GMM report, repeated here for clarity:

$$\Delta\kappa = \int_0^{z_{rock}} \frac{1}{Q(z)V_S(z)} dz \quad (2.2)$$

where z is depth measured from the surface, z_{rock} is the depth of the elastic halfspace, V_S is shear wave velocity, and Q is the quality factor, which is related to small-strain damping D_{min} by:

$$D_{min} = \frac{1}{2Q} \quad (2.3)$$

As explained in Section 7.5 of the V4 GMM report, the damping in the profiles at the stations is selected such that, on average across the field, the damping matches the $\Delta\kappa$ values measured at the ZLV borehole. EQL analyses with the target values of D_{min} readily return the target values of $\Delta\kappa$. On the other hand, this is not the case with nonlinear methods because of numerical issues related to the modelling of frequency-independent damping.

We explored this issue by creating a V_S profile that matches the travel-time averaged V_S profile of the BKAN station, but with a lower number of layers (the choice of this particular station was arbitrary). We established a damping profile identical to the inferred profile at the ZLV down-hole array. For this case, the $\Delta\kappa$ computed using

Eq.(7.20) is 0.0346 s. We performed linear analyses in Deepsoil v7.0 (Hashash *et al.*, 2016) using the frequency domain and the time domain approach with frequency-independent damping. We then computed the values of κ from the high-frequency slope of the Fourier Amplitude spectra at the surface. The value of $\Delta\kappa$ was computed by subtracting the surface κ value from that of the input motion. The results for two input motions are shown in Table 2.2. The time-domain analyses clearly result in values of kappa higher than the target values. This is likely due to the approach used in Deepsoil to model frequency independent damping (Phillips & Hashash, 2009). We not that alternative damping formulations would have resulted in larger discrepancies.

Table 2.2. Values of $\Delta\kappa$ obtained for a synthetic profile with different methods and two input motions.

Input Motion	Analytical	Frequency-Domain	Time-Domain
Groningen motion (M=4.1, R=4.81km)	0.0337 s	0.0355 s	0.0437 s
Northridge EQ motion (M=6.7, R _{cl} =26.8 km)	0.0337 s	0.0343 s	0.0777 s

Obtaining consistent values of $\Delta\kappa$ for the profiles is important in order to have compatibility between the site response analyses and the treatment of κ in the seismological model used to develop the ground motion model at the NS_B boundary.

Another comparison that would provide insight into the suitability of equivalent-linear analyses would be to compare site amplification results derived from both equivalent-linear and nonlinear methods for at least to one site, using common sets of dynamic properties. Even if nonlinear analysis methods were ultimately not adopted in V5, this exercise would provide insight into the epistemic uncertainties associated with the equivalent-linear results.

We compared equivalent linear and nonlinear methods for two soil columns: one with Pleistocene sediments surfacing in the south of Groningen (Zone 320) and one with shallow Holocene sediments (Zone 2001). Site response analyses were conducted for 15 input motions using Deepsoil using the equivalent linear (EQL) option, the non-linear (NL) option with frequency-independent damping, and the linear (L) option. The modulus reduction and damping (MRD) curves of Darendeli were used for sands and clays, and the project-specific peat curve was used for peats. Both the EQL and the NL options were run with the same MRD curves. Results are shown for the input motions listed in Table 2.3. Note that Motions #1 and #15 are low intensity motions, while Motions 11 and 13 are strong input motions.

Table 2.3. Characteristics of input motions used in the comparison of EQL and NL site response analyses

Motion number in this analysis	Filename	M	R (km)	Motion rank	PGA at reference rock horizon (g)
1	m2.9r3.51z3.00n2527_u	2.9	3.51	2527	0.02
15	m7.0r31.93z3.00n2880_cb	7.0	31.93	2880	0.04
11	m6.0r4.81z3.00n3543_u_el	6.0	4.81	3543	0.27
13	m7.0r3.00z3.00n3599_u	7.0	3.00	3599	0.46

A comparison of the results is shown in Figures 2.22 and 2.23. Observe that for the lowest intensity motion (Motion 1) the EQL solution is consistently higher than the NL solution. This difference is higher for the softer (Holocene) profile. We attribute this difference to numerical damping in the NL solution. It is also possible that the frequency-dependent damping implementation does not work well for deep, soft profiles. This is further explored in paragraphs below. For the stronger input motions, we observe that the amplification functions (AFs) computed using EQL are consistently higher than those computed using the NL option. This is consistent with previous observations compiled in Section 8.1 of the GMM V4 report. These observations also justify the choice of the modelling team to limit the amount of model error because of the consistently observed biases of the EQL analyse with respect to the NL analyses (see Figure 9.11 and the accompanying discussion in the GMM V4 report).

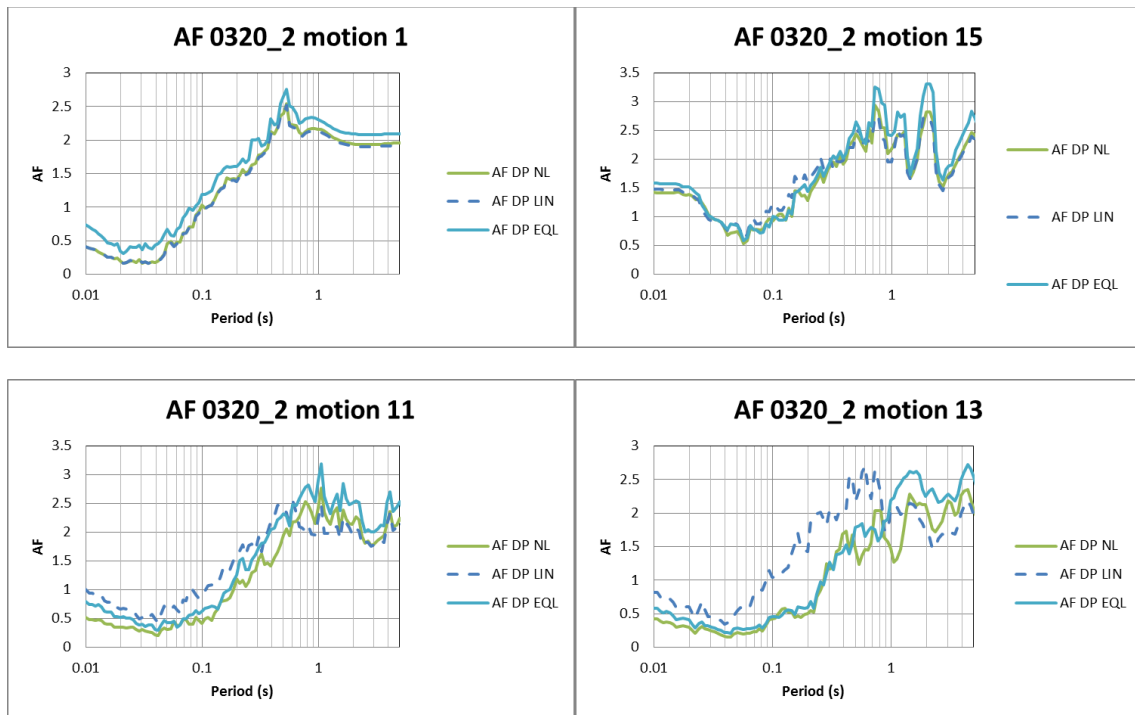


Figure 2.22. Results of linear (LIN), non-linear (NL) and equivalent linear (EQL) site response analyses for a profile in Zone 320. The analyses were run using Deepsoil.

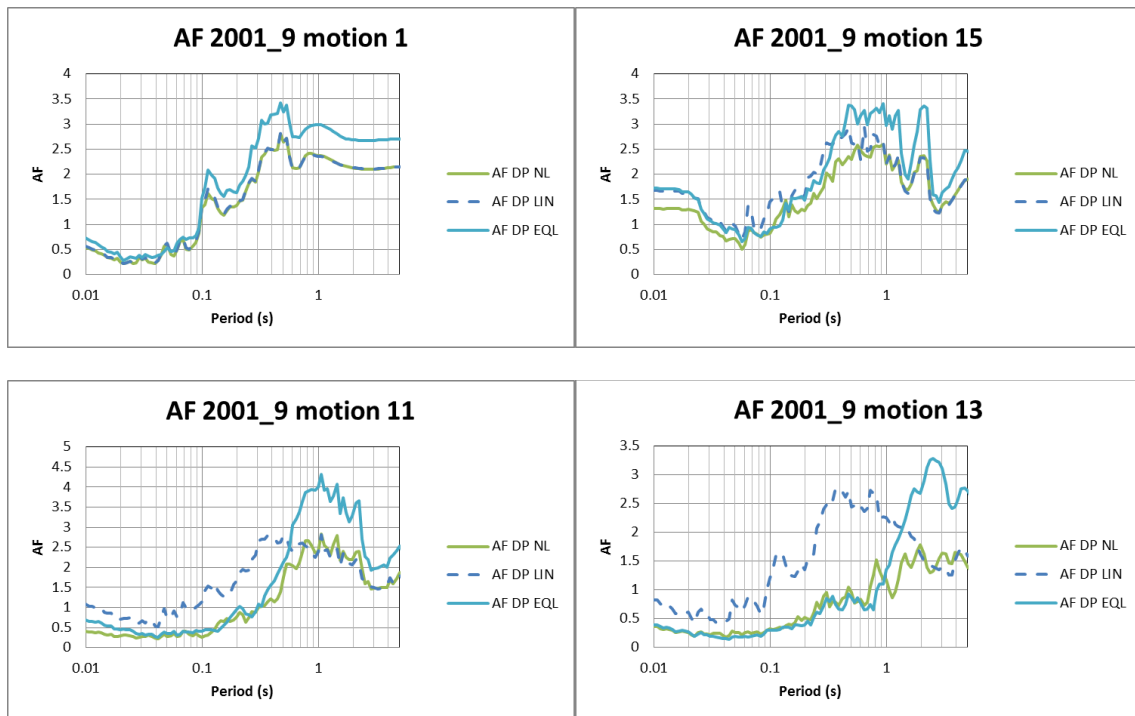


Figure 2.23. Results of linear (LIN), non-linear (NL) and equivalent linear (EQL) site response analyses for a profile in Zone 2001. The analyses were run using Deepsoil.

For comparison, Figures 2.22 and 2.23 also include the results of linear site response analyses using the Deepsoil time domain solution. As expected, the Linear solutions and the NL solution coincide for the lowest intensity motion (Motion 1), and the differences between the Linear and NL solutions increase with the intensity of the input motion.

To evaluate the implementation of small strain damping we develop a synthetic profile with the typical characteristics of the Groningen profiles. The synthetic V_s profile was obtained from the V_s profile at the BAPP ground motion station by computing the time-averaged V_s using a reduced number of layers (Figure 2.24). The small strain damping profile is developed using the field-estimated damping profile described in Figure 4.8 of the GMM V4 report. For this profile, the theoretical $\Delta\kappa$ is computed using Eq.(7.20) in the GMM V4 report (see also the response to the previous comment) and its value is 0.0337.

The linear site response for this profile was computed using the linear, time-domain method and the frequency-domain EQL option in Deepsoil. The value of $\Delta\kappa$ for both cases was computed from the high-frequency portion of the transfer function and is given in Table 2.4. Observe that the frequency domain approach results in an approximately correct $\Delta\kappa$, while the time domain approach results in significantly larger values of $\Delta\kappa$. The difference between the theoretical and the observed $\Delta\kappa$ in the time-domain approach increases for a longer (*i.e.*, larger magnitude) input

motion. The resulting AFs are also shown in Figure 2.25. Note that the effect of larger damping in the time-domain approach is seen as a lower value of AF.

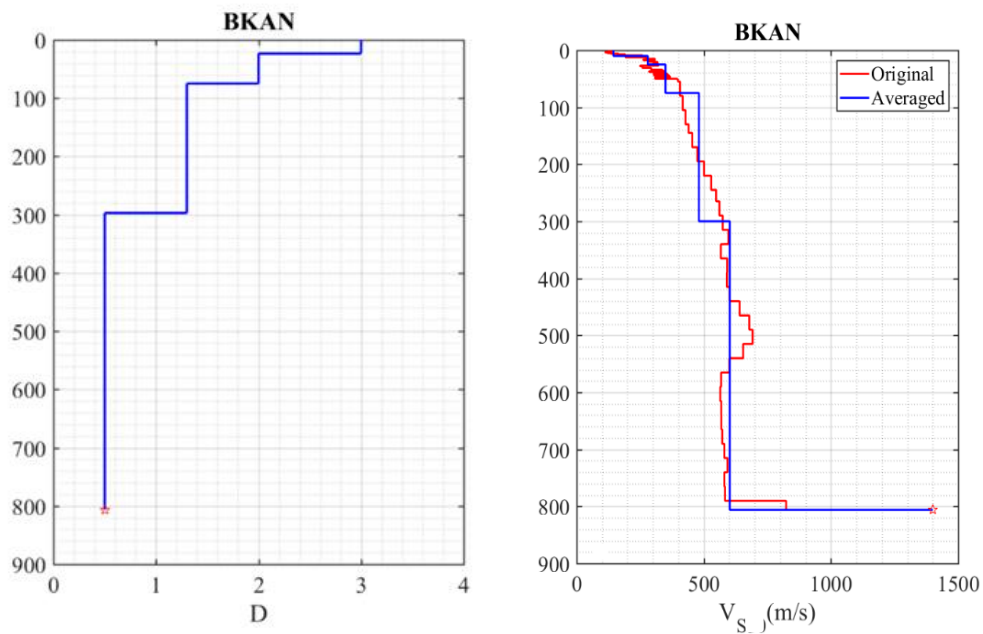


Figure 2.24. Profiles of small strain damping and V_s used to evaluate the implementation of small-strain damping.

Table 2.4. Values of $\Delta\kappa$ for a synthetic profile obtained by different methods and two input motions.

Input Motion	Analytical	Frequency-Domain	Time-Domain
Groningen motion (M=4.1, R=4.81 km)	0.0337 s	0.0355 s	0.0437 s
Northridge EQ motion (M 6.7, R_{cl} =26.8 km)	0.0337 s	0.0343 s	0.0777 s

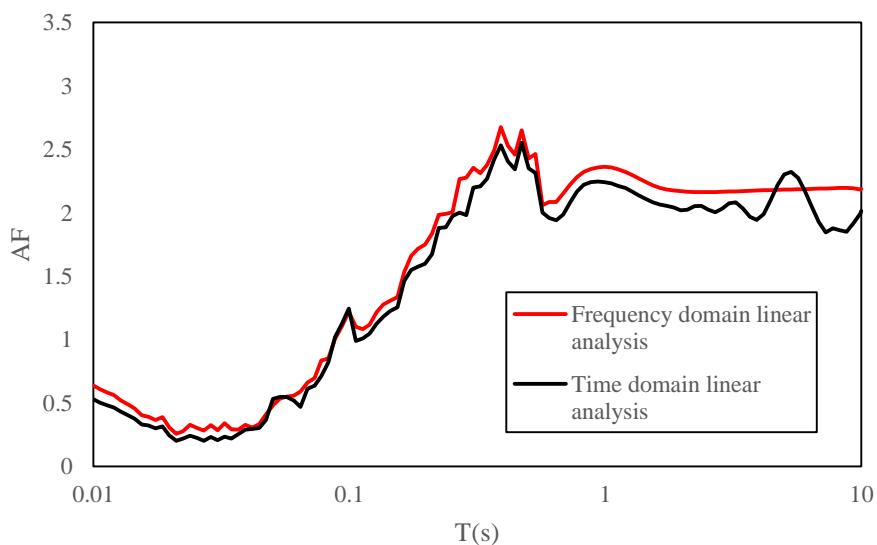


Figure 2.25. Results of linear site response analyses conducted on the profile shown in Figure 2.24 using frequency domain and time domain approaches in Deepsoil.

Overall, these results illustrate that the time-domain implementation in Deepsoil results in higher damping than expected for the deep, soft, and high-damping profiles of the Groningen regions. As indicated before, this is possibly due to numerical damping or with issues with the frequency-independent damping formulation for this type of profiles (*i.e.*, soft, deep profiles).

2.12. Component-to-component variability

Component-to-component variability is considered as variability across azimuths, which is the standard approach. The component-to-component variability can get very large if the signal is polarized so that there is a small value on one component and a large value for another, which seems to be the case with the data from Groningen field. The authors may want to consider: (1) is the polarization producing the strongest component consistently in the same direction (the examples seem to have this in the EW direction), or is the direction of the strongest component random? (2) what is the H1/H2 ratio at the orientation that gives the median SA value?

Our interpretation of the large component-to-component variances observed for the Groningen ground motions is indeed related to strong polarisation of the recorded accelerograms. This is thought to be the result of the radiation patterns from these small, very shallow earthquakes being preserved on the ground surface at locations close to the source. With the relatively dense recording networks operating in the Groningen field, many of the earthquakes have produced near-source recordings that often display strong polarisation, although there is not a consistent pattern of the stronger component being in the NS or EW direction. This is clearly illustrated in Figure 2.26 (based on Figures in Appendix I of the V5 GMM report) that shows peak horizontal motions recorded in the 2017 Slochteren earthquake. In terms of both PGA and PGV, the recordings from G460 and G500 are polarised to the extent of one horizontal component being three times stronger than the other. However, whereas for G500 it is the EW component that is stronger, at G460 the NS component is the stronger. Another interesting observation from these plots is that the remaining recordings show very little polarisation (other than a factor of about 2 between the horizontal components of the G340 recording); this observation has influenced our modelling choices, as discussed below. One point to note here is that adding the large numbers of recordings from the Slochteren earthquake—the vast majority of which are not strongly polarised—to the V5 database and deriving the component-to-component variability model in the same way as for the V3 and V4 models resulted in about a 10% reduction of the variance. However, this updated model has not been adopted for the V5 model because an alternative formulation was adopted to capture the distance-dependence of the component-to-component variability. Before discussing this, however, we present some work conducted in response to the reviewers' suggestions regarding component orientation.

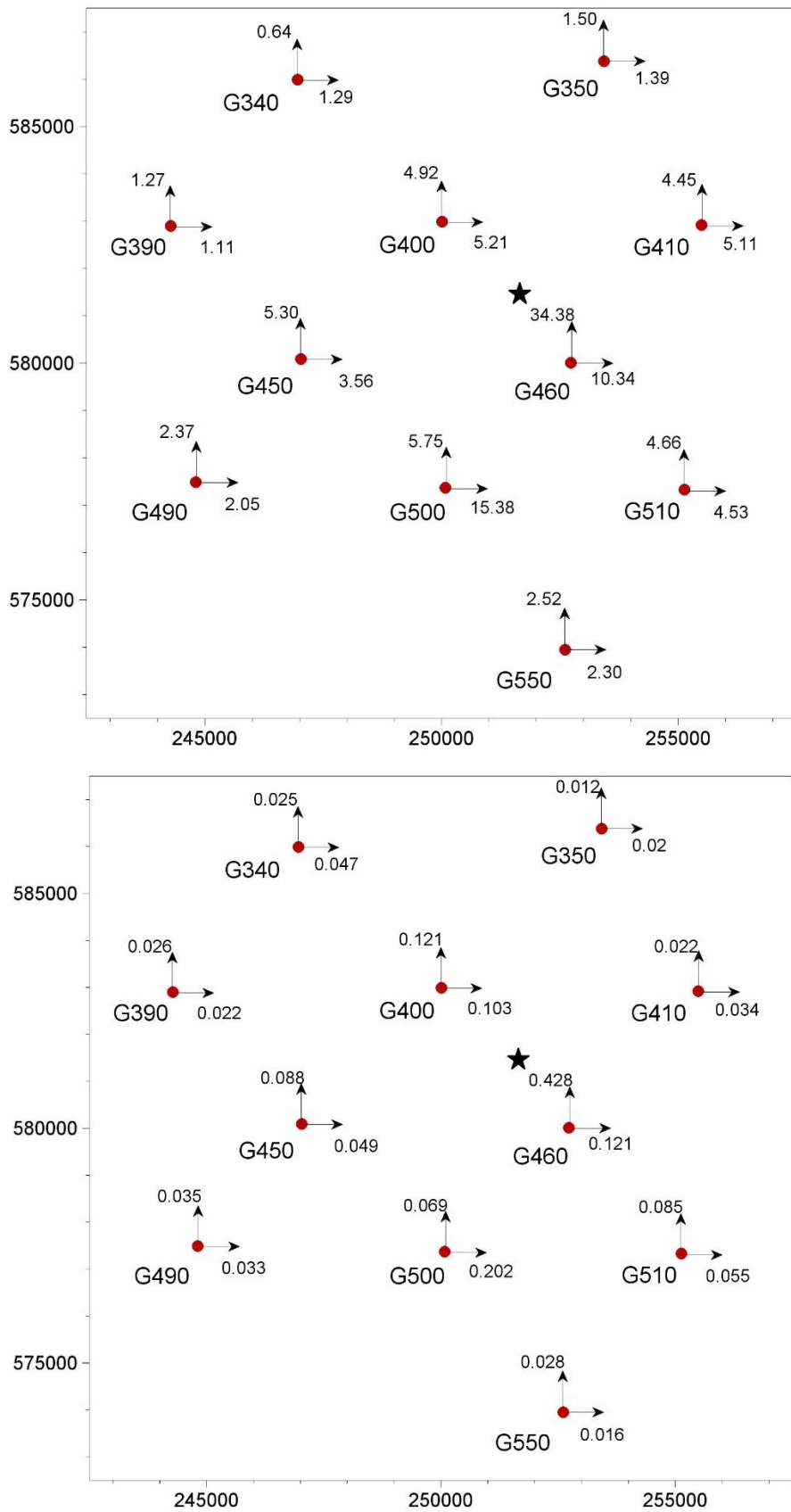


Figure 2.26. Peak amplitudes of horizontal components of near-source (< 10 km) recordings of the Slochteren earthquake in terms of PGA in cm/s^2 (top) and PGV in cm/s (bottom)

Returning to the panel's suggested investigation into the potential influence of the orientation of the sensors to the polarisation observed, some work has been undertaken along these lines. The surface sensors of the KNMI network are set up with a nominally NS-EW orientation (with an average error of a few degrees, particularly for the G-stations). Were it the case that ground motions generated in the Groningen field tend to be more polarised in this orientation than in other orientations, then the sensor orientation is part of the causes of the high variability values observed. Such a scenario is within the realms of possibility given that most of the mapped faults in the field are oriented E-W or NNW-SSE (Figure 2.27).

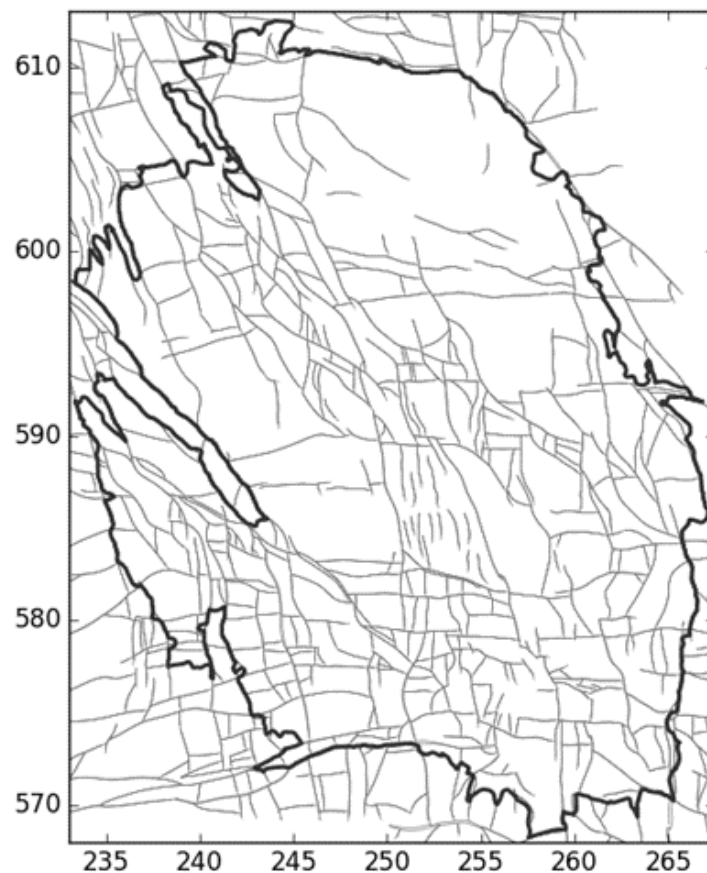


Figure 2.27. Mapped faults in the Groningen field.

The first course of investigation consisted of simply changing the global orientation of the records to observe how the variability values calculated are affected. The component-to-component variances calculated after rotating at 15° intervals are compared to the values corresponding to the existing orientation in Figure 2.28; the equivalent variability values are compared in Figure 2.29. In these plots, the “V5 model” is that obtained using the same approach as for V3 and V4 but with the V5 database; this is not the final model adopted for V5. Figures 2.30 and 2.31 show how the variance and variability change with rotation for the periods of 0.01s, 0.05s, 0.1s, 0.25s, 0.5s and 1s.

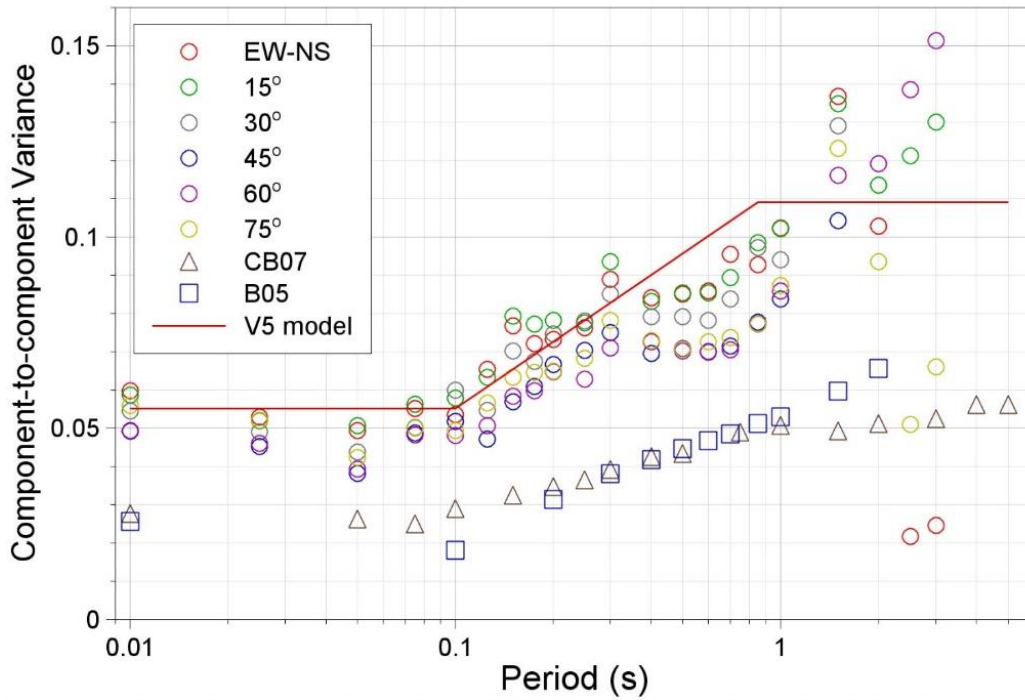


Figure 2.28. The component-to-component variances of the Groningen records rotated at 15° intervals, compared to the tri-linear V5 model and the models of Campbell & Bozorgnia (2007) and Boore (2005).

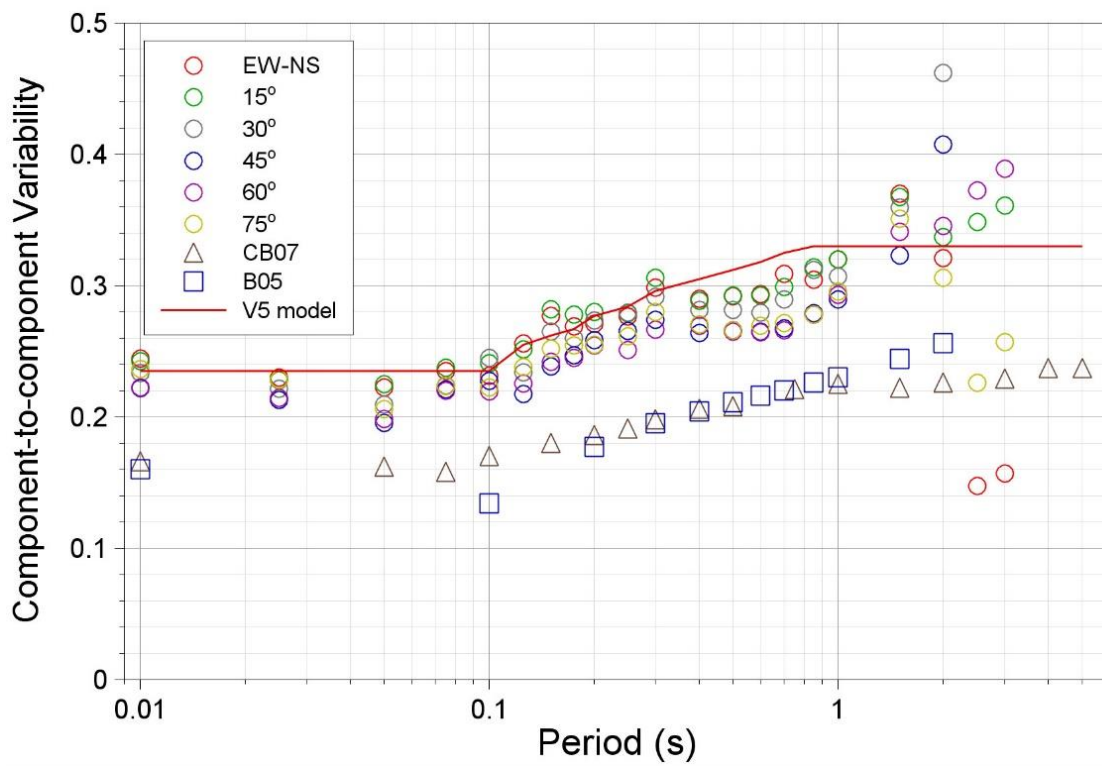


Figure 2.29. The component-to-component variabilities of the Groningen records rotated at 15° intervals, compared to the trilinear V5 model and the models of Campbell & Bozorgnia (2007) and Boore (2005).

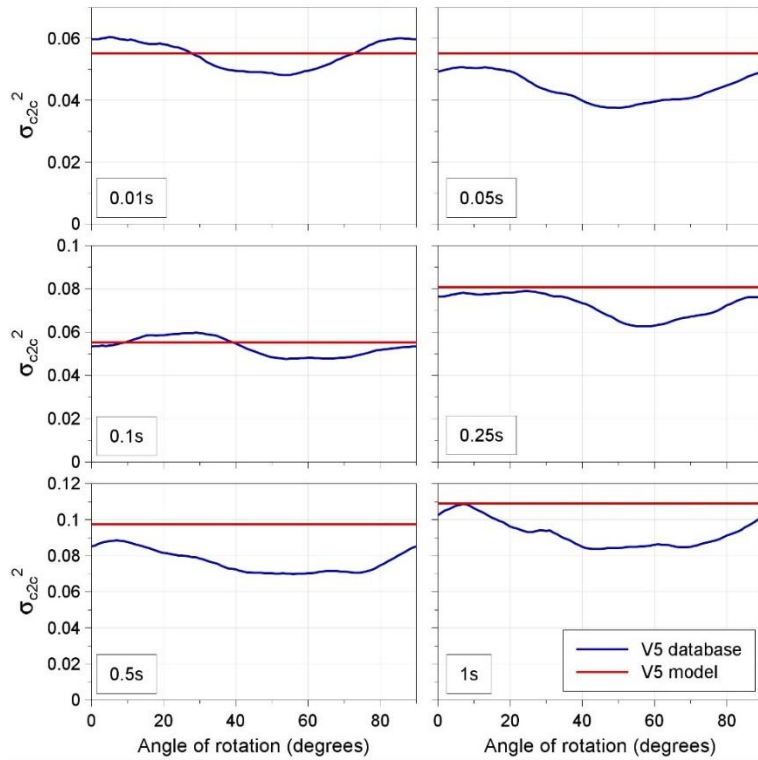


Figure 2.30. The component-to-component variances of the Groningen records at six periods and at angles of rotation from 0° to 90°, compared to the tri-linear V5 model.

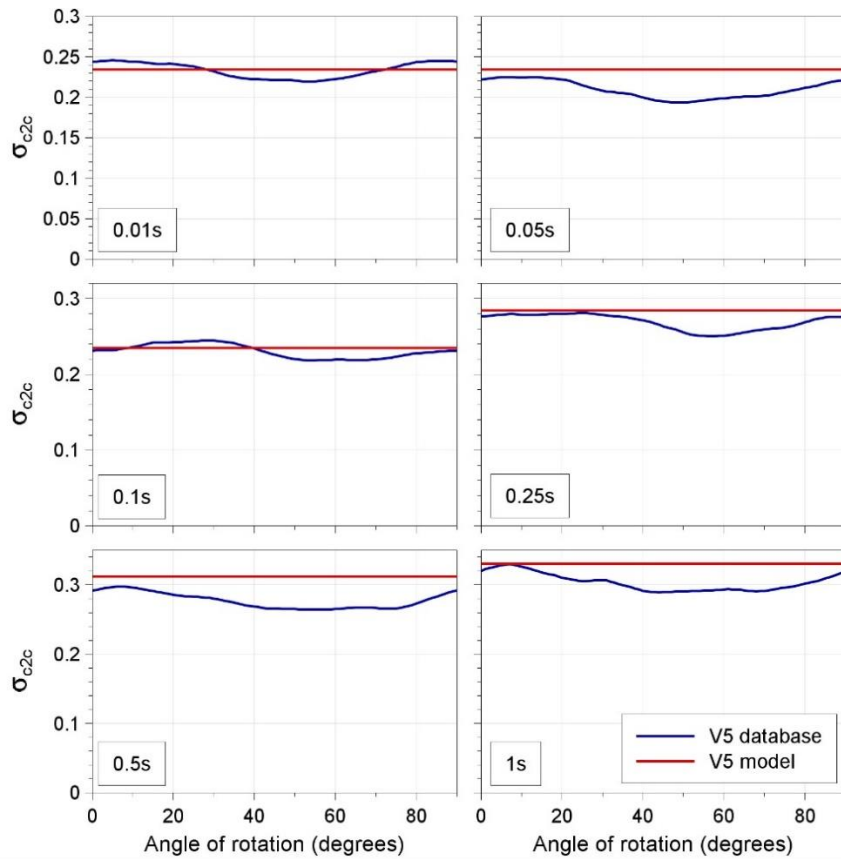


Figure 2.31. The component-to-component variabilities of the Groningen records at six periods and at angles of rotation from 0° to 90°, compared to the tri-linear V5 model.

As can be observed in these four figures, the component-to-component variances calculated at the EW-NS orientation are indeed generally higher than those calculated for most other orientations. However, the differences are very small. The median values are typically only 5% lower and the smallest values only 10% lower than the variance values at the EW-NS orientation. As a result, the behaviour of the simple tri-linear V5 model remains similar with respect to all orientations and identical to the behaviour of the V3 model with respect to the V3 data: it provides a good fit at the period of 0.01s and between 0.1s and 0.2s, while it remains slightly conservative between 0.01s and 0.1s and between 0.2s and 1s. In all cases, the differences are so small that the values calculated remain almost double the values of the Boore (2005) and Campbell & Bozorgnia (2007) models.

The second course of investigation with respect to the influence of sensor orientation involved calculation of the variability after rotating the records separately instead of simultaneously. As the reviewers suggested, the variability was calculated while choosing—for all records and at each period—the orientation which gives the median geometric-mean spectral acceleration among the geometric mean spectral accelerations of all orientations. This is defined by Boore *et al.* (2006) as GMRotD50. For completeness, we will also examine the variability values calculated at the orientations of GMRotD0 and GMRotD100 (the largest and smallest geometric means).

The component-to-component variances and variabilities at the orientations of GMRotD50, GMRotD0 and GMRotD100 are compared to the values calculated for EW-NS and the tri-linear V5 model in Figures 2.32 and 2.33. The records exhibit very low polarisation at the orientation where the strongest geometric mean spectral acceleration is recorded, and, conversely, very high polarisation at the orientation of the weakest geometric mean. The geometric mean of the as-recorded components appears to be situated in the middle between the two extremes and close to the values calculated for the median geometric mean. Therefore, we can conclude that the component-to-component variabilities of the as-recorded ground-motions are representative of the values that would result under different sensor orientations and not biased. Since all the GMMs have been developed in terms of the geometric mean horizontal component, and consequently all hazard maps have been derived in terms of that component definition, we opted to retain this definition going forward.

The focus of our work for the development of the final component-to-component variability in the V5 model was to capture the clear distance dependence, note previously. This results in very large values at very short distances in the magnitude range of the existing Groningen records. However, we do not believe that this degree of polarisation would be expected to persist for larger triggered earthquakes associated with fault ruptures of greater length that also propagate downwards from the gas reservoir into the underlying Carboniferous and Triassic rocks. Consequently, the distance dependence was modelled to decay with increasing

magnitude from the upper limit of the data (M 3.6) so that after two magnitude units the component-to-component variability becomes constant and assumes the values obtained from recordings of tectonic earthquakes. The derivation of the distance- and magnitude-dependent component-to-component variability is explained in detail in Appendix III of the VG GMM report (Bommer *et al.*, 2017e).

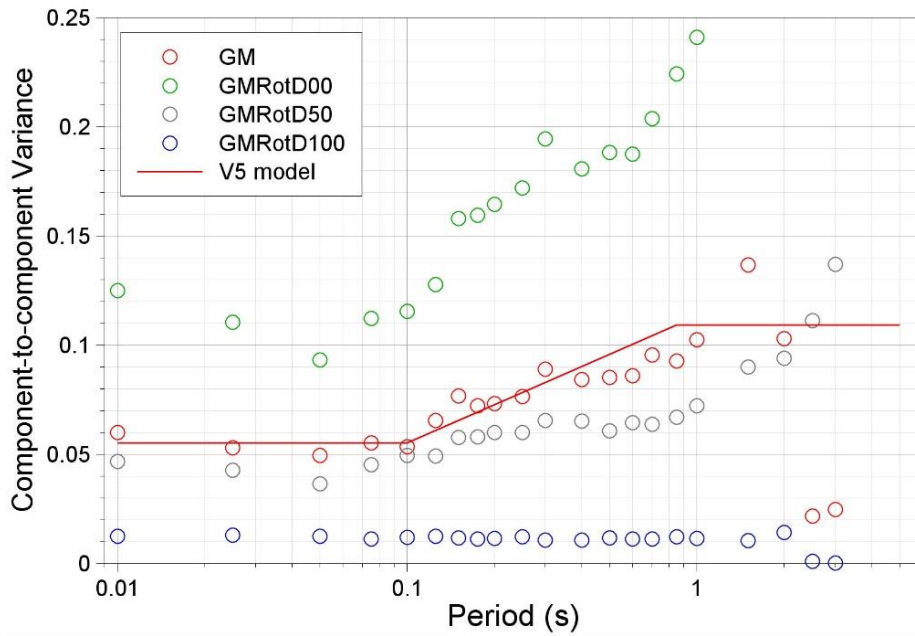


Figure 2.32. Component-to-component variances of the Groningen records for different definitions of the geometric mean spectral acceleration

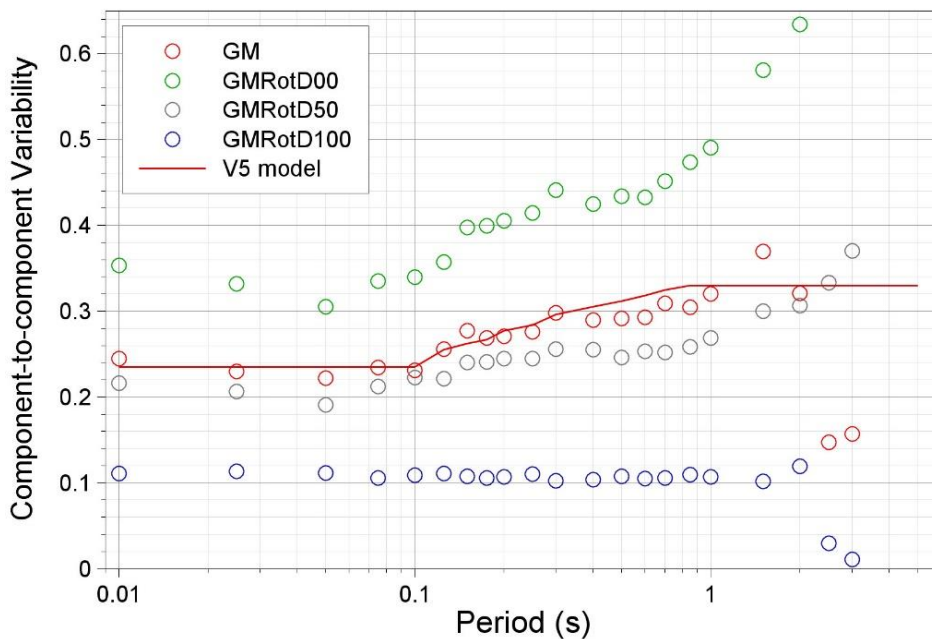


Figure 2.33. Component-to-component variabilities of the Groningen records for different definitions of the geometric mean spectral acceleration

2.13. Function for duration model

Eq. 12.1 shows the function used for the duration model. The function sums source, path, and site terms in ln units, which is multiplicative in arithmetic units. We recognize that such a model can be calibrated to fit a data set, but we consider this form to be suboptimal in representing the physics of the program. Source and path durations are better taken as additive in arithmetic units. Constructing the function in this manner should allow the model to extrapolate better beyond the data range.

We understand the perspective of the reviewers, but we also believe that our chosen functional form is actually consistent with the idea of additive duration contributions. The EXSIM simulations that are used to generate the synthetic data to which the functional form is fit is based upon the same underlying physical model that the reviewers refer to – additive source and path durations. These EXSIM simulations are deliberately performed to ensure that the synthetic data more than cover the full magnitude and distance ranges that might be considered for the Groningen field. Because this is a region-specific model, we do not have to worry about issues like how the function performs under extrapolation. Furthermore, the use of EXSIM to constrain the duration scaling was introduced in the development phase between V3 and V4 of the model specifically to ensure that we achieved more physically-consistent duration scaling when making predictions from large magnitude, long distance scenarios.

We do not attempt to interpret any of the regression coefficients as having any physical meaning, we simply employ a suitably flexible functional form that can capture the scaling embodied by the physics embedded within EXSIM. The functional form clearly captures the resultant scaling well, as can be appreciated from Figure 2.34 which shows the EXSIM predictions along with model estimates for the lower central stress drop branch.

The model that we adopt makes use of the Afshari & Stewart (2016) site response model which is *not* additive and so we need to depart from the ‘optimal’ physics in order to make use of that site response component.

Eq.(12.1) of the V4 GMM report (referred to by the reviewers) shows the functional form expressed as:

$$\ln D = g_{src}(M) + g_{path}(R_{rup}, M) + g_{site}(V_{S,30}) \quad (2.4)$$

If we were to follow the advice of the reviewers, but to still make use of the site response component in the same manner as the ‘physically parameterized’ equations of Afshari & Stewart (2016) then we could do something like:

$$\ln D = \ln[D_E(M) + D_P(R_{rup})] + g_{site}(V_{S,30}) \quad (2.5)$$

where D_E and D_P are the additive source and path durations, which are exclusively functions of magnitude and distance respectively. However, this equation is mathematically equivalent to:

$$\ln D = \ln D_E(M) + \ln \left[1 + \frac{D_P(R_{rup})}{D_E(M)} \right] + g_{site}(V_{S,30}) \quad (2.6)$$

which has exactly the same form as our Eq.(12.1).

In order to be physically consistent, we therefore need to ensure that our $g_{src}(M)$ function (which is equivalent to $\ln D_E$) reflects source durations depending upon the source rise time, and that our additive path duration D_P is being factored down by a term that increases with the source duration. Our $g_{src}(M)$ functional form is equivalent to the stress-drop/rise-time formulation of Afshari & Stewart (2016) with the exception that they use a piecewise linear model for logarithmic stress drop and we use a continuous polynomial to achieve the same scaling. Our $g_{path}(R_{rup}, M)$ term contains strong magnitude dependent coefficients that ensure that we mimic the necessary physical scaling.

We are therefore satisfied that our chosen functional form is capturing the physical processes that the reviewers are advocating. There are also advantages from an implementation point-of-view to make use of functional expressions that are similar between the response spectral and duration models. We believe that by using similar expressions the chances of implementation issues decrease. Similarly, given that we do not perceive any advantages to changing the functional form we believe that there are advantages for the implementation in refining parameters of the same functional expression over implementing a new untested function.

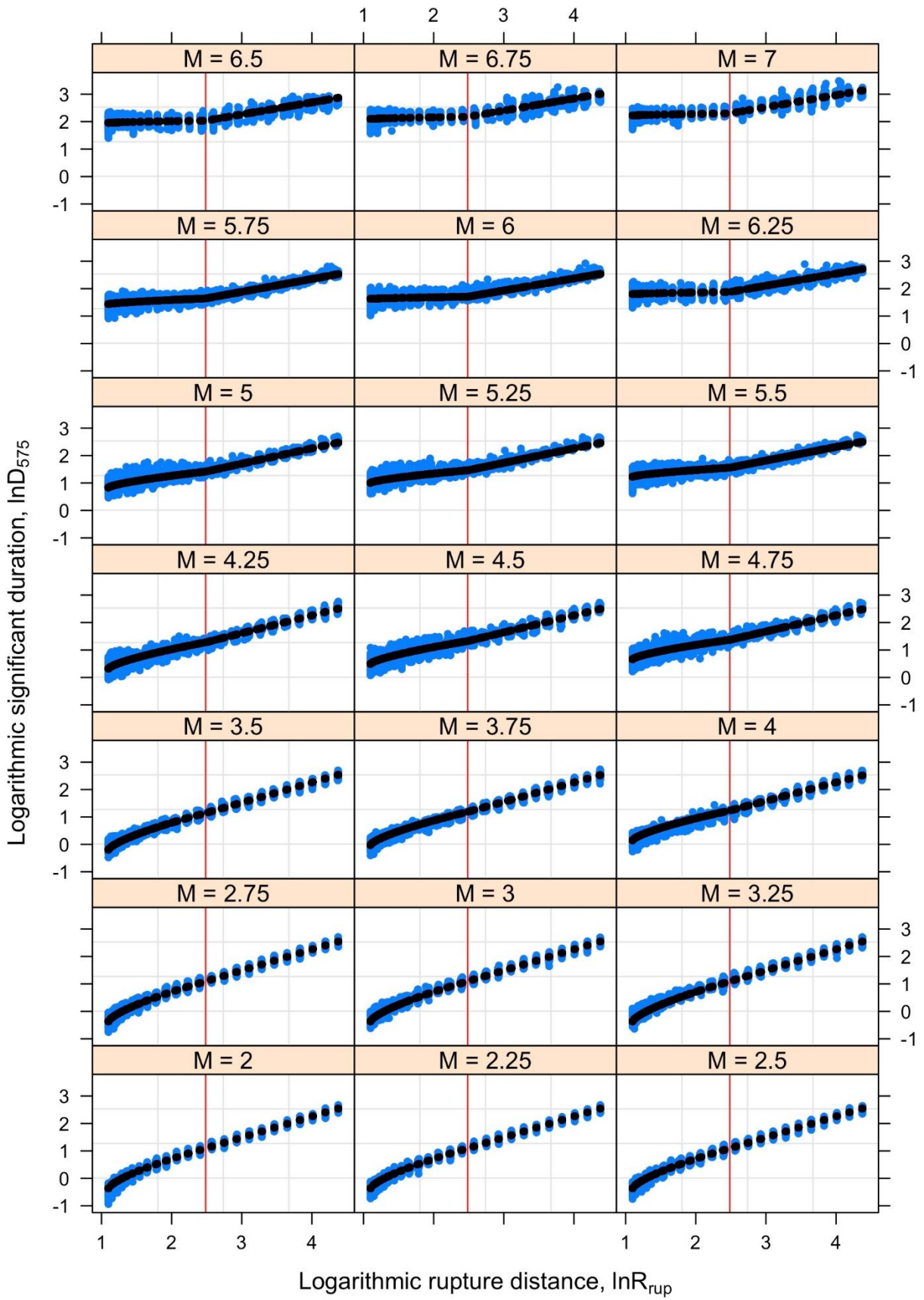


Figure 2.34. Behaviour of the functional form for duration with distance for a very broad range of magnitude values.

3. Additional Review Comments

In addition to the main comments addressed in Chapter 2, the review panel provided other comments grouped by the chapters of the V4 GMM report. The responses to these additional comments are detailed in the following sections.

3.1. Chapter 1: Introduction

Can it be verified from the available data that PGA is well approximated by 0.01 sec spectral acceleration?

We responded to this comment in producing the revised version of the V4 GMM report, displaying in Figure 1.3 the correlation between PGA values and $S_a(0.01s)$ of all individual horizontal components in the Groningen ground-motion database. The plot is reproduced here as Figure 3.1 for ease of reference and we believe it convincingly demonstrates that PGA is very well approximated by $S_a(0.01s)$, which is not surprising for these soft soil sites.

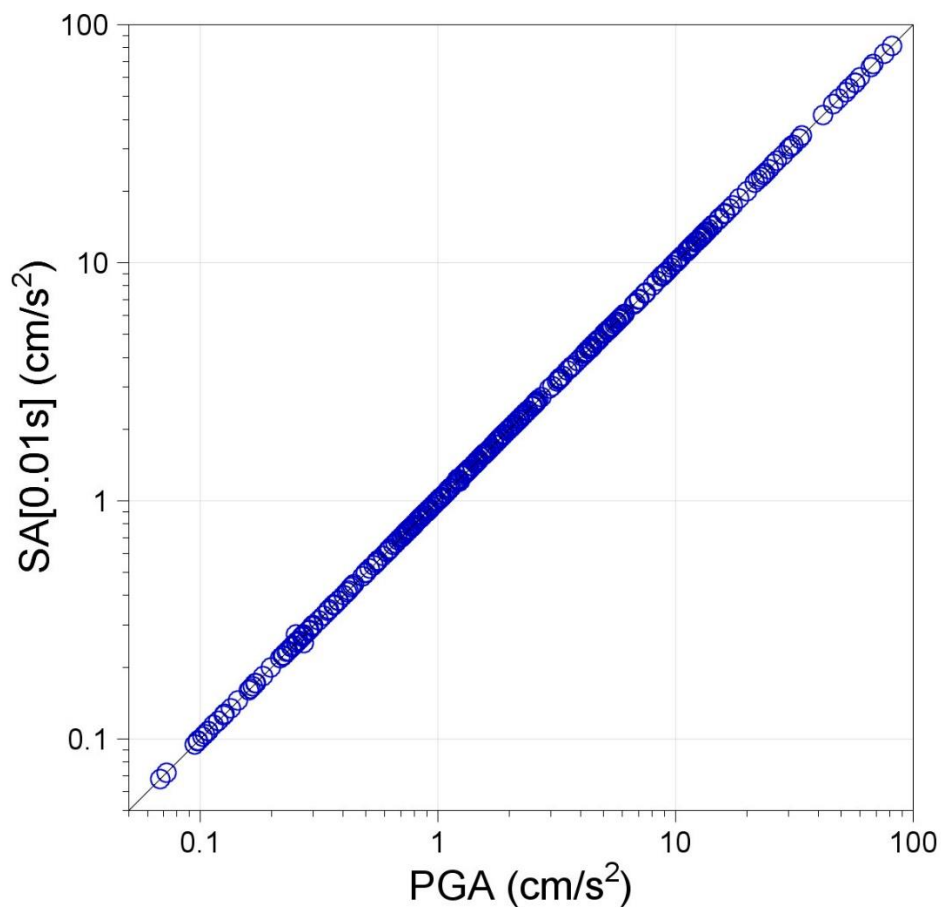


Figure 3.1. Correlation between PGA and $S_a(0.01s)$ values for individual horizontal components of the Groningen ground-motion database

3.2. Chapter 2: Overview of V4 GMM

Please provide better justification for the half-space properties below NS_B. The damping (κ) is chosen to be consistent with $Q=150$, which seems low. The V_s of 1.5 km/s seems to be suitably justified from Figure 2.5 – the only question in this case is how uniform that condition is likely to be across the field.

The uniformity of the 1400 m/s of the half-space is described in Section 7.2 of the V4 GMM report. On page 152 of the report, in Figure 7.12 the histograms of V_s values just above, at and just below the voxels containing the NS_B are shown for the entire field. Figure 7.12(f) shows the distribution around 1400 m/s. Table 7.2 on p.153 provides the average (1402 m/s) and standard deviation (92) m/s. All of these values were obtained from sonic profiles obtained as part of the field characterization needed for gas extraction. With these considerations, we assumed that it was reasonable to assume an elastic half-space (EHS) with $V_s = 1400$ m/s.

The value of damping used for the EHS does not affect the values of the transfer function. As indicated in the report, we used a damping consistent with $Q=150$, which was a relic of the V1 model. The actual value of Q in the V5 model is $Q=220$. However, since the damping of the EHS does not change the amplification functions, the previous damping value was retained for the EHS.

3.3. Chapter 3: Groningen ground-motion database

Please indicate that geophones record velocity. Is the frequency range covered by these instruments sufficient to obtain accurate peak accelerations and short-period spectral accelerations?

We addressed this question in revised version of the V4 GMM report, confirming that the geophones at 50, 100, 150 and 200 m depth at the G-stations do indeed record velocity. Since these record with 200 samples per second, it was possible to differentiate the velocity traces to obtain accelerations. Figure 3.7 in the revised GMM report showed the transfer function of the geophone transducer, which clearly indicates that they are suitable to yield reliable values of PGA and high-frequency spectral accelerations. This is further confirmed by Figure 3.2, which compares the raw and filtered FAS of the NS components recorded during a single event by the surface accelerograph and the 200 metre-depth geophone at station G30. The similar high-pass filter frequency can be seen to be very similar in both cases and the shape of the FAS in the high-frequency range is practically identical in both cases.

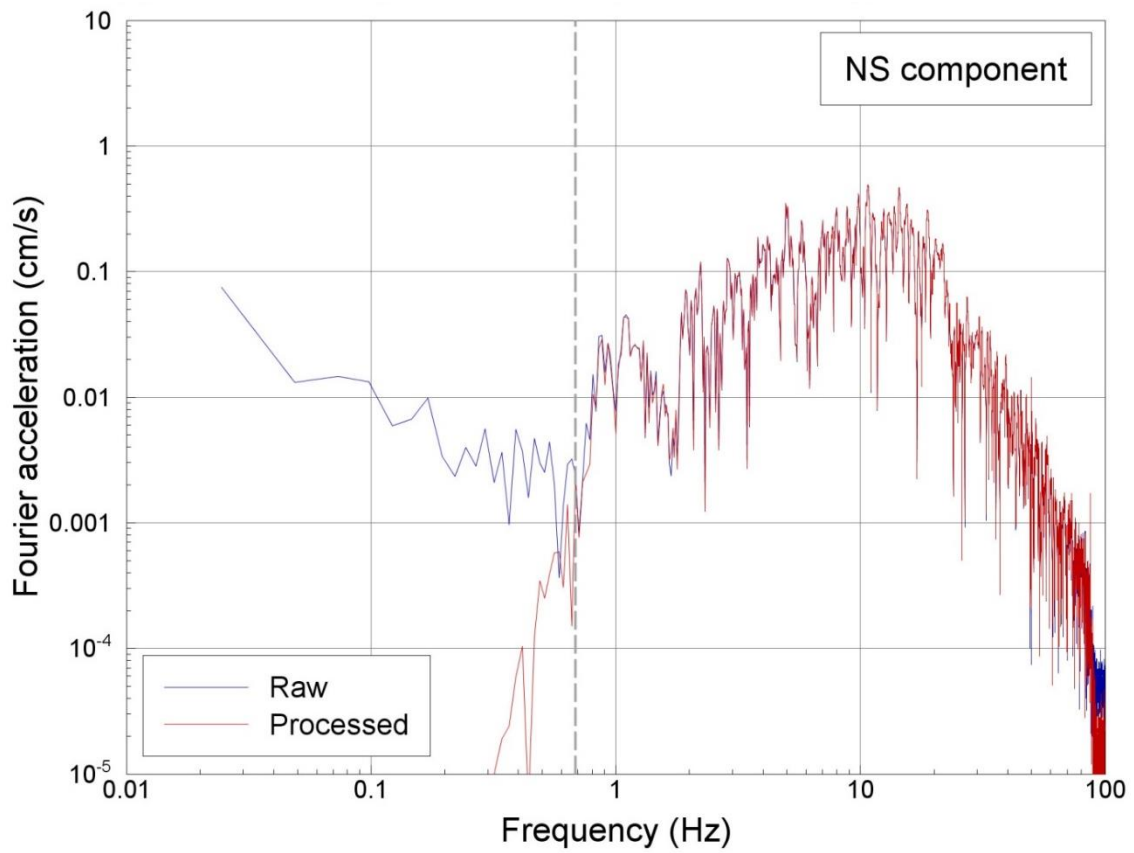
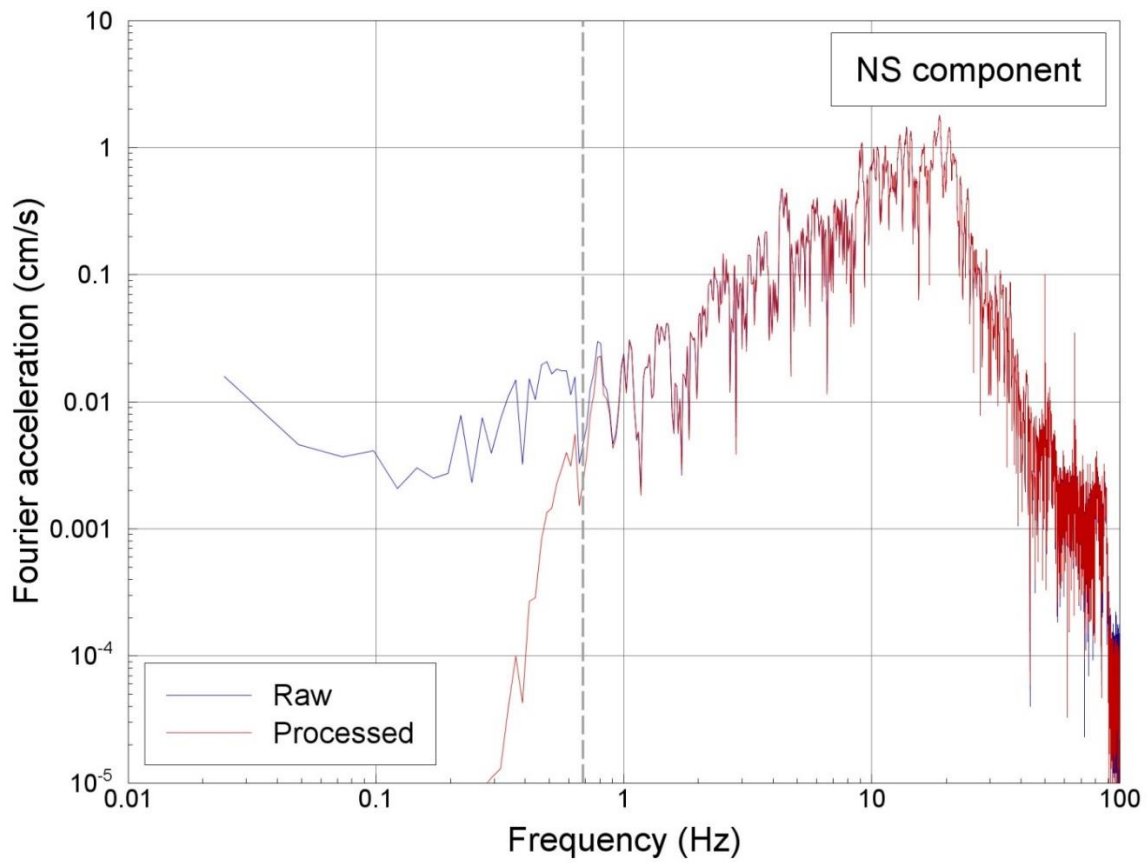


Figure 3.2. Raw (*grey*) and filtered (*red*) FAS of horizontal recordings from the surface accelerograph (*upper*) and the geophone at 200 m depth (*lower*) at the G30 station. The dashed vertical line is the filter cut-off frequency.

3.4. Chapter 4: Characterisation of recording stations

Figure 4.1 shows the selection of limiting frequencies for the calculation of kappa from surface records. Frequency f_1 is based on theoretical corner frequency. Were there visual inspections to make sure that the FAS near f_1 are not affected by resonant peaks or other effects in the FAS?

The frequency f_1 was based on estimates for the source corner frequency in two magnitude ranges (M_L 2.5-2.7 and 2.8-3.6). Spectra were visually inspected to ensure that there were no significant resonant peaks in this range. However, due to the low velocity of the sites it is indeed likely that these estimates are influenced by amplification effects (see Appendix II of the V4 GMM report). As mentioned the κ_0 values calculated at the surface were simply used to test the selection of damping profiles to ensure that, upon deconvolution to the NS_B, that unphysical negative κ_0 was avoided. Kappa fits discussed for the surface data are not used beyond this qualitative comparison. The general assumption is that the spectra are free from significant resonance effects for the data deconvolved to the NS_B rock reference, as presented later in the report.

To as great extent as possible subjective decisions, such as including data or not, are avoided such that bias is not imposed. For example, some data from malfunctioning instruments was excluded, but data that simply do not look like a perfect Brune model are not excluded. We argue that the kappa measurement is a pseudo-physical parameter, in that it describes principally the attenuation of the upper layers, but is ultimately an empirical shaping parameter. Therefore the filter should reflect a least squares fit to available data.

Please compare results for kappa0 of surface stations to published models to see if the results are in the range previously observed.

Figure 3.3 presents exactly what is requested by the reviewers: a plot of established relationships between V_{S30} and κ_0 , on which the Groningen data have been superimposed. As can be observed, the Groningen values are entirely consistent with those found in other studies and with the published relationships, particularly those of Edwards & Fäh (2013). This was a useful exercise to provide us with assurance that our site kappa estimates are perfectly reasonable and also consistent with estimates of this parameter from other equally soft recording sites.

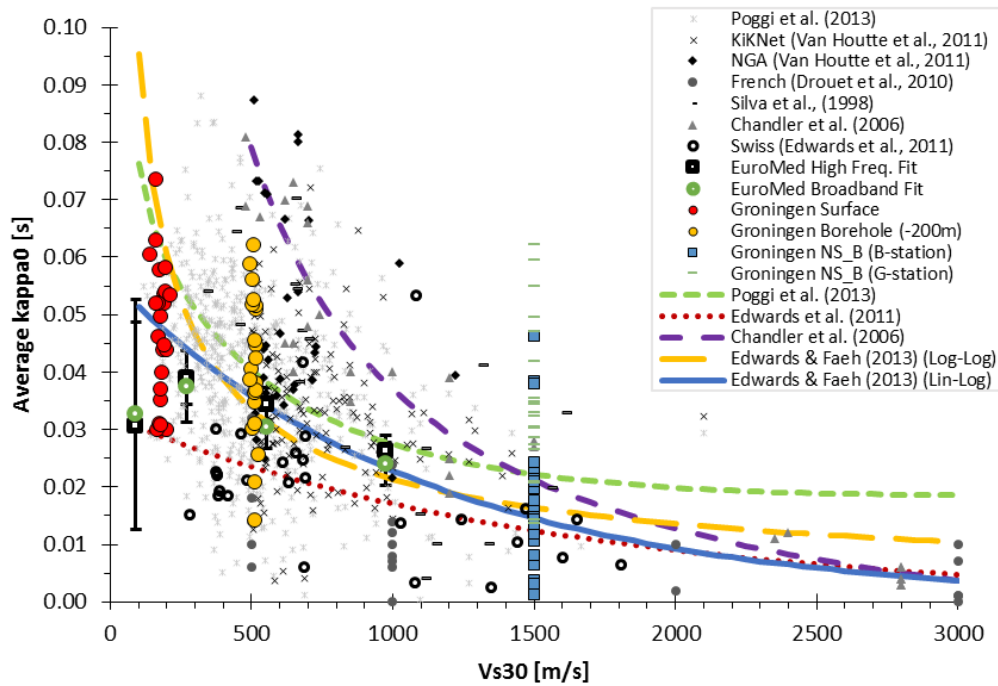


Figure 3.3. V_{s30} versus κ_0 for Groningen surface data (red circles) compared to data from other regions and existing V_{s30} - κ_0 relationships. The Edwards & Fäh (2013) log-log and lin-log fits indicated show the fit to all data in the plot (excluding Groningen). Figure modified after Edwards & Fäh (2013).

P 45, 1st para. It would have been useful to see comparisons of the MASW and SCPT V_s profiles. As stated in the text between the two approaches, MASW provides profiles that are more global in nature and therefore more relevant to frequencies of engineering relevance. It would be useful to average the SCPT and MASW V_s profiles to capture the epistemic uncertainty in both the measurement techniques and the measurements themselves.

For the purposes of constructing the ground-motion model, all that matters is the final measured V_s profile for each recording station, and we have not wanted to greatly expand the GMM report with all the details of the measurement campaign and the interpretation of the results. The *in situ* measurements and the comparisons between the results obtained with different techniques are presented and discussed in great detail in a standalone report that can be downloaded from this link:

<https://nam-feitenencijfers.data-app.nl/download/rapport/8b6a8566-027c-4802-a464-894e1b641f21?open=true>

Additionally, the results have been submitted for publication in *Journal of Seismology* (Noorlandt *et al.*, 2017). Following the initial review, modifications were made and the paper is now undergoing re-review; the changes required were modest.

P 46-47. Explain how damping was inferred from boreholes for derivation of the station-specific transfer functions. Two references in Danish are provided (De Crook & Wassing, 1996, 2001), but these references are not familiar to the panel and the details of how this was done are an important detail of the project.

The revised version of the V4 GMM report (Bommer *et al.*, 2017c) includes a more in-depth discussion of the methodology to obtain damping, and includes an English-language reference to the method (Hauksson *et al.*, 1987). Additional references to the method can be found in Tonn (1991), who trace the method to work by Engelhard *et al.* (1986) and Engelhard (1996).

The text in the GMM V4 is included below for the benefit of the reviewers:

“De Crook and Wassing (1996) measured Q-values for KNMI borehole FSW, located at the eastern rim of the study area (Figure 3.2), at depths between 75 and 300 m. This borehole was the first experimental borehole deployed in 1991 and is equipped with four levels of geophones at 75 m spacing. In addition, a near-surface geophone was deployed for some time at 2.5m depth. Following Hauksson et al. (1987), using a simple spectral ratio technique, damping was measured and the average Q factor between 75 and 300 m was found to be Q=40, or its equivalent in terms of a damping factor 0.013 (1.3%). Attenuation in the upper 75 m could not be determined.

In a follow-up of this study, de Crook & Wassing (2001) measured damping in the upper 25m near the borehole ZLV (Zuidlaarderveen, at the southern rim of the study area, Figure 3.2). This borehole is equipped with two strings with 50m spacing between the geophone levels. Strings are co-located but at a vertical offset of 25m, resulting in a 25m spacing between the geophone levels. Using a seismic vibrator and recording the signal in a cone at depth intervals of 1 m, average damping in the upper 25 m was calculated, again using Hauksson et al. (1987). From the comparison between the modelled and the measured damping values, the results indicate a damping factor of 2-3%.”

It is also noteworthy that ongoing studies of data recently collected at KNMI down-hole arrays renders similar values of Q. These data were analysed by Dr Elmer Ruigrok of KNMI using the same method. These studies are still undergoing hence these data was not available for use in the development of the V5 GMM.

In passing we note that the original references to which the review comment allude were in Dutch (the language of the Netherlands) rather than Danish.

Were alternative damping models considered to investigate sensitivity to damping in the ground response simulations?

The uncertainty in damping is included along with the uncertainty in the modulus reduction and damping (MRD) curves. The uncertainty of MRD curves was the result of coupling the measuring error reported in Darendeli (2001) and the uncertainty in index properties of the soils, as described in Section 9.3, page 211 of the V4 GMM report (Bommer *et al.*, 2017c). The model discussed in this section is also presented in a recently submitted paper (Bahrapouri *et al.*, 2017). The resulting additional uncertainty due to uncertainty in the MRD curves is shown in Figures 9.6 and 9.7 of the V4 GMM report. The uncertainty due to low intensity ground motions is largely due to uncertainty in small strain damping. The contribution to total uncertainty varies across zones, and is large at around $T=0.2$ s for some of the zones.

Despite the introduction of the uncertainty of damping in the model, some aspects of the damping model were not fully explored. For example, low-strain damping was scaled by a constant factor to make the damping compatible with field-estimates of the attenuation parameter Q (Section 4.2 in the V4 GMM report). Alternative formulations, such as a depth-dependent scaling factor, were not investigated. However, it is also important to note that the most important aspect of the damping model is that it needs to be self-consistent. As illustrated in Figure 2.7 of the V5 GMM report (Bommer *et al.*, 2017e), linear transfer functions for each of the recording stations are used to convert surface recordings into ground motions at the NS_B boundary. These motions are then used to generate the GMPE for the NS_B boundary horizon. The NS_B motions are then modified by the zone amplification functions. As long as the same damping model used in the transfer functions for the recording stations and the zone amplification functions, the model is self-consistent. A validation of this approach is the consistency of the high-frequency portion of the inverted seismological model to the transfer functions computed for the stations (Figure 4.3 in the V4 GMM report).

Sec. 4.2. What is the source of $\beta=2.6$ km/s? This was assumed in the derivation of κ . Is this consistent with the value of β used in the simulations? See also comment below for Chapter 5.

The value of $\bar{\beta}=2.6$ km/s is the 'average shear-wave velocity' between the reservoir and surface for typical travel paths (*i.e.*, $R_{\text{epi}} < 25$ km) as determined from NAM's 3D V_s model. This value was used for all calculations (simulations and inversions) where an average path V_s was required.

Sec. 4.3. The trends of site response with M and R are interesting. As presented, the trends are the outcome of simulations. Is this seen in data? It is mentioned that something like this was seen at Kik-net sites (reference to a publication under review), but we cannot tell from what is written whether those features are observation- or simulation-based.

The referenced publication has now been accepted and is available online (Stafford *et al.*, 2017). As indicated in the V4 GMM report, the KiK-net data supports the simulation results. More specifically, we postulated that if there is a magnitude dependence in the amplification functions, this amplitude dependence would be seen in the event-corrected residuals at a single station. Moreover, because the magnitude dependence is the result of damping, the magnitude-dependence of the site term would be a function of the site kappa (*i.e.*, κ_0) or V_{S30} , as the result of the correlation of κ_0 with V_{S30} . Figure 3.4, extracted from Stafford *et al.* (2017), illustrated this dependence for four selected stations in the KiK-net database. The simulations had suggested a positive slope with magnitude (increase in amplification with magnitude). This is the case for the softer sites, but not for the stiffer sites. This is very likely because some of the magnitude dependence of the site term is taken by the magnitude scaling term in the GMM that is used to compute the residuals. Figure 3.5 shows the slope of within event residuals versus magnitude for all the KiK-net stations that have sufficient data. This plot shows that, as expected, the slope is stronger for sites with larger κ_0 or lower V_{S30} . Moreover, the slope is close to zero for the centre of the data.

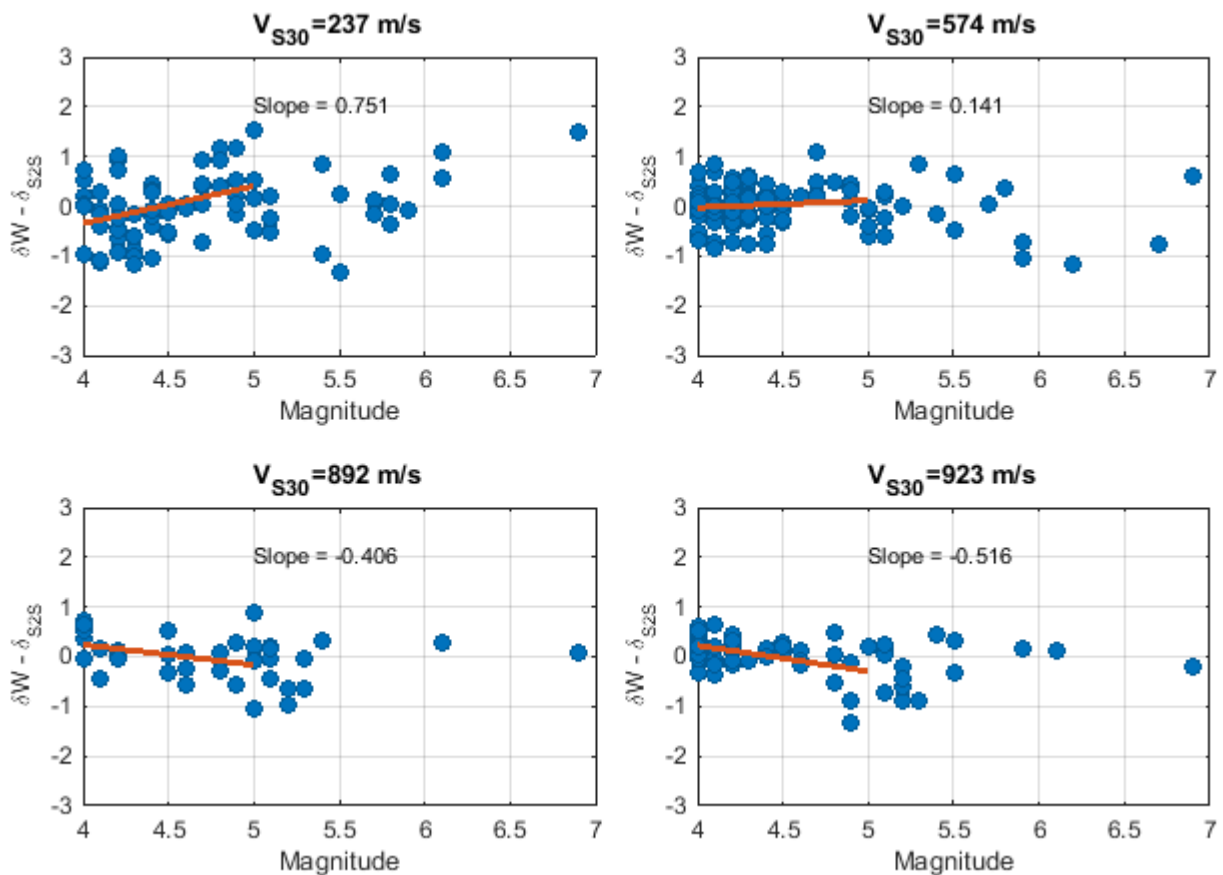


Figure 3.4. Within event residuals (δW) corrected by the average site term for selected KiK-net stations. Values shown are for an oscillator period of 0.04. The V_{S30} of each station is shown, as well as the average slope for the event corrected residuals for $M \leq 5$. From Stafford *et al.* (2017).

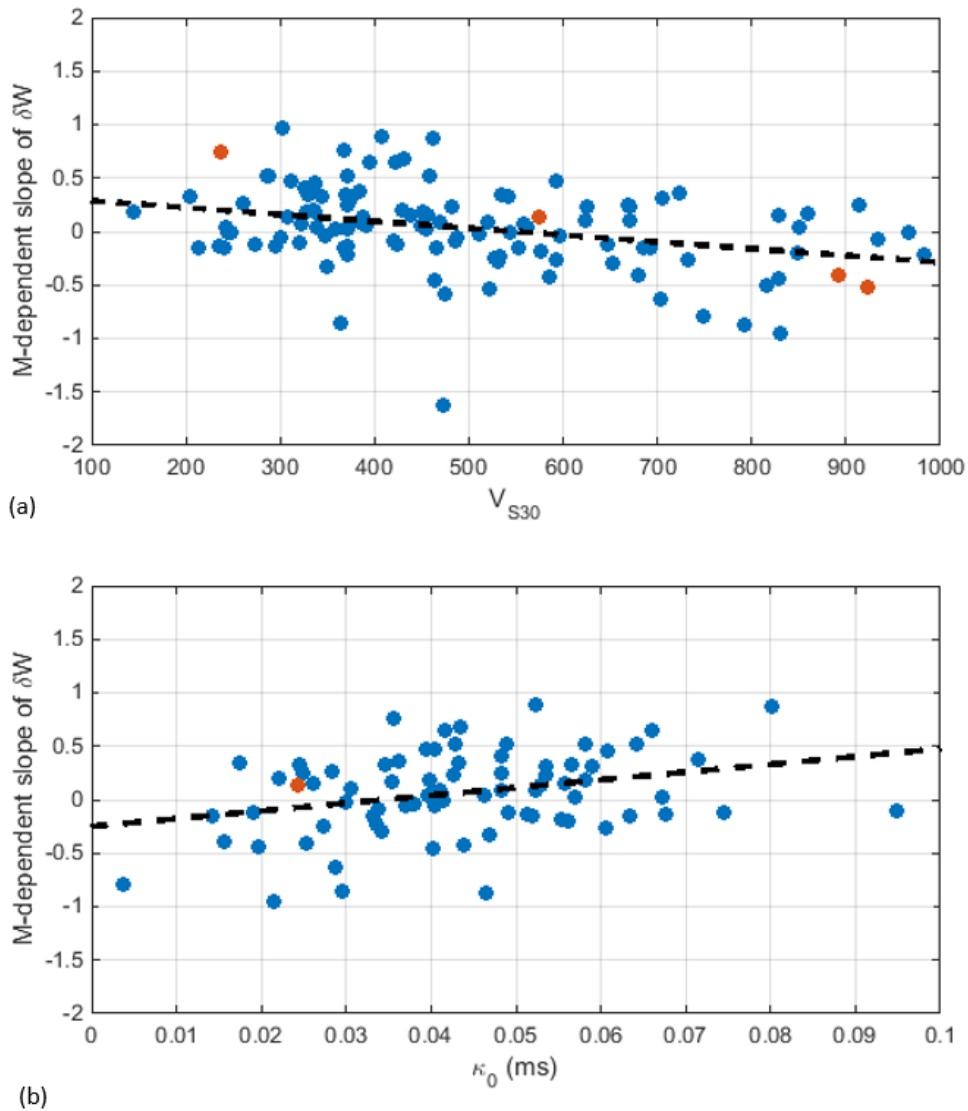


Figure 3.5. Slope of the within event residuals for 118 KiK-net stations with at least 30 records. Data in red identifies the stations shown in Figure 3.4. The dashed line corresponds to a linear fit to the data. a) plotted versus V_{S30} , b) plotted versus estimates of the site diminution parameter κ_0 (not all of the 118 stations had estimates of κ_0). From Stafford et al. (2017).

An indirect validation of the simulation results can also be obtained by comparing the estimates of site-to-site variability (ϕ_{S2S}) for different magnitude ranges. If the site terms ($\delta S2S$) are magnitude dependent for magnitudes lower than 5, as shown in the simulations discussed in Section 4.3, then we expect larger site-to-site variability for the lower magnitudes. The larger variability would result because the rate of magnitude-dependence is likely different for each station, thus adding to the site-to-site variability when magnitude dependence is expected (for $M < 5$). Figure 3.6 shows estimates of ϕ_{S2S} from the KiK-net data for $M \leq 5$ and $M > 5$. Observe that, as expected, at short periods there is a stark difference in values. Similar observations were made on the NGA data by Linda Al Atik (*personal communication*).

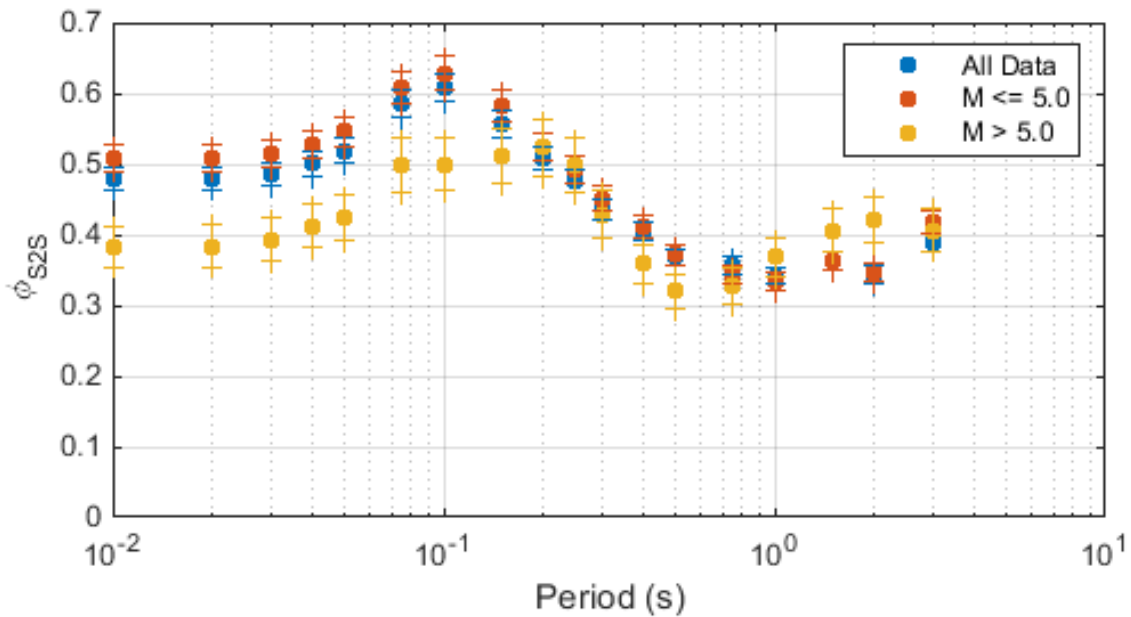


Figure 3.6. Site-to-site standard deviation (ϕ_{S2S}) for the KiK-net database, considering only stations with at least 10 recordings. The data is shown separately for different magnitude ranges. From Stafford et al. (2017).

3.5. Chapter 5: Inversion for source, path and site parameters

Text following Eq. (5.5). Please provide a stronger reference for $\beta=2.0$ km/s. As noted previously, this value is not consistent with the value from Chapter 4 (2.6 km/s). Is this a typo or is there a mismatch between these calculations?

It is noted that ‘the shear-wave velocity at the source, $\beta = 2.0$ km/s. This differs to the path average $\bar{\beta} = 2.6$ km/s and is taken with a high degree of confidence from NAM’s 3D V_s model. To avoid confusion we changed average shear-wave velocity symbol to $\bar{\beta} = 2.6$ km/s at these locations: (1) p.39, 2nd paragraph; (2) Figure 5.8 caption; (3) Equation (4.2); (4) Changed row ‘shear-wave velocity’ to ‘shear-wave velocity at source’ and add row with ‘average shear-wave velocity’ $\bar{\beta} = 2.6$ km/s to Table 6.1, which is reproduced in this document as Table 2.1).

P 60-61. The frequency-independent Q that is used is likely not correct, but may not be consequential for the distance range for which the simulations are performed. The discussion could be simplified in this regard – instead of justifying why Q is frequency-independent (which is likely not correct), it could be indicated that the frequency-dependence, while likely present, is not important.

There seems to be an inconsistency between $Q=150$ in the NS_B half-space and $Q=200$ in the simulations.

In the V4 report we added after p.61, line 8 “...reject the null hypothesis of frequency independent Q. Furthermore, while the influence of Q and its frequency dependence may be an issue at regional scales, the short path lengths relevant to the seismic risk of the field do not justify trying to constrain a more complex functional form for Q. We would note that while Q models are frequently presented frequency dependence, it is still a debated phenomenon – a trade off with geometrical spreading occurs that presents artefacts appearing to be frequency dependence. This is highlighted in Figure 5.4 [V4 GMM report, shown as Figure 3.7 here], where the effect of damping due to Q is shown for the frequency independent model adopted, and for a corresponding frequency dependent model. Frequencies up to 10 Hz are shown as above these frequencies PSA is controlled by increasingly lower-frequency ground motion. The differences shown are significantly below the uncertainties of other parameters (such as stress-drop).”

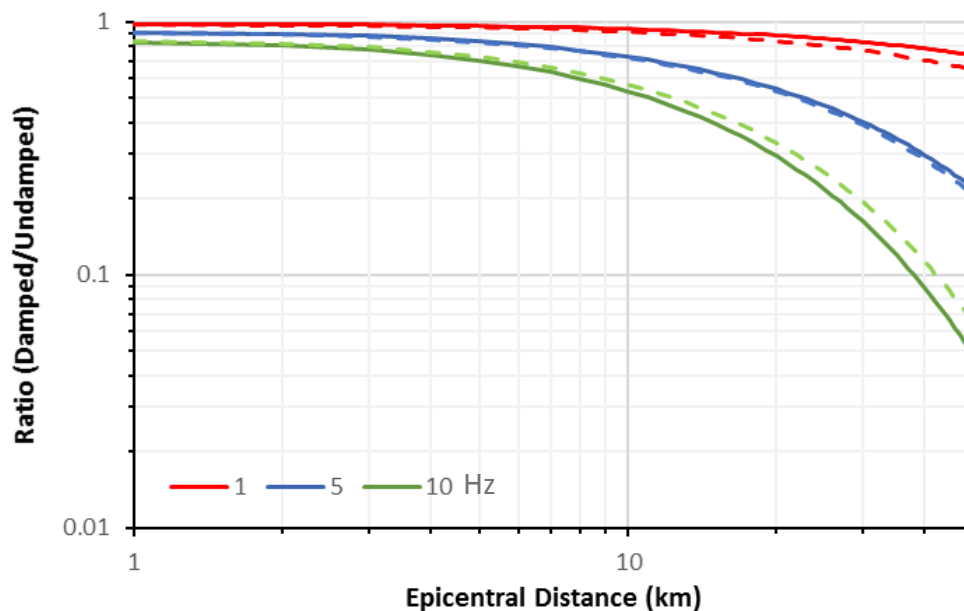


Figure 3.7. Effect of damping due to crustal Q. Solid lines indicate a frequency independent $Q = 200$; dashed lines are for $Q(f) = 140f^{0.2}$. Note that data is available to ~ 25 km.

A quality factor Q of 150 is the value given to the top of the half-space (*i.e.*, at the NS_B with 1.4 km/s velocity). It is consistent that this is lower than the value representative of the model space between the reservoir and the NS_B since Q typically decreases toward shallower depths.

[Fig 5.11](#) shows an apparent positive trend in the residual misfit for kappa vs distance; by eye, the slope appears to be $\sim +0.0013$, which would be significant for $R > 15$ km. Please plot a trend line and test the significance of the slope.

This comment was addressed in the revision of the V4 GMM with the inclusion of Figure 5.12, reproduced here as Figure 3.8 for convenience of the reviewers. The residuals obtained with $Q = 200$ are zero-centred, by definition, but show a very small trend with distance that is not considered to be important, especially within the range of application of the model in the Groningen hazard and risk modelling.

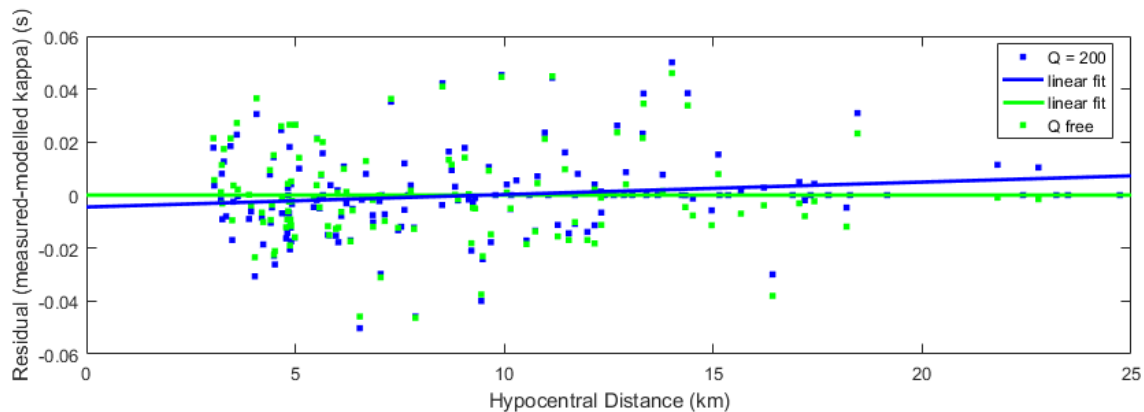


Figure 3.8. Residual misfit of the κ values as a function of distance using the V3 Q model ($Q = 200$, average velocity 2.6 km/s) and with a free Q determined as part of the inversion.

Section 5.4. The simulations show frequency-dependent geometric spreading (apparent), but data does not. There needs to be a clear statement in the text on whether frequency-dependent geometric spreading was applied in the final model or not.

On p.68 at the end of the 1st paragraph in the revised V4 GMM report we added the following text: “*Frequency-independent geometrical spreading (in terms of FAS) was used in the simulations.*”

Figures 5.6-5.7 show PGV for different frequency bands. It is not clear what this means. Are these plots of the FAS or of a band-passed filtered PGV, or are the plots mis-labelled and these are spectral accelerations?

This was clarified in the revision of the V4 GMM report where we added the following text: “*In Figures 5.7 and 5.8, the PGV value are narrow-band limited ground velocities; the frequency indicates the central frequency.*” In other words, the signals are narrow-band filtered and then the PGV of the filtered signal is determined. This was also clarified in the captions of the figures (now Figures 5.7 and 5.8).

Figure 5.19. Comments on the inverted stress parameters:

- Is the stress calculation based on the fitted corner frequency (or did it incorporate the amplitude level)? It would be useful to plot corner frequency vs M. The relationship of the stress parameter to the spectra needs clarification.

- Regarding Figure 5.19, are the stress parameters from alternate versions of the model comparable? If not, please make a version of this figure that shows only the stress estimates for V4, so that trends (if any) will be more apparent.

Figure 5.19 considers only the corner frequency, f_0 (Eq. 5.4). Amplitude level trades off with M_0 so cannot see the advantage for these events with uncertain M_0 . Figure 5.19 now shows corner frequency vs M . Figures 5.18 and 5.19 were updated to show only the V4 values.

3.6. Chapter 6: GMPEs for reference rock horizon

Fault dimensions (p 75). Why not use Leonard 2011 for the fault dimensions (more recent than Wells and Coppersmith, 1994)? Whatever reference is used, the source areas that are used should be checked for compatibility with stress parameters.

We noted in the revised V4 GMM report our reasoning that all fault scaling models are equally inapplicable to the unique setting of Groningen, or at least their applicability is entirely unproven and, for now, cannot be substantiated. The Wells & Coppersmith (1994) relations were chosen as a commonly used model for this purpose; little consideration was put into improving this aspect due to the fact that we do not believe any tectonic model is particularly relevant in this setting.

Fault dimensions were not adjusted for the stress parameter. Our reasoning here was that (a) the stress parameter is not necessarily a physically meaningful value; (b) even if our stress parameter represents a 'stress drop', the link to static stress drop is not fully understood; and (c) our use of stress parameter was designed to capture the range of epistemic uncertainty in our ground-motion predictions, and adjusting the fault dimensions would counteract this aim.

Seismogenic depth (p 75). Is the seismogenic depth of 13 km (see also Table 6.1) justified? What fault aspect ratio is obtained for the largest M ? The studies shown in the Mmax workshop should be cited.

The basis for the seismogenic depth was presented in the revised V4 GMM report, at the foot of p.78: "*Ruptures grow downwards (i.e., $Z_{top} = 3$ km), limited by the seismogenic depth (13 km). This depth is inferred from two sources of information: Cacace (2008) developed rheological models that identified increasing crustal strength down to about 10 km followed by weakening due to elevated temperatures, which might indicate a seismogenic depth on the order of 10 km. Yudistira (2015) estimated crustal velocity profiles from ambient noise measurements, and from the profiles developed a seismogenic depth of 10-13 km would be inferred; at 13 km, there is a marked velocity contrast, with V_S increasing from 3.1 to 4.0 km/s.*"

The maximum aspect ratio realised in the EXSIM simulations was 9.5.

Durations used in simulations (p 76). Report states “Since the input duration for EXSIM_dmb is not the same as that used for the V3 duration model (i.e., $T_{5,75}$), an initial calibration step is undertaken to ensure that the duration of simulated events (at small magnitude) is, on average, as defined by the V3 duration model.” This is difficult to follow. Is the intent to make the duration of simulated event match the V3 $T_{5,75}$ duration model? The subsequent text in the report suggests otherwise: “The calibration showed that $T_{TEEXXSSIIMM} = T_{5,75}/0.383$ ($R^2 = 0.98$) which was then used along with the V3 duration model for $T_{5,75}(R, M=3, VS30=1500 \text{ m/s})$ to define $T_{TEEXXSSIIMM}$ at the NS_B reference horizon.” It appears from this sentence that the EXSIM durations are modified relative to those from the V3 model.

Related to the above, the duration model used in the simulations is based on the V3 duration model. As noted in the text and comment M13, the V3 duration model uses multiplicative source and path durations, which is different from EXSIM durations in which source and path durations are additive. This leaves us confused on how the calibration was done. Was the path duration changed or the source duration changed? The calibration done to make the V3 model work with the EXSIM input is only valid for the range of the data and would not appear to be valid for any extrapolation.

EXSIM requires an input duration for the individual sub-faults. However, this is not exactly $T_{5,75}$ – but a duration (T_{EXSIM}) somewhere between $T_{5,75}$ and $T_{5,95}$. We have simply modified the V3 model for $T_{5,75}$ such that, when input into EXSIM (as T_{EXSIM}), it produces output waveforms that have duration equal to the V3 $T_{5,75}$ model. In the revised V4 GMM report we changed the text as follows:

“The input duration for subfault motions in EXSIM_dmb (T_{EXSIM}) is not equal to $T_{5,75}$ (as provided by the V3 duration model). Therefore, an initial calibration step is undertaken to ensure that the output duration of simulated waveforms (at small magnitude) is consistent with the V3 $T_{5,75}$ duration model. The calibration showed that $T_{EXSIM} = T_{5,75}/0.383$ ($R^2 = 0.98$). The input duration for subfault motions in EXSIM was therefore defined as: $T_{5,75}(R, M=3, VS30=1500 \text{ m/s})/0.383$, with $T_{5,75}$ given by the V3 Groningen duration model.”

The V3 duration model provides durations ($T_{5,75}$) that are consistent with Groningen seismicity and considered valid at $M=3$. Since we need only define the shaking duration for sub-faults (small ruptures, $M \sim 3$) this is sufficient (no extrapolation is needed or performed). The simulation then computes the total duration through summation of the contributions from individual sub-faults.

Bias expression (p 77, Eq 6.2) and subsequent optimization exercise. We do not understand the terminology used for the optimization. RMS bias seems like it is the standard deviation of the Bias(T) averaged over T. What is the sigma(RMS bias)? Equations should be written to define these two terms.

These comments were addressed in the revision of the V4 GMM report, with equations introduced as suggested: see Eqs.(6.1) onwards on p.80. For additional clarity, the relevant equation numbers were added to the captions of Figures 6.2, 6.3 and 6.5.

Note that Eq. 6.1 will generally require a constant term to force the mean of the event terms to be zero. How is this constant term considered in the RMS bias calculations?

There is no reason for the mean of the event terms to be zero for these simulations: η_i simply defines a weighted event-term: this is what the bias is measuring. The subsequent analysis of the bias terms allows us to select models that do have average event terms that are, on average, zero (or minimised).

We do not understand how the best fitting model was selected based on the smallest RMS average misfit and sigma. What is RMS average misfit? How are these combined? An equation should be added to the text to show how these two terms are combined.

The RMS bias (or $|b|$) simply means the modulus of the bias, and the average is the average over the 23 periods; this is now presented in detail in the revised V4 GMM report, as explained above. These terms are not (and cannot, without some subjectivity) be combined. They are used independently to assess the behaviour of individual models. Both average RMS bias (*i.e.*, period-independent $\overline{|b|}$), and the spread of those values $\sigma_{|b|}$ with respect to period were considered by the GMM development team.

Figure 6.5 (p81). We do not understand the terminology of RMS bias and sigma(RMS bias) so we cannot comment on the model selection.

The explanation of this terminology has now been refined and expanded in the revised V4 GMM report (see responses to comments above).

Figure 6.6 (p81). Are all the stress parameter estimates from V1, V2, V3 and V4 strictly comparable because the other parameters of the different versions of these stochastic models are different? If not then it is suggested to delete those from V1 to V3 from this plot because they are confusing and do not add to the discussion.

This suggestion was implemented in the revised V4 GMM report.

Figure 6.14-6.29 and 6.48-6.53. Most of the graphs show a rapid increase in ground motion until about 4.5 and then much reduced magnitude scaling until 5.5 and then a much steeper increase again. This is unusual and not commonly seen in stochastic (e.g. Douglas and

Jousset, SRL, 2011) or empirical models. What is the physical reason for this reduced magnitude scaling in the magnitude range 4.5-5.5? At short periods, we expect that this is due to the magnitude-dependent stress parameter (from M3 to M5). We don't understand why there is a break at long periods (e.g. 5 sec shown in Fig 6.53). This would be lower than the corner frequency, so the reason for the break is unclear. Did the authors consider a model with a monotonically decreasing slope with increasing magnitude?

We do not believe that we should expect to see scaling consistent with analyses like those of Douglas & Jousset (2011). That analysis—and the vast majority of other analyses like it—assumes constant stress drop, constant rupture velocity and point-source rupture dimensions (or some effective distance to adjust the point-source predictions). Similarly, we should not expect empirical models to capture these field-specific breaks in scaling as most empirical datasets have far deeper hypocentres, preferentially rupture up-dip, and do not have such a significant difference in stratigraphy (or at least such differences are smoothed over the ergodic dataset).

The breaks in scaling that are incorporated within the EXSIM simulations relate to the magnitude-dependent stress drop (as the reviewers note), but also to changes in the rupture velocity for sources starting in the reservoir but propagating down into the carboniferous, and changes in the source scaling dimensions going from a Brune-style source for the smaller events into Wells & Coppersmith (1994) source dimensions for larger events. Furthermore, the rupture geometry is such that ruptures always initiate within the reservoir and propagate down into the carboniferous. Examples of the EXSIM simulations for long response spectral ordinates are shown in Figure 3.9 where it can be seen that the model predictions represent the simulated scaling very well. It is therefore clear that the breaks in scaling observed in the report are not some artefact of the regression analyses. As noted by the reviewers, the changes in stress drop and, to a lesser extent, rupture velocity (if its impact is assumed to be linked just corner frequency) should impact short-periods more so than longer periods. However, the rupture velocity changes significantly when moving from within to below the reservoir and impacts upon the triggering of the EXSIM sub-faults, and hence both the spectral amplitudes and the source durations.

We did consider a model with decreasing slope with increasing magnitude. In fact, our spectral model is precisely of this form. We have quadratic scaling at both small and large magnitudes. The only linear magnitude scaling exists of the small section between the red vertical lines shown in Figure 3.9.

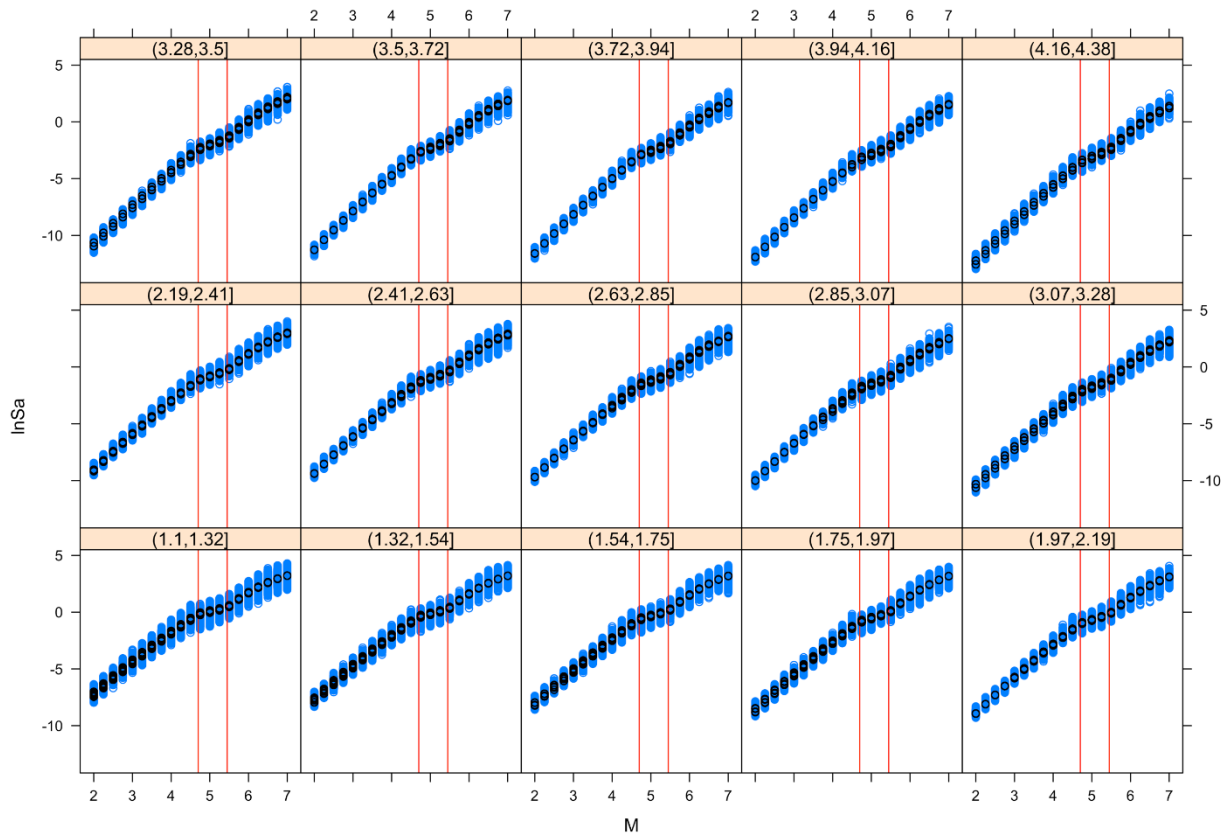


Figure 3.9. Long-period ($T=5.0s$) response spectral scaling with magnitude. Each panel shows EXSIM simulations (*blue markers*) and model predictions (*black markers*) for the natural logarithmic distance bins noted in the header.

[Figure 6.54-6.59](#). The spectra consistently show a bump at about 1.5 sec. We did not find any discussion of this unusual feature in the report. Any explanation?

We are not entirely sure what the origin of this ‘bump’ is, but it has been persistent throughout the model development, and, if anything, has strengthened in going from V4 to V5. The presence of this feature is now noted and acknowledged in the GMM reports (see p.136 of the revised V4 GMM report) although we are not yet able to provide a definitive explanation for its appearance.

We are confident that this is not an artefact of inappropriate site response modelling that has influenced the transformation of surface and borehole motions to the NS_B horizon because we see this ‘bump’ as a field-wide characteristic and it is observed as an output of the EXSIM simulations. These simulations do not explicitly include any such ‘bump’. However, regression coefficient m_4 at $T=1.5$ seconds is very slightly higher than one might expect and this causes this bump to manifest for these larger magnitude values. This issue needs further exploration and will be part of ongoing work in the future. As far as the V5 GMM is concerned, our view is that bump may well have a genuine physical origin and therefore we prefer to retain it rather than attempt to remove it or smooth its influence out of the predicted spectra.

Figure 6.61. The final range of the four models captures the increase in the uncertainty as the model is extrapolated to large magnitudes, but the range seems too narrow at M3 for some periods (e.g. T=1 sec). There is data in this range, but does the range capture the statistical uncertainty from the regression?

The statistical uncertainty from the regression is extremely small because we make use of 436,800 EXSIM simulations within our 'statistical analysis'. However, some estimate of the statistical uncertainty for the M=3 data can be appreciated from Figure 6.42 of the revised V4 GMM report, where the bias for each stress drop is presented as a function of period. Note that this is the bias, given the fixed model calibrated from the EXSIM simulations. This figure indicates that we have something like a 10% range in predicted medians at the longer periods. While it may not immediately evident from Figure 6.61 that is showing over 5 decades of amplitude, this ~10% spread is consistent with that figure.

Working with the empirical data directly, if we compute the standard error in the estimate of the mean for the records that are available at 1.0 seconds then we find a good degree of consistency with the spread implied by our four model branches.

This is also corroborated to some extent by the fact that our V4 and V5 model predictions for small magnitude events at relatively long periods are extremely similar. Therefore, the act of adding more new data to our analyses has not caused introduced any volatility for these longer period ordinates at these small magnitudes.

3.7. Chapter 7: Site response model

P 160, 2nd para, 3rd bullet. Why was randomization only applied to the GeoTOP depth range? Variability below this range was not considered - please explain why? The impact on site response is not insignificant at these greater depths.

The choice to ignore uncertainty in the V_s profile below the GeoTOP depth range was dictated by the fact that the properties of these layers were expected to be relatively uniform across the Groningen field, especially at small spatial scales. If there was an error in the V_s model, and the error was systematic across the entire field, then the effects on site response of this error would be mapped to the site-wide site response term used in the inversions for the NS_B motions. For this reason, we considered that details of the site response of these layers would not be as important as the details of site response of shallower layers. What this approach does not capture is the potential effects on site-to-site variability of spatial variations in the V_s profile. We believe that the minimum epistemic uncertainty (e.g., the model error, see Figure 9.11 in the revised V4 GMM report) that is imposed on the site-to-site variability accounts for this potential source of error. We note that the uncertainty in the amplification functions computed from the 1D site response analyses is generally

lower than this minimum epistemic uncertainty value at long periods (where the details of the deeper velocity structure would have a larger impact).

Sec 7.6. Kishida et al. 2009 claim there were problems with the MRD curves in Wehling et al. 2003, so it is maybe better to not use those data points in your regression of the peat model.

After reading this comment, we have reviewed the Kishida *et al.* (2009a,b) publications and we have not found anything that we can interpret as being the said claims. The reviewers might have been referring to the fact that the Wehling *et al.* (2003) peats had different behaviour than the Sacramento-San Joaquin Delta peats. However, the data in Wehling *et al.* (2003) is consistent with the data from other peats (see Figures 7.17, 7.18, and 7.20 in the revised V4 GMM report), thus we believe it is adequate to include it in our regressions. Kishida *et al.* (2009a) do indicate that their own data for peats from the Sacramento-San Joaquin Delta, for which the model was intended, show less dependence on consolidation stress than the data from Sherman Island peats in Wehling *et al.* (2003). However, peats from other regions show a confining stress dependence that is more similar to that of Wehling *et al.* (2003) than to the peats tested by Kishida *et al.* (2009a). This is also the reason why we did not adopt directly the Kishida *et al.* (2009b) model, as indicated in the report (Section 7.6). It is also important to note that there is now data available for Groningen peats, and these data were used in the development of the V5 model to update the MRD model for Holland Peats in the Groningen field. (Konstantinou *et al.*, 2017).

3.8. Chapter 8: Site response analyses

Input motion duration (p 190). Why use Boore and Thompson 2014 durations and not those for the duration model developed in this study? There also seems to be an incompatibility with the durations used in the simulations for GMM development (Chapter 6, p 76).

We concur that there was, in the original V4 model development, a degree of incompatibility in so much that the input motions were calculated using the V3 GMM. This was simply due to timing constraints: the models have been developed over short time intervals that did not allow for iteration. However, the duration input was subsequently updated to be consistent with the V4 model. For the V5 model, this problem has been overcome and all elements use the same base seismological model for the GMM.

In the revised V4 report (p.197, last paragraph) we now note that “*The durations are calculated by using the V3 duration model (calibrated to the small M Groningen data) as input for the subfault duration in EXSIM, with the average reported over 500 time-*

histories randomly generated for each FAS.” Figure 8.30 in the original V4 GMM report was incorrect: it should effectively be (very similar to) the V4 duration model (Figure 12.21) and has now been removed.

Figure 8.33. The figure shows a strikingly low level of ground motion producing nonlinear site response (approximately 10-3g). Could the apparent nonlinearity at these low amplitudes be related to the same phenomena that produce the magnitude- and distance-dependent linear site response? Is there a double-counting effect occurring here if this is included both in the linear and nonlinear site response terms?

The reviewers are correct in indicating that the apparent nonlinearity is largely related to the scenario dependency of the amplification factors. This is addressed in the V4 GMM report (see Section 8.3, explanation after Figure 8.30). The text from the report is extracted below:

“A notable aspect of the AFs shown in Figure 8.30 is that the nonlinearity for very short oscillator periods is initiated at very low input motions. This occurs due to two primary reasons. First, we note that the input motions in the x-axis refer to motions that are applied at a depth of about 800 m. These motions amplify prior to reaching the surface layers where nonlinearity is triggered. Another reason for this apparent initiation of nonlinearity at low input motions is the magnitude and distance dependence of amplification factors discussed in Section 4.3. In particular, the distance dependence implies that the linear AF increase in value as the distance increases, which implies that for a given magnitude the AFs would increase in value for lower values of input motions. The net effect gives the appearance of nonlinearity. This is clearly seen in Figures 8.32 and 8.33. Figure 8.32 plots the AF for a selected zone and an oscillator period of 0.05 s, both using linear site response analyses and equivalent linear (EQL) site response analyses. In both cases, the observed AFs appear to be intensity dependent. When the same exercise is repeated for longer oscillator periods (where scenario-dependence is not expected), the linear AF behave as expected (Figure 8.33).”

As explained in the V5 GMM report (Bommer *et al.*, 2017e), the model for magnitude and distance dependence of the AFs was considerably improved with respect of that used in the V4 GMM. As a result of better accounting for magnitude and distance dependency, the value of the parameter f_3 in model for AF [Eq.(8.4) in the V4 GMM report] changed. This parameter is an indication of the level of input motion that leads to the initiation of nonlinear behaviour. The values at short periods increased

by nearly an order of magnitude from those of the V4 model, indicating that nonlinearity starts at higher input motions, as expected (Figure 3.10).

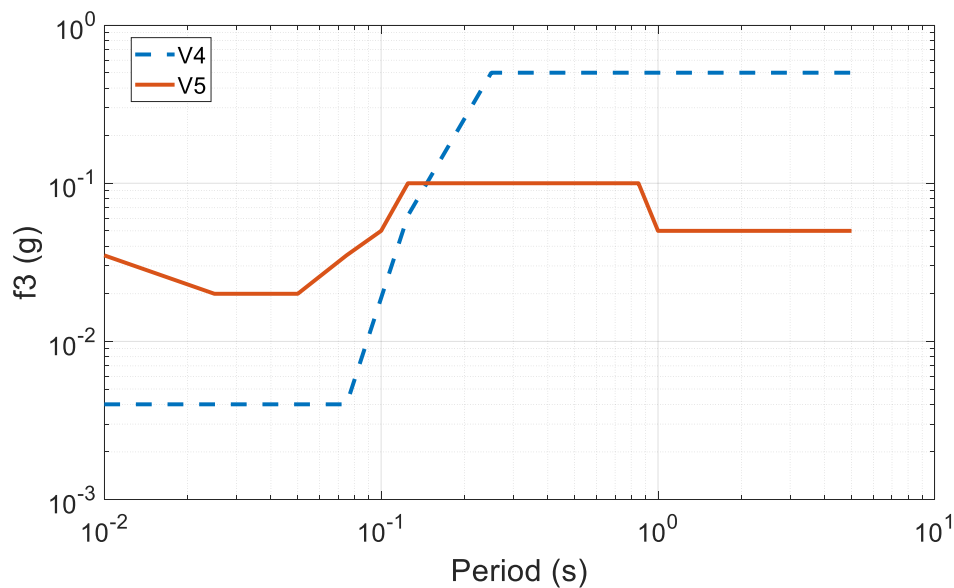


Figure 3.10. Models for parameter f_3 in the V4 GMM and V5 GMM.

3.9. Chapter 9: Zonation for site amplification functions

P 201. The report states that a single randomization per voxel stack was used and that multiple randomizations resulted in “not much difference in the resulting factors”. Isn’t it important to capture the distribution of the amp factors and so can you show that it doesn’t make a difference in the distribution whether a single or multiple randomizations are used?

A single randomisation per voxel stack was used, and all the voxel stacks within a zone were grouped to compute the amplification factors for the zone. This approach was adopted because the median and the standard deviation of V_S profiles across a zone are relatively uniform, and the alternative (*i.e.*, to generate multiple randomisation for each voxel-stack within a zone) would render similar results, but at a larger computational cost.

A simple exercise can illustrate how this approach works. We simulate N normal random variables with a standard deviation of 1 and a mean that is allowed to vary over a narrow range around zero (the means of the N random variables are normally distributed around zero with a standard deviation of 0.1). This mimics the distributions of AFs for all voxel stacks over a zones. Our objective is to obtain the mean and standard deviation of the union of the N random variables. We achieve this in two ways:

1. For each of the random variables, generate 50 realizations, and then pool all of the realizations to compute the pooled mean and standard deviation (equivalent to using multiple randomizations).
2. For each of the random variables, generate a single realization, and then pool these realizations to compute the pooled mean and standard deviation.

Approach 2 is the one adopted in the model (*i.e.*, a single randomisation per voxel stack). Table 3.1 shows the percentage of times that this approach resulted in an error greater than a given threshold. Since most of the zones have more than 1000 voxel stacks, the approach adopted results only in negligible errors (the mean is off by more than 10% only 0.3% of the times).

Table 3.1. Results of the exercise described above in terms of the expected percentage of times that Approach 2 can exceed certain error thresholds. The errors indicated are estimates of the error in computing the mean and standard deviation of the zones from using the “single randomisation per voxel stack” approach.

Sample size n	Number of zones with less than n voxel stacks	Error in mean $> 0.1\sigma$	Error in mean $> 0.05\sigma$	Error in Std > 0.1	Error in Std > 0.05
500	1	2.7%	26.3%	0.2%	11.8%
1000	15	0.3%	12.7%	0	2.3%
2000	38	0%	2.2%	0	0.1%

3.10. Chapter 10: Sigma model

Sec. 10.3. The ϕ_{SS} model as currently formulated is independent of distance. The simulated data in Figures 6.7-6.13 seem to show a higher dispersion at 3 km than at 32 km. Similarly, the residuals in Figures 11.49-11.67 seem to show higher dispersion inside of about 7 km than at greater distance. The formulation of a distance-dependent ϕ_{SS} model is worth considering in the V5 model development.

The selected models for ϕ_{SS} include an upper and a lower branch. These branches were selected to cover the epistemic uncertainty in the values of ϕ_{SS} , as described in the V4 GMM report (Bommer *et al.*, 2017c). The data computed using Groningen recordings matches relatively well the Upper Branch, as shown in Figure 3.11. On the other hand, the lower branch is consistent with ϕ_{SS} models developed from worldwide data and used in many hazard studies for critical facilities (see, for example, the review by Al Atik, 2015). There are also reasons to believe that the earthquakes in the Groningen region would sample a relatively uniform path, hence arguments could be made for the use of a single-path sigma, in particular when considering that the path-attenuation model from Groningen was carefully calibrated using recordings and simulations. The single-path sigma values could be

significantly lower than the single-station phi values. For this reason, the V5 Lower Branch is given equal weight to the Upper Branch in the logic tree.

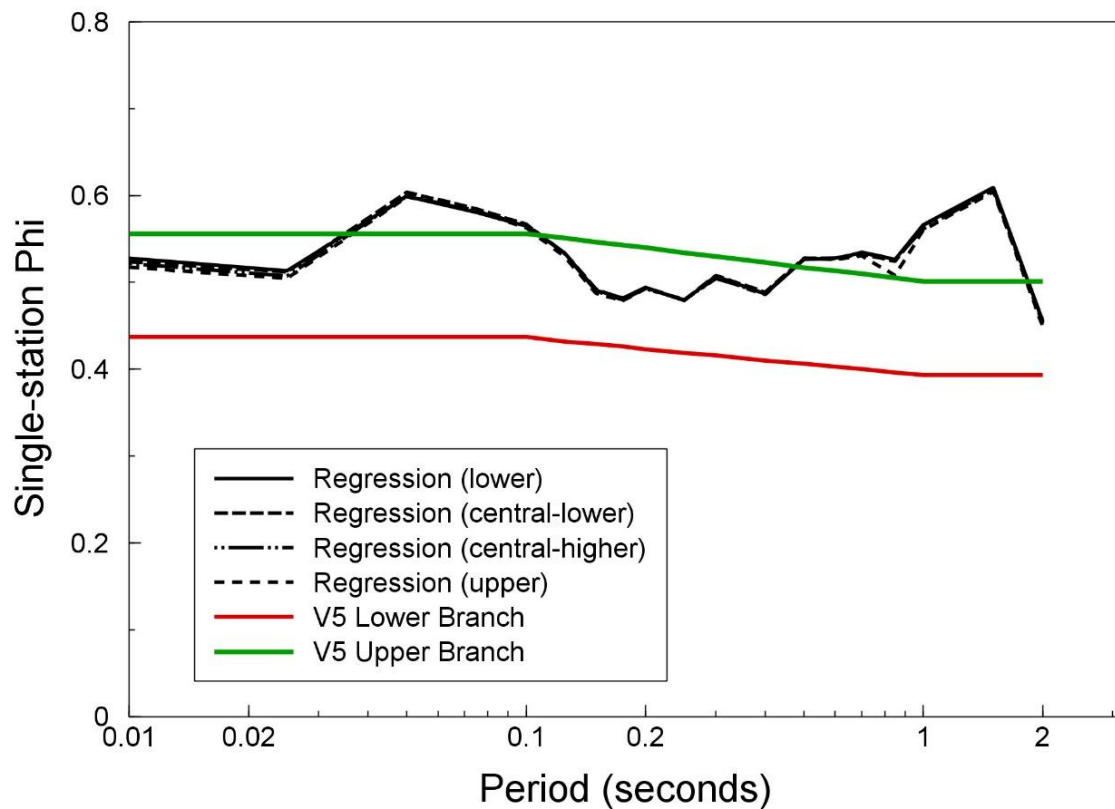


Figure 3.11. Single-station phi (ϕ_{ss}) models. Both the selected models (V5 Lower and Upper branches) and the values computed from regressions are shown.

Figure 3.12 plots the V5 models (Upper and Lower Branches) along with the ϕ_{ss} values from the magnitude- and distance-dependent model of Rodriguez-Marek *et al.* (2013), which were computed for the PEGASOS refinement project (PRP). Note that the PRP model includes distance dependence for low magnitude earthquakes ($M < 5$), but not for large magnitude earthquakes ($M \geq 7$). The V5 Upper Branch model matches the low M, short distance PRP model for short and long periods, while the V5 Lower Branch model matches the low M, large distance PRP model at both short and long periods. These observations imply that the range of selected models does cover the possibility of higher ϕ_{ss} values for shorter distances.

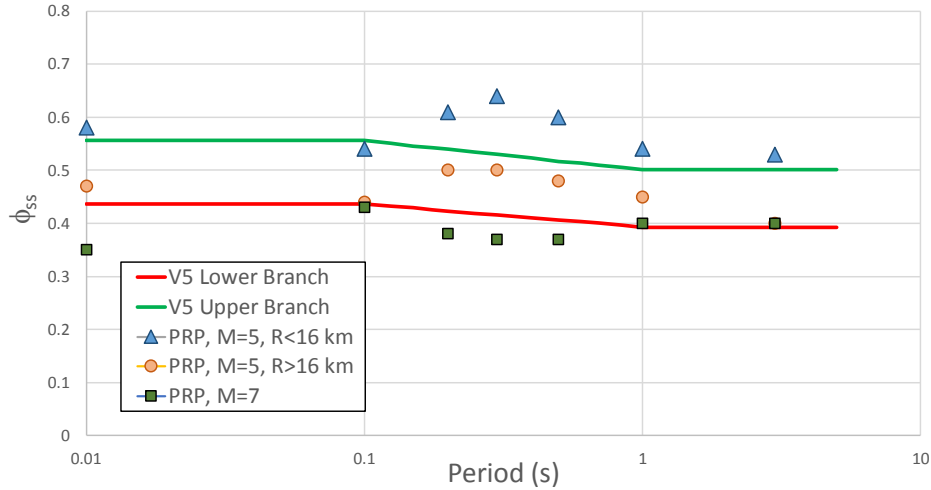


Figure 3.12. Single-station phi (ϕ_{SS}) models. Both the selected models (V5 Lower and Upper branches) are shown. The PRP data are from the magnitude and distance dependent models of Rodriguez-Marek *et al.* (2013).

Sec. 10.4. It would be useful to see a comparison of the reduction in ϕ_{S2S} for the individual zones compared to what would be obtained if all the zones were combined and a simple V_{S30} model, possibly coupled with site period, were used (see also comment M8). This is likely a consideration for the V5 model development.

We explore the suggestion of the reviewers by grouping all zones within a range of V_{S30} and site period (T_{ZONE}) values into a large zone (which we will call a ‘super-zone’). We compute the overall mean of amplification functions (AF) of the super-zone. We also compute the resulting standard deviation by assuming that each of the zones would contribute equally to the super-zone (*e.g.*, each zone has the same number of voxels), in which case the overall standard deviation is given by:

$$\sigma = \sqrt{\sum_{i=1}^n [(\mu_i - \mu)^2 + \sigma_i^2]} \quad (3.1)$$

where σ is the overall standard deviation of the natural log of the AFs, μ_i and σ_i are the mean and standard deviation, respectively, of the $\ln(AF)$ s of each zone, and μ is the overall mean of all the super-zone. Figure 3.13 plots the mean AFs for low-intensity ground motions for zones belonging to a selected range of V_{S30} and site periods. Observe that the overall average would imply that for voxel in certain zones, the mean is under-predicted, while it is over-predicted in other zones.

Figure 3.14 plots the standard deviations for each of the zones belonging to the same range of V_{S30} and site periods, along with the overall standard deviation. Observe that the overall standard deviation is larger than the standard deviation for most zones; however, it underestimates the standard deviation for some zones. This would imply that creating super-zones would lead to biased estimates of the mean and standard deviation for some regions of the Groningen field.

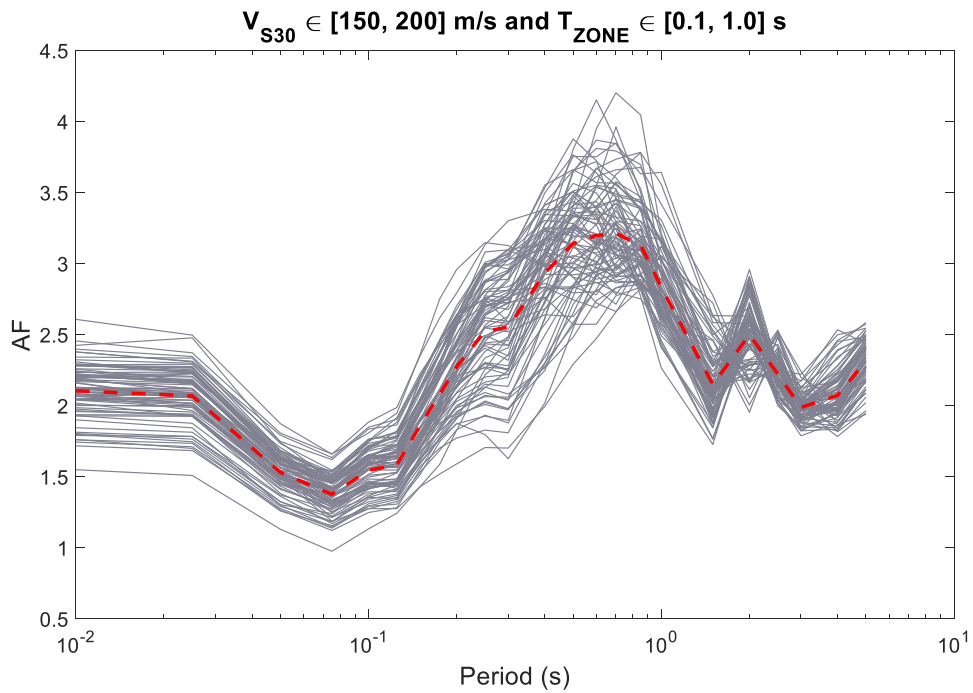


Figure 3.13. Mean AFs for zones with V_{S30} and site periods belonging to the indicated range. The red line is the mean AF for the super-zone created by joining all the selected zones.

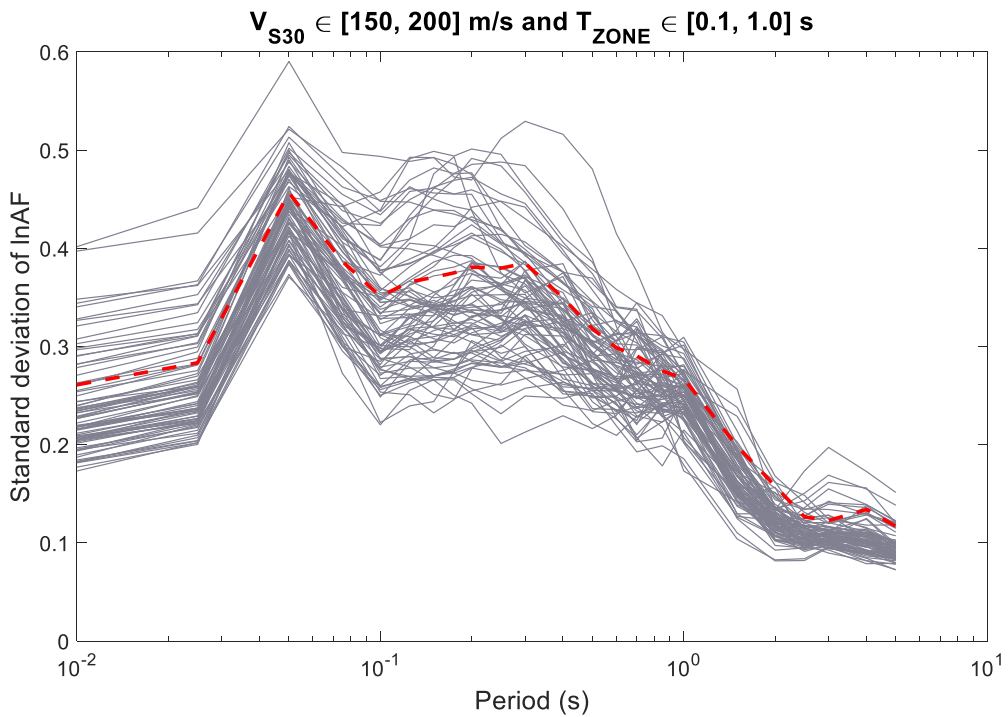


Figure 3.14. Standard deviation of the AFs for zones with V_{S30} and site periods belonging to the indicated range. The red line is the standard deviation for the super-zone created by joining all the selected zones.

3.11. Chapter 11: Application and extension of GMM for Sa(T)

Sec. 11.1, P 252. What was the rationale for imposing minimum and maximum amplifications?

The rationale for imposing minimum and maximum amplifications is discussed in Section 8.3 of the V4 GMM report. To reiterate, the minimum value is a conservative choice that limits the reduction in ground motions resulting from the extreme nonlinear behaviour in soil layers that yield under the applied loading. The maximum AF applies to cases when non-linear behaviour results in an increase in predicted median AFs with increasing spectral input spectral acceleration (S_{aNSB}), which implies a positive value of parameter f_2 (this can be seen for $T=3$ s in Figure 8.30). Positive values of f_2 occur in some cases for long periods ($T \geq 1.5$ s), and are observed because soil-nonlinearity pushes the soil into resonance at these long periods. However, this increase occurs only for a narrow range of strains (i.e., for a limited range of S_{aNSB}), hence an extrapolation of an upward trend in the median AF into higher values of S_{aNSB} is not warranted. Hence, the limit on AF is set to prevent this unwarranted extrapolation of the model in Eq. (8.4).

Figure 11.48. What is the explanation for a much greater spread in PGV (from near 0 to almost 150cm/s) than for SA(0.01s) for nonlinear response? We suspect that this parameter may not be well constrained and perhaps the manner in which it is being set may be unstable (especially for PGV).

The influence of nonlinearity on the amplification of PGV varies considerably across the zones. Some zones have a positive f_2 value (implying that nonlinear behaviour can lead to an increase in PGV), while others have negative values, yet others have values close to zero (nearly linear behaviour). For this reason, the spread of PGV values that can lead to nonlinearity is large. Rather than reproducing Figure 11.48 from the version 1 of the V4 GMM model, which was removed from the revised and updated version of the V4 GMM report in response to this review comment, we include below (Figure 3.15) a plot of the f_2 values for PGV for all the zones. The plotted values of f_2 explain the spread seen in Figure 11.48 from the original V4 GMM report. We note that for SA(0.01s), the values are always negative, with values ranging from -0.6 to -0.2.

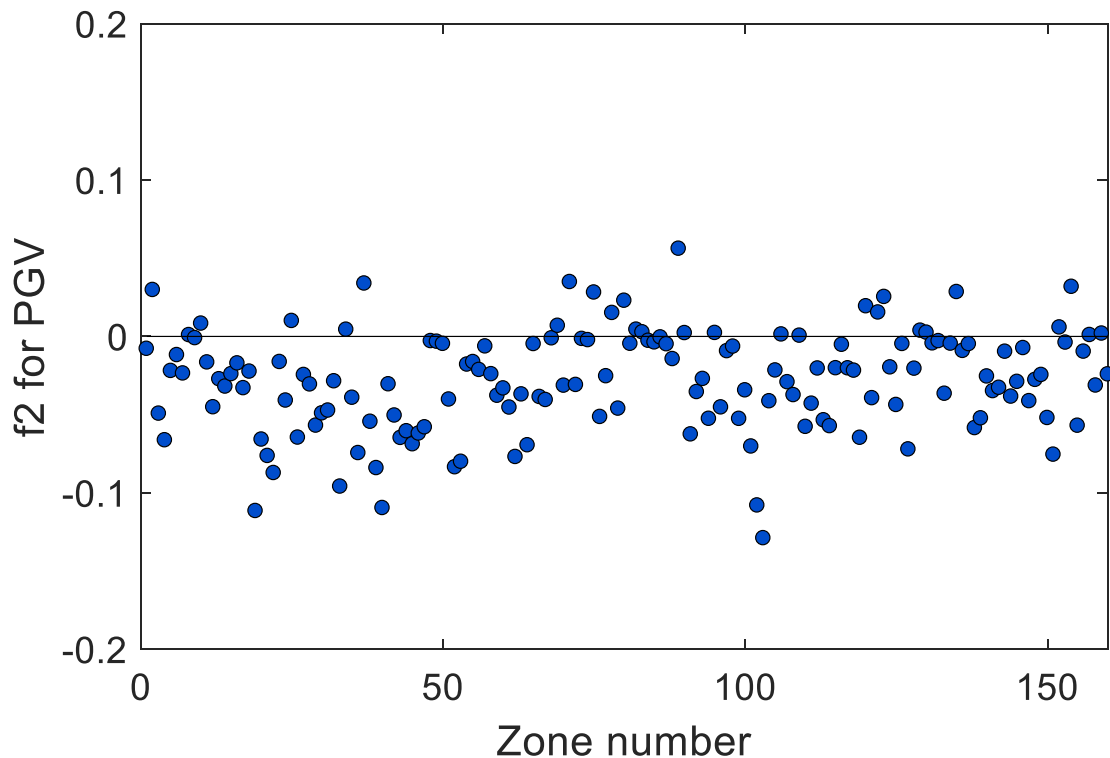


Figure 3.15. Values of parameter f_2 for PGV for all zones.

[Sec. 11.2, Figures 11.49-11.67](#). It would be useful to compute and report the overall bias as a function of period. Often this is removed from the residuals and then the event terms and within-event residuals both have zero mean.

The combination of Figure 6.42 and Figure 11.66 shows precisely the overall bias as a function of period. Figure 6.42 takes the total residuals at the NS-B horizon and partitions these while at the same time computing the bias. This bias is shown in the figure as a function of period. The figure shows that the central models are essentially unbiased at short periods and a deliberately biased for the extreme branches.

The series of figures from 11.47 to 11.65 in the revised V4 GMM report then shows the surface residuals computed after fixing the residuals associated with the NS_B horizon. These are plotted as a function of distance and by site for these figures. Figure 11.66 then takes the average of these surface residuals and plots them against period.

Clearly, from Figure 11.66, we have not removed the bias from the surface residuals in order to give zero-centred residuals because we report clear biases as a function of period in that figure. However, in the V5 model these biases have largely been removed.

Sec. 11.5, P 291. The V/H ratio is generally thought to be strongly dependent on site, in particular H/V peaks at a predominant frequency (e.g. Nakamura, 1989; Lermo and Chavez-Garcia, 1993) that is linked to the depth to bedrock and stiffness. The plots in Fig. 11.71-11.72 appear to confirm that M and R are not the controlling factors, suggesting that V/H may be controlled by site response. We suspect that noticeable V/H trends indicative of site response are smeared out by averaging the V/H ratio over all sites. Thus V/H may be inversely related to your computed amplification functions. Consider plotting V/H, averaged over all earthquakes, at each station and compare its inverse to your amplification functions. It may also work to group V/H by zone. The statement on p. 293 that a usable V/H prediction model is unlikely to be derived from local data may be untrue - it is quite possible that V/H is linked to site amplification and thus can be usefully determined from the local data (at least for linear response). The nonlinear component of site response affects the H component much more than the V component, which could be used as a refinement of a model based on local V/H data.

The first thing we need to state in regards to this comment is that to date the vertical components of motion have proven to be of limited importance for the Groningen seismic hazard and risk assessment. The following points can be noted in this regard:

- The vertical component is not considered in the hazard and risk calculations. Both for estimating building damage and liquefaction hazard, only the horizontal component of motion is considered.
- In the structural analyses performed for the derivation of the fragility functions, a suite of three-component accelerograms has been used; however, these are not scaled or adjusted to target spectra in the horizontal or vertical directions but used as recorded (Crowley & Pinho., 2017).
- In the shake-table tests for full-scale Groningen buildings, only those performed at LNEC in Lisbon were able to consider vertical loading; two scenario inputs were considered, the larger basing the vertical component on the V/H ratios of Campbell & Bozorgnia (2016) and the smaller, following the recommendations made for the V3 GMM (Bommer *et al.*, 2016b), used the same model but with higher ratios—by a factor of about 2—applied to the spectral ordinates at periods of less than 0.2 seconds. Currently there no plans to conduct any more shake table tests including vertical excitation.

For these reasons, and in view of pressured schedule to complete the V5 GMM, we have not invested effort in modifying the V/H model presented as part of the V4 GMM. However, we have given due consideration to these comments and suggestions from the reviewers with a view to possible future work on this topic, and we explain herein our responses.

The first point is that while the plots referred (Figures 11.71 and 11.72 in the original V4 GMM report) do suggest that magnitude and distance exert a limited influence on the V/H ratio for the Groningen data, the magnitude range covered by the data is

only 1.1 units and therefore it would be unwise to discard magnitude-dependence on this basis. Several models for V/H response spectral ratios do indicate a clear dependence on magnitude, especially for soft soil sites where strong non-linearity will affect, as the reviewers mention, the horizontal component of motion. To illustrate the point, we reproduce in Figure 3.16 plots from the study of Gülerce & Abrahamson (2011).

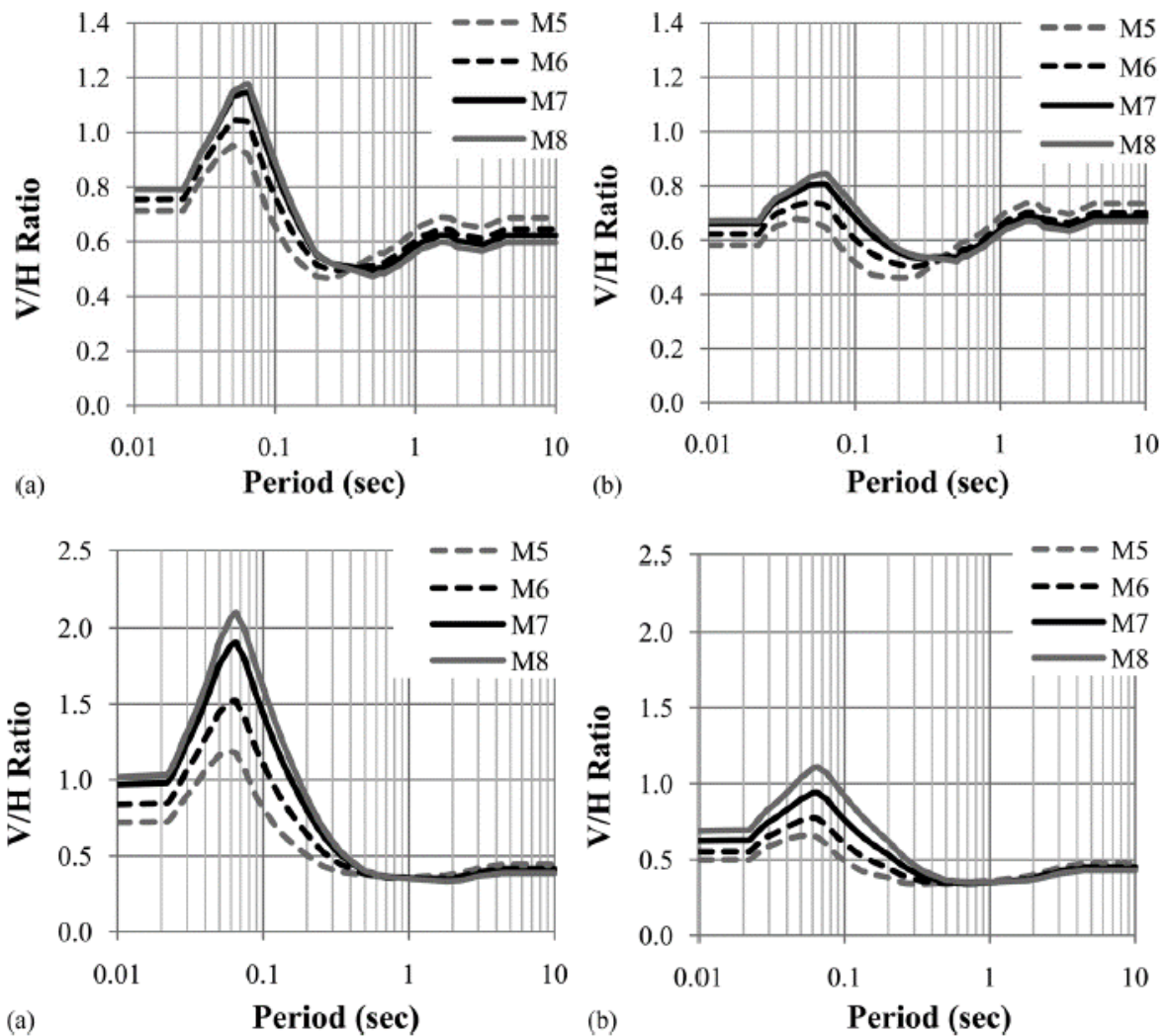


Figure 3.16. Predicted median V/H ratios from the model of Gülerce & Abrahamson (2011) as a function of period. *Upper*: Rock sites with $V_{S30} = 760$ m/s at (a) 5 km and (b) 30 km from earthquakes of different magnitude; *Lower*: Soft soil sites with $V_{S30} = 270$ m/s at (a) 5 km and (b) 30 km from earthquakes of different magnitude;

The plots also show that there is a very pronounced dependence on distance, even within the range of distance relevant to the Groningen hazard and risk analyses. The rapid decay of short-period V/H peaks with distance is common to most models and is reflected in the upper bound of the data points plotted in the figures to which the review comment alludes. We therefore find it difficult to conceive of a V/H model

for Groningen, applicable for magnitudes from 2.5 to 7.25 and for rupture distances from 3 to ~60 km, that is defined exclusively in terms of site characteristics.

We do note that in some projects, in particular the PEGASOS Refinement Project, V/H ratios were related to site response characteristics, invoking the work of Sanchez-Sesma *et al.* (2011) and Kawase *et al.* (2011) as providing the theoretical basis for such relationships. However, the report also acknowledged that “*while these theoretical relationships are valid only for average ratios, empirical observations do evidence the sensitivity of the V/H ratio to other non-site parameters: source-site distance, focal mechanism, and to a lesser degree magnitude*” (Renault *et al.*, 2014).

Notwithstanding our reservations regarding the feasibility of developing a useable model defined only in terms of site characteristics, we have explored the relationship between the V/H spectral ratios of the recorded motions and the reciprocals of the amplification factors calculated for the recording sites. For both of these quantities, the average values were calculated over all recordings from each station and some examples are plotted in Figures 3.17 to 3.19.

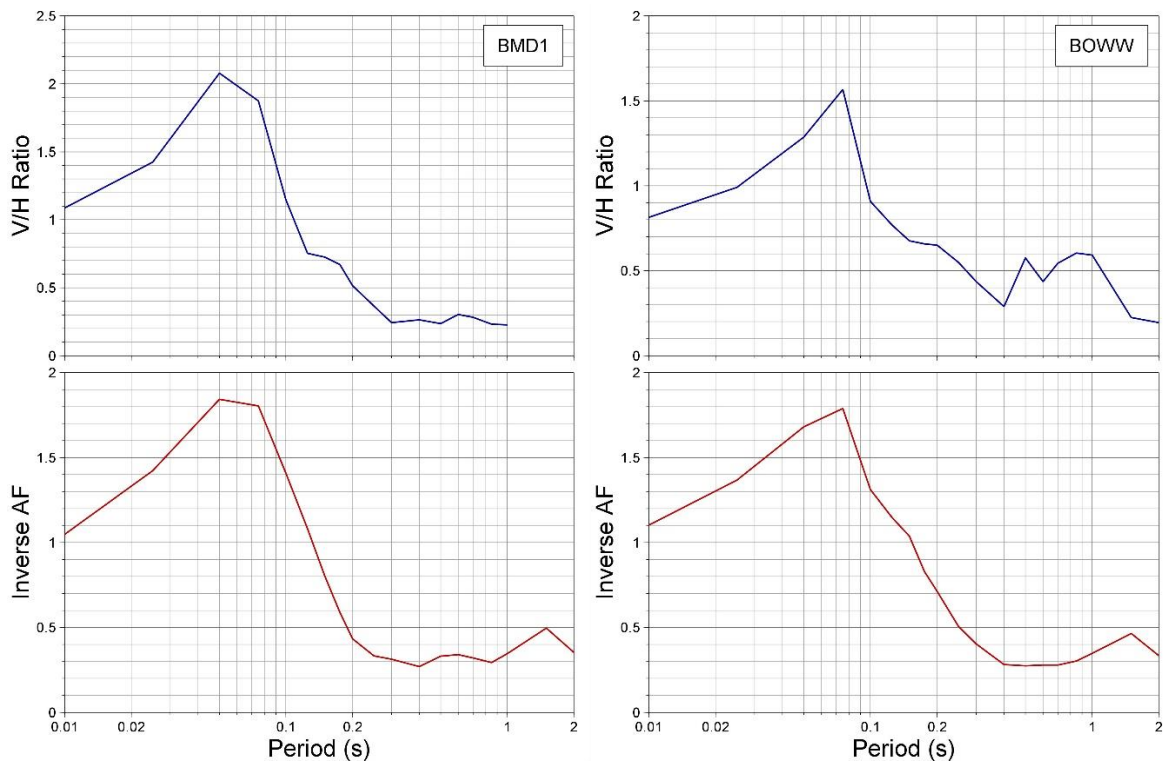


Figure 3.17. Examples of two accelerograph stations for which the average V/H ratios calculated from recordings (*upper*) provide a good match in both shape and amplitude with the inverse of the average AF for the site (*lower*)

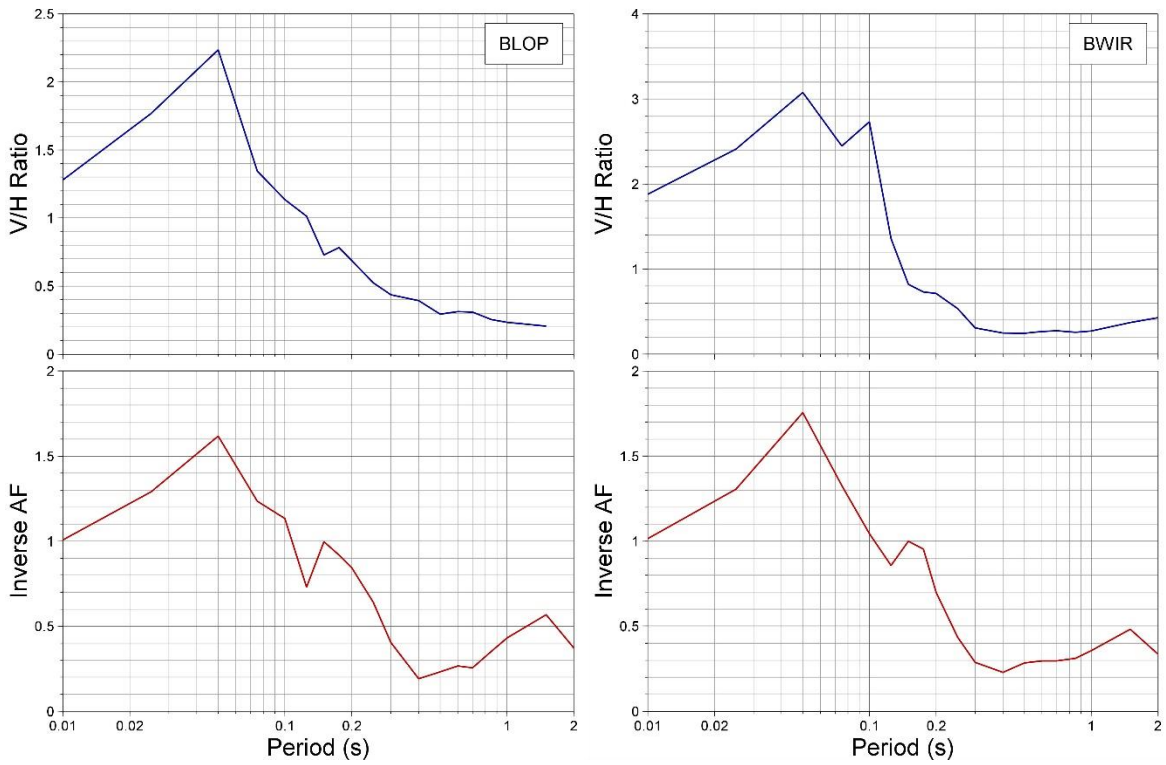


Figure 3.18. Examples of two accelerograph stations for which the average V/H ratios calculated from recordings (*upper*) provide a good match in shape but not amplitude with the inverse of the average AF for the site (*lower*)

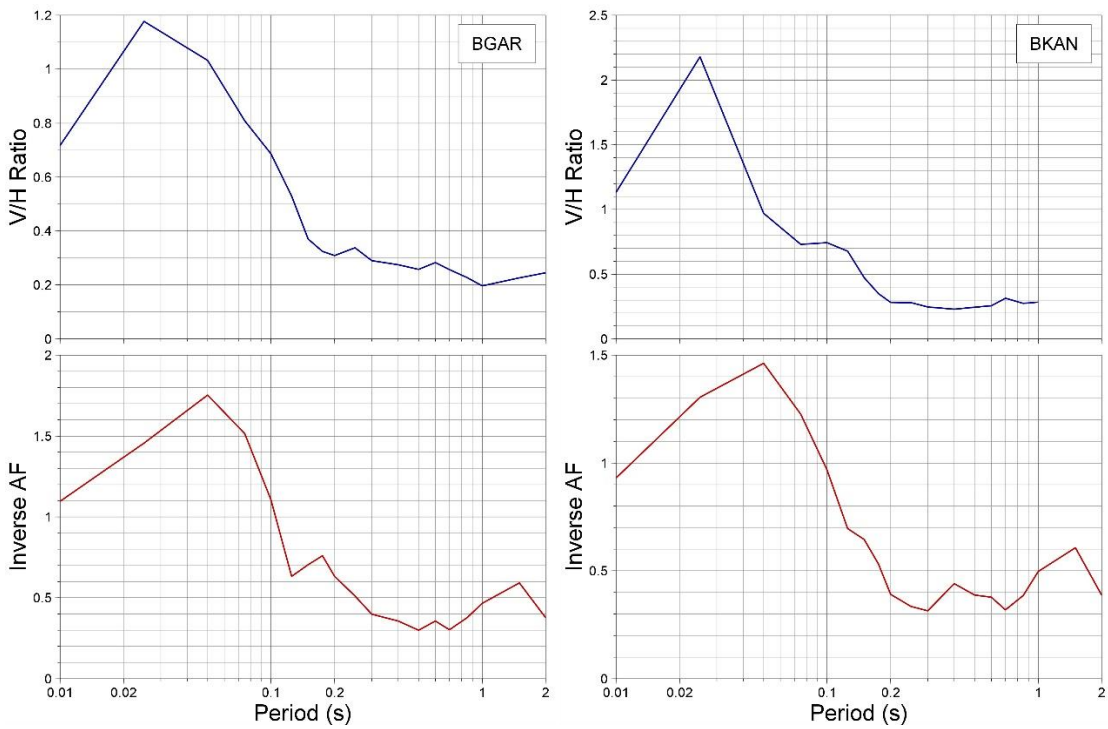


Figure 3.19. Examples of two accelerograph stations for which the average V/H ratios calculated from recordings (*upper*) do not provide a good match in either shape or amplitude with the inverse of the average AF for the site (*lower*)

The different patterns illustrated in these figures are representative of the database as a whole, as summarized in Figure 3.20, which shows the ratios of the response periods associated with the peaks of the V/H ratios and the inverse AFs and the ratios of the actual peaks, for all stations contributing at least two records to the V5 database. The figure also indicates the V_{S30} value for each station and the corresponding median V_{S30} for the zone hosting the station.

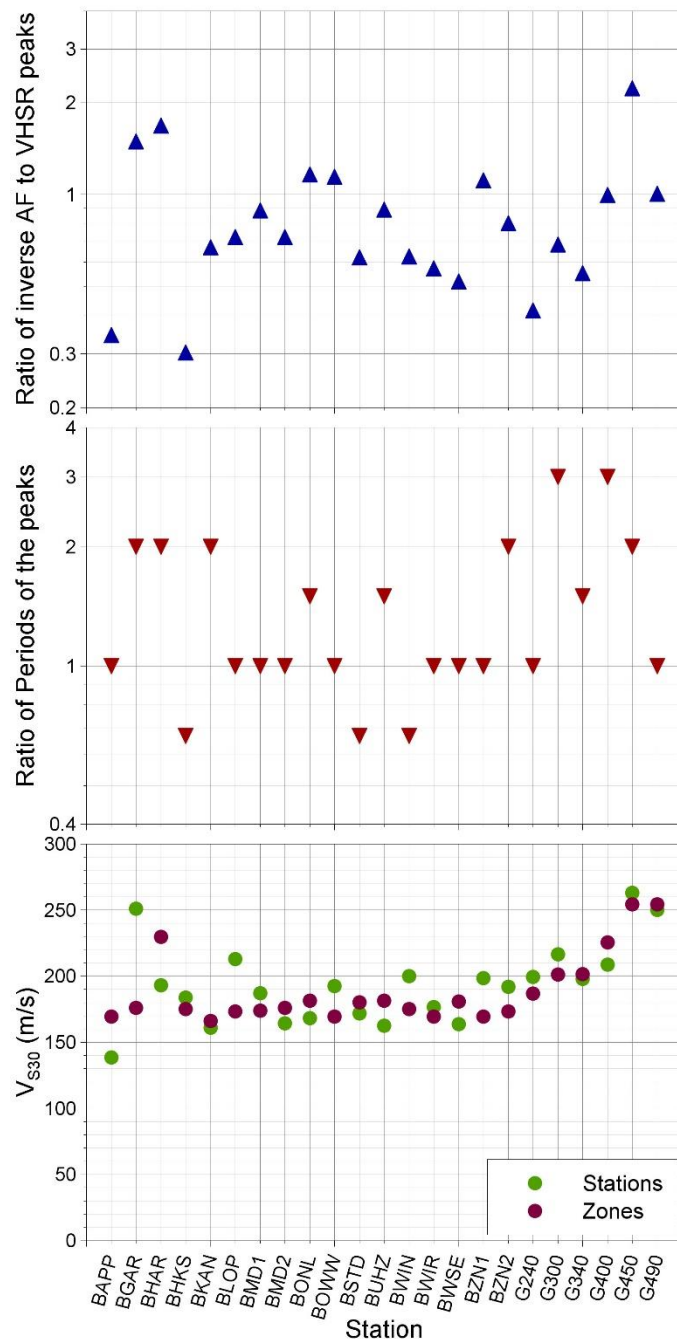


Figure 3.20. *Upper:* Ratios of the peak of the inverse AF to the peak V/H from recordings; *Middle:* Ratios of the periods associated with these peaks; *Lower:* V_{S30} estimates for stations and the host site response zones.

For 10 of the 23 stations, the period associated with the maximum V/H ratio coincides exactly with the peak of the inverse AF, which in itself is encouraging. However, for several of the other stations, the divergence between these two estimates of the peak periods is quite large. In terms of the amplitudes of these peaks, for only one third of the stations is the peak of the inverse AF within 20% of the measured peak of V/H. There are no easily discernible trends of the divergence with the site characteristics. On the basis of these simple exploratory analyses, our initial conclusion would be that pursuing a V/H prediction model based only on site characteristics does not look very promising.

[Figure 11.73](#). What is the explanation for the adjusted ratios beyond 4s? This is not described in the text.

The model of Akkar *et al.* (2014b) that was adjusted to match the V/H ratios from the Groningen data only provides coefficients for oscillator periods up to 4 seconds, hence there was a need to apply an extrapolation up to 5 seconds. In view of the small period-to-period fluctuations in the longer period range, it was decided that the simplest way to achieve this extrapolation was to maintain the V/H ratios constant beyond 4 seconds. Text was added (p.302) to the revised V4 GMM report to explain this modelling choice.

3.12. Chapter 12: GMPE for duration

See main comment M13.

An extensive discussion is provided in Section 2.13 of this report in response to the main review comment M13.

[Figure 12.2](#). The high level of noise in the pre-event portion of this record may indicate that the computed durations are not correct. This record seems to need a high-cut filter to remove that noise before calculation the duration.

This figure to which the reviewers refer was included in some exploratory analyses carried out as part of the V2 model derivation in order to identify the optimal duration parameter for the duration prediction equation. The record belongs to an earthquake with magnitude smaller than 2.5, which, due to the relative scarcity of data at that time, was included in the V2 database but not used in the regressions. Subsequent Groningen GMMs also predict the same duration parameter, D_{S5-75} , hence this section was carried over from the V2 GMM report to the V3 GMM report and then into the initial version of the V4 GMM report. However, the Groningen GMM ground-motion database has been since re-structured, with new event ID codes assigned to

the earthquakes and with events of magnitude smaller than 2.5 completely removed. Hence any mention of this and similar records has been removed from the updated V4 GMM report and the issue of the noise levels in the recording previously shown in Figure 12.2 is now moot.

3.13. Chapter 13: Concluding remarks

Related to the proposed future work on spatial correlation, some recent studies suggest that spectral correlations models may be magnitude-dependent (e.g., Kotha et al. 2017). This should be considered in the future work.

As explained in the V5 GMM report, explicit instructions for the sampling of variability components within each site response zone have now been included as part of the model to ensure that an approximation to spatial correlation of the ground-motion fields is achieved in the model implementation. Work is ongoing to develop a comprehensive spatial correlation model for the field using recordings from several different networks and also finite rupture-based simulations carried out by colleagues from ExxonMobil using the 3D velocity model for the field. We are aware of unpublished work by Nico Kuehn and Norm Abrahamson that incorporates magnitude-dependence into spatial correlations and we will be considering such effects in these analyses (although our empirical data have a very limited magnitude range). However, we are not aware of any other magnitude-dependent spatial correlation models. The finite difference ground-motion simulations may be able to provide insight into magnitude dependence of spatial correlation in the Groningen field.

Studies such as that of Kotha *et al.* (2017), and earlier contributions, include magnitude-dependence for inter-period response spectral correlations; but these are not directly relevant for the spatial correlation model.

4. Concluding Remarks

The V5 GMM for Groningen is the product of several developmental cycles and iterations to achieve a model that satisfies all of the basic requirements that were established at the outset of this work:

- A model for estimating median values and the associated aleatory variability of spectral accelerations at a wide range of oscillator periods, peak ground velocity and significant durations in the Groningen field
- The model should be applicable to earthquakes from magnitude 2.5 to 7.25, reflecting the specific characteristics of Groningen events initiating at depths of 3 km, while capturing the epistemic uncertainty associated with the extrapolations from observations in the range 2.5-3.6 to the larger triggered earthquakes that would propagate downwards from the gas reservoir
- The model should reflect the growth of source rupture dimensions with magnitude and the resulting spatial distribution of the ground-motion field due to larger events
- The model should be applicable at distances ranging from directly above the seismic source to about 60 km from the epicentre, and accurately reflect the influence of the unique upper crustal velocity profile in the Groningen field, especially the presence of the high-velocity Zechstein salt layer—and the very high-velocity anhydrite layers within the Zechstein—above the gas reservoir
- The model should capture the influence of the soft near-surface deposits in the field, including their non-linear response to stronger levels of shaking and the lateral variation of the soils over the field

The process through which all of these objectives have now been met involved producing complete models, with full documentation, at intervals of about 7 months on average following the introduction of the V1 GMM. While this schedule was very aggressive and meant that the advances from one version to the next had to be carefully limited, the sequence of iterative stages of development has had some advantages. The first of these is that each version of the model has been implemented in the hazard and risk engine, providing very valuable feedback on its performance. The second advantage has been that each developmental stage has provided an opportunity for critical peer review and the incorporation of suggestions and recommendations in the subsequent version. The V2 GMM was the subject of the review workshop held in London in October 2015, while the V3 model was presented and discussed at the workshop on finite rupture simulations convened in London in July 2016. The V4 GMM report was then subjected to critical review by the combined review panels from the two workshops. Many of the comments and suggestions of the review panel were incorporated into a revised version of the V4 GMM report; we also submitted responses explaining how we had implemented all of

the editorial comments. More substantial comments were taken into account in the V5 GMM development, as we have explained in this document.

The V5 GMM has now been implemented in Groningen hazard and risk analyses, and is expected to be retained as the current model for estimation of ground-motions due to induced and triggered earthquakes in the field for some time to come. There will be future versions of the model but these will not be issued at the same frequency as has been the case to date. The procedure rather will be to evaluate all new data—ground-motion recordings and geotechnical dynamic characterisation of the sub-surface—regarding its potential impact on the model, and then to modify the GMM only when such new data (or key developments in ground-motion modelling in general) warrant the issue of a new version. Until such time, the V5 GMM is considered a stable and reliable model for use in the Groningen.

The review comments on the V4 GMM noted several important advances that had been made with respect to the previous versions and how these had improved the model. The panel also noted that while several comments were offered on the V4 GMM, *“none of these comments represents major issues that would cause us to recommend against application of the GMM for hazard analysis in the Groningen field”*. The V5 GMM represents further refinements and improvements of the model but no fundamental changes to its formulation from the V4 model. The only substantial change has been the replacement of the $M-M_L$ relationship that was used in the V4 GMM development and which additional work using an expanded dataset has shown to be inappropriate.

Since the V5 GMM is really a refinement of the V4 GMM rather than a substantially different model in terms of simulations, reference rock horizon and characterisation of the near-surface deposits in the field, the report on the V5 GMM is considerably shorter than the documentation of earlier versions of the model (indeed, this report explaining our responses to the review comments is slightly longer than the main body of the report). The full documentation of the V5 GMM is therefore considered to be the revised V4 GMM report and the V5 GMM report together, although for implementation purposes only the latter is required. Should the review panel deem it necessary, a revised version of the V5 GMM report may be issued accommodating any changes, corrections or additions that the panel suggest.

We close by thanking all of the reviewers for their efforts in providing very valuable feedback and suggestions at many stages of the work, and also we offer our thanks once again in anticipation of your time and effort in perusing these responses and the V5 GMM report. To have been able to benefit from the feedback and insights of eight such distinguished individuals in the discipline of engineering seismology for this endeavour has been a genuine privilege.

5. References

- Afshari, K. & J.P. Stewart (2016). Physically parameterized prediction equations for significant duration in active crustal regions. *Earthquake Spectra* **32**(4), 2057-2081.
- Akkar, S., M.A. Sandıkkaya & J.J. Bommer (2014a). Empirical ground-motion models for point- and extended-source crustal earthquake scenarios in Europe and the Middle East. *Bulletin of Earthquake Engineering* **12**(1), 359-387. Erratum: **12**(1), 389-390.
- Akkar, S., M.A. Sandıkkaya & B.Ö. Ay (2014b). Compatible ground-motion prediction equations for damping scaling factors and vertical-to-horizontal spectral amplitude ratios for the broader European region. *Bulletin of Earthquake Engineering* **12**(1), 517-547.
- Al Atik, L. (2015). *NGA-East: Ground-motion standard deviation models for central and eastern United States*. PEER Report 2015/07, Pacific Earthquake Engineering Research Center, UC Berkeley, June 2015, 217 pp.
- Bahrampouri, M., A. Rodriguez-Marek, & J.J. Bommer (2017). Mapping the uncertainty in modulus reduction and damping curves onto the uncertainty of site amplification functions. Submitted to *Soil Dynamics and Earthquake Engineering*, July 2017.
- Bindi, D., M. Massa, L. Luzi, G. Ameri, F. Pacor, R. Puglia & P. Augliera (2014). Pan-European ground-motion prediction equations for the average horizontal component of PGA, PGV, and 5%-damped PSA at spectral periods up to 3.0 s using the RESORCE dataset. *Bulletin of Earthquake Engineering* **12**(1), 391-430.
- Bommer, J.J., B. Dost, B. Edwards, P.J. Stafford, J. van Elk, D. Doornhof & M. Ntinalexis (2016a). Developing an application-specific ground-motion model for induced seismicity. *Bulletin of the Seismological Society of America* **106**(1), 158-173.
- Bommer, J.J., B. Dost, B. Edwards, P.P. Kruiver, P. Meijer, M. Ntinalexis, A. Rodriguez-Marek & P.J. Stafford (2016b). *Development of V3 GMPEs for response spectral accelerations and significant durations from induced earthquakes in the Groningen field*. Version 0, 8 July 2016, 476 pp.
- Bommer, J.J., P.J. Stafford, B. Edwards, B. Dost, E. van Dedem, A. Rodriguez-Marek, P. Kruiver, J. van Elk, D. Doornhof & M. Ntinalexis (2017a). Framework for a ground-motion model for induced seismic hazard and risk analysis in the Groningen gas field, The Netherlands. *Earthquake Spectra* **33**(2), 481-498.
- Bommer, J.J., B. Dost, B. Edwards, P.P. Kruiver, P. Meijers, M. Ntinalexis, A. Rodriguez-Marek, E. Ruigrok, J. Spetzler & P.J. Stafford (2017b). *V4 Ground-Motion Model (GMM) for Response Spectral Accelerations, Peak Ground Velocity, and Significant Durations in the Groningen Field*. Version 1, 29 March 2017, 522 pp.
- Bommer, J.J., B. Dost, B. Edwards, P.P. Kruiver, P. Meijers, M. Ntinalexis, A. Rodriguez-Marek, E. Ruigrok, J. Spetzler & P.J. Stafford (2017c). *V4 Ground-Motion Model (GMM) for Response Spectral Accelerations, Peak Ground Velocity, and Significant Durations in the Groningen Field*. Version 2.1, 23 June 2017, 541 pp.
- Bommer, J.J., B. Dost, B. Edwards, P.P. Kruiver, M. Ntinalexis, A. Rodriguez-Marek, P.J. Stafford & J. van Elk (2017d). Developing a model for the prediction of ground motions due to earthquakes in the Groningen gas field. *Netherlands Journal of Geoscience*, in press.

Bommer, J.J., B. Edwards, P.P. Kruiver, A. Rodriguez-Marek, P.J. Stafford, B. Dost, M. Ntinalexis, E. Ruigrok & J. Spetzler (2017e). *V5 Ground-Motion Model for the Groningen Field*. 30 October, 161 pp.

Boore, D.M. (2005). Erratum: Equations for estimating horizontal response spectra and peak acceleration from western north American earthquakes: A summary of recent work, by D.M. Boore, W.B. Joyner and T.E. Fumal. *Seismological Research Letters* **76**(3), 368-369.

Boore, D.M. (2009). Comparing stochastic point-source and finite-source ground-motion simulations: SMSIM and EXSIM. *Bulletin of the Seismological Society of America* **99**, 3202-3216.

Boore, D.M. & G.M. Atkinson (2008). Ground-motion prediction equations for the average horizontal component of PGA, PGV, and 5%-damped PSA at spectral periods between 0.01s and 10.0 s. *Earthquake Spectra* **24**(1), 99-138.

Boore, D.M., Watson-Lamprey, J. & Abrahamson, N.A. (2006). Orientation-independent measures of ground motion. *Bulletin of the Seismological Society of America* **94**(4A), 1502-1511.

Boore, D.M., J.P. Stewart, E. Seyhan & G.M. Atkinson (2014). NGA-West2 equations for predicting PGA, PGV, and 5% damped PSA for shallow crustal earthquakes. *Earthquake Spectra* **30**(3).

Bozorgnia, Y. & K.W. Campbell (2016). Ground motion model for the vertical-to-horizontal (V/H ratios) of PGA, PGV, and response spectra. *Earthquake Spectra* **32**(2), 951-978.

Brune, J.N. (1970). Tectonic stress and spectra of seismic shear waves from earthquakes. *Journal of Geophysical Research* **75**, 4997-5009.

Brune, J.N. (1971). Correction. *Journal of Geophysical Research* **76**, 5002.

Campbell, K.W. & Y. Bozorgnia (2007). *Campbell-Bozorgnia NGA Ground Motion Relations for the Geometric Mean Horizontal Component of Peak and Spectral Ground Motion Parameters*. PEER Report 2007/02, Pacific Earthquake Engineering Research Center, University of California at Berkeley, 240 pp.

Campbell, K.W. & Y. Bozorgnia (2014). NGA-West2 ground motion model for the average horizontal components of PGA, PGV, and 5%-damped elastic pseudo-acceleration response spectra. *Earthquake Spectra* **30**(3), 1087-1115.

Chiou, B.S.J. & R.R. Youngs (2014). Update of the Chiou and Youngs NGA model for the average horizontal component of peak ground motion and response spectra. *Earthquake Spectra* **30**(3), 1117-1153.

Crowley, H. & R. Pinho (2017). *Report on the v5 Fragility and Consequence Models for the Groningen Field*. Report for NAM, October 2017.

Darendeli, M. (2001). *Development of a new family of normalized modulus reduction and material damping curves*. Ph.D. Thesis, Dept. of Civil Eng., University of Texas, Austin, TX.

De Crook, T. & B. Wassing (1996). Opslingering van trillingen bij aardbevingen in Noord-Nederland, *KNMI-RGD interim report*, 14pp.

De Crook, T. & B. Wassing (2001). Voorspelling van de opslingering van trillingen bij aardbevingen, *Geotechniek*, 47-53.

Douglas, J., S. Akkar, G. Ameri, P-Y. Bard, D. Bindi, J.J. Bommer, S. Singh Bora, F. Cotton, B. Derras, M. Hermkes, N.M. Kuehn, L. Luzi, M. Massa, F. Pacor, C. Riggelsen, M.A. Sandikkaya, F. Scherbaum, P.J. Stafford & P. Traversa (2014). Comparisons among the five ground-motion models developed using RESORCE for the prediction of response spectral accelerations due to earthquakes in Europe and the Middle East. *Bulletin of Earthquake Engineering* **12**(1), 341-358.

Edwards, B. & D. Fäh (2013). Stress parameter and kappa from recordings of large earthquakes in Europe and the Middle East. *Geophysical Journal International* **194**(2), 1190-1202.

Edwards, B., A. Rietbrock, J. J. Bommer & B. Baptie (2008). The acquisition of source, path, and site effects from micro-earthquake recordings using q tomography: Application to the United Kingdom. *Bulletin of the Seismological Society of America* **98**, 1915-1935.

Engelhard, L. (1996). Determination of the seismic wave attenuation by complex trace analysis. *Geophysical Journal International* **125**, 608-622.

Engelhard, L., D. Doan, G. Dohr, P. Drews, T. Gross, F. Neupert, J. Sattlegger & U. Schönfeld (1986). Determination of the attenuation of seismic waves from actual field data as well as considerations to fundamental questions from model and laboratory measurements. *DGMK Report* **254**, 83-119.

Grünthal, G., D. Stromeje & R. Wahlstrom (2009). Harmonization check of M_w within the central, northern, and northwestern European earthquake catalogue (CENEC). *Journal of Seismology* **13**, 613-632.

Gülerce, Z. & N.A. Abrahamson (2011). Site-specific design spectra for vertical ground motion. *Earthquake Spectra* **27**(4), 1023-1047.

Hashash, Y.M.A., M.I. Musgrove, M.I., J.A. Harmon, D.R. Groholski, C.A. Phillips, C.A., and D. Park (2016). "*DEEPSOIL 6.1, User Manual*". Urbana, IL, Board of Trustees of University of Illinois at Urbana-Champaign.

Hauksson, E., T. Teng & T.L.Henyey (1987). Results from a 1500m deep, three-level downhole seismometer array: site response, low Q values and f_{max} . *Bulletin of the Seismological Society of America* **77**, 1883-1904.

Kawase, H., F. J. Sánchez-Sesma & S. Matsushima (2011). The optimal use of horizontal-to-vertical spectral ratios of earthquake motions for velocity inversions based on diffuse-field theory for plane waves. *Bulletin of the Seismological Society of America* **101**(5), 2001-2014.

Kishida, T., R.W. Boulanger, N.A. Abrahamson, M.W. Driller & T.M. Wehling (2009a). Site effects for the Sacramento-San Joaquin delta. *Earthquake Spectra* **25**(2), 301-322.

Kishida, T., R.W. Boulanger, N.A. Abrahamson, T.W. Wehling & M.W. Driller (2009b). Regression models for dynamic properties of highly organic soils. *Journal of Geotechnical and Geoenvironmental Engineering* **135**(4), 533-543.

Konstantinou, M., C. Zwanenburg, & P. Meijers (2017). *Dynamic behaviour of Groningen peat. Analysis and parameter assessment*. Deltares report 1209862-011.

- Kotha, S.R., D. Bindi & F Cotton (2017). Site-corrected magnitude and region-dependent correlations of horizontal peak spectral amplitudes. *Submitted to Earthquake Spectra*.review.
- Kruiver, P. P., E. van Dedem, E. Romijn, G. de Lange, M. Korff, J. Stafleu, J.L. Gunnink., A. Rodriguez-Marek, J.J. Bommer, J.J. van Elk & D. Doornhof (2017). An integrated shear-wave velocity model for the Groningen gas field, The Netherlands. *Bulletin of Earthquake Engineering* **15**(9), 3555-3580.
- Kuehn, N.M. & N.A. Abrahamson (2017). The effect of uncertainty in predictor variables on the estimation of ground-motion prediction equations. *Bulletin of the Seismological Society of America* DOI: <https://doi.org/10.1785/0120170166>.
- Landwehr, N., N.M. Kuehn, T. Scheffer & N.A. Abrahamson (2016). A nonergodic ground-motion model for California with spatially varying coefficients. *Bulletin of the Seismological Society of America* **106**, 2574-2583.
- Munafò, I., L. Malagnini & L. Chiaraluce (2016). On the relationship between M_w and M_L for small earthquakes, *Bulletin of the Seismological Society of America* **106**, 2402-2408.
- Noorlandt, R.P., P.P. Kruiver, M.P.E. de Kleine, M. Karaoulis, G. de Lange, A. Di Matteo, J. von Ketelhodt, E. Ruigrok, B. Edwards, A. Rodriguez-Marek, J.J. Bommer, J. van Elk & D. Doornhof (2017). Characterisation of ground-motion recording stations in the Groningen gas field. *Accepted for publication in Journal of Seismology*.
- Phillips, C. & Y.M.A. Hashash (2009). Damping formulation for nonlinear 1D site response analyses. *Soil Dynamics and Earthquake Engineering* **29**, 1143-1158.
- Renault P.L.A., N. Abrahamson & SP3 Experts (2014). *Volume 5 SP3 - Site Response Characterization - Evaluation Summaries and Hazard Input Documents*, PEGASOS Refinement Project Report, SwissNuclear, Olten, Switzerland.
- Rodriguez-Marek, A., F. Cotton, N.A. Abrahamson, S. Akkar, L. Al Atik, B. Edwards, G.A. Montalva & H. Dawood (2013). A model for single-station standard deviation using data from various tectonic regions, *Bulletin of the Seismological Society of America* **103**, 3149-3163.
- Sánchez-Sesma, F.J., M. Rodríguez, U. Iturrarán-Viveros, F. Luzón, M. Campillo, L. Margerin, A. García-Jerez, M. Suarez, M.A. Santoyo & A. Rodríguez-Castellanos (2011). A theory for microtremor H/V spectral ratio: application for a layered medium. *Geophysical Journal International* **186**(1), 221-225.
- Spetzler, J. & B. Dost (2017). Hypocentre estimation of induced earthquakes in Groningen. *Geophysical Journal International* **209**, 453-465.
- Spica, Z. J., M. Perton, N. Nakata, X. Liu & G.C. Beroza (2018). Site characterization at Groningen gas field area through joint surface-borehole H/V analysis. *Geophysical Journal International*, doi: <http://dx.doi.org/10.1093/gji/ggx426>
- Stafford, P.J., Rodriguez-Marek, A., B. Edwards, P.P. Kruiver & J.J. Bommer (2017). Scenario dependence of linear site effect factors for short-period response spectral ordinates. *Bulletin of the Seismological Society of America*, **107**(6), 2859-2872.
- Tonn, R. (1991). The determination of the seismic quality factor Q from VSP data: a comparison of different computational methods. *Geophysical Prospecting* **39**, 1-27.

Wehling, T.M., R.W. Boulanger, R. Arulnathan, L.F. Harder, & M.W. Driller (2003). Nonlinear dynamic properties of a fibrous organic soil. *Journal of Geotechnical and Geoenvironmental Engineering* **129**(10), 929-939.

Wells, D.L. & K.J. Coppersmith (1994). New empirical relationships among magnitude, rupture length, rupture width, rupture area, and surface displacement. *Bulletin of the Seismological Society of America* **84**, 974-1002.

Yenier, E. & G.M. Atkinson (2015). Regionally adjustable generic ground-motion prediction equation based on equivalent point-source simulations: Application to central and eastern North America. *Bulletin of the Seismological Society of America* **105**, 1989-2009.

APPENDIX X

Review Comments and Responses on the V5 GMM Report

The first version of the V5 GMM report was issued on 30 October 2017 and was submitted to the international review panel (see Appendix I) on 15 December 2017, together with the responses to the V4 GMM review comments (see Appendix IX). Editorial and technical comments were received from the panel on 15 January 2018. The responses to the editorial comments have been communicated to the review panel separately.

This Appendix presents all of the technical comments from the review panel, which refer to the first issue of V5 GMM report and to the V4 comments responses (Appendix IX), together with the comprehensive responses developed by the GMM development team. These are all included here for a transparent and complete record of the development of the GMM to the V5 stage. As noted in the closure letter issued by the review panel—which is presented in Appendix I—the review comments presented herein do not challenge the validity and applicability of the V5 GMM: “*Our overall assessment of the modeling effort to date is that it has produced a state-of-the-art model that is well suited for its purpose of regional ground motion prediction to support hazard and risk studies in the Groningen field. While our most recent review of the draft Version 5 report resulted in some technical and editorial comments, these issues do not impact the fundamental viability of the model that has been developed.*”

The figures and references within this Appendix are self-contained as would be the case if these responses were to be submitted to the review panel as a stand-alone document. However, the page numbers have been made sequential with the rest of this report.

TABLE of CONTENTS

1. INTRODUCTION	273
2. TECHNICAL ISSUES AFFECTING THE GMM	274
2.1. Non-ergodic framework for path effects	274
2.2. Tau model and its uncertainty	275
2.3. Duration function	280
3. ADDITIONAL COMMENTS	282
3.1. Comments on V4 response document	282
3.2. Comments on V5 GMM report	290
4. CONCLUDING REMARKS	297
5. REFERENCES	298

1. Introduction

The V4 GMM report was revised to take into account all of the editorial comments and some of the technical feedback from the review panel, the latter being included herein as Appendix IX. The revised V4 GMM report (version 2.1) was submitted to the review panel together with responses to the editorial comments. Subsequently, the first draft of the V5 GMM report was submitted to the panel together the full suite of responses to the original technical comments, which are also presented in Appendix IX. The panel responded with new comments, both on the V5 report itself and on the V4 responses document. In this document, responses are presented to both sets of comments.

2. Technical Issues Affecting the GMM

The review report issued by the expert panel highlighted three technical issues that are identified as affecting the GMM. These three issues are addressed in the following sections.

2.1. Non-ergodic framework for path effects

A goal of the GMM should be to capture a wide enough epistemic uncertainty range so that as new data, models, and methods are implemented, the new results fall within the epistemic uncertainty range of the current model. Over the last 30 years, this has not been the case, leading to large changes in the hazard as models are updated. As the Groningen ground-motion data sets increase with new earthquakes and the 3-D velocity model is improved, there will likely be a move toward GMMs that incorporate path-specific effects. To avoid having risk results falling outside the current epistemic uncertainty range as future GMMs with path-specific results are developed, the panel recommends setting up a framework for future GMMs that will be able to smoothly incorporate path-specific effects. Initially, the GMM can be kept simple, but with an appropriately broad epistemic uncertainty.

We concur that such a framework is indeed desirable and as indicated in the revised Chapter 8 of the V5 GMM report, we envision the development of such a framework as being part of the future refinements of the model. However, we also reiterate our view that such developments should not be implemented in the same aggressive schedule that has marked the successive phases of the model development to date.

In the next model, the authors are encouraged to set up a framework for the GMM that uses non-ergodic aleatory variability (e.g., single path sigma) with broad epistemic uncertainty that can be reduced over time to incorporate azimuthal dependencies taking advantage of increasing data inventories and insights from 3D simulations. We recognize this is impractical for incorporation into the V5 model.

We do not disagree with this proposal and intend to explore the development of a fully non-ergodic version of the GMM as part of the ongoing future refinements. We are also cautious, however, about adopting excessive epistemic uncertainty ranges because of the potential impact on the risk estimates and social and political consequences of any inflation of these estimates. We would prefer to develop the framework for azimuthal dependent path-effects and only implement it into the model when the database and simulation results permit sufficient constraint to keep the uncertainties to acceptable levels. While the approach proposed by the panel would make perfect sense in the context of a research project, the sensitivities of the Groningen case need to be borne in mind.

2.2. Tau model and its uncertainty

Tau model: As in our V4 review, we remain concerned with the use of inconsistent magnitudes across the period range of the model in the computation of tau. We understand the authors' point in the response document that the variability of the magnitude random effect is fixed, but allowing magnitude to change from period to period artificially lowers tau relative to what would have been obtained for a fixed magnitude. Magnitude measurement error should be removed in the calculation of tau as a single value applicable to all spectral periods. We recognize the effect may be small, and Figure 2.12 in the response document is instructive in this regard.

Further consideration of this issue has made us realise that this issue is not easy to resolve in any formal manner with the current dataset. As noted in our response to the original concerns raised by the review panel, there are particular features of this field-wide dataset that complicate the treatment of magnitude uncertainties. In our previous response we focused upon comparisons with other estimates of tau from (ergodic) tectonic ground-motion models, as well as the statistical uncertainty in our estimates of tau.

However, there are additional factors that complicate this analysis. The main issue is that the implied contribution of magnitude uncertainty to the overall variance of ground-motion observations is unrealistically high for our current dataset. Because we are working with very small magnitudes in the empirical dataset, the partial derivative of the ground-motion model with respect to magnitude is very strong. Figure 2.1 shows the mean of the partial derivatives computed for each earthquake and for each response period.

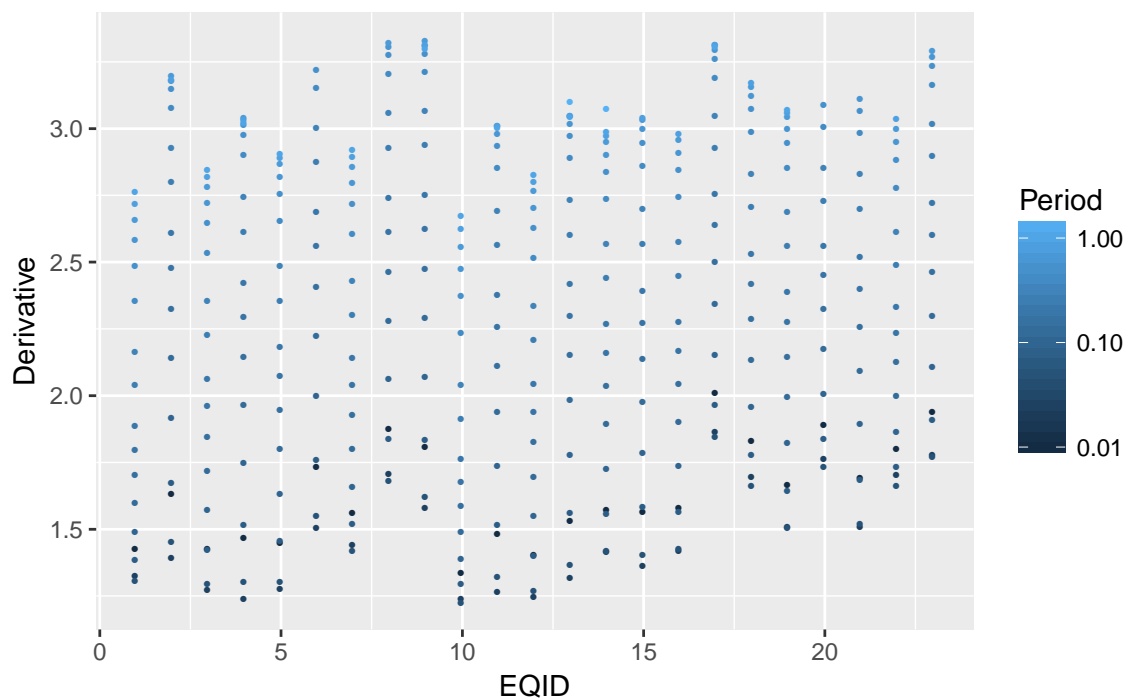


Figure 2.1. Mean partial derivatives with respect to magnitude for each period and event

This figure shows that the derivatives are very strong, especially for the longer response periods. In most cases where magnitude uncertainties have been considered in previous studies, these studies have been conducted for larger magnitude events where the scaling with respect to magnitude is much weaker and hence the derivatives are generally much smaller.

The reason why this is important is that the contribution to the overall variance associated with magnitude uncertainty is:

$$\Delta\sigma^2 = \left(\frac{\partial\mu}{\partial m}\right)^2 \sigma_m^2 \quad (2.1)$$

In the current database, the estimates of the magnitude uncertainty range from 0.1 to 0.3, with an average value of 0.22. The starting point when performing the variance decomposition is to regard the total observed variance as comprising real aleatory components, such as event-to-event variations, site-to-site variations, *etc.*, and artificial variation that arises from computing total residuals using inexact magnitude estimates.

Figure 2.2 shows the total variance as a function of period that is found from the total residuals of the V5 GMM with respect to the empirical observations in the field. This total variance is labelled ‘Total’ in the figure. At each period, the line labelled ‘Magnitude’ is obtained by taking the mean derivative for each earthquake along with the magnitude uncertainty for that event and computing the variance contribution according to the above equation. The mean of these contributions (computed on the scale of the standard deviation) is then plotted as a function of period in the figure.

What this then shows is how much of the total variance observed in the Groningen motions is supposed to arise from the use of inexact magnitude estimates. The line labelled ‘Aleatory’ is found as the difference of the ‘Total’ and ‘Magnitude’ lines. This ‘Aleatory’ level of variance is supposed to be the total *true* aleatory variability that remains (assuming that all other predictor variables are perfectly known). This ‘Aleatory’ level must be partitioned among event-to-event contributions (τ), site-to-site contributions (δ_{S2S}), and site-corrected within event contributions (ϕ_{SS}). However, the green line in the figure associated with ‘PhiSS’ relates to the lower bound level of ϕ_{SS} used in our model, and this should be one of the most well-constrained components of the overall variability. Assuming that this level of ϕ_{SS} is correct then we can remove this from the ‘Aleatory’ component to leave the ‘Remainder’ variance shown with the blue line in Figure 2.2. What can be appreciated from the figure is that the level remaining is far too low, and in some cases there is nothing remaining. Recall, that this ‘Remainder’ line must account for τ^2 as well as δ_{S2S}^2 , and that the smallest level of ϕ_{SS} has been considered here.

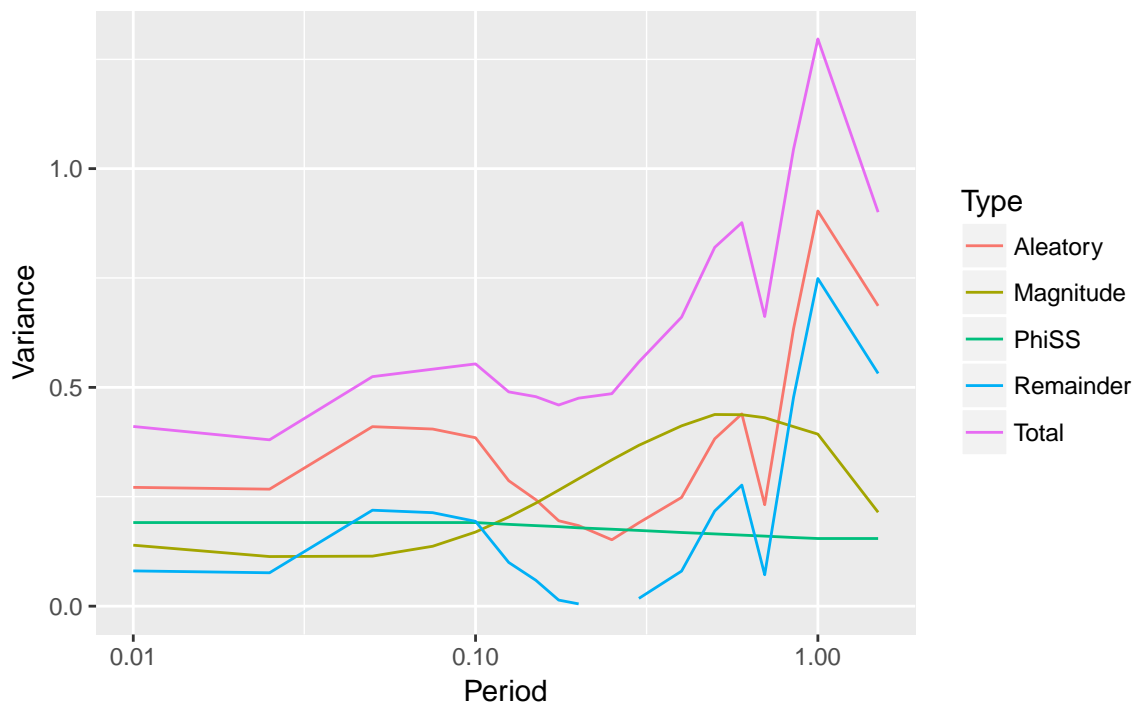


Figure 2.2. Components of variance in Groningen ground motions

The above figures and discussion suggests that we do not currently have consistency among all of the various components of variability. Most likely the estimates of magnitude uncertainty are currently too high, but the main issue that we currently face is that objective/statistically based corrections or adjustments cannot really be applied until we better understand the overall picture with respect to how variability is partitioned among all of the components in the field. Note also that the key issue for the current hazard and risk model is to ensure that the overall estimates of variability are reasonable. Issues associated with partitioning of the variance are not critical right now given the focus upon local personal risk.

The panel realizes that re-working the regression with a best-estimate magnitude to formally re-compute tau is likely not feasible in the available time. However, an approximate adjustment of the existing tau model for this effect would appear to be workable. The authors could compute the variance of the standard deviations of the random effect terms for magnitude, averaged over all earthquakes. This variance could be added to τ^2 to estimate a combined variance that would account for the fixed magnitude effect. We recommend to consider such a change in the tau used for the V5 model.

We appreciate the suggestion for a 'quick-fix' adjustment to the V5 tau model. However, in addition to the argument made in the previous response comment, there is another compelling reasons for us not to implement this suggestion, that being that the V5 model was actually issued in September 2017 and has been implemented in hazard and risk calculations that have been presented to the relevant authorities in the Netherlands in late 2017 and in more recent updates; to release an updated

version of the model at this stage would create unnecessary difficulties. Having already gone through five rapid development stages, we are very reluctant to make further changes on a rushed schedule—we have reached the stage where developments to the model need to be thoroughly explored and investigated before further releases. While implementation of the panel’s recommendation would as likely lead to increased hazard and risk estimates from inflating the between-event variance, we can only apply statistical constraints on the basis of the small-magnitude data we have available. As noted above, the use of this small magnitude data presents challenges that need more careful attention when partitioning variance components. The current model deliberately holds the between-event variance constant for all magnitudes and so any inflation at small magnitudes also impacts between-event variability at large magnitudes as well. Given that most current models for tectonic events predict lower tau values at larger magnitudes. As noted previously, the key for the current approach to hazard and risk computations is to ensure that the total variability is at the right level, and we believe that it is most likely conservative to retain the current model until the time is right for a new version to be released.

Tau uncertainty: The panel would like to see more careful consideration given to the epistemic uncertainty on tau in subsequent versions of the model. Some members of the panel are concerned that the current levels of uncertainty, reflected by the ranges in Figure 3.15, are too small. The V4 to V5 variation in tau shown in Figure 3.16, which was produced by the addition of a single event, highlights the problem.

We agree that this is an issue that clearly needs to be within the scope of ongoing work for refinement of the model. Working without the same degree of pressure to revise the model and to issue complete hazard and risk estimates, the opportunity now exists to develop a more complete uncertainty model and to accommodate a GMM logic-tree with more branches, hence uncertainty on the tau model could be incorporated. As indicated in the previous response, we expect that this is most likely to lead to reduced hazard and risk estimates through the incorporation of lower branches. As noted later in the document, we also wish to complete investigations of the apparent trend of decreasing event terms in recent earthquakes before refining the tau model (see Section 3.2 and response to the comment “V5. Page 92”).

In addition, when constructing the current logic tree for ground-motion uncertainty we developed branches and weights in a manner that intended to reflect the overall variation in ground-motions over the field. We opted to only branch on within-event components of variability rather than also branching on between-event components (for computational reasons). When revisiting this issue in the future we will need to consider the full logic tree for variability and not simply isolate just tau.

The panel understands the argument that a region-specific tau should be smaller than a global tau. However, the epistemic uncertainty in tau for this data set should not be much smaller than for other regions with much larger data sets. As an example, the epistemic range of tau from global models as applied in the SWUS Project is about 0.15 natural log unit (from high to low). This corresponds to a coefficient of variation (COV) of about 0.17 (taking COV as half the range divided by the median value of tau).

In the response to the review comments, the COV for tau is given as 0.35 to 0.60 depending on the period. This is larger than the COV from the global models used in the SWUS Project which makes sense. However, the epistemic range of tau used in V5 is much smaller (e.g. between 0.2 and 0.25 at T=0.1 sec, as shown in Figure 3.15), which is only a range (low to high) of 25% (COV of about 0.1).

As noted above, the treatment of the magnitude uncertainties is causing problems with the partitioning of the variance components and so our estimates of COV should also be interpreted with care. Another issue that complicates the comparison of COV estimates among models is that these estimates actually depend upon the size and balance of the datasets being used. Ultimately, these external estimates of COV can help to also constrain (or at least inform) the partitioning of the total variance in Groningen.

While we accept that our COV estimates appear low compared with the other numbers quoted above, we again have to emphasise that we are not branching on tau in the logic tree and that we really need to be checking our overall COV for the total variance rather than just tau. As our ϕ_{S2S} terms are zone specific, this is not an easy comparison to make with other studies.

The panel recognizes that there is a trade-off between event terms and site terms so the variance components are correlated. Accordingly, if the epistemic range on tau was increased, the epistemic range on phiS2S would be reduced. One way to address this would be to fix tau at three different values (central, upper, lower) and estimate the other variance components. In terms of the average total sigma for a single site, this does not matter, but this could have an effect on risk calculations that consider a region of sites for loss estimates. For such an application, this partitioning of the variance would lead to different ranges of losses.

Yes, we agree with the comment that the partitioning can matter for certain types of risk calculations (portfolio based assessments, or spatially aggregated losses). However, as noted above, the current hazard and risk model targets local personal risk and so the total variance is most important. As noted above, the construction of the logic tree for the variance consciously placed more epistemic uncertainty into ϕ_{S2S} for computation reasons to avoid having to branch at both between event and within event levels.

The approach suggested is one way that we can look to revise our overall partitioning approach. However, it is based upon fixing components of the variability

that are arguably the least well-constrained. Currently, we've fixed components like ϕ_{SS} and ϕ_{S2S} that historically are more readily constrained.

In consideration of the limited data and the other factors described here, the authors should consider in future work not allowing the epistemic uncertainty on tau to be less than that for relatively data-rich regions (e.g., as found in the SWUS Project). Other variance terms could then be adjusted to the fixed values of tau.

Of all of the components within the variability model, the tau values currently have the lowest amount of constraint. The site terms are relatively well constrained from the high-quality velocity model that we have, and we've seen excellent agreement with empirical observation and numerical prediction of the site response. The site-corrected within-event variability is constrained using global data and these are arguably the best constrained components of the overall variability model. However, we are still branching on these values to reflect some epistemic uncertainty. The proposal above suggests that we fix tau values and then adjust the other components to target some overall variance. As noted in the previous response comment, we can certainly attempt this in the future. However, we will also consider refinements to other components that we feel we can constrain with more certainty. For example, the database currently has 23 events and it will take some time to change this number to a level that makes a large impact statistically. However, the expanding network means that we obtained relatively large number of new recordings per event. With the ongoing work on path variability and spatial correlation it is probably more realistic to target constraining field specific levels of ϕ_{SS} and path variability and back-calculating the corresponding levels of τ .

2.3. Duration factor

The panel acknowledges the argument in the response document about the path and source durations being additive in a sense. However, the selected formulation comes with the cost of the path model being dependent on the source duration. In the additive form, the duration is separable in magnitude and distance. Using the multiplicative form, the magnitude and distance scaling are no longer separable. The panel considers this an unnecessary complexity that could have been avoided with a better choice of functional form. Nonetheless, the panel recognizes that the selected function works with the simulation data, so the model is suitable for application within the parameter space of the data set that was considered.

We appreciate the comments and understand the perspectives of the review panel. We can certainly consider using the additive functional form in future versions, but we do not currently believe that our choice has come at any significant 'cost'. The functional form we've adopted is similar in complexity to the models for the spectral ordinates, and the agreement with the simulated data is excellent.

Its also worth noting that the argument of being theoretically rigorous with the functional form cannot only be applied to the median model. The additive functional form suggested has significant implications for the manner in which the variability model should be constructed. While the functional form for the median can arguably become simpler, the variance model certainly becomes far more complicated.

The panel is of mixed opinion regarding whether site term should be additive or multiplicative. A classical Green's function approach requires an additive site effect, so some members of the panel advocate for this form. The basic formulation used in EXSIM requires that the linear site effects also lead to additive duration terms. While acknowledging those mathematical principles for linear systems, other panel members have found the site effect to differ with the duration of shaking on reference rock (hence not strictly additive). The authors are encouraged to comment on this issue in the V5 report so as to support their selected function for the site term.

We are grateful for the acknowledgement that there is not a clear consensus on this issue within the engineering seismology community and that this divergence of views is reflected in the positions adopted by different members of the review panel.

We also do not have strong views upon this issue, and are aware of the arguments for additive and multiplicative terms. However, in this particular study we have not developed our own site model, but have simply directly adopted the site term from Afshari & Stewart (2016). This was a conscious decision because we could not meaningfully compute the site-specific adjustment using the equivalent linear site response modelling that has been adopted and our sites also have a very limited range of $V_{S,30}$ values and so we have very little chance of developing a robust model from the local data. For the same reason, its highly unlikely that our present dataset can be used to contribute to this issue of whether site terms should be additive or multiplicative.

What we can state, however, is that from our own analyses in the past (Bommer et al., 2009), as well as in Kempton & Stewart (2006) and Afshari & Stewart (2016), there are not obvious empirically driven reasons to reject multiplicative site response in favour of additive contributions, despite the theoretical arguments related to Green's functions (or to thinking that site response is simply an extension of the path). It is worth noting however, that the arguments related to Green's functions make most sense when thinking in terms of total duration of the signal and the definition of significant duration certainly complicates those theoretical arguments.

3. Additional Comments

The panel also provided several more short comments, which referred both to the V4 response document and the V5 report. These are dealt with separately in the next two sub-sections. The first four issues related to the V4 response document were all highlighted by the panel as items that should be brought into the project documentation; these were presented under a separate heading in the panel's report but are combined herein with the other comments on the V4 response document.

3.1. Comments on V4 response document

RD. 2.2, Page 8. Based on the response, it appears that even though the stress parameter is set by the fit, the fit is imperfect across frequencies and is better customized to the data through this transfer function. It would be good for this information to appear in the project documentation.

We concur that this is valuable additional information regarding the model derivation. However, since we are now including the full V4 response document is now included as Appendix IX of the revised V5 report, we do not see the need to also insert the information in the main body of the report and thus increase the length of the document. We have added a reference to Appendix IX in the main body of the report where these topics are discussed.

RD. 2.7, Pages 23-24. The information in the response on event depths should appear in the project documentation.

We concur with this recommendation and have added a brief summary of this information, together with the reference to the paper by Spetzler & Dost (2017), to the main body of the report.

RD. 2.9, Pages 35-38. Interesting results on the limitations of time-domain results. Consider bringing these into the project documentation.

We concur that this is valuable additional information regarding the model derivation. However, since we are now including the full V4 response document is now included as Appendix IX of the revised V5 report, we do not see the need to also insert the information in the main body of the report and thus increase the length of the document. We have added a reference to Appendix IX in the main body of the report where these topics are discussed.

RD. 3.9, Page 69. The response shows that randomization for a voxel stack does not affect the results, which is what had been asked for. Moving this into the report is advised.

We concur that that the example justifying the randomization choice would help clarify the report. However, since the full V4 response document is now included as Appendix IX of the revised V5 report, we do not see the need to also insert the information in the main body of the report and thus increase the length of the document. We have added a reference to Appendix IX in the main body of the report where these topics are discussed.

RD. Sec 2.1, Pages 4-5: Is there an explanation for the apparent decay in EXSIM amplitudes as the R_{JB} distance decreases from 1 to 0.1, as evidence on Figures 2.1, 2.2 and 2.3?

The decay in EXSIM values apparent in V4 review response document Figures 2.1-2.3 below $R_{JB} = 1$ km is an artefact of plotting PSA versus R_{JB} for a narrow range of magnitude rather than a single value (we acknowledge that this was not clear in the original figures) and the simulated station distribution.

The station configuration used in the simulations is radial with origin and the centre of strike surface-projection and logarithmically increasing separation distance. The sampling of motions in the strike-direction therefore jumps from $R_{JB} = 0$ km (over fault) to > 1 km (beyond fault surface projection) since the station spacing is already greater than 1 km at the end of the fault strike. For the strike-normal direction the first station is at 0.1 km and the second at 1 km. Only few non- strike-parallel and non-strike-normal azimuths (22.5, 45 degrees, etc.) depending on geometry (fault size is varied randomly) therefore contribute recorded motions in this $R_{JB} = 0.1-1$ km region – in the case of the V4 review response document figures these motions were from the smaller of the range of events giving the impression of decreasing motion below $R_{JB} = 1$ km.

Figures 3.1-2.3 show the simulated data in question from the V4 review response document Figures 2.1-2.3 for a single **M**6.0 event. In this case it is clear that no systematic decrease in the range 0.1 – 1 km exists. We note that since the GMPE was developed for R_{rup} , any **M**– R_{JB} sampling issues are avoided.

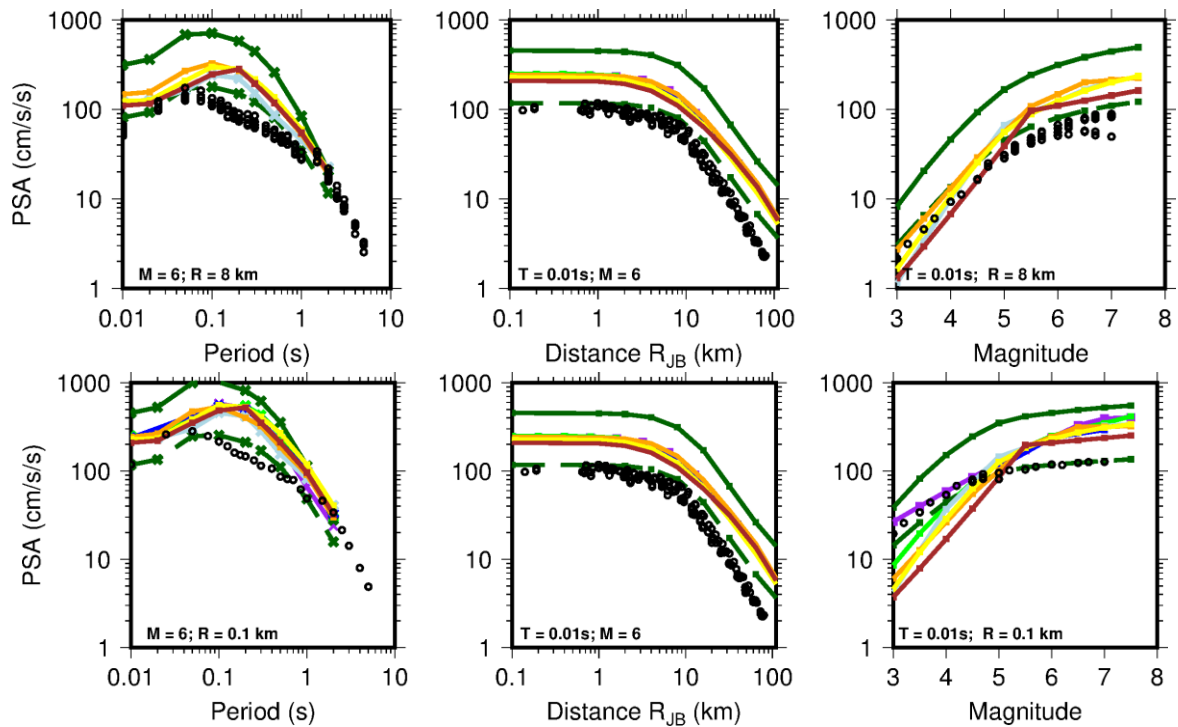


Figure 3.1. EXSIM simulations (circles) for the lower GMM compared against several GMPEs. Scenarios are indicated in the labels. Dark green: Yenier & Atkinson (2015) (dashed = 3 km source, solid = 10 km source); yellow: Campbell & Bozognia (2014); orange: Chiou & Youngs (2014); purple: Akkar *et al.* (2014a); light green: Bindi *et al.* (2014); brown: Boore *et al.* (2014); light-blue: Abrahamson *et al.* (2014)

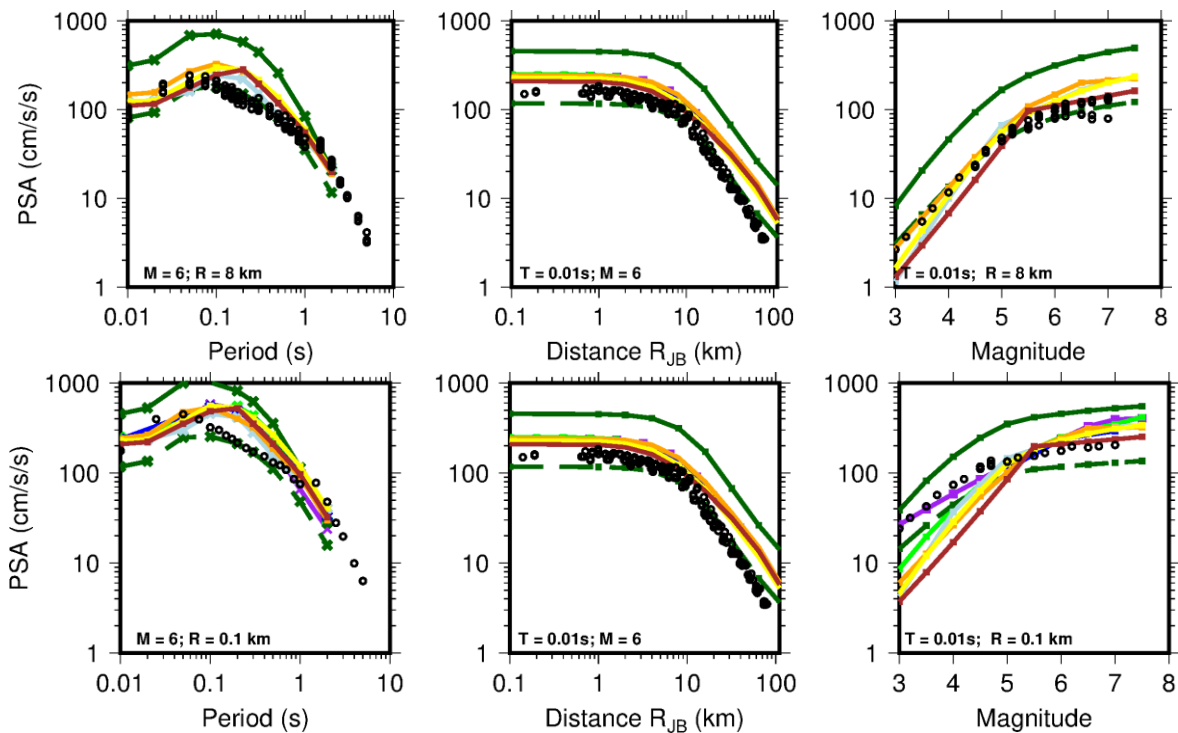


Figure 3.2. EXSIM simulations for the central-a GMM compared against several GMPEs. See Figure 3.1 for details

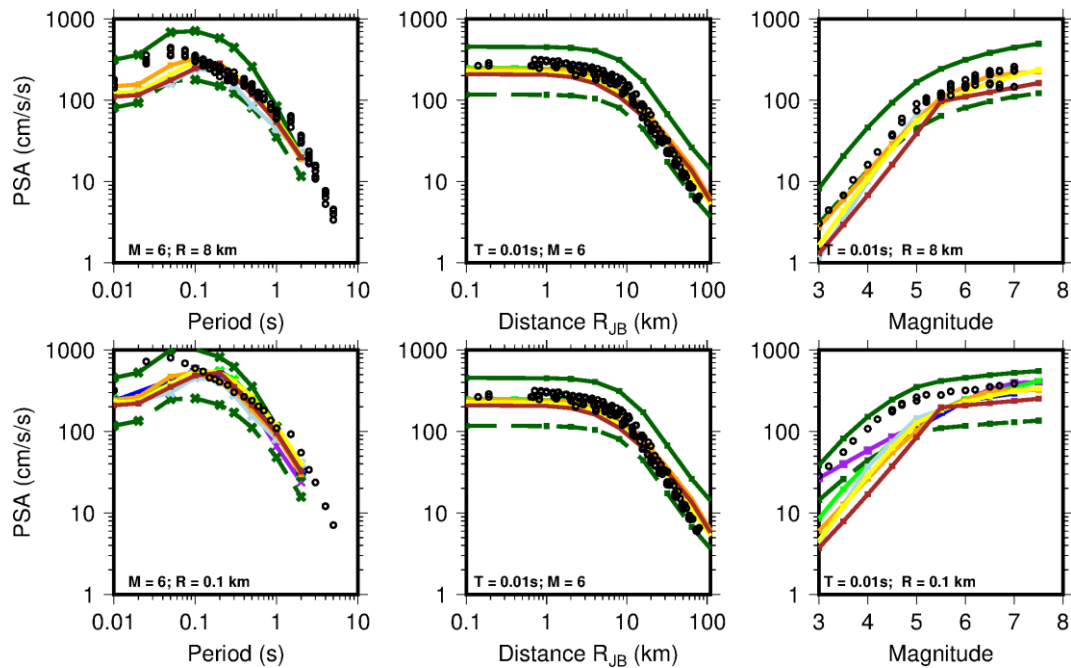


Figure 3.3. EXSIM simulations for the upper GMM compared against several GMPEs. See Figure 3.1 for details

RD. Sec 2.7, Page 24: 2.7: The panel agrees with responses to comments on source depth. One question, in the application of the model to large earthquakes ($M > 5$), it is stated that the initiation depth is 3 km and the rupture propagates downward. For the largest magnitudes considered ($\sim M 7$), has any consideration been given to the rupture also propagating upwards to near the surface? Is there a basis for precluding that this occurs for the largest events?

These modelling decisions reflect the outcomes of both the workshop on Mmax for the Groningen field (Amsterdam, March 2016) and the workshop on the incorporation of finite rupture simulations into the GMM (London, July 2016). Directly above the sandstone layer housing the gas reservoir is a thick layer of Zechstein salt, which is not considered capable of rupturing seismogenically. Therefore, triggered earthquakes that would exceed the available rupture area within the Rotliegend sandstone would be expected to propagate downwards into the Carboniferous. The Mmax panel did not specify that such events would necessarily have a focal depth of 3 km since they also considered the possibility of events initiating within the underlying rock layer. However, for modelling purposes, it was considered appropriate to maintain the initiation of all ruptures within the Rotliegend and then to propagate the ruptures laterally and downwards, albeit that fault ruptures that propagate only downwards are unusual.

RD. Sec 2.8, Pages 30-31. The response presented here, and subsequently in Section 3.10 (page 72), is essentially that because the simulation results are different in different zones, the site response too must be different. As the authors demonstrate quite nicely, a model

conditioned on V_{s30} or V_{s30} in combination with site period, will necessarily smooth through these features and miss some attributes of the simulation results. What the panel comment was trying to get at is whether the data (as interpreted through residuals) support the more refined modeling.

The authors' responses do not address this issue. It is possible that the additional complexity in the modeling does not actually improve model performance relative to the data.

We do appreciate the panel's comment that a V_{s30} -based model may have been sufficient for the Groningen field, and our exploratory analyses did indeed indicate that in some respects this simple proxy does explain the trends in the site amplification factors. However, it was also observed that in some cases, the scatter of the site amplification factors remained large with respect to V_{s30} . Most importantly, the response in Section 3.10 of the V4 responses (Appendix IX) showed how treating the field as a single zone and grouping AFs by V_{s30} and site period resulted in standard deviations that were often larger than those we find for individual zones but sometimes gave lower values.

In terms of how well the model is supported by residuals, if we interpret these in the strict sense of the residuals of the recorded motions at the surface, we are not convinced that this is the most important consideration for calibrating the model. The recordings are from small-magnitude earthquakes that are generally below the levels that contribute to hazard and risk estimates in the field, and they are dominated by linear site response because of the low amplitudes of the motions. We believe that a model that is calibrated to perform well over a wide range of magnitudes is the real objective in this work. The widespread use of V_{s30} is understandable but its basis is historical rather than scientific and we would be reluctant to revert to the use of such a simple proxy for this situation where we have reliable V_s profiles down to much greater depths. In particular, if we consider the panel's suggestion to adopt a framework for a fully non-ergodic (see Section 2.1), then we may create a model that is specific to source-path-site combinations, for which it would be logical to also use the local V_s profiles across the field rather than represent them by a rather crude proxy that is of physical relevance to the seismic radiation in a rather narrow frequency range.

RD. Sec 2.9, Pages 31-32. It's good to see some progress in this regard. The panel is curious if the results of the ground response simulations are very sensitive to shear strength? If so, incorporation of this uncertainty into the logic tree (by varying N_k) could be considered in future work.

The site response analyses were sensitive to the shear strength of the soil for the cases when very soft soil layers were present and when the input motions were strong enough to induce large strains in these layers. As indicated in Section 9.3 of the V4 report, the uncertainty in the undrained strength was included in the

simulations used to constrained the uncertainty in AF due to uncertainty in MRD curves ($\sigma_{\ln AF, MRD}$). Hence, the model described by Figures 9.8 and Equation 9.3 includes the uncertainty in undrained strength.

This issue is already addressed in the revised V4 GMM report, so we do not believe that it is necessary to modify the V5 GMM report in response to this comment, since the V5 and V4 reports together are intended as the final GMM documentation. For completeness, we note this paragraph that is included on p.211 of the revised (version 2.1) report on the V4 model:

“An additional uncertainty on the MRD curves for clays results from the value of the undrained strength of the soil. As indicated in Chapter 7, the methodology of Yee et al. (2013) was used to modify the MRD curves such that its larger strain behaviour is compatible with the dynamic shear strength of the soil. The same approach was used in this exercise. The standard deviation of the undrained strength of the soil was assumed to be 0.5 (in natural log units). Such a high value is warranted because of the lack of measurements of undrained strength in Groningen soils. The undrained strength was assumed to be fully correlated to the modulus reduction curve (i.e., if the modulus reduction curve was higher than the median, the undrained strength was also assumed to be higher than the median).”

Additional tests were being conducted on peats from the Groningen field (Zwanenburg & Konstantinou, 2016; Zwanenburg et al., 2017). These tests resulted in Groningen specific MRD curves for Holland peat. Additionally, more information was gathered about the undrained shear strength of Holand peat. This data was used to update the geomechanic look up table. The adjustments are described in a section now added to Section 4.1 the revised V5 report in Section 4.1.

RD. Sec 2.12, Page 45. In Figures 2.32 and 2.33 the y-axis is the component-to-component variance, but what does that mean for RotD0, RotD50, and Rot100? What is the relationship between component-to-component variance and RotD0, RotD50, and Rot100? If this figure is intending to show the variance between components measured in the RotD0 direction, then the component-to-component variance at the RotD100 direction would be the same as the RotD0 direction. An explanation of what is plotted in these figures is needed.

Figures 2.32 and 2.33 show, respectively, the component-to-component variance and variability of the Groningen database, calculated using the equation of Boore (2005), after each record of the database has been rotated individually to a specific orientation, using the spectral acceleration values calculated at that orientation. In this particular case, the orientations are the as-recorded orientation and three orientations that correspond to the GMRotDpp component definition of Boore et al. (2006). Boore et al. (2006) define GMRotDpp as “the pp^{th} percentile of the set of

geometric means for a given oscillator period. For example, *GMRotD00*, *GMRotD50*, and *GMRotD100* correspond to the minimum, median, and maximum values, respectively". To calculate the *GMRotDpp* values for any percentile, each record must be rotated by small increments (one degree or less) to angles from 0° to 90° of its as-recorded orientation. At each angle, the geometric mean spectral accelerations for each period of interest are calculated. Then, for each period independently, the angles are ranked according to the ranking of the geometric mean spectral accelerations calculated, from smallest to largest. The largest geometric mean is the 100th percentile for a period, and the smallest is the 00th and the corresponding angles at which these values were calculated are the orientations of *GMRotD100* and *GMRotD00* respectively. As, this process is repeated independently for each period and each record, the ranking of the angles may be different from period to period as well as from record to record.

In light of these clarifications, we do not concur with the panel's comment that the component-to-component variance should be the same in the *RotD0* and *RotD100* directions. The component-to-component variance will be largest at the orientation for which the polarisation of the horizontal components is greatest, and this will also correspond to the lowest value of the geometric mean (*i.e.*, *RotD0*). The reason can be understood considering the difference between arithmetic means (AM) and geometric means (GM): the latter measure is more strongly influenced by the smaller of the two values. Figure 3.4 shows how the geometric and arithmetic means of two values vary with the ratios of those values, which confirms how the geometric mean tends to be small for polarised horizontal components.

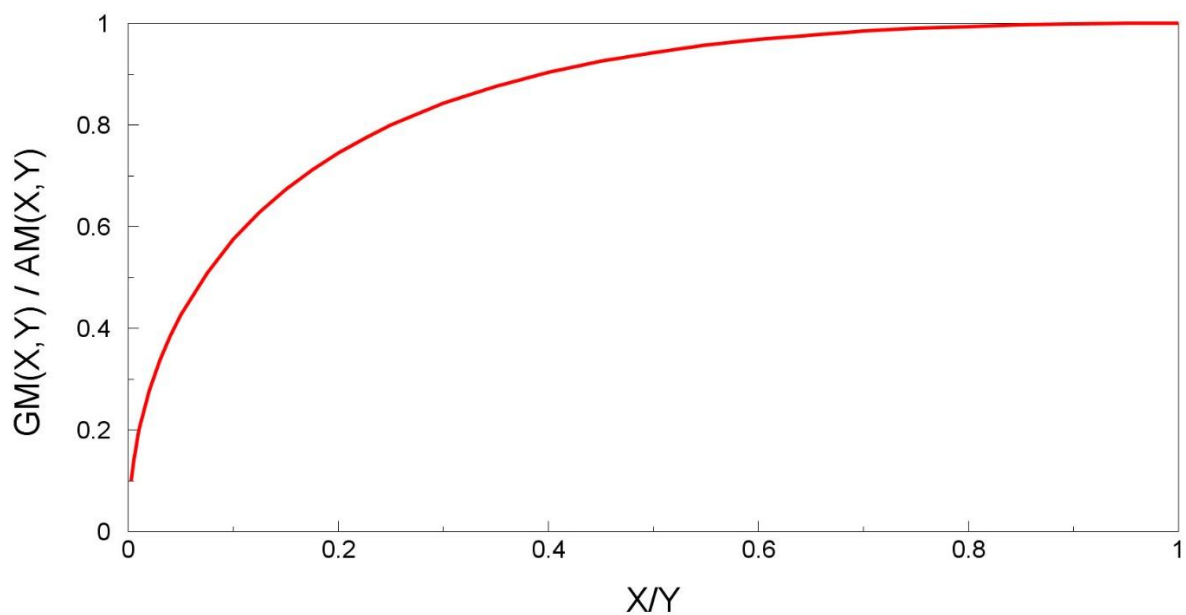


Figure 3.4. Ratio of geometric to arithmetic means of two values as a function of the ratio of the two values

In conclusion, the patterns observed in the figures are clear and also expected. We have not made any change to the report in response to this comment.

RD. Sec 3.4, Page 53. The panel's intent with the original comment was more focused on D_{min} (small strain damping) than what would be obtained by the variations in an MRD model. Nonetheless, the point about consistency between the inversion and forward application is well taken, and it seems that in totality epistemic uncertainties are reasonably captured so no further response needed.

We are glad that the panel concurs with the approach taken to characterize D_{min} and its uncertainty. As indicated by the panel, the consistency of the D_{min} profile in the inversions and forward analyses is a key component of the Groningen GMM model. Just to reiterate, the small-strain damping component of the MRD curves was randomized separately from the large-strain components of the curves, thus resulting in additional uncertainty in D_{min} than for other portions of the curve. This is explained in more detail in a recently-accepted paper (Bahrampour *et al.*, 2018).

[Note: This comment actually refers to p.55 rather than p.53].

RD. Sec 3.10, Page 70. Do the authors consider the available data to be too sparse to evaluate distance-dependence of Φ_{SS} empirically? This is not addressed in the response.

We acknowledge that we did not discuss the possibility of empirical evaluation of the distance-dependence of single-station sigma but we do recognise that this is clearly worthwhile and have added a comment to this effect in the revised Chapter 8, identifying such analyses as an element of the plan for future refinements. With the expanded networks now yielding consistently large numbers of records (> ~50) in most significant earthquakes—as attested by the cases presented in Appendix II and Appendix VIII of the revised report—covering a slightly extended distance range, such an empirical analysis should be possible and certainly should be part of the future refinement work.

RD. Sec 3.10, Pages 71-72. For the sigma model, the range of Φ_{SS} used to capture single-path sigma (nonergodic model) is a good simplified approach for the non-ergodic case. Figure 3.11 shows the smoothed model and the estimated Φ_{SS} . With the estimated values from the regression, the panel does not see the basis for a reduction in Φ_{SS} with period. A constant, period-independent Φ_{SS} seems to fit the data. Please explain the justification for including a reduction at long periods or consider using a constant value.

Previous versions of the Groningen GMM model (V2) used a period-independent ϕ_{SS} . This was modified in the V3 model to account for work conducted for the NGA-East ground-motion modelling project (Al Atik, 2015). The *global* model in Al Atik (2015) shows higher ϕ_{SS} values for short periods and small magnitudes or,

conversely, lower ϕ_{ss} for long periods for the same range of magnitudes (Figure 10.12). A similar trend of lower ϕ_{ss} values for long periods is also evident in the data for the Central and Eastern North America (Figure 10.13). The panel is correct in pointing out that this reduction in ϕ_{ss} for long periods is not evident in the Groningen data. However, given that the Groningen data is well constrained only for small magnitude earthquakes (that are smaller than those that control hazard and risk estimates), the GMM team opted for adopting the period-dependency observed in the better constrained global ϕ_{ss} models.

3.2. Comments on V5 GMM report

V5. Page 14, last paragraph: Are the deconvolved motions taken as outcropping?

Yes, because the STRATA site response analyses use outcropping bedrock motions. A note has been added to the report to clarify this point.

V5. Page 21. Both 300 bars and 100 bars are mentioned on this page as the basis for the stress drop for upper branch simulations. It requires multiple readings to understand that the former is for large M and the latter for small M . This detail could be more clearly explained.

The observation is valuable and the text has been modified to make it easier to follow. The key point is that there is broad epistemic in the stress drop values associated with larger-magnitude earthquakes but we have also included non-trivial ranges of uncertainty in the magnitude range of the data in recognition of the limited number of earthquakes in the database.

V5. Page 21. Figure 3.7. The panel suspects that differences between upper model simulations and Yenier and Atkinson are due to more than differences in Q as Q differences should have minimal impact at 1 km.

The simulations from the Groningen model in the middle frame of Figure 3.7 (the red crosses) lie between the curves from active tectonic regions and the curve Yenier & Atkinson (2015) curve at short distances. The difference between the Groningen simulations and the median ENA predictions increases considerably with distance, hence our commentary regarding the influence of Q . We acknowledge that it is also the case that at very short distances, the Groningen motions are below the ENA predictions and differences in Q are not likely to explain the disagreement so close to the earthquake source. We expect that the difference between the Groningen GMM and ENA model of Yenier & Atkinson (2015) at very short distances is likely due to a source effect: *i.e.*, higher stress-drop for ENA, although equivalently it may be due to a κ_0 effect (lower κ_0 for ENA). We nevertheless see no convincing reason

to model Groningen motions to match records from high stress-drop, mid-crustal earthquakes in mid-plate cratonic regions – and rather see these as a bounding limit.

V5. Figure 3.15. Is there are reason for the low tau for the upper branch at 0.85 sec?

This particular value is discarded from the analysis as it is clearly erroneous (and an explanatory note on this point has been added to the text). This low number is almost certainly the result of the stochastic nature of the MCMC sampling. For each period the model fitting makes use of four independent Markov chains, and a tau estimate (distribution) is obtained from each chain. However, the final result combines the results from the chains. In this sampling approach it is possible for one or more chains to get 'stuck' in a particular region of the multivariate sampling distribution (when acceptance ratios keep rejecting candidates). This shouldn't normally happen when the algorithms are set in a normal manner, but probably in this particular case it has happened and one particular chain has given a poor tau estimate that dragged down the overall mean estimate.

The analysis for this particular period has been re-run using the exact same dataset and the same MCMC sampling conditions. The new tau estimates at this period for each chain are 0.3334, 0.2750, 0.3372, 0.3082 which corresponds to an overall estimate of 0.3134. This revised estimate is very consistent with other estimates at similar periods and across other stress drop branches.

V5. Figure 3.19. In the text discussing this figure, indicate whether the effect shown here includes both the impact of the magnitude definition change and the addition of the Slochteren event data.

The figures shows the ratio of simulated motions from the V4 and V5 models, and therefore the patterns reflect the influence of both the change in the magnitude definition and the addition of the recordings from the Slochteren earthquake. However, in terms of influence of the Slochteren event on the final stochastic model terms it is only $1/23^{\text{rd}}$ since the misfit of spectra was minimised based on event terms rather than individual records. Therefore, the figure is primarily reflecting the effect of the magnitude change. Some text has been added to clarify these points.

V5. Figures 3.20-3.22. The text and caption should note that the NGA values for **M** 2 represent significant extrapolations of those models.

We acknowledge that this is the case and have added a note to this effect.

V5. Page 47. The relatively small differences shown in this plot seem to be at odds with slightly larger differences shown in Figure 4.16 at short periods. In particular, while Fig 4.16 is difficult to read, it appears the difference is 0.26 at 0.05 sec, whereas the difference here seems smaller (0.2 or less).

We suspect that the reviewers may have misread these plots since we do not see the discrepancy to which they allude. On the upper row of Figure 4.16, there is a difference of 0.25, which matches peak on the left-hand plot of Figure 4.12.

V5. Page 60, first paragraph. Why is model applicability described using M_L and not moment magnitude? Differences are likely appreciable at large magnitudes.

This is a good question and since the GMM is effectively based on moment magnitude (through the simulations and the matching of the upper branch to predictions from GMPEs calibrated in terms of M), a justified question as well. Our motivation for maintaining the reference to M_L is simply that the earthquake catalogue used in the derivation of the seismic source model for the Groningen field is still expressed in terms of local magnitudes as determined by KNMI. Now that a stable relationship between the two magnitude scales has been derived for the Groningen field, it is likely that future refinements of the hazard and risk model will involve a wholesale shift to moment magnitude, but for the time being we think it is correct to acknowledge the use of the local magnitude scale in the earthquake catalogue.

V5. Page 63, Figure 6.1. Please explain why different weights are used for the upper and lower branches, or give a reference to a prior report in which that was discussed.

At the top of p.31 of the original V5 report it was stated that branch weights were unchanged from V4 since there had been no reason to modify the rationale behind those weights. In essence, the rationale is that we have quite low confidence in the lower branch—although we think it should be retained since the hypocentres of Groningen earthquakes are very shallow and this may lead to persistently low stress drops—and hence assigned it only a 10% weight. The other branches are all considered equally likely and were thus assigned equal weights. We have added some brief text along these same lines to the revised V5 report.

V5. Page 72, following Eqn 6.18. For duration, it would be more appropriate to not use the ss subscripts on Φ , since the model is ergodic.

Perhaps the text below Equation 6.18 is not as clear as it could have been, but the text currently says that ‘the total variability on the duration is *conceptually* also decomposed into these different elements...’ (emphasis added). The sentence then

goes on to say that really for duration we simply have ϕ because we are assuming a known site response. So, we never actually use ϕ_{SS} in reference to the duration model.

V5. Page 75, Item 4. Are ε_z values not spatially correlated?

The values of this random variable are indeed spatially correlated and this was clearly stated within the V5 report. The final sentence of Chapter 6 stated the following in this regard: *“the same value of ε_z should be invoked at every grid point within a zone in order to represent spatial correlation.”*

V5. Page 92. Is a possible reason for the low ground motions from this recent event that average stress drops of the Groningen earthquakes are decreasing with time or that there is spatial variability in stress drops? The panel encourages consideration of these possible effects in future work.

This is a question that also interests us greatly. We have not been able to identify any systematic spatial variability in stress drops but there is an apparent temporal trend with recent events showing consistently lower event terms. This is also seen in the most recent earthquake—documented in Appendix VIII of the final V5 report—that occurred very close to the highest hazard area in the field but also displays apparently lower-than-average motions. A possible cause for these differences over time may be related to the fact that early events were recorded exclusively on the stations of the B-network whereas the recordings of more recent earthquakes are dominated by the G-network. Although the accelerographs deployed in both networks are the same, we have begun some work to explore if there are systematic differences between the two networks and this is now noted in Chapter 8 as part of the ongoing work of model refinement.

V5. Pages 112-114. The spectral shapes appear to do the opposite to what would generally be expected: period of the peak for **M** 6.5 is lower (~0.1s) than for **M** 4.5 (~0.25s). The panel’s interpretation is that this initially non-intuitive effect results from the increase of stress drop with magnitude above **M** 4.5. We suggest adding a brief discussion to present an appropriate interpretation.

The reason for the decrease in peak of the response spectrum is due to the transition of path Q with increasing fault depth (a function of fault width and therefore magnitude) which leads to damping that is lower than would be applied in a homogeneous (or near homogeneous) medium for larger events. This results in a subsequent shift of the response spectral peak (relative to the expectation for homogeneous Q) to shorter periods as magnitude increases from **M**4.5 to 5.5. Effectively, small events (dominated by high-frequency motions) originating in the

reservoir and propagating through the low Q sediments are damped more effectively than larger (and therefore lower-frequency) events that penetrate the Carboniferous.

Figure 3.5 shows the central-a GMM EXSIM predictions for a strike-normal location at 1 km (green lines). The increase in stress-drop (compare Figure 3.5, *top right* [red lines: using $\Delta\sigma(\mathbf{M})$, other terms constant] and *top left* [black lines: using constant $\Delta\sigma$]) with magnitude does appear to slow the increase in spectral peak with magnitude (note the dotted lines), however this does not lead to a systematic decrease of the peak (in period) with magnitude. The limited influence of with $\Delta\sigma(\mathbf{M})$ is partially due to the fact that the change in $\Delta\sigma$ occurs over a short magnitude range (**M**4.5 to 5.5): both below **M**4.5 and above 5.5 $\Delta\sigma$ is constant.

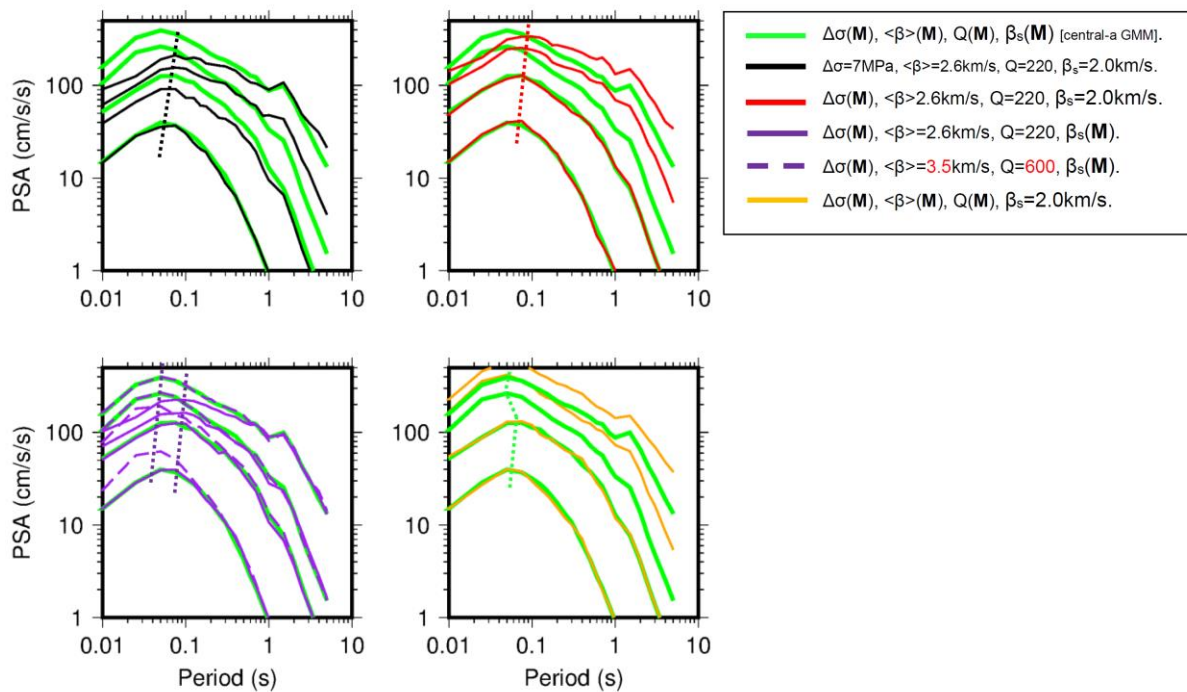


Figure 3.5. Comparison of EXSIM predictions for events with $\mathbf{M} = 3.5, 4.5, 5.5$ and 6.5 at $R_{JB} = 1$ km in the strike-normal direction as a function of period. *Green*: central-a GMM – magnitude dependent stress parameter $\Delta\sigma(\mathbf{M})$, average shear velocity $\langle\beta\rangle(\mathbf{M})$, $Q(\mathbf{M})$ and source velocity $\beta_s(\mathbf{M})$. *Black*: No magnitude dependent parameters – constant $\Delta\sigma = 7$ MPa, constant $\beta_s = 2$ km/s; constant $Q = 220$ and $\langle\beta\rangle = 2.6$ km/s. *Red*: as black, but with $\Delta\sigma(\mathbf{M})$. *Purple*: as green (central-a GMM), but without $\langle\beta\rangle(\mathbf{M})$, $Q(\mathbf{M})$ [dashed, $Q=220$, $\langle\beta\rangle=2.6$ km/s; solid $Q=600$, $\langle\beta\rangle=3.5$ km/s]. *Orange*: as green (central-a GMM), but without $\beta_s(\mathbf{M})$. Dotted lines indicate the change of spectral peak with magnitude – *bottom left*: two trends are shown, one for each end-member.

On the other hand, the effect of fault-size (magnitude) dependent Q (and corresponding average shear-wave velocity $\langle\beta\rangle$ used to calculate the damping term) has a significant impact on the peak (Figure 3.5, *bottom left* [purple solid/dashed lines: constant $Q=220/600$, $\langle\beta\rangle=2.6/3.5$ km/s]). The influence of Q is somewhat

counter-intuitive, since for larger faults in a homogeneous medium we expect higher overall damping (due to the increased distance to sub-faults along strike). However, the change from the $Q = 220$, $\langle\beta\rangle = 2.6$ km/s regime for $M < 4.5$ to $Q = 600$, $\langle\beta\rangle = 3.5$ km/s for $M > 5.5$ clearly outweighs this. It appears that the impact of this transition in the response spectral domain is more complex than would be anticipated in the Fourier domain – since in the latter case we would not expect a decrease in period of the spectral peak with increasing path length (irrespective of the change in Q over part of the path). However, due to the fact that a range of frequencies drive the oscillator response at a particular period (*i.e.*, $SA(T)$), and dominant frequencies decrease for larger events, this may lead to a magnitude dependent sensitivity of the response spectrum to the changes in Q , which manifests as a decrease in the period of peaks in SA.

V5. Page 136 onwards (Appendix VII). The plots of the predicted surface motions indicate spectral accelerations at periods of ~ 0.03 sec that are lower than those at PGA (0.01sec period). Is this behavior physically reasonable or an artifact of the fitting process? The plots of the NS_B spectra in Appendix IV do not appear to show this effect.

The panel is correct in this observation. However, this is not a result of an artefact of the fitting. Rather, it is a result of the scenario dependence of the linear amplification functions. For small magnitudes, the linear AF at a period of about 0.03 to 0.05 s are lower than at higher periods and lower than for PGA ($T=0.01$ s). This can be shown analytically for a simple two-layer system (see Figure 3.6 below). While this figure corresponds to rather arbitrary values of site properties and input motions (although the V_s and kappa values are in the same ballpark as those found for Groningen), it does illustrate the phenomena that leads to the rather peculiar shape of the predicted spectral accelerations. The theory and assumptions associated with this figure are explained in more detail in Stafford *et al.* (2017).

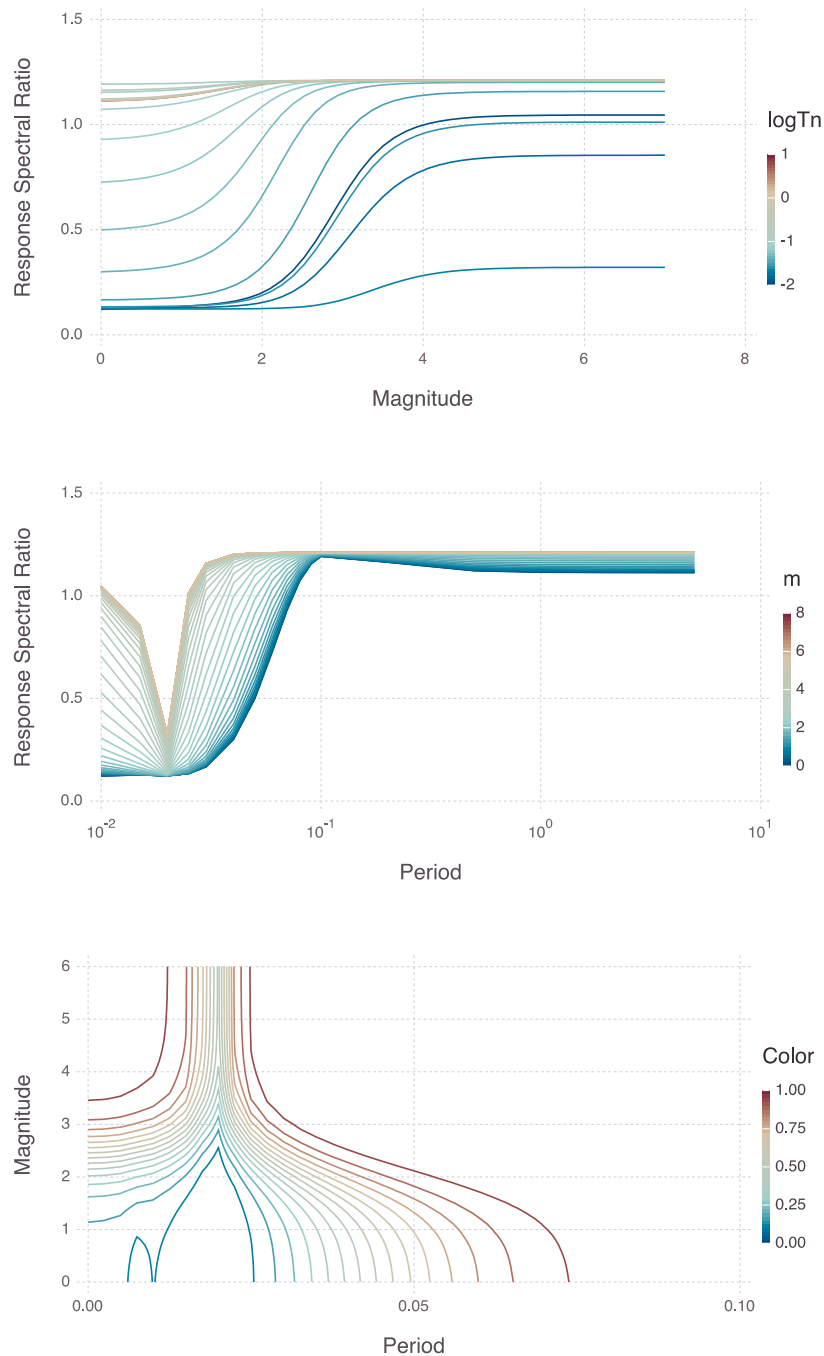


Figure 3.6. Ratios of response spectral ordinates at the base of a 50 m column of Vs 200 m/s soil overlying bedrock. The damping ratio within the soil column is assumed to be 0.035, while the κ_0 value within the underlying bedrock is assumed to be 0.01. Response spectra at the base of the column and surface are obtained from a seismological representation of the underlying Fourier spectrum, with a 100bar stress parameter, and essentially no path attenuation (the scenario is essentially very near source so that the Fourier spectrum is controlled by the source spectral shape and the κ_0 value). The upper panel shows surface/bedrock ratios against magnitude for a broad range of response periods. The central panel shows the same ratios plotted against period for a broad range of magnitudes, and the lower panel plots the contours of these ratios with respect to both magnitude and period. The tendency for the additional damping in the soil column to lead to a relative reduction in the spectral amplitudes over a range of short periods is clear.

4. Concluding Remarks

The comments that have been addressed in this document do not alter the fundamental validity of the V5 GMM report although they have enabled several features of the model to be better explained and more fully justified. The revised V4 and V5 reports, together with the two full sets of review comments and responses in this Appendix and Appendix IX, provide a complete and comprehensive documentation of the ground-motion model. Additionally, the comments have provided additional insights and suggestions that will be of great value in guiding future refinements and enhancements of the GMM for seismic hazard and risk assessment in the Groningen field.

We close by thanking all of the reviewers for their efforts in providing very valuable feedback and suggestions at many stages of the work, and also we offer our thanks once again in anticipation of your time and effort in perusing these responses and the V5 GMM report. To have been able to benefit from the feedback and insights of eight such distinguished individuals in the discipline of engineering seismology for this endeavour has been a genuine privilege.

5. References

- Abrahamson, N.A., W.J. Silva & R. Kamai, R., (2014). Summary of the ASK14 ground motion relation for active crustal regions. *Earthquake Spectra* **30**(3), 1025-1055.
- Afshari, K. & J.P. Stewart (2016). Physically parameterized prediction equations for significant duration in active crustal regions. *Earthquake Spectra* **32**(4), 2057-2081.
- Akkar, S., M.A. Sandikkaya & J.J. Bommer (2014). Empirical ground-motion models for point- and extended-source crustal earthquake scenarios in Europe and the Middle East. *Bulletin of Earthquake Engineering* **12**(1), 359-387. *Erratum: 12*(1), 389-390.
- Bahrampouri, M., A. Rodriguez-Marek & J.J. Bommer (2018). Mapping the uncertainty in modulus reduction and damping curves into the uncertainty of site amplification factors. *Soil Dynamics & Earthquake Engineering*, *in press*.
- Bindi, D., M. Massa, L. Luzi, G. Ameri, F. Pacor, R. Puglia & P. Augliera (2014). Pan-European ground-motion prediction equations for the average horizontal component of PGA, PGV, and 5%-damped PSA at spectral periods up to 3.0 s using the RESORCE dataset. *Bulletin of Earthquake Engineering* **12**(1), 391-430.
- Bommer, J.J., P.J. Stafford & J.E. Alarcón (2009). Empirical equations for the prediction of the significant, bracketed and uniform duration of earthquake ground motion. *Bulletin of the Seismological Society of America* **99**(6), 3217-3233.
- Boore, D.M. (2005). Erratum: Equations for estimating horizontal response spectra and peak acceleration from western north American earthquakes: A summary of recent work, by D.M. Boore, W.B. Joyner and T.E. Fumal. *Seismological Research Letters* **76**(3), 368-369.
- Boore, D.M., J.P. Stewart, E. Seyhan & G.M. Atkinson (2014). NGA-West2 equations for predicting PGA, PGV, and 5% damped PSA for shallow crustal earthquakes. *Earthquake Spectra* **30**(3), 1057-1085.
- Boore, D.M., J. Watson-Lamprey & N.A. Abrahamson (2006). Orientation-independent measures of ground motion. *Bulletin of the Seismological Society of America* **94**(4A), 1502-1511.
- Campbell, K.W. & Y. Bozorgnia (2014). NGA-West2 ground motion model for the average horizontal components of PGA, PGV, and 5%-damped elastic pseudo-acceleration response spectra. *Earthquake Spectra* **30**(3), 1087-1115.
- Chiou, B.S.J. & R.R. Youngs (2014). Update of the Chiou and Youngs NGA model for the average horizontal component of peak ground motion and response spectra. *Earthquake Spectra* **30**(3), 1117-1153.
- Kempton, J.J. & J.P. Stewart (2006). Prediction equations for significant duration of earthquake ground motions considering site and near-source effects. *Earthquake Spectra* **22**(4), 985-1013.
- Stafford, P.J., Rodriguez-Marek, A., B. Edwards, P.P. Kruiver & J.J. Bommer (2017). Scenario dependence of linear site effect factors for short-period response spectral ordinates. *Bulletin of the Seismological Society of America* **107**(6), 2859-2872.

Yenier, E. & G.M. Atkinson (2015). Regionally adjustable generic ground-motion prediction equation based on equivalent point-source simulations: Application to central and eastern North America. *Bulletin of the Seismological Society of America* **105**, 1989-2009.